Methods in Pharmacology and Toxicology

Springer Protocols

Mike Clements
Liz Roquemore *Editors*

Stem Cell-Derived Models in Toxicology

EXTRAS ONLINE

Humana Press

Methods in Pharmacology and Toxicology

Series Editor
Y. James Kang
University of Louisville
School of Medicine
Prospect, Kentucky, USA

For further volumes:
http://www.springer.com/series/7653

Stem Cell-Derived Models in Toxicology

Edited by

Mike Clements

Axion BioSystems, Inc., Atlanta, GA, USA

Liz Roquemore

Cell Applications, GE Healthcare, Cardiff, UK

Humana Press

Editors
Mike Clements
Axion BioSystems, Inc.
Atlanta, GA, USA

Liz Roquemore
Cell Applications
GE Healthcare
Cardiff, UK

Videos can also be accessed at http://link.springer.com/book/10.1007/978-1-4939-6661-5

ISSN 1557-2153 ISSN 1940-6053 (electronic)
Methods in Pharmacology and Toxicology
ISBN 978-1-4939-6659-2 ISBN 978-1-4939-6661-5 (eBook)
DOI 10.1007/978-1-4939-6661-5

Library of Congress Control Number: 2016957355

Cover Illustration: Confocal microscopy image of a spheroid microtissue of hiPSC-derived cardiomyocytes (Cellular Dynamics International, Madison, USA) and human umbilical vein endothelial cells (Zen-Bio Inc., Durham, USA) produced using the GravityTrap hanging drop method (InSphero AG, Schlieren, Switzerland), and immunostained for von Willebrand factor (green), sarcomeric protein myomesin (red), and DNA (blue); from Chapter 11, Zuppinger. Overlaid is a field potential transient signal recorded from spontaneously beating hSC-derived cardiomyocytes on the multielectrode array (MEA) platform (Axion BioSystems Inc., Atlanta, USA); from Preface, Clements.

Printed on acid-free paper

This Humana Press imprint is published by Springer Nature
The registered company is Springer Science+Business Media LLC
The registered company address is: 233 Spring Street, New York, NY 10013, U.S.A.

Preface

Unexpected adverse toxicity findings in drug development or postlaunch have resulted in numerous costly late-stage drug development failures and market withdrawals. To mitigate this risk, the pharmaceutical industry has adopted a range of assays to probe the liability of compounds earlier in the drug development process consistent with the mantra "fail faster, fail cheaper". In the drug discovery process, lead optimization is the ideal phase to screen for safety issues, since at this point failure is relatively cheap and the number of potential compounds for selection (~1000) is greatest. The currently available standard testing models include primary tissue and immortalized cell lines. While immortalized cell lines lend themselves to screening applications (e.g. relatively inexpensive, abundant, easy to handle), the assay end point can be overly simplistic, leading to false positives (i.e. compounds flagged as toxic which are in fact safe) and false negatives (i.e. compounds misidentified as safe when actually toxic). Primary tissue (typically rodent) is often useful for small investigative studies but is not applicable for screening applications, due to both cost and ethical concerns with regard to animal consumption (3Rs). Concerns also persist with the translation of this data to humans due to possible species differences. Consequently, there is increasing demand for more relevant and predictive nonclinical models for in vitro toxicity testing (see Chap. 1, Gintant and Braam).

Since the first descriptions of the differentiation of cardiomyocytes from human embryonic stem cells (hESC) more than a decade ago, there has been much speculation over the utility of these cells for drug safety assessment [1]. Human ESC and human-induced pluripotent stem cell-derived (hiPSC) models, together termed human stem cell-derived (hSC) models, offer an opportunity to provide a more predictive, integrated human model system that is amenable to high-throughput screening in preclinical drug safety assessment. The relative immaturity of these stem cell-derived models is well documented (e.g. [2]), which has led some to question the applicability of hSC-derived models in toxicological studies (i.e. "they are not old enough for drugs").

Although methods to produce hSC-derived models with more "adultlike" phenotypes are currently the focus of intensive research efforts, there is considerable data in the literature to suggest a role for the current iteration of this technology. Accordingly, the potential application of hSC-cardiomyocytes (hSC-CMs) in advancing the development of more predictive preclinical cardiac safety assessment is now the subject of extended testing in the regulatory communities. This includes proposals such as the Japan iPS Cardiac Safety Assessment (JiCSA) consortium with the objective to validate hiPSC-CM assay for regulatory purposes and HESI's Comprehensive in vitro Proarrhythmia Assay (CiPA) which aims to obviate the need for clinical QT studies. The core components of CiPA will include a mathematical (i.e. in silico) model of cardiac muscle electrical activity based on in vitro ion channel data to predict whether new drugs will cause dangerous changes to heart rhythm (i.e. proarrhythmia). A complementary in vitro hSC-CM assay will be integrated into this process with the aim of confirming or casting doubt on the in silico predictions and to broaden the cardiac safety assessment of the candidate drug to include additional proarrhythmic mechanisms not discoverable by the in silico analysis. This is a very promising development for the acceptance

of hSC-derived models in drug discovery and toxicology, and with increased characterization of these hSC-derived models and validation of their associated assays, they will surely grow in prominence.

The majority of this book is focused on differentiated tissues, but we begin the protocol chapters with a high-throughput screen designed to predict embryonic-foetal developmental toxicity using hESCs (Chap. 2, Kameoka and Chiao). One of the first applications of pluripotent stem cells in toxicology was the mouse embryonic stem cell test (mEST), which has been deemed of sufficient value for consideration in regulatory acceptance and submission documents. Here, Kameoka and Chiao describe an improved human embryonic stem cell test (hEST) thus avoiding the extrapolation of responses from animals to humans.

Over half of the chapters in this volume are focused on cardiotoxicity applications. The underlying reason for this bias towards hSC-CM assays is severalfold. Firstly, the cardiomyocyte differentiation process was one of the first to be characterized (hESC-CMs in 2003 and hiPSC-CMs in 2009) and can now be employed to manufacture these cells on an industrial scale suitable for screening applications. Secondly, a human primary model is not readily available (e.g. unlike for hSC-hepatocytes), so there is a large unmet need from the cardiotoxic field. Thirdly, the hSC-CM model has been demonstrated to add value over and above existing model systems (e.g. the antihistamine, terfenadine, produces the expected prolongation of the cardiac action potential in hSC-CMs at clinical relevant concentrations, unlike the false-negative result observed in both canine and porcine Purkinje fibres even at supra-therapeutic concentrations). Finally, cardiotoxicity is one of the most prevalent forms of drug-induced toxicity. Although the recent regulatory guidelines have been successful in reducing the release of proarrhythmic drugs coming to market, there is a general consensus that the extensive focus on a single ion channel (hERG K^+ channel) has resulted in an overly high attrition rate (false positives) in drug development, prematurely halting the development of otherwise promising candidate drugs. CiPA proposes that safety studies using multiple ion channel effects (MICE) models, such as hSC-CMs, are likely to be more predictive of clinical drug response where compensatory drug actions on one or more other ion channels mitigate the effects due to hERG blockade.

Manual patch-clamp remains the “gold-standard” for probing drug-induced cardiac ion channel effects (see Chap. 3, Renganathan et al.), and an automated method for increasing assay throughput is also described here (Chap. 4, Obergrussberger et al.). However, manual patch-clamp is very labour intensive, and the difficulties translating automated patch-clamp protocols to hSC-derived models have resulted in the CiPA initiative focusing on analogous emerging electrophysiology-based technologies, namely, multi-electrode array (MEA; see Chap. 5, Millard et al., and Chap. 10 Obergrussberger et al.) and voltage-sensitive optical probes (i.e. genetically encoded voltage indicators, GEVIs (see Chap. 6, Dempsey et al.), and voltage-sensitive dyes, VSDs (see Chap. 7, Kettenhofen)). These techniques present their own strengths and limitations as discussed in the relevant chapters.

Not all cardiotoxicity can be observed by changes in hSC-CM excitability with the aforementioned electrophysiology-based assays. Full and efficient assessment of new drug development liabilities must take a holistic account of both the structural and functional aspects of cell biology. The relative complexity of stem cell-derived models makes them applicable to surveying a wide range of mechanisms whereby a new chemical entity may perturb cell function. Accordingly, this has sparked the development of a diverse range of innovative analytical platforms with the potential to probe previously inaccessible features of cell function (Fig. 1).

Cardiomyocyte excitability (i.e. an action potential) initiates calcium release into the cell and is subsequently removed from the cytoplasm prior to the next contraction event.

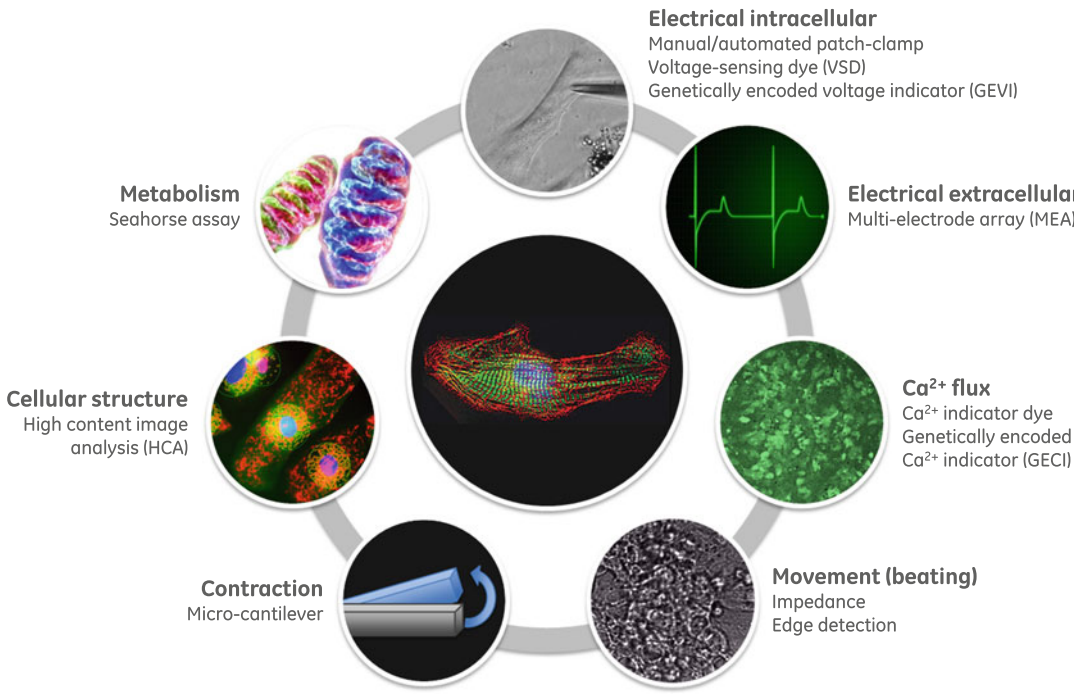

Fig. 1 One cell to bind them all: bridging analytical platforms. As well as providing a more relevant nonclinical model for in vitro toxicity testing, hSC-derived models have the potential to bridge analytical platforms and in doing so provide an integrated model for probing many possible causes and mechanisms of toxicity. The example of hSC-cardiomyocytes (*centre*) and some of the possible associated assays are illustrated here

Compound-induced effects on these calcium transients can be measured with high-throughput calcium imaging platforms as either the mean response of the hSC-CM monolayer (see Chap. 7, Kettenhofen) or with single-cell resolution (see Chap. 8, Pfeiffer et al., and Chap. 9, George et al.). In turn, this calcium signal is converted into the mechanical contraction of the cardiomyocyte. The physical movement of a layer of beating cardiomyocytes can be continuously monitored with the impedance assay (see Chap. 10, Obergrussberger et al.) or image-based edge detection of a beating spheroid (see Chap. 11, Zuppinger et al.). Measuring this downstream hSC-CM movement can be advantageous since compounds can perturb the cell's contractile machinery, without impacting its electrophysiology, e.g. the myosin II inhibitor blebbistatin. These platforms, however, do not measure the direct force of contraction, which would be advantageous when screening for unwanted compound-induced changes to the strength of cardiac contractility (i.e. inotropic effects). This requirement is addressed in Chap. 12 (Oleaga et al.), where a novel microcantilever-based device is employed to detect perturbations in the force of hSC-CM contractions.

In addition to altering the acute mechanical function of the heart (functional toxicity), cardiotoxicity can also occur due to morphological damage to cardiomyocytes, damage to intracellular organelles, or loss of cardiomyocyte viability (structural toxicity), resulting in cardiomyopathy and heart failure. Methods for screening for compound-induced changes to cell morphology are described in Chap. 13 (Roquemore et al., high-content image analysis, HCA) and Chap. 14 (Kriston-Vizi et al., hypertrophy).

Human SC-neurons similarly offer a novel method of screening for neurotoxins. The MEA assay can be employed to predict neurotoxic risk associated with drugs or compounds present in the environment by monitoring subtle perturbations to the spontaneous firing patterns of hSC-neuronal cultures (e.g. insecticides; see Chap. 15, Kraushaar et al.).

Hepatotoxicity is a major cause of drug attrition, and consequently, in vitro liver-based assays are an integral part of preclinical safety assessments. Primary human hepatocytes are currently the model of choice but are limited by donor-to-donor variability and the short period of time they are functional in culture (i.e. they are unsuitable for assessing the effects of prolonged compound exposure). Human SC-hepatocytes could potentially address these concerns, but their implementation in toxicity assays has been hindered largely due to difficulties in obtaining a mature metabolic phenotype. The expression of CYP3A4, the most abundant cytochrome P450 in the liver, is expressed at lower levels in hSC-hepatocytes compared with primary human hepatocytes. This is of concern since CYP450-dependent formation of toxic metabolites is a cause of drug-induced liver injury. That said, promising hSC-hepatocyte data has emerged from methods attempting to replicate the cellular microstructure of the liver (see Chap. 16, Ware and Khetani).

With the first commercially available hSC-derived models, there was an initial drive to produce >95% "pure" cell models. The rationale behind this approach was that it would be preferable if drug-induced effects observed in biochemical assays could be assigned to a single-cell type. However, recent findings suggest that the presence of stromal (e.g. fibroblast) cells in the culture of interest adds functionality and ultimately increases predictivity. The precise mixing of different highly pure cell types with stromal cells now allows the end user to titre the performance of the model to achieve the desired functionality (see Chap. 11, Zuppinger, for hSC-CMs; and Chap. 16, Ware and Khetani, for hSC-hepatocytes). The advent of technologies that facilitate self-assembling 3D spheroids and self-ordering patterns of cells in 2D culture has helped limit the inevitable increase in assay set-up time and cost associated with the added complexity of these co-culture models.

For the first time, this volume brings together a diverse collection of stem cell-derived model-based toxicity assays, from those routinely used to those deemed to have considerable potential. Key opinion leaders from academia and industry have been invited to contribute their preferred assay protocols with accompanying rationale and example output data. Our goal is to enable adoption of these protocols in laboratories that are interested in entering the field as well as to facilitate the transfer of best practices between laboratories that are already actively pursuing these technologies. The use of stem cell-derived models in safety pharmacology and toxicology is in their infancy, but their potential for improving risk assessment will inevitably drive the development of even more innovative methods to probe toxicity.

Atlanta, GA, USA — *Mike Clements*
Cardiff, UK — *Liz Roquemore*

References

1. Davila JC, Cezar GG, Thiede M, Strom S, Miki T, Trosko J (2004) Use and application of stem cells in toxicology. Toxicol Sci 79(2):214–223
2. Veerman CC, Kosmidis G, Mummery CL, Casini S, Verkerk AO, Bellin M (2015) Immaturity of human stem-cell-derived cardiomyocytes in culture: fatal flaw or soluble problem? Stem Cells Dev 24(9):1035–1052

Contents

Preface . . . . . *v*
Contributors . . . . . *xi*

1 Stem Cell-Derived Models for Safety and Toxicity Assessments: Present and Future Studies in the "Proclinical Space" 1
Gary Gintant and Stefan Braam

2 Human Pluripotent Stem Cell Test for Assessing the Potential Teratogen Risk 17
Sei Kameoka and Eric Chiao

3 Cardiac Action Potential Measurement in Human Embryonic Stem Cell Cardiomyocytes for Cardiac Safety Studies Using Manual Patch-Clamp Electrophysiology 37
Muthukrishnan Renganathan, Haiyang Wei, and Yong Zhao

4 Automated Patch Clamp Recordings of Human Stem Cell-Derived Cardiomyocytes 57
Alison Obergrussberger, Claudia Haarmann, Sonja Stölzle-Feix, Nadine Becker, Atsushi Ohtsuki, Andrea Brüggemann, Michael George, and Niels Fertig

5 The CiPA Microelectrode Array Assay with hSC-Derived Cardiomyocytes: Current Protocol, Future Potential. 83
Daniel C. Millard, Mike Clements, and James D. Ross

6 Optogenetic Approach to Cardiotoxicity Screening: Simultaneous Voltage and Calcium Imaging Under Paced Conditions. 109
Graham T. Dempsey and Christopher A. Werley

7 HTS-Compatible Voltage- and Ca^{2+}-Sensitive Dye Recordings from hiPSC-Derived Cardiomyocytes Using the Hamamatsu FDSS Systems 135
Ralf Kettenhofen

8 Kinetic Image Cytometry for Predicting Arrhythmias Using Human Stem Cell-Derived Cardiomyocytes 153
Emily R. Pfeiffer, Ross Whittaker, Raquel Vega, Fabio Cerignoli, Patrick M. McDonough, and Jeffrey H. Price

9 Decoding Ca^{2+} Signals as a Non-electrophysiological Method for Assessing Drug Toxicity in Stem Cell-Derived Cardiomyocytes 173
Christopher H. George and David H. Edwards

10 Combined Impedance and Extracellular Field Potential Recordings from Human Stem Cell-Derived Cardiomyocytes 191
Alison Obergrussberger, Ulrich Thomas, Sonja Stölzle-Feix, Nadine Becker, Krisztina Juhasz, Leo Doerr, Matthias Beckler, Michael George, and Niels Fertig

11 Edge-Detection for Contractility Measurements with Cardiac Spheroids 211
Christian Zuppinger

12 Contractile Force Readout of hESC-Cardiomyocytes 229
Carlota Oleaga, Gregg Legters, L. Richard Bridges, Lee Kumanchik, Candace Martin, Yunqing Cai, Mark Schnepper, Christopher W. McAleer, Christopher J. Long, and James J. Hickman

13 In Vitro Cardiotoxicity Investigation Using High Content Analysis and Human Stem Cell-Derived Models. 247
Liz Roquemore, M. Ariel Kauss, Catherine Hather, Nick Thomas, and Hirdesh Uppal

14 Structural Toxicity: Hypertrophy Models of Human Pluripotent Stem Cell-Derived Cardiomyocytes. 271
Janos Kriston-Vizi, Sian E. Harding, and Gábor Földes

15 Addressing Functional Neurotoxicity Using the Microelectrode Array (MEA) 293
Udo Kraushaar, Elke Guenther, and Dietmar Hess

16 Micropatterned Co-Cultures of Induced Pluripotent Stem Cell-Derived Hepatocytes and Stromal Cells for Drug Toxicity Studies 311
Brenton R. Ware and Salman R. Khetani

Index *335*

Contributors

Nadine Becker • *Nanion Technologies GmbH, Munich, Germany*
Matthias Beckler • *Nanion Technologies GmbH, Munich, Germany*
Andrea Brüggemann • *Nanion Technologies GmbH, Munich, Germany*
Stefan Braam • *Pluriomics BV, BD Leiden, The Netherlands*
L. Richard Bridges • *NanoScience Technology Center, University of Central Florida, Orlando, FL, USA*
Yunqing Cai • *NanoScience Technology Center, University of Central Florida, Orlando, FL, USA*
Fabio Cerignoli • *Vala Sciences, San Diego, CA, USA*
Eric Chiao • *Regeneron Pharmaceuticals, Tarrytown, NY, USA*
Mike Clements • *Axion BioSystems, Inc., Atlanta, GA, USA*
Graham T. Dempsey • *Q-State Biosciences, Cambridge, MA, USA*
Leo Doerr • *Nanion Technologies GmbH, Munich, Germany*
David H. Edwards • *School of Medicine, Cardiff University, Cardiff, UK*
Gábor Földes • *National Heart and Lung Institute, Imperial Centre for Experimental and Translational Medicine, Imperial College London, London, UK; Heart and Vascular Center, Semmelweis University, Budapest, Hungary*
Niels Fertig • *Nanion Technologies GmbH, Munich, Germany*
Michael George • *Nanion Technologies GmbH, Munich, Germany*
Christopher H. George • *School of Medicine, Cardiff University, Cardiff, UK*
Gary Gintant • *AbbVie, Integrative Pharm., Integrated Science and Technology, North Chicago, IL, USA*
Elke Guenther • *Department of Electrophysiology, NMI Natural and Medical Sciences Institute at the University of Tuebingen, Reutlingen, Germany*
Claudia Haarmann • *Nanion Technologies GmbH, Munich, Germany*
Sian E. Harding • *National Heart and Lung Institute, Imperial Centre for Experimental and Translational Medicine, Imperial College London, London, UK*
Catherine Hather • *GE Healthcare, Cardiff, UK*
Dietmar Hess • *Axiogenesis AG, Cologne, Germany*
James J. Hickman • *NanoScience Technology Center, University of Central Florida, Orlando, FL, USA*
Krisztina Juhasz • *Nanion Technologies GmbH, Munich, Germany*
Sei Kameoka • *Vertex Pharmaceuticals, Boston, MA, USA*
M. Ariel Kauss • *University of California at San Francisco, San Francisco, CA, USA*
Ralf Kettenhofen • *Axiogenesis AG, Cologne, Germany*
Salman R. Khetani • *School of Biomedical Engineering, Colorado State University, Fort Collins, CO, USA; Department of Bioengineering, University of Illinois at Chicago, Chicago, IL, USA; Department of Mechanical Engineering, Colorado State University, Fort Collins, CO, USA*

Udo Kraushaar • *Department of Electrophysiology, NMI Natural and Medical Sciences Institute at the University of Tuebingen, Reutlingen, Germany*
Janos Kriston-Vizi • *MRC Laboratory for Molecular Cell Biology, University College London, London, UK*
Lee Kumanchik • *NanoScience Technology Center, University of Central Florida, Orlando, FL, USA*
Gregg Legters • *NanoScience Technology Center, University of Central Florida, Orlando, FL, USA*
Christopher J. Long • *NanoScience Technology Center, University of Central Florida, Orlando, FL, USA*
Candace Martin • *NanoScience Technology Center, University of Central Florida, Orlando, FL, USA*
Christopher W. McAleer • *NanoScience Technology Center, University of Central Florida, Orlando, FL, USA*
Patrick M. McDonough • *Vala Sciences, San Diego, CA, USA*
Daniel C. Millard • *Axion BioSystems, Inc., Atlanta, GA, USA*
Alison Obergrussberger • *Nanion Technologies GmbH, Munich, Germany*
Atsushi Ohtsuki • *Nanion Technologies GmbH, Tokyo Laboratory, Medical Innovation Laboratory, Tokyo Women's Medical University and Waseda University Joint, Institution for Advanced Biomedical Sciences, Shinjyuku-ku, Tokyo, Japan*
Carlota Oleaga • *NanoScience Technology Center, University of Central Florida, Orlando, FL, USA*
Emily R. Pfeiffer • *Vala Sciences, San Diego, CA, USA*
Jeffrey H. Price • *Vala Sciences, San Diego, CA, USA*
Muthukrishnan Renganathan • *Eurofins Pharma Inc., St Charles, MO, USA*
Liz Roquemore • *GE Healthcare, Cardiff, UK*
James D. Ross • *Axion BioSystems, Inc., Atlanta, GA, USA*
Mark Schnepper • *NanoScience Technology Center, University of Central Florida, Orlando, FL, USA*
Sonja Stölzle-Feix • *Nanion Technologies GmbH, Munich, Germany*
Ulrich Thomas • *Nanion Technologies GmbH, Munich, Germany*
Nick Thomas • *GE Healthcare, Cardiff, UK*
Hirdesh Uppal • *Medivation Inc., San Francisco, CA, USA*
Raquel Vega • *Vala Sciences, San Diego, CA, USA*
Brenton R. Ware • *School of Biomedical Engineering, Colorado State University, Fort Collins, CO, USA; Department of Bioengineering, University of Illinois at Chicago, Chicago, IL, USA*
Haiyang Wei • *Eurofins Pharma Inc., St Charles, MO, USA*
Christopher A. Werley • *Q-State Biosciences, Cambridge, MA, USA*
Ross Whittaker • *Vala Sciences, San Diego, CA, USA*
Yong Zhao • *Eurofins Pharma Inc., St Charles, MO, USA*
Christian Zuppinger • *Cardiology, Department of Clinical Research MEM G803b, Bern University Hospital, Bern, Switzerland*

Chapter 1

Stem Cell-Derived Models for Safety and Toxicity Assessments: Present and Future Studies in the "Proclinical Space"

Gary Gintant and Stefan Braam

Abstract

The promise of human, stem cell-derived models for safety and toxicity assessments remains great. Using such preparations it should be possible to provide preclinical assessments of drug effects with human-derived cells and engineered tissues, creating a new "proclinical" paradigm to study human responses without administering drugs to human volunteers or patients. Along with this promise come challenges related to more fully characterizing, standardizing, and understanding these novel preparations, developing the experimental platforms necessary for efficient and reproducible studies, and validation studies demonstrating overall utility of various models. This chapter describes some issues encountered with the development of human-induced stem cell-derived cardiomyocytes for safety and toxicity studies with evolving drug candidates, along with a discussion of the role of future proclinical studies as part of an integrated package of more traditional safety and toxicology assessments.

Key words Preclinical studies, Translational, Stem cell-derived cardiomyocytes, Proclinical studies, CiPA, Phenotypic assays, Drug screening

1 The Promise of Human-Induced Pluripotent Stem Cell-derived Cardiomyocytes

Over the past two decades, two seminal scientific breakthroughs, namely, (1) the first report of long-term culture of human *embryonic* stem cells by Jamie Thomson [1] and (2) the discovery of human-*induced* pluripotent stem cell-derived cells (iPSCs) by Shinya Yamanaka [2], led to the birth of a completely new field of translational science focused on the derivation of personalized fully functional human cells (both healthy and diseased) of many different organs. Many major technical advances followed quickly. In particular, major improvements have been made in the process of deriving these cells in culture and the development of reproducible differentiation strategies to produce functional cells like cardiomyocytes, neurons, and hepatocytes in numbers and purities amenable for functional assays. These advances sparked interest in the

Mike Clements and Liz Roquemore (eds.), *Stem Cell-Derived Models in Toxicology*, Methods in Pharmacology and Toxicology, DOI 10.1007/978-1-4939-6661-5_1,

development of novel preclinical in vitro testing strategies (to evaluate drug safety and efficacy) as well as the development of novel cellular therapies for human diseases.

The functional cell types derived from "healthy" (representing non-diseased states) iPSCs in combination with novel assay strategies have now found their way to the safety/ADME/toxicology departments of biopharmaceutical companies and CROs where they are being used to study effects of evolving drugs in human cellular models in the preclinical R&D space. Besides being useful for the generation of healthy cells, this technology is very amendable to the generation of "disease-in-a-dish" models. Congenital diseases are at the forefront of these applications, in part because existing genome-wide association datasets for many diseases enable functional assessment in experimental in vitro human models. Furthermore, rapid advances in genome engineering now allow the construction of isogenic control cell lines which increase confidence that observed cellular phenotypes are directly correlated to the genetic variant of interest. In particular, in the case of cell autonomous diseases like cardiac arrhythmias, this technology is exceptionally well placed to study molecular mechanisms that drive disease progression and putative targets for reversal of disease symptoms. It has been demonstrated in many articles that arrhythmic phenotypes can be observed in human-induced pluripotent stem cell-derived cardiomyocytes (hiPSC-CMs) derived from LQT patients [3], a concept inconceivable a decade ago. In conclusion rapid advances in iPSC biology have resulted in novel in vitro models that are already impacting today's drug discovery process.

Most chapters in this book describe platforms and methodological approaches used or being developed for in vitro stem cell human-derived cellular models. It is important to not only understand the strengths and limitations of these various methodological approaches but also to understand the strengths and limitations of the preparations themselves. Both components (preparations and methodological approaches) will define the utility, best applications, and adoption of the models. This chapter will discuss some general principles and concepts regarding the use and translation of phenotypic models employing stem cell-derived preparations for drug discovery and safety, as well as considerations regarding the influence (and promise) of evolving stem cell-derived therapies. While the focus in this chapter may be on cardiomyocytes, comparable issues are applicable with neuronal and hepatocyte models, two areas of intense interest. Finally, while the perspectives and opinions in this chapter are centered primarily on the use of human-derived models for evaluating drug safety and toxicity, these concepts are also applicable to the use of these preparations as disease models in drug discovery.

2 Understanding The Preparations

For decades, biomedical and pharmaceutical researchers have used model systems to study human biology, development, disease, and drug therapy. In particular, model organisms are widely used to investigate treatments and potential causes of human disease when experiments directly on humans are not feasible or are unsafe and therefore unethical. Examples of commonly used laboratory model systems include the fruit fly *Drosophila melanogaster*, the zebrafish *Danio rerio*, the rat *Rattus norvegicus*, and the mouse *Mus musculus*. Largely because of the ability to perform reverse genetics, the mouse has evolved as the favorite model to study human genes and disease processes [4]. Although all of these model organisms have their own specific advantages and disadvantages, they have one major disadvantage in common, namely, they are not human and thus may not possess systems similar to humans. Care must always be taken when extrapolating from any model system to humans.

3 The iPSC-Derived Cardiomyocyte Model

Ideally, human iPSC model systems overcome this major "translational" issue and fulfill the main criteria of an experimental system: simple, idealized, readily accessible, and easily manipulated [5]. With experimental animal models, it is clearly more challenging to study mechanisms that may involve multiple cellular systems and multiple organs, where multiple interactions modulate and define the cellular phenotype through autocrine, paracrine, and endocrine/exocrine factors, as well as physical/mechanical characteristics of the microenvironment and mechanotransduction (see section on Maturation, below). However, processes "at the cellular level" like transcriptional regulation, proliferation, differentiation, cell migration, and specific cellular functions (e.g., electrophysiology and contractility) are very well suited to being studied in human-derived in vitro cellular models [6–8].

Despite higher-level similarities, it remains crucial to recognize cellular differences between acutely isolated primary cells and stem cell-derived cardiomyocytes used in in vitro models. For studies involving ex vivo-derived cells and tissues, nature provides the necessary quality control standards, as the preparations were properly functioning in (presumably) a healthy integrated animal. Consider adult rat papillary muscles as an example. Given identical experimental protocols and reagents, studies conducted with adult rat papillary muscles harvested from a particular strain of healthy rats today would be expected to provide the same experimental result as those generated some 50 years ago. Assuming standardized (and

generally agreed-upon "best practices" in the field), this outcome is possible because the animal provides a stable, mature phenotype (fully developed in vivo) necessary to sustain a healthy rat.

At present, the situation with hiPSC-CMs is quite different than the rat papillary muscle example. hiPSC-CMs are derived from different (often unidentified) sources (including "normal" vs. disease patients) and are likely differentiated using a wide variety of (often) proprietary protocols yielding (sometimes) heterogeneous cell populations with different levels of maturation. Even if one assumes a consistent supply of large batches of quality-controlled and cryopreserved hiPSC-CMs delivered for experiments, variations in cell culture conditions, media (oftentimes not fully defined), and duration of maturation may lead to experimental preparations with different functional or morphological characteristics. For example, it is well recognized that different protocols and culture conditions give rise to different electrophysiologic phenotypes of atrial and ventricular hiPSC-CMs [9, 10]. It is not unexpected that culture conditions should influence cellular phenotypes, as the electrophysiology of simplified (scaffold-free) 3D spheroid cultures of hiPSC-CMs (and even cultured neonatal rat cardiomyocyte monolayers) has been shown to be dependent on culture substrate [11, 12].

Clearly, there is a need for cell manufacturing under a stringent quality management system and well-defined release criteria, along with a well-defined maturation pathway for in vitro studies with hiPSC models. This could involve a panel of cell identity and functionality assays, thereby mimicking or even improving the quality control that one will get "for free" using in vivo material. An extensive list of criteria for structural phenotyping of hiPSC cardiomyocytes has recently been proposed [13], and the need for positive and negative functional controls in assay development and implementation is obvious.

It is well known that present-day commercial hiPSC-CM preparations either provide a heterogeneous population of atrial, ventricular, and nodal myocytes based on electrophysiologic phenotype or an enriched or even pure (ventricular) phenotype. Such disparities can lead to potentially different responses (both qualitatively and quantitatively) to test interventions or pharmacologic challenges and may confound comparisons of results obtained with hiPSC-CM preparations compared with those from native cells or tissues. Until more standardized practices are in place, there is a need to demonstrate assay reproducibility and assay sensitivity for studies involving hiPSC-CMs, such as would be accomplished through the routine use of positive (and negative) controls. Such demonstrations will define "fit-for-purpose" applications for stem cell-derived models and provide confidence in the benefit of using hiPSC-CMs (still viewed by many with skepticism and needing validation as a research tool). Such efforts will need to be repeated

with each refinement of the hiPSC-CM preparation, for example, with the evolution from simpler single-cell and monolayer cultures to more matured and defined 2D structures and onward to more complex 3D cultures/cocultures recapitulating aspects of organ physiology [14].

4 Evolution of the hiPSC-CM Model: Maturation

Despite the close resemblance to primary human cardiomyocytes, a major hurdle for the field remains the fact that hiPSC-CM gene expression, electrophysiologic phenotypes, metabolism, and contractile and structural organization do not fully match that of mature adult human cardiomyocytes (see [15, 16]). Indeed, current hiPSC-CM preparations more closely resemble fetal/neonatal human primary cardiomyocytes than adult cardiomyocytes ([17, 18], reviewed by Veerman et al. [19]).

Recently, studies designed to improve hiPSC-CM maturation have revealed that solutions can be developed to overcome many of the developmental barriers encountered with hiPSC-CMs. Approaches that have so far been (partly) successful include prolongation of time in culture, application of mechanical stretch and strain, novel flexible substrates that mimic heart tissue, growth in three-dimensional tissue configuration, exposure to electrical (or optogenetic) stimulation, improved culture media, and addition of fibroblasts, endothelial cells, and vascular smooth muscle to generate an organotypic culture system [19]. Key functional and structural criteria for defining a mature myocyte phenotype could include decreased spontaneous automaticity (reduced beat frequency), hyperpolarization of the resting membrane potential, improved sarcomeric structure and organization, the presence of T-tubules, and increased force of contraction.

With these novel culture systems promoting maturation, new challenges and specific advantages and disadvantages emerge. These challenges include among others (1) compatibility with assay systems/platforms and (2) maintenance of cells in culture. The most widely applicable method is optimizing culture media to improve cardiomyocyte function. Using this approach, functional improvements like increased upstroke velocities and action potential amplitudes, lower (more negative) resting membrane potentials, improved sarcomeric organization, and alterations in cardiac-specific gene expression have been reported [20]. At the other end of the spectrum is long-term culture. Although several studies have shown (small) improvements in cardiac phenotype, the industrial (and practical) applicability of long-term culture is questionable and technologically challenging. One study showed Z- and I-bands in 30-day-old hiPSC-CM, while cardiomyocytes between 30 and 90 days

developed sarcomeres that included Z-, I-, and A-bands, and some cardiomyocytes showed M-bands in 360-day hiPSC-CMs. However, as expected the authors demonstrated considerable variability after long-term culture [21].

The task becomes more challenging when the culture environment has to be changed. Irrespective of whether one is using engineered heart tissue, mechanical stretch and strain systems, flexible substrates, 3D culture, or heterotypic cocultures involving multiple cell types, classical assays like the multielectrode array (MEA) or high-throughput calcium assays are no longer functionally optimal. In the case of multielectrode arrays, it is important to culture pure populations of cardiomyocytes in a monolayer directly on the electrodes, and deviations from this condition render the system less robust. For example, (1) 3D constructs generate both field potentials and far-field potentials, which have a major effect on signal shape, (2) stretch and strain and flexible culture substrates are difficult to combine with rigid electrode material, and (3) heterotypic cultures minimize low-resistance electrical contact between cardiomyocytes and electrodes. Novel technologies are emerging to address these issues.

Finally a general concern is how to deal with the functional maturation of hiPSC-CMs to a state that they no longer spontaneously contract. It is anticipated that the absence of spontaneous electrical activity in these cells in culture could lead to the downregulation of sarcomeric proteins and proteins related to the contractile machinery, which could retard or even reverse cellular maturation in the long term [21]. This dedifferentiation phenomenon has been very well documented for primary isolated cardiomyocytes, which can typically only be used for studies within 24 h [22]. Novel stimulation techniques and optogenetic stimulation techniques will surely play a role in the successful resolution of these issues [23].

Thus, it is anticipated that the biology and technology components should be developed hand in hand to generate the next generation of hiPSC-CM-based in vitro assays. This notion is already embraced in the rapidly developing field of "organ-on-a-chip" field where bioengineers (along with cell biologists) use techniques like microfluidics, pacing and recording electrodes, optical grade material, and automated culture and assay procedures to optimize functional endpoints.

5 Consideration of Different Electrophysiologic Phenotypes in Study Models

Just as there are differences between electrophysiologic phenotypes across different species, so it is now expected that there will be differences in electrophysiologic phenotypes between different hiPSC-CMs. Hortigon-Vinagre et al. [24] recently compared

baseline electrophysiological characteristics of two commercially available hiPSC-CMs using the voltage-sensing dyes. They reported mean action potential durations of 229 and 427 ms obtained in cells cultured in a monolayer when paced at 1 Hz stimulation rate under identical experimental conditions. By way of comparison, APD90 values for undiseased single-cell human endocardial action potentials are approximately 275 ms [25]. Both cardiomyocyte preparations showed a rate dependence analogous to that of adult human cardiac cells (prolonging at slower stimulation rates), and both showed qualitatively similar prolongation to the IKr blocker E-4031 and APD shortening with the calcium channel blocker nifedipine. Studies measuring extracellular field potentials using multielectrode array techniques or contractile force using engineered heart tissue have also shown differences in field potential durations and contraction of different hiPSC-CMs (*see* Chap. 5, Millard et al.). For example, Mannhart et al. used their engineered heart tissue model both under 1 Hz pacing and spontaneous contraction conditions and found up to 50% differences in contraction duration between in-house prepared hiPSC-CMs and two commercially available hiPSC-CMs [26].

Differences in baseline electrophysiological characteristics may modulate (either qualitatively or quantitatively) effects of various ion channel agonists and antagonists, depending on the characteristics and densities of various ionic currents in the myocytes. The extent to which differences in the electrophysiological characteristics will impact the ability to predict clinical responses will depend on the importance of the individual currents in defining the electrogenesis of the action potential as well as the concentration- and time-dependent characteristics of block of the multiple ion currents affected. Published data suggests that hiPSC-CMs can routinely detect block of IKr/hERG (current block carried by the hKv11.1 channel) using various platforms and multiple drugs shown to block this current [27, 28], demonstrating this current plays a prominent role in affecting repolarization of hiPSC-CMs presently used in studies. However, detecting block of fast sodium current may be more difficult [29], due (at least in part) to the reduced resting membrane potential typical of most hiPSC-CMs resulting from a paucity of IK1 [30], the current largely responsible for terminal repolarization, and setting the resting potential of ventricular cells. The partially depolarized resting membrane potential of hiPSC-CMs results in less sodium channels being available for opening (more sodium channel inactivation), thereby reducing the amount of current available for the fast upstroke of the action potential with each beat. Work by multiple groups is ongoing to enhance IK1 in an attempt to modify the electrophysiologic phenotype toward a more mature ventricular myocyte (*see*, e.g., [31]). Nonetheless, the different characteristics

of repolarization obtained with different hiPSC-CM preparations (and experimental methodologies) do not negate the utility of hiPSC-CMs to detect drugs that affect repolarization.

As with all experimental models, differences in characteristics and responses need to be considered within the context of use of the model. For example, it is well known that the electrophysiologic properties of ventricular myocytes differ across different species (as well as translation to man). One often-cited difference is the predominant role which hERG/IKr current plays in ventricular repolarization in human, dog, rabbit, and guinea pig ventricle that is not shared in the rat and mouse ventricle (where the transient outward current (Ito, through the Kv4.3 channel) predominates). Such differences reflect distinctly different requirements of the different species. For example, resting heart rates of dogs and humans are typically near 60–90 beats per minute, while those for rat and mouse are 300 and 600 beats per minute, respectively. These differences can exist due to the fact that different currents restrict action potential duration. Despite such differences, each species has provided valuable information toward understanding cardiac physiology, and appreciating these differences provides the framework to interpret experimental results in the context of human physiology and pharmacology. The same arguments apply to stem cell-derived cardiomyocytes. In the context of drug discovery efforts, one must characterize and understand the strengths and limitations of the preparations under study in order to properly interpret drug responses and their translation (prediction) to humans. This represents a continuing effort with human stem cell-derived cardiomyocytes, as we (in parallel) learn more about cardiac development from hiPSC-CMs.

Much has been written (and is expected) of the utility of hiPSC-CMs derived from diseased individuals. Various authors have commented on the promise of such preparations for efficacy (as well as safety studies) within the context of personalized medicine [32]. For more "simpler" monogenic diseases, the concept is fairly straightforward, with concerns focused more on reproducibility of hiPSC-derived cells. For more complex diseases, it is likely that the multiple factors that contribute to disease will not be fully or adequately reproduced in monocultures of cultured stem cell-derived preparations. Thus, it is likely that one needs to be more careful regarding which aspects of the disease are recapitulated in the more complex 3D engineered tissues that are evolving [33].

6 Approaches to Screening Drug Effects Using hiPSC-CMs: Black Box (Phenotypic) Screening vs. Targeted, Mechanistic Studies

In general, one can distinguish two general categories or approaches for in vitro drug screening assays. We will call the first the "phenotypic approach" and the second the "mechanistic approach."

Traditionally the phenotypic approach is more broadly embraced for early drug discovery projects, whereas targeted mechanistic studies are often more narrowly focused and applied for translational studies (often later during drug discovery/development). These terms also apply to screening campaigns for drug efficacy (e.g., using "diseased myocytes," so-called disease in a dish, as well as screening of "normal myocytes" for drug safety).

The phenotypic screening approach can be compared to the engineer's "black box," in that the cell generates an integrated response by a mechanism (or mechanisms) inherent in a system not fully characterized or understood. In the case of hiPSC-CMs, the integrated response may be electrophysiologic (e.g., delayed repolarization, cellular arrhythmias), contractile (movement, force, duration of contraction), structural (morphological changes), or biochemical, with effects often interrelated. While some functional systems in cells or tissues may be better characterized and understood (e.g., generation of contraction and relaxation), the complete integration of this system in the cell (e.g., understanding modulation by kinases, phosphatases, and other signaling pathway modulators) is likely less well understood. Thus, the phenotypic screening approach actually involves testing both the "black box" response and known (and unknown) actions of compounds under evaluation.

Ideally, the set of test compounds used for phenotypic screening represents a large, broad range of known, well-characterized, and understood "gold standards" reflecting a balanced mixture of (clinically) used drugs with and without known untoward/adverse effects. Using this approach, results from the "black box" are compared to known clinical responses (after consideration of drug exposures) and 2×2 contingency tables constructed defining diagnostic and prognostic performance, including receiver-operator curves as employed in clinical medicine [34]. Generally, if assay performance meets or exceeds that of assays presently available, one would consider replacing earlier assays with the newer assay for safety/toxicity testing. This ideal scenario is often difficult to achieve, as (a) consensus for a test set of "gold standards" is often not available, (b) the number of compounds typically tested is often low (consisting of a few recognized "standards" that fall short of the larger number necessary to provide a useful test of assay performance), (c) tests are often performed unblinded (leading to potential bias), and (d) compound selection is often biased in favor of likely adverse compounds (typically of more interest and worthy of publication). Despite the difficulties and uncertainties of phenotypic screening, it remains highly attractive to use phenotypic screening to test for drug safety and toxicology testing, providing a more global, overall assessment of multiple potential cellular liabilities (many not necessarily the focus of mechanistic studies), and provides potential opportunities for "discovering" novel effects and mechanisms prior to advancing compounds into early clinical studies.

In contrast, a "mechanistic approach" involves a more focused assessment of a drug's effect using a biological process that is (almost) completely understood. In this scenario, one does not need to test a larger number of compounds, as one understands the process and is not testing the "black box" (since it is a well-understood experimental system), but simply testing the drugs on the well-defined system. In the case of hiPSC-CMs as a model for cardiac safety and proarrhythmia, one would need to know that the cells/myocytes reliably express the system(s) responsible for the adverse effects, that the mechanisms are not influenced by other processes, and that an appropriate endpoint is readily and reproducibly measurable. Needless to say, few adverse effects are understood well enough to declare that the "mechanistic approach" represents a complete, stand-alone investigational strategy.

Realistically, it is difficult to rely fully on mechanistic studies as the sole preclinical test regime to predict proarrhythmic safety in humans. The reductionist approach embraced in mechanistic studies can no longer cope with the levels of integration reflected in the enormous amount of information derived from so-called "-omics" sciences and technologies—genomics, proteomics, lipidomics, metabolomics, and so on. Furthermore, even within a single cell, the activity of ion channels is locally modulated by second messengers like cyclic AMP, which is in turn compartmentalized by the function of specific phosphodiesterases [35]. Such details in the levels of complexity are difficult to capture in a single mechanistic assay.

To overcome the issues cited above, scientists are now embracing smart combinations of mechanistic and phenotypic screening approaches. One example is provided by the ongoing Comprehensive In Vitro Proarrhythmia Assay (CiPA) initiative, in which the mechanism of proarrhythmia (torsades de pointes) is well understood on a cellular level and provides the foundation for combined in vitro and in silico approaches to define proarrhythmic risk based on ion channel data [36–38]. Confidence in the CiPA approach is provided by various studies demonstrating that drugs that are known to elicit delayed repolarization and proarrhythmia clinically, also elicit delayed repolarization and arrhythmias on a cellular level with hiPSC-CMs [28, 39–41], coupled with demonstrated electrophysiologic similarities between hiPSC-CMs and native human ventricular myocytes [9, 42] and a firm understanding of the electrophysiologic processes responsible for initiating and perpetuating torsades de pointes. Within CiPA, the use of hiPSC-CMs provides an integrated physiologic (phenotypic) screening system more representative of the human response than those derived from simple ionic current (mechanistic approach) measures (typically limited to the hERG/IKr current) in heterologous expression systems.

7 Future Studies in the "Proclinical Space"

As with all new models, their use and adoption depend on adequate characterization and demonstration of utility for the questions being addressed. hiPSC-CMs are in the midst of such testing. This is occurring with more "established" preparations (such as 2D monolayers) as well as novel preparations (such as cocultures and 3D constructs). Characterization of these different cell preparations on different assay platforms and their "fit-for-purpose" evaluations will provide a better understanding of the strengths and limitations of the available combinations of cell preparations and platforms. For some uses a more immature phenotype may be sufficient (or possibly beneficial), while others will require more mature electrophysiologic, structural, or metabolic phenotype.

Traditionally, drug discovery/development efforts have been generally categorized as either preclinical or clinical. Preclinical studies typically employ either in vivo animal studies (and more integrated responses) or in vitro preparations (typically, less integrated responses derived from different levels of system integration ranging from organ to subcellular) with animal-derived preparations. In contrast, clinical studies involve human subjects (or patients) with a focus on meaningful clinical endpoints (or alternatively surrogate markers/biomarkers for longer-term responses). Due to physiologic and pharmacologic differences across species or imperfect disease models, preclinical study results are often questioned in regard to their ability to translate to human responses.

The advent of hiPSC-CM-based in vitro assays is promoting a paradigm shift for drug discovery and development. We shall use the term "proclinical space" to define this new experimental arena. Within this space, proclinical studies bridge the traditional preclinical findings with clinical responses by utilizing human-derived preparations in nonclinical studies positioned earlier in the drug discovery process. The promise (and benefits) of proclinical studies is simply that one can test for human responses (representing clinical responses) with human-derived preparations in vitro without placing human subjects and patients at risk and without requiring valuable "ex vivo" human preparations difficult (or impossible) to procure. Examples of proclinical studies ongoing today include (1) the use of human hepatocytes for early drug metabolism studies and (2) identification of retigabine as a novel therapeutic strategy to correct hyperexcitability in iPSC-derived ALS neurons carrying a superoxide dismutase 1 (*SOD1*) mutation [43]. Other examples are screening studies for cystic fibrosis drug efficacy using human bronchial epithelial cell lines [44], three-dimensional bronchospheres derived from primary human airway basal cells [45], and rectal organoids [46]. Such studies represent the vanguard of future studies involving hiPSC preparations. Experiments may

involve "normal" or "diseased" cells, the later providing for investigations related to "personalized medicine" initiatives. Indeed, patient-specific hiPSC-CMs represent a promising experimental preparation to model cardiovascular disease in vitro and specific pharmacologic therapies and toxicities [47, 48].

It is likely that future proclinical studies will use stem cell-derived tissues (and organs) to characterize more integrated responses. The use of gene-editing techniques (such as CRISPR-Cas9), as well as cell and tissue engineering [49], will undoubtedly play a role in such studies. The well-publicized "organ-on-a-chip" initiatives represent one future aspect of proclinical studies. Proclinical studies will not eliminate preclinical studies any time soon, due to the wealth of knowledge available regarding animal physiology and uncertainties regarding the ability of human stem cell-derived preparations to recapitulate human responses expected based on ex vivo or in vivo studies. However, proclinical studies will first compliment preclinical studies and eventually replace many in vitro and in vivo preclinical studies as preparations evolve and "fit-for-purpose" applications are better defined.

The challenges for the successful application of human stem cell-derived preparations in proclinical studies are great and will require continuous testing and reevaluation as the field progresses. However, the vision for proclinical studies can already be seen on the horizon, and the use of human stem cell-derived cardiomyocytes will pave the way for such future efforts.

References

1. Thomson JA, Itskovitz-Eldor J, Shapiro SS, Waknitz MA, Swiergiel JJ, Marshall VS, Jones JM (1998) Embryonic stem cell lines derived from human blastocysts. Science 282(5391):1145–1147. Erratum in: Science 1998 Dec 4;282(5395):1827
2. Takahashi K, Yamanaka S (2006) Induction of pluripotent stem cells from mouse embryonic and adult fibroblast cultures by defined factors. Cell 126:663–676
3. Shinnawi R, Gepstein L (2014) iPCS cell modeling of inherited cardiac arrhythmias. Curr Treat Options Cardiovasc Med 16(9):331. doi:10.1007/s11936-014-0331-4
4. Mak TW (2007) Gene targeting in embryonic stem cells scores a knockout in Stockholm. Cell 131:1027–1031
5. Rosenblueth A, Wiener N, Rosenblueth A, Wiener N (1945) The role of models in science. Philos Sci 12:316–321
6. Avior Y, Sagi I, Benvenisty N (2016) Pluripotent stem cells in disease modelling and drug discovery. Nat Rev Mol Cell Biol 17(3):170–182. doi:10.1038/nrm.2015.27
7. Davis RP, van den Berg CW, Casini S, Braam SR, Mummery CL (2011) Pluripotent stem cell models of cardiac disease and their implication for drug discovery and development. Trends Mol Med 17(9):475–484. doi:10.1016/j.molmed.2011.05.001
8. Pouton C, Haynes J (2007) Embryonic stem cells as a source of models for drug discovery. Nat Rev Drug Discov 6:605–616
9. Ma J, Guo L, Fiene SJ, Anson BD, Thomson JA, Kamp TJ, Kolaja KL, Swanson BJ, January CT (2011) High purity human-induced pluripotent stem cell-derived cardiomyocytes: electrophysiological properties of action potentials and ionic currents. Am J Physiol Heart Circ Physiol 301(5):H2006–H2017. doi:10.1152/ajpheart.00694.2011
10. Uesugi M, Ojima A, Taniguchi T, Miyamoto N, Sawada K (2014) Low-density plating is sufficient to induce cardiac hypertrophy and electrical remodeling in highly purified human iPS cell-derived cardiomyocytes. J Pharmacol Toxicol Methods 69(2):177–188. doi:10.1016/j.vascn.2013.11.002

11. Beauchamp P, Moritz W, Kelm JM, Ullrich ND, Agarkova I, Anson BD, Suter TM, Zuppinger C (2015) Development and characterization of a scaffold-free 3D spheroid model of induced pluripotent stem cell-derived human cardiomyocytes. Tissue Eng Part C Methods 21(8):852–861. doi:10.1089/ten.TEC.2014.0376
12. Boudreau-Béland J, Duverger JE, Petitjean E, Maguy A, Ledoux J, Comtois P (2015) Spatiotemporal stability of neonatal rat cardiomyocyte monolayers spontaneous activity is dependent on the culture substrate. PLoS One 10(6), e0127977. doi:10.1371/journal.pone.0127977
13. Pasqualini FS, Sheehy SP, Agarwal A, Aratyn-Schaus Y, Parker KK (2015) Structural phenotyping of stem cell-derived cardiomyocytes. Stem Cell Rep 4(3):340–347. doi:10.1016/j.stemcr.2015.01.020, Epub 2015 Feb 26
14. Nirmalanandhan VS, Sittampalam GS (2009) Stem cells in drug discovery, tissue engineering, and regenerative medicine: emerging opportunities and challenges. J Biomol Screen 14:755–768
15. Liu J, Laksman Z, Backx PH (2016) The electrophysiological development of cardiomyocytes. Adv Drug Deliv Rev 96:253–273
16. Turnbull IC, Karakikes I, Serrao GW, Backeris P, Lee JJ, Xie C, Senyei G, Gordon RE, Li RA, Akar FG, Hajjar RJ, Hulot JS, Costa KD (2014) Advancing functional engineered cardiac tissues toward a preclinical model of human myocardium. FASEB J 28(2):644–654. doi:10.1096/fj.13-228007
17. van den Berg CW, Okawa S, Chuva de Sousa Lopes SM, van Iperen L, Passier R, Braam SR, Tertoolen LG, del Sol A, Davis RP, Mummery CL (2015) Transcriptome of human foetal heart compared with cardiomyocytes from pluripotent stem cells. Development 142(18):3231–3238. doi:10.1242/dev.123810
18. van den Heuvel NH, van Veen TA, Lim B, Jonsson MK (2014) Lessons from the heart: mirroring electrophysiological characteristics during cardiac development to in vitro differentiation of stem cell derived cardiomyocytes. J Mol Cell Cardiol 67:12–25. doi:10.1016/j.yjmcc.2013.12.011
19. Veerman CC, Kosmidis G, Mummery CL, Casini S, Verkerk AO, Bellin M (2015) Immaturity of human stem-cell-derived cardiomyocytes in culture: fatal flaw or soluble problem? Stem Cells Dev 24(9):1035–1052. doi:10.1089/scd.2014.0533
20. Ribeiro MC, Tertoolen LG, Guadix JA, Bellin M, Kosmidis G, D'Aniello C, Monshouwer-Kloots J, Goumans MJ, Wang YL, Feinberg AW, Mummery CL, Passier R (2015) Functional maturation of human pluripotent stem cell derived cardiomyocytes in vitro—correlation between contraction force and electrophysiology. Biomaterials 51:138–150. doi:10.1016/j.biomaterials.2015.01.067, Epub 2015 Feb 18
21. Kamakura T, Makiyama T, Sasaki K, Yoshida Y, Wuriyanghai Y, Chen J, Hattori T, Ohno S, Kita T et al (2013) Ultrastructural maturation of human-induced pluripotent stem cell-derived cardiomyocytes in a long-term culture. Circ J 77:1307–1314
22. Volz A, Piper HM, Siegmund B, Schwartz P (1991) Longevity of adult ventricular rat heart muscle cells in serum-free primary culture. J Mol Cell Cardiol 23(2):161–173
23. Zhuge Y, Patlolla B, Ramakrishnan C, Beygui RE, Zarins CK, Deisseroth K, Kuhl E, Abilez OJ (2014) Human pluripotent stem cell tools for cardiac optogenetics. Conf Proc IEEE Eng Med Biol Soc 2014:6171–6174. doi:10.1109/EMBC.2014.6945038
24. Hortigon-Vinagre MP, Zamora V, Burton FL, Craig MA, Green J, Gintant GA, Smith GL. The use of ratiometric fluorescence measurements of the voltage sensitive dye di-4-ANEPPS to examine action potential characteristics and drug effects on human induced pluripotent stem cell-derived cardiomyocytes. Toxicol Sci 2016: [Epub ahead of print]. doi:10.1093/toxsci/kfw171
25. O'Hara T, Virág L, Varró A, Rudy Y (2011) Simulation of the undiseased human cardiac ventricular action potential: model formulation and experimental validation. PLoS Comput Biol 7(5), e1002061. doi:10.1371/journal.pcbi.1002061
26. Mannhardt I, Breckwoldt K, Letuffe-Brenière D, Schaaf S, Schulz H, Neuber C, Benzin A, Werner T, Eder A, Schulze T, Klampe B, Christ T, Hirt MN, Huebner N, Moretti A, Eschenhagen T, Hansen A (2016) Human engineered heart tissue: analysis of contractile force. Stem Cell Rep pii:S2213-6711(16)30036-4. doi:10.1016/j.stemcr.2016.04.011
27. Asakura K, Hayashi S, Ojima A, Taniguchi T, Miyamoto N, Nakamori C, Nagasawa C, Kitamura T, Osada T, Honda Y, Kasai C, Ando H, Kanda Y, Sekino Y, Sawada K (2015) Improvement of acquisition and analysis methods in multi-electrode array experiments with iPS cell-derived cardiomyocytes. J Pharmacol Toxicol Methods 75:17–26. doi:10.1016/j.vascn.2015.04.002
28. Braam SR, Tertoolen L, Casini S, Matsa E, Lu HR, Teisman A, Passier R, Denning C, Gallacher DJ, Towart R, Mummery CL (2013) Repolarization reserve determines drug responses in human pluripotent stem

cell derived cardiomyocytes. Stem Cell Res 10(1):48–56. doi:10.1016/j.scr.2012.08.007

29. Qu Y, Gao B, Fang M, Vargas HM (2013) Human embryonic stem cell derived cardiac myocytes detect hERG-mediated repolarization effects, but not Nav1.5 induced depolarization delay. J Pharmacol Toxicol Methods 68(1):74–81. doi:10.1016/j.vascn.2013.03.001
30. Satin J, Kehat I, Caspi O, Huber I, Arbel G, Itzhaki I, Magyar J, Schroder EA, Perlman I, Gepstein L (2004) Mechanism of spontaneous excitability in human embryonic stem cell derived cardiomyocytes. J Physiol 559(Pt 2):479–496
31. Vaidyanathan R, Markandeya YS, Kamp TJ, Makielski JC, January CT, Eckhardt LL (2016) IK1-enhanced human-induced pluripotent stem cell-derived cardiomyocytes: an improved cardiomyocyte model to investigate inherited arrhythmia syndromes. Am J Physiol Heart Circ Physiol 310(11):H1611–H1621. doi:10.1152/ajpheart.00481.2015
32. Bellin M, Marchetto MC, Gage FH, Mummery CL (2012) Induced pluripotent stem cells: the new patient? Nat Rev Mol Cell Biol 13(11):713–726. doi:10.1038/nrm3448
33. Benam KH, Dauth S, Hassell B, Herland A, Jain A, Jang KJ, Karalis K, Kim HJ, MacQueen L, Mahmoodian R, Musah S, Torisawa YS, van der Meer AD, Villenave R, Yadid M, Parker KK, Ingber DE (2015) Engineered in vitro disease models. Annu Rev Pathol 10:195–262. doi:10.1146/annurev-pathol-012414-040418
34. Zweig MH, Campbell G (1993) Receiver-operating characteristic (ROC) plots: a fundamental evaluation tool in clinical medicine. Clin Chem 39(4):561–577
35. Perera RK, Nikolaev VO (2013) Compartmentation of cAMP signalling in cardiomyocytes in health and disease. Acta Physiol (Oxf) 207(4):650–662. doi:10.1111/apha.12077
36. Fermini B, Hancox JC, Abi-Gerges N, Bridgland-Taylor M, Chaudhary KW, Colatsky T, Correll K, Crumb W, Damiano B, Erdemli G, Gintant G, Imredy J, Koerner J, Kramer J, Levesque P, Li Z, Lindqvist A, Obejero-Paz CA, Rampe D, Sawada K, Strauss DG, Vandenberg JI (2016) A new perspective in the field of cardiac safety testing through the comprehensive in vitro proarrhythmia assay paradigm. J Biomol Screen 21(1):1–11
37. Gintant G, Sager PT, Stockbridge N (2016) Evolution of strategies to improve preclinical cardiac safety testing. Nat Rev Drug Discov. doi:10.1038/nrd.2015.34
38. Sager PT, Gintant G, Turner JR, Pettit S, Stockbridge N (2014) Rechanneling the cardiac proarrhythmia safety paradigm: a meeting report from the Cardiac Safety Research Consortium. Am Heart J 167(3):292–300. doi:10.1016/j.ahj.2013.11.004
39. Harris K, Aylott M, Cui Y, Louttit JB, McMahon NC, Sridhar A (2013) Comparison of electrophysiological data from human-induced pluripotent stem cell-derived cardiomyocytes to functional preclinical safety assays. Toxicol Sci 134(2):412–426. doi:10.1093/toxsci/kft113
40. Rajamohan D, Matsa E, Kalra S, Crutchley J, Patel A, George V, Denning C (2013) Current status of drug screening and disease modelling in human pluripotent stem cells. Bioessays 35(3):281–298. doi:10.1002/bies.201200053
41. Rajamohan D, Kalra S, Duc Hoang M, George V, Staniforth A, Russell H, Yang X, Denning C (2016) Automated electrophysiological and pharmacological evaluation of human pluripotent stem cell-derived cardiomyocytes. Stem Cells Dev 25(6):439–452. doi:10.1089/scd.2015.0253
42. Honda M, Kiyokawa J, Tabo M, Inoue T (2011) Electrophysiological characterization of cardiomyocytes derived from human induced pluripotent stem cells. J Pharmacol Sci 117(3):149–159
43. Wainger BJ, Kiskinis E, Mellin C, Wiskow O, Han SS, Sandoe J, Perez NP, Williams LA, Lee S, Boulting G, Berry JD, Brown RH Jr, Cudkowicz ME, Bean BP, Eggan K, Woolf CJ (2014) Intrinsic membrane hyperexcitability of amyotrophic lateral sclerosis patient-derived motor neurons. Cell Rep 7(1):1–11. doi:10.1016/j.celrep.2014.03.019
44. Gottschalk LB, Vecchio-Pagan B, Sharma N, Han ST, Franca A, Wohler ES, Batista DA, Goff LA, Cutting GR (2016) Creation and characterization of an airway epithelial cell line for stable expression of CFTR variants. J Cyst Fibros 15(3):285–294. doi:10.1016/j.jcf.2015.11.010
45. Hild M, Jaffe AB (2016) Production of 3-D airway organoids from primary human airway basal cells and their use in high-throughput screening. Curr Protoc Stem Cell Biol 37:IE.9.1–IE.9.15. doi:10.1002/cpsc.1
46. Dekkers JF, Berkers G, Kruisselbrink E, Vonk A, de Jonge HR, Janssens HM, Bronsveld I, van de Graaf EA, Nieuwenhuis EE, Houwen RH, Vleggaar FP, Escher JC, de Rijke YB, Majoor CJ, Heijerman HG, de

Winter-de Groot KM, Clevers H, van der Ent CK, Beekman JM (2016) Characterizing responses to CFTR-modulating drugs using rectal organoids derived from subjects with cystic fibrosis. Sci Transl Med 8(344):344ra84. doi:10.1126/scitranslmed.aad8278

47. Burridge PW, Li YF, Matsa E, Wu H, Ong SG, Sharma A, Holmström A, Chang AC, Coronado MJ, Ebert AD, Knowles JW, Telli ML, Witteles RM, Blau HM, Bernstein D, Altman RB, Wu JC (2016) Human induced pluripotent stem cell-derived cardiomyocytes recapitulate the predilection of breast cancer patients to doxorubicin-induced cardiotoxicity. Nat Med 22(5):547–556. doi:10.1038/nm.4087
48. Karakikes I, Ameen M, Termglinchan V, Wu JC (2015) Human induced pluripotent stem cell-derived cardiomyocytes: insights into molecular, cellular, and functional phenotypes. Circ Res 117(1):80–88. doi:10.1161/CIRCRESAHA.117.305365
49. Feric NT, Radisic M (2016) Maturing human pluripotent stem cell-derived cardiomyocytes in human engineered cardiac tissues. Adv Drug Deliv Rev 96:110–134. doi:10.1016/j.addr.2015.04.019

Chapter 2

Human Pluripotent Stem Cell Test for Assessing the Potential Teratogen Risk

Sei Kameoka and Eric Chiao

Abstract

In order to reduce the reliance on animal studies, both the pharmaceutical and chemical industries have been investigating new human cell-based in vitro assays capable of predicting a chemical's potential harm to humans. Here we describe a human pluripotent stem cell test (hPST) capable of identifying compounds that pose teratogenic risk to humans such as thalidomide. Given the complexity of human development and the broad spectrum of compounds correctly classified based on their known in vivo teratogenic risk, the hPST is a remarkably simple assay. Following 3 days of directing the differentiation of a monolayer of human pluripotent stem cells toward the mesendoderm fate, the nuclear localization of a single transcription factor, SOX17, is quantitated. The reduction of SOX17 in the presence of test compounds is used to stratify the compounds' teratogenic risk. However, as is the case with many human pluripotent stem cell experimental systems, careful optimization of the differentiation conditions is required in order to obtain reproducible results. Therefore, in addition to outlining the methodology of the hPST, we describe in detail various techniques we have used to optimize the assay.

Key words Teratogen, Embryotoxicity, Developmental toxicity, Human pluripotent stem cell

1 Introduction

Teratogens disturb the normal development of the embryo or fetus. Assessing the risk of drug- or chemical-induced teratogenicity in animals is both costly and imperfect [1–4]. In the 1970s, an unrecognized teratogen, thalidomide, was given to pregnant women as a treatment for morning sickness. Although thalidomide had been tested in pregnant rodent models and failed to exhibit teratogenic risk, in humans it proved to cause debilitating birth defects [5, 6]. In recent years, several in vitro methods for assessing compound- and chemical-driven teratogenic risk have been developed [7–19]. One widely used model uses mouse embryonic stem cells differentiated toward the cardiac lineage, the mouse embryonic stem cell test (mEST) [20]. Disruption of the number of beating cardiomyocytes

Mike Clements and Liz Roquemore (eds.), *Stem Cell-Derived Models in Toxicology*, Methods in Pharmacology and Toxicology,
DOI 10.1007/978-1-4939-6661-5_2,

is used as a marker of teratogenicity. In 2013, our group sought to refine this method with the goal of developing a higher-throughput, more quantitative assay using human embryonic stem cells that would ideally be capable of detecting human teratogens such as thalidomide that may be missed by rodent models [21].

The human pluripotent stem cell test, hPST, is a 3-day monolayer differentiation of human pluripotent stem cells toward the mesendoderm lineage. The degree of disruption of the germ layer specification, as judged by cell loss and loss of nuclear protein localization of the transcription factor SOX17, is compared to the effects seen at similar concentrations with known teratogens, thereby extrapolating the risk of an unknown compound's potential teratogenicity.

Conceptually, two primary hypotheses guided our assay development. The first hypothesis was that if we could examine the specification of pluripotent stem cells into the three primary germ layers, endoderm, ectoderm, and mesoderm, we would capture more teratogenic compounds than a single lineage differentiation protocol such as the cardiomyocyte differentiation used in the mEST. Much to our surprise, at least based on our training set of 70 compounds, a single differentiation protocol toward the mesendoderm lineage was able to provide sufficient predictive value.

The second hypothesis was that maximal sensitivity could be achieved if we were able to quantify the protein expression of key developmental regulators at the very onset of lineage specification—the stage where approximately half of the cells express the pluripotency markers such as Oct4 and NANOG and the other half express the mesendoderm markers SOX17 and EOMES. The theory was that, at this stage, multiple developmentally important pathways would be active, and increases or decreases in expression of the regulators may be easier to detect at this stage compared to later when lineage specification had already occurred and expression of signaling pathways may be more restricted. While not formally proven, we believe that this conjecture is key to the assay performance. In our hands, we have found that assay performance is suitable as long as around 30–60% of the cells express SOX17, but we observed reduced sensitivity when we tested compounds at a stage where 80–100% of the cells in the well expressed the mesendoderm markers at the conclusion of the differentiation. Unfortunately, determining the conditions where all wells in the plate exhibit 50% expression of the lineage marker is perhaps the most difficult aspect of the assay. Conditions for achieving this can vary between individual human pluripotent stem cell lines. Nevertheless, by carefully optimizing seeding densities and growth factor concentrations, we have been able to reproduce the assay with multiple human ES cell lines and a human iPSC line.

2 Materials

2.1 Reagents for Pluripotent Stem Cell Culture

1. mTESR1 (05850, STEMCELL Technologies). Store the 5× supplement in −80 °C. Once the supplement is mixed with media, store it at 4 °C and use it within 7 days. Do not warm the entire bottle in the 37 °C water bath. Warm only the amount of media needed each day.
2. hESC-qualified Matrigel Matrix, LDEV-Free (354277, BD Biosciences). Matrigel should be stored at −80 °C and thawed on ice overnight in 4 °C refrigerator before use.
3. PBS without calcium and magnesium (10010-023, Thermo Fisher).
4. 100 mm dishes. Polystyrene, clear, sterile, and tissue culture-treated surface. We used Corning 430167, but a similar product from different company should work.
5. Accutase cell detachment solution (07920, STEMCELL Technologies).
6. Falcon disposable polystyrene serological pipettes (5, 10, 25 ml) (13-668-2, 13-675-20, 13-675-22, Thermo Fisher). Individually wrapped.
7. Y-27632 dihydrochloride (1254, Tocris). Dissolve it to 10 mM for 2000× stock solution in DMSO or PBS. It should be aliquoted into multiple tubes and stored at −20 °C for up to 3 years.

2.2 Reagents for Mesendoderm Differentiation

1. TC-coated, polystyrene, black, clear flat bottom 96-well plates. We have used Corning (3603) and BD Falcon (353948, 353219) plates successfully.
2. Advanced RPMI Medium 1640, no glutamine (12633-012, Thermo Fisher). Store at 4 °C. Once glutamine is added, use it within 3 months.
3. Recombinant human/mouse/rat activin A (338-AC-005, R&D Systems). Aliquot at 40 μg/ml and store at −80 °C. Avoid multiple freeze-thaw cycles to minimize protein degradation.
4. Recombinant human Wnt-3a (5036-WN-010, R&D Systems). Aliquot at 40 μg/ml and store at −80 °C. Avoid multiple freeze-thaw cycles to minimize protein degradation.
5. Fetal bovine serum (FBS) (ES009B, ES cell qualified, Millipore). FBS should be aliquoted into smaller volumes and stored at −80 °C. The same lot should be used for all studies for consistency.
6. L-Glutamine, 200 mM (25030–081, Thermo Fisher). Store at −20 °C. Once it is thawed, store at 4 °C and use it within 3 months.
7. SB 431542 hydrate (S4317, Sigma).

8. Thalidomide (T144-100MG, Sigma).
9. Imatinib mesylate (SML1027, Sigma).
10. All-trans retinoic acid (554720, Calbiochem).

2.3 Reagents for Immunofluorescence Staining

1. Human SOX17 NorthernLights NL557-conjugated Antibody, Goat IgG, polyclonal (NL1924R, R&D Systems). Store at 4 °C. We tested six different SOX17 antibodies from different sources; this antibody was most specific and showed highest signal-to-noise ratio. Dilute 1:20 in blocking solution right before use. We occasionally found small precipitated particles which resulted in strong background. To prevent this, make sure to filter antibody with 0.22 μm syringe filter (SLGP033RB, Millipore).
2. Human Brachyury NorthernLights NL557-conjugated Antibody, Goat IgG, polyclonal (NL2085R, R&D Systems).
3. Human SOX2 NorthernLights NL493-conjugated Antibody, Goat IgG, polyclonal (NL20181G, R&D Systems). Brachyury and SOX2 antibodies are only used for supplementary experiment to optimize the hPST for new cell lines.
4. Formaldehyde solution, 16%, 10×10 ml ampule (28908, Thermo Fisher). Store at room temperature (RT). Open ampule on the day of experiment.
5. 30% albumin solution from bovine serum (A9576-50ML, Sigma). Store at 4 °C.
6. Donkey serum (S30-100ML, Millipore). Store at −20 °C.
7. Sheep serum (S22-100ML, Millipore). Store at −20 °C.
8. Image-iT FX Signal Enhancer (I36933, Thermo Fisher). Store at 4 °C.
9. Triton X-100, Sigma (T8787, Sigma). Store at RT.
10. SlowFade Gold antifade reagent with DAPI (S36938, Thermo Fisher). Store at 4 °C.
11. DPBS with calcium and magnesium (14040-133, Thermo Fisher). Store at RT.

2.4 Blocking Solution for Immunostaining

Mix the following reagents and store at 4 °C up to 3 days.

1. DPBS.
2. 10% donkey serum.
3. 2% sheep serum.
4. 0.2% Triton X-100.
5. 1% BSA.

2.5 Mesendoderm Differentiation Medium I

Make fresh media on the day of experiment. Final concentrations are shown below:

1. Advanced RPMI Medium 1640.

2. 2 mM L-glutamine.
3. 80 ng/ml human activin A.
4. 20 ng/ml human Wnt-3a.
5. 80 units/ml (0.08 mg/ml) penicillin-streptomycin (P0781, Sigma).

2.6 Mesendoderm Differentiation Medium II

1. Advanced RPMI Medium 1640.
2. 2 mM l-glutamine.
3. 80 ng/ml human activin A.
4. 0.1% FBS.
5. 80 units/ml (0.08 mg/ml) penicillin-streptomycin (P0781, Sigma).

3 Methods

3.1 General Technical Guidelines

1. Routine stem cell culture
   Pluripotent stem cells were maintained in mTESR1 media on Matrigel-coated 100 mm plates. Passaging was performed by nonenzymatic dissociation with 2 mM EDTA in PBS. Antibiotics (penicillin, streptomycin) or antifungal reagents were not used during pluripotent stem cell maintenance. We primarily used the human ES cell line H9 (from WiCell) for our studies.
2. Mycoplasma
   Absence of mycoplasma contamination was regularly confirmed using the MycoAlert Detection Kit (LT07-118, Lonza).
3. Karyotype analysis
   Karyotype analysis should be performed around every 10–20 passages of pluripotent stem cell culture. For most experiments, only cells between passages 20 and 40 were used. An abnormal karyotype can affect proliferation rate and mesendoderm differentiation efficiency.
4. Cell culture
   All cell culture procedures were performed at 37 °C, 5% CO_2. It is recommended that one use a CO_2 incubator capable of on-demand, high-temperature decontamination cycle (e.g., Forma Steri-Cycle CO_2 incubator, 201370, Thermo Fisher). All manipulations of cells were performed inside a Class II biosafety cabinet using standard sterile technique.
5. Pipetting
   Pipetting for 96-well plates should be performed with 12-channel electronic pipettes. We use E4 Multi Pipette Multi E12-200XLS+ (17013800, Thermo Fisher). In general, reverse pipetting is recommended to increase the accuracy. Use pipette tips with filters, as it is difficult to sterilize inside the pipette

and it becomes an easy source of contamination. An automated liquid handler can be used for the hPST assay except when performing serial dilutions with DMSO, as low surface tension of DMSO makes the handling of liquid significantly inaccurate due to the adhesion of solution to the pipette tips.

6. Adapting pluripotent stem cells to mTESR1 on Matrigel
   If the stem cell line was maintained on feeder fibroblast cells in media other than mTESR1, it is recommended that the line be adapted to feeder-free conditions with mTESR1 media for several passages prior to beginning the differentiation protocol.

   When pluripotent stem cell colonies are sufficiently large on feeder cells, scrape the small pieces off and transfer to a Matrigel-coated dish with media composed of 20% mTESR1, 80% old media, and 10 μM Y-27632.

   Next day (Day 2), change media to 40% mTESR1 and 60% old media without Y-27632.

   On Day 3, change media to 60% mTESR1 and 40% old media.

   On Day 4, change media to 80% mTESR1 and 20% old media.

   On Day 5, change media to 100% mTESR1.

   When cells reach about 80% confluence, wash with PBS once; incubate cells in 5 ml of dissociation buffer (2 mM EDTA in PBS) for 3 min at room temperature. Aspirate dissociation buffer and add mTESR1 media. Manually dissect uniform pluripotent regions from the colonies using either a sterile pipette tip, sterile scalpel or pulled glass Pasteur pipette. Transfer small pieces to a new Matrigel-coated plate, and culture with mTESR1 with 5 μM Y-27632. Y-27632 is only required for cell attachment, not subsequent feedings.

   Repeat this dissociation process for an additional two passages.

7. Preparation of cell bank
   To prevent batch-to-batch effects across differentiations, large banks of pluripotent stem cells should be generated. We usually make a bank from 8×100 mm dishes of pluripotent stem cell (approximately 80 million cells), dissociated with 2 mM EDTA in PBS, suspended in mFreSR (05854, STEMCELL Technologies) , and dispensed at a concentration of 1.5 million cells per tube in a total of 50 tubes. These can be stored in liquid nitrogen indefinitely.

8. Preparation of stock solution of compounds
   All hydrophobic and hydrophilic small chemical compounds should be dissolved in DMSO and PBS, respectively, and stored as stock solutions in amber glass bottles or 1.5 ml polypropylene tubes at −20 °C for up to 2 years. If the compound is known to be unstable in these forms, it should be kept as a lyophilized form. Repeated freeze-thaw should be avoided. If cLogP data is available, compounds with cLogP larger than 5

should not be used due to potential solubility problems in the aqueous media across the full dose-range study. Concentration of stock solution should be 20 mM. After dissolving a compound in DMSO or PBS, it should be sonicated for 5–30 min at 30–37 °C, until compound is dissolved completely. We use Branson Ultrasonics Bransonic MH Series Ultrasonic Baths 1800 (15-336-110, Thermo Fisher), but any alternative sonicator should work. The standard dose range we used for the hPST assay encompassed six doses with 1:2 dilution (100, 50, 25, 12.5, 6.3, and 3.1 μM).

3.2 Standard Protocol

We delineate the day that we switch from mTESR to "Differentiation Medium I" with test compound as Day 0 of differentiation. At Day 0, the cells should be at the predetermined optimal density (see the Notes section below for optimization tips) that results in approximately 50% SOX17-positive cells at the end of the experiment. For our stocks of the H9 human ES cell line, the optimal starting density at Day 0 was approximately 30–60% confluency. For the standard protocol outlined in Fig. 1, we initiate the differentiation 48 h after plating and growing the pluripotent stem cells in the 96-well dish.

3.2.1 Day 2: Plate Pluripotent Stem Cells on 96-Well Plates

1. Preparation of Matrigel-coated 96-well plates.

Thawing

Thaw hESC-qualified Matrigel on ice inside the refrigerator overnight. After thawing, swirl the bottle and make sure the liquid solution does not contain any solid granules or precipitation.

Dilution of Matrigel

Add prechilled 300 ml PBS to a prechilled 500 ml storage bottle (we use 455-0500, Thermo Fisher). Add 5 ml Matrigel to this (1:60 dilution) and gently swirl the bottle until the Matrigel is uniformly dissolved.

Transfer to 96-well plate

Dispense 70 μl Matrigel per well on all wells of black/clear 96 plate using a 12-channel electronic pipette. Make sure to perform this process quickly, as Matrigel solidifies at room temperature.

Matrigel solidification

Incubate plates at 37 °C in CO_2 incubator for 60–90 min. Do not incubate too long, as the coated surface may become too thick and could inhibit optimal cell attachment.

Washing

Discard the Matrigel by flipping the plate to eject the Matrigel solution into a waste container. Dispense 100 μl of PBS into each well. Be careful not to pipette directly on the surface, as

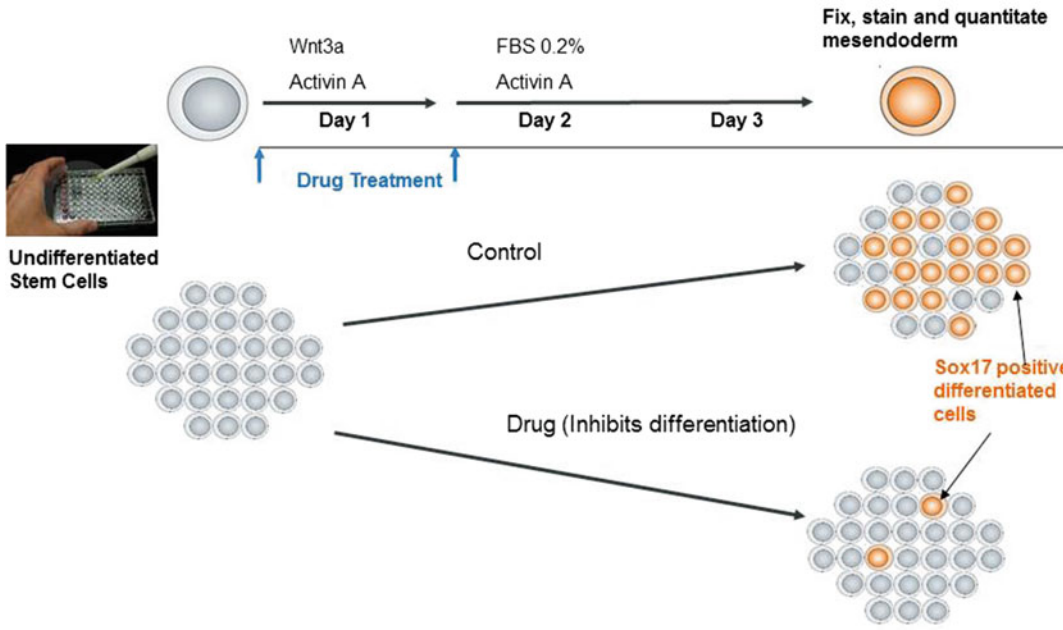

Fig. 1 Differentiation protocol in a 96-well plate

Matrigel forms a very fragile coat on the surface which can be disrupted easily by pipetting. Shake the plate at 650 rpm for 2 min. Discard PBS again by flipping the plate.

Storage

The Matrigel-coated 96-well plates can be prepared up to 5 days prior to plating the PSCs. If prepared ahead of time, dispense 100 μl of PBS per well, replace the lid, and store plates at 4 °C.

2. Seed pluripotent stem cells onto Matrigel-coated 96-well dishes

Our standard method requires approximately 3 × 100 mm pluripotent stem cell plates to test three drugs in duplicate wells in duplicate plates.

Dissociate cells

When pluripotent stem cells in 100 mm plate become about 60–70% confluent, remove media, rinse with PBS once, and then add 3 ml of Accutase per 100 mm plate. Cells should detach within 3–5 min. Immediately add 17 ml mTESR1 with 5 μM Y-27632 to stop the reaction, transfer it to a 50 ml tube, and centrifuge at 400 × g for 5 min.

Count cells

Remove supernatant. Add 10 ml mTESR1 with 5 μM Y-27632. Pipette up and down gently to suspend cell pellet. Perform cell

counting and check cell viability. This can be done by automated machine such as Vi-CELL cell counter or manual counting with Trypan Blue method using a hemocytometer (we use INCYTO C-Chip DHC-N01). Note that it is not unusual for cell numbers obtained by two methods to differ significantly (>50%).

Dilute cells

To obtain uniform conditions for the assay, one must first optimize the plating cell density for each cell line, since the doubling times of individual cell lines may vary. The optimal seeding density is empirically determined by finding the density that results in 30–70% SOX17+ cells at the end of the differentiation (*see* Sect. 4.1). In our hands with the H9 hESC line, the ideal plating density resulted in 40–50% confluence 48 h after plating. Dilute the optimized cell number per well so that 100 μl of media contain the appropriate number of cells and plate the cells as described below.

Plate cells

Bring the Matrigel-coated 96-well plates prepared in the previous section from 4 °C to room temperature. Pipette up and down to resuspend the cell mixture. Swirl 50 ml tubes gently and transfer cells to 50 ml reagent reservoirs (individually wrapped, 2321–2530, USA Scientific) using a 30 μm strainer (SmartStrainer, 130-098-458, Miltenyi) to remove potential cell clumps. It is preferable to use a 50 ml tube instead of a 15 ml tube, as cell mixing can be done more gently by swirling. Set the multichannel electronic pipette to 8 × 100 μl multi-dispense mode and dispense 100 μl of cells to eight rows. Make sure that all 12 pipette tips dispensed equal volume of media at same rate, as air leakage due to loose contact between pipette and pipette tips may cause uneven pipetting.

Incubate the plate at 37 °C in CO_2 incubator for 24 h. If necessary place four water-filled trays surrounding the plates to further reduce evaporation-mediated edge effects.

3.2.2 Day 1: Change Media

1. Change mTESR media
   Twenty-four hours after seeding, observe the plate under a phase-contrast microscope and record the confluency. Discard media by flipping the plate quickly and pressing it on a kimwipe gently to remove liquid from the top of the plate. Add 100 μl mTESR1 media without Y27632 per well to the side wall of 96-well plate.

3.2.3 Day 0: Initiation of Differentiation and First Compound Treatment

1. Preparation of compounds

   A typical plate map layout is shown in Fig. 2. Rows A and H are not used as they are most affected by edge effects. We use 12 wells (columns 2, 7) of DMSO controls as vehicle control and also to quantify the edge effect, 6 wells of the TGF-beta inhibitor SB-431542 as a positive control to inhibit mesendoderm differentiation, and 6 wells of imatinib as an internal reference compound, as its SOX17-IC_{50} is 10–30 μM, near the safety threshold of hPST. It is important to always have these three internal controls on the same plate as the experimental test compounds.

   The example in Fig. 2 investigates compounds in dose ranged from 3 to 100 μM in duplicates, but one can modify the doses and the number of replicates depending on the goals of the study. In addition to this, column 1 contains DMSO controls which can be specifically used to confirm the quality of immunofluorescence staining. This edge column is not used for IC_{50} calculation, as peripheral wells are often affected by an edge effect, but are still suitable as control wells that can be used to optimize image acquisition and analysis without worrying about photobleaching.

   Prepare a 200× compound dilution series master plate

   Dispense 50 μl of DMSO or PBS in rows C to G (2nd to 7th) of a 96-well plate except column 12. Dispense 100 μl of a 20 mM stock compound solution into top row B (second row) according to the plate map (Fig. 2). Transfer 50 μl of row B to row C and mix ten times with an electronic pipette. Repeat this process for row C to row G. For column 12, add 50 μl of 5 μM SB-431542 for all wells, which serves as a positive control for the inhibition of SOX17 expression and mesendoderm formation.

   Aliquot into 2 ml deep 96-well plates for final dilutions

   Transfer 2.5 μl from the wells of the compound plate to two new sterile 2 ml deep 96-well plates (e.g., 1896–2110, USA Scientific). Make two plates: plate 1 for Differentiation Medium I and plate 2 for Differentiation Medium II. For plate 1, proceed to next step immediately. For plate 2, seal it with sealing foil (2923–0110, USA Scientific) and keep it at room temperature for 24 h. Do not put this plate in 4 °C or −20 °C as low temperature may cause precipitation of some compounds.

   Add Differentiation Medium I to the aliquoted compounds in the 2 ml deep 96 -well plates

   Add 497.5 μl of warm Differentiation Medium I media (1:200 dilution) to all 96 wells of the compound plate and gently mix

a

	1	2	3	4	5	6	7	8	9	10	11	12
A	empty	empty	empty	empty	empty	empty	empty	empty	empty	empty	empty	empty
B	DMSO	DMSO	Imatinib	Drug 1	Drug 2	Drug 3	DMSO	Imatinib	Drug 1	Drug 2	Drug 3	SB-431542
C	DMSO	DMSO	Imatinib	Drug 1	Drug 2	Drug 3	DMSO	Imatinib	Drug 1	Drug 2	Drug 3	SB-431542
D	DMSO	DMSO	Imatinib	Drug 1	Drug 2	Drug 3	DMSO	Imatinib	Drug 1	Drug 2	Drug 3	SB-431542
E	DMSO	DMSO	Imatinib	Drug 1	Drug 2	Drug 3	DMSO	Imatinib	Drug 1	Drug 2	Drug 3	SB-431542
F	DMSO	DMSO	Imatinib	Drug 1	Drug 2	Drug 3	DMSO	Imatinib	Drug 1	Drug 2	Drug 3	SB-431542
G	DMSO	DMSO	Imatinib	Drug 1	Drug 2	Drug 3	DMSO	Imatinib	Drug 1	Drug 2	Drug 3	SB-431542
H	empty	empty	empty	empty	empty	empty	empty	empty	empty	empty	empty	empty

b

	1	2	3	4	5	6	7	8	9	10	11	12
A	empty	empty	empty	empty	empty	empty	empty	empty	empty	empty	empty	empty
B	0	0	100	100	100	100	100	100	100	100	100	5
C	0	0	50	50	50	50	50	50	50	50	50	5
D	0	0	25	25	25	25	25	25	25	25	25	5
E	0	0	12.5	12.5	12.5	12.5	12.5	12.5	12.5	12.5	12.5	5
F	0	0	6.3	6.3	6.3	6.3	6.3	6.3	6.3	6.3	6.3	5
G	0	0	3.1	3.1	3.1	3.1	3.1	3.1	3.1	3.1	3.1	5
H	empty	empty	empty	empty	empty	empty	empty	empty	empty	empty	empty	empty

Fig. 2 Example of plate map and corresponding result. (**a**) 96-well plate map 1, compound plate; (**b**) map 2, drug dose (μM); (**c**) result (raw data) (number of SOX17+ cells/well, % of average of DMSO control); and (**d**) result (summary)

10 times immediately. Since both Differentiation Media contain high amount of proteins, care should be taken while pipetting to avoid foaming.

2. Treat cells with compound

   Remove the cell plate from incubator. Discard the media by flipping the plate over a waste container to expel the media.

c

	1	2	3	4	5	6	7	8	9	10	11	12
A	NA	NA	NA	NA	NA	NA	NA	NA	NA	NA	NA	NA
B	NA	100.6	0.0	0.0	0.5	3.3	97.7	0.0	0.0	0.0	4.9	0.0
C	NA	101.8	0.0	0.0	0.0	85.4	98.8	0.0	0.7	0.0	69.1	0.0
D	NA	91.8	0.2	0.0	0.0	91.5	89.1	2.3	0.3	0.0	88.1	0.0
E	NA	103.6	59.2	0.0	0.5	93.5	100.6	89.0	0.0	0.4	83.0	0.0
F	NA	101.5	88.2	1.2	11.8	108.2	98.5	107.5	0.0	39.3	93.0	0.0
G	NA	109.6	92.9	0.0	79.4	107.4	106.4	103.1	0.0	69.8	121.5	0.0
H	NA	NA	NA	NA	NA	NA	NA	NA	NA	NA	NA	NA

d

Compound	SOX17-IC50 (uM)	Call
Imatinib	16.5	toxic
Drug 1	< 3.1	toxic
Drug 2	4.7	toxic
Drug 3	68.0	safe

Fig. 2 (continued)

Wash plate with 100 µl/well DPBS (with calcium and magnesium) four times. It is important to remove mTESR completely as it may inhibit differentiation. Each wash was done by shaking the plate at 650 rpm for 3 min using an Eppendorf MixMate or similar plate shaker. Do not pipette directly on the surface of cells, as that may disrupt the fragile monolayer. Ideally, the entire washing steps should not exceed 30 min, since maintaining cells in PBS at room temperature for a prolonged duration is not optimal.

Following the final wash, replace the PBS with 100 µl media containing compounds in Differentiation Medium I from the compound plate. Shake the plate at 650 rpm for 3 min. Place the plate in 37 °C CO_2 incubator overnight.

3.2.4 Day 4: Media Change and Second Compound Treatment

1. Second compound treatment

   Prepare the second compound plate by warming the Differentiation Media II to 37 °C and adding 497 μl to the compound plate made in the previous section, gently mixing by pipetting up and down ten times without bubble formation.

   Take the cell plate from the incubator, discard the media by flipping the plate, and transfer 100 μl media containing compounds in Differentiation Media II. Place the plate in 37 °C CO_2 incubator for next 48 h.

3.2.5 Day 6: Terminate Differentiation and Fix and Stain Cells

1. Stop the differentiation

   Seventy-two hours after the start of differentiation, discard the media by flipping the plate. Add 200 μl DPBS per well and discard immediately. Repeat this two more times. This washing step is needed to remove dead cell debris and potential compound precipitation on the top of monolayer. At this point, cells are not fixed and the monolayer can be disputed very easily. Care must be taken not to pipette PBS directly on the cell surface. Discard DPBS at the last step.

2. Fix cells

   Add 100 μl of freshly prepared 3% formaldehyde in DPBS per well, shake the plate at 650 rpm for 1 min, and incubate for 15 min at room temperature. Fixing cells for extended periods should be avoided as this may damage the antigen epitope. Incomplete fixation may also be problematic, as it may result in incomplete attachment of cells on the plate, leading to the loss of cells during the multiple washing steps of subsequent immunostaining.

   Discard formaldehyde by flipping the plate, adding 200 μl DPBS and then discarding it. Repeat this washing step two times, leaving a final 100 μl of DPBS in each well until ready to proceed with the antibody staining.

   Although at this stage the fixed cell plate can be stored up to 3 days at 4 °C, performing immunofluorescence staining immediately usually produces better results.

3. Immunofluorescence staining of cells.

   Permeabilize cells

   Discard DPBS from the plate and add 100 μl of DPBS with 0.1% Triton X-100 per well. Shake the plate at 650 rpm for 1 min. Leave the plate for 15 min at room temperature.

   Pre-blocking

   Discard the DPBS/Triton X-100 solution from the plate and add 30 μl Image-iT FX solution per 96 well. Shake the plate at 650 rpm

for 1 min. Incubate with the pre-block solution for 30 min at room temperature. Discard the solution by flipping the plate.

Blocking

Add 100 μl blocking solution per well and shake the plate at 650 rpm for 1 min. Block for 1 h and then discard the blocking solution by flipping the plate over a waste container.

Antibody binding

Filter the antibody solution as described in the reagent section. Add 60 μl of SOX17 antibody solution per well and shake the plate at 650 rpm for 3 min. Incubate the plate for 1 h at room temperature. Then shake the plate at 650 rpm for 3 min again. Incubate the plate for another 1–2 h at room temperature.

Wash

Discard the antibody by flipping the plate and add 100 μl of antibody blocking solution. Shake the plate at 650 rpm for 3 min to wash. Repeat this one more time and wash with DPBS two more times.

Discard DPBS and add 35 μl of SlowFade with DAPI per well very slowly as it is very viscous. The plate can be immediately used for fluorescence microscopy or stored at 4 °C for 1–2 weeks.

3.2.6 Microscopic Image Analysis to Quantify SOX17-IC_{50}

Note on plate reader use

We found that once the assay conditions had been optimized, the high content image analysis (Cellomics ArrayScan VTI HCS Reader, Thermo Fisher) readout (number of SOX17+ cells per well) and plate reader (PerkinElmer Envision) readout (580 nm Rfu per well) were highly associated ($R = 0.89$, $P < 0.0001$) and the IC_{50} values determined by both methods were similar. However, the plate reader reading is more easily affected by background fluorescence noise generated by non-specific binding of SOX17 antibody, cell debris, and autofluorescence of compounds. Because of this, it is recommended to use the plate reader as a first quick scan tool and microscope-based image analysis as a more robust investigative tool.

Excitation and emission filters for the anti-SOX17 antibody conjugated to NL557

For immunofluorescence of NL557 fluorochrome (557/574 nm), use Krypton (568 nm) or HeNe (543 nm) for laser excitation and use filter sets for phycoerythrin (565/575), Rhodamine Red (570/590), or Cy3 (548/562).

3.2.7 Analyzing the Data and Calculating Compound IC_{50} Values

1. Quality assessment of the differentiation run
   First, check the DMSO control wells in column 1 with a manual fluorescence microscope. This column is not used for IC_{50}

quantitation, but is specifically designed for quality assessment of the plate. Do not observe any well except column 1 at this stage, as fluorescence excitation causes photobleaching that may affect the proper quantitation of test sample wells. Since SOX17 is a transcription factor, only the nucleus should be stained, while the cytoplasm is free of signal. All column 1 wells should have 30–70% SOX17+ cells, although the column may contain non-optimized wells due to edge effects. If there is a significant aberration from the ideal 30–70% SOX17+ cells (e.g., less than 10% SOX17+ cells or near 100% SOX17+ cells), it is likely that the differentiation or immunostaining was sub-optimal and may yield inconsistent results.

2. Capture images of all 96 wells and quantify the SOX17+ cell number and DAPI+ cell number

   When setting up the parameters such as excitation strength, exposure time, *z*-axis focusing, and intensity histogram threshold, use wells in the column 1 to prevent photobleaching of other wells. After setting these benchmarks, quantify SOX17+ cell numbers and DAPI+ cell numbers for all other wells.

   To define the background level for SOX17 signal, six wells in column 12 (Fig. 2) on each plate were treated with 5 μM SB-431542 which inhibits mesendoderm differentiation. These wells should show 0% SOX17+ cells. Columns 2 and 7 are all DMSO vehicle controls, and the average of these wells should be used to normalize against the test compounds when calculating the IC_{50} values (i.e., % inhibition = ((compound)/(DMSO)) × 100). An example of the number calculated is shown in Fig. 2c.

3. Calculate IC_{50} values

   Determine SOX17-IC_{50} and DAPI-IC_{50} using a curve fit program such as GraphPad Prism or TableCurve (Fig. 2d). In the example shown in Fig. 2d, where we used H9 cells and 30 μM as a safety threshold, drug 1 and drug 2 were determined as potentially toxic and drug 3 as nontoxic. One should set a safety threshold based on IC_{50} values of the reference compounds and the individual goals of the experiment. As with any in vitro safety assessment, one should interpret the data while taking into account the appropriate risk tolerance given the investigation context. For instance, if an investigator is interested in identifying only chemicals that exhibit the highest risk of teratogenicity in humans, one could flag only those compounds that exhibit the most complete inhibition of SOX17, without reducing the number of DAPI positive cells.

3.2.8 Interpreting the Quality of Each hPST Experiment

The following points should be considered in judging whether the particular run of the assay is successful:

DMSO negative control

Standard deviation of all 12 wells of DMSO control should be lower than 15–20%, and averages of columns 2 and 6 should be similar. If this is not the case, an edge effect during cell culture or uneven immunostaining may be the cause.

TGF-beta inhibitor SB-431542 positive control

SOX17-IC_{50} for SB-431542 is less than 1 μM (about 0.1 μM in H9 ES cell) and DAPI-IC_{50} is known to be higher than 50 μM. All wells in column 12 should have no cell death (near 100% DAPI+ cell numbers) and 0% SOX17+ cell number.

Internal reference compound control

SOX17-IC_{50} of imatinib, which is an internal reference compound in Fig. 2a, in our batch of H9 cell is 10–30 μM. Each run of the hPST assay should produce a result consistent with this. SOX17-IC_{50} of imatinib may vary depending on cell line. Therefore it may be desirable to choose additional reference compounds that better suit the goals of your study.

4 Notes

4.1 Optimization of the hPST Assay with a New Cell Line

Many parameters have to be optimized before running the first hPST using a new cell line, as the efficiency of mesendoderm differentiation and the responsiveness to growth factors vary among cell lines.

Differentiation should be stopped at the time when about 30–70% of cells are SOX17+ mesendoderm. To achieve this, the duration of differentiation may vary between cell lines and needs to be determined empirically. In addition, ideally cells should not reach 100% confluence during the assay since contact inhibition may affect the differentiation.

When differentiation is stopped, well-to-well variance of SOX17+ cell number should be minimum. Coefficient of variance (CV) of SOX17+ cells should be less than 20%.

To optimize conditions for a new cell line, the seeding cell density, differentiation duration period, and growth factor concentrations should be optimized. We optimize our assay by running the standard protocol without test compounds with the following parameters modified as described below.

Differentiation duration

Stop the differentiation at Days 1, 2, 3, 4, and 5 from the start of differentiation to do time course analysis to determine the optimal duration that results in 30–70% SOX17+ cells.

Cell density

Test five different cell seeding densities: 4k, 8k, 16k, 32k, and 48k/well. Choose the cell density that results in about 20–70% confluence at Day 0. Some cell lines proliferate significantly after the start of differentiation. Observe cells under a phase-contrast microscope every day to record the confluence and identify the starting density that results a sub-confluent density at the end of the differentiation.

Activin concentration

One problem we observed frequently was that the number of SOX17-positive cells reaches too high a level (nearly 100%) by Day 3. This is usually solved by decreasing activin concentration and/or stopping the differentiation at Day 2.5.

Like many recombinant growth factors, the specific biological activity of activin at a given concentration may vary between individual productions lots or different commercial sources. Therefore, one may need to test a range of activin concentrations when switching to a new lot or new vendor. We typically tested three concentrations of activin: 20 ng, 80 ng, and 200 ng/ml.

Run Each hPST Assay with the Selected Conditions and with Multiple Standard Compounds

After setting up the baseline differentiation parameters, perform the hPST with multiple compounds in triplicate over a full dose range (usually 3.1–100 μM). At least three replicate wells for each condition are required to determine reproducibility. The following compounds are recommended as useful internal controls.

Caffeine or saccharin
These compounds serve as a negative control and should not show any toxicity; both SOX17-IC_{50} and DAPI-IC_{50} should be higher than 200 μM.

All-trans retinoic acid (RA) and SB-431542
These compounds should serve as positive controls for differentiation inhibition. SOX17-IC_{50} of both should be less than 1 μM. Cytotoxicity of RA is usually higher than that of SB-431542. DAPI-IC_{50} of RA and SB-431542 is usually between 30 and 200 μM.

Thalidomide
Also a positive control for differentiation inhibition. SOX17-IC_{50} is around 1 μM, while it shows no cytotoxicity up to 100 μM. However, unlike retinoic acid or SB-431542, even relatively high doses of 20–50 uM do not inhibit differentiation completely, and about 5–25% cells remain SOX17+. This is a unique feature of thalidomide that is most probably due to its

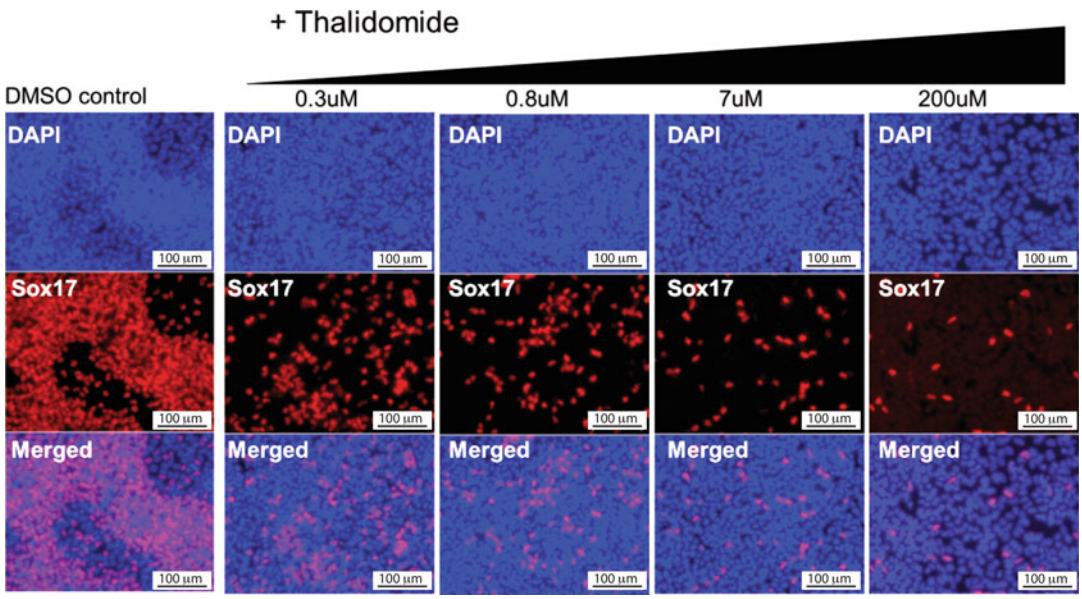

Fig. 3 Thalidomide dose response illustrating the reduction of SOX17-positive cells

toxic mechanism being very different from that of SB-431542 or retinoic acid. An example of a thalidomide dose response experiment is shown in Fig. 3.

Imatinib

This serves as a convenient reference compound for us, as it is commercially available and both SOX17-IC_{50} and DAPI-IC_{50} fall within the full dose range (3.1–100 μM).

5 Future Directions

The hPST described above is capable of correctly identifying human teratogens including thalidomide, which had not been identified using rodent systems. Furthermore, this assay holds the promise of being adapted to an HTS format that could assist in efforts to triage chemicals and rank order compounds during drug development. Adapting the assay to a higher density plate format is possible but would certainly require optimizing the plating density of the cells and the duration of the assay. In order to eliminate the requirement for immunostaining the cells, it may be possible to engineer a human pluripotent stem cell line to carry a reporter capable of measuring SOX17 nuclear localization. If validated, such a system may significantly increase the assay throughput.

Although the field clearly could benefit from novel in vitro human cellular systems, given the extraordinarily high stakes involved when making risk assessments of potential human

teratogens, new assays should be rigorously validated by independent laboratories. Driven largely by the breakthrough for creating human-induced pluripotent stem cells [22], the increased availability of human pluripotent stem cell lines and recent advances allowing routine growth of the cells have lowered the barrier researchers previously faced when considering initiating new human pluripotent stem cell studies in their labs. Hopefully, this will facilitate greater adaptation of this technology into the field of toxicology and the broader investigation and validation of human pluripotent stem cell-based assays such as the one described here.

References

1. Rezvanfar MA, Hodjat M, Abdollahi M (2016) Growing knowledge of using embryonic stem cells as a novel tool in developmental risk assessment of environmental toxicants. Life Sci 158:137–160
2. Rovida C et al (2015) Toxicity testing in the 21st century beyond environmental chemicals. ALTEX 32(3):171–181
3. Shuey D, Kim JH (2011) Overview: developmental toxicology: new directions. Birth Defects Res B Dev Reprod Toxicol 92(5):381–383
4. Rovida C, Hartung T (2009) Re-evaluation of animal numbers and costs for in vivo tests to accomplish REACH legislation requirements for chemicals—a report by the transatlantic think tank for toxicology (t(4)). ALTEX 26(3):187–208
5. Newman CG (1986) The thalidomide syndrome: risks of exposure and spectrum of malformations. Clin Perinatol 13(3):555–573
6. Vargesson N (2015) Thalidomide-induced teratogenesis: history and mechanisms. Birth Defects Res C Embryo Today 105(2):140–156
7. Robinson JF et al (2010) Embryotoxicant-specific transcriptomic responses in rat postimplantation whole-embryo culture. Toxicol Sci 118(2):675–685
8. Schumann J (2010) Teratogen screening: state of the art. Avicenna J Med Biotechnol 2(3):115–121
9. Mayshar Y, Yanuka O, Benvenisty N (2011) Teratogen screening using transcriptome profiling of differentiating human embryonic stem cells. J Cell Mol Med 15(6):1393–1401
10. Marshall VA, Carney EW (2012) Rabbit whole embryo culture. Methods Mol Biol 889:239–252
11. Panzica-Kelly JM, Zhang CX, Augustine-Rauch K (2012) Zebrafish embryo developmental toxicology assay. Methods Mol Biol 889:25–50
12. Venters SJ, Ordahl CP (2012) Somite unit chronometry to analyze teratogen phase specificity in the paraxial mesoderm. Methods Mol Biol 798:103–123
13. Kojima T, Asano S, Takahashi N (2013) Teratogenic factors affect transcription factor expression. Biosci Biotechnol Biochem 77(5):1035–1041
14. Teixido E et al (2013) Assessment of developmental delay in the zebrafish embryo teratogenicity assay. Toxicol In Vitro 27(1): 469–478
15. Ball JS et al (2014) Fishing for teratogens: a consortium effort for a harmonized zebrafish developmental toxicology assay. Toxicol Sci 139(1):210–219
16. Kappen C, Salbaum JM (2014) Gene expression in teratogenic exposures: a new approach to understanding individual risk. Reprod Toxicol 45:94–104
17. Schulpen SH et al (2015) Comparison of gene expression regulation in mouse- and human embryonic stem cell assays during neural differentiation and in response to valproic acid exposure. Reprod Toxicol 56:77–86
18. Xing J et al (2015) A method for human teratogen detection by geometrically confined cell differentiation and migration. Sci Rep 5:10038
19. Warkus EL et al (2016) Use of in vitro morphogenesis of mouse embryoid bodies to assess developmental toxicity of therapeutic drugs contraindicated in pregnancy. Toxicol Sci 149(1):15–30
20. Seiler AE, Spielmann H (2011) The validated embryonic stem cell test to predict embryotoxicity in vitro. Nat Protoc 6(7):961–978
21. Kameoka S et al (2014) A high-throughput screen for teratogens using human pluripotent stem cells. Toxicol Sci 137(1):76–90
22. Takahashi K et al (2007) Induction of pluripotent stem cells from adult human fibroblasts by defined factors. Cell 131(5):861–872

Chapter 3

Cardiac Action Potential Measurement in Human Embryonic Stem Cell Cardiomyocytes for Cardiac Safety Studies Using Manual Patch-Clamp Electrophysiology

Muthukrishnan Renganathan, Haiyang Wei, and Yong Zhao

Abstract

Human stem cell-derived cardiomyocytes present numerous advantages over isolated primary cardiac cells or tissues to study action potential (AP) prolongation by drug candidates for cardiac safety studies. Human stem cell-derived cardiomyocytes (hSC-CMs) express ionic channels that underlie cardiac action potentials and exhibit typical electrophysiological and mechanical characteristics of native human cardiomyocytes. Here, we demonstrate that the hSC-CMs are optimal for assessing dl-sotalol- and quinidine-induced action potential repolarization delay and nifedipine-induced shortening of action potential repolarization, and thus hSC-CMs exhibit the required electrophysiological and pharmacological profile at the cellular level.

Key words I_{Kr}, Action potential, EAD, QT interval, Human stem cell-derived cardiomyocytes, TdP and drug-induced proarrhythmia

1 Introduction

Prolongation of the QT interval on the electrocardiogram is caused by the lengthening of the ventricular myocyte action potential due to a reduction of outward K^+ currents, enhancement of inward late Na^+ current during phase 2, and/or enhancement of inward Ca^{2+} current during phase 3 of the cardiac action potential (Fig. 1). This reduction in net outward current and/or an increase in net inward current can facilitate prolongation of the action potential and the development of early afterdepolarizations (EAD). EAD are secondary voltage depolarizations which occur during the repolarizing phase of the cardiac action potential (AP) and are often associated with arrhythmias such as torsade de pointes (TdP) in cardiac diseases [1–3] including acquired and congenital long QT syndromes [4, 5] and heart failure.

EAD can occur due to reactivation of the L-type Ca^{2+} current and/or due to failure of Na^+ current to inactivate completely

Mike Clements and Liz Roquemore (eds.), *Stem Cell-Derived Models in Toxicology*, Methods in Pharmacology and Toxicology, DOI 10.1007/978-1-4939-6661-5_3,

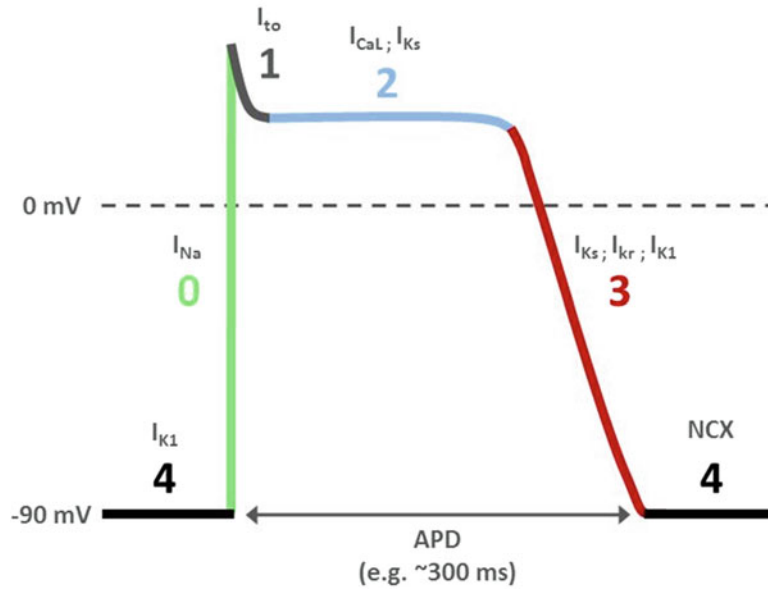

Fig. 1 Cardiac action potential and ionic currents during depolarization. The action potential, here depicted for a typical ventricular cell, reflects the changing electrical potential differences across cardiac cell membranes as a function of time and is controlled by the flow of ions through ion channels (different colored lines depict the flow of different currents). Resting (4), upstroke (0), early repolarization (1), plateau (2), and final repolarization (3) are the five phases of the action potential. The time elapsed between AP upstroke and the return to the resting potential is referred to as AP duration (APD)

during the repolarizing phase of the cardiac action potential and/or activation of the Na^+-Ca^{2+} exchange current during the action potential plateau [6–9]. When coincident with an increase in transmural dispersion of repolarization, this EAD-induced extrasystole can trigger reentry, torsade de pointes (TdP) [10–13], and, if uncorrected, sudden cardiac death.

Similarly, drug-induced delay in ventricular repolarization can induce TdP and is a leading cause of adverse clinical events and withdrawal of drugs (e.g., antipsychotics, antihistamines, and fluoroquinolone antibiotics) from the market [14]. Primarily all drugs that have been shown to induce TdP show inhibition of the I_{Kr} current (mediated by the hERG K^+ channel), but the possibility remains that any drug that reduces net repolarizing currents, either by reduction of outward current or increase in inward current, may induce TdP. In response to this concern, the ICH E14 and S7B guidelines were issued in May 2005 as a preclinical electrophysiology test against the hERG K^+ channel and a clinical QT measurement, respectively [15, 16]. These guidelines have effectively reduced the risk of bringing drugs to market that have the potential to cause TdP, but are imperfect, since these nonclinical and clinical

studies still identify many drugs as "positive" despite a lack of demonstrable proarrhythmic risk [17–20]. In a workshop held in July 2013 by the US Food and Drug Administration (FDA), the Cardiac Safety Research Consortium, and the nonprofit Health and Environmental Sciences Institute (HESI), a new paradigm was proposed focusing on a comprehensive assessment of multi-ion channel effects to improve the proarrhythmic risk assessment of drugs [21]. This new approach includes human stem cell-derived cardiomyocyte (hSC-CM) technology that has the potential to improve upon the currently employed cardiotoxicity assays [21]. Human stem cell-derived cardiomyocytes (both human embryonic stem cell-derived cardiomyocytes, hESC-CMs, and human-induced pluripotent stem cell-derived cardiomyocytes, hiPSC-CMs) have been shown to express ionic channels that underlie the cardiac action potential and exhibit typical electrophysiological and mechanical characteristics of native human cardiomyocytes [22–24].

Whole-cell current clamp of hSC-CMs offers the most complete and accurate assessment of the proarrhythmic liability of a drug candidate and in-depth exploration of its arrhythmogenic mechanisms at the cellular level. Here we demonstrate that hESC-CMs provide a biologically relevant alternative to transfected cell line models, primary cells, or tissues for predictive cardiac safety testing in a manual patch-clamp setup. Using three well-characterized drugs, (1) sotalol, a hERG K^+ channel blocker; (2) quinidine, a multiple cardiac ion channel blocker and the first drug to be clearly associated with QT interval prolongation and TdP; and (3) nifedipine, an L-type Ca^{2+} channel blocker, we show that the measurement of action potential parameters using hSC-CMs provides a useful model of drug-induced cardiac risk.

2 Materials

2.1 Cell Culture Components

- hESC-CMs, GE Cytiva™ Cardiomyocytes 1×10^5 cells 28-9774-35 (one cryovial of 1×10^5 cells was used to plate two 35 mm petri dishes each containing 10–12 coverslips (5 mm)).
- 15 ml centrifuge tubes, Corning 430052.
- 50 ml centrifuge tubes, Corning 430290.
- Serological pipettes—5 ml, Corning 4487.
- Serological pipettes—10 ml, Corning 4488.
- Serological pipettes—25 ml, Corning 4489.
- 500 ml cellulose acetate filter units, Corning 430769.
- Coverslips—electrophysiological applications, VWR 631–0149.
- RPMI 1640 + glutamine, Gibco 21875034.
- B27™ supplement, Gibco 17504–044.

- Matrigel™, Becton Dickinson 356231.
- KnockOut™ DMEM (KO-DMEM), Gibco 10829–018.
- DMEM, Gibco 41965–039.

2.2 Equipment Needed for Cell Culture

- Adjustable pipettes
- Liquid nitrogen vapor cryostore
- Biosafety cabinet (BSC)
- Centrifuge
- Vacuum pump and line
- Hemocytometer or automated cell counting instrument

2.3 Patch-Clamp Instrumentation

- Microscope, Nikon Eclipse TE2000-S
- Patch-clamp amplifier, Axon Instruments, MultiClamp 700B
- Digitizer, Axon Instruments, Digidata 1322A
- pCLAMP, Axon Instruments, Version 10
- Micropipette puller, Sutter Instrument, P-97
- Motorized manipulator, Sutter Instrument MP-225
- Dual channel heating system, Warner Instruments TC-344B
- High-performance air table and Faraday cage, Kinetic Systems 5704-3648-21
- Glass pipette, WPI TW150F-4
- 24-well cell culture plate, Corning 3524
- Coverslip 5 mm, Warner Instruments
- Falcon sterile 35 mm petri dishes, Corning 353001

3 Methods

For the proposed schedule for this hESC-CM manual path-clamp assay, *see* Fig. 2.

Fig. 2 Action potential duration measurement assay schedule

3.1 Preparation of RPMI 1640/B27 Medium

3.1.1 Thaw frozen 10 ml B27 supplement vial(s) in a 37 °C water bath. Remove the B27 from the water bath when the material has completely thawed. Do not incubate at 37 °C for extended periods of time. Perform the following steps aseptically inside the biosafety cabinet (BSC).

3.1.2 Wipe the required number of RPMI 1640 + glutamine medium bottles and B27 supplement vials with 70% isopropanol and transfer to a BSC.

3.1.3 Place the filtration unit into the BSC.

3.1.4 Carefully transfer 500 ml of the RPMI 1640 + glutamine medium followed by 10 ml of B27 supplement into the reservoir of the filter unit and filter it.

3.1.5 Place sterile cap on the bottle portion of the filter unit.

3.1.6 Store the medium at 2–8 °C. Use within 1 week of preparation.

3.1.7 Avoid repeated warming of the RPMI 1640/B27 medium. Warm only the required volume of medium to complete the task.

3.2 Preparation of 1:2 Diluted Matrigel Aliquots

Growth factor-reduced Matrigel (Becton Dickinson # 356231) is the cell attachment substrate used for coating the surface the coverslips (**Note 1**).

3.2.1 Slowly thaw Matrigel overnight at 2–8 °C to avoid the formation of a gel.

3.2.2 Wipe the Matrigel and KO-DMEM bottles with 70% isopropanol and transfer to a BSC.

3.2.3 Cool a sterile 10 ml pipette by drawing and releasing 10 ml of cold KO-DMEM into the pipette repeatedly without removing the pipette from the bottle of KO-DMEM. (Alternatively store 10 ml pipettes at 2–8 °C before use).

3.2.4 Add 10 ml of cold KO-DMEM to the vial containing 10 ml Matrigel.

3.2.5 Working quickly, mix the Matrigel and KO-DMEM with a 10 ml pipette, avoiding the formation of bubbles.

3.2.6 Aliquot 2 ml of diluted Matrigel into each prechilled sterile 50 ml tube; store at −20 °C until required. Matrigel that has been diluted 1:2 is stable for 3 months when stored at −20 °C.

3.3 Preparation of 1:30 Diluted Matrigel Solution

3.3.1 Perform the following steps aseptically (**Note 1**).

3.3.2 Slowly thaw a 2 ml diluted Matrigel aliquot prepared in step 3.2.6 at 4 °C for at least 2 h to avoid the formation of a gel. Once thawed transfer it to BSC.

3.3.3 Cool a sterile 5 ml pipette by drawing 5 ml of cold KO-DMEM into the pipette (**Note 1**).

3.3.4 Dilute the Matrigel aliquots with 5 ml cold KO-DMEM. Carefully mix Matrigel solution, avoiding the formation of bubbles.

3.3.5 Cool a sterile 25 ml pipette by drawing 25 ml of cold KO-DMEM into the pipette (**Note 1**).

3.3.6 Add a further 23 ml cold KO-DMEM (for a final dilution of 1:30). Carefully mix Matrigel solution, avoiding the formation of bubbles.

3.4 Preparation of Matrigel-Coated Coverslips

3.4.1 Perform the following steps aseptically.

3.4.2 For a 35 mm petri dish, 6–10 coverslips can be added. Coverslips should be sterilized by soaking in 70% ethanol for a minimum of 24 h in a sealed sterile 50 ml tube. Ensure complete wetting of both sides of each coverslip by making sure there is no air bubble under each coverslip.

3.4.3 Air dry coverslips by placing plate into BSC for a minimum of 2 h before adding Matrigel.

3.4.4 Add 2 ml of diluted Matrigel from 3.3.6 to the 35 mm petri dish containing 6–10 coverslips. Ensure the coverslips are completely immersed in the Matrigel solution.

3.4.5 Incubate the plates and coverslips overnight at 2–8 °C.

3.4.6 Before thawing cells, take the Matrigel-coated coverslips out of 2–8 °C storage. Leave the coverslips at room temperature for 1 h before use. Aspirate the Matrigel solution from the petri dish immediately before the addition of cells (*see* **Note 2** and Fig. 3).

3.4.7 Matrigel-coated coverslips are stable for 2 days when stored at 2–8 °C.

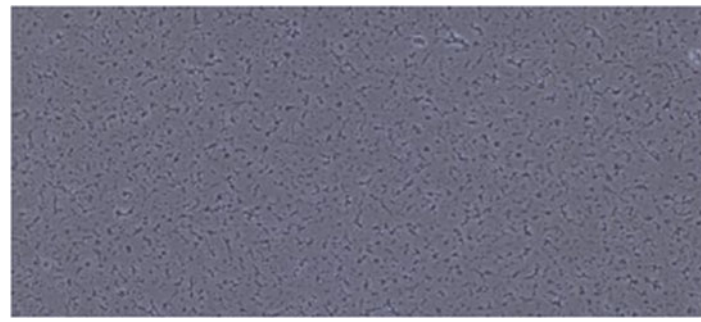

Fig. 3 Matrigel is present uniformly on the surface of a coverslip ready to receive hSC-CMs. © 2014 General Electric Company—reproduced with the permission from the owner

3.5 Thawing hSC-CMs (Cytiva Cardiomyocytes)

3.5.1 Perform the following steps aseptically.

3.5.2 Remove the cryovial of hSC-CMs from the cryostore and place onto dry ice for 2–3 min.

3.5.3 Thaw cell suspension in a 37 °C water bath with gentle agitation until ice crystals just disappear (2–3 min). To avoid contamination of the cells, take care not to immerse the whole cryovial into the water bath. Avoid extended incubation at 37 °C.

3.5.4 Wipe the outside of the cryovial with 70% isopropanol and transfer to BSC.

3.5.5 Carefully transfer the cell suspension into a sterile 50 ml centrifuge tube.

3.5.6 Rinse the cryovial with 1 ml of pre-warmed RPMI 1640/B27 and combine with the cell suspension. Transfer the rinsings dropwise with gentle mixing of the tube containing the cells.

3.5.7 Slowly (over the course of 2–3 min) add the 8 ml of pre-warmed RPMI 1640/B27 drop by drop to the centrifuge tube. Centrifuge at 400 g for 4 min at room temperature.

3.5.8 Carefully, aspirate the supernatant using a 10 ml serological pipette. Resuspend the cells in the residual liquid by gently swirling the tube.

3.5.9 Resuspend the cell pellet in 1 ml of pre-warmed RPMI 1640/B27 with gentle agitation.

3.5.10 If using the 1×10^5 cardiomyocyte pack size, dilute the cell suspension further with another 1 ml.

3.5.11 Determine viability and viable cell number using a hemocytometer and trypan blue. Cell viability is usually between 92 and 97%.

3.5.12 Add 10 µl trypan blue solution to the 10 µl of the cell suspension in an Eppendorf tube. Incubate the mixture for 3 min at 37 °C.

3.5.13 Apply 10 µl of the 1:1 mixture into a Neubauer hemocytometer and count viable (clear), dead (blue), and total cells.

3.5.14 Take the average cell count from each of the sets of 16 corner squares and the central square.

3.5.15 Calculate the number of cells—multiplying the average number of cells counted in the chamber squares by the volume of each square (1×10^4 ml^{-1}), dilution factor [2], and total volume of the suspension (1 ml). For example, if the mean number of cells counted per square is equal to 5, then:

$$5 \text{ cells} \times 1 \times 10^4 \text{ ml}^{-1} \times 2 \text{ dilution factor} \times 1 \text{ ml} = 1 \times 10^5$$

cells total (i.e., 100,000 cells in the cell suspension).

3.5.16 Dilute viable cells to final required concentration using pre-warmed RPMI 1640/B27 as in Sect. 3.6.

3.6 Plating Cells onto Matrigel-Coated Coverslips

A petri dish containing 10–12 coverslips will accommodate 5×10^4 cells, dispensed in a minimum volume of 1 ml. 5×10^4 cells should be added to the center of the dish such that the suspension will cover all the coverslips. A 1×10^5 cryovial of cells can seed two petri dishes each containing 10–12 coverslips (**Note 3**).

3.6.1 Dispense another 1 ml of pre-warmed RPMI 1640/B27 into the petri dish after 2 h incubation at 37 °C/5 % CO_2.

3.6.2 Incubate all coverslips at 37 °C/5 % CO_2 for a minimum of 48 h (typically 72 h) before use.

3.6.3 Refeed cardiomyocyte cultures every other day after the plating of cells. Remove 1 ml of media from the petri dish and replace it with 1 ml of pre-warmed RPMI 1640/B27 media for a partial media change.

3.7 Test Compound Preparation

All chemicals used in the validation tests were purchased from Sigma-Aldrich Co. LLC. (St. Louis, MO). Compound stocks were prepared either in dimethyl sulfoxide (DMSO) or deionized water, at 400× the highest test concentration, and stored frozen (−80 °C). Prior to the experiments, the stock solution was thawed, sonicated, and vortexed. Compounds were then serially diluted in DMSO or in deionized water into glass vials at 400× the lowest concentrations to be tested. Finally, the compound stocks were diluted at 1:400 into extracellular solution (*see* Sect. 3.8). DMSO concentration was 0.25 % for negative control, test compound, and washout solutions.

3.8 Extracellular and Intracellular Solution Compositions

- Extracellular solution contained (mM): NaCl 137, KCl 4, $CaCl_2$ 1.8, $MgCl_2$ 1, HEPES 10, glucose 10, pH 7.4, adjusted with NaOH (stored at 2–8 °C, Table 1).

Table 1
Extracellular (bath) solution

Solution name	Chemicals	Concentration (mM)	FW	g/l
Extracellular solution	NaCl	137.0	58.44	8.006
	KCl	4.0	74.55	0.298
	$CaCl_2$	1.8	110.98	0.200
	$MgCl_2.6H_2O$	1.0	203.3	0.203
	D(+)-Glucose	10.0	180.2	1.802
	HEPES	10	238.3	2.383 or (10 ml/1 M solution)

pH adjusted to 7.4 with NaOH, stored at 4 °C (expiration date: 1 month after preparation)

Table 2
Intracellular (pipette) solution

Solution name	Chemicals	Concentration (mM)	FW	mg/0.1 l
Intracellular solution	KCl	130	74.55	969.15
	$MgCl_2.6H_2O$	5	203.3	101.7
	HEPES	10	238.3	238.30
	EGTA	5	380.4	190.2

pH adjusted to 7.2 with KOH stored at –20 °C (expiration date: 6 months after preparation)

- Intracellular solution contained (mM): KCl 130, $MgCl_2$ 5, EGTA 5, HEPES 10, pH 7.2, adjusted with KOH (aliquoted and stored –20 °C, Table 2). The intracellular solution was freshly supplemented with 50 μg/ml gramicidin for perforated patch clamp on the recording day.

3.9 Reference Compounds and Gramicidin

- Sotalol hydrochloride, Sigma-Aldrich Inc. S0278; storage, room temperature; solubilization, 60 mM in distilled H_2O; aliquots stored, –80 °C; test concentrations, 10, 30, 100 μM.
- Quinidine hydrochloride monohydrate, Sigma-Aldrich Inc. Q0750; storage, room temperature; solubilization, 20 mM in distilled H_2O; aliquots stored, –80 °C; test concentrations, 0.3, 1, 3 μM.
- Nifedipine, Sigma-Aldrich Inc. N7634; storage, 2–8 °C; solubilization, 30 mM in DMSO; aliquots stored, –80 °C; test concentrations, 0.1, 0.3, 1 μM.
- Gramicidin from *Bacillus aneurinolyticus* (FW = 1880), Sigma-Aldrich Inc. G5002; storage at 2–8 °C, ≤ 3 years; gramicidin (50 mg/ml) DMSO stock solution was prepared, aliquoted, and stored at 2–8 °C.

3.10 Assay Protocol

3.10.1 The hSC-CMs are plated on Matrigel-coated coverslips in a petri dish (Sect. 3.6). The cells are ready for manual patch-clamp testing after 2-day culture at 37 °C with 5% CO2, but we typically wait 3 days before use to allow the cardiomyocytes to mature and become electrically excitable.

3.10.2 Prior to the patch-clamp assay, in a biosafety cabinet, transfer a coverslip (on which the hSC-CMs are seeded) from the petri dish to another petri dish containing pre-warmed RPMI 1640/B27 media using sterile forceps. Next transfer this coverslip to a glass bottom culture dish containing pre-warmed extracellular solution. Change the solution once with 1 ml of extracellular solution before loading the glass culture dish onto a heater adapter under a patch-

clamp microscope. Turn on the temperature controller TC-344B dual channel heating system (Warner Instruments, USA) and adjust the temperature to 35 ± 2 °C (Fig. 4a).

3.10.3 Pull the glass pipette (thin-walled glass capillaries with filament, TW150F-4, World Precision Instruments, USA) using a micropipette puller (Sutter Instrument, P90) and polish with a microforge (Narishige Microforge MF-830, Japan). The pipette resistance can be in the range of 4–8 MΩ.

3.10.4 Backfill the glass pipette with intracellular solution without gramicidin by tipping the backend (non-pulled end) of the pipette into intracellular solution until a small bead of intracellular solution is apparent at the pipette tip (**Note 4** and Fig. 4b). A cap from an Eppendorf tube or a small screw cap top can be used as a reservoir for intracellular solution.

3.10.5 Prepare a 50 mg/ml gramicidin stock solution in DMSO. Make 10 µl aliquots and store them at −20 °C for up to 1 month.

3.10.6 Prepare 50 µg/ml gramicidin by diluting 1 µl of 50 mg/ml gramicidin stock solution in 1 ml of intracellular saline solution.

3.10.7 Fill the glass pipette with the intracellular solution containing gramicidin (50 µg/ml) and place it on an electrode holder on the manual patch-clamp setup.

3.10.8 Under the microscope, select a healthy, single beating cell (*see* Fig. 5, e.g., cell morphology). After the pipette slightly touches the cell, apply negative pressure to the pipette to form a GΩ seal. After achieving GΩ seal with a glass pipette, monitor capacity current transients (in voltage clamp mode) for alteration in access resistance. An access resistance ≥10 MΩ indicates achievement of a perforated patch-clamp recording (**Notes 5** and **6**).

3.10.9 Switch from voltage clamp mode to current clamp mode and apply a brief stimulating pulse (about twice the stimulating threshold, 2–5 ms duration, at 1 Hz) to induce action potentials (**Note 7**). The cells that spontaneously beat can be injected with −10 to −40 pA current amplitude to suppress the spontaneous activity. Disregard cells that cannot be paced at 1 Hz.

3.10.10 The typical ventricular-like action potential is defined as (Fig. 6):

- Resting membrane potential (RMP) is ≤−72 mV.
- Action potential amplitude ≥ 100 mV.
- Vmax > 10 V/s.

Fig. 4 (**a**) Manual patch-clamp setup for APD measurements with a glass culture dish on the heater adapter under the microscope. 1, Air table; 2, Faraday cage; 3A, solution perfusion controller; 3B, syringe reservoirs for vehicle and test compound storage and perfusion; 4, inverted microscope; 5A, Axon MultiClamp amplifier; 5B, digitizer; 5C, headstage with pipette holder; 6A–C, micromanipulator; 7A, dual channel heater controller; 7B, inline solution heater; 7C, cable assemblies with connector for heater adapter for dish; 8, computer; 9, pipette puller; and 10, microforge. (**b**) Image of glass pipette being backfilled with intracellular solution using the cap of screw cap tube. 11, Backend of glass tube (non-pulled end); 12, arrow points to a small bead of intracellular solution at the pipette tip

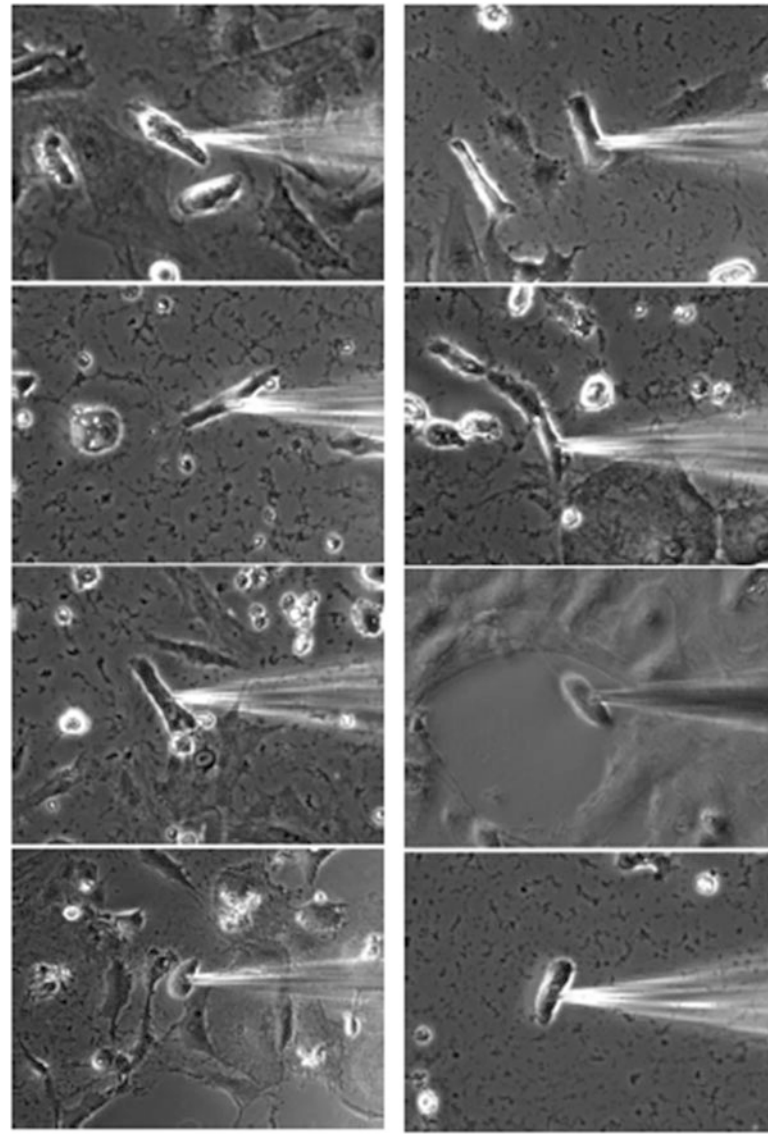

Fig. 5 Examples of hSC-CM cell morphologies seen when patching manually. © 2014 General Electric Company—reproduced with the permission from the owner

- Action potential duration at 90% repolarization (APD_{90}) ≥ 150 ms.

3.10.11 Patch-clamp recordings are performed using MultiClamp 700B and pCLAMP 10 software. Filter the analog signals with a low-pass filter at 10 kHz before digitization at 50 kHz and save the data to a PC computer.

3.10.12 After the induced action potential has stabilized (3–5 min within ±5% variability of RMP and action potential amplitude), continuously perfuse the recorded cell with

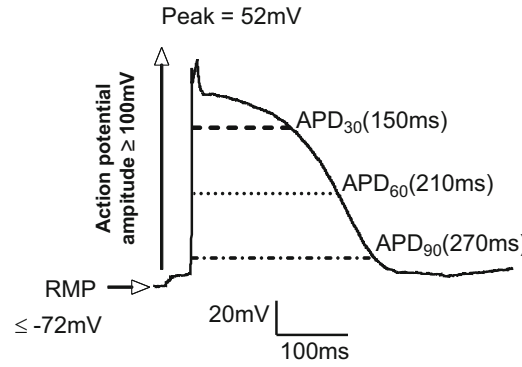

Fig. 6 hSC-CM action potential with the following parameters labeled: RMP, action potential amplitude, Vmax, and APD_{30}, APD_{60}, and APD_{90}

vehicle control solution (flow rate of 2 ml/min). Only cells showing a stable baseline (2–5 min, within ±5% variability of RMP and action potential amplitude) during this vehicle control application period are selected for further study.

3.10.13 Sequentially perfuse the recorded cell with test compound, starting from the lowest and progressing to the highest test concentration (**Note 8**). When the steady-state of action potential prolongation or shortening is obtained or the cell has been incubated with test compound for 5 min and action potential duration remains unchanged, apply the next ascending concentration. After completion of the test compound application, washout the compound with vehicle control (0.25% DMSO in extracellular solution by default) for 5 min to determine whether the compound's effect is reversible.

3.10.14 If the effect of compound on action potential duration is reversible, perfuse 100 μM dl-sotalol to the same cell so that the effect of the reference compound can be observed. If the effect of the compound is not reversible, test the effect of the reference compound in a separate cell ($n = 1$).

3.10.15 If possible, check the access resistance and membrane resistance of the recorded cell after the test has been completed to confirm that the seal was satisfactory throughout the experimental period (*see* list 3.11.5 for acceptance criteria).

3.10.16 In a typical working day, 2–4 cardiomyocytes with three concentration measurements with a washout can be recorded.

3.11 Data Analysis

Use ClampFit 10 software (Molecular Devices, Sunnyvale, California) to analyze the recorded action potentials.

3.11.1 Average the responses from five recorded action potentials from each perfusion group (vehicle control, compound concentration #1, compound concentration #2, compound concentration #3, and washout).

3.11.2 Quantify the following parameters (Fig. 6):

- RMP
- Action potential amplitude (APA)
- Maximum rate of action potential depolarization (Vmax)
- Action potential duration at 60 and 90% repolarization (APD_{60} and APD_{90})

3.11.3 The data acceptance criteria for a ventricular-like action potential were set as follows:

- RMP is ≤ -72 mV.
- Action potential amplitude ≥ 100 mV.
- Vmax ~ 12 V/s.
- There is a noticeable action potential plateau (phase 2).
- Action potential duration at 90% repolarization (APD_{90}) ≥ 150 ms.
- 100 μM dl-sotalol should induce ≥25% change in APD_{90} vs. vehicle control values.

3.11.4 Present data as mean ± standard error of mean (SEM). Compare data from the compound test groups to that from the vehicle control group using a paired *t*-test. A statistically significant difference is defined as $p < 0.05$.

3.11.5 Assay data integrity verification was determined by confirming the following:

- Access resistance ≤ 15 MΩ.
- Membrane resistance ≥ 500 MΩ.
- Concentration-dependent effect on AP90 duration was observed.
- Compound-induced effect was partially or completely reversed by washout.
- Cell morphology appears healthy after final test compound or washout solution has been perfused.

4 Notes

1. Do not allow the Matrigel solution to reach room temperature as this will reduce its performance as a cell attachment substrate. Keep the solution, pipettes, and KO-DMEM cold at all stages of handling. Avoid room temperature plastic coming

into contact with Matrigel. Avoid repeated freeze-thawing of diluted Matrigel aliquots.

2. Examine the Matrigel coating using a 10× objective to ensure a uniform layer of Matrigel is present on the surface to receive the cardiomyocytes (Fig. 3). If the Matrigel layer is uneven or contains large aggregates, discard and prepare fresh coverslips.
3. Do not rinse the Matrigel-coated coverslips before addition of cells because this will reduce the performance of the cell attachment substrate. Avoid direct contact with the Matrigel-coated surface(s) as this could scratch the surface coating.
4. The presence of gramicidin in the pipette solution can prevent seal formation if it leaks from the patch pipette onto the cell membrane. Consequently, the tip of the patch pipette is filled with antibiotic-free solution to allow seal formation and backfilled with intracellular solution containing gramicidin. Giga seal formation should occur before the gramicidin reaches the tip and perforates the membrane.
5. If the cell capacitance increases suddenly within 2 min without a gradual increase in capacitance over 5–7 min, it indicates cell has gone into "whole-cell" mode instead of perforated patch mode. Discard the cell and move to another cell.
6. If seal is not >1 GΩ, then apply further pressure in an attempt to increase the seal resistance to >1 GΩ or release pressure altogether. If this does not work, discard the pipette and begin the process again on a new cell with a new pipette.
7. Record the current amplitude that triggers an action potential, using a pulse duration of 5–10 ms. This is the threshold stimulus, which typically is in the range of 10–100 pA. Set the current amplitude to twice the threshold that triggers the action potential and pace the cell at a frequency of 1 Hz.
8. Typically, three concentrations and a washout (5 min application for each of the three concentrations and the washout) will be applied to a single cell. The limiting factors are the stability of the recording and cell health.

5 Results

Recorded action potentials were stimulated in hSC-CMs at a frequency of 1 Hz. Similar to human cardiomyocytes, three types of action potentials were recorded in hSC-CMs: nodal-like (data not shown), atrial-like (data not shown), and ventricular-like. Only the cells with action potentials that met all ventricular-like action potential criteria (*see* list 3.10.8) were used for this validation study. Three drugs that selectively block different cardiac ion channels were

tested and their pharmacological effects on the action potential from hSC-CMs were characterized in the experiments.

Sotalol, a K^+ channel blocker, induced a marked prolongation of the recorded action potential duration (APD), and this drug-induced delay in repolarization was concentration dependent: when compared to vehicle control values, APD_{90} was prolonged by 7.8%, 21.2%, and 54.6% with 10 μM, 30 μM, and 100 μM sotalol applications, respectively. The other recorded parameters were unchanged (*see* Fig. 7 and Table 3).

Nifedipine is an L-type Ca^{2+} channel blocker. In contrast to sotalol, nifedipine consistently shortened action potential duration in a concentration-dependent manner. When compared to vehicle control values, APD_{90} was shortened by −17.9%, −35.2%, and −52.6% in 10 μM, 30 μM, and 100 μM nifedipine, respectively. Moreover, after washout, the effect of nifedipine on action potential duration was partially reversed (*see* Fig. 8, Table 4).

Quinidine, a multiple ion channel blocker, significantly prolonged APD_{60} and APD_{90}, in a concentration-dependent manner. When compared to vehicle control values, APD_{90} was prolonged by 18.7%, 36.8%, and 51.9% in 0.3, 1, and 3 μM quinidine, respectively. Quinidine at 3 μM was also found to reduce the RMP and action potential amplitude and slowed Vmax (*see* Fig. 9, Table 5).

To verify the validation results, APD_{90} values obtained from this study were compared with those reported in literature. The results derived by us and others are comparable (*see* Table 6). Furthermore, the effects of quinidine on RMP, action potential amplitude, and Vmax observed in our tests are also similar to those reported in literature [23, 24].

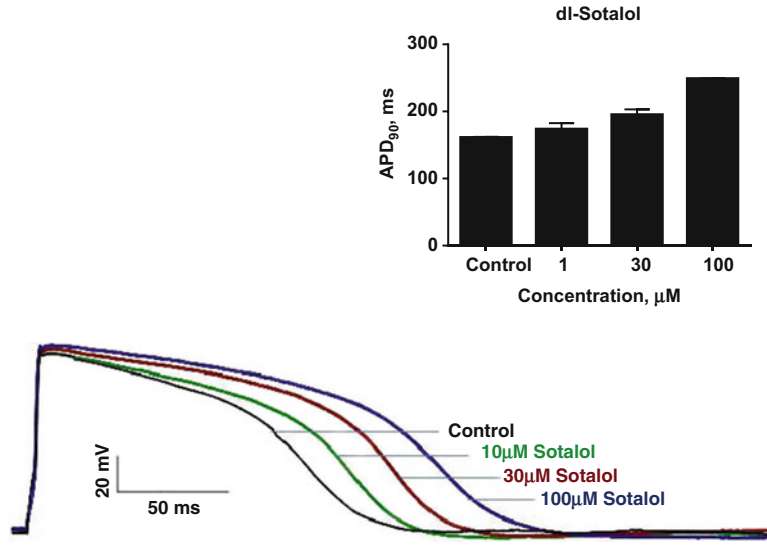

Fig. 7 (**a**) Pharmacological effects of sotalol on action potentials from hSC-CM. Scale bars indicate amplitude (mV) and duration (ms). (**b**) Bar chart summary of the effect of sotalol on APD_{90}

Table 3
Effect of dl-sotalol on action potential parameters

	RP (mV)	APA (mV)	Vmax (V/s)	APD_{60} (ms, % of change)	APD_{90} (ms % of change)
Control	−86 ± 3.3	102 ± 0.3	21.3 ± 0.4	111.5 ± 2.3	161.1 ± 1.1
10 μM sotalol	−84.2 ± 2	105.2 ± 2.0	19.8 ± 0.5	129.2 ± 6.5	173.5 ± 9.2 (7.8%)
30 μM sotalol	−85.2 ± 4.7	104.3 ± 1.9	18.6 ± 0.1	133.8 ± 9.5	195.2 ± 7.8* (21.2%)
100 μM sotalol	−84.7 ± 1.7	101.9 ± 1.9	18.3 ± 0.2	150.3 ± 3.3* (34.8%)	248.9 ± 0.4* (54.6%)

* indicates a statistically significant difference ($P < 0.05$)

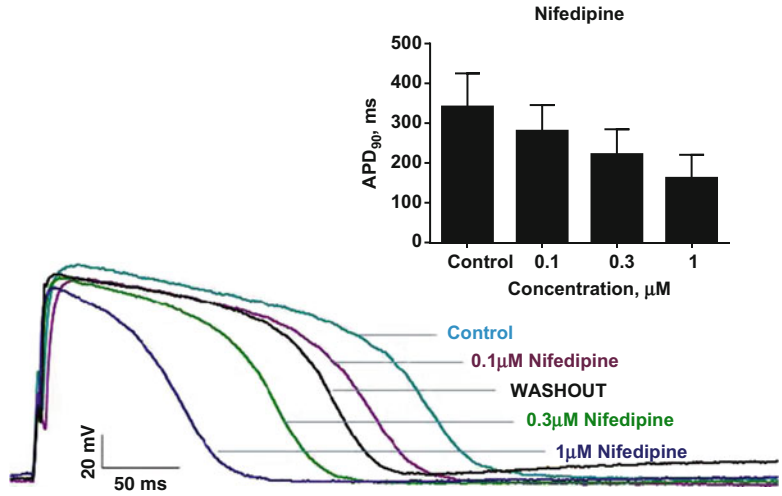

Fig. 8 (**a**) Pharmacological effects of nifedipine on action potentials from hSC-CM. Scale bars indicate amplitude (mV) and duration (ms). (**b**) Bar chart summary of the effect of nifedipine on APD_{90}

Table 4
Effect of nifedipine on action potential parameters

	RP (mV)	APA (mV)	V_{max} (V/s)	APD_{60} (ms, % of change)	APD_{90} (ms, % of change)
Control	−95.6 ± 1.6	125.0 ± 6.7	11.9 (±0.9)	249.3 ± 28.0	340.7 ± 84.7
0.1 μM nifedipine	−94.9 ± 2.1	118.5 ± 5.8	10.9 (±0.7)	206.9 ± 23.2	279.7 ± 66.0 (−17.9)
0.3 μM nifedipine	−94.7 ± 2.6	114.0 ± 5.5	10.6 (±1.0)	144.7 ± 13.6* (−42.0%)	220.9 ± 64.0* (−35.2%)
1 μM nifedipine	−93.4 ± 1.1	110.7 ± 8.0* (−11.4%)	11.4 (±1.1)	98.2 ± 16.5* (−60.6%)	161.4 ± 59.4* (−52.6%)

* indicates a statistically significant difference ($P < 0.05$)

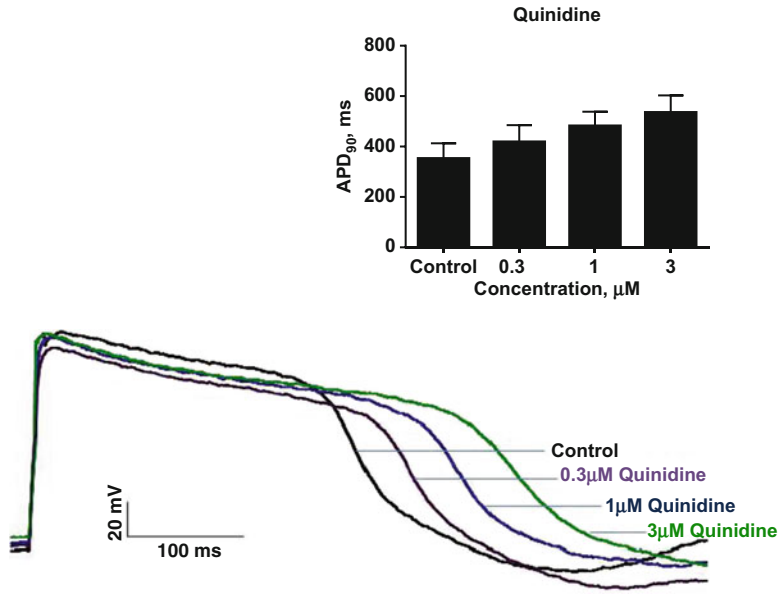

Fig. 9 (**a**) Pharmacological effects of quinidine on action potentials from hSC-CM. Scale bars indicate amplitude (mV) and duration (ms). (**b**) Bar chart summary of the effect of quinidine on APD_{90}

Table 5

Effect of quinidine on action potential parameters

	RP (mV, % of change)	APA (mV, % of change)	Vmax (V/s, % of change)	APD_{60} (ms, % of change)	APD_{90} (ms, % of change)
Control	−97.2 ± 2.5	123.0 ± 5.0	12.1 ± 1.4	287.8 ± 65.1	352.1 ± 61.1
0.3 µM quinidine	−95.4 ± 4.9	116.8 ± 8.3	10.7 ± 0.7	332.0 ± 73.6	418.1 ± 67.1 (18.7%)
1 µM quinidine	−90.3 ± 2.4	117.4 ± 5.7	10.3 ± 1.0	376.3 ± 78.3* (30.7%)	481.7 ± 56.4* (36.8%)
3 µM quinidine	−87.8 ± 1.7* (−9.7%)	110.2 ± 5.7* (−10.5%)	8.7 ± 0.9* (−28%)	409.8 ± 87.7* (42.8%)	534.7 ± 68.2* (51.9%)

* indicates a statistically significant difference ($P < 0.05$)

Table 6

Comparison of Eurofins's results with published literature values

	APD_{90} (% of change)		
	Eurofins	Peng et al. [18]	Ma et al. [21]
100 µM sotalol	54.6	57.2	–
1 µM nifedipine	−52.6	−41.3	−54.6*
3 µM quinidine	51.9	79.9	–

* indicates the value was obtained at a test concentration of 100 nM nifedipine

6 Discussion

hERG encodes I_{Kr} (cardiac rapidly activating delayed rectifier potassium channel current) in the heart [25]. This K^+ channel current is a key contributor to action potential repolarization. Blockade of the I_{Kr} current delays cardiac repolarization [26]. Sotalol and quinidine, both of which are I_{Kr} blockers, were found to prolong hESC-CM action potential duration in this study. The Ca^{2+} current contributes to the plateau phase (phase 2) of the cardiac action potential. Blockade of this current shortens action potential duration [23, 24]. The L-type Ca^{2+} channel blocker, nifedipine, was found to dramatically shorten the action potential duration in this study. Furthermore, quinidine blocks Na^+ and Ca^{2+} channels. As a result of this blockade, RMP and action potential amplitude may be decreased and Vmax may become slower. All of these effects were observed after quinidine application in this validation study.

In conclusion: (1) Ventricular-like action potentials were stably recorded from hSC-CMs with the manual patch-clamp technique. (2) The responses of hSC-CMs to the known drugs were consistent with the drug's mode of action. For example, action potential duration was prolonged by hERG K^+ channel blockers, sotalol and quinidine, and shortened by the Ca^{2+} channel blocker, nifedipine. (3) The effect of nifedipine on action potential duration was reversed following washout. (4) The results from our validation study are comparable to those reported in literature. (5) The action potential measurement from hSC-CMs provides valuable and reliable information on the cardiac safety of a test compound and can help to elucidate the mechanism of drug action on cardiac ion channels.

Acknowledgments

We thank Shimin Wang for collecting the action potential data.

References

1. Cranfield PF (1977) Action potentials, afterpotentials, and arrhythmias. Circ Res 41:415–423
2. Rosen MR, Moak JP, Damiano B (1984) The clinical relevance of afterdepolarizations. Ann N Y Acad Sci 427:84–93
3. Weiss JN, Garfinkel A, Karagueuzian HS, Chen PS, Qu Z (2010) Early afterdepolarizations and cardiac arrhythmias. Heart Rhythm 7:1891–1899
4. Keating MT, Sanguinetti MC (2001) Molecular and cellular mechanisms of cardiac arrhythmias. Cell 104:569–580
5. Liu GX, Choi BR, Ziv O, Li W, de Lange E, Qu Z et al (2012) Differential conditions for early after-depolarizations and triggered activity in cardiomyocytes derived from transgenic LQT1 and LQT2 rabbits. J Physiol 590:1171–1180
6. Antzelevitch C, Sicouri S (1994) Clinical relevance of cardiac arrhythmias generated by afterdepolarizations. Role of M cells in the generation of U waves, triggered activity and torsade de pointes. J Am Coll Cardiol 23:259–277

7. Viswanathan PC, Rudy Y (1999) Pause induced early afterdepolarizations in the long QT syndrome: a simulation study. Cardiovasc Res 42:530–542
8. Carlsson L, Abrahamsson C, Andersson B, Duker G, Schiller-Lindhardt G (1993) Proarrhythmic effects of class III agent almokalant: importance of infusion rate. QT dispersion and early after depolarizations. Cardiovasc Res 27:2186–2193
9. Burashnikov A, Antzelevitch C (1998) Acceleration-induced action potential prolongation and early afterdepolarizations. J Cardiovasc Electrophysiol 9:934–948
10. El-Sherif N, Caref FB, Yin H, Restivo M (1996) The electrophysiological mechanism of ventricular arrhythmias in the long QT syndrome tri-dimensional mapping of activation and recovery patterns. Circ Res 79:474–492
11. Surawicz B (1989) Electrophysiological substrate for Torsade de pointes: dispersion of refractoriness or early afterdepolarizations. J Am Coll Cardiol 14:172–184
12. Verduyn SC, Vos MA, Van der Zande J, Van der Hulst FF, Wellens HJJ (1997) Role of interventricular dispersion of repolarization in acquired torsade-de-pointes arrhythmias: reversal by magnesium. Cardiovasc Res 34:453–463
13. Antzelevitch C, Shimizu W, Yan GX et al (1999) The M cell: its contribution to the ECG and to normal and abnormal electrical function of the heart. J Cardiovasc Electrophysiol 10:1124–1152
14. Brown AM, Rampe D (2000) Drug-induced long QT syndrome: is HERG the root of all evil? Pharm News 7:15–20
15. ICH Harmonized Tripartite Guideline (2005) The non-clinical evaluation of the potential for delayed ventricular repolarization (QT interval prolongation) by human pharmaceuticals S7B. Recommended for adoption at step 4 of the ICH process on 12 May 2005 by the ICH Steering Committee. ICH; (http://www.ich.org/fileadmin/Public_Web_Site/ICH_Products/Guidelines/Safety/S7B/Step4/S7B_Guideline.pdf)
16. ICH Harmonized Tripartite Guideline (2005) The clinical evaluation of QT/QTc Interval prolongation and proarrhythmic potential for non-antiarrhythmic drugs E14. Recommended for adoption at step 4 of the ICH process on 12 May 2005 by the ICH Steering Committee. ICH; (http://www.ich.org/fileadmin/Public_Web_Site/ICH_Products/Guidelines/Efficacy/E14/E14_Guideline.pdf)
17. Darpo B (2010) The thorough QT study four years after the implementation of the ICH E14 guidance. Br J Pharmacol 159:49–57
18. E14 Implementation Working Group ICH E14 Guideline (2012) The clinical evaluation of QT/QTc interval prolongation and proarrhythmic potential for non-antiarrhythmic drugs questions & answers (R1) (http://www.ich.org/fileadmin/Public_Web_Site/ICH_Products/Guidelines/Efficacy/E14/ E14_Q_As_R1_step4.pdf)
19. Sugiyama A, Hashimoto H, Nakamura Y, Fujita T, Kumagai Y (2014) QT/QTc study conducted in Japanese adult healthy subjects: a novel xanthine oxidase inhibitor topiroxostat was not associated with QT prolongation. J Clin Pharmacol 54(4):446–452
20. Giorgi MA, Bolaños R, Gonzalez CD, Di Girolamo G (2010) QT interval prolongation: preclinical and clinical testing arrhythmogenesis in drugs and regulatory implications. Curr Drug Saf 5:54–57
21. Rechanneling the cardiac proarrhythmia safety paradigm (2014) A meeting report from the Cardiac Safety Research Consortium. Am Heart J 167:292–300
22. Clements M, Thomas N (2014) High-throughput multi-parameter profiling of electrophysiological drug effects in human embryonic stem cell derived cardiomyocytes using multi-electrode arrays. Toxicol Sci 140(2):445–461
23. Pen S, Lacerda AE, Kirsch GE, Brown AM, Bruening-Wright A (2010) The action potential and comparative pharmacology of stem cell- derived human cardiomyocytes. J Pharmacol Toxicol Methods 61(3):277–286
24. Ma J et al (2011) High purity human-induced pluripotent stem cell-derived cardiomyocytes: electrophysiological properties of action potential and ionic currents. Am J Physiol Heart Circ Physiol 301:H2006–H2017
25. Sanguinetti MC, Changan J, Curran MC, Keating MT (1995) A mechanistic link between an inherited and an acquired cardiac arrhythmia: HERG encodes the Ikr potassium channel. Cell 81(2):299–307
26. Sanguinetti MC, Tristani- Firouzi M (2006) hERG potassium channels and cardiac arrhythmia. Nature 440:463–469

Chapter 4

Automated Patch Clamp Recordings of Human Stem Cell-Derived Cardiomyocytes

Alison Obergrussberger, Claudia Haarmann, Sonja Stölzle-Feix, Nadine Becker, Atsushi Ohtsuki, Andrea Brüggemann, Michael George, and Niels Fertig

Abstract

Patch clamp remains the gold standard for studying ion channel activity within cell membranes. Conventional patch clamp is notoriously low throughput and technically demanding making it an unsuitable technique for high-throughput screening (HTS). Automated patch clamp (APC) devices have done much to increase throughput and improve ease of use, particularly when using standard cell line cells such as HEK and CHO. In recent years, however, the use of human-induced pluripotent stem cells (hiPSCs) has become increasingly important, especially for safety screening in response to the Comprehensive In Vitro Proarrhythmia Assay (CiPA) initiative introduced in 2013. The goal of this initiative is to standardize assays, targets, and cell types. One part of the paradigm focuses on the use of APC and hiPSC cardiomyocytes. This chapter describes two automated patch clamp devices recording from up to 8 or 384 cells simultaneously using hiPSC cardiomyocytes. In the voltage clamp mode, voltage-gated Na^+ (Na_V), Ca^{2+} (Ca_V), and K^+ (K_V) channels could be recorded, and pharmacology using tetracaine, a Na_V channel blocker, is described. Additionally, action potentials in the current clamp mode were recorded, and examples are shown including the effect of nifedipine, a Ca_V channel blocker. Detailed methods are provided for cell culture and harvesting of hiPSCs for use on APC devices. Protocols are also provided for voltage and current clamp recordings on the Patchliner, and voltage clamp experiments on the SyncroPatch 384PE APC instruments.

Key words Automated patch clamp, Patchliner, SyncroPatch 384PE, hiPSC-derived cardiomyocytes, Voltage clamp, Current clamp, Ion channels, Voltage-gated Na^+, Voltage-gated K^+, Voltage-gated Ca^{2+}

1 Introduction

In the 1970s, Neher and Sakmann first described the patch clamp technique using fine glass pipettes to make giga-ohm seals [1]. More than 30 years later, patch clamp still remains the gold standard for obtaining information about ion channels. However, conventional patch clamp is technically demanding and unsuitable for high-throughput screening (HTS) experiments. Over the

Mike Clements and Liz Roquemore (eds.), *Stem Cell-Derived Models in Toxicology*, Methods in Pharmacology and Toxicology,
DOI 10.1007/978-1-4939-6661-5_4,

last decade or so, automated patch clamp (APC) devices have appeared on the market to facilitate ease of use and increase throughput of patch clamp experiments [2, 3]. Automation of the technique using a planar substrate has proven to be the most successful method and has seen the introduction of small semiautomated devices recording from a single cell at a time, for example, the Port-a-Patch (Nanion Technologies GmbH, Munich, Germany) [4, 5], through to fully automated robotic systems recording from multiple cells simultaneously including the Patchliner (Nanion Technologies GmbH) [6], QPatch (Biolin Scientific/Sophion A/S) [7, 8], Patch Express (Molecular Devices, LLC, Sunnyvale, CA) [9, 10], SyncroPatch 96 (Nanion Technologies GmbH) [11, 12], IonWorks (Molecular Devices, LLC) [13, 14], IonWorks Barracuda (Molecular Devices, LLC) [15, 16], Qube (Biolin Scientific/Sophion A/S), CytoPatch (Cytocentrics AG, Rostock, Germany) [17], IonFlux (Fluxion Biosciences, Inc., South San Francisco, CA) [18], and SyncroPatch 384PE (Nanion Technologies GmbH) [19, 20].

Human-induced pluripotent stem cells (hiPSCs) are receiving increasing interest as an alternative to acutely dissociated cells from animal tissue. For example, hiPSC cardiomyocytes (hiPSC-CMs) may provide a viable alternative to acutely isolated cardiac myocytes for safety testing of potential drug candidates. The CiPA initiative introduced in 2013 [21–23] is an ongoing international collaboration to reassess aspects of safety screening in terms of standardizing technology, cell types, and ion channel targets to gain a more complete safety profile of a drug candidate. One important aspect of this is the evaluation of hiPSC-CMs on APC platforms [21, 23]. This chapter describes the methods for hiPSC culture and harvesting for use on APC systems. The APC systems used were the Patchliner (Fig. 1a) and SyncroPatch 384PE (Fig. 1b–d). So far, hiPSC-CMs from a number of different providers have been used on the Patchliner and SyncroPatch 384PE including Cor.4U (Axiogenesis AG, Cologne, Germany) [20, 24], iCell Cardiomyocytes [11] and iCell Cardiomyocytes^2 (Cellular Dynamics International, Madison, WI) [20], Pluricytes (Pluriomics), and Cellectis (Takara, Clontech), among others, including patient-specific hiPSCs [25]. hiPSC neurons have also been used on the Patchliner [26]. Four examples of hiPSC-CMs have been used to compile this chapter: Cor.4U (Axiogenesis AG), Pluricytes (Pluriomics), iCell Cardiomyocytes (Cellular Dynamic International), and cells from Tokyo Women's Medical University (TWMU). The chapter goes on to give a detailed description of performing voltage and current clamp experiments on the Patchliner and voltage clamp experiments on the SyncroPatch 384PE.

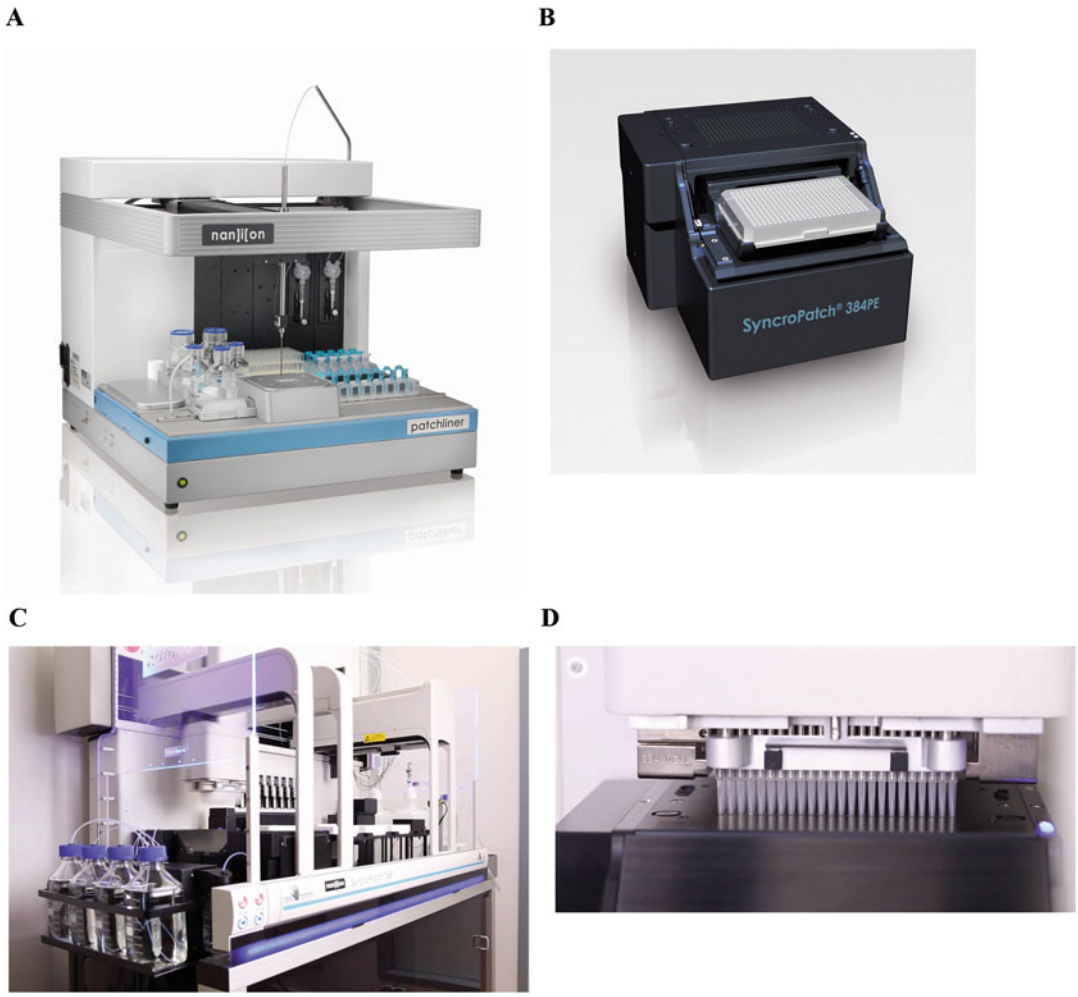

Fig. 1 The Patchliner and SyncroPatch 384PE instruments. (**a**) The Patchliner pipetting robot with borosilicate glass chip located inside the measure head. Computer and amplifiers required for running the system are not shown (reproduced with permission from [12]. (**b**) The SyncroPatch 384PE recording module with borosilicate glass chip located outside of the measure head. (**c**) The SyncroPatch 384PE located inside the Biomek FX^P (Beckman Coulter) during a recording. The glass bottles containing internal solution and the pipettor with 384 pipettes can be seen. (**d**) The 384 pipetting head of the Biomek FX^P shown positioned inside the chip while dispensing solution to the chip (**b**–**d**, reproduced with permission from [20])

2 Materials

2.1 hiPSC Cardiomyocyte Culture Reagents

1. hiPSC-CMs: Cor.4U (Axiogenesis AG), iCell Cardiomyocytes (Cellular Dynamics International), Pluricytes (Pluriomics), hiPSC-CMs from TWMU.
2. Manufacturer-specific culture medium.
3. Stock solution of fibronectin (1 mg/ml; sterile).

4. Phosphate-buffered saline (PBS) including Ca^{2+} and Mg^{2+} (Dulbecco's PBS, Gibco, cat. no. 14040-166; Ca^{2+}/Mg^{2+} not stated).

2.2 hiPSC Cardiomyocyte Harvesting Reagents

1. Washing buffer: PBS without Ca^{2+}/Mg^{2+} (Dulbecco's PBS, Gibco, cat. no. 14190-094), 2 mM EDTA.
2. Detachment enzyme: TrypLE (Invitrogen, 1x, cat. no. 12605-010) or Dispase (50 U/ml, Corning, cat. no. 354235).
3. Manufacturer-specific culture medium.
4. Calcium-free Hank's balanced salt solution (HBSS; Gibco, cat. no. 14175-053) with 2 mM $MgCl_2$ added.

2.3 Planar Patch Clamp Electrophysiology Using the Patchliner

1. Patchliner recording station (Nanion Technologies GmbH).
2. 2× EPC10 Quadro amplifiers (HEKA Elektronik).
3. NPC®-16 chips, resistance 2–3.5 MΩ (Nanion Technologies GmbH).
4. PatchControlHT software (Nanion Technologies GmbH).
5. PatchMaster software (HEKA Elektronik).
6. Igor software (WaveMetrics).
7. Internal K^+ solution: 60 mM KF, 50 mM KCl, 10 mM NaCl, 2 mM $MgCl_2$, 20 mM EGTA, 10 mM HEPES, pH 7.2 (sterile filtered).
8. External buffer: 140 mM NaCl, 4 mM KCl, 2 mM $CaCl_2$, 1 mM $MgCl_2$, 10 mM HEPES, pH 7.4 (sterile filtered).
9. High Ca^{2+} solution: 120 mM NaCl, 3 mM KCl, 5 mM $MgCl_2$, 10 mM $CaCl_2$, 10 mM HEPES (Na^+-salt), pH 7.4 (sterile filtered).
10. Tetracaine stock: 10 mM stock solution in external buffer.
11. Nifedipine stock: 10 mM stock solution in DMSO (*see* **Note 1**).

2.4 Planar Patch Clamp Electrophysiology Using the SyncroPatch 384PE

1. SyncroPatch 384PE recording module (Nanion Technologies GmbH) including digital 384 channel amplifier (Tecella).
2. Biomek FX^P pipetting robot (Beckman Coulter GmbH, Krefeld, Germany)
3. NPC®-384 chips, resistance 3.5–4.5 MΩ (Nanion Technologies GmbH).
4. PatchControl 384 software (Nanion Technologies GmbH).
5. DataControl 384 software (Nanion Technologies GmbH).
6. Internal K^+ solution: 120 mM KF, 20 mM KCl, 10 mM NaCl, 5 mM EGTA, 10 mM HEPES, pH 7.2 (sterile filtered). Freshly added just before the measurements: 2 mM Mg-EDTA, 25 μM escin, and 1 mM Na-ATP.

7. External buffer: 140 mM NaCl 4 mM KCl, 2 mM $CaCl_2$, 1 mM $MgCl_2$, 10 mM HEPES, pH 7.4 (sterile filtered).
8. Reference buffer: 60 mM N-methyl-d-glucamine (NMDG), 80 mM NaCl, 4 mM KCl, 2 mM $CaCl_2$, 1 mM $MgCl_2$, 5 mM glucose, 10 mM HEPES (Na^+-salt), pH 7.4 (sterile filtered).
9. High Ca^{2+} solution: 60 mM NMDG, 70 mM NaCl, 3 mM KCl, 5 mM $MgCl_2$, 10 mM $CaCl_2$, 10 mM HEPES (Na^+-salt), pH 7.4 (sterile filtered).
10. Nifedipine stock: 10 mM stock solution in DMSO (*see* **Note 1**).

3 Methods

hiPSC-CMs are typically received from the manufacturer as frozen aliquots, for example, iCell Cardiomyocytes (Cellular Dynamics International) and Pluricytes (Pluriomics), or as live cultures, for example, Cor.4U (Axiogenesis AG). The cardiomyocytes are typically used 4–10 days after thawing (sometimes up to 28 days post-thaw) to allow formation of a beating network of cells or 4–14 days following arrival as live cultures to allow recovery of the cells after transport. For planar patch clamp recordings, cells must be harvested into a cell suspension, and suction is used from underneath the patch clamp chip to attract a cell to the patch clamp aperture in order to get a good seal between the cell membrane and the borosilicate glass of the chip. Suction is used to rupture the patch of membrane blocking the patch clamp aperture to gain whole-cell access. The Patchliner is a fully automated patch clamp robot and the SyncroPatch 384PE a patch clamp module situated inside a state-of-the-art pipetting robot, e.g., the Biomek FX^P (Beckman Coulter). The positions of solutions and compounds are programmed within the software, and once cells, solutions, and the patch clamp chips are brought into the correct position, experiments proceed unattended, progressing through the steps programmed in the software. Importantly, however, particularly for current clamp recordings, the user is free to pause the running of the experiment at any time and can adjust the amplifier commands manually (e.g., start and stop recordings, change the holding potential, etc). A detailed description of the steps involved in cell culture, harvesting, and voltage clamp experiments using cell line cells on the Patchliner is provided in [12]. The relevant steps for hiPSC-CMs are provided in this section but may need to be adapted for the cell type used and the experiment performed (*see* **Notes 2** and **3**).

3.1 hiPSC Cardiomyocyte Culture

3.1.1 Defrosting Frozen Aliquots

1. Dilute the fibronectin stock (1 mg/ml) 1:100 with PBS (including Ca^{2+} and Mg^{2+}), e.g., 50 µl fibronectin in 5 ml PBS (including Ca^{2+} and Mg^{2+}). Gently resuspend the fibronectin solution using a pipette (*see* **Note 4**). Coat the required number of T25 culture flasks (or T75 flasks for SyncroPatch 384PE experiments)

by adding 5 ml of the diluted fibronectin solution per T25 flask and incubate at 37 °C for 1.5 h or overnight at 4 °C.

2. Frozen cells should be thawed as specified by the cell supplier. The common steps are briefly outlined here but should be adjusted according to the cell manufacturer's recommendations.
3. Put the vial of cells in a 37 °C water bath for exactly 4 min.
4. Remove the vial of cells from the water bath, spray with 70% ethanol, and place into the sterile cell culture laminar flow hood.
5. Gently transfer the hiPSC-CMs to a new sterile 50 ml centrifuge tube using a 1 ml pipette (*see* **Note 5**).
6. Rinse the empty hiPSC-CM vial with 1 ml of plating/thawing medium (at room temperature) to recover any residual cells from the vial. Add the 1 ml plating/thawing medium rinse from the cryovial dropwise over 90 s (i.e., one drop every 4–5 s) to the 50 ml centrifuge tube containing the hiPSC-CM cell suspension. Gently swirl the tube while adding the media to ensure that the solution mixes completely; this also minimizes osmotic shock to the thawed cells.
7. Slowly add 8 ml of plating/thawing medium (at room temperature) to the 50 ml centrifuge tube containing the hiPSC-CM and the 1 ml of media. Add the first 1 ml dropwise over 30–60 s. Then add the remaining volume over the next ~30 s. Gently swirl the centrifuge tube while adding the medium.
8. Gently mix the contents of the 50 ml centrifuge tube by inverting 2–3 times. Gentle mixing is critical to ensure maximum viability. Avoid vigorous shaking or vortexing of the cell suspension.
9. Carefully remove the fibronectin from the T25 flask made in Step 1 (*see* **Note 4**). Gently mix the cells and add 4–5 ml of the cell suspension to each T25 fibronectin-coated flask.
10. Put the flasks in the incubator overnight (37 °C). Exchange media 24 h after plating to remove dead cells.
11. Exchange media to maintenance media (supplied by the manufacturer) 48 h after plating (*see* **Note 6**).

3.1.2 Maintaining Live Cultures (Cor.4U)

1. Cardiomyocytes were transported in T25 or T75 culture flasks filled to the brim with media. Discard superfluous media and allow flasks to settle in the incubator for at least 4 h.
2. Check if the cardiomyocytes have resumed beating before harvesting them for experiments.

3.2 hiPSC Harvesting Procedure

1. Remove media and wash twice with PBS/EDTA.
2. Add PBS/EDTA and incubate for 5 min at room temperature.
3. After the 5 min incubation step, remove PBS/EDTA, add 3 ml of pre-warmed TrypLE (1x) or Dispase (50 U/ml), gently swirl

the solution around so that it is evenly distributed over the plate, and immediately remove most of the enzyme solution so that only a thin film of solution is left covering the cells.

4. Incubate 2–5 min at 37 °C until the cells start to float.
5. Tap the flask gently to dislodge the remaining cells.

3.2.1 Harvesting hiPSC-CMs for Use on the Patchliner

1. For use on the Patchliner, add 2 ml of the appropriate culture media (at 4 °C) and 2 ml calcium-free HBSS including 2 mM $MgCl_2$ (at 4 °C) to the T25 flask. The cell density at the end should be ideally >200,000 cells/ml. Do not pipette the cells up and down to avoid shear stress.
2. Gently transfer the cell suspension into a low-binding 1.5 ml Eppendorf tube.
3. Incubate for 20 min at 4 °C.
4. Gently pipette the cells up and down using a 1 ml pipette with disposable tip to remove clusters.
5. Leave the cells in the low-binding Eppendorf tube and put the tube in position C1 of the Patchliner; set the cell position to C1 in PatchControlHT (*see* **Note** 7). Pipette the cells up and down manually shortly before the robotic pipette adds the cells to the chip.

3.2.2 Harvesting hiPSC-CMs for Use on the SyncroPatch 384PE

1. For use on the SyncroPatch 384PE, add 8 ml of the appropriate culture media (at 4 °C) and 8 ml Ca^{2+}- free HBSS plus 2 mM $MgCl_2$ (at 4 °C) to the T75 flask. The cell density at the end should be ideally >200,000 cells/ml. Do not pipette the cells up and down to avoid shear stress.
2. Gently transfer the cell suspension into a one-well Teflon reservoir and place it on the Inheco shaker. Alternatively, a multi-well Teflon reservoir, e.g., 2-, 3-, or 6-well, can be used if more than one cell type is used during one experiment.
3. Incubate for 30 min at 10 °C.
4. Before the measurement gently pipette the cells up and down using a 1 ml pipette with disposable tips to remove clusters.

3.3 Planar Patch Clamp Electrophysiology Using the Patchliner

On the Patchliner, cells were recorded in voltage clamp and current clamp modes, allowing for ion channel pharmacology and pharmacology on action potentials, respectively.

3.3.1 Cell Capture and Sealing Procedure

1. Start up the system (computer, Patchliner, amplifiers) before harvesting the cells to allow the amplifiers to reach operating temperature, optimizing signal-to-noise ratio.
2. After launching PatchControlHT, which automatically starts up PatchMaster,loadthepre-programmedtree“CurrentClamp_1509.xml” from the PatchControlHT menu. Running the tree will

automatically load the associated PatchMaster files (pgf, onl, and pro files). Select the Edit mode to check the experiment steps and modify settings (e.g., compound positions, joblist, online analysis parameters) as appropriate.

3. Prepare compounds and solutions and place them in the appropriate rack. *See* Fig. 2a for an annotated picture of the Patchliner showing positions for internal and external solutions and compound plates. Figure 2b shows an example of the rack layout and compound dialog for tetracaine.
4. Place three chips (resistance 2–3.5 MΩ) on the chip wagon. Each chip has 16 channels (i.e., recording chambers); hence, three chips correspond to six runs on a Patchliner Octo or 12 runs on a Patchliner Quattro. Each channel is composed of the planar patch clamp borosilicate chip and individual microfluidics for internal and external recording solutions.
5. Place harvested cells in the low-binding Eppendorf tube and put the tube in position C1 of the Patchliner, set the cell position to C1. Pipette the cells up and down manually just before the robotic pipette adds the cells to the chip, ideally while the external recording solution is added (*see* **Note** 7).
6. Run the tree from the topmost position (Initialize Hardware folder). This will initialize the robot and wash the pipette several times. This also generates a new data file in PatchMaster and resets all amplifier and robot parameters.
7. Several dialog boxes will automatically appear. First, a checklist will appear for whether cells, compounds, and solutions are in the correct positions. All boxes must be clicked for the experiment to proceed. Next, a dialog box will appear showing the joblist. Here, compound positions, names, and voltage protocols are checked or selected if not done previously.
8. A dialog box will appear for the chip position. Once this is defined, the robot will start filling the chip with solutions at the selected chip position.
9. All eight internal positions of the chip are filled with internal solution automatically by the pipette using the internal solution defined in the Dispense Settings. This step occurs outside of the measure head.
10. Chip wagon moves into the measure head and measure head moves down.
11. External position of the chip is filled with external solution automatically by the pipette using the external solution defined in the Dispense Settings.
12. Negative pressure is applied briefly to the hole to ensure the hole is free. Chip resistance is measured in PatchMaster and the values appear in the PatchControlHT window. Atmospheric

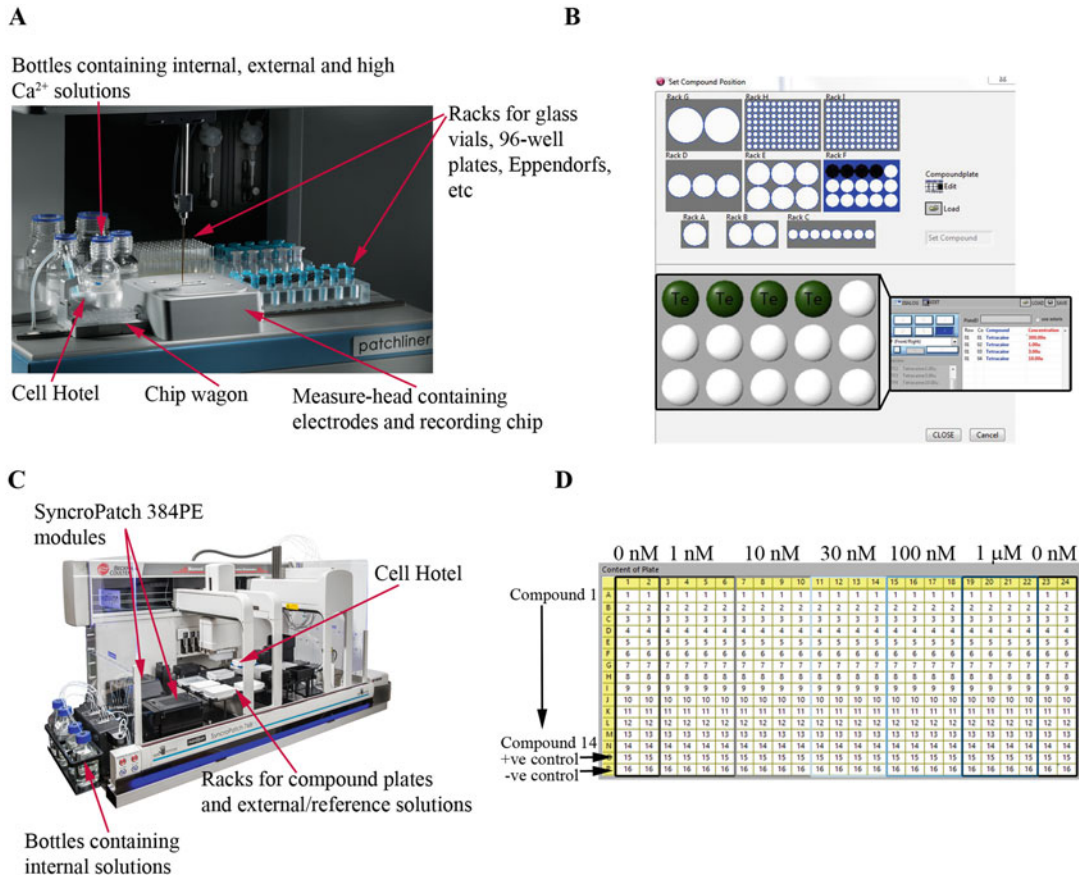

Fig. 2 Annotated picture of the Patchliner (**a**) and an example of the compound plate layout in PatchControlHT (**b**). Different plates can be selected in racks A – I). Rack A is the cell hotel; rack D usually contains internal, external, and high Ca^{2+} solutions. In this example, rack F contains the compound tetracaine in Eppendorfs. The inset shows the compound dialog where compound name and concentration are added. (**c**) Annotated picture of the SyncroPatch 384PE showing the positions of internal and external solutions and compound plates. (**d**) An example of a compound plate layout in PatchControl 384. For this example, generic compounds (named Compound 1 to Compound 14), positive control (+ve control), and negative control (–ve control) are present in rows A–P. Four columns contain the same concentration with four columns (1, 2, 23, and 24) containing no compound (control solution). In this example, the cells received one concentration of compound per well and the concentration-response curve calculated across the whole plate. If cumulative concentration-response curves were constructed, i.e., multiple concentrations of compound per cell, the compound plate setup would be different

pressure is applied. A slight negative holding potential (−20 mV) is applied for catching the cells (*see* **Note 8**).

13. The pipette picks up cells from position C1 for the first channel. Suction is applied to the first channel as the pipette adds the cells. Once a cell is captured as assessed by seal resistance crossing a threshold value (typically 10 MΩ), suction is reduced (*see* **Note 9**). The pipette repeats this for all other channels; cells are picked up individually for each channel of the chip.

14. Holding potential is reduced to –40 mV.
15. High Ca^{2+} solution is added to all eight channels automatically by the pipette (*see* **Note 10**).
16. Holding potential is reduced to –80 mV.
17. Suction is applied to the cells until the whole-cell configuration is reached.
18. Atmospheric pressure is applied to each cell; CSlow and RSeries are compensated automatically.
19. External solution is exchanged to normal external buffer.

3.3.2 Voltage-Gated Recordings of hiPSC-CMs on the Patchliner

1. An L-type Ca_V protocol is performed using the command "start L-type CaIV" in PatchControlHT (as part of the tree). *See* Fig. 3a for the voltage protocol, a recording from an example cell and the average IV from 24 iCell Cardiomyocytes (Cellular Dynamics International).
2. The command "start NaIV" is run in PatchControlHT (as part of the tree). PatchMaster runs the pgf NaIV. *See* Fig. 3b for the voltage protocol, a recording from an example cell and the average IV from 41 iCell Cardiomyocytes (Cellular Dynamics International).
3. Once the IV plots have been completed, PatchControlHT will automatically start the pharmacology protocol. The voltage protocol "NaPharm" is started. In this case, the voltage was stepped from the holding potential of –100 mV to 0 mV for 20 ms and then back to the holding potential. Sweep interval was 2 s. The online analysis "NaPharm" is run simultaneously during the recording, the peak amplitude is plotted against time, and the peak amplitude is automatically exported to an Excel spreadsheet in the correct format to load into Igor at a later stage for analysis.
4. The pipette of the Patchliner adds the concentrations of tetracaine defined in the joblist. The solutions are added in increasing concentrations. The pipette is washed in between each addition. In this case, the cells were incubated for approximately 120 s in each concentration. Incubation times will vary depending on how long the effect takes to reach steady state. In the case of compounds acting on Na_V channels, this tends to be relatively fast (within 60–120 s), whereas compounds acting on hERG can take a lot longer (up to 5 min).
5. Once all the concentrations of tetracaine have been added, an optional washout step where normal external buffer is added can also be integrated in the tree. If this has been integrated, the wash step will be performed now. Alternatively, a control blocker (a compound known to result in full block) can be added to serve as a standard for normalizing the data. Depending on the typical recording stability of a target, vehicle controls can be run

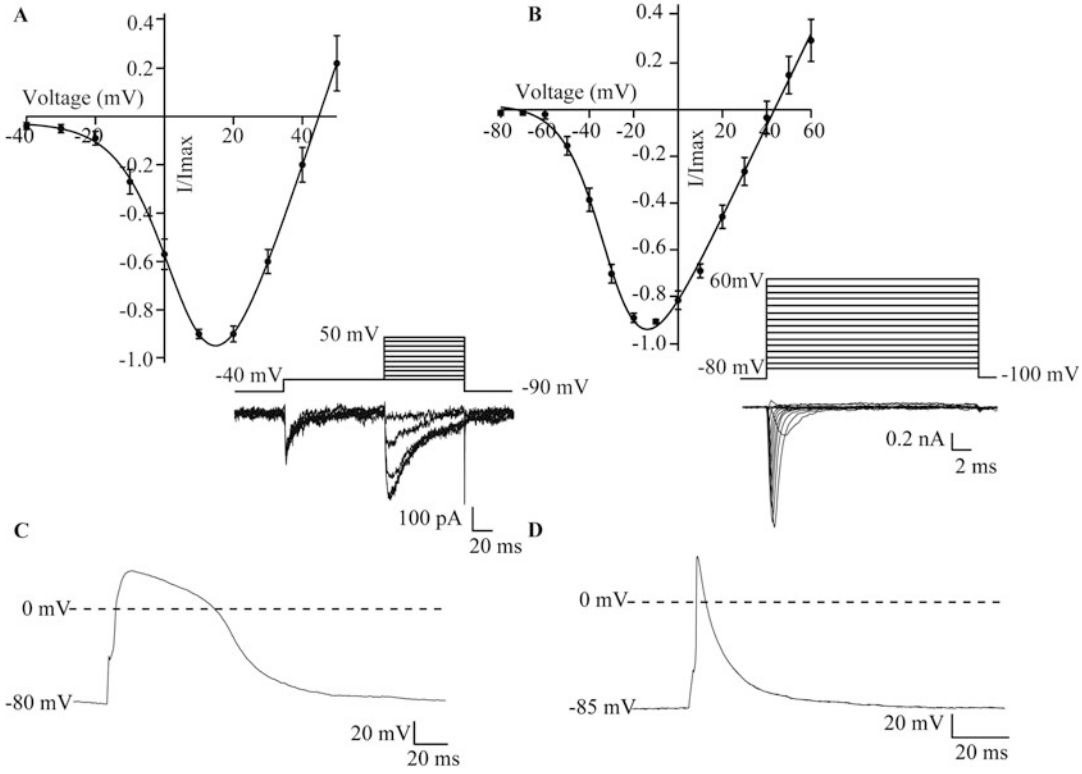

Fig. 3 Recordings in voltage and current clamp modes on the Patchliner. (**a**) Ca_V current-voltage plot for an average of 24 iCell Cardiomyocytes (Cellular Dynamics International) recorded on the Patchliner. The raw current traces from an example cell are shown in the inset. The voltage step protocol used to elicit the Ca_V current is also shown. An 80 ms pre-pulse to −40 mV for 100 ms was used to inactivate Na_V and T-type Ca_V channels followed by a second step to the test potential from −40 mV to 50 mV for 80 ms increasing in 10 mV increments. Holding potential was −90 mV and sweep interval was 5 s. The points were normalized to the peak current and shown are mean values ± SEM. A Boltzmann equation was fitted revealing a Vhalf of activation of 6.8 mV consistent with values found in the literature for the cardiac $Ca_V1.2$ channel [30, 31] using a 10–20 mM Ca^{2+} concentration as the charge carrier (*see* **Note 16**). (**b**) NalV plot for an average of 41 iCell Cardiomyocytes (Cellular Dynamics International) recorded on the Patchliner. The raw current traces from an example cell are shown in the inset. The voltage step protocol used to elicit the Na_V current is also shown. From a holding potential of −100 mV, the voltage was stepped to −80 mV for 20 ms and returned to the holding potential. The voltage was then increased by 10 mV with every sweep (sweep interval 1 s) up to 60 mV. The points were normalized to the peak current and shown are mean values ± SEM. A Boltzmann equation was fitted revealing a Vhalf of activation of −29 mV. (**c**) Action potentials elicited using a 1 ms current pulse to 650 pA for the cell shown in Panel A. Cell was held at a potential of −80 mV. When a mixture of Na_V and Ca_V channels were expressed, the action potentials tended to have an APD90 in the range of 50–100 ms, in the example shown approximately 70 ms. (**d**) Action potential elicited using a 1.5 ms current pulse to 480 pA for the cell shown in Panel B. Cell was held at a potential of −85 mV. When primarily Na_V was expressed in the cells, the action potentials tended to be shorter with an APD90 approximately 12 ms

in parallel (simultaneously on the same chip). This option is recommended when recording cell types/ion channels susceptible to desensitization or rundown. Linear rundown can be accounted for by the data analysis tools provided in Igor Pro.

6. The experiment is now finished (if the robot has been programmed to perform just one experiment); the chip wagon will move out of the recording chamber, and the pipette will be washed at the wash station (*see* **Note 11** for an estimation of time required for the experiment and, thus, throughput).

Data Analysis

1. Open Igor. Go to the "Patchliner" tab and choose "Load Experiment"—"Load single experiment." Browse the computer folders to find the relevant Excel file.
2. Choose the relevant analysis type from the drop-down menus; in this case the analysis should be set as "blocker."
3. Data will be loaded into Igor. Press "Display" in the Data Browser window, and the data will be displayed showing all successful concentration-response curves for each cell for that experiment. Press "Raw" to display the raw data traces and "Time" to display the time courses. Visually inspect data. If any cells look faulty, i.e., peak amplitude is very small (less than about 30 pA) or cannot be distinguished from noise, peak amplitude is positive (under the experimental conditions, the peak amplitude should be negative), or a spike in the data has been used as the peak amplitude by mistake, unclick the channel, and this cell will no longer be used in the analysis.
4. In the Data Browser window, press "Average result." The concentration-response curves for all active channels will be averaged and displayed. The average IC_{50} value ± SEM taken from the individual IC_{50} values is displayed. The IC_{50} value of the average plot is also displayed. *See* Fig. 4 for the concentration-response curve for an average of five iCell Cardiomyocytes (Cellular Dynamics International) generated using Igor and the raw traces from an example cell showing inhibition of the Na_V current by increasing concentrations of tetracaine. The IC_{50} of tetracaine was 2.9 ± 1.4 μM ($n = 5$) in good agreement with the value found in the literature for block of $Na_V1.5$ by tetracaine [14] and with $Na_V1.5$ overexpressed in HEK293 cells recorded on the SyncroPatch 384PE (unpublished observations).
5. Click "show summary" in the Data Browser window to generate a table of results showing average IC_{50} values for each of the compounds loaded into Igor. The data can be saved as an Igor experiment.

3.3.3 Current Clamp Recordings of hiPSC-CMs on the Patchliner

For the start of the experiment, please refer to Sect. 3.3.1.

1. Once the cells are in whole-cell configuration and have been washed with external recording solution, three different IV protocols are applied to specifically check for the presence of Na^+, Ca^{2+}, and K^+ currents. Note that the AP shape, especially the AP duration (APD), can strongly vary depending on the

expression of these ion channels (*see* Fig. 3c, d, and **Note 9**). Online analysis parameters such as AP amplitude, action potential duration at 50% of repolarization (APD50), and action potential duration at 90% of repolarization (APD90) can be measured and monitored. Depending on the experiment, APs with a short APD90, e.g., as shown in Fig. 3d, can be acceptable, e.g., for compounds expected to block Na_V channels. We implement no general selection criteria based on APD50 or APD90; APs are included or excluded from the analysis depending on the experiment performed.

2. After the IVs in the voltage clamp mode, all channels are switched to the current clamp mode without any current injection, i.e., without manipulation of the cells' native resting potential, by setting the gentle switch function to inactive. A continuous sweep is recorded to document the resting membrane potentials.
3. To make use of the gentle switch function, i.e., the amplifiers' ability to determine the current that needs to be injected in the current clamp mode to achieve a predefined membrane potential, all channels need to be switched back to voltage clamp. Here, a holding potential of –80 mV is set, then the gentle

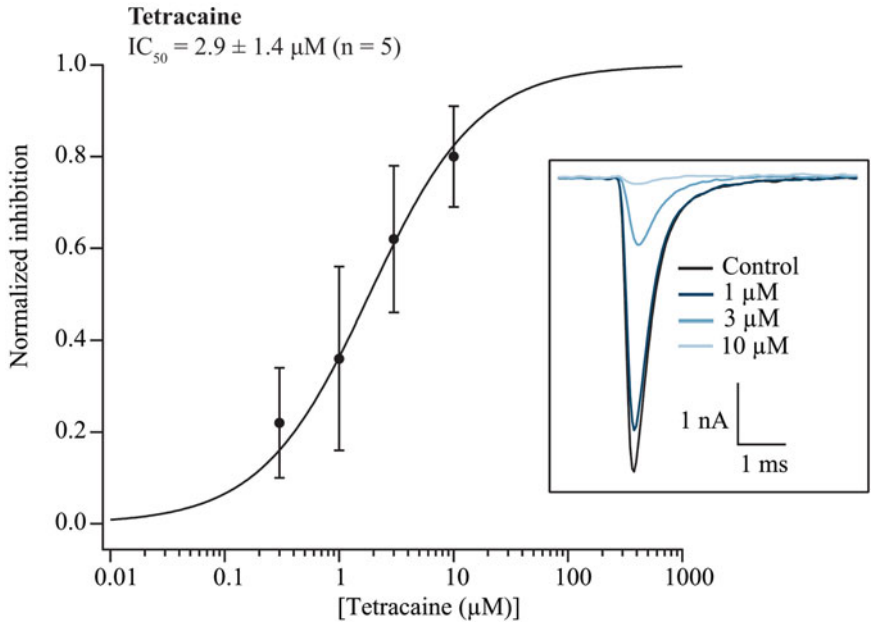

Fig. 4 Concentration-dependent inhibition of $Na_V1.5$ by tetracaine expressed in iCell Cardiomyocytes (Cellular Dynamics International). Shown is the concentration-response curve for tetracaine for an average of five cells. The raw traces from an example cell in control solution (*black*) and in increasing concentrations of tetracaine (1, 3, and 10 µM) are shown in blue. The IC_{50} calculated from the average of the five individual concentration-response curves was 2.9 ± 1.4 µM ($n = 5$) in good agreement with the literature value for $Na_V1.5$ expressed in HEK cells [14]

switch function is set to active, and the amplifiers are switched back to the current clamp mode. Now each cell is supplied with the current injection required to maintain a membrane potential of –80 mV. hiPSC-CMs have a higher resting membrane potential than adult ventricular myocytes, in part due to lower IK1 channel expression [27]. Consequently, to fully activate Na^+ channels, current is injected to lower the resting membrane potential to –80 mV.

4. Ideally, the tree should be paused here, and the experimenter should check manually whether the membrane potential is adjusted correctly to –80 mV and, if not, adjust the current injection as appropriate.
5. Next, the folder "Find threshold to evoke APs" is run to determine and set individual stimulation intensities for each cell (*see* **Note 12**).
6. Once stable conditions are established, the action potential pharmacology can be performed by running the folder "Start AP Pharm Recording." Here, APs are elicited every 20 s, while first a wash, then the defined concentrations of a compound, and then two washes to check for washout are applied. During these recordings, all key AP features (APD90, upstroke slope, overshoot, amplitude, etc.) are analyzed, recorded with the *.dat file and written to a Microsoft Excel file.
7. Compounds can be added in the same way as described for voltage clamp experiments in Sect. 3.3.2 and data analysis performed as described in section "Data Analysis". An example of the effect of the Ca_V channel inhibitor, nifedipine, on the action potentials recorded from an iCell Cardiomyocyte (Cellular Dynamics International) is shown in Fig. 5.

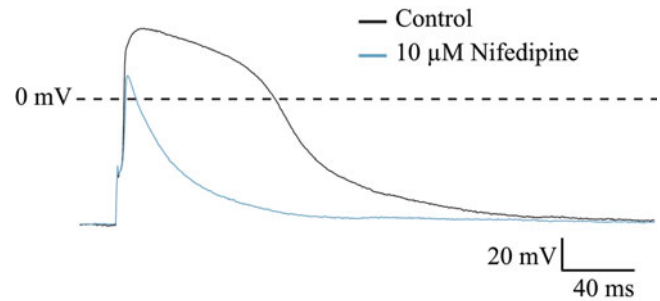

Fig. 5 Effect of nifedipine on action potentials recorded from iCell Cardiomyocytes (Cellular Dynamics International). Shown is an example action potential in control conditions (*black*) and in the presence of 10 µM nifedipine (*blue*). Nifedipine caused a drastic shortening of the action potential and a reduction of action potential amplitude consistent with a block of the $Ca_V1.2$ channel

3.4 Planar Patch Clamp Electrophysiology Using the SyncroPatch 384PE

3.4.1 General Experimental Setup

1. Turn on the system. This involves pushing all three buttons sequentially (in any order) integrated in the front of the machine for the robot itself, the Biomek computer and the Nanion computer.
2. On the Nanion computer, open the remote desktop connection to the Biomek computer so you can control the whole system with just one set of mouse and keyboard.
3. Double click on the PatchControl 384 icon on the desktop of the Nanion computer and wait until the software launches.
4. Double click on the Biomek software icon on the desktop of the Biomek computer. The software in which the experiments are programmed appears.
5. Home all axes (i.e., initialize the robot).
6. Place a used chip in the chip tray and put all tubes for internal solution intake (on the left-hand side of the SyncroPatch 384PE) into a bottle of distilled water. Run System Flush in PatchControl 384 from the menu bar under Manual Control.
7. Make any changes to the method, adding functions by drag and drop.
8. Open the Compound Dialog (Setup->Compound) and edit the compound positions.
9. Prepare solutions and place them at the appropriate positions, i.e., internal solutions in bottles on the left-hand side and external solution and compounds in the appropriate rack. *See* Fig. 2c for an annotated picture of the plate deck of the Biomek FX^P and an example of the compound plate dialog in PatchControl 384 (Fig. 2d).
10. Place tube 1 for the internal solution intake into the bottle containing the internal recording solution.
11. Prepare cells, place the cells in a one-well Teflon reservoir (or multi-well Teflon reservoir if more than one cell type is used in the experiment) and place on the Inheco shaker.
12. Start cell hotel. Do not set the temperature below 10 °C
13. Place a new chip in the chip tray.
14. Press play.

3.4.2 Cell Capture and Sealing Procedure

1. The chip is first filled with external solution. The pipette picks up External buffer for all 384 wells and fills the external wells of the chip (*see* **Note 13**).
2. The chip is then filled with Internal K^+ solution. This step occurs independently of the pipette as the internal solution is filled via tubing lines underneath the chip. If different internal solutions are used to fill the chip or will be used in the experiment if performing an internal exchange, these solutions need

to be in the correct positions and correctly programmed in PatchControl 384.

3. In the acquisition window of PatchControl 384, the 384 wells show the square current pulse and the corresponding resistance of the aperture. The background of each well is color-coded; the thresholds are set in the method but can also be changed manually by using the slider bar. At the beginning of an experiment, thresholds are set by default: light blue indicates resistance <3 MΩ, blue indicates resistance 3–6 MΩ, and green indicates resistance >6 MΩ.
4. Holding potential is reduced to −20 mV.
5. The pipette moves to the cell position, pipettes the cells up and down once, and then picks up the cell suspension for all 384 channels. The cells are added, and simultaneously suction is applied to attract a cell to each aperture (default value = −150 mBar). The pressure is changed back to −50 mBar at the end of the cell catch. *See* **Note 14**.
6. Holding potential is reduced to −40 mV.
7. High Ca^{2+} solution is added by the pipette to all 384 wells (*see* **Note 10**). This is directly followed by removal of solution by the pipettes so each well contains 40 µl again (*see* **Note 15**).
8. Voltage is reduced to −120 mV.
9. Atmospheric pressure is applied to each cell; CSlow and RSeries are compensated automatically.
10. Solution is exchanged for Reference solution (*see* **Note 15**). In the experiments presented here, the wells were then washed three times with Reference solution. The number of times that the cells are washed with reference solution depends on the cells and ion channel used for the experiment. At least one wash with reference solution is required for correct analysis of the data and we recommend, where possible, to perform three washes with reference solution to ensure steady state current amplitude for the control recording.

3.4.3 Voltage-Gated Recordings of hiPSC-CMs on the SyncroPatch 384PE

1. Voltage step protocol for Na^+ and Ca^{2+} activation curve (shown in Fig. 6) is run automatically. The online analysis is performed simultaneously, and the user can toggle between the raw data traces and online analysis tab within the recording software. *See* Fig. 7 for an annotated screenshot of the PatchControl 384 software during recording of a NaIV using Pluricytes (Pluriomics) and Fig. 8 for examples of raw traces and average IV curves for Na^+, Ca^{2+}, and K^+ currents recorded from Pluricytes. Figure 9 shows a screenshot of the PatchControl 384 software during a recording of a NaIV using Cor.4U (Axiogenesis AG). Figure 10 shows examples of raw traces and

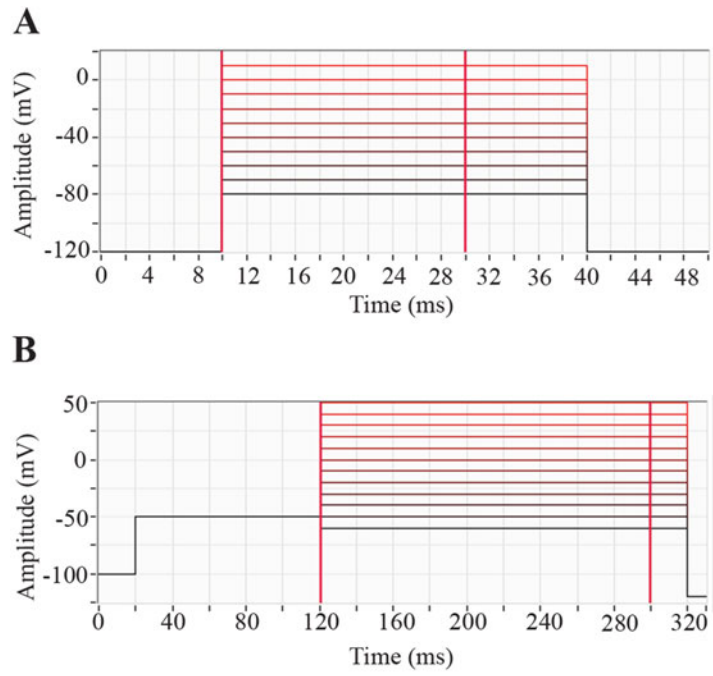

Fig. 6 Voltage protocols used on the SyncroPatch 384PE to record Na_V currents (**a**) and Ca_V currents (**b**)

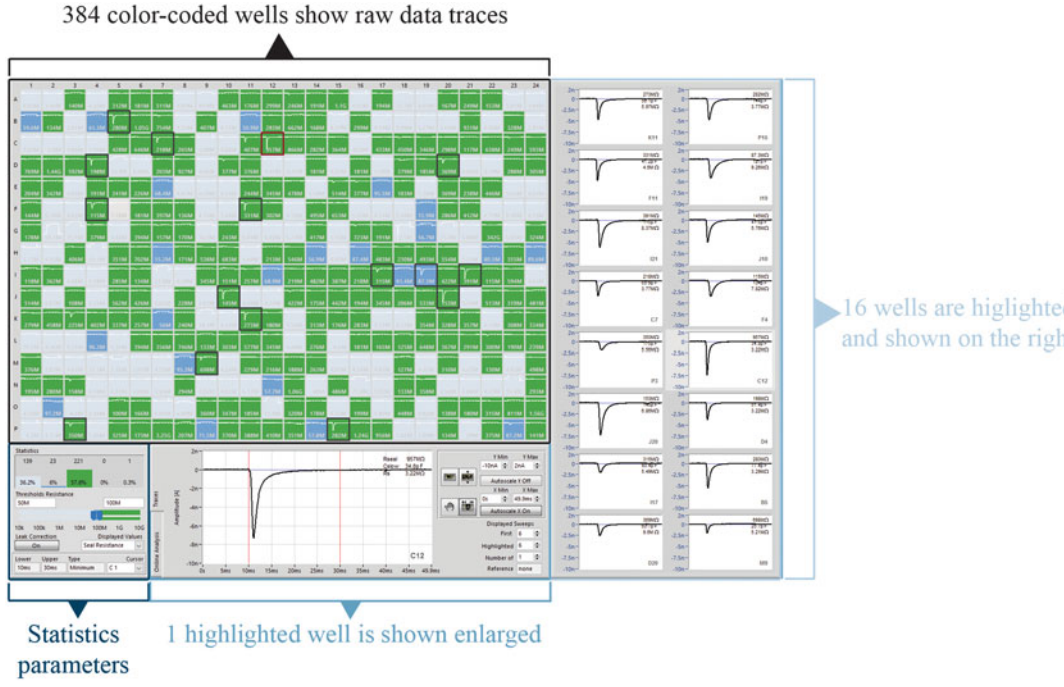

Fig. 7 Screenshot showing the PatchControl 384 software during a recording of Pluricytes (Pluriomics). The screenshot is annotated to show the different aspects including the 384 color-coded wells, statistics box, and highlighted traces which are shown enlarged. Shown are Na_V currents elicited using the voltage protocol shown in Fig. 6a

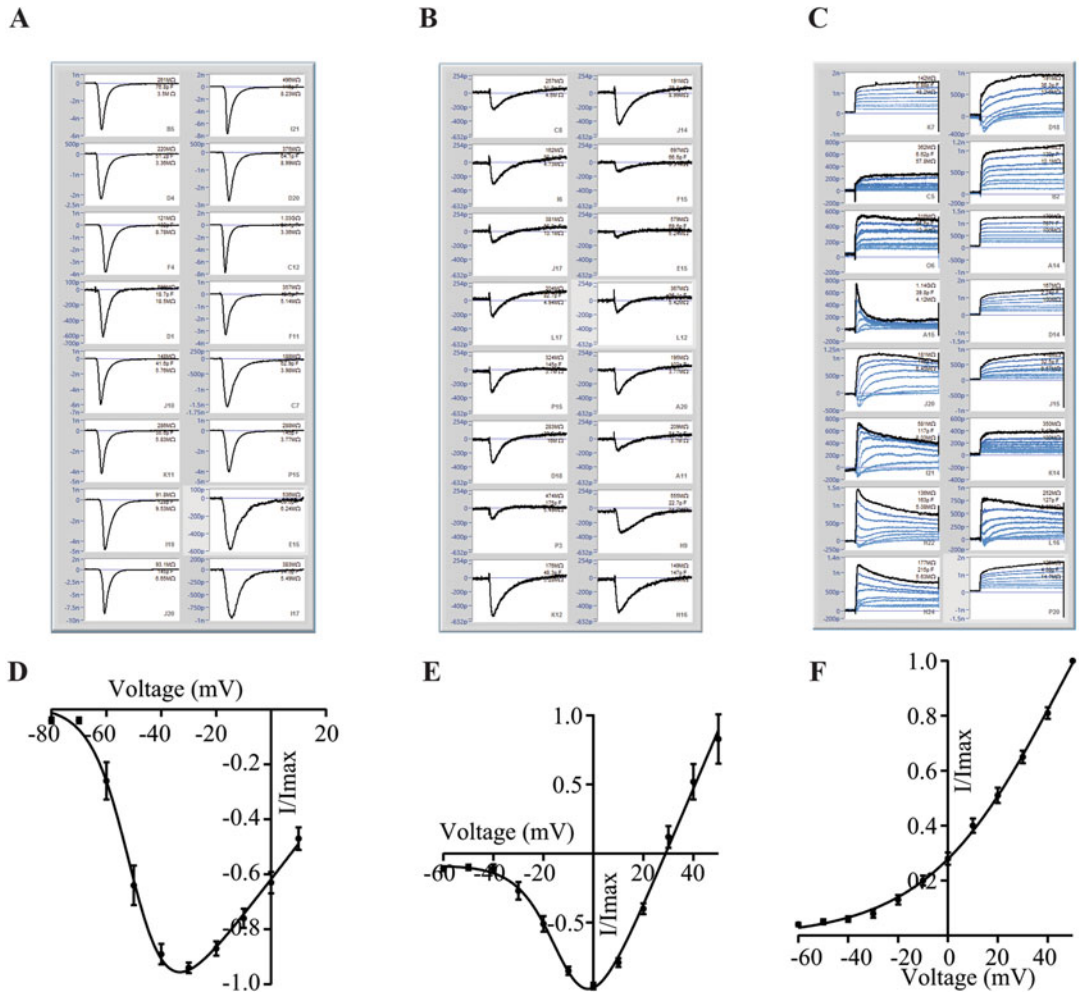

Fig. 8 (**a**) Sixteen examples of Na_V currents from Pluricytes (Pluriomics). The current response to a voltage step from −100 to −50 mV is shown. (**b**) Sixteen examples of Ca_V currents from Pluricytes (Pluriomics). The voltage step used was from −100 to −50 mV (to inactivate Na_V channels) and then to −10 mV. The current response to the step from −50 to −10 mV is shown. (**c**) Sixteen examples of the current responses to a voltage step protocol are shown. In some examples K_V, Na_V, and Ca_V currents are seen. (**d**) IV curve for Na_V for an average of 16 Pluricytes. Each point is average ± SEM. A Boltzmann curve, fitted to the averaged data, revealed a Vhalf of activation of −50 mV in good agreement with the literature [32]. (**e**) IV curve for Ca_V for an average of 16 Pluricytes (Pluriomics). A Boltzmann curve, fitted to the averaged data, revealed a Vhalf of activation of −9.8 mV, in good agreement to values found in the literature for the cardiac $Ca_V1.2$ channel [30, 31]. (**f**) IV curve for K_V for an average of 17 Pluricytes (Pluriomics)

average IV curves of Na^+ and K^+ currents recorded from Cor.4U. *See* **Notes 14** and **16**.

2. When testing unknown compounds we recommend always to include positive and negative controls on each plate to ensure that the cells and the system perform as expected. Also reference

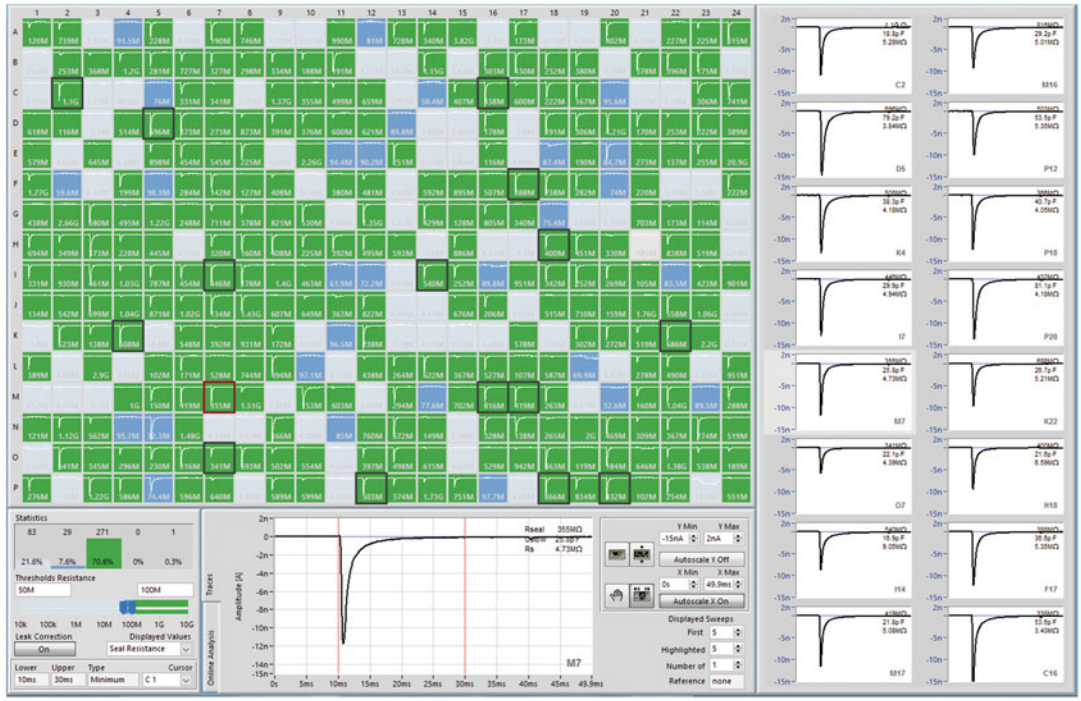

Fig. 9 Screenshot showing the PatchControl 384 software during a recording of Cor.4U (Axiogenesis AG). Shown are Na_V currents elicited using the voltage protocol shown in Fig. 6a

washes at the beginning of the recording for each cell to establish stable baselines. The system allows automated quality control (QC) of the measurements. These can be included as deemed appropriate by the user. Common QCs at the end of the reference period would be performed on the current size and seal and at the end of the experiments on the seal. Signal rundown is not automatically taken into account. *See* **Note 17** for an estimation of time required for the experiment and, thus, throughput.

3.4.4 Data Analysis: Concentration-Response Curve Analysis

1. Open DataControl 384 by double clicking on the icon on the desktop of the computer.
2. Select the appropriate recording in the data tree.
3. Click onto the CRC Results tab.
4. Choose "Start with Dialog" and adjust the settings in the upcoming window to: Analysis Type (Activator), Normalization (Common Reference), First Fit (C1), OA Point Selection Rule (Mean End 1), and Parameters to Fit (Only Minimum, Fixed to 0). Press Apply and Close.
5. On the CRC Results tab, the analyzed data for each individual cell and the average over all cells are shown. *See* Fig. 11 for

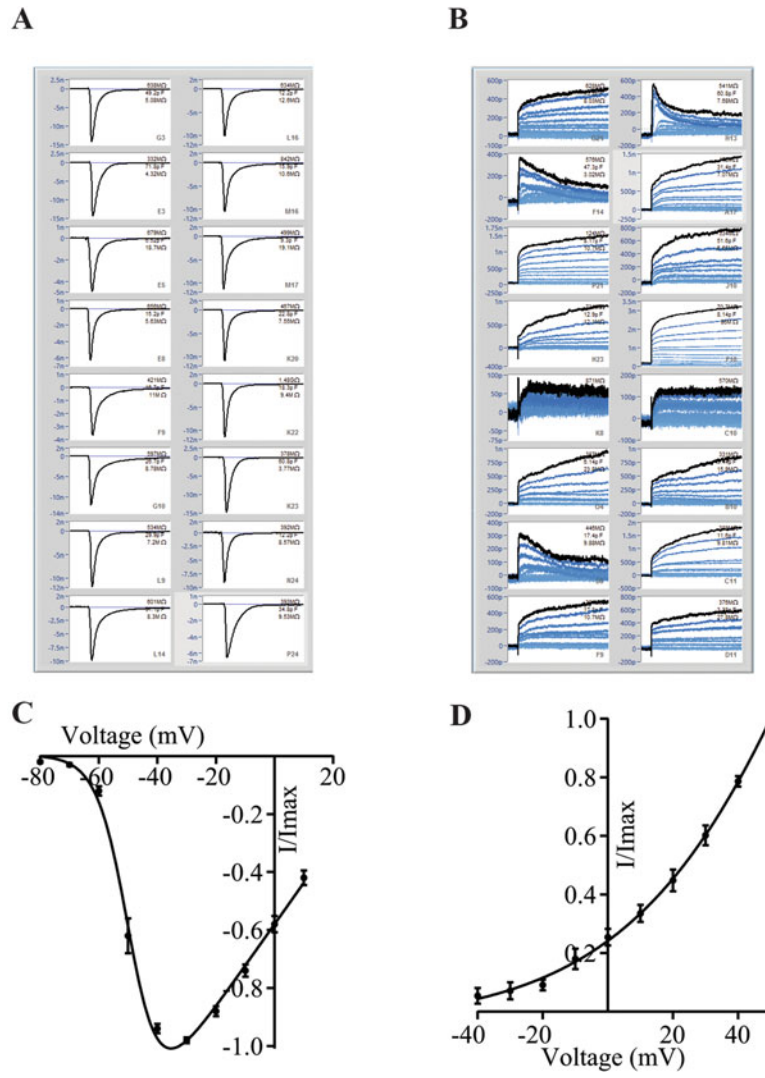

Fig. 10 (**a**) Sixteen examples of Na_V currents from Cor.4U. The current response to a voltage step from −100 to −50 mV is shown. (**b**) Sixteen examples of the current responses to a voltage multistep protocol are shown. The outward K_V-mediated currents can be seen. (**c**) IV curve for Na_V for an average of 16 Cor.4U cells (Axiogenesis AG). Each point is average ± SEM. A Boltzmann curve, fitted to the averaged data, revealed a Vhalf of activation of −49 mV in good agreement with the literature [32]. (**d**) IV curve for K_V for an average of 15 Cor.4U cells (Axiogenesis AG)

concentration-response curve for nifedipine block of the Ca_V currently recorded from TWMU stem cell-derived cardiomyocytes. The IC_{50} of 84.1 nM calculated from the average concentration-response curve of 11 cells is in good agreement with the literature value for block of nifedipine on guinea pig myocytes [28].

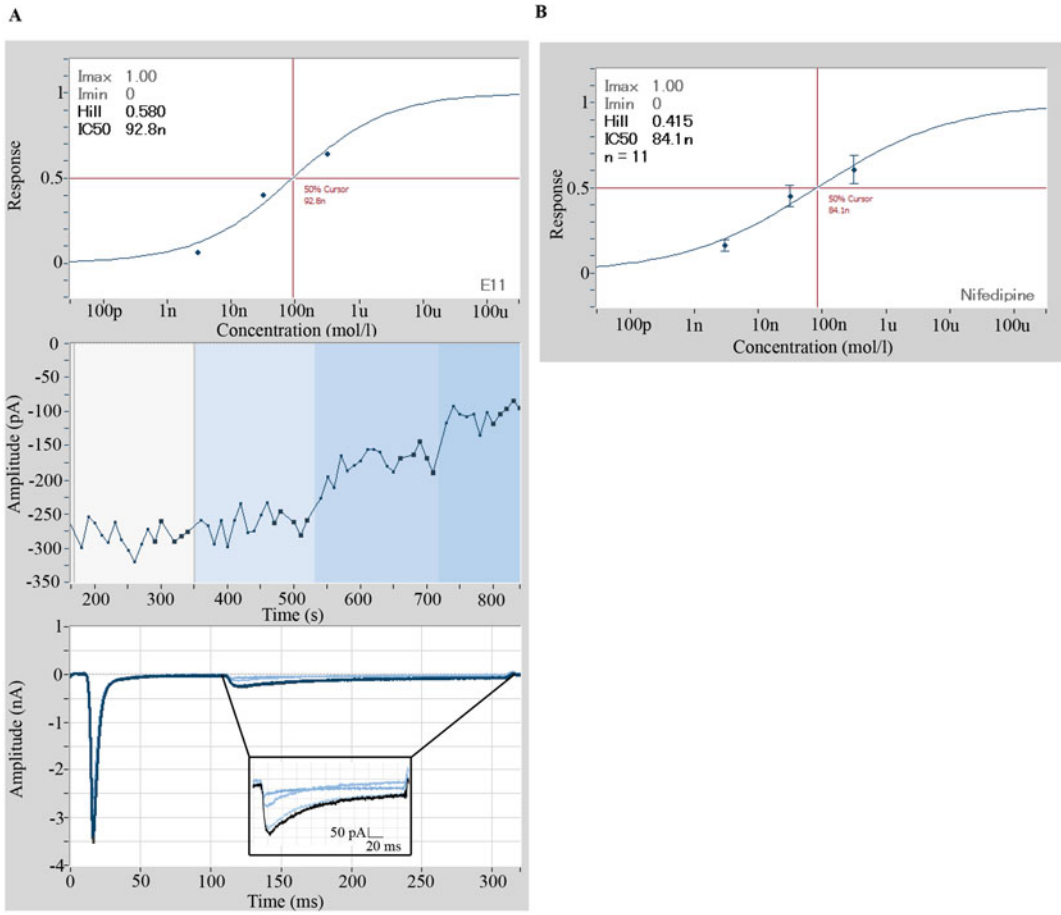

Fig. 11 Screenshot of the DataControl software showing block of Ca_V current recorded from TWMU stem cell-derived cardiomyocytes by nifedipine. (**a**) An example of the raw data traces (*bottom*), time course of the experiment in increasing concentrations of nifedipine (white = control solution, darkening blue = increasing concentrations of nifedipine), and concentration-response curve (*top*). (**b**) Concentration-response curve for nifedipine for an average of 11 cells. A Hill equation was fitted to the averaged points, the $IC_{50} = 84.1$ nM, in good agreement with the literature value for nifedipine block of Ca_V recorded from guinea pig myocytes [28]

4 Notes

1. Nifedipine is light sensitive and should be stored in a vessel which protects it from light.
2. The capture rate and ultimately thereby the success rate of an experiment strongly depend on good-quality cells; hence, it is advisable to optimize the harvesting protocol for each channel and cell type. Adapting the recording solutions to optimize current and seal stability also greatly contributes to high success rates.

3. Typical problems associated with automated patch clamp robots are that the cell catch does not perform sufficiently. Reasons for this tend to be the same on both systems, the Patchliner and the SyncroPatch 384PE. (1) The solutions (especially problems with the internal solution) are often a cause of this. Also (2) insufficient cell density or quality as well as (3) insufficient pipetting (e.g., empty system water in the case of the Patchliner) could be causes. Also, cells might not seal or seals do not last long enough for the experiment. This might be caused by cell quality or inappropriate solutions. As previously mentioned (*see* **Note 2**), optimization of the cell quality is one significant factor. Also smaller patch aperture sizes could also be chosen for the experiment.
4. Fibronectin should be pipetted very gently as it is sensitive to shear stress. Additionally, fibronectin in the culture flasks should not be allowed to dry out at any point.
5. The use of a 50 ml centrifuge tube facilitates mixing of cells with plating/thawing media to minimize osmotic shock and increase cardiomyocyte viability. Precise timing is critical for maximizing viable cell recovery; the cells should not spend more than a few minutes thawed in the vial before adding plating media. Avoid repeated pipetting of the thawed hiPSC-CM cell suspension.
6. In our hands, cells started to beat within 24 h after plating; however, several days were required for synchronous beating of the monolayer.
7. When using standard cell lines such as HEK or CHO, cells can be placed in the cell hotel of the Patchliner where the cells are periodically (every 30 s or so) pipetted up and down by the robot using a 1 ml disposable pipette. In our experience, the success rate for cell capture of the hiPSC-CMs is better when the cells remain in the low-binding Eppendorf and the cell hotel is not used. The cells should be pipetted up and down manually just before the robot adds the cells to the chip, ideally while the external recording solution is added to the chip.
8. Applying negative holding potential improves the success rate, particularly if the cells spontaneously enter the whole-cell configuration, i.e., the patch of membrane blocking the patch clamp aperture is ruptured allowing physical and electrical access to the whole of the cell, when captured to the chip.
9. The expected success rate for cardiomyocytes is considerably lower than for standard cell lines such as HEK or CHO. Seal resistances >100 MΩ can be achieved in ~50% of the cells; however, ideally, GΩ seals are required for good AP recordings without APD90 rundown—L-type Ca^{2+} channels, which greatly contribute to the AP duration and are particularly

susceptible to current rundown if the seals are, or become, leaky. For voltage clamp experiments, seal resistances >100 MΩ are acceptable as long as they are stable throughout the recording protocol. Of the cells that were captured with seal resistance >100 MΩ, approximately 80% expressed Na^+ currents (>−100 pA, mean peak amplitude −10 nA) and approximately 50% Ca^{2+} currents (>−50 pA, mean peak amplitude −169 pA).

10. The combination of F^- in the internal solution and Ca^{2+} in the external solutions increases and stabilizes the seal resistance. The mechanism appears to relate to the very low solubility of CaF_2 although this is not yet fully understood.
11. A typical Patchliner experiment usually requires less than 1 h of preparation time, involving setting up recording protocols, preparing compounds, and dissociating the cells. A standard experiment runs for 15–30 min, recording eight cells in parallel. With an established assay, 5–10 compounds can be tested in 1 day.
12. For cells with strongly shifting resting potentials due to changes in seal or ion channel activity, the stimulus may not be appropriate for the entire duration of the pharmacology experiment. In those cases, the experimenter may choose to observe the cells' responses over a few seconds to a minute and adjust the stimulation intensity and/or current injection for the membrane potential as appropriate.
13. The external buffer (NaCl) is used to fill the chip; the solution is then exchanged to the reference buffer containing NMDG once the cells are captured. If the reference buffer (NMDG) is used to fill the chip, cells will not be caught. The reason for this is unknown.
14. As noted for the Patchliner (*see* **Note 9**) the seal rate for hiPSC-CMs is considerably less than for cell lines such as HEK or CHO. The percentage of cells with a seal resistance (RSeal) >100 MΩ for the Pluricytes was 57.6% and for the Cor.4U > 70.6%. Ion channel expression also differs between cell types. For the Pluricytes, of the cells that were captured with a RSeal > 100 MΩ (57.6%; 221 cells), in 96% (212 cells) of cells a K_V could be measured (mean peak amplitude 763 pA), in 19% (40 cells) a Ca_V could be measured (mean peak amplitude −212 pA), and in 14% (30 cells) a Na_V could be measured (mean peak amplitude −2 nA). For the Cor.4U, of the cells that were captured with RSeal > 100 MΩ (70.6%; 271 cells), in 95% (257 cells) a K_V could be measured (mean peak amplitude 494 pA), in 8% (23 cells) a Ca_V could be measured (mean peak amplitude −183 pA), and in 88% (239 cells) a Na_V could be measured (mean peak amplitude −8 nA). In the Cor.4U cells, the Na_V current was very large (*see* Figs. 9 and 10), often > −10 nA.

15. When solution is exchanged, 40 µl of solution is added and immediately afterwards 40 µl solution is removed from the well.
16. In order to improve the seal resistance and increase Ca_V current to a measurable amplitude, sometimes a higher concentration of Ca^{2+} (5–10 mM) was used for the NaIV and CaIV recordings. A higher concentration of Ca^{2+} can shift the IV curves for these channels to more positive potentials [29–31].
17. The time it takes to set up a typical SyncroPatch 384PE experiment strongly depends on whether the compounds are already delivered in 384-well plates or not. If not those could also be prepared on the pipetting robot. However, this takes time. Assuming 5 h of measurement time, the number of compounds tested in this time very much depends on the plate layout. Assuming a plate layout as shown in Fig. 2d and an experiment time of 30 min, this would mean that 150 compounds could be tested in a day.

5 Future Prospects

hiPSC-CMs are an attractive alternative to cardiac ion channels overexpressed in cell lines because of their closer representation of the native environment. They are also a more viable alternative to acutely isolated cardiomyocytes which are difficult to obtain and difficult to use in automated electrophysiology. However, these cells need to be well characterized before they can be routinely used for safety screening. As part of the CiPA initiative, APC providers are working together with hiPSC-CM providers to characterize the cells further and standardize protocols. The capability for temperature control and current clamp of APC devices, already available on the Patchliner [11], and under development on the SyncroPatch 384PE, will also be an important consideration for safety testing in the future. Novel technologies such as impedance, described in Chap. 10 in this book, will most likely provide complementary information for safety testing using hiPSC-CMs.

Acknowledgments

We thank Cellular Dynamics International (CDI), Madison, Wisconsin, for the collaboration and for providing us with cardiomyocytes (iCell cardiomyocytes). We also thank Axiogenesis AG, Cologne, Germany, for the collaboration and for providing us with cardiomyocytes (Cor.4U). We also thank Pluriomics for providing us with the Pluricytes.

The authors disclosed receipt of the following financial support for the research, authorship, and/or publication of this article: The work presented here was funded in part by the Bundesministerium fuer Bildung und Forschung (BMBF, grant 01QE1502).

References

1. Neher E, Sakmann B (1976) Single-channel currents recorded from membrane of denervated frog muscle fibres. Nature 260:799–802. doi:10.1038/260799a0
2. Dunlop J, Bowlby M, Peri R et al (2008) High-throughput electrophysiology: an emerging paradigm for ion-channel screening and physiology. Nat Rev Drug Discov 7:358–368. doi:10.1038/nrd2552
3. Farre C, Haythornthwaite A, Haarmann C et al (2009) Port-a-patch and patchliner: high fidelity electrophysiology for secondary screening and safety pharmacology. Comb Chem High Throughput Screen 12:24–37. doi:10.2174/138620709787047966
4. Brüggemann A, George M, Klau M et al (2003) The NPC © Technology. Assay Drug Dev Technol 1:665–673
5. Brueggemann A, George M, Klau M et al (2004) Ion channel drug discovery and research: the automated Nano-Patch-Clamp © technology. Curr Drug Discov Technol 1:91–96
6. Brüggemann A, Stoelzle S, George M et al (2006) Microchip technology for automated and parallel patch-clamp recording. Small 2:840–846. doi:10.1002/smll.200600083
7. Jones KA, Garbati N, Zhang H, Large CH (2009) Automated patch clamping using the QPatch. In: Janzen WP, Bernasconi P (eds) High throughput screening: methods and protocols, 2nd edn. Humana Press, a part of Springer Science & Business Media, Totowa, pp 209–223
8. Mathes C, Friis S, Finley M, Liu Y (2009) QPatch: the missing link between HTS and ion channel drug discovery. Comb Chem High Throughput Screen 12:78–95. doi:10.2174/138620709787047948
9. Tao H, Santa Ana D, Guia A et al (2004) Automated tight seal electrophysiology for assessing the potential hERG liability of pharmaceutical compounds. Assay Drug Dev Technol 2:497–506. doi:10.1089/adt.2004.2.497
10. Xu J, Guia A, Rothwarf D et al (2003) A benchmark study with SealChip™ planar patch-clamp technology. Assay Drug Dev Technol 1:675–684. doi:10.1089/154065803770381039
11. Stoelzle S, Obergrussberger A, Brüggemann A et al (2011) State-of-the-art automated patch clamp devices: heat activation, action potentials, and high throughput in ion channel screening. Front Pharmacol 2:1–11. doi:10.3389/fphar.2011.00076
12. Obergrussberger A, Haarmann C, Rinke I et al (2014) Automated patch clamp analysis of nAChα7 and NaV 1.7 channels. Curr Protoc Pharmacol 65:11.13.1–11.13.48. doi:10.1002/0471141755.ph1113s65
13. Schroeder K, Neagle B, Trezise DJ, Worley J (2003) IonWorks HT: a new high-throughput electrophysiology measurement platform. J Biomol Screen 8:50–64. doi:10.1177/1087057102239667
14. Finkel A, Wittel A, Yang N et al (2006) Population patch clamp improves data consistency and success rates in the measurement of ionic currents. J Biomol Screen 11:488–496. doi:10.1177/1087057106288050
15. Gillie DJ, Novick SJ, Donovan BT et al (2013) Development of a high-throughput electrophysiological assay for the human ether-à-go-go related potassium channel hERG. J Pharmacol Toxicol Methods 67:33–44. doi:10.1016/j.vascn.2012.10.002
16. Kuryshev YA, Brown AM, Duzic E, Kirsch GE (2014) Evaluating state dependence and subtype selectivity of calcium channel modulators in automated electrophysiology assays. Assay Drug Dev Technol 12:110–119. doi:10.1089/adt.2013.552
17. Scheel O, Himmel H, Rascher-Eggstein G, Knott T (2011) Introduction of a modular automated voltage-clamp platform and its correlation with manual human Ether-à-go-go related gene voltage-clamp data. Assay Drug Dev Technol 9:600–607. doi:10.1089/adt.2010.0352
18. Spencer CI, Li N, Chen Q et al (2012) Ion channel pharmacology under flow: automation via well-plate microfluidics. Assay Drug Dev Technol 10:313–324. doi:10.1089/adt.2011.414
19. Obergrussberger A, Stölzle-Feix S, Becker N et al (2015) Novel screening techniques for ion channel targeting drugs. Channels 9:367–375. doi:10.1080/19336950.2015.1079675
20. Obergrussberger A, Brüggemann A, Goetze TA et al (2015) Automated patch clamp meets high-throughput screening: 384 cells recorded

in parallel on a planar patch clamp module. JLabAutom.doi:10.1177/2211068215623209

21. Sager PT, Gintant G, Turner JR et al (2014) Rechanneling the cardiac proarrhythmia safety paradigm: a meeting report from the Cardiac Safety Research Consortium. Am Heart J167:292–300.doi:10.1016/j.ahj.2013.11.004
22. Fermini B, Hancox JC, Abi-Gerges N et al (2015) A new perspective in the field of cardiac safety testing through the comprehensive in vitro proarrhythmia assay paradigm. J Biomol Screen. doi:10.1177/1087057115594589
23. Cavero I, Holzgrefe H (2014) Comprehensive in vitro proarrhythmia assay, a novel in vitro/in silico paradigm to detect ventricular proarrhythmic liability: a visionary 21st century initiative. Expert Opin Drug Saf 13:745–758. doi:10.1517/14740338.2014.915311
24. Becker N, Stoelzle S, Göpel S et al (2013) Minimized cell usage for stem cell-derived and primary cells on an automated patch clamp system. J Pharmacol Toxicol Methods 68:82–87. doi:10.1016/j.vascn.2013.03.009
25. Rajamohan D, Kalra S, Hoang MD et al (2016) Automated electrophysiological and pharmacological evaluation of human pluripotent stem cell-derived cardiomyocytes. Stem Cells Dev 25. doi:10.1089/scd.2015.0253
26. Haythornthwaite A, Stoelzle S, Hasler A et al (2012) Characterizing human ion channels in induced pluripotent stem cell-derived neurons. J Biomol Screen 17:1264–1272. doi:10.1177/1087057112457821
27. Meijer van Putten RME, Mengarelli I, Guan K et al (2015) Ion channelopathies in human induced pluripotent stem cell derived cardiomyocytes: a dynamic clamp study with virtual IK1. Front Physiol 6:Article 7. doi:10.3389/fphys.2015.00007
28. Shen JB, Jiang B, Pappano AJ (2000) Comparison of L-type calcium channel blockade by nifedipine and/or cadmium in guinea pig ventricular myocytes. J Pharmacol Exp Ther 294:562–570
29. Klugbauer N, Lacinova L, Flockerzi V, Hofmann F (1995) Structure and functional expression of a new member of the tetrodotoxin-sensitive voltage-activated sodium channel family from human neuroendocrine cells. EMBO J 14:1084–1090
30. Kass RS, Krafte DS (1987) Negative surface charge density near heart calcium channels. Relevance to block by dihydropyridines. J Gen Physiol 89:629–644. doi:10.1085/jgp.89.4.629
31. Charnet P, Bourinet E, Dubel SJ et al (1994) Calcium currents recorded from a neuronal alpha 1C L-type calcium channel in Xenopus oocytes. FEBS Lett 344:87–90
32. Sheets MF, Hanck DA (1999) Gating of skeletal and cardiac muscle sodium channels in mammalian cells. J Physiol 514(Pt 2):425–436

Chapter 5

The CiPA Microelectrode Array Assay with hSC-Derived Cardiomyocytes: Current Protocol, Future Potential

Daniel C. Millard, Mike Clements, and James D. Ross

Abstract

The Comprehensive In Vitro Proarrhythmia Assay (CiPA) initiative, led by the US Food and Drug Administration (FDA), aims to improve preclinical cardiac safety evaluation and reduce unwarranted drug attrition by utilizing more comprehensive model systems. A major component of CiPA is the development of an electrophysiological assay using human stem cell-derived cardiomyocytes (hSC-CMs), which provide an integrated assessment of the multiple ion channels contributing to the cardiac action potential (AP). This chapter details the current CiPA protocol for evaluating drug-induced changes in hSC-CM electrophysiology using microelectrode array (MEA) technology. In this assay, electrodes embedded in a cell culture substrate noninvasively interface with established cardiomyocyte networks, providing functional, mechanistically based measures of the cardiac action potential without perturbing the cellular network. Introduction of multiwell MEA technology has significantly increased assay throughput, enabling development efforts that further demonstrate the predictivity and reliability of MEA assays for evaluation of cardiac safety liability. Following a review of MEA theory and the field potential (FP) signal, this chapter provides a step-by-step protocol for MEA plate preparation and maintenance, assay execution, and data analysis according to the current CiPA guidelines. Alternative approaches to the MEA assay are also discussed, along with commentary on emerging advances in MEA technology for the assessment of cardiac safety liability in vitro.

Key words Cardiomyocyte, Stem cell, Microelectrode array, Drug safety, Field potential, High throughput, Multiwell, Electrophysiology

1 Introduction

Microelectrode array (MEA) technology has been used to study electroactive cells, such as neurons and cardiomyocytes, for decades [1]. Electrodes embedded in a cell culture substrate noninvasively interface with established cardiomyocyte networks, providing functional, mechanistically based measures of the cardiac action potential without perturbing the cellular network. The electrophysiological signal obtained from the microelectrodes, termed the cardiac field potential (FP), arises from the propagation of the cardiac action potential (AP) across the electrode array, providing measures of the depolarization

Mike Clements and Liz Roquemore (eds.), *Stem Cell-Derived Models in Toxicology*, Methods in Pharmacology and Toxicology, DOI 10.1007/978-1-4939-6661-5_5,

and repolarization of the cardiomyocyte network that are directly correlated to corresponding measures from the cardiac action potential waveform. Existing commercial MEA systems provide direct voltage recordings of high spatial and temporal resolution across multiple wells simultaneously, providing an effective and efficient platform technology for evaluation of cardiomyocyte activity.

Early studies with MEA technology utilized rodent cardiomyocyte networks [2, 3]. More recently, however, the emergence of stem cell techniques has enabled the study of human cardiomyocyte models in vitro. Human stem cell-derived cardiomyocytes (hSC-CMs) are now widely available and reproduce appropriate ion channel distributions and cardiac phenotypes [4]. The concomitant introduction of multiwell MEA technology facilitated the development and evaluation of hSC-CMs, leading to recent assay development efforts that demonstrate the *predictivity* and *reliability* of CM-MEA assays for evaluation of cardiac safety liability [5–9].

This chapter will detail the CM-MEA assay protocol that was established by a Health and Environmental Sciences Institute (HESI)-driven scientific committee for use in the pilot study of the Comprehensive In Vitro Proarrhythmia Assay (CiPA) initiative. In doing so, we will discuss the past, present, and future of the CM-MEA assay. First, a review of MEA theory from the literature will establish the foundations of the field potential measurement and its advantages for cardiac safety evaluation. Next, the Protocol and Notes sections will provide step-by-step instructions for the consensus protocol, along with a detailed discussion of alternative or optional methods. Finally, advanced techniques, such as paced or chronic assays, and recent technological developments will be explored as they pertain to current and future implementations of the CM-MEA assay for assessment of proarrhythmic risk.

1.1 MEA Theory

The electrophysiological signal obtained from the microelectrodes, termed the cardiac field potential, arises from the propagation of the cardiac action potential across the electrode array, much as the electrocardiogram is derived from propagation of electrical signals across the heart. All three signals—the action potential, in vitro field potential, and ECG field potential—provide clear fiducial markers indicating the onset of depolarization and the conclusion of repolarization. The action potential of an isolated cardiomyocyte comprises the sum of inward and outward ionic currents, including sodium (NaV1.5), calcium (CaV1.2), and potassium (hERG) currents. An example of the cardiac action potential, as measured by patch clamp recording, is presented in Fig. 1, along with the corresponding extracellular field potential (FP) and electrocardiogram (ECG), which integrates the propagation of the action potential across a network of cardiomyocytes.

Classical models of the extracellular field potential describe the signal as the second derivative of the transmembrane voltage with

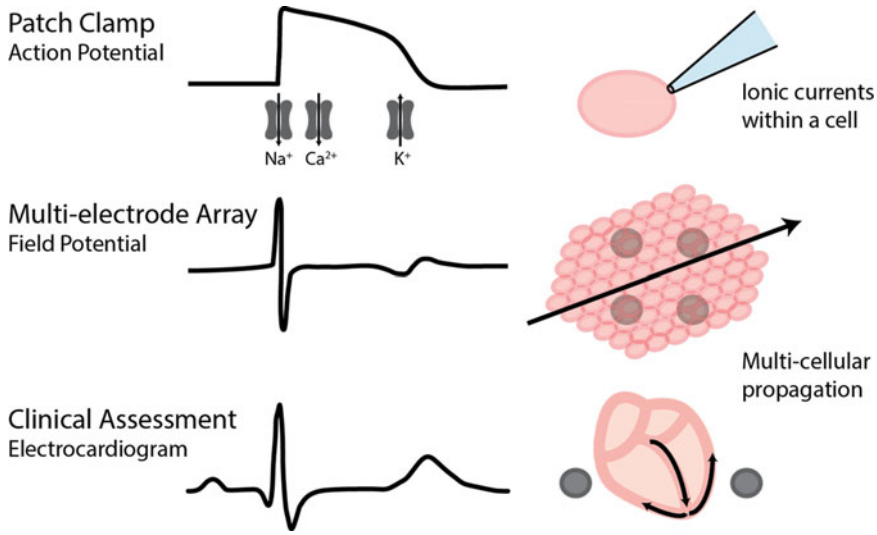

Fig. 1 Cardiac electrophysiology signals indicate onset of depolarization and repolarization from in vitro studies to the clinic. The cardiomyocyte action potential (*top*) results from the transmembrane currents through multiple ion channels (e.g., sodium, calcium, and potassium). The field potential signal (*middle*) arises from the multicellular propagation of the cardiomyocyte action potential across a microelectrode. Similarly, the electrocardiogram is driven by the propagation of the cardiomyocyte action potential across the heart

respect to space along the cardiac tissue; this model is often simplified to the second derivative, with respect to time, of the cardiac action potential, under the assumption of spatial uniformity [10]. The example field potential waveform in Fig. 1 utilizes this assumption and illustrates a "second derivative" shape in the field potential. In this case, the peak of the repolarization feature demarcates the maximum rate of repolarization in the cardiac action potential, which typically occurs near 90% of complete repolarization.

These second derivative models were derived for extracellular probe electrodes positioned near tissue slices, and not with adherent cells in close contact to a planar surface electrode, as is the case with MEAs. For MEAs, experimental and computational work has shown that the coupling between the electrode and electroactive cell significantly impacts the size and shape of the detected signal [11–13]. Figure 2 depicts an example MEA, a dense cardiomyocyte monolayer, and a spectrum of the possible field potential signal shapes. All three field potential shapes were recorded from electrodes in the same well and thus sample different portions of the same cardiomyocyte network. The top signal (1) resembles an AP-like shape, whereas the bottom signal (3) corresponds to the "second derivative shape," and the middle signal (2) represents an intermediate waveform. At greater than 10 mV in amplitude, the extracellular electrode captures over 10% of the full intracellular voltage change in the AP-like shape. Although it is important to recognize the distinct field potential shapes that may occur, the "second derivative" shape (3) is the most commonly observed and will be the focus throughout the rest of the chapter.

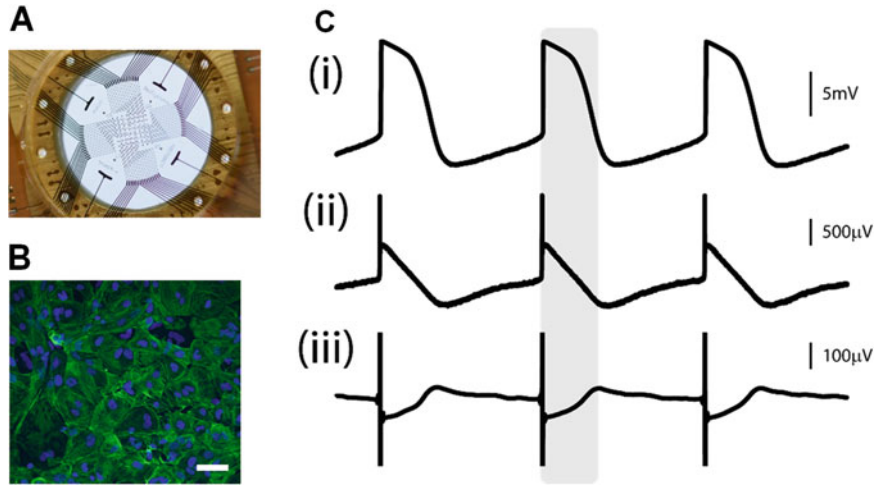

Fig. 2 Field potential shape is dependent on the coupling between the syncytium and electrode. (**a**) A microelectrode array contains multiple electrodes embedded in the substrate of a culture well. (**b**) hSC-CMs form an interconnected syncytium when seeded onto the microelectrode array. Scale bar is 50 µm. (**c**) Depending on the coupling strength of the syncytium to the electrode, action potential-like signals (1), "first derivative signals" (2), or "second derivative signals" (3) can be acquired

The field potential end points provide information on the following features of the cardiac AP: (1) depolarization, (2) repolarization, (3) beat timing, (4) arrhythmia occurrence, and (5) propagation. An example of the cardiac field potential, with the associated measurement definitions, is shown in Fig. 3. The onset of cardiac depolarization is marked by a sharp deflection in the field potential signal, termed the depolarization spike. The peak-to-peak amplitude (AMP) of the depolarization spike provides a measure of the speed of depolarization in the cardiomyocyte network. Repolarization timing of the cardiac network is indicated by the repolarization feature of the field potential. The field potential duration (FPD), analogous to the QT interval in clinical ECGs, is given by the timing interval between the depolarization spike and the peak of the repolarization feature. A cardiac beat, encompassing depolarization and repolarization of the cardiac action potential, is defined as the signal between two consecutive depolarization spikes, and the duration of this time interval is referred to as the beat period (BP). Irregularities in beat timing indicate arrhythmic beating and are often associated with early afterdepolarization (EAD) events, as shown in Fig. 3. Finally, the detection of a beat on multiple electrodes in the well enables quantification of the origin, speed, and direction of propagation within the cardiomyocyte network on a beat-by-beat basis.

1.2 Cardiac Safety Evaluation with MEA Technology

The CM-MEA assay incorporates the human biology from hiPSC-CMs with a label-free, noninvasive electrophysiological assay, allowing a comprehensive evaluation of cardiac safety liability

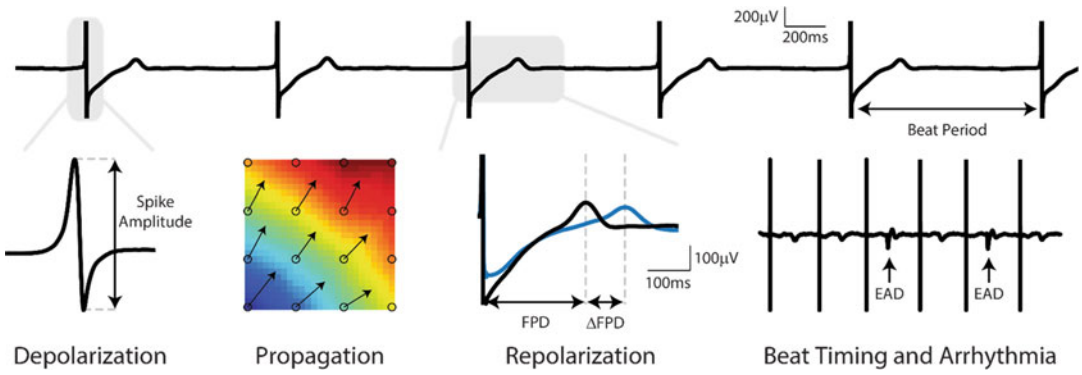

Fig. 3 The field potential signal provides multiple end points of cardiac electrophysiology. Each beat provides information on the depolarization, propagation, and repolarization of the hSC-CM monolayer. Information on beat timing and arrhythmia is extracted from the relative timing of consecutive beats

in vitro with increased throughput. Toward this end, recent studies have evaluated the CM-MEA assay across an array of compounds with known clinical risk and mechanism of action [5–8] in an effort to evaluate clinical concordance. Specifically, early studies using single-well MEA systems demonstrated consistent results for changes in field potential duration in response to well-described single- and multi-ion channel blockers [6–8]. Additionally, CM-MEA-based risk ranking of 21 compounds on a multiwell MEA platform [5] showed good agreement with Redfern scores [14], while multi-parametric assessment of field potential profiles classified probable mechanisms of action. Finally, recent studies have extended beyond measures of repolarization and quantified aspects of arrhythmic beating to more directly target the specific phenotype of interest in proarrhythmia risk assessment [9].

These efforts have led to the inclusion of the CM-MEA assay into the ongoing development and evaluation of the CiPA initiative, led by the US Food and Drug Administration (FDA), which aims to redefine preclinical evaluation of torsades de pointes (TdP) liability. Current regulatory guidance focuses on block of the potassium channel encoded by the human Ether-à-go-go related gene (hERG) and QT prolongation in the clinical ECG, both of which are surrogate markers of TdP risk. Instead, the CiPA proposal will define a proarrhythmia risk ranking using a multifaceted in vitro approach that combines (1) in silico modeling of the cardiac action potential, derived from patch clamp studies of multiple individual ion channels, and (2) direct evaluation with integrated human cellular studies, utilizing the electrophysiological response of human stem cell-derived cardiomyocytes acquired from instrumentation including MEA technology [15, 16]. Ongoing collaborations led by the Health and Environmental Sciences Institute (HESI) have developed a core CM-MEA protocol, which has been

evaluated in a multi-site pilot study and will soon be incorporated within a 28-compound validation study.

In a related effort, the Japan iPS Cardiac Safety Assessment (JiCSA) consortium has performed rigorous pilot and validation studies to evaluate the utility of the CM-MEA assay in assessing cardiac safety liability. A recent cross site reliability study demonstrated reproducible results for compound-induced prolongation of repolarization for E-4031 at three independent sites [17], with a follow-up study demonstrating high intra- and inter-facility reliability across seven compounds and ten facilities [18].

This chapter will detail the core CM-MEA protocol developed for the CiPA initiative and informed by the JiCSA studies, including culturing hSC-CMs on MEA plates, experimental procedures, data analysis, and quality control measures. Key decision points for the protocol will be detailed in Sect. 4, including alternative approaches (Fig. 4). As there are minor variations in cell culture, hardware, and software across commercial multiwell MEA systems, this chapter will focus on the Maestro multiwell MEA platform (Axion BioSystems, Inc.), allowing a more detailed description of how to execute the CiPA protocol without a loss in generality. The Maestro contains 768 microelectrodes distributed across 12-, 48-, or 96-well MEA plates and the fully functional AxIS software suite (Fig. 5). A brief introduction to advanced applications, such as pacing and chronic assays, will be described after the CiPA protocol, along with a commentary on the future direction of CM-MEA assays and instrumentation.

2 Materials

2.1 Cell Plating and Culture

1. 12-, 48-, or 96-well MEA plate (Axion BioSystems, Inc.)
2. One vial of hSC-CMs: Cor.4U (Axiogenesis AG), iCell CM² (Cellular Dynamics International, a Fujifilm company), Pluricyte (Pluriomics), and Cytiva Plus (GE Healthcare)
3. Cell culture medium (cell manufacturer specific)
4. Stock solution of fibronectin (1 mg/ml; sterile) or other surface coating materials (cell manufacturer specific)

2.2 Compound Addition and Data Acquisition

1. Maestro multiwell MEA platform (Axion BioSystems, Inc.)
2. Cell culture media (cell supplier specific)

2.3 Data Analysis and Results

1. AxIS software suite v2.3 (Axion BioSystems, Inc.)
2. CiPA Analysis Tool (Axion BioSystems, Inc.)
3. AxIS Metric Plotting Tool (Axion BioSystems, Inc.)

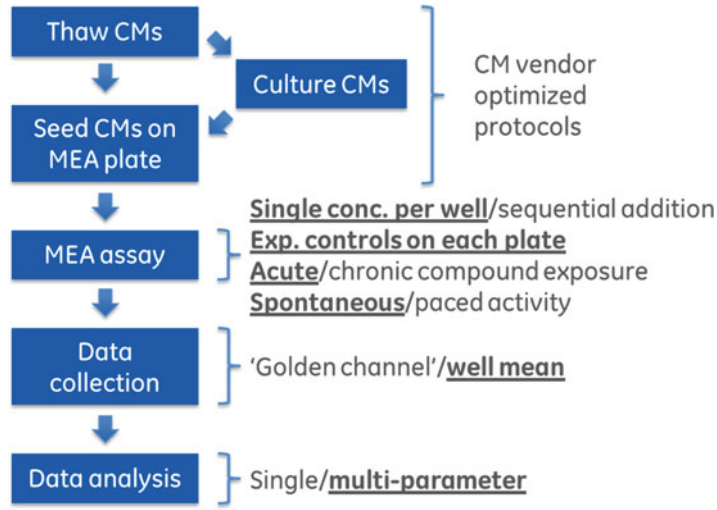

Fig. 4 Recommended options for the CiPA CM-MEA assay. Following vendor-optimized protocols for seeding hSC-CMs on the MEA plate, there are multiple options in executing a CM-MEA assay. The CiPA assay recommends a single-dosing scheme with a positive control on each plate and acquisition of acute time-point spontaneous data. It is recommended to aggregate end points from multiple electrodes in the well, with an emphasis on multiple MEA parameters describing depolarization, repolarization, and beat timing

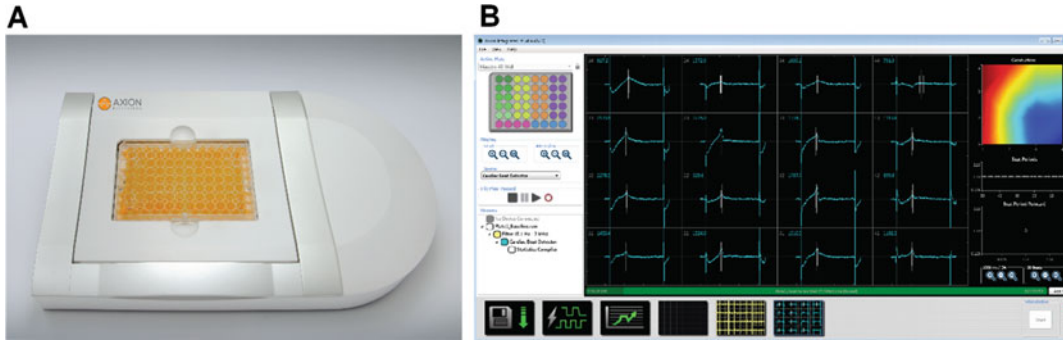

Fig. 5 The Maestro multiwell MEA platform. (**a**) The Maestro (Axion BioSystems, Inc.) simultaneously samples 768 electrodes distributed across 12-, 48-, or 96-well plates. (**b**) The AxIS software suite (Axion BioSystems, Inc.) records and processes data in real time from the Maestro system. The cardiac dashboard displays averaged beats for each electrode in a well, as well as processed end points including the FPD, propagation map, beat timing, and real-time arrhythmia detection

3 Methods

3.1 CiPA Protocol

3.1.1 Cell Plating and Culture

1. Wipe the package of the sealed MEA plate with 70% ethanol (EtOH) and then place it in a biological tissue culture hood.
2. Pull the MEA plate from the sealed package and wipe the top, bottom, and sides of the plate with a Kimwipe soaked in 70% EtOH.

3. Add ~6 ml of sterile distilled water to the area surrounding the wells (MEA reservoirs) of the MEA plate to prevent substrate evaporation. Do not allow the water into the wells of the MEA plate.
4. Prepare surface coatings according to cell manufacturer recommendations and spot the surface coatings directly onto the MEA in each well. To do so, first tilt the MEA plate at an angle (~30° from level) such that all wells are visible and then bead a droplet from the pipet tip and touch onto the center of the array (Fig. 6a–b). The droplet volume is typically 4–10 μL and should follow cell manufacturer recommendations. Apply the surface coating in every well.
5. Place the lid on the MEA plate and incubate according to cell manufacturer recommendations in a standard cell culture incubator at 37 °C.
6. Thaw and resuspend the cells in media according to the cell manufacturer recommendations. Generally, this process involves thawing the cells in a 37 °C water bath, centrifuging the cells, aspirating the supernatant, and adding the appropriate media volume to achieve the desired cell density.
7. Remove the MEA plate from the cell culture incubator and aspirate the surface coating from each well. Tilt the plate at an angle and add a droplet of the cell suspension directly onto the MEA in the center of the well (Fig. 6c). Aspiration and cell addition should be performed one row at a time across the plate to prevent drying and crystallization of the surface coating. The droplet volume is typically 4–10 μL and should follow cell manufacturer recommendations.
8. Place the lid on the MEA plate and incubate according to cell manufacturer recommendations in a standard cell culture incubator at 37 °C. The incubation time is typically 1–3 h.

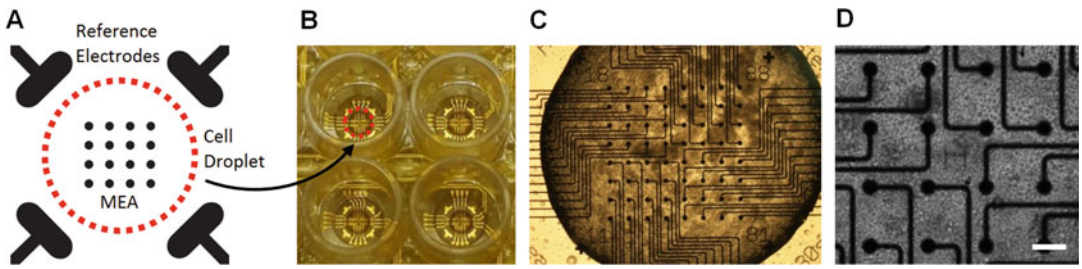

Fig. 6 A spotting technique is used to seed cells on an MEA plate. (**a**) Cells are seeded by placing a droplet of the cell suspension directly onto the array and within the space circumscribed by the reference electrodes. (**b**) Example droplets placed on a multiwell MEA plate. (**c**) Microscope image of a cell droplet seeded onto a 12-well MEA plate, with 64 electrodes per well. Accurate placement results in the droplet covering the entire array. (**d**) Microscope image of a cell culture 5 days after thaw and plating, at which point the cells have formed a functional beating syncytium. Scale bar is 100 μm

9. Remove the MEA plate from the cell culture incubator and add medium to each well (500 µL per well for a 12-well plate, 300 µL per well for a 48-well plate, and 200 µL per well for a 96-well plate). To do so, tilt the MEA plate at an angle (~30° from level) and add half of the media volume down the side of the well (Fig. 7). Adding the media too quickly may dislodge the cardiomyocytes. Slowly return the MEA plate to a flat position such that the media covers the cell droplet. Repeat this procedure to add the second half of the media volume to each well. These steps may be performed one row at a time using a multichannel pipet.
10. Place the lid on the MEA plate and then store in a cell culture incubator at 37 °C and 5 % CO_2. The media should be changed regularly, according to cell manufacturer recommendations.
11. Evaluation of the hSC-CMs typically occurs 4–14 days after seeding on the MEA plate, according to cell manufacturer recommendations. At this point, the cellular phenotype will have matured to exhibit stable beating and repolarization across the plate.

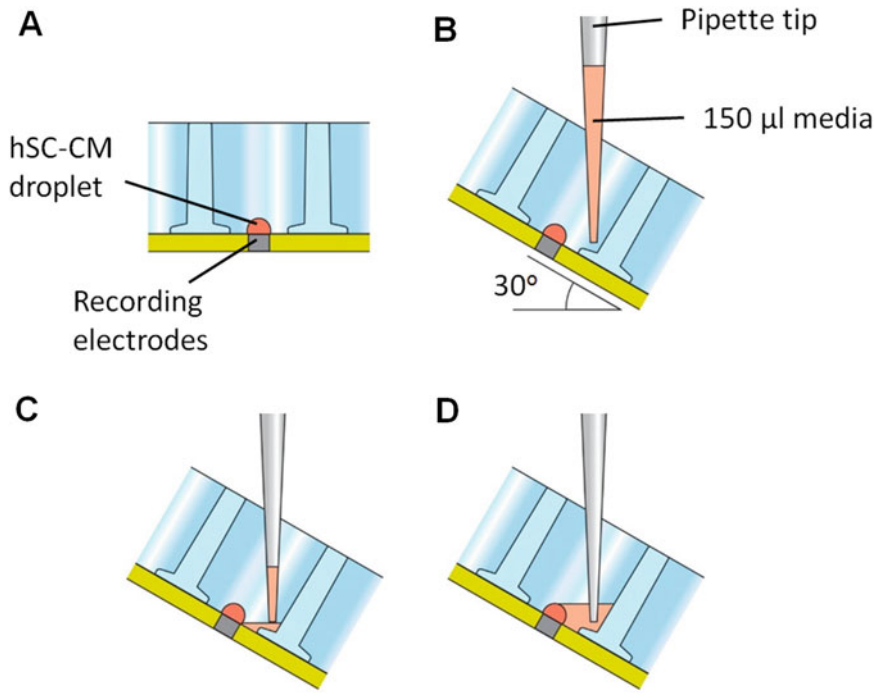

Fig. 7 Media addition technique following spotting an MEA plate. (**a**) The cell droplet is first placed on the MEA. (**b**) Tilt the plate at a 30° angle, such that the media may be deposited in the corner of the well. (**c**) and (**d**) Slowly add media to the well. Reproduced with permission from Clements, 2016 [19]

3.1.2 Compound Addition and Data Acquisition

1. The media should be changed at least 2 h prior to the experiment to allow for cell culture equilibration.
2. Compounds should be prepared fresh on the day of testing. The compounds are prepared in cell media at 10× the desired final concentration on a standard compound plate and allowed to incubate for >30 min to ensure temperature and pH equilibration. If DMSO is required to solubilize the compound, care should be taken to maintain less than 1% DMSO in the solution. The compound will be diluted 10× when added to the well volume, such that the final DMSO concentration is less than 0.1%.
3. Move the cell culture plate directly from the incubator to the MEA device for a baseline recording, with environmental controls (37 °C and 5% CO_2) used to maintain the temperature and pH (*see* **Note 1**). The ECmini device provides 5% CO_2 to the recording chamber when seated on the Maestro platform (Fig. 8). The recommended flow rate for CO_2 is 0.5 L/min.
4. The cultures should be allowed to equilibrate for 15 min to ensure a stable beating profile. After equilibration, it is recommended to acquire a 5 min baseline recording.
5. The dosing may be performed on the MEA instrument or in a biosafety cabinet. Dosing in a biosafety cabinet maintains sterility, which is important for chronic experiments, whereas dosing on the MEA instrument minimizes perturbation to the cell cultures, such as fluctuations in temperature and pH or mechanical disturbances.
6. A single dose is applied to each well by removing 10% of the well volume (30 µL for a 300 µL well volume in a 48-well

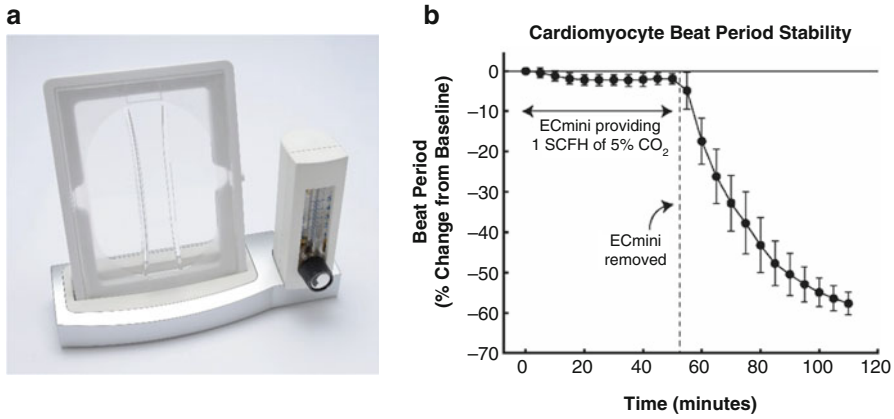

Fig. 8 Environmental controls maintain stable beating. (**a**) The ECmini (Axion BioSystems, Inc.) forms a sealed chamber over the MEA plate for continuous delivery of CO_2 to maintain culture pH. (**b**) The beat period of the hSC-CMs remains stable with proper pH management, but rapidly decreases when the ECmini is removed

plate) and replacing with the same volume drawn from the compound plate, which contains 10× the desired final concentration of the compound. Rather than mixing, which may affect cell physiology, the compound is allowed to diffuse naturally through the well. As an alternate approach, sequential/cumulative dosing may be performed (*see* **Note 2**).

7. If the plate was dosed in the biosafety cabinet, the plate should be immediately returned to the MEA instrument. As a minimum, a 5 min recording should be made 30 min following dosing to allow sufficient time for the cells and compound to equilibrate. A continuous recording following dosing is recommended for enhanced detection and quantification of arrhythmic indicators, such as EADs.

3.1.3 Data Analysis and Results

1. In the AxIS software, beat detection parameters define the algorithms for detecting cardiac beats and quantifying the end points described above (Fig. 3). A beat is initiated as the raw voltage signal passes the detection threshold (default = 300 μV) and completed when the raw voltage signal again passes the detection threshold. Quality control criterion defining the minimum and maximum beat period may be defined based on known limits of the physiology, such that beats not meeting these criteria are discarded from analysis.
2. A continuous recording provides the greatest flexibility in identification of the collection of beats from which to extract the field potential end points of interest. The standard CiPA protocol prescribes the end points be extracted at 30 ± 2 min following dosing or >15 min after placement on the recording device for baseline measurements. The end points may be derived from each beat within this time window and averaged to produce the well measures. Alternately, an algorithm may be used to identify the most stable region of beating, such that the average well measures may be computed from an optimally stable collection of beats, as illustrated in Fig. 9 (*see* **Note 3**). Additional parameters, such as propagation pattern, may be important for informing beat selection depending on the end point of interest (*see* **Note 4**).
3. The AxIS software automatically computes the metrics defined in Fig. 3, among others, from the collection of beats selected for analysis. Multiple algorithms are included for detecting the peak of the repolarization feature, which is used in computing the field potential duration. The polynomial regression algorithm is tailored for sensitivity when dealing with small signals, whereas the inflection search algorithm is highly robust for strong signal features. It is important to ensure the same signal feature is being tracked between the baseline and dosed conditions.

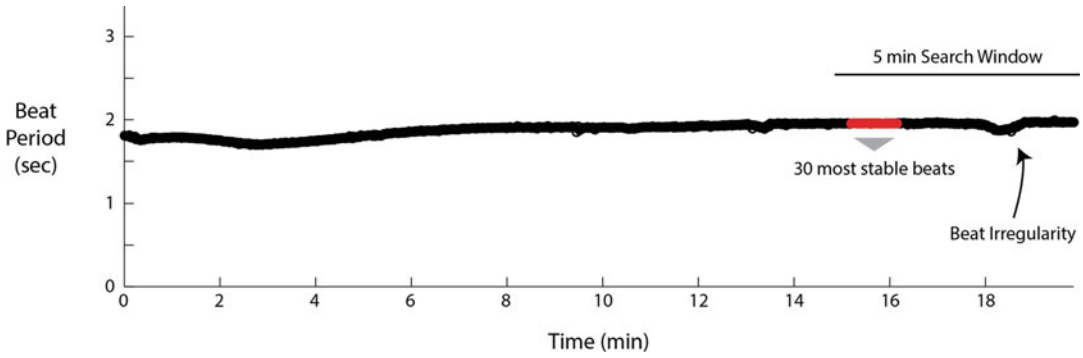

Fig. 9 End points are automatically derived from regions of stable beating. AxIS employs an automated algorithm to identify the most stable region of beating within a specified search window. In this way, transient beating irregularities do not influence important end point computations

4. With multiple electrodes sampling the activity of the cardiac monolayer in each well, the redundancy across measurements may be used to enhance reliability and accuracy in the average well measurement of field potential duration. Quality control settings may be defined in AxIS to eliminate statistical outliers from the average computation according to three criteria: (1) beat to beat FPD consistency, (2) electrode FPD consistency, and (3) well FPD consistency. Alternatively, a "golden channel" approach may be used to identify a single electrode signal to compare across the baseline and dosed conditions (*see* **Note 5**).
5. The presence or absence of arrhythmic indicators, such as EADs or triggered activity, is typically noted by manual inspection of the data. Automated algorithms for detecting unstable beat timing may be used to improve the identification and classification of arrhythmic indicators. In the CiPA Analysis Tool, an automated algorithm performs a running estimate of the probability distribution for beat period in a well, such that regions of bistability may be easily detected. A collection of beats exhibiting a bistable beat period (*see* Fig. 10) is indicative of an alternans pattern (A-B-A-B beat pattern, where A and B represent distinct beat shapes) and highly predictive of the onset of arrhythmic indicators like EADs.
6. Quality control criteria may be defined for baseline measurements to eliminate unhealthy cultures before dosing and analysis. Figure 11 illustrates the distribution across wells and plates for common MEA end points. The cultures exhibit high well-to-well reliability, such that outlier wells may be easily identified. As an example, a range of acceptable beat periods may be defined, such as 1–2 s, and wells falling outside of this range in the baseline measurement are excluded from the study before dosing. The range of acceptable beat periods should be defined according to the specific cell preparation in use, as different commercial cell types exhibit distinct beating profiles (*see* **Note 6**).

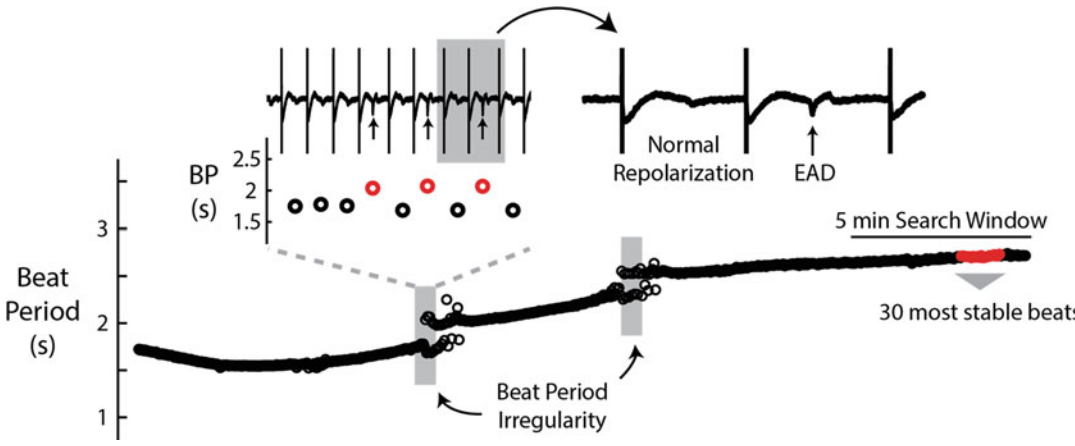

Fig. 10 Alternans patterns are automatically detected to inform arrhythmia classification. AxIS employs an automated algorithm to identify alternans patterns (bistable beating), which are often associated with proarrhythmic phenotypes, such as EADs (inset)

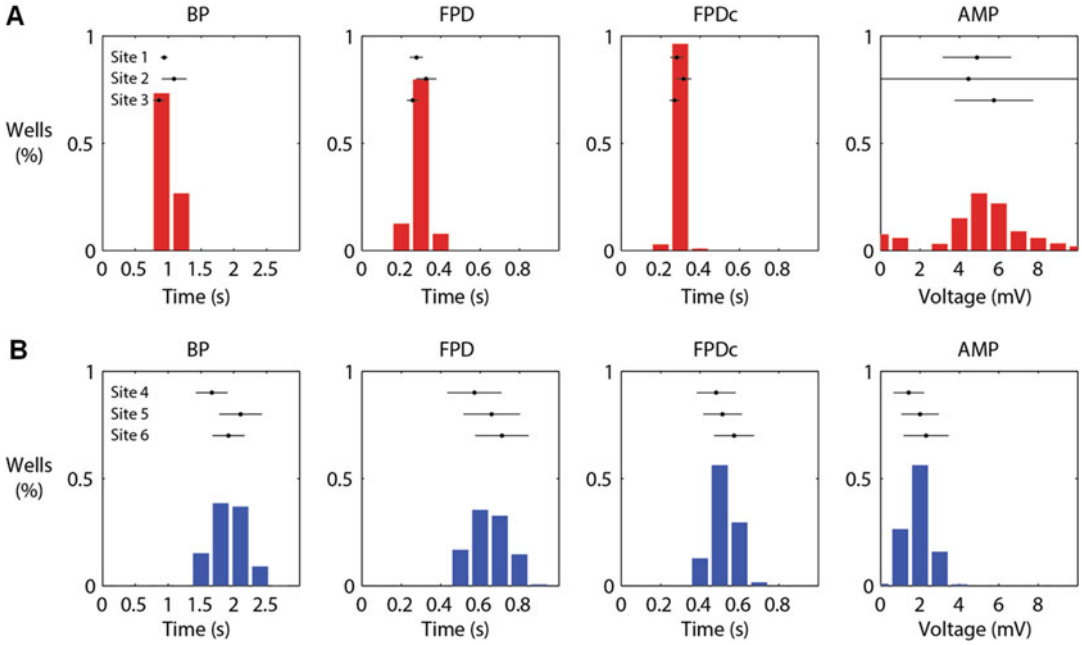

Fig. 11 MEA end points are consistent across wells, plates, and sites. Baseline end points of BP, FPD, FPDc, and AMP were consistent across wells, plates, and sites in the CiPA pilot study for two cell types (Cor.4U - red; iCell CM - blue) evaluated on the Maestro across six sites. Histograms represent data from ~300 wells aggregated across three sites for each cell type, with the mean (*dot*) and standard deviation (*bar*) represented for each individual site by the inset. Error bars represent ±1 standard deviation across replicates

7. To compute final end point measurements, a comparison is made between the baseline and dosed conditions. Most MEA studies to date have utilized a normalized comparison, whereby the percent change between the baseline and dosed measurement is

computed for each metric (e.g., $\%FPD = 100 * (FPD_{dosed} - FPD_{baseline})/FPD_{baseline}$). The percent change is then averaged across replicates of a compound and dose, and then average percent change from the vehicle control is subtracted from the measurement (e.g., $\Delta\%FPD = \%FPD_{compound} - \%FPD_{vehicle}$). Alternatively, a "double delta" calculation may be used (*see* **Note** 7).

8. Repolarization timing is intrinsically linked to the beating rate in cardiomyocytes, such that the field potential duration is corrected for spontaneous beat rate. Typically, clinical formulae, such as the Fridericia or Bazett corrections, are used to correct field potential duration. Rate correction should be performed before averaging across replicates. Alternatively, pacing experiments, as described in the Advanced Techniques section, may be used to collect data for computation of a custom rate correction curve, which provides a more robust approach than blindly applying other correction factors.
9. Evaluation of positive control compounds serves as a final quality control procedure to validate cell health, experimental protocol, and analysis methods. Typically, one potent hERG blocker, such as dofetilide or E-4031, and one potent calcium blocker, such as nifedipine or diltiazem, may be used as positive control compounds. For these compounds, previous literature supports that a ≥20 % change in FPDc (vehicle corrected), or the onset of arrhythmic activity for hERG blockers, should be readily detected in a well-executed study (*see* Fig. 12) at or near (1×–3×) the clinical free drug concentration [5–8, 17]. In addition, the response to positive control compounds may be used to calibrate results across different preparations of a given cell type, or across cell types altogether, and to track assay consistency over time.

3.2 Advanced Techniques

3.2.1 Electrical Pacing

Repolarization timing is intrinsically linked to the spontaneous beat rate of cultured cardiomyocyte monolayers (Fig. 13a), which can vary across wells and pharmaceutical manipulations. Clinical correction factors, such as the Bazett and Fridericia formulae, can be used to account for this relationship, but their applicability to stem cell-derived cardiomyocytes remains unknown.

Reliable electrical pacing of a cardiomyocyte culture addresses these unknowns. Pacing stabilizes the beat rate across wells, thus improving the reliability of the preparation for quantifying effects on repolarization timing. Furthermore, control of the beat rate enables exploration of the intrinsic relationship between the field potential duration and the beat rate for stem cell-derived cardiomyocytes and how this relationship manifests under pharmacological manipulation (i.e., reverse-use dependence). This section of the chapter provides a protocol for performing pacing experiments and analysis.

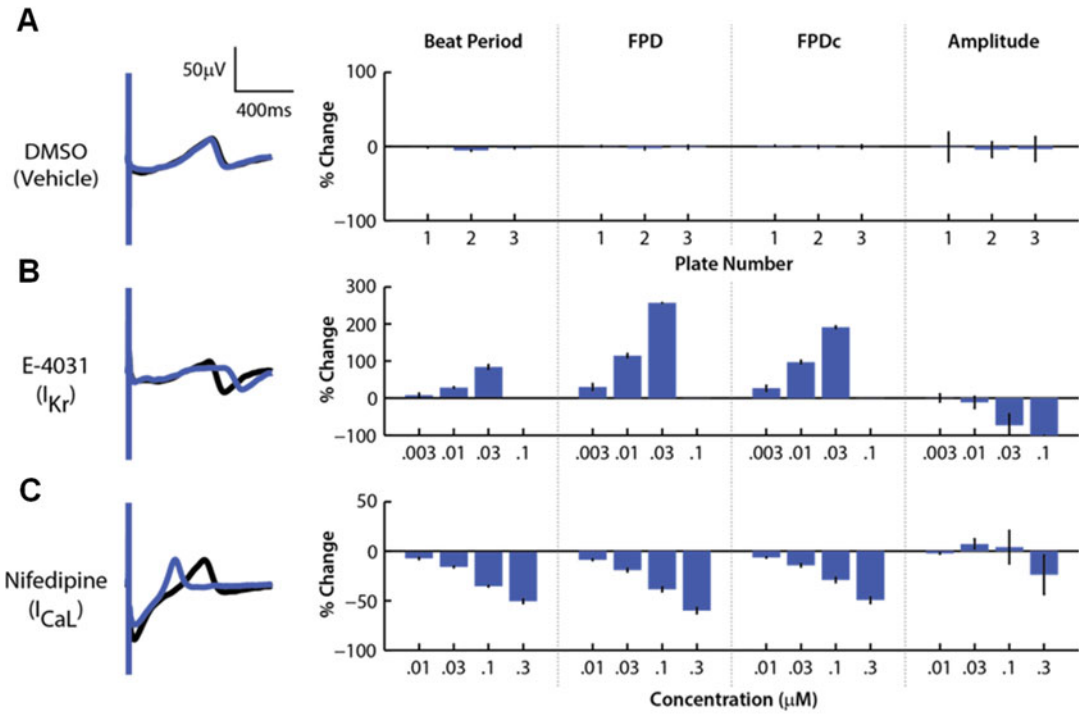

Fig. 12 MEA end points reflect expected responses to positive control compounds. The four primary MEA end points (BP, FPD, FPDc, and AMP) are shown for the vehicle control (**a**), E-4031 (**b**), and nifedipine (**c**) from a single site in the CiPA pilot study. (**a**) The vehicle control showed no change in field potential morphology (*left*) or end points (*right*), with high reliability within and across plates. (**b**) E-4031, a potent I_{Kr} blocker, produced a dose-dependent increase in BP, FPD, and FPDc, with high reliability across replicates ($N=3$). (**c**) Nifedipine, a potent I_{CaL} blocker, produced a dose-dependent decrease in BP, FPD, and FPDc, with high reliability across replicates ($N=3$). All error bars represent ±1 standard deviation across replicates

1. Establish hSC-CM cultures in vitro according to the recommended plating procedure (see above).
2. Choose the desired pacing rates based upon the specific application (*see* **Note 8**).

   - Reducing well-to-well variability—By forcing each well to beat at the same rate, the well-to-well variability of field potential duration may be reduced, as illustrated in Fig. 13c. In this case, pacing at 1 Hz is appropriate for most baseline and dosed conditions.
   - Beat rate correction of FPD—By pacing at a variety of rates, the relationship between rate and field potential duration may be measured and used for calculation of a custom rate correction formula (Fig. 13b). Rates should span from the spontaneous rate to 2 Hz (e.g., 0.7, 1.0, 1.2, 1.5, and 2.0 Hz).
   - Reverse-use dependence—Some compounds produce greater FPD prolongation at slow rates, termed reverse-

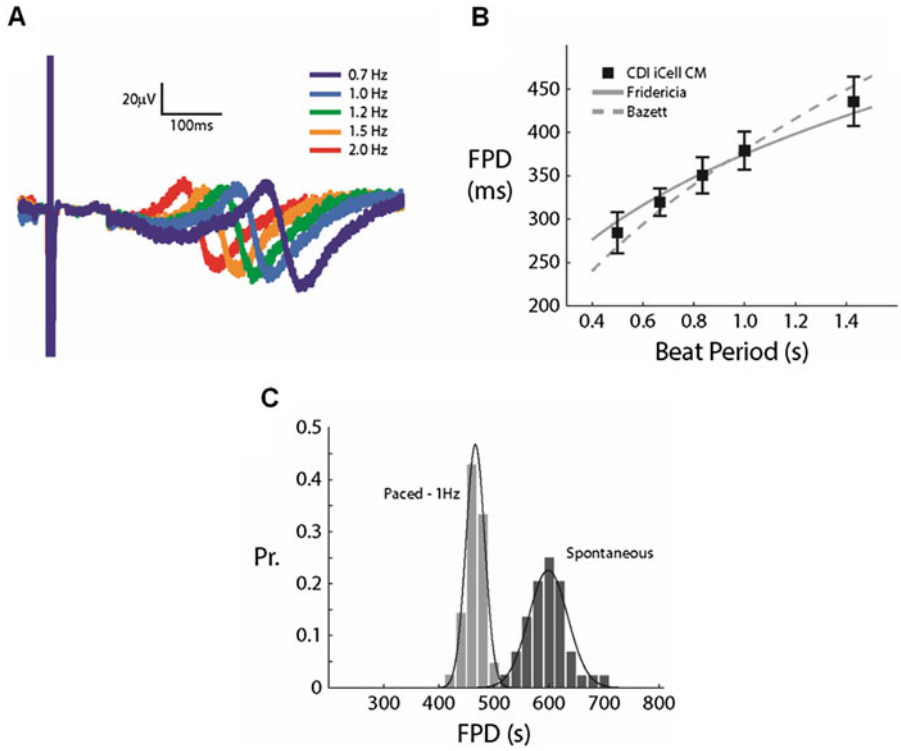

Fig. 13 Repolarization timing is rate dependent and controllable through pacing. (**a**) Electrical microstimulation from the embedded electrodes can be used to control the beating rate of hSC-CM cultures. The FPD is directly modulated by pacing rate, as illustrated by the example paced field potential traces. (**b**) The relationship between FPD and BP is highly reliable across wells in a plate, but may differ from existing clinical correction formulae. (**c**) Pacing standardizes the beating rate, and subsequently FPD, across wells leading to reduced well-to-well variability

use dependence, which may be an important predictor of proarrhythmic risk. Pacing rates should be biased toward the spontaneous rate if the compound of interest prolongs beat period and FPD (e.g., 0.5, 0.6, 0.7, 0.8, and 1.0 Hz).

- Optimize the pacing stimulus to ensure a 100% capture fraction across wells, where capture fraction is defined as the percentage of stimuli that elicit a cardiac beat. Increasing the current intensity or stimulus duration will improve the capture fraction. Evaluate the pacing stimulus at the fastest rate designated by the experimental plan, as higher pacing rates require a stronger stimulus to achieve complete capture. If capture is achieved, consider reducing the current intensity or stimulus duration to lessen the artifact. If capture is not achieved, increase the current intensity or stimulus duration (Fig. 14). For cultures with poor cell coverage, using a different stimulating electrode may also improve capture.

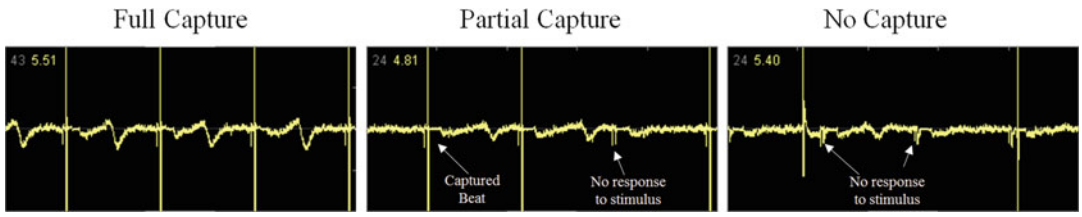

Fig. 14 Each stimulus elicits a beat for successful pacing. (**a**) In full capture, each electrical stimulus produces a beat, leading to a consistent and controlled beat rate. (**b**) In partial capture, some stimuli do not elicit a beat, leading to an inconsistent beat rate. (**c**) In the case of no capture, none of the stimuli elicit a beat, such that the spontaneous beat rate remains. A stronger stimulus must be utilized for cultures with partial capture or no capture

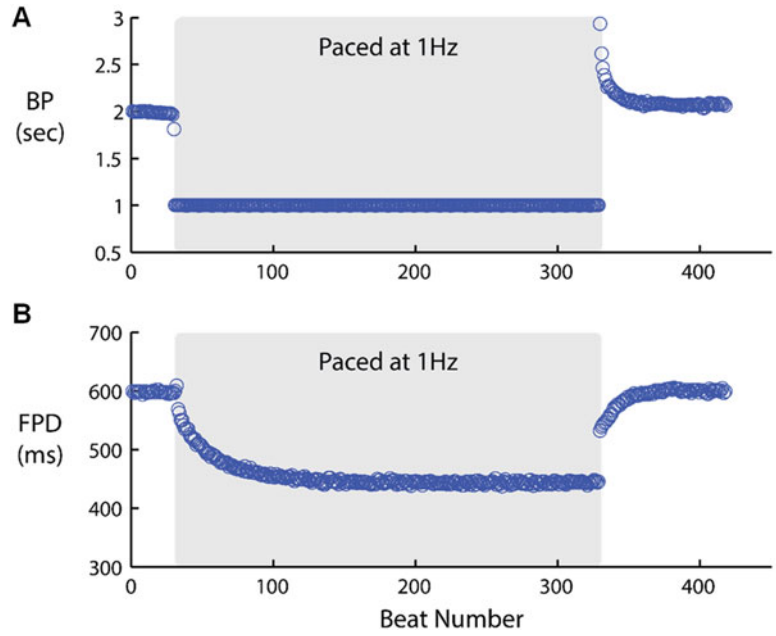

Fig. 15 Repolarization timing slowly approaches steady state after pacing onset. (**a**) The beat period of the hSC-CM culture changes instantaneously when full capture is achieved. (**b**) FPD slowly approaches a steady state after successful pacing onset. Measurements of FPD should be made after the steady state has been reached in pacing experiments

- Record at least 3 min of paced activity at each rate in the experimental plan. As shown in Fig. 15, the FPD will slowly approach a new steady-state value when the beat rate is changed. Recording at least 3 min of paced data will ensure that the FPD has reached a steady state.
- Dose the cultures and repeat the paced recordings at least 30 min after dosing. The pacing experiment may take as long as 15 min to achieve all desired rates, therefore it is important to allow enough time for the drug effect to equilibrate.

3.2.2 Chronic Assays

Direct ion channel effects are detected on acute timescales using the CM-MEA described above. However, many compounds exert non-ion channel effects over chronic timescales due to intracellular signaling or ion channel trafficking, which may be missed in acute measurements. The CM-MEA assay is label-free and non-invasive, allowing long-term monitoring of the cellular phenotype in response to chronic compound exposure. This section of the chapter provides a protocol for performing chronic experiments and analysis.

1. Establish hSC-CM cultures in vitro according to the recommended plating procedure (see above).
2. Choose the desired chronic recording intervals based upon the specific application. Chronic recordings may be made over the timescale of hours to days.
3. Follow the procedure described in the "Compound Addition and Data Acquisition" section to acquire a baseline recording and an acute dosed recording.
4. For chronic measurements 1–4 h post-dose, it is recommended to leave the plate on the MEA instrument with environmental controls (37 °C and 5 % CO_2) used to maintain the temperature and pH. For chronic measurements 1–4 days post-dose, the plate may be placed in the incubator between recordings to allow for use of the MEA instrument to perform additional assays. In this case, return the MEA plate directly from the incubator to the MEA device for chronic recordings, with environmental controls (37 °C and 5 % CO_2) used to maintain the temperature and pH. The cultures should be allowed to equilibrate for 15 min to ensure a stable beating profile. After equilibration, it is recommended to acquire a 5 min recording.
5. Continue to change the media according to manufacturer recommendations. For each media change, the compound should be replenished to maintain a constant exposure.
6. Vehicle control replicates should be included on each plate to adjust for changes in the cell phenotype over chronic time points. However, as the MEA assay is label-free and noninvasive, the cellular phenotype is typically stable over chronic time points, as illustrated in Fig. 16.

3.3 Future Directions

3.3.1 Optogenetics

Optogenetics is a technique whereby light-sensitive ion channels, referred to as opsins (e.g., channelrhodopsin 2, ChR2), are genetically targeted to a cell population, such that incident light of the correct wavelength produces a transmembrane current and depolarizes the cells [20, 21]. Although originally developed in the neuroscience community, optogenetic techniques have seen early proof of concept and utility for pacing in vitro cardiac electrophysiology assays and hSC-CMs [22]. Recently introduced optical

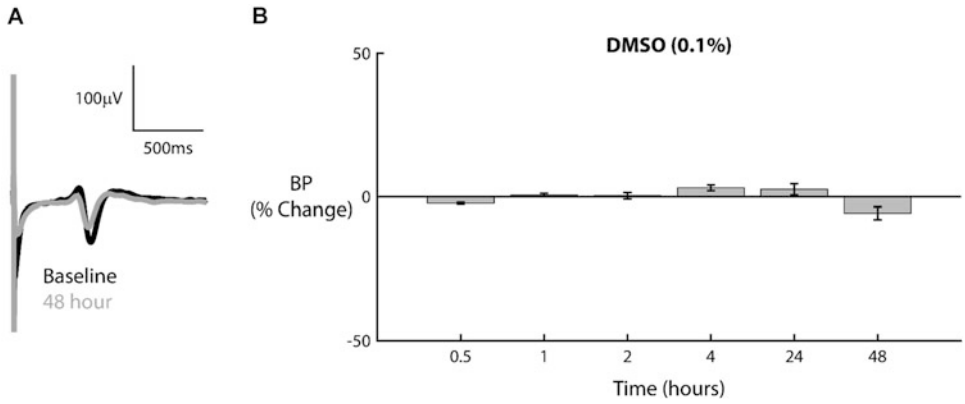

Fig. 16 Cardiomyocyte beating is stable over chronic time points in the MEA assay. (**a**) There is no qualitative change in the raw field potential between the baseline (*black*) and the 48 h chronic time point for the vehicle control (DMSO, *gray*). (**b**) Quantitatively, the beat period was stable over the chronic experiment for the vehicle control ($N = 5$), with less than a 10 % deviation from baseline at all time points

stimulation hardware, Lumos (Axion BioSystems, Inc., Fig. 17a), provides the capability to deliver temporally precise optical stimulation independently and simultaneously from 192 LEDs distributed across 48 wells, enabling turnkey optogenetic pacing assays with hSC-CMs.

ChR2 expression may be driven by a variety of well-established gene delivery techniques. Most commonly, a viral vector (e.g., AAV-CAG-ChR2-GFP, UNC Viral Vector Core) is used to deliver the genetic material encoding ChR2, under the control of a general or cell-specific promoter. The viral vector may be added to the cell suspension before seeding the hSC-CMs or to individual wells 1–5 days after plating. Typically, 7–14 days are required to achieve maximal ChR2 expression, but optically evoked experiments may be possible at earlier time points.

An example of optically paced hSC-CM activity is shown in Fig. 17. The culture is immediately entrained by the pulsed optical stimulus (Fig. 17b), with the expected decrease in FPD occurring for faster pacing rates (Fig. 17c). As with electrical pacing, the relationship between BP and FPD was consistent across wells in the plate ($N = 24$, Fig. 17d).

3.3.2 *Automation*

Although software packages, such as the AxIS software suite, allow for automated analysis of electrophysiological data from CM-MEA assays, culture and maintenance of hSC-CMs has traditionally been a labor-intensive and time-consuming task. Automation of traditional cell culture tasks has existed for years, yet the cost of hSC-CMs necessitates efficient handling of the cells. The recently introduced APEX, an automated MEA workstation (Axion BioSystems, Inc., Fig. 18), has optimized key processes such as mixing and drop placement to ensure efficient and accurate automation

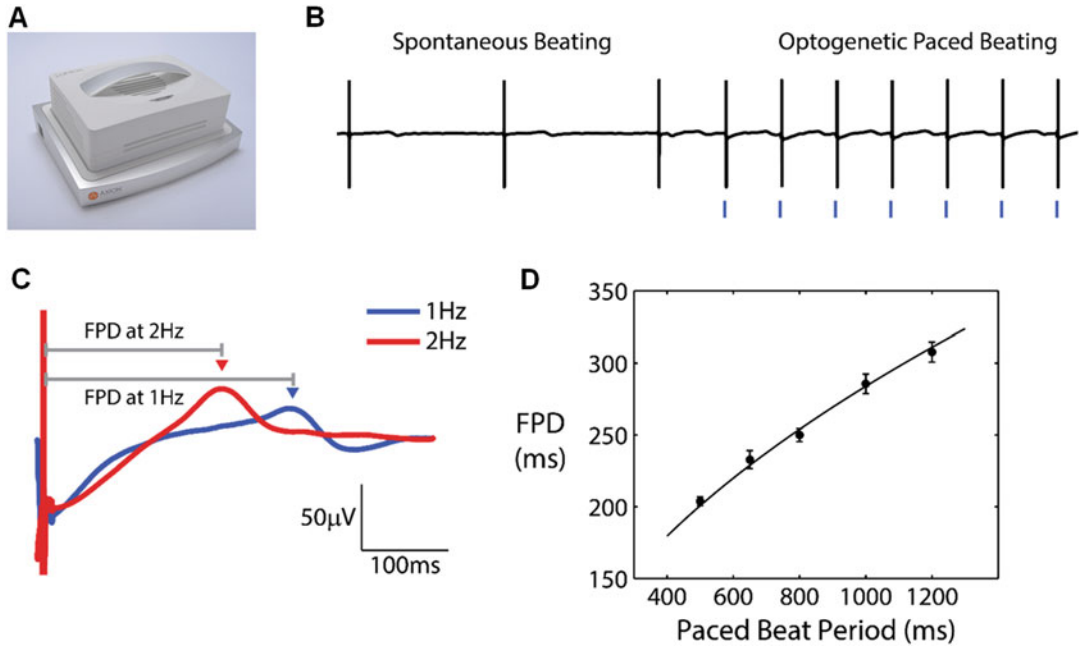

Fig. 17 ChR2-expressing cultures allow optogenetic pacing. (**a**) Lumos multiwell optical stimulator (Axion BioSystems, Inc.). (**b**) Each pulse of blue (470 nm) light stimulates a paced beat from hSC-CM cultures expressing ChR2. (**c**) As with electrical pacing, the FPD is modulated by optogenetic pacing rate. (**d**) The relationship between FPD and paced BP is reliable across wells for optogenetic pacing

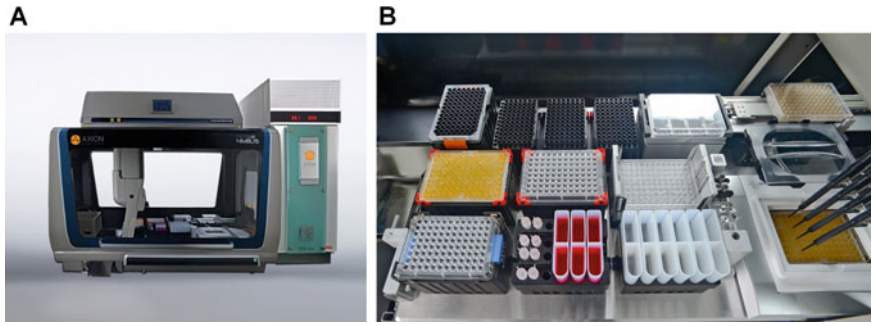

Fig. 18 Automation of the CM-MEA assay to improve reliability and throughput. (**a**) Maestro APEX (Axion BioSystems, Inc.) includes an automated liquid handler, 44-plate incubator, on-deck gas mixer, HEPA filtration system, and Maestro multiwell MEA platform. (**b**) A custom deck layout contains all equipment required for automated plating, maintenance, and dosing of cardiomyocytes

of hSC-CM culture and maintenance on MEA plates. The combination of automated cell culture, experimentation, and analysis now allows a completely automated CM-MEA assay workflow.

3.3.3 Drug-Drug Interactions

While CiPA is designed to assess effects on multiple ion channels for an integrated evaluation of proarrhythmic risk, the hSC-CM model has the possibility to detect non-ion channel-mediated

effects, such as ion channel trafficking or calcium handling perturbations that may occur over acute or chronic timescales. Pharmacokinetic drug-drug interactions, where a perpetrator drug affects the metabolism of a victim drug, may be assessed through in vitro assays and knowledge of drug transporter and metabolic systems in the body. Pharmacodynamic drug-drug interactions, however, are much more difficult to predict and isolate and thus often go unnoticed through preclinical and clinical testing. Recent evidence evaluating the interaction between sofosbuvir and amiodarone suggests that hSC-CMs could provide a simple and cost-effective model for screening candidate compounds against a library of commonly prescribed, FDA-approved drugs to identify potential pharmacodynamics drug-drug interactions, allowing further investigation in secondary assays [23].

3.3.4 Structure-Function Relationships

As with pharmacodynamic drug-drug interactions, hSC-CMs provide a model for multimodal assays assessing the structure-function relationship after exposure to candidate pharmaceuticals. Recent work utilized a transparent MEA plate (Axion BioSystems, Inc.) to compare electrophysiological and structural end points on the same cardiac monolayers using MEA recordings and high content imaging (HCI, a.k.a. HCA) analysis [24]. Such multimodal assays take advantage of the integrated biology of hSC-CMs to provide added value from each assay and advanced mechanistic information.

4 Notes

1. pH Sensitivity: The spontaneous beat period of hSC-CMs is exquisitely sensitive to temperature and pH. The beat frequency increases as temperature and pH increase and decreases as temperature and pH decrease. This phenomenon is illustrated in Fig. 8, as a constant beat period is maintained under with CO_2 delivery, but rapidly decreases (faster beat frequency) when the CO_2 delivery is removed.
2. Single vs. Sequential Dosing: Single dosing and sequential dosing each have advantages and disadvantages. The CiPA protocol recommends single dosing as it eliminates the concern of time-dependent effects that may accumulate over a long sequential dosing experiment. However, a single-dosing experiment requires more plates and cells to test and thus can be more expensive to run. Sequential, or cumulative, dosing utilizes repeated measurements of the same plate, with increasing concentrations of the compounds added at regular intervals (e.g., every 30 min). This method allows more compounds to be tested per plate, leading to a more cost-effective use of cells and plates. However, time-dependent effects may accumulate over time, such that phenotype observed for high concentrations of

the compounds may be influenced by the previously dosed lower concentrations.

3. Optimizing Assay Quality: The beat timing across multiple beats may also be used as a quality control measure for ensuring reliable data. Other metrics, including the field potential duration, are affected by modifications in the beat period. Therefore, it may be important to ensure the beat period has been stable for some time before analyzing the cardiac metrics. A healthy culture will exhibit low variability in beat period from beat to beat. However, spontaneous changes in beat period may occur. An example of this is shown in Fig. 9, in which the beat period transiently decreases at ~18 min and returns to the steady-state BP by ~19 min. The measurements of the field potential should not be made during such a spontaneous change in beat period, but rather should be made when the beat period is stable, as indicated by the red dots. To do so, a measure of stability is defined as the standard deviation of the beat period for a collection of N beats, where a lower value indicates greater stability. The collection of N beats that minimize the stability metric are then selected for analyzing the cardiac metrics of interest. $N = 30$ is recommended for the CiPA protocol and is the default in the AxIS software. In the CiPA protocol, wells exhibiting a coefficient of variation for beat period greater than 5% in the baseline condition are excluded from dosing and analysis. For reference, healthy cultures typically exhibit a coefficient of variation for beat period less than 1%, and often as low as 0.1%, when the most stable beats are analyzed.
4. Conduction Velocity Metrics: Conduction velocity and other propagation metrics are a function of the beat origin, or pacer location, in a cardiac monolayer. Thus, for improved sensitivity in analyzing propagation metrics, it is important to control for spontaneous changes in the beat origin, which may occur on a beat-by-beat basis. The AxIS software provides an option for limiting the analysis of cardiac metrics to the dominant propagation pattern present in a collection of beats.
5. Golden Channel vs. Well Mean: The "golden channel" (a.k.a. the "golden electrode") approach entails selecting a single electrode signal from a given well to be compared across the baseline and dosed conditions and ignoring information from other electrodes in the well. This procedure typically requires manual oversight by the user to select the "golden channel" in each well and may also be accompanied by manual adjudication of the FPD identified by an automated algorithm. While the "golden channel" approach is more labor-intensive, it may provide more accurate results for extreme effects on FPD (>50%ΔFPD). Finally, the "golden channel" approach may be required for low-electrode-count MEA systems, but is more

flexible for high-electrode-count systems due to increased flexibility in selection of the "golden channel."

6. Cell Type-Specific Beating Characteristics: As shown in Fig. 11, the iCell (CDI) and Cor.4U (Axiogenesis) cardiomyocytes exhibit distinct beating profiles in the baseline condition. iCell cardiomyocytes exhibited spontaneous beating at ~0.5 Hz, whereas Cor.4U cardiomyocytes beat at ~1 Hz. Meanwhile, the Cytiva Plus cardiomyocytes (GE Healthcare) have previously exhibited an intermediate beat rate at ~0.75 Hz [19].
7. Double Delta Calculation: A "double delta" calculation is often used for electrocardiogram data in clinical trials. Rather than computing the percent change in a measurement, the difference in the raw value between the dosed and baseline conditions is calculated for each treatment and then adjusted by the same value for the vehicle control. The term "double delta" is used to indicate the two "subtraction" steps (e.g., ΔΔFPD), rather than a subtraction of a percent change calculation (Δ%FPD). The percent change calculation normalizes to the specific beating profile of cell preparation in baseline and thus generally allows more direct comparison across cell preparations.
8. Selecting Pacing Rate: As most commonly used cardiac cell preparations are spontaneously active, pacing rates must be carefully chosen because it is not possible to pace slower than the spontaneous beat rate. So, for compounds that reduce the spontaneous beat rate, it may be possible to pace at slower rates in the dosed condition than was possible to in the baseline condition. By contrast, it may not be possible to achieve the same pacing rate in the dosed condition as baseline if the treatment increases the spontaneous beat rate.

5 Conclusion

The MEA assay provides reliable and predictive measures of cardiac electrophysiology in hSC-CMs using a label-free approach capable of operating at high throughput scale. The protocol described above reflects the current CiPA study guidelines for culturing hSC-CMs, collecting the required electrophysiological end points, and compiling the data analysis. The selected results from the CiPA pilot study included in this chapter highlight the high degree of well-to-well and site-to-site reliability afforded by the protocol and the Maestro multiwell electrophysiological platform, which is essential for effective evaluation of cardiac safety liability in the CiPA framework. In addition, recent technological advances in the MEA assay, including automation and optogenetics, support the extension of MEA-based assays beyond CiPA for evaluation of chronic toxicities, drug-drug interactions, and structure-function relationships.

References

1. Thomas CA, Springer PA, Loeb GE, Berwald-Netter Y, Okun LM (1972) A miniature microelectrode array to monitor the bioelectric activity of cultured cells. Exp Cell Res 74(1):61–66
2. Reppel M, Igelmund P, Egert U, Juchelka F, Hescheler J, Drobinskaya I (2007) Effect of cardioactive drugs on action potential generation and propagation in embryonic stem cell-derived cardiomyocytes. Cell Physiol Biochem 19(5–6):213–224
3. Meiry G, Reisner Y, Feld Y, Goldberg S, Rosen M, Ziv N, Binah O (2001) Evolution of action potential propagation and repolarization in cultured neonatal rat ventricular myocytes. J Cardiovasc Electrophysiol 12(11):1269–1277
4. Ma J, Guo L, Fiene SJ, Anson BD, Thomson JA, Kamp TJ, January CT (2011) High purity human-induced pluripotent stem cell-derived cardiomyocytes: electrophysiological properties of action potentials and ionic currents. Am J Physiol Heart Circ Physiol 301:2006–2017
5. Clements M, Thomas N (2014) High-throughput multi-parameter profiling of electrophysiological drug effects in human embryonic stem cell derived cardiomyocytes using multi-electrode arrays. Toxicol Sci 140(2):445–461
6. Harris K, Aylott M, Cui Y, Louttit JB, McMahon NC, Sridhar A (2013) Comparison of electrophysiological data from human-induced pluripotent stem cell-derived cardiomyocytes to functional preclinical safety assays. Toxicol Sci 134(2):412–426
7. Navarrete EG, Liang P, Lan F, Sanchez-Freire V, Simmons C, Gong T, Wu JC (2013) Screening drug-induced arrhythmia events using human induced pluripotent stem cell-derived cardiomyocytes and low-impedance microelectrode arrays. Circulation 128(11 Suppl 1):S3–S13
8. Braam SR, Tertoolen L, van de Stolpe A, Meyer T, Passier R, Mummery CL (2010) Prediction of drug-induced cardiotoxicity using human embryonic stem cell-derived cardiomyocytes. Stem Cell Res 4(2):107–116
9. Gilchrist KH, Lewis GF, Gay EA, Sellgren KL, Grego S (2015) High-throughput cardiac safety evaluation and multi-parameter arrhythmia profiling of cardiomyocytes using microelectrode arrays. Toxicol Appl Pharmacol 288(2):249–257
10. Spach MS, Barr RC, Serwer GA, Kootsey JM, Johnson EA (1972) Extracellular potentials related to intracellular action potentials in the dog Purkinje system. Circ Res 30(5):505–519
11. Breckenridge LJ, Wilson RJ, Connolly P, Curtis AS, Dow JA, Blackshaw SE, Wilkinson CD (1995) Advantages of using microfabricated extracellular electrodes for in vitro neuronal recording. J Neurosci Res 42(2):266–276
12. Asakura K, Hayashi S, Ojima A, Taniguchi T, Miyamoto N, Nakamori C, Sawada K (2015) Improvement of acquisition and analysis methods in multi-electrode array experiments with iPS cell-derived cardiomyocytes. J Pharmacol Toxicol Methods 75:17–26
13. Bove M, Grattarola M, Martinoia S, Verreschi G (1995) Interfacing cultured neurons to planar substrate microelectrodes: characterization of the neuron-to-microelectrode junction. Bioelectrochem Bioenerg 38(2):255–265
14. Redfern WS, Carlsson L, Davis AS, Lynch WG, MacKenzie I, Palethorpe S, Hammond TG (2003) Relationships between preclinical cardiac electrophysiology, clinical QT interval prolongation and torsade de pointes for a broad range of drugs: evidence for a provisional safety margin in drug development. Cardiovasc Res 58(1):32–45
15. Sager PT, Gintant G, Turner JR, Pettit S, Stockbridge N (2014) Rechanneling the cardiac proarrhythmia safety paradigm: a meeting report from the Cardiac Safety Research Consortium. Am Heart J 167(3):292–300
16. Gintant, G. et al. (2016) Evolution of strategies to improve preclinical cardiac safety testing. Nat. Rev. Drug Discov., 15, 457–71
17. Nakamura, Y. et al. (2014) Assessment of testing methods for drug-induced repolarization delay and arrhythmias in an iPS cell-derived cardiomyocyte sheet: multi-site validation study. J. Pharmacol. Sci., 124, 494–501
18. Kitaguchi T, Moriyama Y, Taniguchi T, Ojima A, Ando H, Uda T, Miyamoto N (2015) CSAHi study: evaluation of multi-electrode array in combination with human iPS cell-derived cardiomyocytes to predict drug-induced QT prolongation and arrhythmia—effects of 7 reference compounds at 10 facilities. J Pharmacol Toxicol Methods 78:93–102
19. Clements M (2016) Multielectrode array (MEA) assay for profiling electrophysiological drug effects in human stem cell-derived cardiomyocytes. Curr Protoc Toxicol 68:22.4.1–22.4.32
20. Boyden ES, Zhang F, Bamberg E, Nagel G, Deisseroth K (2005) Millisecond-timescale, genetically targeted optical control of neural activity. Nat Neurosci 8(9):1263–1268
21. Yizhar O, Fenno LE, Davidson TJ, Mogri M, Deisseroth K (2011) Optogenetics in neural systems. Neuron 71(1):9–34

22. Clements, I.P., Millard, D.C., Nicolini, A.M., Preyer, A.J., Grier, R., Heckerling, A., Blum, R.A., Tyler, P., McSweeney, K.M., Lu, Y.F. and Hall, D., 2016, March. Optogenetic stimulation of multiwell MEA plates for neural and cardiac applications. In SPIE BiOS (pp. 96902C-96902C). International Society for Optics and Photonics
23. Millard DC, Strock CJ, Carlson CB, Aoyama N, Juhasz K, Goetze TA, Stoelzle-Feix S, Becker N, Fertig N, January CT, Anson BD, Ross JD. (2016) Identification of Drug-Drug Interactions In Vitro: A Case Study Evaluating the Effects of Sofosbuvir and Amiodarone on hiPSC-Derived Cardiomyocytes. Toxicol. Sci., kfw153
24. Clements M, Millar V, Williams AS, Kalinka S (2015) Bridging functional and structural cardiotoxicity assays using human embryonic stem cell-derived cardiomyocytes for a more comprehensive risk assessment. Toxicol Sci 148(1):241–260

Chapter 6

Optogenetic Approach to Cardiotoxicity Screening: Simultaneous Voltage and Calcium Imaging Under Paced Conditions

Graham T. Dempsey and Christopher A. Werley

Abstract

We have developed an in vitro cardiotoxicity assay using genetically encoded, engineered protein sensors and actuators (Dempsey et al., J Pharmacol Toxicol Methods, doi:10.1016/j.vascn.2016.05.003, 2016). The assay, based on the Optopatch platform for all-optical electrophysiology (Hochbaum et al., Nat Methods 11:825–833, 2014), incorporates simultaneous measurement of the action potential (AP) waveform and Ca^{2+} transient (CT) in human-induced pluripotent stem cell (hiPSC)-derived cardiomyocytes (CMs) under light-controlled, optogenetic pacing. A syncytium of hiPSC-derived CMs is prepared in a mixed monolayer culture, where a subset of CMs expresses a genetically encoded, dual-function calcium and voltage reporter, CaViar (Hou et al. Front Physiol 5:1–10, 2014), while others express a channelrhodopsin variant, CheRiff. Optical pacing of the CheRiff-expressing cells synchronizes the syncytium and provides a stable electrophysiological background. In this chapter, we discuss details of the Cardiac Optopatch methodology, including cell preparation, Optopatch imaging, and data analysis. We have used this platform to screen the cardiotoxic effects of compounds, both acutely and chronically; examples will be shown. The Optopatch platform provides a robust assay to measure APs and CTs in hiPSC-CMs. This assay will facilitate comparisons of cell-based assays to human clinical data with the goal of a more accurate in vitro predictor of clinical torsades de pointes (TdP).

Key words Optogenetics, Optopatch, QuasAr, GCaMP, CheRiff, CaViar, Human-induced pluripotent stem cell-derived cardiomyocytes, CiPA, Torsades de pointes, Arrhythmia, Early after depolarization, Genetically encoded fluorescence indicator

1 Optogenetic Probes

Since the development of GFP as a tool for live-cell imaging in the 1990s [1, 2], there has been an explosion of research using engineered fluorescent proteins to report on cellular physiology. Because genetically encoded probes often harness the finely evolved and diverse native machinery of the cellular environment (see [3] for an overview of mechanisms), they can report highly varied parameters with exquisite specificity. Reviewed in [3] and [4], genetically encoded fluorescent indicators (GEFIs) have been

Mike Clements and Liz Roquemore (eds.), *Stem Cell-Derived Models in Toxicology*, Methods in Pharmacology and Toxicology, DOI 10.1007/978-1-4939-6661-5_6,

constructed, which report on enzyme activity [5], small-molecule concentration [6], and electrophysiological state [7]. In addition to reporters, there exists a battery of optical actuators (reviewed in [8, 9]) which can be used to change a cell's membrane potential [10], induce intracellular aggregation [11], or trigger signaling pathways [12]. Table 1 shows a small selection of sensors and actuators relevant to cardiotoxicity measurements.

There are a number of advantages to using GEFIs for studying cellular physiology. An inherent advantage of GEFIs is that they are genetically encoded: they can be targeted to subsets of cells using specific promoters and used to tease out the interactions between different cell types in signaling networks. These indicators have minimal cellular toxicity so that they can be used in longitudinal studies at multiple time points spanning days or weeks without the constraints of small-molecule dyes. In addition, all-optical measurements can be multiplexed for high-throughput studies. Furthermore, the broad spectral range of genetically encoded actuators and reporters enables the combination of different modalities for simultaneous stimulation and readout of key physiological parameters.

Voltage and calcium are critical readouts of cardiac electrophysiology, and the ability to stimulate the response of cardiac cells

Table 1
Example GEFIs for sensing different aspects of cellular physiology

GEFI name	Sensing target	Excitation λ (nm)	Emission λ (nm)	References
CheRiff	Voltage stimulation	470	N. A.	[13]
QuasAr2	Voltage	635	710	[13]
ASAP1	Voltage	488	510	[14]
Ace2N-mNeon	Voltage	506	517	[15]
GCaMP6f	Calcium	488	510	[16]
RCaMP-2, jRCaMP1a, jRGECO1a	Calcium	561	600	[17, 18]
Mitycam	Mitochondrial calcium	500	520	[19]
GCaMPer	ER calcium	488	510	[20]
Grx1-roGFP2	Redox state	488	510	[21]
mito-roGFP2-Grx1	Mitochondrial redox state	488	510	[21]
Grx1-roGFP1-iE$_{ER}$	ER redox state	488	510	[22]
PercevalHR	ATP	500	520	[23]

Included are name, sensing target, excitation and emission wavelengths, and literature reference for each

enables controlled beat rates and a stable electrophysiological background. To this end, we have focused on a particular subset of the large pallet of genetically encoded actuators and reporters to enable stimulation and pacing with simultaneous voltage and calcium recording in human-induced pluripotent stem cell (hiPSC)-derived cardiomyocytes (CMs) [24]. Light-controlled stimulation and recording of action potentials (APs) are implemented using a pair of transmembrane proteins, CheRiff and QuasAr2, respectively [13]. Recording of calcium transients (CTs) is implemented using GCaMP6f [16], which is fused to the intracellular side of the QuasAr2 protein. This fusion protein is called CaViar for "calcium and voltage indicator" [25]. We call this platform Cardiac Optopatch (Fig. 1a), which can be utilized for the investigation of drug-induced toxicity and disease phenotyping in cardiac myocytes and more broadly in other electrically excitable cells.

At the heart of the technology is the voltage sensor QuasAr2 [13], a red-light excitable archaerhodopsin variant with near-infrared (NIR) fluorescence that is sensitive to the transmembrane voltage: the balance between darker and brighter chemical states is shifted by the electric field across the protein. QuasAr2 exhibits a number of highly desirable properties as a fluorescence voltage indicator [13, 27]: (1) the relative change in fluorescence intensity is linearly proportional to the voltage change across the physiological voltage range; (2) the response time of the indicator is fast (0.3 ms) at 34 °C; (3) the response is highly sensitive to voltage changes, exhibiting a 90% $\Delta F/F$ per 100 mV; and (4) the expression of the reporter does not perturb the basal electrical properties of the cells. As CMs beat, the fluorescence change tracks the action potential (AP) (Fig. 1b, black spontaneous trace), here in hiPSC-derived CMs from Cellular Dynamics International (CDI).

To stimulate AP firing and pace the cells, we use CheRiff, a highly sensitive channelrhodopsin variant [13]. CheRiff is a blue-light-activated channel and thus has excellent spectral separation from QuasAr2 (red/NIR imaging). When blue light is absorbed by CheRiff, it opens the cation channel, allowing nonspecific flow of ions across the membrane. At typical cardiac resting membrane potentials (−90 mV to −60 mV, depending on cell type), the increased sodium conductance through CheRiff upon blue-light activation is the most relevant component, and as a result the cell becomes depolarized. Six millisecond pulses of blue light are sufficient to trigger a cardiac AP, which propagates across the syncytium outward from the site of stimulation. Periodic trains of blue stimuli reliably pace the syncytium (Fig. 1b, blue and red traces), lock the interspike interval, and reduce variability in AP shape parameters (Fig. 1c).

In addition to triggering and recording voltage, we also measure changes in calcium signaling. As a major mediator of intracellular signaling and the control signal for contraction strength,

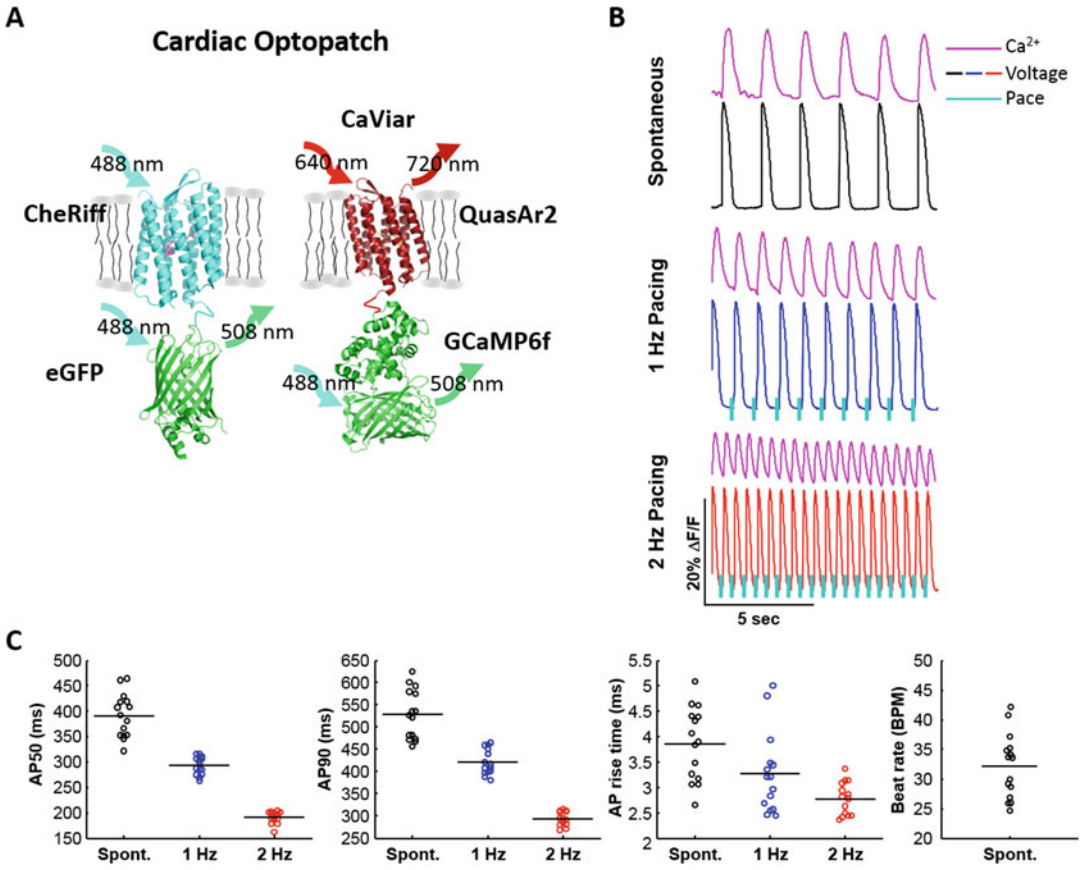

Fig. 1 Optogenetic constructs for simultaneous pacing, voltage, and Ca^{2+} measurement. (**a**) Schematic structures of optogenetic proteins used for pacing and detection of voltage and intracellular Ca^{2+}. The crystal structures of CheRiff and QuasAr2 have not been solved; the diagrams show homologous proteins. Pacing of CMs is achieved through pulsed 488 nm LED illumination of CheRiff. The CheRiff construct is coupled to an eGFP tag for detection of CheRiff expression. A fusion protein called CaViar [25], consisting of QuasAr2 [13] fused to GCaMP6f [16], was used for simultaneous voltage and Ca^{2+} imaging. QuasAr2 was excited via red laser light. GCaMP6f was excited via blue laser light. Cells were separately transduced with either CheRiff or CaViar vectors. (**b**) Voltage traces for spontaneous beating (*black*), paced beating at 1 Hz (*blue*), and paced beating at 2 Hz (*red*). Optical pacing stimuli are shown as *cyan dashes*. The simultaneous measurement of Ca^{2+} (*magenta*) is shown at each pacing condition. (**c**) Dot density plots for the AP50, AP90, AP rise time, and spontaneous beat rate showing dish-to-dish variability across different beat rates. AP parameters show reduced variability with pacing, as indicated by the tighter clustering of data points. *Black horizontal lines* indicate the mean of the distributions. Reproduced from Dempsey et al. [26] with permission

calcium plays a significant role in cardiac function and disease. We used GCaMP6f [16], a popular calcium sensor that is highly responsive to changes in cytosolic calcium levels and non-perturbative to basal calcium handling in CMs [28, 29].

In this chapter, we discuss the details of the Cardiac Optopatch methodology, including cell source, cell preparation, Optopatch imaging, and data analysis. Throughout the text, we highlight

important practical considerations at each stage of the execution of the method and provide detailed protocol information. We also show Optopatch results from applying several well-understood tool compounds, including both acute and chronic treatment. Finally, we highlight the advantages of Optopatch to other approaches and give an outlook on future developments of the technology.

2 Materials

Terminally differentiated iCell cardiomyocytes along with the accompanying plating and culture media were purchased from CDI. Standard six-well, plastic-bottomed plates were used for initial culturing of CMs, and 35 mm dishes (MatTek Corp.; 10 mm glass diameter, #1.5) were used for Optopatch measurements. For spatial segregation of the CheRiff and CaViar cells, Sylgard 184 elastomer was used to make polydimethylsiloxane (PDMS) semicircles. Solutions of 0.1% gelatin and 10 μg/ml fibronectin (powder dissolved in sterile water or PBS) were used for coating dishes. For preparation of Optopatch lentivirus, the following materials are needed: 15 cm plates, HEK293T cells, lentiviral plasmids (Cellecta), transfection reagent (PEI, Polysciences), Opti-MEM serum-free media, and DMEM10.

For Optopatch imaging, all-trans retinal was used to supplement the CDI maintenance media. The Optopatch imaging buffer components in mM are 1.8 $CaCl_2$, 2.5×10^{-4} $Fe(NO_3)_3$, 0.81 $MgSO_4$, 5.3 KCl, 44 $NaHCO_3$, 129 NaCl, 0.91 NaH_2PO_4, 1 sodium pyruvate, and 10 D-(+)-galactose. The key optical components required are red laser source, blue laser source, blue LED, high numerical aperture objective, dichroic and emission filters, and a scientific CMOS camera. See below for recommended specs for each component.

3 Methods

3.1 Cell Source and Preparation

The development of hiPSC-CMs has created an exciting new opportunity for investigating human cardiac electrophysiology, in particular in vitro cardiotoxicity. HiPSC-CMs can now be differentiated into cultures that are predominantly (95%) cardiomyocytes, which express most cardiac ion channels, replicate characteristic changes in AP duration, are more species relevant than animal models, and are easier to obtain in large amounts than are primary CMs [30, 31]. Cellular preparations can now create spontaneously beating cultures and are able to recapitulate the action potential (AP) waveform of ventricular, atrial, and nodal cells [32–34], although recent measurements with voltage-sensitive dyes

suggested a continuous, cell density-dependent distribution of AP morphologies [35]. These cells also provide an inherently more physiological model system for AP studies than heterologous, single-channel expression systems, which do not account for the impact of different combinations of channels and channel subunits, alternative splicing, and posttranslational modifications. Because of these developments, regulatory agencies are considering the use of hiPSC-derived CMs for preclinical cardiotoxicity screening, as has been shown through the Comprehensive In Vitro Proarrhythmia Assay (CiPA) initiative [36, 37]. One concern that has been raised about hiPSC-CMs is their degree of physiological maturation [38]. Thus, as the technology of stem cell-derived CMs continues to progress in the coming years, it will be crucial to understand how their properties translate toward clinical outcomes. Thorough characterization of the electrophysiological profile and ion channel content of these cells will thus be an essential part of their adoption for use in cardiotoxicity assays and other preclinical assessments.

With the prospects of preclinical cardiotoxicity screening and disease modeling, there are now a number of commercial sources of hiPSC-derived CMs that can be purchased for use in a variety of assays. We have applied Optopatch to several different sources of CMs from multiple vendors including CDI, Axiogenesis, Takara-Clontech, GE Healthcare, and Pluriomics. Each cell source typically provides cells as frozen stocks that can be thawed using the vendor-provided protocols and plated into a variety of dish and well formats depending on the application (*see* **Note 1**). In this chapter, we present the detailed protocols and data examples for CDI iCell cardiomyocytes. We first plate CMs in six-well plates to allow transfection of pools of cells with different lentiviruses and then replate cells in glass-bottomed dishes with half the dish expressing CheRiff and half the dish expressing CaViar. As detailed later in this section, we segregate the pacing cells from the readout cells to ensure that the Optopatch recordings are free of stimulus artifacts.

3.1.1 Culturing of Cardiomyocytes

Six-well plates (Falcon # 353046) are coated with gelatin (Millipore # ES-006-B) for improved cell adherence. Plates are incubated overnight with 0.1% gelatin at 4 °C with the top parafilmed to prevent evaporation and ensure sterility. The gelatin solution should be fully aspirated prior to cell plating. Cells should be handled gently and thawed explicitly according to the manufacturer's protocol. We store cell stocks in liquid N_2 and keep them on dry ice until the moment of thawing. In this case, we plate CMs into each well at a density of 2.4×10^4 cells/cm^2 in 1.25 ml of plating medium (CDI) (*see* **Note 2**). The manufacturer instructions recommend slowly adding the plating media dropwise to the cells to minimize osmotic shock and improve cell viability. Cells are incubated at 37 °C in 5% CO_2. After 48 h, cells are rinsed to remove

non-adherent cells and other debris, switched to maintenance medium (CDI), and fed every 48 h until replating, described below.

3.1.2 Transduction with Optopatch Vectors

An essential step for Optopatch is introduction of the optogenetic vectors into the cells to enable stable and efficient expression of CaViar and CheRiff. We experimented with a number of different transfection methods, including viral transduction and lipophilic-based delivery methods. Lentiviral infections with VSV-g pseudotyped particles have been the most robust method we have encountered, giving high, relatively uniform expression efficiencies with minimal compromise to cell health (*see* **Note 3**).

Lentivirus is prepared in-house generally following established protocols [39]. Low-passage number HEK293T cells in 15 cm plates at ~80% confluence are transfected with the lentiviral expression plasmid (CaViar or CheRiff) as well as lentiviral packaging and capsid plasmids (Cellecta # CPCP-K2A). Transfection is mediated with polyethyleneimine (PEI, Polysciences # 20170-170). For each 15 cm plate, the transfection solution comprises 500 µl Opti-MEM serum-free media, 25 µg packaging plasmids, 20 µg expression vector, and 180 µg PEI diluted from a stock solution. After 10 min, the Opti-MEM mixture is added to 25 ml DMEM10 (or other HEK culture media) and exchanged with the current culture media. Virus is harvested 2 days after transfection, aliquoted, and stored at −80 °C for later use (*see* **Note 4**).

Five days after plating, hiPSC-derived CMs are transduced with lentivirus. CaViar is expressed in some wells, CheRiff in other wells. Cells are left overnight in the viral medium at 37 °C in 5% CO_2. Virus is then removed from the cells and 1.5 ml of maintenance medium added to each well. The efficiency of viral delivery is ~80–90%, typically resulting in 8–10 expressing cells in each 100 µm × 100 µm field of view (FOV).

3.1.3 Preparation of Plates for Voltage Imaging with Pacing

For voltage imaging alone, CMs expressing either CaViar or CheRiff can be interspersed because the stimulus light source will not excite the red/NIR QuasAr2. For this experiment, MatTek dishes (MatTek Corp.; 10 mm glass diameter, #1.5) are incubated with 10 µg/ml fibronectin (Sigma # F2006-1 mg) in 0.1% gelatin overnight at 4 °C, and media is fully aspirated prior to cell plating. Cells expressing CaViar and CheRiff are trypsinized according to the manufacturer's protocol, mixed at a volume ratio of 5:1 CaViar-CheRiff, and then pelleted at 180 g for 5 min (*see* **Note 5**). The combined cells are then resuspended in 2.1 ml of maintenance medium, counted with a live-dead stain using a hemocytometer to determine the available number of cells, and plated at a density of 4×10^4 cells/cm^2 in 100 µl of plating medium directly onto the center of the recessed glass (*see* **Note 6**). Cells are kept at 37 °C in 5% CO_2 overnight to adhere to the glass. Maintenance medium

(1.0 ml) is added to each dish, and the cells are fed every 48 h by replacing 750 µl of medium with fresh maintenance medium.

3.1.4 Preparation of Plates for Voltage and Calcium Imaging with Pacing

One challenge associated with pacing and calcium imaging is that the absorption spectra of CheRiff and GCaMP6f are spectrally overlapped, where both require blue-light excitation to function. Although new red/orange calcium sensors [17, 40] have the potential to eliminate this problem, the method presented here uses cell patterning (Fig. 2a). Half the dish expresses CheRiff, which can be stimulated by one blue-light source, evoking an AP that propagates across the dish. The other half of the dish expresses CaViar enabling imaging of voltage and calcium transients using red light and a second blue source (Fig. 2b). Cell patterning is implemented using a semicircle of elastomer, which masks half the dish while the CheRiff cells are plated. After the cells adhere, CaViar-expressing cells are plated everywhere (described below). This enables voltage and calcium imaging in one half of the dish and simultaneous CheRiff pacing in the other, both with blue light but without optical cross talk.

For simultaneous voltage and calcium imaging, MatTek dishes (10 mm glass diameter) are prepared to segregate CheRiff-expressing cells from CaViar-expressing cells as follows. Polydimethylsiloxane (PDMS) semicircles are prepared from roughly 5 mm thick sheets of Sylgard 184 elastomer. Circles slightly smaller than 10 mm diameter are punched from the sheet, bisected with a razor, and sterilized with UV exposure (30 min) followed by ethanol submersion (10 min). The semicircles are treated on one side by applying a solution of 10 µg/ml fibronectin in 0.1% gelatin for 10 min at room temperature before aspirating to remove the solution. The semicircles are then placed onto one side of the recessed MatTek dish glass surface, carefully applying pressure across the top of the PDMS until a complete seal is observed. The remaining exposed area of the glass is then coated with 10 µg/ml fibronectin in 0.1% gelatin at 4 °C overnight. Immediately after its placement, the location of the PDMS semicircle is marked to guide dish orientation and the placement of the pacing light during imaging.

Cells expressing the CheRiff are trypsinized according to the manufacturer's protocol and resuspended in 50 µl of maintenance medium per dish. For plating, 50 µl of the CheRiff cells are then added to the exposed portion of the glass surface and allowed to sit for 40 min at 37 °C in 5% CO_2 to allow the cells to adhere. The PDMS discs are then removed, the glass surface washed with 150 µl of maintenance medium, and the remaining volume aspirated. Trypsinized CaViar cells are then resuspended in 100 µl of maintenance medium per dish and plated at a density of 4.0×10^4 cells/cm^2 in 100 µl to cover the entire glass surface. Cells are kept at 37 °C in 5% CO_2 overnight to adhere to the glass. 1.0 ml of

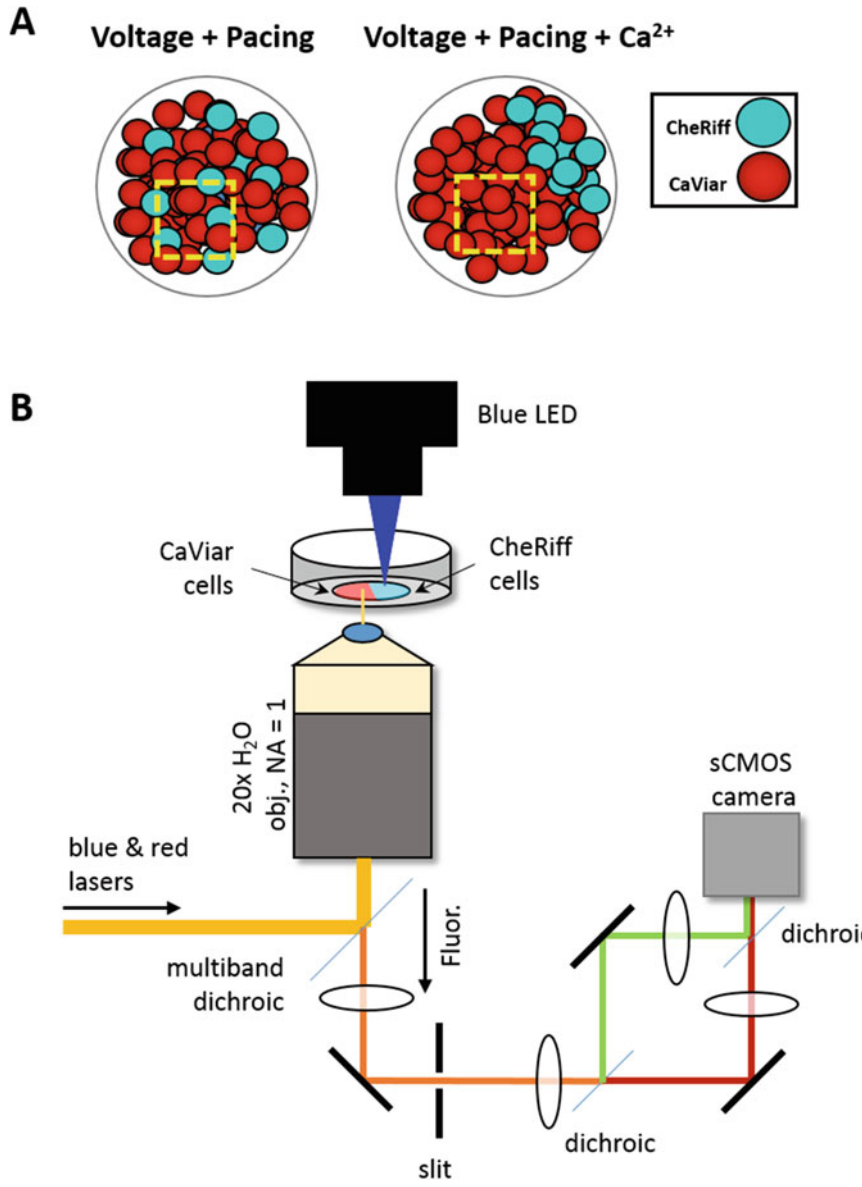

Fig. 2 Schematic of plating schemes and custom instrument for Optopatch measurements. (**a**) CM plating configurations. For simultaneous optical pacing and voltage imaging, CheRiff cells (*solid cyan circles*) were comingled with CaViar cells (*solid red circles*). The *yellow dotted line* indicates a microscope field of view. For simultaneous optical pacing and imaging of both Ca^{2+} and membrane voltage, cells were plated to spatially segregate CheRiff-expressing cells to avoid optical cross talk. The CheRiff-expressing cells lay outside the imaging region. (**b**) Red (640 nm) or blue (488 nm) laser light was directed toward the sample (as shown in *yellow*) through a 20× water immersion objective lens, with NA of 1.0, in an epifluorescence format. Fluorescence was collected by the same objective and passed through a dichroic mirror. A home-built dual-view detection scheme was used to image each fluorescent band (shown as *red* and *green*) onto adjacent halves of a scientific CMOS (sCMOS) camera. This approach enabled simultaneous detection of QuasAr2 and GCaMP6f fluorescence. For pacing of CMs, a blue LED source was positioned above the dish. (**a**) Reproduced from Dempsey et al. [26] with permission

maintenance medium is added to each dish, and the cells are fed every 48 h by removing 750 μl of media from the dish and adding 750 μl fresh maintenance medium.

3.2 Optopatch Imaging

It takes approximately 1 week for full expression of the reporter proteins after lentiviral infection; cells can be reliably imaged between 8 and 20 days post-thaw. Depending on the choice of CM source, cells can be ready for conducting assays as early as 1 week post-thaw (*see* **Note 7**).

3.2.1 Sample Treatment Prior to Imaging

For the CDI cells, we incubate with 5 μM retinal (Sigma-Aldrich # R2500) in maintenance medium for >30 min at 37 °C in 5% CO_2 immediately prior to recording. Alternatively, one can use 1 μM retinal for 24–48 h prior to imaging. Be sure to confirm the media components with each cell provider prior to use (*see* **Note 8**).

Following the incubation with retinal, the medium is completely removed from the dish and replaced with 1.5 ml of warmed cardiac imaging buffer, which matches the salt and sugar concentrations of maintenance medium but lacks phenol red, vitamins, and amino acids (*see* **Note 9**). The formula in mM is 1.8 $CaCl_2$, 2.5×10^{-4} $Fe(NO_3)_3$, 0.81 $MgSO_4$, 5.3 KCl, 44 $NaHCO_3$, 129 NaCl, 0.91 NaH_2PO_4, 1 sodium pyruvate, and 10 D-(+)-galactose. The buffer is adjusted to pH 7.3 by placing the initial solution at 37 °C in 5% CO_2 for 30 min to equilibrate, removing and immediately adjusting the pH to the desired value and returning to 37 °C in 5% CO_2 to ensure a stable pH value. Cells are kept at 37 °C in 5% CO_2 for 30 min in the buffer prior to imaging. Alternatively, other imaging buffer formulations could be used, but one should confirm that the media components do not adversely impact the performance of the CMs. We have performed Optopatch imaging of CMs in full maintenance media and obtained successful recordings, albeit at reduced signal-to-noise ratio (SNR) compared to the cardiac imaging buffer formulation without phenol red, vitamins, and amino acids.

3.2.2 Spontaneous Beating and Paced Action Potentials

For Cardiac Optopatch instrumentation, one must consider the appropriate excitation light sources, filters, objective lens, and fluorescence detection element to ensure the highest assay performance. We have tested a variety of instrument designs and highlight some of the appropriate hardware choices in each case.

For measurement of spontaneous activity, hiPSC-derived CMs expressing CaViar are exposed to whole-field, constant illumination with red laser light ($\lambda = 640$ nm, 50 W/cm^2) to excite fluorescence of the QuasAr2 voltage indicator. Red lasers can be purchased from a variety of vendors including Coherent, MPB Communications, Dilas, or CNI with tradeoffs between cost, performance, and laser power. Fluorescence is collected via either a 20× water immersion objective with a numerical aperture (NA) of

1.0 (Zeiss # 421452-9700-000) or a 60× oil immersion objective with NA of 1.49 (Olympus APON 60XOTIRF). The higher NA objective provides increased SNR, though the water immersion objective allows for sufficient SNR to resolve critical features of the AP and calcium waveform. The collected fluorescence is separated from illumination light via a Cy5 or Alexa 647 band-pass emission filter (Chroma) that is matched to the emission band of QuasAr2; the optimized filter is Semrock FF01-736/128. The preferred sensor technology is a scientific CMOS (sCMOS) camera (e.g., Hamamatsu ORCA-Flash4.0) because it can record with low noise with a large FOV at the high, ~500 Hz frame rates required to resolve the upstroke of the cardiac AP (*see* **Note 10**). Alternative options to sCMOS cameras include EMCCD cameras or sensitive photodiode detectors. The use of high-quantum efficiency, low-noise detectors is critical for achieving high SNR Optopatch recordings. For pacing, pulses of blue LED illumination (6 ms, 0.5 W/cm^2, 470 nm wavelength) are delivered to the dish to stimulate the CheRiff optogenetic actuator, which pace the entire syncytium through gap junction-mediated conduction. Fluorescence is recorded from the CaViar-expressing cells under constant red illumination (as described above).

3.2.3 Simultaneous Imaging of Voltage and Ca^{2+}

Simultaneous pacing and measurements of voltage and Ca^{2+} are performed by plating CheRiff-expressing CMs on half the dish and CaViar-expressing CMs on the other half (as described above, and *see* Fig. 2a). Pulses of intense 470 nm LED illumination (Thorlabs # M470L3) are delivered to the CheRiff half of the cells to pace the dish (Fig. 2b). Continuous blue and red illumination are delivered to the central cells to monitor Ca^{2+} and voltage simultaneously. Blue laser light ($\lambda = 488$ nm, 0.15 W/cm^2, Coherent OBIS 488 LX; **Note 11**) excites fluorescence of the GCaMP6f genetically encoded Ca^{2+} indicator, and red laser light ($\lambda = 640$ nm, 50 W/cm^2) excites fluorescence of the QuasAr2 voltage indicator. Several vendors sell 488 nm laser sources that can be used with the same tradeoffs as mentioned above for the red laser. A dual-view imaging system projects emission from GCaMP6f (500–550 nm) and from QuasAr2 (660–760 nm) onto adjacent halves of a sCMOS camera, operating at a frame rate of 100–500 Hz. Typically, we send blue and red laser illumination up through the objective lens of our inverted microscope to excite the fluorescent sensors. We use a blue LED mounted from above and focused several mm away to excite the CheRiff-expressing cells.

Custom software is written to control and synchronize the illumination, camera, and optogenetic stimuli and enable the application of arbitrary optical waveforms. We use scripts written in either LabVIEW (National Instruments) or MATLAB (MathWorks).

3.2.4 Comparison of QuasAr2 with FluoVolt

When using an exogenous sensor, it is of critical importance to confirm that the sensor is accurate and does not perturb the cells being studied. To confirm this, we use the voltage-sensitive dye FluoVolt, whose sub-millisecond response time ensures accurate reproduction of the cardiac AP.

MatTek dishes are prepared as described in "Preparation of Plates for Voltage Imaging with Pacing" and plated with unlabeled cardiomyocytes at a density of 8.5×10^4 cells/cm^2. After 8 days in culture, QuasAr2 is expressed in a sparse subset of CM via lipofection (Mirus LT-1) with a construct comprising: CMV-CamKII-QuasAr2-mOrange [13]. For each MatTek dish, the transfection mixture (400 ng DNA, 7.5 μl LT-1, 500 μl Opti-MEM) is mixed and incubated for 15 min at room temperature. The mixture is added dropwise to the cells after 8 days in culture, and the feedings proceeded normally. QuasAr2 is expressed in <5 % of the cells. The overall expression levels are lower than with lentivirus due to the distant CMV promoter in the CamKII construct.

Measurements are performed 4 days after transfection. FluoVolt (Life Technologies) is added to the dish according to the manufacturer's instructions. This dye labels every cell in the dish. QuasAr2-expressing cells are located using red excitation and near-infrared fluorescence. Green fluorescence from FluoVolt and near-infrared fluorescence from QuasAr2 are imaged simultaneously using a dual-wavelength imaging system (Fig. 2b). FluoVolt signals are compared between cells expressing and not expressing QuasAr2. Measurements are performed on spontaneously beating cells.

The top traces in Fig. 3a–b show the overlaid fluorescence readout from QuasAr2 and FluoVolt. The excellent agreement verifies the linear response of both (which have independently been characterized using patch clamp [13, 41]). The bottom traces (Fig. 3a–b) show no difference between cells with and without QuasAr2 expression, indicating that our voltage reporter does not perturb CM electrophysiology. Furthermore, extended red imaging, although it does cause slight photobleaching of the fluorescent sensor, does not perturb the cardiac AP (Fig. 3c–d). In fact, we routinely record cumulative five-point dose responses, including multiple pacing frequencies at each drug concentration, with no appreciable change in the AP waveforms in controls (Fig. 4).

3.2.5 Preparation and Storage of Drug Stocks

Compound handling is a critical component of performing a reliable assay. For the data shown in this chapter, compounds were purchased as dried powders, with the exception of DMSO (Sigma-Aldrich). Each compound was dissolved in DMSO to achieve a stock concentration of 10 mM. Be sure to confirm solubility properties and safe handling procedures for each compound prior to testing. Here compounds were solubilized in DMSO by vortexing the solution at room temperature until completely dissolved,

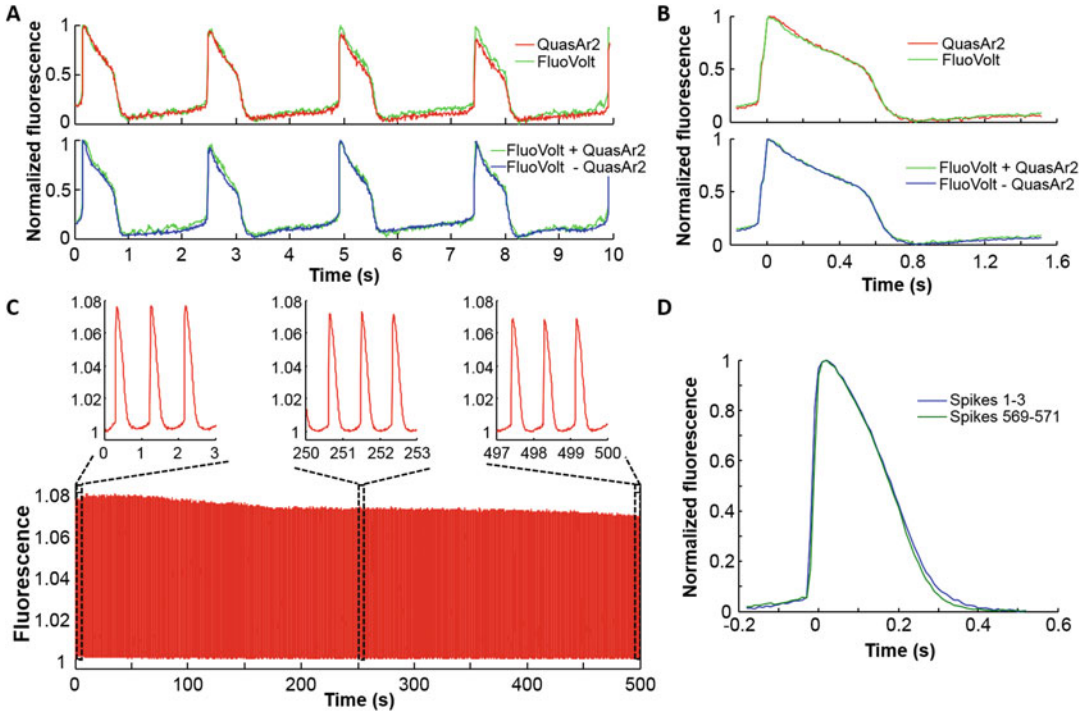

Fig. 3 QuasAr2 reports cardiomyocyte (CM) action potentials (APs). (**a**) Comparison of the CM AP waveforms, as measured by the genetically encoded voltage indicator QuasAr2 and the voltage-sensitive dye, FluoVolt. Cells were sparsely transfected with the QuasAr2 construct and then treated with FluoVolt dye. QuasAr2 was excited by 640 nm laser light with fluorescence detection centered at 720 nm. FluoVolt was excited by 488 nm laser light with fluorescence detection centered at 525 nm. The top panel shows the simultaneously recorded AP waveforms from a cell expressing QuasAr2 (*red line*) and labeled with FluoVolt (*green line*). The lower trace compares the FluoVolt AP waveform in the presence (FluoVolt$^+$, QuasAr2$^+$, *green*) and absence (FluoVolt$^+$, QuasAr2$^-$, *cyan*) of QuasAr2 expression. (**b**) Plots of the average waveforms from the traces in (**a**). (**c**) Phototoxicity and photobleaching measurement of QuasAr2. Cells were imaged under continuous red laser illumination (~50 W/cm^2) for 500 s. Expanded views of the fluorescence recording are shown in the lower panels. (**d**) The average AP waveform shapes for the beginning (*blue*) and end (*green*) of the trace in (**c**). (**b**–**d**) Reproduced from Dempsey et al. [26] with permission

typically 2–3 min. One hundred microliter aliquots (of 10 mM stock) were prepared and immediately stored at −20 °C until use. The catalog numbers (Sigma-Aldrich) for the compounds shown in this chapter are as follows: DMSO (D8418), quinidine (Q3625), nifedipine (N7634), cisapride (C4740), and pentamidine (P0547).

For each compound and each concentration, stocks are prepared by dilution from the 10 mM stock in cardiac imaging buffer and kept at 37 °C in 5% CO_2 prior to use. The diluted stocks are made such that the final drug concentration could be achieved upon addition of 100 μl to the dish containing 1.0 ml of custom cardiac imaging buffer. A "blank" containing cardiac imaging

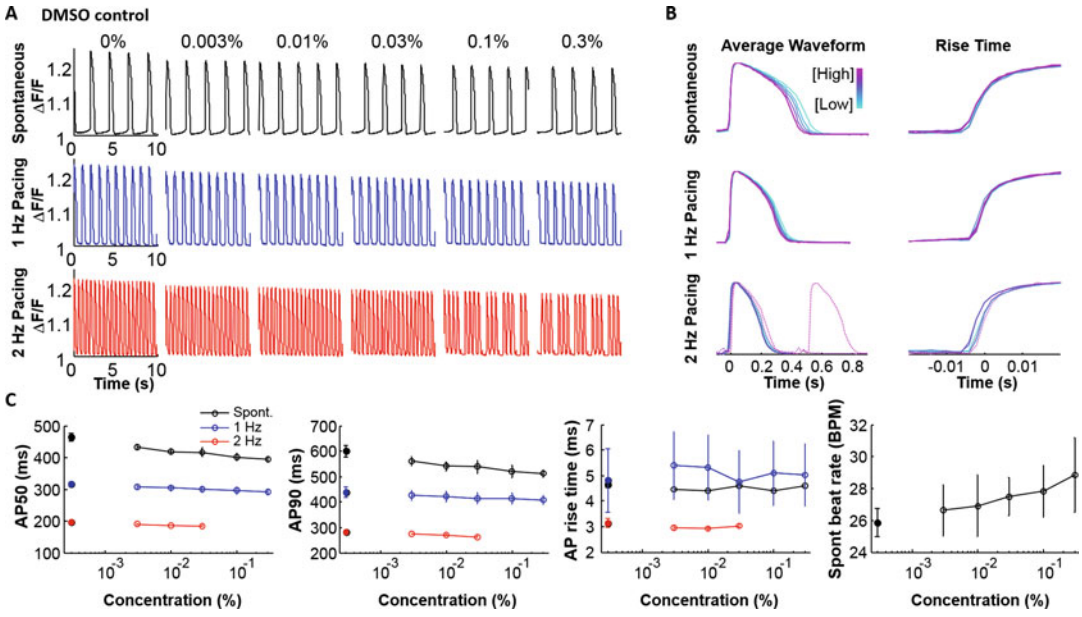

Fig. 4 Treatment of CMs with a DMSO control. (**a**) Fluorescence ($\Delta F/F$) versus time as a function of DMSO concentration, for spontaneously beating cells (*top*, *black*) and the same cells paced at 1 Hz (*middle*, *blue*) and at 2 Hz (*bottom*, *red*). Traces are taken from a single dish of cells and a single field of view. Data acquired at 100 Hz frame rate. Cells were treated with sequentially increasing concentrations of DMSO. (**b**) The average waveform (*left panels*, acquired at 100 Hz frame rate) and average upstroke (*right panels*, acquired at 500 Hz frame rate) for the concentrations tested (cyan to magenta, lowest to highest concentration). *Dashed lines* indicate that the cells did not beat at the specified pacing rate. In the case of spontaneous beating, this criterion did not apply. (**c**) Dose dependences of the AP50, AP90, AP rise time, and spontaneous beat rate. *Closed circles* represent the "blank" addition of imaging buffer; *open circles* represent addition of compound. Beat rates correspond to spontaneous (*black*), 1 Hz (*blue*), and 2 Hz (*red*). In the case of 1 and 2 Hz pacing, data points are omitted when the cells did not beat at the specified pace rate. Error bars represent standard error of the mean

buffer alone was also prepared for each drug and kept at 37 °C in 5% CO_2 prior to use. All dilutions were prepared fresh from a 10 mM frozen stock on the day of the measurement.

3.2.6 Drug Addition and Imaging

Imaging is performed on a custom-built epifluorescence microscope (Fig. 2b). The beat rate properties of CMs can change dramatically depending on the temperature and environmental conditions used for imaging. For this reason, cells are maintained at a temperature of 35–37 °C on the microscope using a heated stage (Warner Instruments) and objective collar (Bioptechs). The microscope is equipped with an *xy*-translation stage (Ludl Electronic Products) that allows for precise recording and retrieval of stage positions. This can be used to identify different regions of the dish, store their positions, and return to those regions for cumulative dosing of the same cells with compound. A home-built

environmental chamber maintains cell cultures in air with high humidity and 5 % CO_2 throughout the experiments. This is critical for maintaining a stable pH in the carbonate-based imaging buffer system described above.

Each cumulative drug addition is performed as follows. A MatTek dish is placed on the microscope for 10 min to allow the cells to stabilize in the environmental chamber. Cells are then pre-paced at 2 Hz for 1 min, followed by continuous illumination with red light for 20 s. This serves to expose all the cells in the dish to the same pacing stimulus before drug addition and to ensure that cells are able to follow the desired pacing frequency. A "blank" negative buffer control of 100 μl is then added to the dish and thoroughly mixed by pipetting ten times. The sample is then allowed to stabilize for 3–5 min before the start of the imaging protocol (see below). The imaging protocol is performed for three fields of view (FOVs) selected by the operator to ensure the presence of QuasAr2- and GCaMP6f-expressing cells and the microscope *xy*-stage positions saved for each. Immediately after, 100 μl of the warmed, diluted stock concentration is added to the dish and mixed by gently pipetting up and down ten times to achieve the lowest desired drug concentration. The imaging protocol is then performed for the same three FOVs. This process is repeated for each drug concentration. A vehicle control is performed for DMSO at concentrations of 0.003, 0.01, 0.03, 0.1, and 0.3% (Fig. 4). For chronic exposure to drug, cells are imaged before and after drug addition and then returned to the incubator for 20–48 h prior to reimaging.

The imaging protocol for each FOV is:

- Three seconds of red laser illumination to reduce the presence of phototransients before the recording
- Thirty seconds of red laser illumination (or red and blue laser when imaging voltage and Ca^{2+}) to record spontaneous beating: 25 s recording at 100 Hz followed by 5 s recording at 500 Hz
- Red (and blue) laser illumination turned off for 4 s to allow for data storage
- Blue LED illumination to pace the cells at 1 Hz for 1 min
- Simultaneous 1 Hz pacing with 15 s of red (and blue) laser illumination: 10 s recording at 100 Hz followed by 5 s recording at 500 Hz
- Red (and blue) laser illumination turned off for 4 s to allow for data storage
- Blue LED illumination to pace the cells at 2 Hz for 1 min
- Simultaneous pacing of the cells at 2 Hz with 15 s of red (and blue) laser illumination: 10 s recording at 100 Hz followed by 5 s recording at 500 Hz

Although we were very conservative in our initial experiments to pace the cells for long periods before recording so they would fully equilibrate, more experience has revealed that the "pre-pacing" can be reduced or even eliminated in some cases. Another protocol that has been informative is a ramped stimulus rate, where the stimulation frequency is gradually increased from the spontaneous beat rate up to where the cells can no longer maintain the pace rate. In addition to measuring how the shape parameters change with beat rate, the frequency at which cells cannot keep pace and their behavior just below this frequency can be very revealing of drug effects.

3.3 Optopatch Data Analysis

Data analysis is performed using custom MATLAB software focused on quantifying (1) changes in AP waveform (early after depolarizations or EADs, alternans, cessation of beating), (2) changes in calcium handling (cessation of Ca^{2+} flux, Ca^{2+} sparks, baseline Ca^{2+}, and Ca^{2+} amplitude), and (3) AP50, AP90, beat rate, and maximal upstroke velocity.

A brief description of the data analysis is given below.

3.3.1 Identification of Action Potentials and Calcium Transients

To identify the timing of the APs, voltage traces are first corrected for photobleaching using a sliding linear interpolation with a 2 s window. Each trace is scaled to report fractional changes in fluorescence relative to baseline ($\Delta F/F$). The first derivative of each trace is used to locate the spike upstroke (maximal dF/dt) and this is recorded as the spike time. An alternative method of finding the rising edges that has proven more robust for noisy data is to convolve the time trace with a step function and find the maxima of the convolution output.

In paced recordings, blue-light stimulus artifacts are removed by linear interpolation between the frames immediately before and after the stimulus pulse. There is typically a 10 ms delay between the onset of the blue pulse and the upstroke of the AP. Given the ~700 μm separation between stimulation and recording regions, we can infer a conduction velocity of ~70 mm/s. Ca^{2+} traces are not corrected for photobleaching. The spike timing is extracted using the information from the voltage traces. Each Ca^{2+} trace is scaled to fractional fluorescence units, $\Delta F/F$.

3.3.2 Classification of Action Potentials and Calcium Transients

The inter-beat interval is calculated by recording the average time, in seconds, between AP upstrokes, whose timing is determined as described above. AP50 and AP90 are calculated from the average beat from each 100 Hz frame-rate movie. AP50 and AP90 are the duration in ms of the AP at 50% and 90% repolarization, respectively. Linear interpolation was used to achieve subframe precision in this timing.

The rise time is determined from the 500 Hz movies. The upstroke is defined as the time for the fluorescence to travel

between 30 and 70% of the full deflection. Timing is calculated with subframe precision using linear interpolation. The reported value is the mean rise time over all beats in a given trace. The Ca^{2+} transient is characterized by the amplitude of $\Delta F/F$ in the CT, averaged over all beats in a given trace.

3.3.3 Statistical Analyses

All error bars reported represent the standard error of the mean across three FOV acquired in each of two dishes (six measurements) unless indicated otherwise. All statistical comparisons are performed using a one-way ANOVA with Dunnett's test for statistical significance. All p values are considered significant if <0.05.

3.4 Baseline Characteristics and Example Drug Effects

Baseline dish-to-dish variability is a critical parameter for an assay, and many iPSC-CM-based assays are particularly sensitive to this because they rely on the highly variable spontaneous beat rate. We quantify this variability across all of the dishes, using "blank" measurements made immediately prior to compound addition. Figure 1c shows dot density plots comparing AP50, AP90, and rise time for both spontaneously beating cultures and those paced at 1 and 2 Hz. As expected, the pacing shortened the AP in a rate-dependent manner. In addition to locking the beat rate, optical pacing also decreased dish-to-dish variability in AP shape parameters, underscoring the importance of pacing when detecting subtle, drug-induced shifts in AP properties. The AP50 was 391 ± 61 ms (mean ± s.d.) in spontaneously beating cultures, 293 ± 24 ms at 1 Hz pacing, and 191 ± 17 ms at 2 Hz pacing. The AP90 showed a similar reduction in variability (528 ± 79 ms for spontaneous beating, 422 ± 40 ms for 1 Hz pacing, 293 ± 23 ms for 2 Hz pacing), as did the rise time, but only at 2 Hz pacing (3.9 ± 1.0 ms for spontaneous beating, 3.3 ± 1.1 ms for 1 Hz pacing, 2.8 ± 0.4 ms for 2 Hz pacing). The final dot density plot shows the spread in the cultures' spontaneous beat rates (32.1 ± 7.6 beats/min). These results highlight the importance of optical pacing with Optopatch to mitigate dish-to-dish variability of AP parameters arising from the natural variability of the spontaneous beat rate of the cultures.

Results from a DMSO vehicle control are shown in Fig. 4. The first noteworthy observation is recording quality: voltage is detected with fractional fluorescence changes of $\Delta F/F = 30\%$ and excellent signal to noise (500:1 at 100 Hz frame rate, 200:1 at 500 Hz frame rate). The pacing fidelity is faithful at 1 Hz and in the first measurements at 2 Hz. The increasing DMSO concentration and effects of repeated imaging have a small but measureable effect on the AP waveforms. The biggest effects are observed in the un-paced cultures where the spontaneous beat rates increased from 25.8 ± 0.9 to 28.8 ± 2.4 beats/min over the course of 75 min measurement. The AP width decreases with increasing DMSO concentration: from 0 to 0.3% DMSO, the AP50 decreased from 464 ± 11 to 394 ± 8 ms, and AP90 decreased from 600 ± 23 to

512 ± 15 ms. Under optical pacing conditions, the AP width also shortens, but the fractional changes are approximately threefold smaller: at 1 Hz the AP50 decreased from 315 ± 8 to 292 ± 10 ms, and AP90 decreased from 439 ± 20 to 408 ± 19 ms. These observations further illustrate the importance of pacing to minimize drift in AP parameters.

To validate the Optopatch platform for use in cardiotoxicity, we have tested a battery of ion channel modulators; the results from a few are shown here. Cisapride, originally developed as a gastroprokinetic, was removed from the market due to cardiac complications arising from hERG block [42], and corresponding effects were detected by Optopatch (Fig. 5a, c). Under spontaneous beating, 0.1 μM cisapride markedly increased both the AP50 and AP90 and also extended the rise time by twofold. At 1 μM cisapride the voltage waveform changed drastically, with slow,

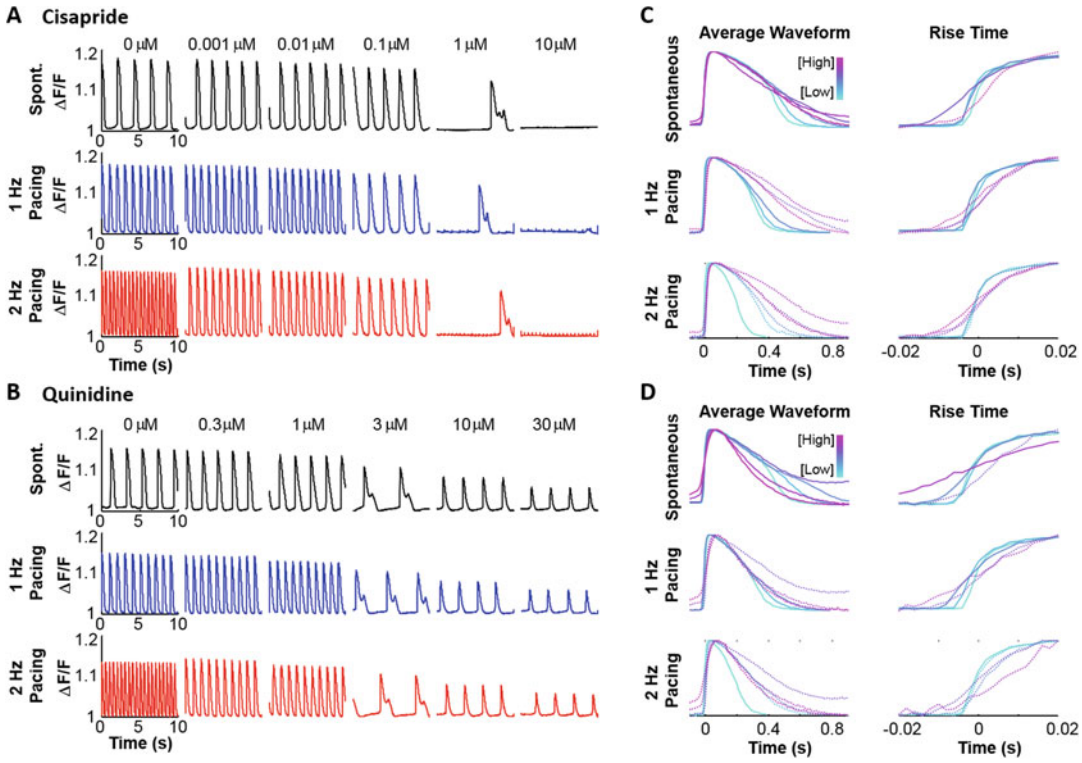

Fig. 5 Alterations in the AP waveform induced by cisapride and quinidine. Fluorescence ($\Delta F/F$) versus time for (**a**) cisapride and (**b**) quinidine, for spontaneously beating cells (*top*, *black*) and cells paced at 1 Hz (*middle*, *blue*) and 2 Hz (*bottom*, *red*). Cells were treated with sequentially increasing concentrations of drug. Both cisapride and quinidine induced EADs. (**c**, **d**) Average AP waveform (*left panels*) and upstroke (*right panels*) for the concentrations tested (*cyan* to *magenta*, *lowest* to *highest* concentration). *Dashed lines* indicate that the cells did not beat at the specified pacing rate. In the case of spontaneous beating, this criterion did not apply. (**a**) Reproduced from Dempsey et al. [26] with permission

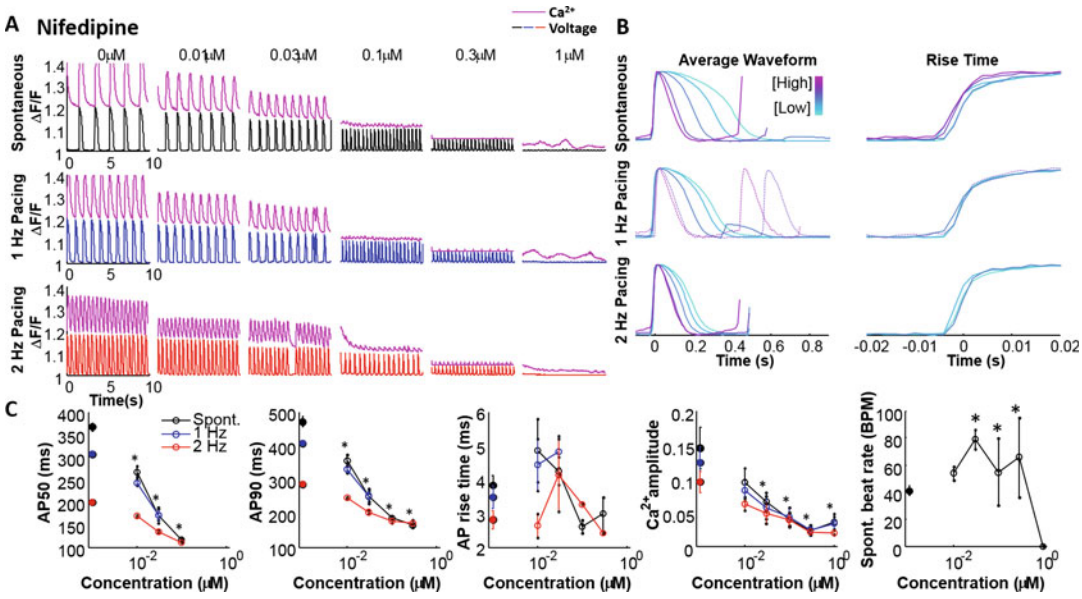

Fig. 6 Alterations in the AP waveform and Ca^{2+} transients induced by nifedipine. (**a**) Fluorescence ($\Delta F/F$) versus time for nifedipine-treated CMs, for spontaneously beating cells (*top*, *black*) and cells paced at 1 Hz (*middle*, *blue*) and 2 Hz (*bottom*, *red*). The Ca^{2+} waveforms (*pink*) for these cells are shown above each of the corresponding voltage waveforms. (**b**) Average AP waveform (*left panels*) and upstroke (*right panels*) for the nifedipine concentrations tested (*cyan* to *magenta*, *lowest* to *highest* concentration). (**c**) Quantification of the AP50, AP90, rise time, CT amplitude, and spontaneous beat rate. (**c**) Reproduced from Dempsey et al. [26] with permission

irregularly spaced spontaneous beats and EADs in both spontaneous and paced APs.

In addition to hERG blockers, Na^+ channel blockers such as quinidine had dramatic effects on the AP waveforms (Fig. 5b, d). At 1 μM, the APs began to widen and the rise time slowed significantly. At 3 μM, EADs were observed. At concentrations >3 μM, cells continued to beat, but with a sharp reduction in AP amplitude and a greatly modified shape. Quinidine's mechanism of action and the changed AP shape are consistent with depolarizations dominated by calcium currents instead of sodium currents.

The calcium channel blocker nifedipine affected voltage and calcium transients in both spontaneously beating and paced cultures (Fig. 6). Most notably, the calcium amplitude decreased with increasing concentration until it was extinguished at higher doses. The spontaneous beat rate increased rapidly with concomitant reduction in AP width and voltage amplitude. The rise time, which is presumably dominated by sodium currents, was not significantly affected. The syncytium stopped beating at a concentration of 1 μM.

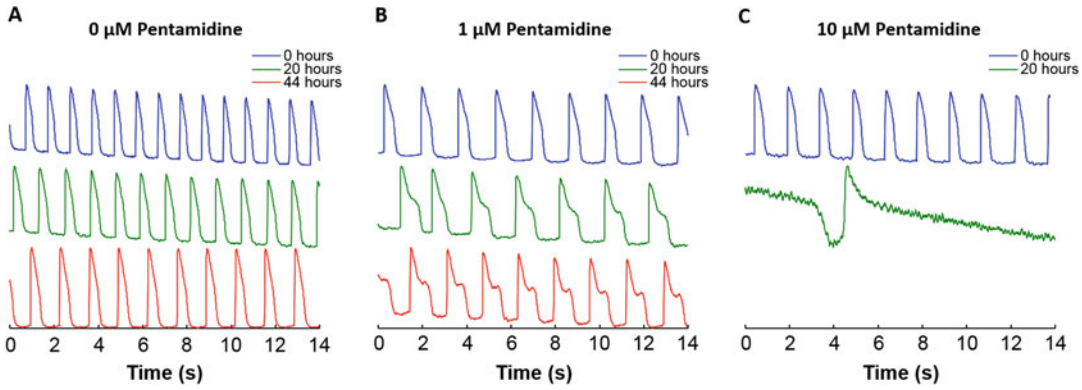

Fig. 7 Alterations in the AP waveform following chronic treatment with pentamidine. Fluorescence ($\Delta F/F$) versus time at immediately after compound addition (0 h), 20 and 44 h after pentamidine addition. Reproduced from Dempsey et al. [26] with permission

In addition to acute effects, we have used the Optopatch system to report effects from chronic drug exposure (>24 h), a procedure that cannot be executed with toxic fluorescent dyes. Pentamidine causes prolonged QT and TdP in patients due to compromised hERG trafficking [43]. We observed a gradual change in the AP waveform on the 10-h timescale in the presence of pentamidine (Fig. 7). In the absence of pentamidine, the AP shape was relatively stable over the measurement period of 44 h (Fig. 7a). At 1 μM pentamidine, the CMs showed no acute change in the AP waveform (Fig. 7b). By 20 h, however, the AP waveform showed clear AP90 prolongation which evolved into EADs by 44 h. At 10 μM pentamidine, we observed a highly distorted AP waveform at 20 h and completely abolished beating by 44 h (Fig. 7c). These measurements demonstrate that the Cardiac Optopatch system can probe long-term effects of drug exposure, which is possible because of the stable expression of the voltage sensor, and the noncontact, optical measurements preserve dish sterility.

4 Notes

1. The most common challenge we have encountered when working with different cell sources is associated with cell adherence to the glass-bottomed dishes we use for Optopatch imaging. We have found that it is likely necessary to re-optimize the surface coating protocol when switching between cell types. One should also consider Matrigel and related products as an alternative coating material.
2. Cell plating efficiency is batch specific. Be sure to check the certificate of analysis and preferably perform a live-dead stain

using a hemocytometer and a standard light microscope to determine the actual number of platable cells per vial.

3. In addition to choice of transfection method, one must also choose the promoter for driving protein expression. There are a variety of options for generalized expression in mammalian cells, including CAG, EF1a, CMV, and SV40 to name a few. Here we use the CMV promoter, which is a strong mammalian expression promoter derived from the human cytomegalovirus.
4. It is important to make robust preparations of lentivirus to ensure homogeneous distribution of Optopatch expression. If the viral titer is too low, cells will not express the optogenetic proteins at sufficiently high levels to ensure high SNR measurements of voltage and calcium and optical pacing. If one chooses to make their own stock of lentivirus, be sure to use some measure of viral titer. We have also encountered highly variable lentiviral titers in some commercially available sources, so be sure to check that the active viral particles are consistent across batches. It is recommended to use single thaws of the virus because viral titre degrades significantly with each freeze-thaw cycle.
5. Not all cell providers have established protocols for trypsinizing CMs. Be sure to check with the manufacturer in each case.
6. To ensure robust optical pacing across the dish when using spatial segregation of the CheRiff- and CaViar-expressing cells, the CMs must maintain a syncytium. If the cells are too sparse, one will not be able to pace. This can easily be detected by testing different pace rates (e.g., 1.5 and 2 Hz) and determining if the CMs can follow the pacing light. When CMs don't follow the pace light, the cells are either too sparse or CheRiff is not expressed sufficiently well (*see* **Note 4**). Different CM sources exhibit different spontaneous beat rates, so be sure to test pacing rates that are higher than the spontaneous beat rate.
7. Be sure to check with the individual CM providers to ensure that the cells are being imaged in the optimal assay window. For CDI iCell CMs, we typically image 14 days post-thaw.
8. An important first step prior to Optopatch imaging is to ensure that the cells have been treated with all-trans retinal, the chromophore used by both QuasAr2 and CheRiff. For many cell providers, the cell culture media is supplemented with retinal and may not require exogenous addition. For others where the retinal is not included, the cells will need to be treated prior to imaging to ensure proper performance of the proteins. Be sure to check the media components with each cell provider. We have used both acute and chronic addition of retinal to the media. However, the retinal concentrations should not exceed the prescribed concentrations to ensure robust cell viability.

9. An important consideration in using hiPSC-derived CMs is the choice of imaging media. For Optopatch imaging, a custom cardiac imaging buffer is used to minimize background autofluorescence while maintaining stable cellular physiology and spontaneous beating. A variety of buffer compositions (Tyrode's, serum containing, serum-free, etc.) have been employed in related techniques (multielectrode array, voltage-sensitive dyes, etc.). These buffers can also be used for Optopatch measurements. However, one will need to validate the choice of imaging media to ensure that the cell physiology and SNR of the optical sensors are unperturbed.
10. One important consideration when designing a microscope for Optopatch imaging is maximizing the FOV that can be recorded at high frame rates. Typical commercial microscopes operate at high magnification and map the center of an objective's imaging area, where aberrations are minimized, onto the full camera sensor. This design is ideal for recording beautiful, static immunofluorescence images, but is very inefficient for simultaneously recording from many cells at high frame rate. In cameras, the smaller the sensor area that is read out, the faster the maximum frame rate. To maximize the number of cells that can be recorded from simultaneously at 500 Hz, then, it is desirable to reduce the magnification of the imaging system. By reimaging the sample (Fig. 2b) with a demagnification factor of 4×, we can record a 300 × 400 μm FOV with the 60× objective (15× actual magnification) or a 750 × 1000 μm FOV with the 20× objective (5× actual magnification).
11. Blue laser intensity should be set as described in the text. Be careful not to set this intensity too high as it can be detrimental to the cell health.

5 Conclusions and Outlook

The Cardiac Optopatch platform has a number of distinct advantages over existing methods for characterization of electrophysiological properties of CMs: (1) The ability to measure both voltage and calcium waveforms under paced conditions within a single cellular preparation has not been possible with other platforms largely due to spectral overlap of available reporters. (2) The use of CheRiff enables robust optical pacing of the CM cultures. Both the AP and CT waveforms are highly sensitive to the beat rate, and in spontaneously beating cultures, drugs can affect this rate. This phenomenon can result in biological "noise" in the waveform parameters that can obscure the direct effects of the drug on the intended targets. Thus, it is important to be able to pace the cells at physiological frequencies. An additional advantage of optical pacing is

the ability to design stimulus protocols that mimic a physiological challenge to the CMs. We have utilized this approach successfully with an optical pacing protocol to detect drug-induced changes in the maximal pacing frequency and map changes in AP shape as a function of frequency. (3) By pacing in one location and recording in another, we can record the propagation time between the locations and extract the conduction velocity. We have found that conduction velocity is highly sensitive to ion channel modulators. (4) The Cardiac Optopatch platform allows for a genetically encoded approach, which removes concerns about phototoxicity from using voltage-sensitive dyes and enables cell type-specific labeling. (5) Drugs with delayed cardiotoxic effects are a major challenge for standard hERG assays. The Optopatch platform can perform chronic measurements of drug-induced toxicity and track longitudinal changes in AP waveform.

While Optopatch measurements precisely reflect the underlying AP and CT waveforms, there are some opportunities for improvement: (1) As with most optical assays, Optopatch measurements do not report absolute voltage or Ca^{2+} and thus are insensitive to subtle shifts in the resting voltage or baseline Ca^{2+}. The AP waveform is, however, sensitive to resting membrane potential, and changes in AP width are expected if compounds induce a shift in resting voltage. We are currently exploring methods for converting fluorescence to absolute voltage. (2) The assays in this study were performed on single-well cultures, which limits current throughput. Parallelization to multiple wells for higher throughput can be achieved through standard engineering measures and is an area of active development at Q-State.

In evaluating the cardiotoxicity assay, one must differentiate between the measurement platform and the cellular substrate. HiPSC-derived CMs replicate some physiological aspects of adult ventricular myocytes, but we have observed a number of shortcomings: (1) Calcium handling—A hallmark of CM maturity is the role of calcium handling in excitation-contraction coupling. For adult primary CMs, it is anticipated that CMs show a shortening of the AP and an increase in the CT amplitude upon elevated beat rate [44]. For the hiPSC-derived CMs, we observe shortening of APs at higher stimulus frequency, but either no apparent change or a decrease in the CT amplitude with increasing beat rate (Fig. 1b). (2) Morphology—In vivo CMs have a brick-like shape with a well-defined orientation to the muscular banding, while in vitro hiPSC-CMs have ill-defined shape and banding orientation [45]. (3) AP shape—We have observed clear changes in AP shape toward a more mature CM waveform (faster rise time, larger voltage, and calcium amplitude) with increased time in culture. This indicates that the cells have not reached their maturation endpoint when the cryovial is thawed and the cells are first placed into culture. (4) Mixed populations—hiPSC-derived CM preparations, as indicated by the

cell provider, are not pure populations of ventricular cells. The cells exhibit spontaneous beating and are a mixture of atrial, ventricular, and nodal cells. Our current analysis averages APs and CTs from all members of a mixed population. Thus, it may be that deviations from anticipated pharmacological response are due to statistical averaging over this population. Future efforts will be to design cell type-specific Optopatch vectors for targeted expression in select cell types. This is a unique capability of the optogenetic approach. (5) Incomplete ion channel expression—We observe a strong response to many compounds with known cardiotoxic profiles, including modulation of the hERG current using known blockers, and exhibited features of arrhythmic behavior, including EADs (Fig. 5a, b). However, some currents such as I_{ks} are difficult to detect in hiPSC-derived CMs with known pharmacological modulators such as chromanol [24], suggesting an absence of substantial current in these cells. In addition to missing ion channels, other proteins such as those associated with the myofibrillar isoforms also show immature expression levels [45]. (6) We observed highly variable spontaneous beat rates (Fig. 1c). We found that the highly variable spontaneous beat rate leads to a large range of AP90 values, whereas pacing greatly reduced this spread. This highlights an important advantage of optical pacing. Variability in the spontaneous beat rate drives variability in AP parameters and optical pacing mitigates this problem. (7) Depolarized resting potential—Manual patch clamp recordings of hiPSC-derived CMs show a more depolarized membrane potential (−50 mV) compared to that expected from adult CMs (−85 mV) [45]. This potential changes with time and culture and exhibits batch-to-batch variability. The result is that the membrane potential is heavily dictated by hERG. As a result, block of the hERG channel leads to changes in membrane potential, which can impact sodium and calcium currents.

Although they are already a powerful tool, the immaturity of these cells currently prevents hiPSC-CMs from reproducing some types of in vivo effects. As the cell culture improves in tandem with measurement platforms, hiPSC-CMs will realize their full potential in cardiotoxicity screening.

This chapter demonstrates the salient features of the Optopatch technology in successfully reporting the electrophysiological response of human iPSC-derived cardiomyocytes to pharmacological perturbations. The Optopatch platform should prove useful in creating an in vitro assay with hiPSC-derived CMs for the accurate reporting of cardiotoxic effects of compounds. Furthermore, as hiPSC technology develops, the Optopatch platform will be invaluable for assessing the electrophysiological function and maturity of improved CM preparations.

References

1. Chalfie M, Tu Y, Euskirchen G et al (1994) Green fluorescent protein as a marker for gene expression. Science 263:802–805. doi:10.1126/science.8303295
2. Heim R, Cubitt AB, Tsien RY (1995) Improved green fluorescence. Nature 373:663–664. doi:10.1038/373663a0
3. Tantama M, Hung YP, Yellen G (2012) Optogenetic reporters: fluorescent protein-based genetically encoded indicators of signaling and metabolism in the brain. Prog Brain Res. doi:10.1016/B978-0-444-59426-6.00012-4
4. Newman RH, Fosbrink MD, Zhang J (2011) Genetically-encodable fluorescent biosensors for tracking signalling dynamics in living cells. Chem Rev 111:3614–3666. doi:10.1021/cr100002u.Genetically-encodable
5. Harvey CD, Ehrhardt AG, Cellurale C et al (2008) A genetically encoded fluorescent sensor of ERK activity. Proc Natl Acad Sci U S A 105:19264–19269. doi:0804598105 [pii]\r10.1073/pnas.0804598105
6. Tewson PH, Quinn AM, Hughes TE (2013) A multiplexed fluorescent assay for independent second-messenger systems: decoding GPCR activation in living cells. J Biomol Screen 18:797–806. doi:10.1177/1087057113485427
7. Kralj JM, Douglass AD, Hochbaum DR et al (2012) Optical recording of action potentials in mammalian neurons using a microbial rhodopsin. Nat Methods 9:90–95. doi:10.1038/nmeth.1782
8. Kim B, Lin MZ (2013) Optobiology: optical control of biological processes via protein engineering. Biochem Soc Trans 41:1183–1188. doi:10.1042/BST20130150
9. Lin JY (2011) A user's guide to channelrhodopsin variants: features, limitations and future developments. Exp Physiol 96:19–25. doi:10.1113/expphysiol.2009.051961
10. Klapoetke NC, Murata Y, Kim SS et al (2014) Independent optical excitation of distinct neural populations. Nat Methods 11:338–346. doi:10.1038/nmeth.2836
11. Kennedy MJ, Hughes RM, Peteya LA et al (2010) Rapid blue-light-mediated induction of protein interactions in living cells. Nat Methods 7:973–975. doi:10.1038/nmeth.1524
12. Airan RD, Thompson KR, Fenno LE et al (2009) Temporally precise in vivo control of intracellular signalling. Nature 458:1025–1029. doi:10.1038/nature07926
13. Hochbaum DR, Zhao Y, Farhi SL et al (2014) All-optical electrophysiology in mammalian neurons using engineered microbial rhodopsins. Nat Methods 11:825–833. doi:10.1038/nmeth.3000
14. St-Pierre F, Marshall JD, Yang Y et al (2014) High-fidelity optical reporting of neuronal electrical activity with an ultrafast fluorescent voltage sensor. Nat Neurosci 17:884–889. doi:10.1038/nn.3709
15. Gong Y, Huang C, Li JZ et al (2015) High-speed recording of neural spikes in awake mice and flies with a fluorescent voltage sensor. Science 350:1361–1366. doi:10.1126/science.aab0810
16. Chen T-W, Wardill TJ, Sun Y et al (2013) Ultrasensitive fluorescent proteins for imaging neuronal activity. Nature 499:295–300. doi:10.1038/nature12354
17. Dana H, Mohar B, Sun Y et al (2016) Sensitive red protein calcium indicators for imaging neural activity. Elife 5, e12727. doi:10.7554/eLife.12727
18. Inoue M, Takeuchi A, Horigane S et al (2014) Rational design of a high-affinity, fast, red calcium indicator R-CaMP2. Nat Methods. doi:10.1038/nmeth.3185
19. Kettlewell S, Cabrero P, Nicklin SA et al (2009) Changes of intra-mitochondrial Ca^{2+} in adult ventricular cardiomyocytes examined using a novel fluorescent Ca^{2+} indicator targeted to mitochondria. J Mol Cell Cardiol 46:891–901. doi:10.1016/j.yjmcc.2009.02.016
20. Henderson MJ, Baldwin HA, Werley CA et al (2015) A low affinity GCaMP3 variant (GCaMPer) for imaging the endoplasmic reticulum calcium store. PLoS One 10:1–17. doi:10.1371/journal.pone.0139273
21. Gutscher M, Pauleau A-L, Marty L et al (2008) Real-time imaging of the intracellular glutathione redox potential. Nat Methods 5:553–559. doi:10.1038/nmeth.1212
22. Birk J, Meyer M, Aller I et al (2013) Endoplasmic reticulum: reduced and oxidized glutathione revisited. J Cell Sci 126:1604–1617. doi:10.1242/jcs.117218
23. Tantama M, Martínez-François JR, Mongeon R, Yellen G (2013) Imaging energy status in live cells with a fluorescent biosensor of the intracellular ATP-to-ADP ratio. Nat Commun 4:2550. doi:10.1038/ncomms3550
24. Dempsey GT, Chaudhary KW, Atwater N et al (2011) Cardiotoxicity screening with simultaneous optogenetic pacing, voltage imaging and calcium imaging. J Pharmacol Toxicol Methods. doi:10.1016/j.vascn.2016.05.003
25. Hou JH, Kralj JM, Douglass AD et al (2014) Simultaneous mapping of membrane voltage and calcium in zebrafish heart in vivo reveals

chamber-specific developmental transitions in ionic currents. Front Physiol 5:1–10. doi:10.3389/fphys.2014.00344

26. Dempsey GT, Chaudhary KW, Atwater N et al (2016) Cardiotoxicity screening with simultaneous optogenetic pacing, voltage imaging and calcium imaging. J Pharmacol Toxicol Methods S1056–8719(16):30044-2
27. Maclaurin D, Venkatachalam V, Lee H, Cohen AE (2013) Mechanism of voltage-sensitive fluorescence in a microbial rhodopsin. Proc Natl Acad Sci U S A 110:5939–5944. doi:10.1073/pnas.1215595110
28. Shang W, Lu F, Sun T et al (2014) Imaging Ca^{2+} nanosparks in heart with a new targeted biosensor. Circ Res 114:412–420. doi:10.1161/CIRCRESAHA.114.302938
29. Kaestner L, Scholz A, Tian Q et al (2014) Genetically encoded Ca^{2+} indicators in cardiac myocytes. Circ Res 114:1623–1639. doi:10.1161/CIRCRESAHA.114.303475
30. Ma J, Guo L, Fiene SJ et al (2011) High purity human-induced pluripotent stem cell-derived cardiomyocytes: electrophysiological properties of action potentials and ionic currents. Am J Physiol Heart Circ Physiol 301(5):H2006–H20017. doi:10.1152/ajpheart.00694.2011
31. Mummery C, Ward-van Oostwaard D, Doevendans P et al (2003) Differentiation of human embryonic stem cells to cardiomyocytes: role of coculture with visceral endoderm-like cells. Circulation 107:2733–2740. doi:10.1161/01.CIR.0000068356.38592.68
32. Burridge PW, Matsa E, Shukla P et al (2014) Chemically defined generation of human cardiomyocytes. Nat Methods 11:855–860. doi:10.1038/nmeth.2999
33. Lan F, Lee AS, Liang P et al (2013) Abnormal calcium handling properties underlie familial hypertrophic cardiomyopathy pathology in patient-specific induced pluripotent stem cells. Cell Stem Cell 12:101–113. doi:10.1016/j.stem.2012.10.010
34. Puppala D, Collis LP, Sun SZ et al (2013) Comparative gene expression profiling in human-induced pluripotent stem cell—derived cardiocytes and human and cynomolgus heart tissue. Toxicol Sci 131:292–301. doi:10.1093/toxsci/kfs282
35. Du DTM, Hellen N, Kane C, Terracciano CMN (2015) Action potential morphology of human induced pluripotent stem cell-derived cardiomyocytes does not predict cardiac chamber specificity and is dependent on cell density. Biophys J 108:1–4. doi:10.1016/j.bpj.2014.11.008
36. Cavero I, Holzgrefe H (2014) Comprehensive in vitro proarrhythmia assay, a novel in vitro/in silico paradigm to detect ventricular proarrhythmic liability: a visionary 21st century initiative. Expert Opinion on Drug Safety 13(6):745–758. doi:10.1517/14740338.2014.915311
37. Sager PT, Gintant G, Turner JR et al (2014) Rechanneling the cardiac proarrhythmia safety paradigm: a meeting report from the Cardiac Safety Research Consortium. Am Heart J 167:292–300. doi:10.1016/j.ahj.2013.11.004
38. Robertson C, Tran D, George S (2013) Concise review: maturation phases of human pluripotent stem cell-derived cardiomyocytes. Stem Cells 31:1–17. doi:10.1002/stem.1331.Concise
39. Geraerts M, Michiels M, Baekelandt V et al (2005) Upscaling of lentiviral vector production by tangential flow filtration. J Gene Med 7:1299–1310. doi:10.1002/jgm.778
40. Inoue M, Takeuchi A, Horigane S et al (2014) Rational design of a high-affinity, fast, red calcium indicator R-CaMP2. Nat Methods 12:64–70. doi:10.1038/nmeth.3185
41. Miller EW, Lin JY, Frady EP et al (2012) Optically monitoring voltage in neurons by photo-induced electron transfer through molecular wires. Proc Natl Acad Sci U S A 109:2114–2119. doi:10.1073/pnas.1120694109
42. Hennessy S, Leonard CE, Newcomb C et al (2008) Cisapride and ventricular arrhythmia. Br J Clin Pharmacol 66:375–385. doi:10.1111/j.1365-2125.2008.03249.x
43. Cordes JS, Sun Z, Lloyd DB et al (2005) Pentamidine reduces hERG expression to prolong the QT interval. Br J Pharmacol 145:15–23. doi:10.1038/sj.bjp.0706140
44. Llach A, Molina CE, Fernandes J et al (2011) Sarcoplasmic reticulum and L-type Ca^{2+} channel activity regulate the beat-to-beat stability of calcium handling in human atrial myocytes. J Physiol 589:3247–3262. doi:10.1113/jphysiol.2010.197715
45. Yang X, Pabon L, Murry CE (2014) Engineering adolescence: maturation of human pluripotent stem cell-derived cardiomyocytes. Circ Res 114:511–523. doi:10.1161/CIRCRESAHA.114.300558

Chapter 7

HTS-Compatible Voltage- and Ca^{2+}-Sensitive Dye Recordings from hiPSC-Derived Cardiomyocytes Using the Hamamatsu FDSS Systems

Ralf Kettenhofen

Abstract

Standard acute cardiac safety pharmacological assays usually comprise high-throughput screening (HTS) of single cardiac ion channels like the hERG channel expressed in tumor cell lines and low-throughput assay systems like ex vivo tissue preparations or Langendorff perfused hearts from animals. These types of model systems typically lack sufficient predictivity and/or throughput.

In contrast, standardized and pure human induced pluripotent stem cell-derived cardiomyocytes (hiPSCM) are commercially available and have already been demonstrated to be predictive human cell models in which to assess cardiotoxicity in vitro (Obejero-Paz et al., Sci Rep 5:17623, 2015; Lu et al., Toxicol Sci 148:503–516, 2015; Kitaguchi et al., J Pharmacol Toxicol Methods 78:93–102, 2015; Gilchrist et al., Toxicol Appl Pharmacol 288:249–257, 2015).

Here it is described how human-induced pluripotent stem cell-derived Cor.4U cardiomyocytes can be implemented in an HTS assay environment using the FDSS plate reader platforms from Hamamatsu and modern fluorescent probes to monitor drug-induced changes to either cardiac cytosolic free calcium ($[Ca^{2+}]_i$) transients or plasma membrane potentials.

Key words Human-induced pluripotent stem cells, Cardiomyocytes, Calcium transients, Fluorescent calcium-sensitive dye, Membrane potential, Fluorescent voltage-sensitive dye, Plate reader, High throughput

1 Introduction

The contraction of cardiomyocytes is induced by a mechanism called excitation-contraction coupling. Cardiac pacemaker cells generate a rhythmic electrical depolarization, which causes plasma membrane potential changes—called action potentials—in cardiac myocytes. In phase 2 of the action potential, L-type calcium channels are opened and small amounts of calcium ions enter the cytosol. These calcium ions are able to bind to and open the ryanodine receptors of the sarcoplasmic reticulum (SR) triggering large amounts of calcium ions to be released from the SR into the cytosol. This second mechanism is called calcium-induced calcium release (CICR) and is finally

Mike Clements and Liz Roquemore (eds.), *Stem Cell-Derived Models in Toxicology*, Methods in Pharmacology and Toxicology, DOI 10.1007/978-1-4939-6661-5_7,

responsible for the induction of myocyte contraction. While the membrane potential of the cardiomyocyte is repolarized to resting membrane potentials, the calcium ions are pumped back into the sarcoplasmic reticulum by the sarco-/endoplasmic reticulum ATPase (SERCA). These periodical changes of the cytosolic free calcium ion concentrations are called calcium transients.

Cor.4U® cardiomyocytes are produced by differentiation of human-induced pluripotent stem cells. A stable integration of the puromycin resistance cassette in the hiPSCs expressed under the control of cardiac alpha-myosin heavy chain promoter allows for the selection of pure cardiomyocytes. These cardiomyocytes exhibit spontaneous rhythmic contraction and typical cardiomyocyte properties including typical cross striation of contractile filaments and connexin 43 expression (*see* Fig. 1) in addition to expected cardiomyocyte electrophysiological properties.

Fluorescent voltage- and calcium-sensitive dyes have been developed which can enter cells and change their fluorescent properties in response to either changes in plasma membrane potential or calcium binding, respectively. Kinetic fluorescence plate reader systems equipped with an excitation light source, the appropriate excitation and emission filter set, and sensitive, fast cameras like the Hamamatsu FDSS μCell and the FDSS7000EX (*see* Fig. 2) are able to detect and record the changes in fluorescence from monolayers of Cor.4U® cardiomyocytes. In addition, both FDSS systems are

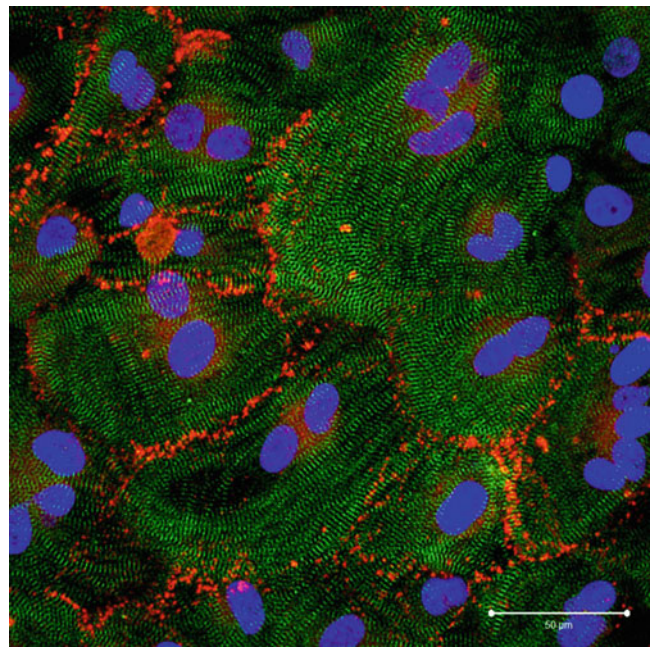

Fig. 1 Immunostaining of Cor.4U® cardiomyocytes against myomesin (*green*) revealing the typical cross striation of cardiomyocytes, the gap junction protein connexin 43 (*red*), and the nuclei (*blue*). Image generated by fluorescence microscopy was kindly provided by Prof. Zuppinger, University of Bern, Switzerland

Fig. 2 Kinetic fluorescence plate reader system: (**a**) Hamamatsu FDSS μCell and (**b**) Hamamatsu FDSS7000

setup with robotics and pipettor head to add compounds to all wells simultaneously. The typical waveforms obtained from the recordings of calcium transient and voltage-sensitive dye (VSD) assays can be used to assess drug-induced changes to cardiomyocyte physiology.

Several consortia including the Japanese initiatives Consortium for Safety Assessment Using Human iPS Cells (CSAHi) and Japanese iPS Cardiac Safety Assessment (JiCSA) [3] and the international Comprehensive In Vitro Proarrhythmia Assay (CiPA) initiative [5] supported by regulatory institutions are currently validating commercially available hiPSCM from several providers, including Cor.4U® cardiomyocytes, with the aim of incorporating these assays into guidelines for safety pharmacological studies, to supplement or substitute the existing ICHS7B guideline.

Microelectrode array recordings and voltage-sensitive dye (VSD) assays are the preferred methods to assess proarrhythmic potential of drugs. However, the calcium transient assay will also be included in the upcoming validation study as a potential backup assay.

2 Materials

The Cor.4U® human-induced pluripotent stem cell (hiPSC)-derived cardiomyocytes (Axiogenesis AG, Cologne, Germany) were either used in fresh cell format pre-seeded in microplates (96- and 384-well plates) or thawed from a frozen vial of four million cells and cultured in Cor.4U® Culture Medium (Axiogenesis AG, Cologne, Germany). For the assays described below, the cells are transferred to Tyrode's solution (cat. no. T2397 Sigma-Aldrich,)

supplemented with 10 mM HEPES and adjusted to potassium ion concentration of 4.2 mM (modified Tyrode's solution).

Trypan blue solution has a concentration of 0.4% and was obtained from Sigma-Aldrich (cat. no. T8154).

Black microplates with flat transparent (μClear®) bottom in either 96- or 384-well format, were obtained from Greiner Bio-One (Frickenhausen, Germany).

The Cal-520-AM dye from AAT Bioquest was used to record calcium transients from Cor.4U cardiomyocytes. The lyophilized dye was reconstituted in a concentration of 5 mM in water-free DMSO and stored in 7 μl aliquots at −20 °C.

For voltage-sensitive dye (VSD), the FluoVolt® dye from Thermo Fisher Scientific was used. The 1000× concentrated dye solution in DMSO is stored at 4 °C in the refrigerator together with the 100× concentrated Power-LOAD™ and the 10× concentrated Neuro Background Suppressor.

As a coating material, fibronectin from bovine plasma is used, preferably the 1 mg/ml stock solution from Sigma-Aldrich.

Furthermore, DPBS with calcium (Ca^{2+}) and magnesium (Mg^{2+}) (Sigma-Aldrich, cat. no. D8662) is required to dilute the fibronectin stock solution as well as DPBS without Ca^{2+} and Mg^{2+}(Sigma-Aldrich, cat. no. D8537), which is used for the washing of the cells before dissociation. For dissociation of fresh Cor.4U® cardiomyocytes, Accumax was obtained from Sigma-Aldrich (cat. no. A7089).

In order to record and analyze either calcium transients or changes in plasma membrane potentials in Cor.4U® cardiomyocytes using fluorescent dyes, the kinetic optical plate reader systems FDSS7000EX and the FDSS μCell with integrated dispensing heads and high-speed imaging-based detectors from Hamamatsu (Hamamatsu, Japan) were used. The FDSS μCell can be equipped either with a pipettor head for 96 or 384 wells or with a 96-well electrical field stimulation (EFS) head, which enables electrical pacing of hiPSCM. Please note that it is note possible to record action potential-like waveforms using voltage sensitive dyes with the stimulation head due to patent issues [6].

Both devices are equipped with temperature control in order to be able to conduct the experiments at physiological temperature.

3 Methods

3.1 Culture of hiPSC-Derived Cor.4U® Cardiomyocytes

3.1.1 Thawing Frozen Cor.4U® Cardiomyocytes and Seeding into Multiwell Plates

Before starting the protocol, please carefully read Sect. 4.1:

1. Dilute fibronectin stock solution (1 mg/ml, Sigma-Aldrich, Munich, Germany) 1:100 in DPBS with Ca^{2+}/Mg^{2+} and then add 25 μl or 50 μl of the diluted solution to each well of a 384- or 96-well black μClear microplate, respectively.
2. Incubate the plate in an incubator at 37 °C in a saturated humidity for 3 h.

3. Transfer 4 ml Cor.4U® Culture Medium into a 50 ml tube and warm to 37 °C.
4. Before thawing the cells, warm 1 ml Cor.4U® Culture Medium in another 50 ml tube (tube B).
5. Quickly transfer the cells from liquid nitrogen directly to a 37 °C water bath and thaw the vial until the frozen cell suspension detaches from the bottom of the vial and only a small ice clump is visible (approx. 2 min). See also Sect. 4.2.
6. Disinfect the outside of the vial and transfer the vial to the laminar flow hood. Pipette the cell suspension carefully into the tube containing 4 ml Cor.4U® Culture Medium. The total volume is now 5 ml.
7. Determine the number of viable cells, e.g., by trypan blue staining of an aliquot of the cell suspension and counting of trypan blue-negative cells in a Neubauer hemocytometer. Please see Sect. 4.3.
8. For seeding into a 384-well plate, adjust the density of viable cells to 2×10^5/ml, discard the fibronectin coating solution in the microplate, and seed 50 µl of the cell suspension into each well. This corresponds to 1×10^4 viable cells per well.

   For a 96-well plate, adjust the cell suspension to 1.5×10^5/ml, discard the fibronectin coating solution in the plate, and seed 200 µl of the cell suspension into each well. This corresponds to 3×10^4 viable cells per well.
9. Leave the plates for 20 min under the laminar hood. See Sect. 4.4.
10. Change the medium on a daily basis to guarantee the highest quality of cardiomyocytes, and culture the cells for at least 3 days before starting the experiment. See also Sect. 4.5.

3.1.2 Dissociation of Cor.4U® Cardiomyocytes from Cell Culture Flasks and Seeding in Microplates

As an alternative to seeding cells direct from frozen vials, here the dissociation from a T75 flask containing three million Cor.4U cardiomyocytes is described. The amount of cells is sufficient to seed a 96-well plate. In order to seed a complete 384-well plate, an additional T25 flask with at least one million Cor.4U cardiomyocytes is required. Please follow the instructions for fibronectin coating of microplates in Sect. 3.1.1 and be aware of Sect. 4.1:

1. Pre-warm 60 ml Cor.4U® Culture Medium to 37 °C.
2. Discard the medium in the T75 flask and wash the cell layer twice with 10 ml DPBS without Ca^{2+}/Mg^{2+}.
3. Incubate the cells for 5–10 min in Accumax solution at 37 °C in the incubator.
4. Stop the digestion reaction by adding 10 ml pre-warmed Cor.4U® Medium and transfer the cell suspension into a 50 ml tube.

5. Rinse the growth surface of the T75 flask with 10 ml of fresh pre-warmed Cor.4U® Culture Medium and transfer the solution into the same 50 ml tube from step 4.
6. Centrifuge the Cor.4U® cardiomyocytes at 180× g for 3 min, discard the supernatant, and resuspend the cardiomyocytes in 1 ml Cor.4U® Culture Medium.
7. Determine the number of viable cells by trypan blue staining and counting the trypan blue-negative cells in, e.g., a Neubauer hemocytometer. The viability should be ≥90%.
8. For a 384-well plate, adjust the cell concentration to 2×10^5 cells/ml and 1×10^5 cells/ml for a 96-well plate.
9. Discard the fibronectin coating solution from the microplate and seed 50 µl of the 2×10^5 cells/ml cell suspension to each well of the 384-well plate (corresponds to 1×10^4 cells/well) or 200 µl of the 1×10^5 cells/ml cell suspension to each well of the 96-well plate (corresponds to 2×10^4 cells per well).
10. Leave the plates for at least 20 min under the laminar hood. See Sect. 4.4.
11. Change the medium on a daily basis to guarantee the highest quality of cardiomyocytes and culture the cells for at least 3 days before starting the experiment. See also Sect. 4.5.

3.1.3 Pre-seeded Multiwell Plates with Fresh Cor.4U Cardiomyocytes

Pre-seeded 96-well or 384-well plates with 2×10^4/well or 1×10^4/well Cor.4U cardiomyocytes, respectively, can be obtained from Axiogenesis. Upon arrival of the microplates, remove the silicon mat under a laminar hood and change the medium with pre-warmed Cor.4U® Culture Medium (200 µl/96 well or 75 µl/384 well). Close the plate with a fresh, sterile lid and let the cells recover overnight in an incubator with 37 °C, 5% CO_2, and a saturated humidity before starting the experiment.

3.2 Recording of Spontaneous Calcium Transient from Cor.4U® Cardiomyocytes

3.2.1 Preparation of the FDSS System

1. Turn on the FDSS system to cool down the camera and to warm up the system to 37 °C. It takes about 30 min to warm up the FDSS µCell to 37 °C, whereas the FDSS7000EX system requires at least 90 min to reach this temperature. When using the FDSS7000EX, make sure that the "Operation Preparation" button is checked to start the dispenser robotics.
2. Start the computer that controls the FDSS system, and launch the FDSS software.
3. Choose the "High Speed" option and select the required 96-well or 384-well pipettor head in the software.
4. Equip the FDSS system with appropriate tips and pipettor head in case drugs have to be applied. This ensures that the pipetting tips are also pre-warmed to 37 °C.
5. In the "Protocol" menu, define the file names of the experiment and adjust the "Total Sample Rate." For baseline and incubation

times, it is advisable to choose at least a 1 min recording time (which corresponds to 3660 samples when using an exposure of 15.6 ms) and 2 min for the drug application.

3.2.2 FDSS Dispenser Setup

The dispenser is only required when drugs are to be applied from the ligand plate to the assay plate.

The FDSS μCell employs one stage for the ligand plate, whereas the FDSS7000EX offers the choice of two stages and one loader position. The latter can be used to load a ligand plate into the device without the need to open the front door.

The "Dispenser Control" window contains the parameters for the dispenser setup.

It is recommended to add the compounds in 10× concentration. For example, for a final reaction volume in the assay plate of 30 μl in a 384 well, set in the "Dispenser Control" window in the menu "Aspirate" the "Volume" to 3 μl, the "Speed" to 10 μl/s, and the "Height" to 0.5 mm. In the "Dispense" menu, set the "Speed" to 50 μl/s and the "Height" to 1.5 mm.

For a 96-well plate, set the aspiration volume to 10 μl.

Then, save the settings in the "FDSS Application" window in the "Assay Protocol File."

3.2.3 Cell Preparation and Dye Loading for the Calcium Transient Assay

1. Pre-warm modified Tyrode's solution to 37 °C.
2. At least 1 h before adding the calcium dye, discard the medium of the multiwell plate into a container and dry the upper part of the multiwell plate on a clean piece of tissue. Take care that the well contains no remaining bubbles that could disturb the medium addition, especially on the 384-well plates.
3. Add modified Tyrode's solution to each well (50 μl per 384 well, 100 μl per 96 well) and place the plate back into the incubator at 37 °C, 5% CO_2, and saturated humidity.
4. In the meantime, prepare a solution containing 2.5 μM Cal-520 dye in modified Tyrode's solution. Then, thaw an aliquot of 5 mM Cal-520 dye and add the 7 μl to 14 ml modified Tyrode's solution and pre-warm the solution to 37 °C in the dark.
5. Ninety minutes before the start of the experiment, discard the medium from the multiwell plate as described above and add the prepared warm dye solution to each well of the plate (25 μl per 384 well, 100 μl to each 96 well).
6. Incubate the cells with dye solution for 45–60 min in the incubator.
7. Afterward, discard the dye solution and wash the cells once with modified Tyrode's solution (see also Sect. 4.6.)
8. Finally, add 27 μl or 90 μl modified Tyrode's solution to each well of a 384-well plate or 96-well plate, respectively, and let the cells recover for 30 min in the incubator before starting the experiment (see Sect. 4.7.)

3.2.4 Calcium Transient Recording in the FDSS

1. Load the assay plate with the cells in the assay plate position of the FDSS μCell, or put the assay plate on the loader tray of the FDSS7000EX and click on the "Load" button in the "Dispenser Control" window of the FDSS software.
2. Check in the "Manual Ctrl" menu that the filters are set to Ex480/Em540 in the "Filter Control" panel.
3. Start the detection by clicking on the "Life On" button in the "Camera Control" panel and visually inspect the detected fluorescence of the calcium transients.
4. Adjust the sensitivity of the camera (usually the sensitivity is between 7 and 9 for calcium transients when using the calcium dye concentration mentioned above and the lowest exposure time of 15.6 ms). The maximum calcium transient fluorescence intensity should not reach camera saturation, which will be indicated by the red color in the "Live Window."
5. Press the "Life Off" button to stop the detection.
6. Switch to the "Protocol" menu and check the "Sensitivity" tab.
7. Set the "Auto Sensitivity" to "Off – Fix" and adjust the "Fix Sensitivity" to the value determined before (usually the value is between 7 and 9). Make sure that these adjustments are saved for all protocols defined for the experiment.
8. Start the recording by clicking on the "Start" button. The raw data will be displayed with a delay and will be saved automatically after the recording is finished.
9. For drug application, load the right "Assay Protocol File" in the FDSS software and place the compound plate in the appropriate position defined in the protocol, or load the compound plate into the FDSS7000EX by using the loader. To do so place the compound plate on the ligand plate loader tray, check in the "Dispenser Control" window of the FDSS software that the tab for the "TH1 + Loader" is active, and then click on the "Load" button.
10. Start the recording by clicking on the "Start" button of the FDSS software.

3.3 Action Potential-Like Recording

Preparation of the FDSS system, dispenser settings, and data recording is the same as described for the calcium transient assay in Sects. 3.2.1, 3.2.2, and 3.2.4, respectively. One exception is the setting for the "Fix Sensitivity," which typically has to be set to the maximum value of 10.

3.3.1 Cell Preparation for VSD Assay: Non-wash Assay

1. Pre-warm modified Tyrode's solution to 37 °C.
2. At least 60 min before loading the cells with dye, discard the medium by flipping the assay plate over a container and drying the upper part of the multiwell plate on a clean piece of tissue.

Take care that the well contains no bubbles that could disturb medium addition.

3. Add warm modified Tyrode's solution to each well (50 µl per 384 well, 100 µl per 96 well).
4. Repeat this procedure and finally place the plate back into the incubator at 37 °C, 5 % CO_2 and saturated humidity.
5. Just before the 60 min have elapsed, prepare the dye solution. Thaw the 1000× concentrated FluoVolt dye stock solution and pre-warm 10 ml modified Tyrode's solution in a 50 ml tube to 37 °C in a water bath.
6. Add 12 µl of the FluoVolt dye, 120 µl of the 100× concentrated PowerLoad™, and 1.2 ml of the 10× concentrated Neuro Background Suppressor to the pre-warmed 10 ml modified Tyrode's solution.
7. Discard the medium from the assay plate by flipping the plate over a container and drying the upper part of the multiwell plate on a clean piece of tissue.
8. Add 27 µl or 90 µl of the dye solution from step 6 to each well of a 384- or 96-well plate, respectively, and quickly place the assay plate back into the incubator.
9. Allow the Cor.4U® cardiomyocytes to load with FluoVolt dye for 15–20 min.
10. Afterwards proceed with the recording in the FDSS system as described in Sect. 3.2.4. Typically the sensitivity has to be set to the maximum value of 10. Please see also Sect. 4.8.

3.4 Data Analysis Using the Hamamatsu Wave Checker Software

Wave Checker is a MATLAB-based analysis tool that can be incorporated into the FDSS software to allow the user to calculate the following parameters (*see* Fig. 3):

1. Beat rate in beats per minute and total peak number per recording
2. Peak-to-peak time (P-P-time; average, standard deviation, min, max)
3. Ratio (average and standard deviation) defined as ratio = (AMP + RMP)/RMP
4. Amplitude (AMP; average and standard deviation)
5. Background fluorescence (RMP; average and standard deviation)
6. Slope (average, standard deviation)
   - Rising slope (from bottom to peak with selection for 0–100 %, 10–90 %, 20–80 %, 30–70 %)
   - Falling slope (peak to bottom)
   - Integration (average, standard deviation)

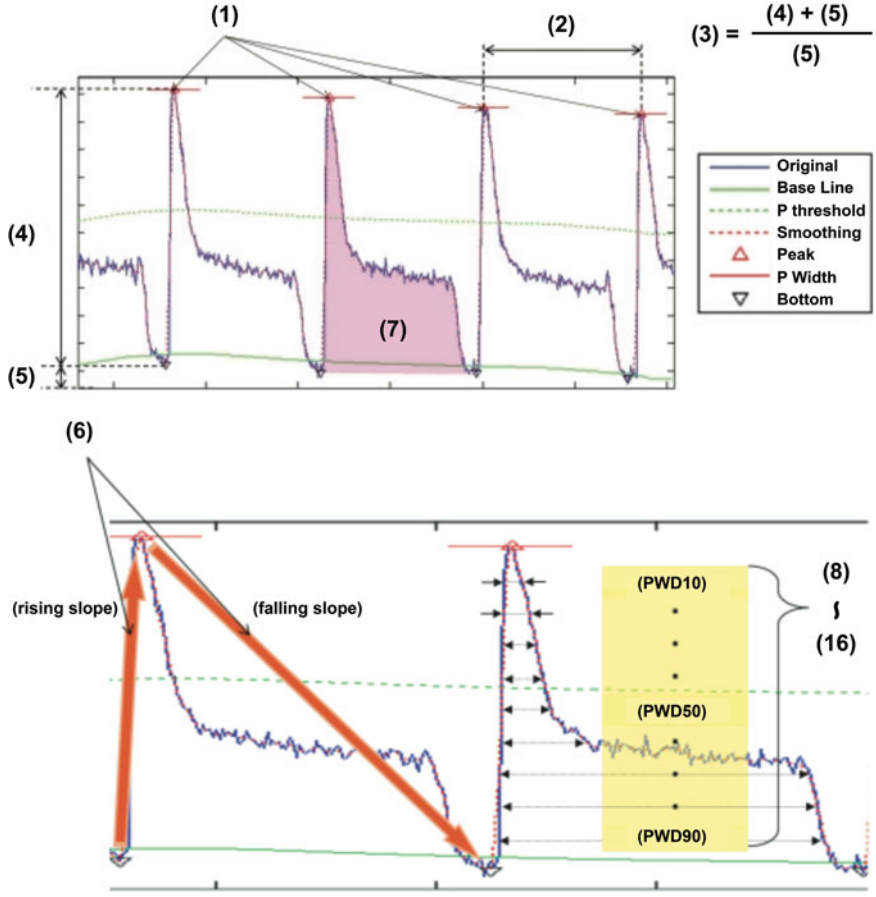

Fig. 3 Fluorescent waveform parameters analyzed using the Hamamatsu Wave Checker software. This analysis is applicable for both calcium transient and voltage-sensitive dye assays

- To (16) peak width durations (PWD10 to PWD90; average, standard deviation)

The analysis can be applied to both calcium transient and voltage-sensitive dye recordings.

3.5 Compound-Induced Changes of Cor.4U® Cardiomyocyte Calcium Transients and Action Potential-Like Recordings

Figure 4 shows typical baseline recordings of calcium transients and voltage-sensitive dye assay from Cor.4U® cardiomyocytes cultured in a 384-well plate.

As illustrated in Fig. 5, the hERG blocker astemizole revealed a dose-dependent prolongation of the calcium transient peak width duration and induction of EAD-like arrhythmic pattern of calcium transients.

Quantification of astemizole-induced effects demonstrated a dose-dependent increase in peak width duration at 90% (PWD90) and beat rate (*see* Fig. 6).

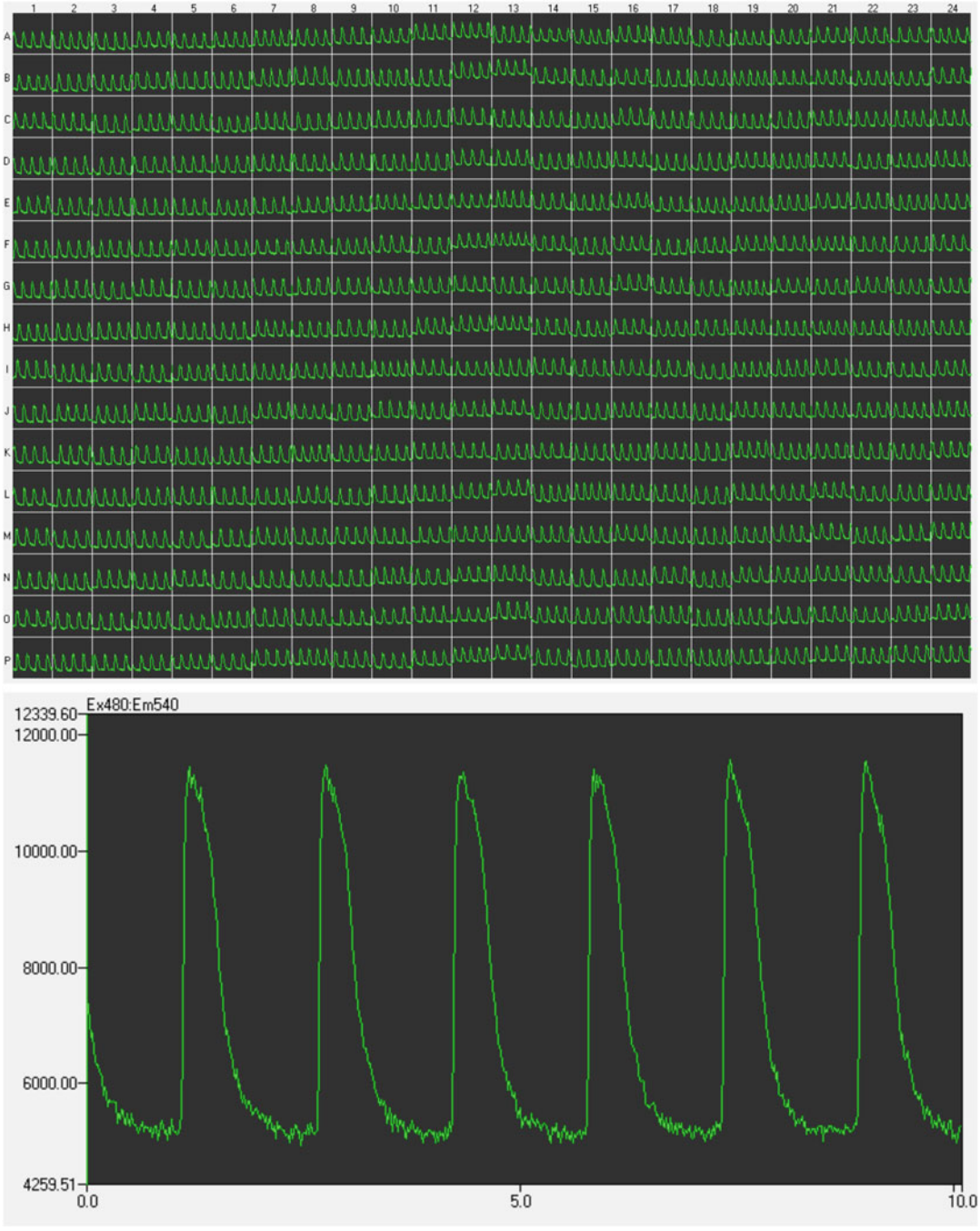

Fig. 4 Graphs from the Hamamatsu FDSS recording software. (**a**) Calcium transient recordings from Cor.4U® cardiomyocytes in 384-well plate. (**b**) Calcium transient recording from a single well. (**c**) Single-well recording from a voltage-sensitive dye assay

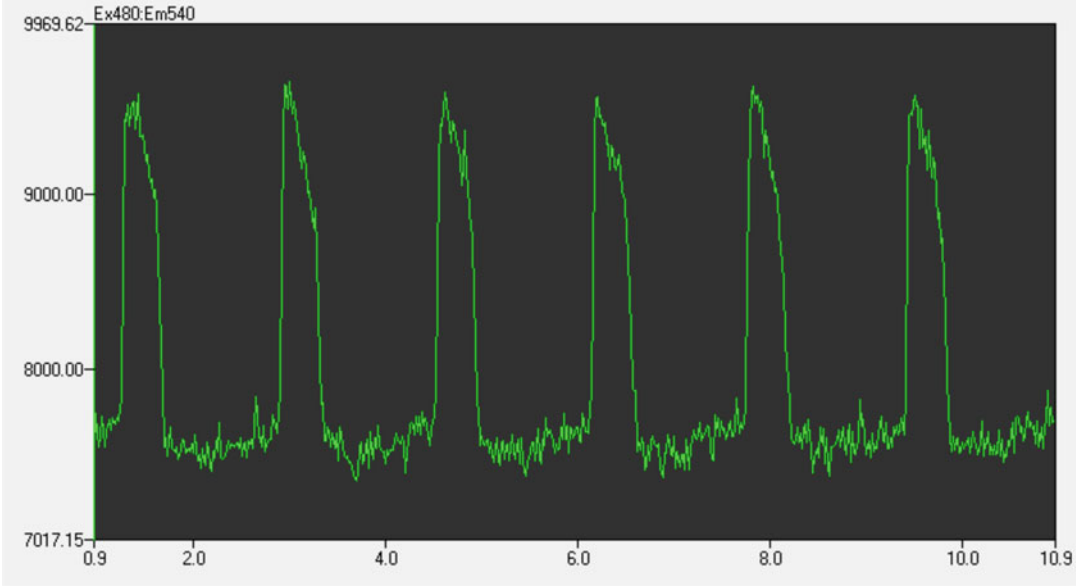

Fig. 4 (continued)

Analysis of the results of 40 reference compounds provides evidence that compounds exhibiting effects on cardiac physiology show the same pattern of effects on the recorded calcium transient parameters in Cor.4U® cardiomyocytes. As an example, the hERG blockers astemizole, cisapride, dofetilide, quinidine, sotalol, and erythromycin group together when the multi-parametric data are analyzed using cluster analysis (*see* Fig. 7).

Figure 8 illustrates the effect of the voltage-gated sodium channel activator ATX-II on action potential-like recordings from Cor.4U cardiomyocytes in the voltage-sensitive dye assay. The compound prolonged the peak width duration at 80%, which shows that Cor.4U cardiomyocytes are also predictive of repolarization delay in addition to hERG block.

4 Notes

4.1 Avoid Electrostatic Charging of Microplates

At least one day before seeding Cor.4U® cardiomyocytes, take the microplates (e.g., black 96-well or 384-well μClear cell culture microplates, Greiner Bio One, Frickenhausen, Germany) out of the plastic packaging to avoid electrostatic charging of the plates, which may cause bubble formation during pipetting, especially when using 384-well plates. Bubble formation during the addition of the fibronectin coating solution or the cell suspension will cause defects in the cardiomyocyte monolayer and lead to a loss of data points.

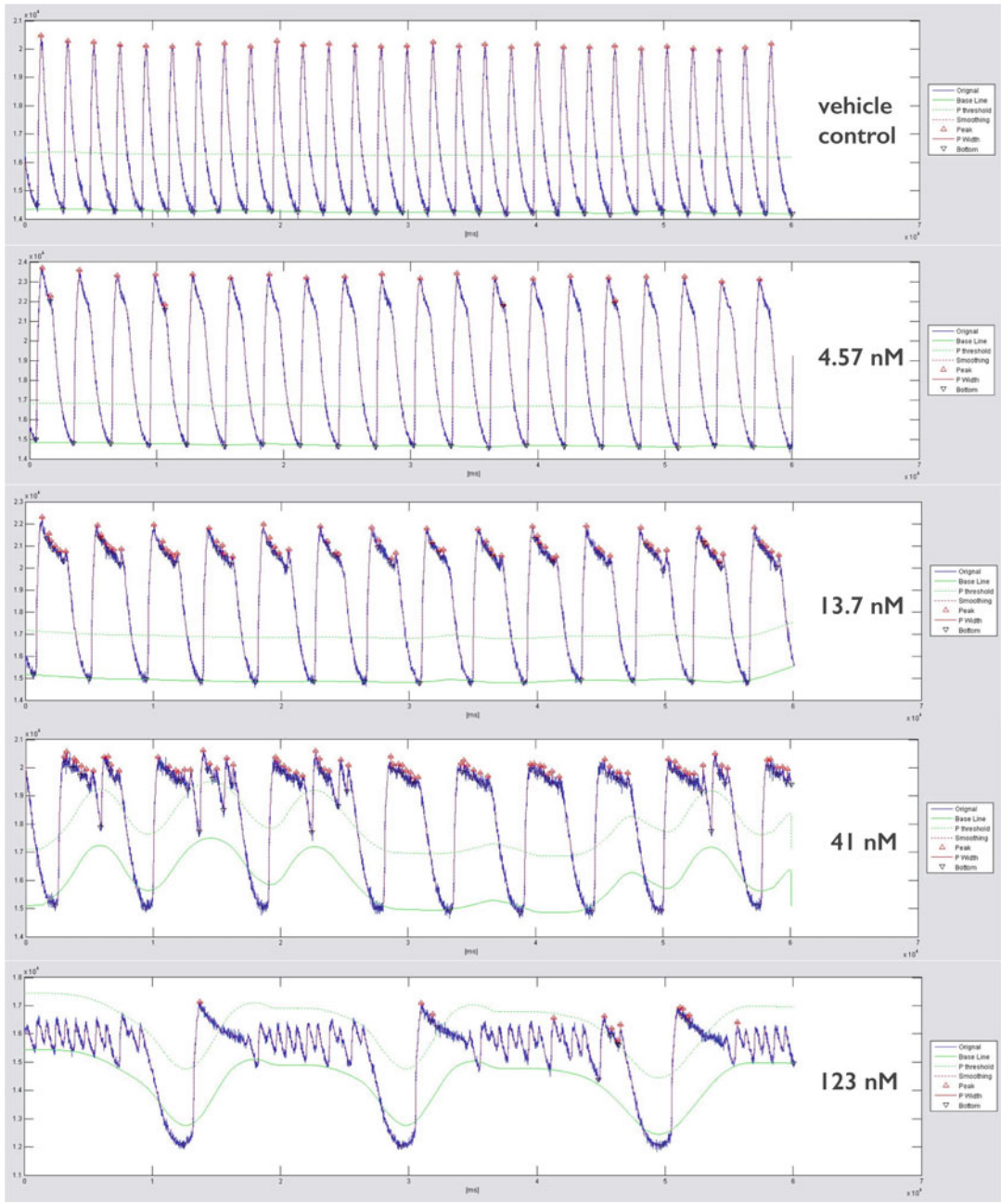

Fig. 5 Dose-dependent effects on Cor.4U® cardiomyocyte calcium transients after 30 min incubation with 4.57 nM, 13.7 nM, 41 nM, or 123 nM astemizole, in comparison to DMSO vehicle control. Calcium transient raw data graphs were obtained after import into the Hamamatsu Wave Checker software

Make sure that antistatic and grounded mats are placed under the laminar hood and that personnel wear antistatic shoes and disposable nitrile gloves during the seeding procedure described below.

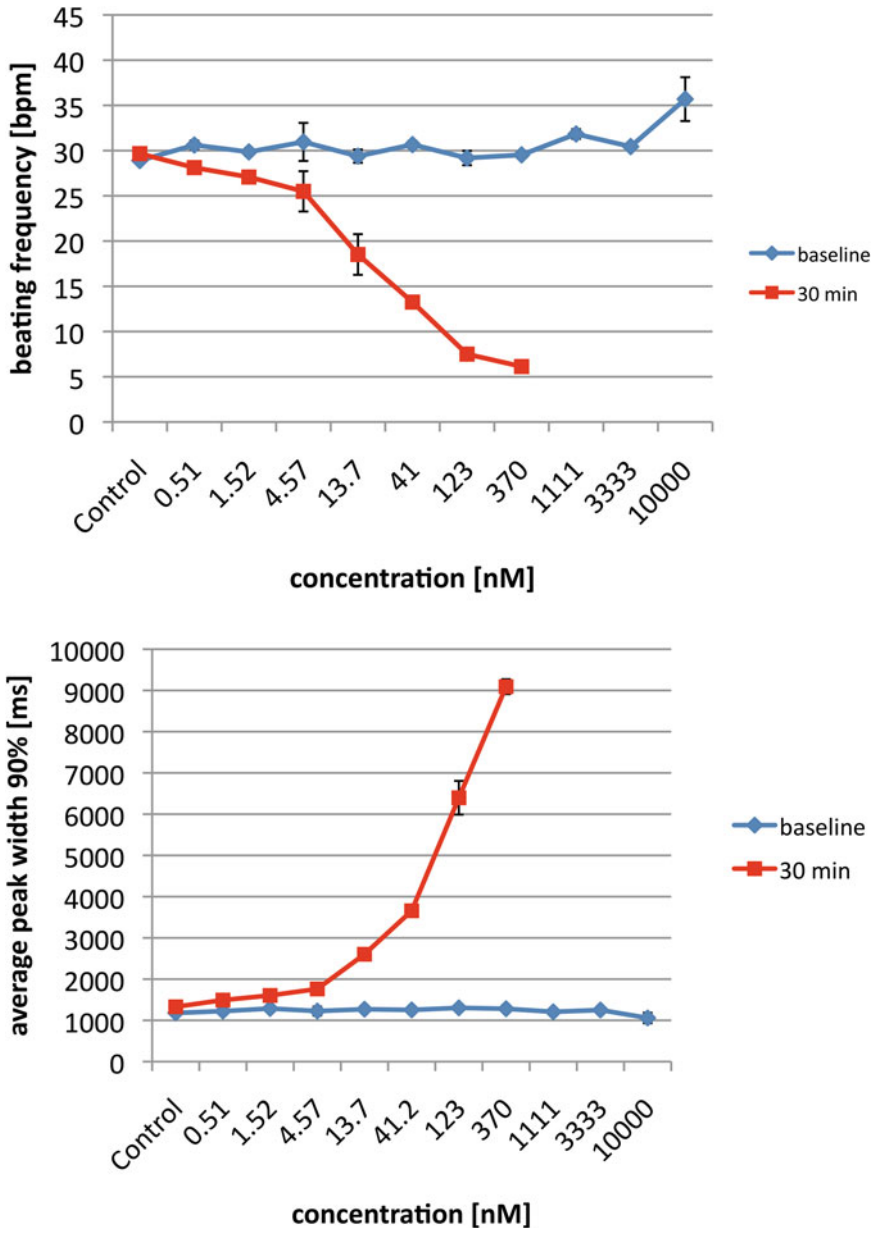

Fig. 6 Quantification of astemizole impact on Cor.4U® cardiomyocyte calcium transient parameter beating frequency and peak width duration at 90 % (PWD90)

4.2 Reduced Viability of Frozen Cor.4U® Cardiomyocytes

Storage of frozen vials of Cor.4U® cardiomyocytes on dry ice or at −80 °C will decrease the amount of viable cells after thawing. Immediately transfer the vials of Cor.4U® cardiomyocytes into the liquid nitrogen or the vapor phase of liquid nitrogen upon arrival. Keep the transport from liquid nitrogen to dry ice as short as possible or transport the cells into the laboratory via a dewar filled with liquid nitrogen.

Fig. 7 Overview of the effects of 40 reference compounds on Cor.4U® cardiomyocyte calcium transient parameters. Classes of compounds like hERG blockers cluster together due to the pattern of their effects on the recorded calcium transient parameters

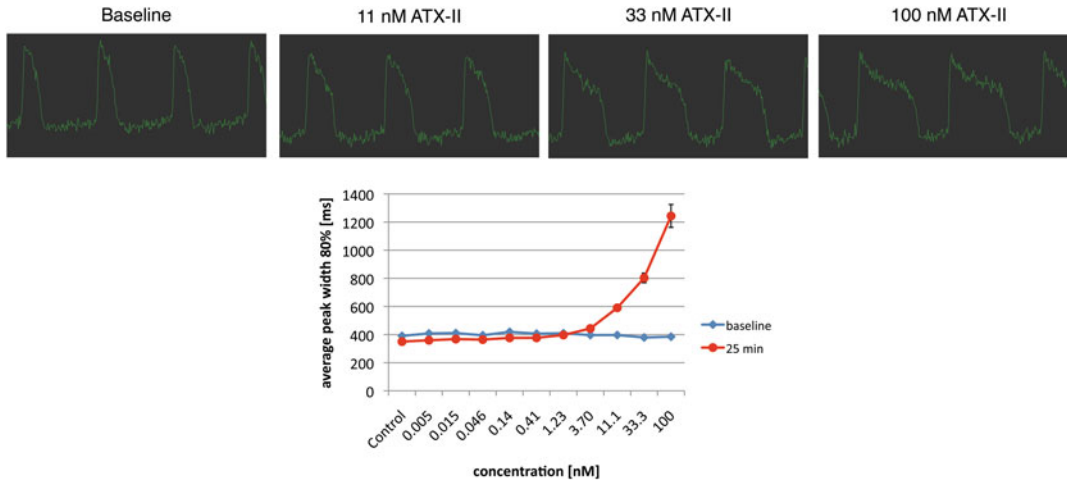

Fig. 8 Dose-dependent ATX-II-induced prolongation of action potential-like recordings from Cor.4U® cardiomyocytes in the voltage-sensitive dye assay

4.3 Centrifugation of Cor.4U® Cardiomyocytes After Thawing Reduces Viability

Do not centrifuge Cor.4U® cardiomyocyte suspensions immediately after thawing! Centrifugation directly after thawing will damage the cells and leads to cell loss.

4.4 Avoid Edge Effects

When a microplate is transferred from room temperature into a heated incubator (usually at 37 °C), a temperature gradient is formed within the microplate, such that higher temperatures occur in the outer wells, while the inner wells will tend to have lower temperatures.

In the case of a microplate freshly seeded with a cell suspension of cardiomyocytes, this can lead to pronounced convection currents in the cell suspension in the outer wells, keeping the cells in suspension instead of settling to the bottom of the well. Furthermore, the cells kept in suspension by these convection currents prefer to settle at the boundary of the well, which reduces the number of cells in the center of the well. The inner wells of the plate heat up more slowly, so convection currents do not occur and the cells settle evenly on the bottom of the well. This phenomenon is known as the "edge effect" where the outer wells of microplate show different results compared to inner wells in a given assay. Keeping the freshly seeded microplate at room temperature for 20 min before transferring to the heated incubator helps the edge effect because the cells in the outer wells will distribute more homogeneously on the bottom of each well [7].

4.5 Harsh Suction and Pipetting Disrupts Cardiomyocyte Monolayers

Medium exchange and washing steps of Cor.4U® cardiomyocytes cultured in microplates have to be conducted very carefully since harsh suction and pipetting causes disruption of the cardiomyocyte monolayer. This is especially true for high-density formats like the

384-well plate. Due to the fact that Cor.4U® cardiomyocytes are not proliferative, defects in the cell monolayer will not be repaired by cell growth.

For the washing steps during the preparation for the assay on the day of experiment, it is recommended to discard the medium by quickly flipping the plate over a container and then tapping the plate onto a clean tissue since sterility is no longer required.

4.6 Non-wash Assay with the Cal-520-AM Dye

The washing step before the start of the experiment increases operator workload and also adds a further 30 min incubation period in the incubator, to allow the cells to recover from the stress associated with this volume change.

It is possible to conduct the calcium transient assay with the Cal-520 dye as a non-wash assay, by adding compounds to the cells with the dye still in the medium. However, the disadvantage of this approach is that the recorded transient amplitudes will increase over time. In this case, time-matched vehicle controls can be used to correct for this effect.

4.7 Calcium Transient Assay Stability

All parameters of the calcium transient wash assay using the Cal-520-AM dye are stable even 4 h after the loading of the dye. Only the beat rate is reduced in the first 30 min after the dye washout so that a recovery time of 45 min is recommended. Together with the dye loading time of 45 min, the experimental window is 2.5 h, which is sufficient to detect acute drug-induced changes of the calcium transient parameters.

4.8 Stability of Action Potential-Like Recordings with the FluoVolt Dye

Do not load the Cor.4U® cardiomyocytes with the FluoVolt dye for more than 20 min because an exposure time longer than 60 min will increase the probability of observing dye-induced side effects like APD prolongation. A maximum 20 min dye loading period will leave an experimental window of about 40 min, which is wide enough to observe acute drug effects without interference of the FluoVolt dye.

5 Conclusion

The identification of proarrhythmic potentials of drug candidates is a critical factor in the complete drug development process. In this regard, the combination of hiPSC-derived Cor.4U® cardiomyocytes with HT- compatible Hamamatsu FDSS systems for fluorescent calcium or voltage-sensitive dye assays is the ideal solution. Compared to other physiologically relevant assays like manual patch clamp, these assays are extremely easy to conduct and do not require highly educated personnel.

The high-throughput capabilities and the high level of predictability allow for placing the assay even early on in the preclinical drug development as a selection filter for subsequent costly and time-consuming ex vivo and/or in vivo studies and will potentially substitute for clinical thorough QT studies.

As a future perspective, integration of genetically encoded fluorescent sensors into commercially available hiPSC-derived cardiomyocytes will eliminate the need for chemical dyes and will allow for studying drug-induced long-term proarrhythmic and cardiotoxic effects.

References

1. Obejero-Paz CA, Bruening-Wright A et al (2015) Quantitative profiling of the effects of vanoxerine on human cardiac ion channels and its application to cardiac risk. Sci Rep 5:17623. doi:10.1038/srep17623
2. Lu HR, Whittaker R et al (2015) High throughput measurement of Ca++ dynamics in human stem cell-derived cardiomyocytes by kinetic image cytometery: a cardiac risk assessment characterization using a large panel of cardioactive and inactive compounds. Toxicol Sci 148(2):503–516. doi:10.1093/toxsci/kfv201
3. Kitaguchi T, Moriyama Y et al (2015) CSAHi study: evaluation of multi-electrode array in combination with human iPS cell-derived cardiomyocytes to predict drug-induced QT prolongation and arrhythmia—effects of 7 reference compounds at 10 facilities. J Pharmacol Toxicol Methods 78:93–102. doi:10.1016/j.vascn.2015.12.002
4. Gilchrist KH, Lewis GF et al (2015) High-throughput cardiac safety evaluation and multi-parameter arrhythmia profiling of cardiomyocytes using microelectrode arrays. Toxicol Appl Pharmacol 288(2):249–257. doi:10.1016/j.taap.2015.07.024
5. Fermini B, Hancox JC et al (2016) A new perspective in the field of cardiac safety testing through the comprehensive in vitro proarrhythmia assay paradigm. J Biomol Screen 21(1):1–11. doi:10.1177/1087057115594589
6. Maher MP, Gonzales JE (2005) Multi well plate and microelectrode assemblies for ion channel assays. US Patent 6,969,449B2, 29 Nov 2005
7. Lundholt BK, Scudder KM, Pagliaro L (2003) A simple technique for reducing edge effect in cell-based assays. J Biomol Screen 8(5):566–570. doi:10.1177/1087057103256465

Chapter 8

Kinetic Image Cytometry for Predicting Arrhythmias Using Human Stem Cell-Derived Cardiomyocytes

Emily R. Pfeiffer, Ross Whittaker, Raquel Vega, Fabio Cerignoli, Patrick M. McDonough, and Jeffrey H. Price

Abstract

Kinetic Image Cytometry™ (KIC™), in which living cells are cultured in multi-well dishes and imaged for electrophysiological transients (such as intracellular calcium or membrane potential) using automated digital microscopy/image analysis, represents an advance in the field of high content analysis. KIC methods, coupled with the use of human stem cell-derived cardiomyocytes (hSC-CMs), are potentially very useful for identifying proarrhythmia activity of test compounds, relevant to cardiosafety. In the present study, a panel of 40 compounds was tested with KIC to quantify the effects of the chemicals on the calcium transients associated with contraction in hSC-CMs, and the results compared to the effects of these compounds on the QT-interval from human electrocardiograms. The kinetics of the calcium transients quantified with KIC identified the chemicals that prolong (commonly associated with proarrhythmic activity) or shorten the QT interval with 100% specificity and 94% sensitivity. These data, along with data obtained in previous studies utilizing KIC and hSC-CMs, demonstrate that this assay platform represents the current "state-of-the-art" in vitro method for testing drug candidates for proarrhythmic tendencies.

Key words Arrhythmia, Induced pluripotent stem cells, Long QT, Action potential, Calcium transient, hERG, Cardiomyocytes, Potassium channel, Sodium channel, Calcium channel, Torsades de Pointes

1 Introduction

Drug-induced arrhythmias are unwanted and sometimes fatal side effect of medications. A common culprit of arrhythmia liability is drug-induced reduction of K^+ current through the human "ether a go-go related" channel (hERG, encoded by *KCNH2*). This hERG K^+ channel block is observed as the prolongation of the QT-interval in the ECG record, and can result in Torsades de Pointes (TdP), a ventricular arrhythmia, which can lead to fibrillation and sudden death. A surge in drug-induced TdP in the 1980s and 1990s, spurred regulatory agencies to require testing of drug candidates for QT-prolonging effects prior to approval [1]. Current FDA guidance (e.g., S7B) [2] recommends non-rodent animals (e.g., guinea pigs,

Mike Clements and Liz Roquemore (eds.), *Stem Cell-Derived Models in Toxicology*, Methods in Pharmacology and Toxicology, DOI 10.1007/978-1-4939-6661-5_8,

rabbits, and canines) for ex vivo (e.g., isolated hearts, Purkinje fibers) and in vivo (e.g., telemetered dogs) studies as well as recombinant heterologous cells expressing cloned human ion channels. However animal models are species-specific, expensive, and low-throughput, and recombinant systems do not recapitulate the full electrophysiological response of human cardiomyocytes. Drug effects on multiple ion channels frequently may result in an overall cardiac effect not predicted by isolated hERG screening, as observed with fluoxetine (Prozac) [3], and verapamil [4, 5]; both fluoxetine and verapamil inhibit hERG and also cardiac calcium channels, which is likely compensatory as these drugs are not arrhythmogenic. With recent advances in stem cell technology, human induced pluripotent stem cells, which are readily differentiated into cardiac myocytes (hSC-CMs), are commercially available. As hSC-CMs are amenable to high-throughput culturing, they can be used for high content phenotypic analysis via recent advancements in imaging methods [6, 7], and can potentially be used to screen drug candidates for arrhythmia liability earlier in the drug discovery process, reducing the cost of drug development. Furthermore, as the cells are human in origin and produce electrophysiological transients integrating the cohort of human ionic currents [8, 9], data obtained using methods customized for these cell types can be more predictive than from recombinant or animal cell models [10]. Consequently, implementation of methods utilizing hSC-CMs for arrhythmia liability testing is anticipated to improve cardiac safety and reduce animal use.

Contractions of the heart result from action potentials that originate in the sinoatrial node and propagate through the atria and ventricles to initiate calcium transients within the cardiac myocytes. This increase in cytoplasmic calcium, in turn, activates myofibrillar proteins to initiate contraction [11, 12]. The action potential initiates first, and is relatively brief; next, the calcium transient originates, and the contractile motion follows (Fig. 1a). Ion currents and channel proteins involved in action potential initiation include, I_{Na}, the inward sodium current mediated by the sodium channel (major subunit encoded by *SCN5A*), and I_{Ca}, the inward calcium current mediated by the L-type calcium channel (major subunit encoded by *CACNA1C*). Repolarization results from closing of the L-type calcium channel, and outward flow of potassium (I_{Kr}, I_{Ks}, and I_{K1}) through channels encoded by *KCNH2*, *KCNQ1*, and *KCNJ2*, respectively (Fig. 1b). Initiation of the calcium transient occurs via Ca^{2+} influx through the L-type calcium channel, which activates further calcium release from the sarcoplasmic reticulum via the ryanodine receptor (i.e., calcium-induced calcium release). The calcium transient is terminated by reuptake of calcium into the SR and extrusion from the cell by SERCA2 and the Na:Ca exchanger, respectively (Fig. 1c). Cardiac electrophysiology is governed by these major ion currents, and an assortment of others, which act in concert to produce the full cardiac action potential and calcium

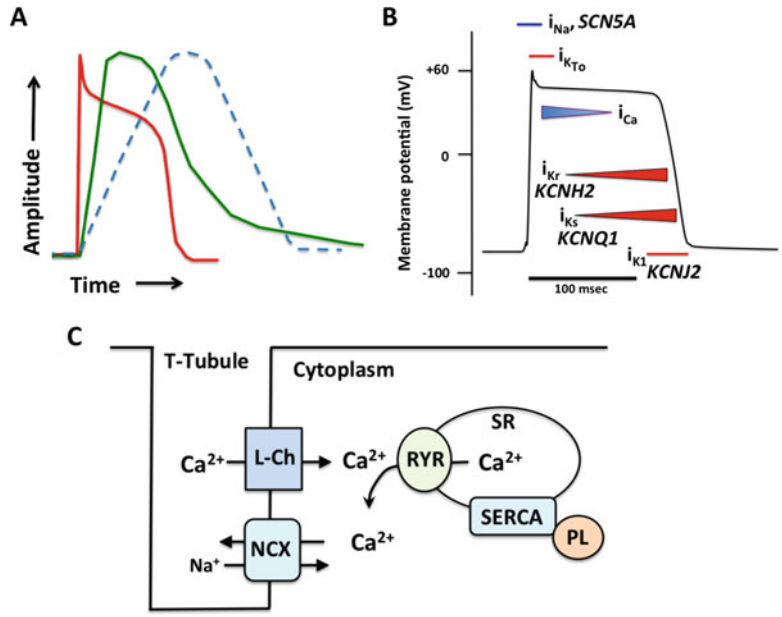

Fig. 1 The relationship between action potentials, calcium transients, and contraction of cardiac myocytes. (**a**) Schematic representation of the kinetics of APs (*red line*), calcium transients (*green line*), and contraction (*dotted blue line*). (**b**) The major ion channels that participate in the AP. Ion currents are designated (e.g., I_{Na} is the inward sodium current), as well as the genes encoding the channel proteins. (**c**) Calcium influx, triggered by opening of the L-type calcium channel, initiates calcium release from the ryanodine receptor to trigger contraction. To initiate relaxation (diastole), calcium is taken back up into the sarcoplasmic reticulum by SERCA2, and removed from the cytoplasm by Na:Ca exchange, and other processes (adapted from Bers [12])

transient. Thus, assays of cardiac effect based only on a single channel type in a heterologous expression system are not optimal for prediction of response in clinic. Similarly, assays that rely on non-human mammalian models, which differ in subtype and relative expression level of the ion channels described here, may not accurately predict compound effects in patients.

In previous studies, KIC was used to assess arrhythmic liability of test compounds based upon the ability of the chemicals to modify calcium transient kinetics in iCell Cardiomyocytes from Cellular Dynamics International [7, 10]. A goal of the present study was to evaluate the effects of a related chemical set on calcium transients in hSC-CMs from an alternative source of commercially available hSC-CMs (Cor.4U hiPSC-Cardiomyocytes from Axiogenesis). This was done to test the suitability of the Cor.4U hiPSC-Cardiomyocytes for use with KIC, and also to explore the generality of the approach, since the cardiac myocytes from the two different suppliers represent different human subjects.

2 Materials

Cor.4U hiPSC-Cardiomyocytes from Axiogenesis (Cologne, Germany) were utilized for this study. These purified cardiac myocytes spontaneously generate action potentials with associated calcium transients and contractions. To label cell nuclei (enabling autofocus of the microscopy workstation and analysis of the cell images) and to load the cells with a fluorescent calcium indicator, the hSC-CMs were incubated with a solution featuring Hoechst 33342 and Fluo-4 AM (Table 1). Data recordings were performed with the cells in Tyrode's buffer (Table 2).

An IC200—Kinetic Image Cytometer (Vala Sciences Inc, San Diego, California), outfitted with a 20× NA 0.75 objective, was used for image acquisition. The IC200-KIC is an automated digital fluorescence microscopy workstation featuring an environmental chamber optimized to acquire video images of cells plated in multi-well plates. Cells were maintained at 37 °C and 5% CO_2 during image acquisition (see detailed protocols, below).

Chemicals utilized in this study were prepared as 1000× stock solutions in DMSO. The final DMSO concentration (0.1%) was kept constant across all wells in every experimental run.

3 Methods: Kinetic Image Cytometry™

Chemicals were tested at seven concentrations in triplicate, along with DMSO-treated controls, to generate 8-point dose-response curves (*see* Fig. 2 for plate map). Reference compounds were included for each plate including a known hERG channel blocker (E4031), a sodium channel blocker (flecainide), and verapamil (an L-type calcium channel antagonist that also has inhibitory effects

Table 1
Calcium dye loading solution

Stock reagent	Working stock	Dye loading solution (10 ml)
Assay buffer: Fluo-4 NW kit component, or 20 mM HEPES in 1× HBSS	Add 10 v 1 M HEPES to 490 v HBSS, store 4 °C	7.5 ml
Probenecid 77 mg/ml: Fluo-4 NW kit component	Suspend 77 mg vial contents in 1 ml assay buffer, store −20 °C	100 µl
HOECHST 10 mg/ml stock	Prepare fresh 1:50 intermediate solution in assay buffer, final 200 ng/ml	10 µl of 1:50 preparation
Fluo-4 NW dye	Suspend bottle contents in 10 ml assay buffer, store 4 °C	2.5 ml

Table 2
Example Tyrode's buffer formulation, pH 7.4

Component	Final (mM)
Distilled water	
NaCl	135
KCl	6
$CaCl_2$	2
$MgCl_2$	1
HEPES	25
Glucose	10

	1	2	3	4	5	6	7	8	9	10	11	12
A												
B												
C	Con	Con	Con	C1 D1	C1 D1	C1 D1	C1 D2	C1 D2	C1 D2	C1 D3	C1 D3	C1 D3
D	C1 D7	C1 D7	C1 D7	C1 D6	C1 D6	C1 D6	C1 D5	C1 D5	C1 D5	C1 D4	C1 D4	C1 D4
E	Con	Con	Con	C2 D1	C2 D1	C2 D1	C2 D2	C2 D2	C2 D2	C2 D3	C2 D3	C2 D3
F	C2 D7	C2 D7	C2 D7	C2 D6	C2 D6	C2 D6	C2 D5	C2 D5	C2 D5	C2 D4	C2 D4	C2 D4
G	Con	Con	Con	E4031	E4031	E4031	FLEC	FLEC	FLEC	VER	VER	VER
H												

Fig. 2 Plate map for the assay. Cells were plated in wells C1 to G12. Each compound was tested at seven different concentrations, in triplicate. Wells exposed to DMSO, only, were also included, with triplicate wells at three positions on the plate. E4031, flecainide, and verapamil were also included on every plate as reference compounds. Images were acquired from the wells in a "serpentine" fashion, from well C1 to C12, then D12 to D1, then E1 to E12, etc., to reduce the time required to scan the plate and minimize differences that might arise between wells due to leakage of Fluo-4 from the cells

on hERG). For each well a single image was first collected of the nuclei at excitation/emission wavelengths appropriate for Hoechst (nuclear image); the optics were then switched to the green fluorescence channel for visualizing the Fluo-4, and images collected at 30 frames per second for 10 s (calcium images). Images were stored to the computer hard drive in user-specified directories in an uncompressed *.tif format.

The images were analyzed with the software program CyteSeer™ (Vala Sciences Inc) [13] utilizing the "Cardiac Two-Channel Time Series" algorithm. This algorithm first identifies the nuclei in the

field of view from the nuclear image, and assigns each nucleus a unique number; the algorithm then averages the Fluo-4 intensity across the calcium images, to identify the cell boundaries, and uses this information, along with the position of the nucleus to identify the "cytoplasmic mask" (pixels corresponding to the region between the cell boundary and nucleus) for each cell. The average pixel intensity for the Fluo-4 signal is then calculated for the cytoplasmic mask at each time point (Fig. 3). It is important to exclude the nuclear region from the analysis, as calcium transients within the nucleus exhibit slower upstroke and downstroke velocities and prolonged duration vs. the cytoplasmic transients. Cells that did not display calcium transients were excluded from further analysis by gating on the time-course data. For the cells exhibiting calcium transients, measurements characterizing each transient such as indices of transient duration and shape, repolarization morphology (Fig. 4), and beat rate were tabulated and grouped for statistical analysis.

A key feature of the approach is that these methods yield a detailed record for each cell. Thus, cells exhibit contractile activities asynchronous with others in the field of view, and the percentage of cells exhibiting contractile activity can be quantified. The records can also potentially be surveyed to identify potential "pacemaker" cells in the field of view, and to track propagation of the contractile events. It is also possible to fix the cells following the KIC analysis, immunolabel for relevant biomarkers, reimage the plate, and correlate biomarker expression to the kinetic events on a cell-by-cell basis; with this strategy, subpopulations of cells within the cultures can be selectively analyzed (unpublished). This degree of analysis is not achieved with systems such as the FLIPR (Molecular Devices, Sunnyvale CA) or FDSS (Hamamatsu, Middlesex, NJ), which average the signals across a well.

3.1 Cardiomyocyte Preparation

For cardiac safety assays, hSC-CMs are cultured in monolayer near 90% confluence, achieving a density of approximately 250–350 cells per recorded field of view. Controlled cell density [14], careful cell handling according to manufacturer's recommendations, and optimal extracellular matrix protein selection are important factors in obtaining a homogeneous, healthy cardiomyocyte culture. In this study, Cor.4U hiPSC-Cardiomyocytes (Axiogenesis, Cologne, Germany) were utilized, with the following protocol:

3.1.1 Preparation

1. Inspect the lot of Axiogenesis Cor.4U hiPSC-Cardiomyocytes to be plated.
   a. Acquire lot-specific plating density from a preliminary experiment (e.g., 35,000–55,000 cells per well, 96-well format).
   b. Use manufacturer's provided plating and maintenance media, and additives.
   c. Thaw frozen media overnight at 4 °C.

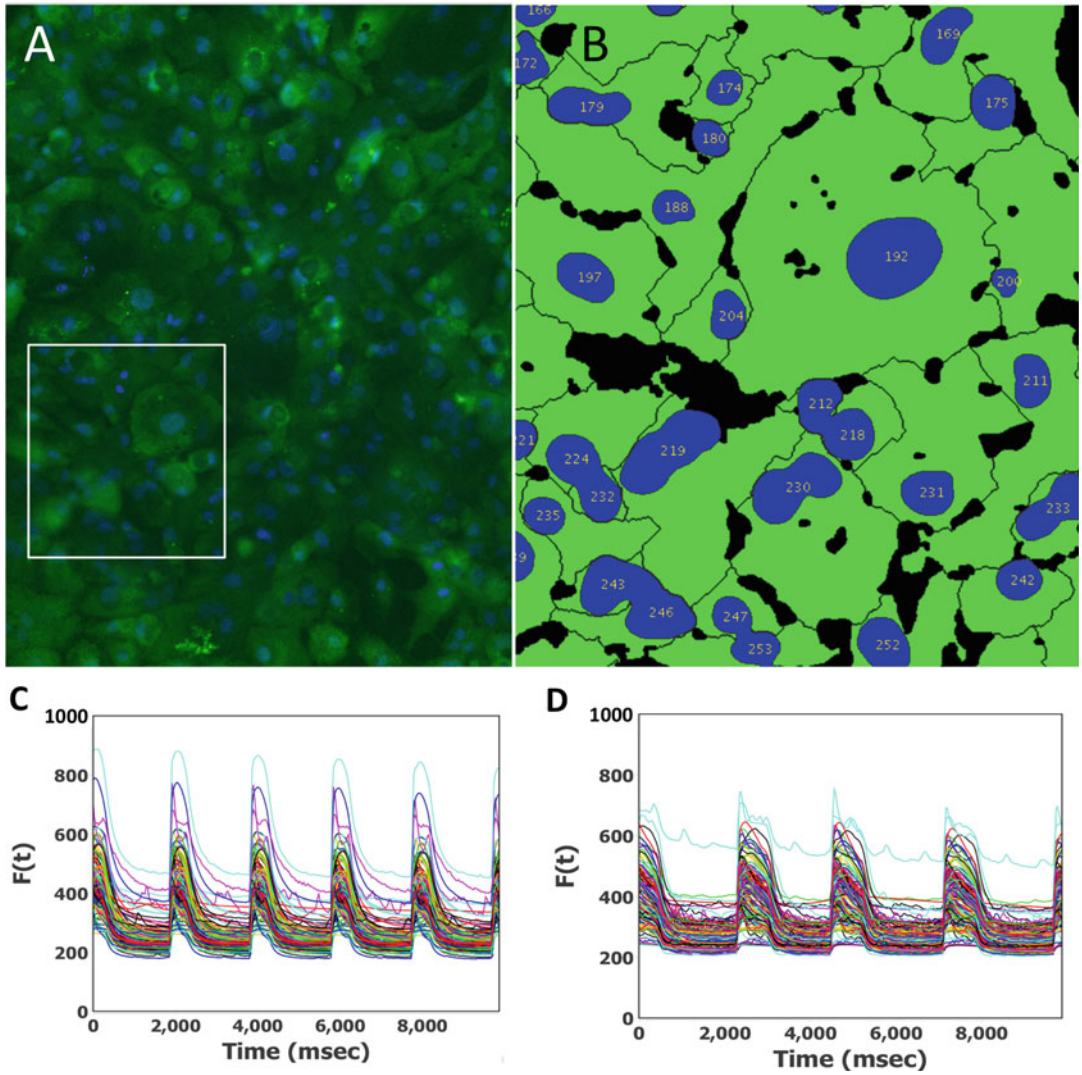

Fig. 3 Basics of kinetic image cytometry. (**a**) A screenshot from CyteSeer™ is shown for a control well of hSC-CMs labeled with Hoechst (nuclei, *blue*) and Fluo-4 (intracellular calcium, *green*). (**b**) The inset region from (**a**), *white rectangle* is displayed at higher magnification to show the identified nuclei and cell boundaries. The cytoplasmic mask regions for each cell are in *green*. (**c**) Traces are displayed of the average pixel intensity (Fluo-4) of the cytoplasmic masks ($n=176$ cells) for a control well. (**d**) Traces are shown for a different well exposed to E4031 (100 nM) which blocks hERG and prolongs the transients ($n=134$ cells)

2. Prepare Plates and Plating Media.

   a. Clean biosafety cabinet and equipment with 70% ethanol solution.

   b. Coat Greiner μClear 96-well plates

      i. Working inside a tissue culture hood, dilute fibronectin (Sigma F1141, 1 mg/ml) to 10 μg/ml in Hank's balanced salt solution (HBSS): 150 μl in 15 ml.

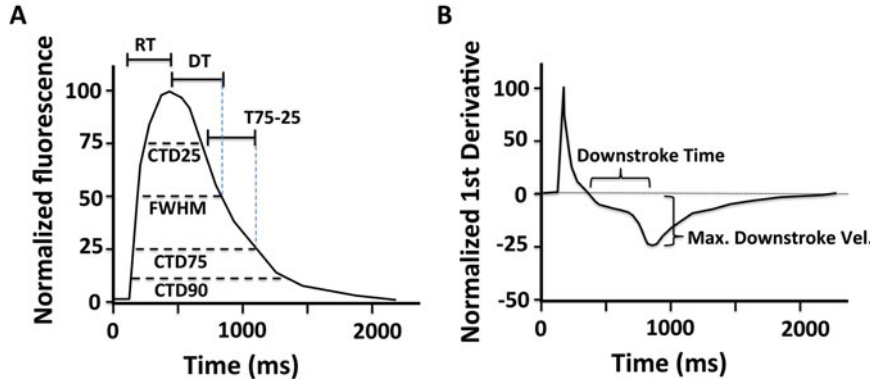

Fig. 4 Definition of calcium transient measurements. (**a**) Data parameters derived from the calcium transient. Rise time (RT): the time elapsed from the start of the upstroke to the peak. Decay time (DT): the time elapsed from the peak to the 50 % point of the downstroke. Full width half maximum (FWHM): the time elapsed from the 50 % point of the upstroke to the 50 % point of the downstroke. CTD25, CTD75, and CTD90 correspond to the calcium transient durations at the 25 %, 75 %, and 90 % magnitude (e.g., CTD75 is the time elapsed from the 25 % point of upstroke to the 25 % point on the downstroke relative to the peak). T75-25: the time elapsed from 75 % to 25 % of maximum on the downstroke. (**b**) Data parameters derived from the 1st derivative of the calcium transient. Downstroke time: the time elapsed from the zero-point of the 1st derivative (corresponds to peak of the calcium transient) to time point of the maximum downstroke velocity (maximum negative value of the 1st derivative)

ii. Add 100 µl of freshly diluted fibronectin solution to each well of the 96-well plate.

iii. Incubate plates at 37 °C 5 % CO_2 tissue culture incubator for 3 h.

iv. After 3 h incubation, aspirate excess fluid, cover plates, and set aside.

c. Add 5 µl Puromycin per 10 ml Thawing Media to make working Plating Media (PM), and bring to room temperature (**Note 1**).

3.1.2 Procedure

1. Clean and place equipment in biosafety cabinet:

   a. Room temperature PM, fibronectin-coated plates, P1000 and multichannel pipettes and tips, media reservoirs, and 50 ml falcon tube.

2. Thaw cells: obtain frozen vial(s) (1–3 vials) of Cor.4U cells from liquid N_2 store, and place in a 37 °C water bath for 4 min exactly.

3. Recover vial, spray with 70 % EtOH and wipe, immediately place in hood.

4. Using a P1000 pipette, collect contents of cell vial(s) and dispense gently into 50 ml falcon tube.

5. Multiply the following volumes per vial thawed, e.g., for three vials, add 1 ml three times:
   a. Add 1 ml of PM into vial to rinse, recover, and add dropwise to 50 ml tube containing the cells (4–5 s per drop, and gently mixing 50 ml tube). Use a maximum of three vials per 50 ml tube.
   b. Add another 1 ml of PM to cell suspension (4–5 s per drop).
   c. Slowly add an additional ~3.5 ml PM per vial, for a total of 6 ml per vial of cells.
6. Mix gently, but well, to disassociate the clumps.
7. Assess viability with an automated cell counter, and calculate live cell density for plating. In this study, cell viability ranged from 55 to 80% at the time of plating.
8. Dilute cells for plating: add plating media to achieve desired concentration, e.g., 45,000 cells per 100 µl (450 k cells/ml).
9. Plate cells, using P200 multichannel pipette (use slow speed for any cell-handling step) and media reservoir, mixing gently before plating each row.
   a. Plate 100 µl per well. Take care not to touch well bottom, e.g., pipette suspension along well wall with plate tipped at approximately 20°.
10. Cover the 96-well plate and allow to rest in tissue culture hood for 10–15 min. Place in an incubator (37 °C, 5% CO_2) at the flattest location possible (**Note 2**).
11. After 3 h, completely replace the plating medium with 200 µl maintenance media, pre-warmed to 37 °C.
12. Culture for 6 days before KIC proarrhythmia assay, changing media at 24 h, and then every 2 days.

3.2 Imaging and Analysis

KIC™ utilizes fluorescent electrophysiological sensitive small molecule probes such as Fluo-4 (intracellular calcium) or FluoVolt (membrane potential). Genetically expressed calcium- or voltage-sensitive proteins may be used as alternatives (**Note 3**). In the protocol described here we will focus solely on intracellular calcium imaging using the Fluo-4 dye (**Note 4**). The dye loading protocol for Fluo-4 is as follows:

3.2.1 Procedure for KIC™ Assay with Fluo-4 No-Wash (NW) (Molecular Probes)

1. Prepare dye loading solution (Table 1). Vortex each component individually, and shield from light. Bring to 37 °C.
2. In biosafety cabinet, remove cell culture media and load 100 µl dye solution per well (use slow speed on multichannel pipettor for all cell-handling steps).

3. Incubate cells in dye for 60 min inside a 37 °C 5% CO_2 tissue culture incubator.
4. Prepare compounds:
   a. Compound stocks are prepared in DMSO at 1000-fold the final test concentration(s), and stored at −20 °C.
   b. Suspend compounds at test concentration(s) in Tyrode's buffer at sufficient volume for replicate analysis, and bring to 37 °C in master plate map format. All vehicle control and compound wells will contain 0.1% DMSO.
5. Remove dye loading solution from cells: do this by removing dye solution, replacing with 200 µl Tyrode's buffer (warmed to 37 °C); the Tyrode's solution is used as a wash solution to remove residual dye.
6. Remove the Tyrode's wash solution and add final imaging solution: 200 µl Tyrode's buffer containing vehicle or compound.
7. Place the plate inside IC200-KIC chamber and equilibrate for 20 min before reading plate.
8. Run KIC image acquisition program, e.g., (per well) Nuclear channel: autofocus protocol and single image of nuclei (**Note 5**). Calcium channel: kinetic image series such as 30 frames per second for 10 s (**Note 6**).

Typical KIC videos are acquired at 30–100 frames per second for recording durations of 10–20 s [6]. Forty-eight to 60 wells are recorded per scan in the protocol described above, avoiding dye leak from the cells that may occur in a longer duration scans. Beat rate control via electrical stimulation may optionally be applied (**Note 7**). Compound effect is judged as a percentage change relative to vehicle controls distributed throughout the plate. Reference compounds (e.g., E4031 (100 nM), a hERG K^+ channel blocker, flecainide (2 µM), a sodium channel blocker, and verapamil (300 nM), a Ca^{2+} channel, and hERG K^+ channel blocker) are typically included on each plate for quality assessment (**Note 8**). Typically acute compound exposure periods (20–30 min) are tested. However, cells may be cultured with compounds included in the media for extended periods (e.g., hours or days) to test effects of chronic exposure.

4 Notes

1. The antibiotic Puromycin was present in plating medium for the initial seeding only. No antibiotics were used in the culture medium after the seeding medium was removed.

2. In our hands, the most even coverage of the wells is obtained by placing the dishes on a level surface (verified with a bubble level) immediately after plating.
3. Genetically encoded calcium or voltage sensing proteins would have advantages over fluorescent dyes in that the expression of the sensor can be targeted using cell-type specific promoters and the cells would not have to be "loaded" with the indicators prior to the experiment. A potential disadvantage is that the genetically encoded reporters sometimes respond slowly to the kinetic transients whereas the fluorescent dyes respond rapidly.
4. Fluo-4 was chosen as the fluorescent calcium indicator because it is the brightest of the dyes that are currently available. Rhod-2, which is a red-channel calcium indicator, also works well with hSC-CMs and KIC.
5. For quantifying potential proarrhythmogenic effects of chemicals on cardiac myocytes, the most often used parameter is the CTD75 value, which is an index of the duration of the calcium transient.
6. Since the calcium transient duration is on the order of 1 s, image acquisition at 30 fps gives sufficient resolution to identify prolonging effects of test compounds.
7. While not used in the present study, the KIC can electrically pace the contractions of hSC-CMs and other cardiomyocytes, via electrodes that are automatically lowered into the wells.
8. Acceptance criteria to monitor the quality of the cell preparation and successful implementation of the KIC experiment include: prolongation of the FWHM and decay time to $\geq 150\%$ by E-4031, prolongation of FWHM and Decay Time $\geq 125\%$ by flecainide, and diminishment of FWHM and Decay Time to $\leq 85\%$ and $\leq 80\%$, respectively, by verapamil.

5 Results

To further validate the usefulness of the KIC methodology in identifying potential cardiotoxic effects of candidate pharmaceuticals, a unique set of 40 compounds was assayed for ability to modify the kinetics of the calcium transients and contraction rate of Cor.4U hiPSC-Cardiomyocytes (*see* Table 3 for effects on calcium transient duration (CTD75), maximally effective concentration, and drug concentration range tested). Consistent with previous results, hERG-blockers such as ibutilide increased the duration of the decay phase of the calcium transient, as did ranolazine, whereas verapamil—which inhibits both the L-type calcium channel and hERG—had the opposite effect, shortening transient decay (Fig. 5). Additionally, rate effects were also quantified, such as

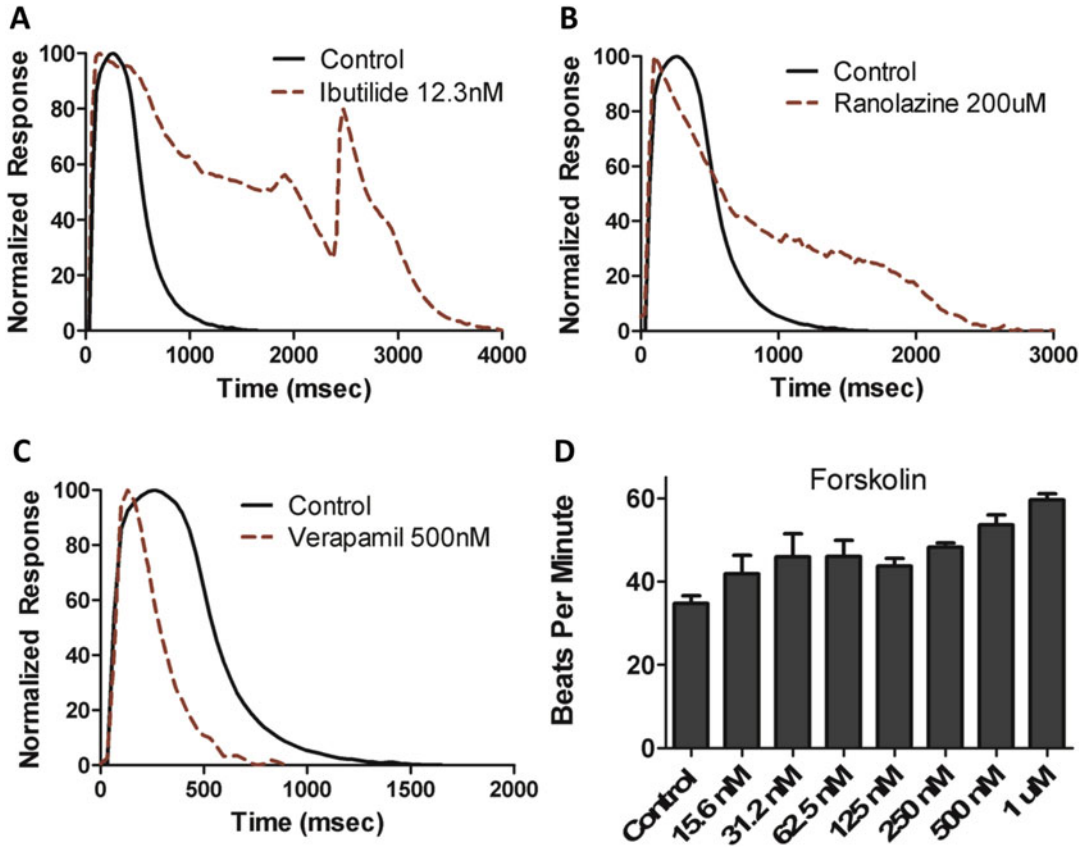

Fig. 5 Representative effects on the calcium transient by cardioactive compounds. hSC-CMs were seeded into 96-well dishes, cultured so that they formed spontaneously contractile monolayers, and assayed for calcium transient kinetics using Fluo-4 and KIC. For kinetic analysis, the transients are normalized to the baseline (0 %, diastole) and maximum (100 %, systole). Traces are shown from a control cell vs. those treated with (**a**) a hERG blocker (ibutilide), (**b**) a mixed channel blocker (ranolazine), and (**c**) a compound that simultaneously inhibits both L-type calcium channels and hERG (verapamil). The dose-dependent effect of forskolin on the spontaneous beat rate of the hSC-CMs is shown in **d** (each bar is the mean ±SD from $n=3$ wells, treated at the indicated concentration

increased contractile frequency elicited by forskolin, which increases cAMP (Fig. 5).

Since the kinetics of the cardiac calcium transients are strongly influenced by ion fluxes associated with the action potential, we postulate that agents that alter the kinetics of the calcium transients have corresponding effects on action potential kinetics and, accordingly, that potential cardiotoxic effects can be identified with KIC and Fluo-4 loaded hSC-CMs. Consistent with this hypothesis, the screen correctly identified 23/23 compounds that prolong the QT interval (calcium transient duration CTD75 prolonged >135 % of vehicle control), 9/11 QT-shortening compounds (calcium transient duration shortening to CTD75 < 85 % vehicle control), and 6/6 of compounds with no effect on the QT interval duration (Fig. 6, Table 3).

Table 3
The panel of 40 compounds assayed for effect on the calcium transient by KIC in Cor.4U hiPSC-Cardiomyocytes

Compound	Expected result	Observed result	Greatest CTD75 effect (%)	Concentration at greatest effect	Concentration range tested
Alfuzosin	Prolonged Transient	Prolonged Transient	189	33 μM	0.14 μM to 100 μM
Amiodarone	Prolonged Transient	Prolonged Transient	145	25 μM	0.78 μM to 50 μM
Astemizole	Prolonged Transient	Prolonged Transient	424	33 nM	0.14 nM to 100 nM
BayK 8644	Prolonged Transient	Prolonged Transient	148	3.67 μM	0.14 μM to 100 μM
Bepridil	Prolonged Transient	Prolonged Transient	177	333 nM	4 nM to 10 μM
Cisapride	Prolonged Transient	Prolonged Transient	256	407 nM	135 nM to 10 μM
Dofetilide	Prolonged Transient	Prolonged Transient	306	37 nM	1 nM to 1 μM
Donepezil	Prolonged Transient	Prolonged Transient	624	6.25 μM	1.6 μM to 100 μM
E4031	Prolonged Transient	Prolonged Transient	551	75 μM	6.25 μM to 150 μM
Flecainide	Prolonged Transient	Prolonged Transient	677	33 μM	0.13 μM to 100 μM
Ibutilide	Prolonged Transient	Prolonged Transient	391	37 nM	1 nM to 1 μM
Moxifloxacin	Prolonged Transient	Prolonged Transient	150	125 μM	7.9 μM to 500 μM
Pentamidine	Prolonged Transient	Prolonged Transient	643	12.5 μM	0.39 μM to 25 μM
Pimozide	Prolonged Transient	Prolonged Transient	282	1 μM	10 pM to 10 μM
Procainamide	Prolonged Transient	Prolonged Transient	667	500 μM	7.8 μM to 500 μM
Quinidine	Prolonged Transient	Prolonged Transient	273	11.1 μM	0.14 μM to 100 μM
Ranolazine	Prolonged Transient	Prolonged Transient	387	100 μM	3.1 μM to 200 μM

(continued)

Table 3
(continued)

Compound	Expected result	Observed result	Greatest CTD75 effect (%)	Concentration at greatest effect	Concentration range tested
Sertindole	Prolonged Transient	Prolonged Transient	136	1 μM	31 nM to 10 μM
Sotalol	Prolonged Transient	Prolonged Transient	432	125 μM	7.8 μM to 500 μM
Sparfloxacin	Prolonged Transient	Prolonged Transient	651	125 μM	7.8 μM to 500 μM
Terodoline	Prolonged Transient	Prolonged Transient	143	3.33 μM	14 nM to 10 μM
Thioridazine	Prolonged Transient	Prolonged Transient	137	2.5 μM	0.16 μM to 10 μM
Tolterodine	Prolonged Transient	Prolonged Transient	283	123 nM	14 nM to 10 μM
Diltiazem	Shortened Transient	Transient Shortened/ Beating Stops	62	5 μM	10 nM to 100 μM
Forskolin	Shortened Transient	Transient Shortened/ Rate Increased	72	1 μM	15.6 nM to 1 μM
Histamine	Shortened Transient	Transient Shortened/ Rate Increased	64	3.67 μM	0.14 μM to 100 μM
Isoprenaline	Shortened Transient	Transient Shortened/ Rate Increased	66	15 nM	15 nM to 1 μM
Mallotoxin	Shortened Transient	Transient Shortened	72	100 μM	0.14 μM to 100 μM
Nifedipine	Shortened Transient	Transient Shortened/ Beating Stops	47	10 μM	100 pM to 100 μM
Nimodipine	Shortened Transient	Transient Shortened	54	500 nM	8 nM to 500 nM
Nitrendipine	Shortened Transient	Transient Shortened/ Beating Stops	81 (68)	333 nM	4 nM to 10 μM
NS1643	Shortened Transient	None, reduced beating	96	25 μM	1.5 μM to 100 μM
Serotonin	Shortened Transient	None	92	1 nM	100 pM to 100 μM
Verapamil	Shortened Transient	Transient Shortened/ Beating Stops	82	312.5 nM	78.1 nM to 5 μM
Ascorbic acid	None	None	113	1 μM	100 pM to 100 μM

(continued)

Table 3
(continued)

Compound	Expected result	Observed result	Greatest CTD75 effect (%)	Concentration at greatest effect	Concentration range tested
Aspirin	None	None	111	50 μM	500 pM to 500 μM
Famotidine	None	None	123	25 μM	1.6 μM to 100 μM
Fluoxetine	None	None	107	1 μM	16 nM to 1 μM
Linezolid	None	None	109	12.5 μM	1.6 μM to 100 μM
Loratidine	None	None	133	50 μM	1.6 μM to 100 μM

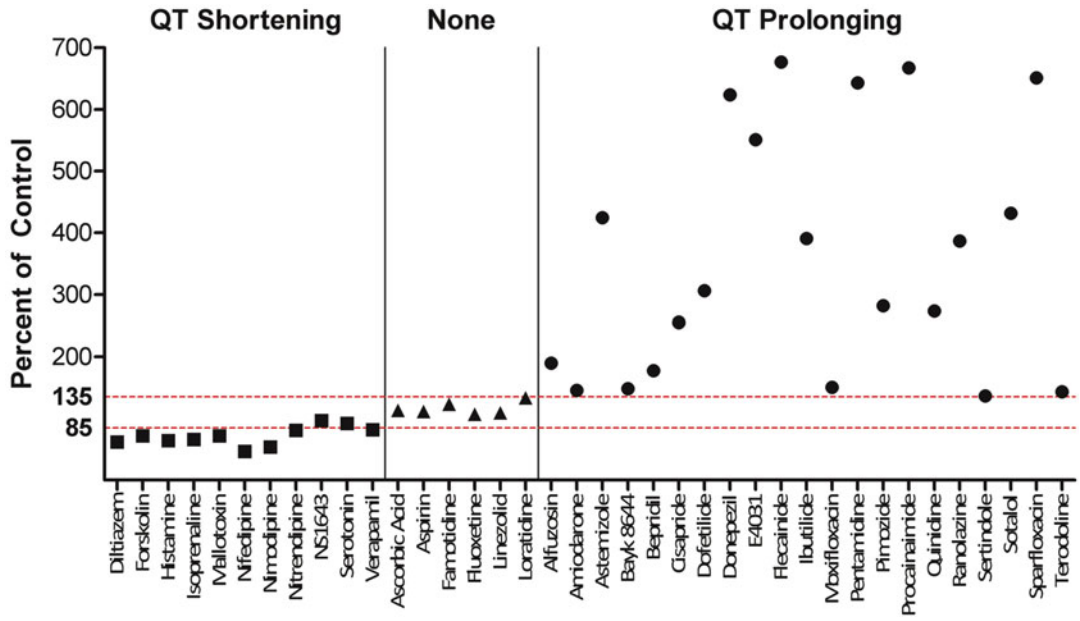

Fig. 6 Greatest effect on calcium transient duration CTD75 caused by test compounds. Maximum transient shortening is presented for compounds which were expected to cause a QT shortening effect (none caused prolongation beyond the 135 % threshold), and maximum transient prolongation is presented for compounds expected to cause no effect or a prolonging effect on the QT interval

Regarding compounds expected to shorten the QT interval, we did not observe significant shortening of calcium transient duration by serotonin. Our expectation that serotonin would reduce transient duration was based upon its positive chronotropic

and ionotropic effects on atrial preparations [15, 16], and its ability to shorten the duration of the calcium transients of isolated human atrial cardiomyocytes, effects which have been linked to increased cAMP [16]. However, serotonin has minimal effects on human ventricular myocardium unless inhibitors of phosphodiesterase are added to prevent breakdown of cAMP [17]. In our study, phosphodiesterase inhibitors were not used, and the hSC-CMs were predominantly ventricular in phenotype, perhaps accounting for the lack of effect of this agent.

Regarding NS1643, this compound is a hERG channel "activator," that increases potassium current through the hERG channel to increase repolarization, thus reducing action potential duration in cell models in which the hERG channel is expressed in non-cardiac myocytes, or in ventricular cardiac myocytes prepared from a variety of mammalian species [18–22]. In this study, NS1643 did not reduce the duration of the calcium transient in the hSC-CMs from Axiogenesis, but relatively high concentrations (≥25 μM) inhibited spontaneous contractile activity, perhaps relating to the ability of this compound to prolong the post-repolarization refractory period [18]. In previous work, NS1643 did reduce calcium transient duration in hSC-CMs from Cellular Dynamics International [7]. Resolving the discrepancy between the results obtained with hSC-CMs from the two suppliers will require further research. To our knowledge, no other data has been published representing the effect of this compound on human cardiac myocytes or heart tissue.

Overall, the assay was highly predictive, predicting the effects of the compounds on the ECG QT interval with 100% specificity and 94% sensitivity. This high diagnostic accuracy surpasses results reported in whole non-rodent in vivo models (specificity 80–100%, sensitivity 33–91%) [23–25] and in recombinant hERG channel screening (specificity 75–88%, sensitivity 64–82%) [25, 26], as well as results in hSC-CM assays using other methods [27]. The results obtained with verapamil are notable, as this compound is clinically safe, despite its hERG-blocking ability, but the L-channel-blocking activity of this compound has a compensatory effect leading to mild effects on the QT interval [28]; thus, while a recombinant hERG channel assay might predict that verapamil would be cardiotoxic, the KIC data are more in-line with the clinical observations.

These results are consistent with the performance of similar assays conducted using KIC with iCell Cardiomyocytes from Cellular Dynamics International [6, 7, 10]. For example, 98% specificity and 80% sensitivity were recently achieved for a panel of 90 compounds [10]. Thus, repeated across time, and with the hSC-CMs from two different suppliers derived from different human donors, these assays have proven to maintain low variability among controls and reference compounds, and demonstrate high reproducibility and fidelity to clinically active compound

concentrations. These findings should not be surprising, considering that phenotypic assays have been shown to be more successful in predicting clinical effects than single target approaches [29].

6 Conclusion

Drug arrhythmogenic liability remains a key safety concern for the pharmaceutical industry. The emergence of hSC-CMs provides scalable human cardiomyocyte models, which allow researchers to assess compound effects across multiple ion channels and signaling pathways simultaneously. The KIC™ assay for arrhythmogenic liability (Vala Sciences, San Diego, CA, USA) uses intracellular calcium transients as an integrated signal to provide a high-throughput cell-by-cell readout of compound effects in order to stratify compounds by arrhythmogenic potential early in the drug development process. Compound effects on the calcium transient or action potential duration, as well as proarrhythmia signals such as early after depolarization (EADs) and irregular rhythms, may be reliably detected with the assistance of automated analysis and high-throughput KIC. By analyzing the alterations in the calcium transients of human iPSC-derived cardiomyocytes, this method provides a kinetic phenotypic assay that can be used to survey for effects across the full complement of ion channels acting in concert.

A potential limitation of the KIC methods used in the present study is that it may be relatively insensitive to inhibitory effects of compounds on the sodium channel during the upstroke ("phase 0") of the action potential due to use of 30 fps image acquisition, which is not fast enough to fully resolve the upstroke, and the use of Fluo-4 to measure calcium, instead of directly monitoring the voltage-transient. To address this limitation additional KIC methods are in development featuring fluorescent voltage-indicators (e.g., FluoVolt™) and increased rates of image acquisition (up to 1500 fps).

The data from this study, and from our previous work [6, 7, 10], demonstrate that KIC of hSC-CMs is likely the most predictive in vitro assay currently available for assessing the potential for chemical compounds to cause human arrhythmias. Notably, KIC, used in conjunction with a variety of cardiac cell models, is also proving suitable for exploring therapeutic strategies relevant to heart failure [30, 31].

Acknowledgements

We would like to gratefully acknowledge Axiogenesis for contribution of the hES-CMs used in this study. Development of KIC instrumentation and methods and CyteSeer™ has been supported by

several grants including the following: NIH/NHLBI FastTrack STTR R42HL086076 "Live cell and HCS assays to quantify production of cardiomyocytes from stem cells"; CIRM RT1-01143 "Optimization in the Identification, Selection and Induction of Maturation of Subtypes of Cardiomyocytes derived from Human Embryonic Stem Cells"; and NIH/NHLBI STTR R42HL112521 "Optogenetic Multiparametric Assay for HT Cardiotoxicity Testing."

References

1. Stockbridge N, Morganroth J, Shah RR, Garnett C (2013) Dealing with global safety issues: was the response to QT-liability of non-cardiac drugs well coordinated? Drug Saf 36:167–182
2. FDA (2005) S7B nonclinical evaluation of the potential for delayed ventricular repolarization (QT interval prolongation) by Human Pharmaceuticals. Guidance for Industry: U.S. Department of Health and Human Services, Food and Drug Administration
3. Magyar J, Rusznak Z, Harasztosi C, Kortvely A, Pacher P et al (2003) Differential effects of fluoxetine enantiomers in mammalian neural and cardiac tissues. Int J Mol Med 11:535–542
4. Matsuoka S, Nawada T, Hisatome I, Miyamoto J, Hasegawa J et al (1991) Comparison of Ca2+ channel inhibitory effects of cibenzoline with verapamil on guinea-pig heart. Gen Pharmacol 22:87–91
5. Zahradnik I, Minarovic I, Zahradnikova A (2008) Inhibition of the cardiac L-type calcium channel current by antidepressant drugs. J Pharmacol Exp Ther 324:977–984
6. Cerignoli F, Charlot D, Whittaker R, Ingermanson R, Gehalot P et al (2012) High throughput measurement of Ca(2)(+) dynamics for drug risk assessment in human stem cell-derived cardiomyocytes by kinetic image cytometry. J Pharmacol Toxicol Methods 66:246–256
7. Lu HR, Whittaker R, Price JH, Vega R, Pfeiffer ER et al (2015) High throughput measurement of Ca++ dynamics in human stem cell-derived cardiomyocytes by kinetic image cytometry: a cardiac risk assessment characterization using a large panel of cardioactive and inactive compounds. Toxicol Sci 148:503–516
8. Ma J, Guo L, Fiene SJ, Anson BD, Thomson JA et al (2011) High purity human-induced pluripotent stem cell-derived cardiomyocytes: electrophysiological properties of action potentials and ionic currents. Am J Physiol Heart Circ Physiol 301:H2006–H2017
9. Peng S, Lacerda AE, Kirsch GE, Brown AM, Bruening-Wright A (2010) The action potential and comparative pharmacology of stem cell-derived human cardiomyocytes. J Pharmacol Toxicol Methods 61:277–286
10. Pfeiffer ER, Vega R, McDonough PM, Price JH, Whittaker R (2016) Specific prediction of clinical QT prolongation by kinetic image cytometry in human stem cell derived cardiomyocytes. J Pharmacol Toxicol Methods 81:263–273
11. Bers DM (2002) Cardiac excitation-contraction coupling. Nature 415:198–205
12. Bers DM (2008) Calcium cycling and signaling in cardiac myocytes. Annu Rev Physiol 70:23–49
13. McDonough PM, Agustin RM, Ingermanson RS, Loy PA, Buehrer BM et al (2009) Quantification of lipid droplets and associated proteins in cellular models of obesity via high-content/high-throughput microscopy and automated image analysis. Assay Drug Dev Technol 7:440–460
14. Uesugi M, Ojima A, Taniguchi T, Miyamoto N, Sawada K (2014) Low-density plating is sufficient to induce cardiac hypertrophy and electrical remodeling in highly purified human iPS cell-derived cardiomyocytes. J Pharmacol Toxicol Methods 69:177–188
15. Gergs U, Bockler A, Ebelt H, Hauptmann S, Keller N et al (2013) Human 5-HT(4)receptor stimulation in atria of transgenic mice. Naunyn Schmiedebergs Arch Pharmacol 386:357–367
16. Christ T, Rozmaritsa N, Engel A, Berk E, Knaut M et al (2014) Arrhythmias, elicited by catecholamines and serotonin, vanish in human chronic atrial fibrillation. Proc Natl Acad Sci U S A 111:11193–11198
17. Kaumann AJ, Levy FO (2006) 5-hydroxytryptamine receptors in the human cardiovascular system. Pharmacol Ther 111:674–706
18. Hansen RS, Diness TG, Christ T, Demnitz J, Ravens U et al (2006) Activation of human

ether-a-go-go-related gene potassium channels by the diphenylurea 1,3-Bis-(2-hydroxy-5-trifluoromethyl-phenyl)-urea (NS1643). Mol Pharmacol 69:266–277

19. Diness TG, Yeh YH, Qi XY, Chartier D, Tsuji Y et al (2008) Antiarrhythmic properties of a rapid delayed-rectifier current activator in rabbit models of acquired long QT syndrome. Cardiovasc Res 79:61–69
20. Szabo G, Farkas V, Grunnet M, Mohacsi A, Nanasi PP (2011) Enhanced repolarization capacity: new potential antiarrhythmic strategy based on HERG channel activation. Curr Med Chem 18:3607–3621
21. Guo J, Cheng YM, Lees-Miller JP, Perissinotti LL, Claydon TW et al (2015) NS1643 interacts around L529 of hERG to alter voltage sensor movement on the path to activation. Biophys J 108:1400–1413
22. Perissinotti LL, Guo J, De Biase PM, Clancy CE, Duff HJ et al (2015) Kinetic model for NS1643 drug activation of WT and L529I variants of Kv11.1 (hERG1) potassium channel. Biophys J 108:1414–1424
23. Vargas HM, Bass AS, Koerner J, Matis-Mitchell S, Pugsley MK et al (2015) Evaluation of drug-induced QT interval prolongation in animal and human studies: a literature review of concordance. Br J Pharmacol 172:4002–4011
24. Morissette P, Nishida M, Trepakova E, Imredy J, Lagrutta A et al (2013) The anesthetized guinea pig: an effective early cardiovascular derisking and lead optimization model. J Pharmacol Toxicol Methods 68:137–149
25. Wallis RM (2010) Integrated risk assessment and predictive value to humans of non-clinical repolarization assays. Br J Pharmacol 159:115–121
26. Gintant G (2011) An evaluation of hERG current assay performance: translating preclinical safety studies to clinical QT prolongation. Pharmacol Ther 129:109–119
27. Sirenko O, Cromwell EF, Crittenden C, Wignall JA, Wright FA et al (2013) Assessment of beating parameters in human induced pluripotent stem cells enables quantitative in vitro screening for cardiotoxicity. Toxicol Appl Pharmacol 273:500–507
28. Johannesen L, Vicente J, Mason JW, Sanabria C, Waite-Labott K et al (2014) Differentiating drug-induced multichannel block on the electrocardiogram: randomized study of dofetilide, quinidine, ranolazine, and verapamil. Clin Pharmacol Ther 96:549–558
29. Swinney DC, Anthony J (2011) How were new medicines discovered? Nat Rev Drug Discov 10:507–519
30. Wahlquist C, Jeong D, Rojas-Munoz A, Kho C, Lee A et al (2014) Inhibition of miR-25 improves cardiac contractility in the failing heart. Nature 508:531–535
31. Wei K, Serpooshan V, Hurtado C, Diez-Cunado M, Zhao M et al (2015) Epicardial FSTL1 reconstitution regenerates the adult mammalian heart. Nature 525:479–485

Chapter 9

Decoding Ca^{2+} Signals as a Non-electrophysiological Method for Assessing Drug Toxicity in Stem Cell-Derived Cardiomyocytes

Christopher H. George and David H. Edwards

Abstract

We describe a new method to profile the Ca^{2+} signalling fingerprint of stem cell-derived cardiomyocytes (CMs) under drug-naïve and drug-exposed conditions. This method, termed SALVO, takes into account (1) the quantification of very low-amplitude Ca^{2+} fluxes that occur *between* large Ca^{2+} spikes that, in the absence of any effect on Ca^{2+} spikes per se, may have a profound impact on cell phenotype and (2) the statistical assessment of the variability in the amplitude and temporal components of Ca^{2+} spike trains. In a previous study, SALVO identified the potential cardiovascular (CV) risk of drugs that had no measurable impact on cellular electrophysiological profile and also yielded a toxicity score that exhibited a better correlation with human QT prolongation liabilities than other conventional electrophysiological readouts.

This chapter sets out a step-by-step protocol for establishing phenotypically consistent CM populations and our method for performing the Ca^{2+} signalling analysis in which the output data are reconciled with phenotypic end points (e.g. cytotoxicity and susceptibility to apoptosis). We present a worked example using two drugs that disrupt Ca^{2+} signalling via different mechanisms; drug A causes the cessation of spontaneous Ca^{2+} oscillation via progressive attenuation in Ca^{2+} spike amplitude, whereas drug B elicits different periodic behaviours. Both drugs have comparable effects on the frequency of Ca^{2+} spikes, but SALVO analysis discriminates their actions. An extensive set of notes is included that will help the reader reproduce our methods with high fidelity.

Key words Ca^{2+}, Signalling, Cardiovascular, Stem cells, Cardiomyocytes, Imaging, Drug toxicity, Screening

1 Introduction

Cardiovascular (CV) drug development needs have led to enhanced screening systems to improve early-stage assessments of potential hazard [1, 2]. The widespread adoption of human stem cell-derived cardiomyocytes (CMs)—a term encompassing both embryonic stem cell-derived CM (ES-CM) and induced pluripotent stem cell-derived CMs (iPSC-CMs)—into the drug screening toolkit goes some way to recreating the cell-to-cell interactions

Mike Clements and Liz Roquemore (eds.), *Stem Cell-Derived Models in Toxicology*, Methods in Pharmacology and Toxicology,
DOI 10.1007/978-1-4939-6661-5_9,

that modulate the behaviour of individual CM in vivo and addresses many of the problems associated with non-human cell-based assays [1, 3–5]. However, these cells will only become a truly useful resource in the drug screening landscape if they are harnessed to new methodologies that move beyond conventional electrophysiological (EP) assessments that sometimes fail to adequately assess the potential hazards of drugs in the clinical setting [1, 2, 6, 7]. In one notorious example, EP measurements during FDA-mandated screening appeared not to identify the CV risk associated with rofecoxib (Vioxx™), a drug that was withdrawn because of unacceptable CV hazard [8] and subject to a $5.8 billion dollar lawsuit [9]. The comprehensive in vitro proarrhythmia assay (CIPA) initiative aims to address these issues [10–12].

We have tackled the problem from a different perspective that complements and extends the current armoury of electrophysiology-based methods. Calcium (Ca^{2+}) signals modulate almost every biological process [13–15], and the normal synchronisation of Ca^{2+} signalling within and between cells in a population is collectively determined by multiple coupled oscillators acting across multiple scales [15–22]. Given the intricacies of these processes, it is perhaps not surprising that disrupted Ca^{2+} signalling is a good index of phenotypic deterioration and drug-induced cytotoxicity in CM [6, 23]. Consequently, the detailed assessment of spatiotemporal organisation of Ca^{2+} signals under normal and drug-exposed conditions is valuable. Although methods do exist for investigating complex phenomena in Ca^{2+} signalling data [17, 24, 25], these tend to focus on very specific aspects of cell behaviour rather than provide a 'holistic' evaluation of the patterns of cellular Ca^{2+} signals.

Our approach is to profile the Ca^{2+} signalling fingerprint of CM under drug-naïve and drug-exposed conditions [18, 26, 27]. This in itself is not especially new because assessments of the characteristics of super-threshold Ca^{2+} signals (e.g. the frequency and amplitude of large Ca^{2+} 'transients' or 'spikes') are commonly employed. However, the novelty of our approach comes from (1) the quantification of very low-amplitude Ca^{2+} fluxes that occur *between* these Ca^{2+} spikes that in the absence of any effect on Ca^{2+} spikes per se may have a profound impact on cell phenotype (e.g. susceptibility to cell death) [15, 28–30] and (2) the statistical determination of the variability in the amplitude and temporal components of Ca^{2+} spike events. In order to integrate the analysis of Ca^{2+} spikes with the information that is encoded by signals occurring *between* these spike events (i.e. in inter-spike intervals), we developed SALVO (an acronym of **s**ynchronisation, **a**mplitude, **l**ength and **v**ariability of **o**scillation), a software program that enables the detailed quantification of the spatiotemporal patterning of Ca^{2+} signals in CM [31].

In a proof-of-concept study using a small panel of drugs, this approach accurately identified those drugs with established

pro-arrhythmogenic liability [23] and confirmed that disrupted cellular Ca^{2+} signalling in vitro is a hallmark feature of drugs with known CV risk in humans. Importantly, this study also validated the use of SALVO to (1) identify the potential CV risk of valdecoxib, an analog of rofecoxib (Vioxx™) and a drug which had no measureable impact on cellular EP profile, and (2) generate drug toxicity scores that exhibit better correlation with QT prolongation liabilities in humans than other conventional electrophysiological readouts (e.g. cardiac action potential duration (APD_{90}) or measurements of cellular impedance) [7, 32–34].

This chapter sets out our protocols for establishing phenotypically consistent CM populations and the systematised approach we take to performing drug toxicity assessments utilising a detailed SALVO-based analysis of super- and subthreshold cellular Ca^{2+} signals. We also include an extensive set of notes ('tips and tricks') that will enable the reader to reproduce our methods with high fidelity.

2 Materials

2.1 Cardiomyocytes

The protocols described in this chapter relate specifically to post-differentiated CM from human ESC and IPS; methods for these differentiation processes have been described previously (e.g. [35–38]). Typically, these protocols do not yield CM exclusively. For example, H7 stem cell-derived Cytiva™ (GE Healthcare), which are produced via a monolayer differentiation protocol adapted from Xu et al. [35], are supplied as a heterogeneous cell population in which CM accounts for approximately half of the cells, whilst fibroblasts and other non-CM cell types comprise the remainder [23]. In our experience, the proportion of cardiac troponin-T (cTnT)-positive CM remains constant in culture, suggesting a stable population of differentiated CMs and the absence of proliferative or differentiation-competent non-CM cells (Fig. 1b). Acknowledging this issue, in this chapter we use the term CM to refer to all cells in stem cell-derived populations (**Note 1**).

Matrigel (Corning) is diluted 1:1 (v/v) in KnockOut DMEM (KO-DMEM, Thermo Fisher Scientific) and is snap frozen on dry ice prior to storage at –80 °C. This solution is further diluted to 1:30 (v/v) in ice-cold KO-DMEM immediately prior to use. We have found that other adhesion matrices (e.g. fibronectin or laminin), presumably because of different adhesion capacities, tend to inhibit axial realignment of CMs on the culture surface (Fig. 1B, C) (**Note 2**).

2.2 Silicon Gaskets

Reusable silicon gaskets (diameter 0.3 mm and depth 1 mm, CultureWell™ MultiWell inserts [Grace Bio-Labs]) are purchased in 10×5 configurations and then cut into 2×2 squares (9.5×9.5 mm) with a razor blade (Fig. 1a).

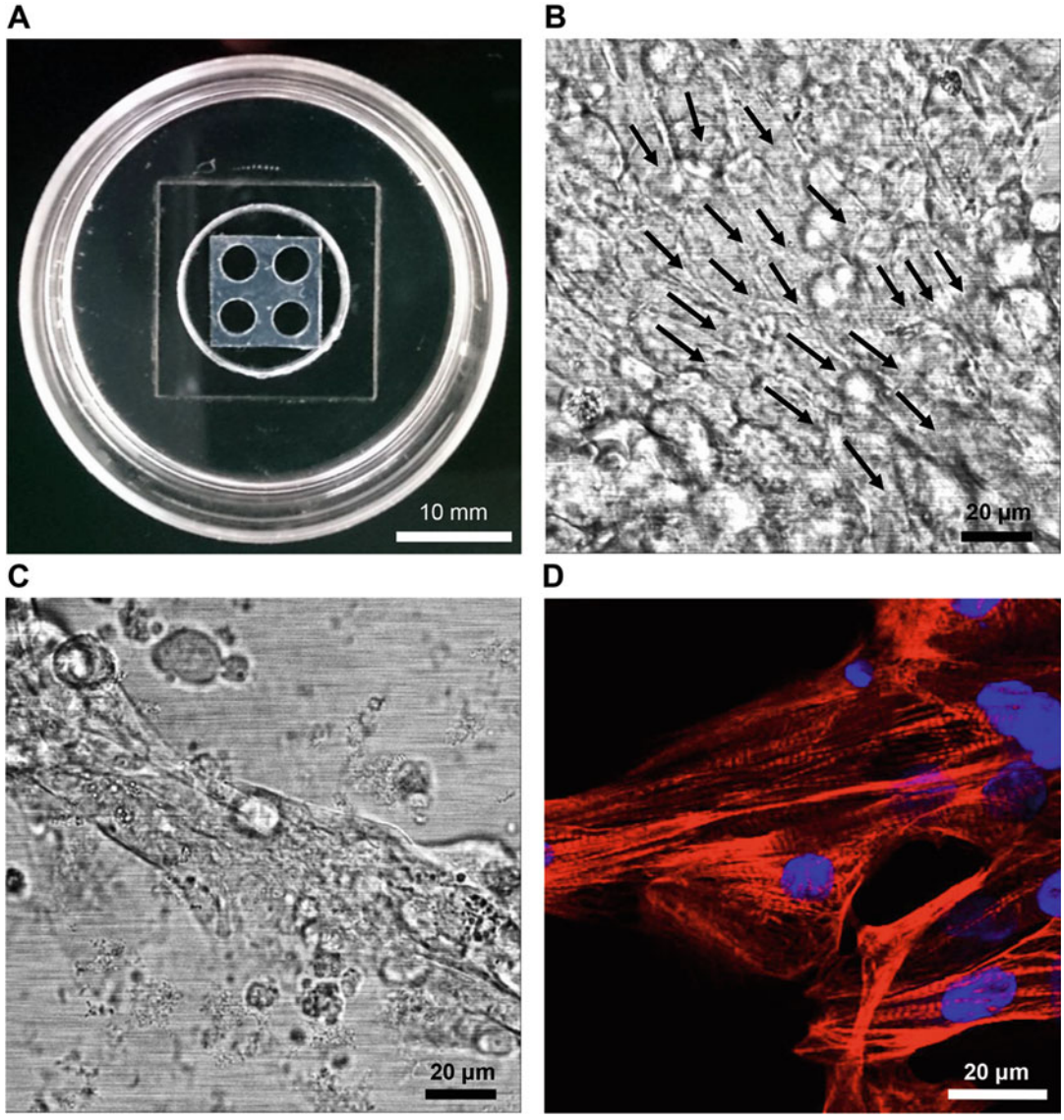

Fig. 1 CM plating and formation of syncytia. (**a**) A silicon gasket, containing four wells each with a surface area each of 7 mm^2, on a glass-bottomed chamber. (**b**) CM between days 4 and 7 post-plating should be confluent and exhibit clear directional alignment (*arrows*). (**c**) In some instances, CMs form highly tensile 'strings' that contract in a unidirectional manner. (**d**) CM alignment is associated with cTnT striation (*red*). Nuclei are counterstained with DAPI (*blue*). From Lewis et al. [23]

2.3 Solutions, Buffers and Media

2.3.1 RPMI Medium

Contains 1× serum-free B27 supplement [39, 40]. The concentration of free Ca^{2+} ($[Ca^{2+}]$), from the dissociation of calcium nitrate, $Ca(NO_3)_2$, is approximately 0.4 mM (**Note 3**). RPMI/B27 is stored at 4 °C for up to 2 weeks and is always prewarmed to 37 °C prior to addition to cells (**Note 4**). The formulation of RPMI is available at the link provided in [41].

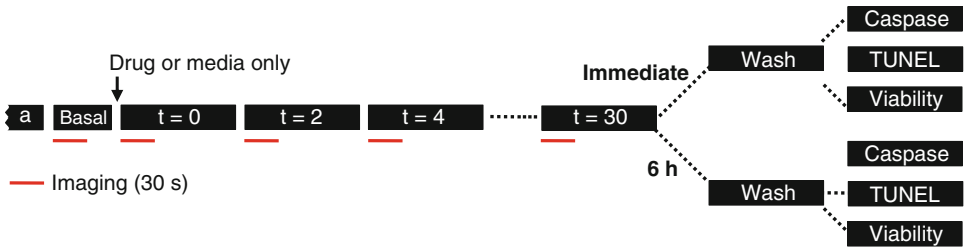

Fig. 2 Experimental protocol. In the initial step (**a**), CMs are transferred to 1.9 ml of prewarmed KRH or Leibovitz L-15 for 20 min prior to imaging baseline Ca^{2+} signals ('Basal', 30 s) (**Notes 19** and **20**). Stock solutions of all drugs in either KRH or Leibovitz L-15 are added to the chamber in a bolus (100 µl; i.e. a 1:20 (v/v) dilution in the chamber) (**Note 29**). For the 6 h incubation after imaging at $t = 30$ min, CMs are transferred to RPMI with or without B27 and with or without the drug under test (**Notes 26** and **27**)

2.3.2 Leibovitz L-15 Medium

This medium is buffered by base amino acids and phosphate, rather than sodium bicarbonate, having been formulated to maintain pH 7.4 in non-CO_2 environments. Free [Ca^{2+}] is approximately 1.3 mM. We find that Leibovitz L-15 provides a better means of maintaining pH levels throughout the protocol (Fig. 2) than the use of a bicarbonate-buffered medium (e.g. RPMI) in conjunction with 5% CO_2 delivered via environmental control of the microscope chamber. To avoid attenuating the fluorescent signal intensity from the Ca^{2+} dye, we use the formulation without phenol red. The full formulation of this medium is available via the link provided in [42]

2.3.3 Krebs-Ringer-HEPES (KRH)-Buffered Solution

We sometimes use this solution for Ca^{2+} imaging; it contains (in mM) NaCl (120), HEPES (25), KCl (4.8), $CaCl_2$ (1.3), KH_2PO_4 (1.2), $MgSO_4$ (1.2) and glucose (5.5) with pH adjusted to 7.4.

2.4 Equipment for Ca^{2+} Imaging

We routinely use a Leica 6000 DMRBE microscope fitted with a resonant-scanning confocal microscope (SP5, Leica Microsystems) that limits photobleaching during relatively prolonged imaging cycles (**Note 5**). We have also validated the method using low-level excitation illumination on a camera-based imaging system (e.g. Hamamatsu Orca attached to a Zeiss Axiovert microscope) and, over shorter imaging periods, on a high-content screening platform (IN Cell Analyzer 2200, GE Healthcare).

3 Methods

3.1 Recovery from Freezing and Plating

For the majority of users, post-differentiated CM will be obtained from commercial suppliers or via collaboration and will be frozen in medium containing a cryoprotectant (e.g. DMSO). This subsection describes our protocols for minimising the variability of the resultant CM on thawing and plating.

1. Silicon gaskets (2 × 2 wells) are sterilised by autoclaving, wetted in 70% (v/v) ethanol and pressed to a 14 mm diameter glass-bottomed coverslip in individual plastic chambers (Cellvis)

(Fig. 1a) (**Note 6**). Chambers strongly adhere to the glass via evaporation and are left to dry completely for 1 h at RT. When completely dry, chambers are chilled at –20 °C for 1 h and then prechilled Matrigel/KO-DMEM solution (1:30 (v/v)) is added to each well of the gasket (15 μl) such that it typically forms a domed meniscus. A 'pocket' of KO-DMEM (250 μl) is pipetted at the periphery of each chamber to preserve the relative humidity of the chamber and prevent evaporation of the Matrigel solution from the gasket. Chambers are stored for 12–15 h at 4 °C until use (step 4). After this time, the Matrigel should have formed a homogeneously dispersed phase across the glass surface which is clearly visible under a light microscope.

2. Cryovials containing CM in a medium/DMSO cryoprotectant are transferred from storage (typically in the vapour phase of liquid N_2) to dry ice for 2–3 min (**Note 7**) before being brought up to 37 °C using a hotblock or water bath.
3. During step 2 and immediately as the last ice crystals disappear, CMs in the freezing solution are taken up into 5 ml syringe fitted with a wide-bore filling tube already containing 2 ml of prewarmed RPMI/B27 (**Note 8**). The resulting cell suspension, in which no attempt is made to mix the DMSO-containing freezing solution with the RPMI/B27 in the syringe, is carefully layered at the bottom of a prewarmed 15 ml conical-bottomed centrifuge tube (**Note 9**). Prewarmed RPMI/B27 (8 ml) is added to the suspension dropwise over the course of 3 min (**Note 10**). The cell suspension is centrifuged at 400 × g for 4 min, and the supernatant containing non-intact cells/ruptured membranes is removed (**Note 9**). Cells are gently resuspended in RPMI/B27 (3–5 ml).
4. A small amount of this CM suspension (≈50 μl) is removed, mixed with an equal volume of Trypan Blue solution and incubated at RT for 1 min. This CM/Trypan Blue solution is applied to the counting chamber of a haemocytometer, and the number of viable cells (i.e. those that are not stained blue) is determined (**Note 11**). The efficiency of plating (i.e. the proportion of viable cells that will adhere to the culture surface and exhibit functional competency post-plating) must also be taken into account. We empirically determine the plating efficiency on a batch-to-batch basis; the protocol described here assumes a typical plating efficiency of approximately 60–70 %. Following an assessment of viability, the CM suspension is subsequently recentrifuged (400 × g, 4 min) and the supernatant is decanted. The resulting pellet is resuspended very gently using a 1000 μl pipette tip to a density of 1000 viable cells per μl (corrected for plating efficiency) in prewarmed RPMI/B27.
5. Matrigel-treated glass surfaces from step 1 are warmed to 37 °C for 1 h in advance of CM plating, and the Matrigel solution is removed from the gaskets < 1 min prior to seeding

(**Note 12**). We have empirically determined the optimal seeding density as 2500 viable CM per mm^2 (adjusted for plating efficiency) (**Note 13**). From the cell suspension in step 4, 15 μl (15,000 CM) is seeded in a single well of the silicon gasket (7 mm^2 surface area) (**Note 14**), and the KO-DMEM 'pocket' from step 1, which should still be present, is retained. Chambers are transferred to 37 °C in a humidified 5 % CO_2 environment. CMs are allowed to adhere to the coverslip for 2 h before prewarmed RPMI/B27 is added (2 ml) (**Note 15**). RPMI/B27 medium is exchanged every 48 h, and cells are allowed to mature 'on plate' for 4–7 days, at which time the CM will exhibit well-ordered spontaneous Ca^{2+} oscillations (**Note 16**).

3.2 Ca^{2+} Imaging

1. The excitation and emission profiles, signal-to-noise characteristics, kinetics and Ca^{2+}-binding affinity of Fluo-4 [43] make it our fluorescent Ca^{2+} indicator dye of choice for these studies (**Note 17**). Cells are incubated under a small volume (100 μl) of RPMI/B27 containing Fluo-4 AM (5 μM, Molecular Probes) diluted from a freshly prepared stock (1 mM dissolved in DMSO) for 30 min at 37 °C in a humidified 5 % CO_2 environment. These conditions result in homogeneous loading of cell cytoplasm and nuclei, but not the intracellular organelles (**Note 18**).
2. Ca^{2+} dye-loaded CMs are transferred to KRH solution or Leibovitz medium (1.9 ml, i.e. to a final volume of 2 ml) (**Notes 19** and **20**). CMs are allowed to equilibrate in KRH or Leibovitz L-15 for 20 min at 37 °C prior to Ca^{2+} imaging (Fig. 2). Regions of a single CM-containing well of the silicon gasket are selected at random, and imaging is performed using resonant-scanning confocal microscopy (e.g. SP5, Leica Microsystems) or a camera-based system (e.g. ORCA-Flash 4.0, Hamamatsu). All Ca^{2+} imaging is performed using a standardised protocol (Fig. 2) that aims to reduce inter-experimental variability—using 63× or 20× objectives with images acquired at 512×512 or 1024×1024 pixels, respectively (**Notes 21**, **22**, **23**, **28**).

3.3 Determination of Cell Viability and Apoptosis

Immediately following imaging CM viability, cytotoxicity and the extent of apoptosis are determined using Promega's ApoTox-Glo Triplex Assay according to the manufacturer's instructions. Following the ApoTox-Glo Triplex Assay, we also visualise apoptotic nuclei in the same populations using a terminal deoxynucleotidyl transferase dUTP nick end labelling (TUNEL) method according to the manufacturer's instructions (DeadEnd, Promega) (**Note 24**).

We also investigate latent toxicity, which we define as a measureable decrease in cell viability over a longer period of time, in the absence of any increase in cytotoxicity over the standard 30 min imaging protocol (**Note 25**). In parallel experiments, CMs are subject to medium exchange and are incubated for a further 6 h in

RPMI with or without B27 supplement and with or without drug (**Notes 26** and **27**) (Fig. 2).

3.4 Data Extraction and Processing

Numeric data are extracted from an image series using Leica's image acquisition software (Leica LAS AF) or Fiji image analysis tools [44]. We employ two methods for extracting data. For imaging using a 63× objective, we assign regions of interest (ROIs, 50 μm^2) where each ROI corresponds to a single CM within the population (Fig. 4). We usually assign up to 20 ROIs per field of view (FOV). For Ca^{2+} imaging confluent populations using a 20× objective, we use a regional analysis approach based on dividing the FOV into grids (16, 25, 49, etc.) [6] (Fig. 4) (**Note 28**).

SALVO, a Python-based computer program, is used to profile the amplitude and temporal organisation of Ca^{2+} signalling [23, 31]. Ca^{2+} spike signal maxima and minima and inter-spike periods are detected using SALVO's auto-detection algorithms (based on spline detect or threshold detection methods) or by manual assignation of the start, peak and end of each Ca^{2+} spike. SALVO outputs are archived and mined using a linked SQL-based database system (DBMiner).

We cannot cover all aspects of SALVO functionality (e.g. statistical analysis of parametric variation) in this chapter; more detailed information can be obtained from the corresponding author (CG). For the purposes of this chapter, we focus on a nine-parameter description of Ca^{2+} signalling which is given in Fig. 3b, c. A brief explanation of each of the terms:

- Five of these selected outputs parameterise the Ca^{2+} spikes: *frequency, amplitude, duration, area,* and *rate of decay.*
- *Inter-transient noise (ITN)* is a novel descriptor of very low-amplitude Ca^{2+} fluxes during inter-spike periods and is the cumulative signal variability (SV) in a given trace. The calculation of the SV is described in detail elsewhere [23, 45].
- *Temporal heterogeneity index (THI)* and *amplitude heterogeneity index (AHI)* are statistical measurements of the variability in the duration of inter-spike intervals and Ca^{2+} spike signal intensity maxima, respectively. THI and AHI will be zero in trains of Ca^{2+} spikes in which the amplitude and temporal regimentation of sequential Ca^{2+} spikes are perfect and will increase as the Ca^{2+} spikes become more disordered [23].
- *Synchronisation* is the calculation of the extent of intercellular Ca^{2+} spike synchronisation (Fig. 3c).

The data extraction and analytical processes are schematised in Fig. 4. Multiparametric SALVO outputs are amenable to incorporation into a single toxicity score (e.g. Fig. 5 in [23]) or may be subjected to hierarchical cluster analysis (HCA) to discriminate drug-induced effects (e.g. Fig. 6 in [23]), but we do not cover these downstream applications in this chapter.

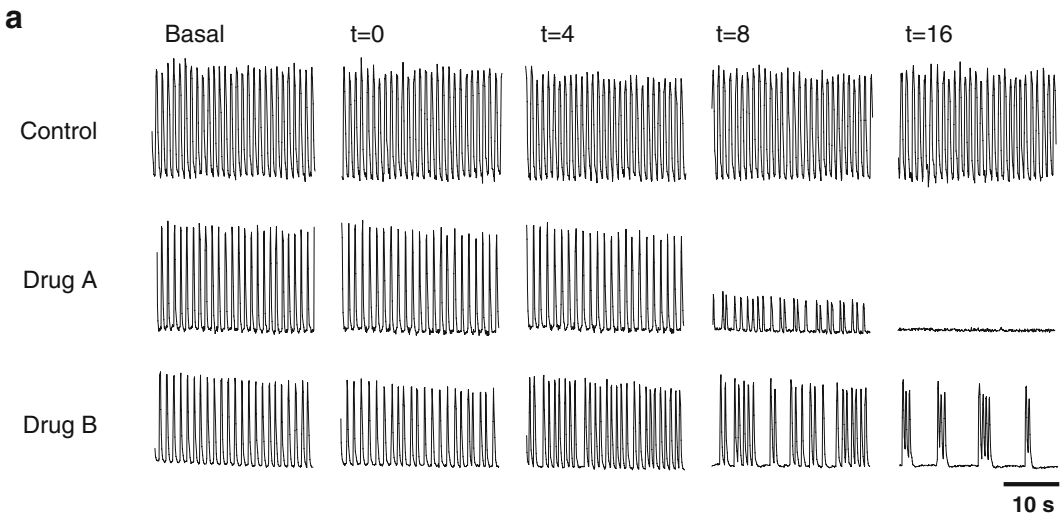

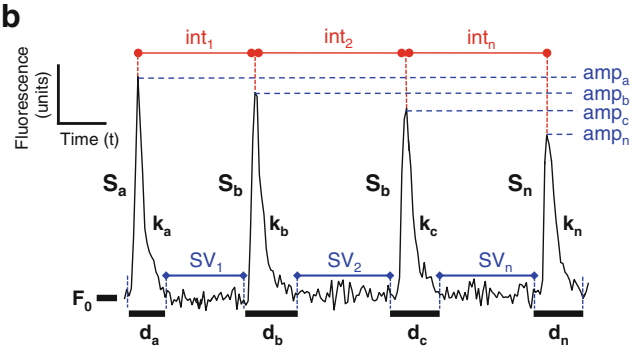

Frequency	= S s^{-1}
Amplitude*	= $(amp_n\text{-}F_0)$ /F_0
Duration	= $(d_a+ d_b+ d_c+ d_n)$ /n
Inter-transient noise (ITN)	= $\Sigma(SV_1....SV_n)$
Area*	= Area under curve / F_0
Rate of decay	= $(k_a+ k_b+ k_c+ k_n)$ /n
Temporal heterogeneity index (THI)	= $\sigma(int_1....int_n)$
Amplitude heterogeneity index (AHI)	= $\sigma(amp_a....amp_n)$
Synchronization	= Coincidence $(S_a.....S_n)$

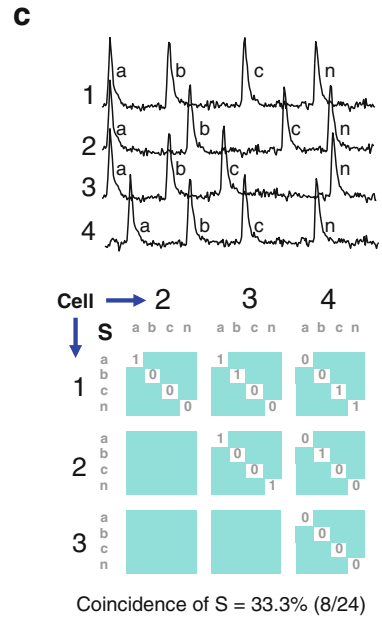

Fig. 3 Quantifying different modes of Ca^{2+} signalling perturbation. (**a**) Ca^{2+} oscillations in single CM under basal (drug-naïve) conditions and following the addition of media only (control) or drugs A and B as per the protocol described in Fig. 2. Ca^{2+} signals immediately following control or drug addition ($t=0$) and subsequently at 4, 8 and 16 min are shown. These data are analysed in Fig. 4. (**b**) The deconstruction of Ca^{2+} spikes, and inter-spike intervals, into eight parameters that describe intracellular Ca^{2+} signalling. *, These descriptors involve the calculation of data for individual spikes which are then averaged across the Ca^{2+} spike train. Adapted from Lewis et al. [23] (**c**) The extent of intercellular synchronisation is calculated using a matrix which quantifies the temporal coincidence of Ca^{2+} spikes across CM. In the given example, using four CMs (1–4) with four Ca^{2+} spikes in each CM (a, b, c, n), the intercellular synchronisation is 33.3 %. Reproduced with permission from Lewis et al. [23]

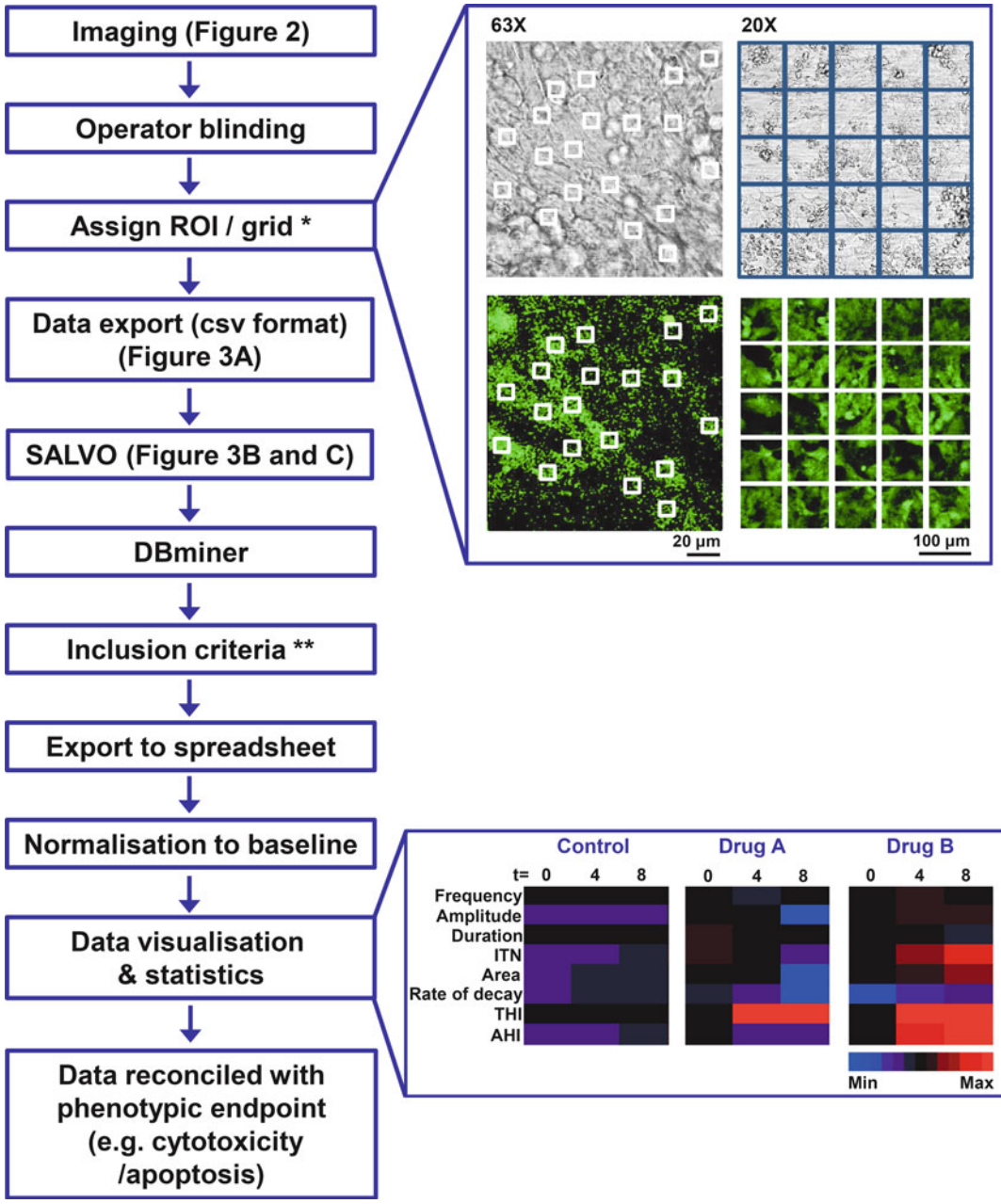

Fig. 4 Scheme for data processing and visualisation. * **Notes 28** and **30**. ** **Note 31**. The upper panel shows typical FOVs obtained from bright-field (*top*) or Fluo-4-dependent fluorescence (*bottom*) imaging of CM using 63× or 20× objectives. For those images acquired using a 63× objective, the white boxes represent 50 μm^2 ROI, whereas for images obtained using a 20× objective, the FOV is divided into grids (*see* **Note 28**). The lower panel shows the visualisation of SALVO analysis corresponding to the Ca^{2+} oscillation traces shown in Fig. 3a. Since these traces are from single cells, the extent of intercellular synchronisation is not given. The absence of Ca^{2+} spikes at $t=16$ with drug A (Fig. 3a) precludes SALVO analysis, so only data from $t=0$, 4 and 8 are shown (**Note 32**)

In the given example, both drugs A and B produced marked disruption of Ca^{2+} signalling, but the modes of perturbation were qualitatively different: drug A caused the cessation of spontaneous Ca^{2+} oscillation via the progressive attenuation in Ca^{2+} spike amplitude, whereas drug B elicited different periodic behaviours (Fig. 3a). Despite these different modes of Ca^{2+} disruption, quantification of Ca^{2+} spike frequency revealed no differences between drugs A and B with both drugs producing values similar to those obtained under control (no drug) conditions (Fig. 4). Clearly, this highlights a real limitation of any method of Ca^{2+} spike analysis that does not take account of the specific temporal distribution of the Ca^{2+} spikes. To this end, our novel indices of Ca^{2+} signal organisation, namely, ITN, AHI and THI, discriminate the different effects of these two drugs (Fig. 4).

4 Notes

1. It is conceivable that contaminant non-CMs influence (a) the development of CM functional competency and (b) the measured effect of drugs on CMs (e.g. EC_{20} values). We previously used a FACS-based strategy to enrich CMs, but although this improved some of functional properties of the CM, it generally resulted in greater phenotypic variability across the population (see Supplementary Fig. 6 in [23]). We also investigated the extent of cell division in these 'non-enriched'/heterogeneous cell populations. In the three years that we have been using Cytiva™ CM, we have found no evidence of cell division. In contrast, when using CM differentiated from patient fibroblasts using the method of Burridge et al. [37], we do observe cell division although this is rare (see Supplementary Movie 8 in [6]). Even then, we have only ever observed cell division on gelatin matrices, possibly indicating a role for the culture matrix (i.e. 'adhesiveness') in this phenomenon.
2. The axial alignment of cells (Fig. 1b, c) is associated with the intracellular redistribution of cardiac TnT into well-organised striatal arrangements and is a characteristic typical of CM on days 4–7 post-seeding (Fig. 1d). In this form, CMs exhibit spontaneous and caffeine-dependent sarcoplasmic reticulum (SR) Ca^{2+} release and are responsive to electrical stimulation at frequencies that exceed the endogenous Ca^{2+} spike frequency. Although these features suggest the relative maturation of the SR [46], cTnT striation is not a good marker of CM functional maturity [6, 23, 47–49].
3. This sub-physiological external $[Ca^{2+}]$ is sufficient to support spontaneous contractility, but helps maintain the cells in a relatively 'quiet' state and avoids overloading the SR which can be

a consequence of longer-term culture in medium where [Ca^{2+}] is higher (i.e. ≈1.3 mM).

4. CM are extremely sensitive to temperature. We prewarm the media to 39 °C so that it is ≈37 °C at the point of addition.
5. On this system operating in unidirectional mode, a scan configuration of 512 × 512 pixels takes 71 ms. The acquisition of an image every 100 ms intervals (10 Hz) thus gives a period of ≈30 ms free from illumination. Under these conditions, the background drift (decay) in fluorescence signal intensity due to photobleaching is typically <5% across the time series.
6. The dimensions of the 'wells' in the silicon gaskets are 3 mm × 1 mm (diameter and depth, respectively) creating a surface area for CM attachment of 7 mm^2. This is comparable to that of a single well of a 384-well plate and very similar to the dimensions of the hemispherical front lens of a standard microscope objective. However, unlike in 384-well format, we find that the high value of 'CM to medium' in these chambers (≈100 μl medium per 1000 cells) facilitates the dilution of some para- and autocrine factors that can interfere with cellular synchronisation. The silicon gaskets survive multiple rounds of autoclaving, but their adhesion to glass is reduced beyond eight cycles.
7. Warming cells directly from liquid N_2 to 37 °C without this intermediate step on dry ice results in a much greater incidence of cell bursting and a poor recovery of intact cells.
8. We avoid the use of pipettes at this stage and typically use a syringe fitted with a 4 mm diameter filling tube to avoid sheering CM.
9. The use of a 'tall' tube, in which the cell pellet is separated from the surface of the 10 ml of solution by ≈8 cm, facilitates the separation of the ruptured/non-intact cells from the intact CM intended for seeding. Post-centrifugation of the supernatant solution is removed from the top, i.e. 'chased down' the tube towards the CM pellet.
10. In our hands, the very slow dilution of the DMSO-containing cryopreservation medium to an eventual ratio of 1:10 (v/v) with RPMI/B27 is essential to avoid 'media shock'—a process by which rapid dilution of the DMSO-containing freezing medium damages CM. We don't fully understand the reasons for this.
11. Since non-intact/ruptured cells should be removed in Sect. 3.1 step 3, CM viability at this stage should exceed 90%.
12. The Matrigel-treated glass surface should not be allowed to dry out, and CM should be seeded as soon as possible after the Matrigel is removed. We typically follow a cycle of removing

approximately 90% of the solution from six chambers (using an automatic pipette set to 14 μl), followed by seeding into these six chambers and so on. It is also important that this step be done as cleanly as possible, since any wetting of the gasket surface will lead to the inability to form a stable meniscus described in step 5.

13. This is the initial seeding density that results in homogeneous dispersion of CM across the culture surface. Subsequent 'self-organisation' and alignment of the CMs (see Fig. 1b, c), especially the dynamic movement of some CM on a gelatin matrix (see Supplementary Movies 6 and 7 in [6]), means that the distribution of cells on the surface can be very heterogeneous after a few days in culture.
14. Although 'low-density' plating of cells (i.e. 500–1200 cells per mm^2) has been reported to drive a phenotype consistent with electrical remodelling and cellular hypertrophy [50], we find no measureable effect on the Ca^{2+} handling behaviour of the cells or on the extent of intercellular synchronisation at cell densities between 200 and 2000 cells per mm^2. CMs are only seeded into one gasket because we use the chambers as 'single use', i.e. to investigate one drug concentration (Fig. 2).
15. We do not remove the solution from the gaskets prior to 'topping-up' with RPMI/B27. For reasons that we do not fully understand, the development of functional competency in the CMs is adversely affected if the few non-adherent cells (which are usually spherical in shape and/or granular in appearance) are removed after 2 h.
16. We have described the progressive reduction in spontaneous activity in CM with continued time in culture which may correlate with an increased maturation of the cellular Ca^{2+} handling machinery [6, 23]. In our view, the most 'adult-like' phenotype will correspond to the absence of spontaneous Ca^{2+} oscillations, but full responsiveness of CM to external electrical stimulation (i.e. 'pacing'). This will involve CM culture beyond 7 days and is not covered in this chapter.
17. We have used several Ca^{2+} dyes including Fluo-3, Fluo-5 and Fluo-8 that work just as well. However, each dye will produce a different 'fingerprint' of Ca^{2+} signalling that precludes inter-dye comparisons. For this reason, it is best to define which Ca^{2+} reporter dye works best in a particular experimental configuration and then perform all experiments with the selected dye. Since SALVO analysis depends on recording low-amplitude Ca^{2+} fluxes, good definition of basal (inter-spike/inter-transient) Ca^{2+} signals is required. We have used some Ca^{2+} dyes that are not good for this purpose (e.g. Ca^{2+} orange and Ca^{2+} crimson).

18. Many researchers use DMSO-containing pluronic F127, a poloxamer nonionic surfactant, to dissolve Fluo-4 AM. We find that good-quality, dessicated-stored DMSO [preferably supplied in low-volume glass vials (1–5 ml)] renders the addition of pluronic F127 unnecessary. We also routinely use Fluo-4 that has been packaged in aliquots of 50 μg, and one of these vials will typically be used within the course of a week's experiment. The accumulation of Fluo-4 into intracellular organelles will be seen between 60 and 90 min post-loading; during experiments we co-ordinate the timings of loading to negate to this limitation. All CMs are imaged within 1 h of Fluo-4 loading.
19. Up to this point, CMs have been maintained in culture for several days and then loaded with Fluo-4 in RPMI/B27 containing low [Ca^{2+}] (≈0.4 mM) (**Note 3**). The transfer of CM to KRH solution or Leibovitz L-15 medium raises [Ca^{2+}] to a physiologically relevant level (≈1.3 mM) and reproducibly results in spontaneous physical contraction and Ca^{2+} oscillation at frequencies >0.3 Hz in >90% of CM populations after 3–5 min.
20. For those drugs with relatively low water solubility (e.g. maximum solubility in water of 10 mM) at pH7.4 and at 23 °C or those first require solubilisation in DMSO or methanol, we use KRH. Otherwise, Leibovitz L-15 is our medium of choice. Neither medium/solution has any effect on the biological activity of any drug we have investigated to date.
21. In this protocol the maximum experimental window is limited to 30 min to avoid the intracellular accumulation of Fluo-4 inside organelles that makes data interpretation difficult (**Note 18**). The use of genetically encoded Ca^{2+} indicators [51] for longer-term studies of Ca^{2+} signalling may avoid this problem. In the study of Lewis et al., drug-induced perturbation in Ca^{2+} signalling was evident after just 3 min [23].
22. Accurate deconstruction of Ca^{2+} signals (Fig. 3b) requires image sampling at rates between 5 and 10 times greater than the frequency of Ca^{2+} spikes. For example, a Ca^{2+} spike frequency of 1 Hz would require image acquisition between 5 and 10 Hz (e.g. every 100 or 200 ms).
23. Sometimes, the extent of physical contractility makes imaging difficult. For example, a CM cluster may move between ROIs on a grid (Fig. 4). In these instances, we have used blebbistatin (5 μM), an agent that inhibits myofilament shortening but preserves normal Ca^{2+} cycling [23, 52]. In our experience, blebbistatin has a small but measurable effect on CM Ca^{2+} signalling, and the impact of this agent must be taken into account when interpreting the effects of subsequent drug additions on blebbistatin-immobilised CMs.

24. Although there is usually an excellent correlation between caspase 3/7 activation and the full induction of apoptosis, we have (rarely) found that data obtained from caspase 3/7 activation assays do not correlate entirely with the extent of apoptosis 'classically' determined by DNA fragmentation assays. Anecdotally, we sometimes observe that caspase activation-dependent signals are disproportionally higher than the number of apoptotic nuclei identified by TUNEL. This may point to reversibility in the caspase activation dependence of apoptosis as others have reported in other cell types [53–55]. To negate this issue, we routinely perform both caspase activation (ApoTox-Glo) and TUNEL (DeadEnd) assays on the same CM population.
25. An investigation of latent toxicity should be a component of CIPA.
26. We have not observed any different concentration-dependent effects of a drug depending on whether the B27 supplement was included in the medium or not during this 6 h incubation. However, it is possible that some drugs do interact with the components of B27, thereby reducing their effective free concentration. To address this, parallel experiments in the absence of the B27 supplement are done.
27. This 6 h incubation in the presence of drug allows the exploration of the more chronic aspects of toxicity. The rationale for performing parallel investigations in the *absence* of drug comes from reports of 'cell memory' in which cell populations can apparently recover from noxious stimuli only to exhibit marked dysfunction at a later time point [15, 56].
28. To avoid artefact, the calculation of ITN requires the analysis of signal intensity from >500 pixels. Using a 63× objective, the FOV corresponds to 21,025 μm^2 (145 × 145 μm). At 512 × 512 pixels (262,144 pixels), user-defined ROIs of 50 μm^2 (white boxes; 63× panels) correspond to 625 pixels. In this configuration, the number of pixels per μm^2 is 12. Using a 20× objective, the FOV corresponds to 207,936 μm^2 (456 × 456 μm). In these data acquired at 1024 × 1024 pixel resolution (1,048,576 pixels), each region of the grid is 1/25th of the FOV and will comprise 8317 μm^2 (41,943 pixels). In this format, the number of pixels per μm^2 is 5.
29. CM are very sensitive to mechanical deformation, and even the addition of drug-containing medium can provoke altered Ca^{2+} signalling. To avoid this, any additions to the chamber are performed well away from the silicon gasket/glass culture surface, and the addition of a typical volume of 100 μl ensures good mixing of the drug.

30. Confocal microscopy generates images of discrete planes of depth (z-sections), and those cells that exhibit very different morphologies (e.g. sphericity) lying above the plane of the adherent monolayer do not contribute to the Ca^{2+}-dependent fluorescent signal. Imaging modalities that capture fluorescent signals throughout the entire depth of the sample (e.g. non-confocal imaging) will not differentiate signals coming from bona fide CM that are adherent to the attachment matrix and those cells which lie above this plane.
31. To avoid artefact from CM that exhibit atypical behaviour under baseline conditions, we apply inclusion criteria: typically frequency > 0.3 Hz, AHI < 0.2, baseline drift < 5% over 30 s and signal to noise > 2. These thresholds typically result in the inclusion of >90% of all data.
32. In those traces in which a concentration of drug produces a cessation of Ca^{2+} spikes (e.g. drug A at t = 16, Fig. 3a), it is not possible to perform SALVO analysis. In these instances it is obvious that these drug concentrations/time points have catastrophic effects on Ca^{2+} signalling in CM.

5 Conclusion

The methods described here, which provide an integrative analysis of Ca^{2+} spike characteristics and low-amplitude inter-spike Ca^{2+} fluxes, comprehensively profile CM Ca^{2+} signalling. However, with some workup, the system could be configured for 'multiplexing' spectrally separated ion-sensitive fluorescent probes or combined with electrophysiological platforms [57]. In addition to enabling enhanced drug safety/toxicology screening in CM, SALVO could be applied to profiling drug toxicity in other cells (e.g. hepatocytes) and to the analysis of other cellular signals that change on different timescales (e.g. pH).

Acknowledgement

Research in the authors' laboratories was funded by the British Heart Foundation, Wellcome Trust, Medical Research Council (Proximity to Discovery) and Cardiff University.

References

1. Silvester NC, George CH (2011) Searching for new cardiovascular drugs: towards improved systems for drug screening? Expert Opin Drug Discov 6:1155–1170
2. Moller C, Slack M (2010) Impact of new technologies for cellular screening along the drug value chain. Drug Disc Today 15:384–390

3. Pouton C, Haynes JM (2007) Embryonic stem cells as a source of models for drug discovery. Nat Rev Drug Disc 6:605–616
4. Braam SR, Tertoolen L, van de Stolpe A et al (2010) Prediction of drug-induced cardiotoxicity using human embryonic stem cell-derived cardiomyocytes. Stem Cell Res 4:107–116
5. Dick E, Rajamohan D, Ronksley J et al (2010) Evaluating the utility of cardiomyocytes from human pluripotent stem cells for drug screening. Biochem Soc Trans 38:1037–1045
6. Jones AR, Edwards DH, Cummins MJ et al (2016) A systemized approach to investigate Ca^{2+} synchronization in clusters of human induced pluripotent stem-cell derived cardiomyocytes. Front Cell Dev Biol 3:89
7. Redfern WS, Carlsson L, Davis AS et al (2003) Relationships between preclinical cardiac electrophysiology, clinical QT interval prolongation and torsade de pointes for a broad range of drugs: evidence for a provisional safety margin in drug development. Cardiovasc Res 58:32–45
8. Zhang J, Ding EL, Song Y (2006) Adverse effects of cyclooxygenase 2 inhibitors on renal and arrhythmia events: meta-analysis of randomized trials. JAMA 296:1619–1632
9. Feeley J (2013) http://www.bloomberg.com/news/articles/2013-07-18/merck-pays-23-million-to-end-vioxx-drug-purchase-suits
10. CIPA (2016) http://www.fda.gov/downloads/AboutFDA/CentersOffices/OfficeofMedicalProductsandTobacco/CDER/UCM420834.pdf
11. Hill AP, Perry MD, Abi-Gerges N et al (2016) Computational cardiology and risk stratification for sudden cardiac death: one of the grand challenges for cardiology in the 21st century. J Physiol. doi:10.1113/JP272015
12. Cavero I, Holzgrefe H (2014) Comprehensive in vitro proarrhythmia assay, a novel in vitro/in silico paradigm to detect ventricular proarrhythmic liability: a visionary 21st century initiative. Expert Opin Drug Saf 13:745–758
13. Berridge MJ, Bootman MD, Roderick HL (2003) Calcium signalling: dynamics, homeostasis and remodelling. Nat Rev Mol Cell Biol 4:517–529
14. Berridge MJ, Lipp P, Bootman MD (2000) The versatility and universality of calcium signalling. Nat Rev Mol Cell Biol 1:11–21
15. George CH, Parthimos D, Silvester NC (2012) A network-oriented perspective on cardiac calcium signaling. Am J Physiol Cell Physiol 303:C897–C910
16. Glass L (2001) Synchronization and rhythmic processes in physiology. Nature 410:277–284
17. Boileau E, George CH, Parthimos D et al (2015) Synergy between intercellular communication and intracellular Ca^{2+} handling in arrhythmogenesis. Ann Biomed Eng 43:1614–1625
18. George CH, Barberini-Jammaers SR, Muller CT (2008) Refocussing therapeutic strategies for cardiac arrhythmias: defining viable molecular targets to restore cardiac ion flux. Expert Opin Ther Pat 18:1–19
19. Kholodenko BN, Hancock JF, Kolch W (2010) Signalling ballet in space and time. Nat Rev Mol Cell Biol 11:414–426
20. Kim J-R, Shin D, Jung SH et al (2010) A design principle underlying the synchronization of oscillations in cellular systems. J Cell Sci 123:537–543
21. Lakatta EG, Maltsev V, Vinogradova TM (2010) A coupled SYSTEM of intracellular Ca^{2+} clocks and surface membrane voltage clocks controls the timekeeping mechanism of the heart's pacemaker. Circ Res 106:659–673
22. Novak B, Tyson JJ (2008) Design principles of biochemical oscillators. Nat Rev Mol Cell Biol 9:981–991
23. Lewis KJ, Silvester NC, Barberini-Jammaers SR et al (2015) A new system for profiling drug-induced calcium signal perturbation in human embryonic stem cell-derived cardiomyocytes. J Biomol Screen 20:330–340
24. Falcke M (2004) Reading the patterns in living cells—the physics of Ca^{2+} signaling. Adv Phys 3:255–440
25. Uhlen P (2004) Spectral analysis of calcium oscillations. Sci STKE 9:pl15
26. George CH, Lai FA (2007) Developing new anti-arrhythmics: clues from the molecular basis of cardiac ryanodine receptor (RyR2) Ca^{2+}-release channel dysfunction. Curr Pharm Des 13:3195–3211
27. Li S, Chen G, Li RA (2013) Calcium signalling of human pluripotent stem cell-derived cardiomyocytes. J Physiol 591:5279–5290
28. George CH, Higgs GV, Lai FA (2003) Ryanodine receptor mutations associated with stress-induced ventricular tachycardia mediate increased calcium release in stimulated cardiomyocytes. Circ Res 93:531–540
29. George CH, Higgs GV, Mackrill JJ et al (2003) Dysregulated ryanodine receptors mediate cellular toxicity: restoration of normal phenotype by FKBP12.6. J Biol Chem 278:28856–28864
30. George CH, Rogers SA, Bertrand BMA et al (2007) Alternative splicing of ryanodine receptors modulates cardiomyocyte Ca^{2+} signaling and susceptibility to apoptosis. Circ Res 100:874–883

31. George CH, Silvester NC, Barberini-Jammaers SR (2010) Method and system for analyzing calcium transients in coupled cells. Patents US8,666,676; JP5,771,194; AU2010252792
32. Harris K, Aylott M, Cui Y et al (2013) Comparison of electrophysiological data from human-induced pluripotent stem cell-derived cardiomyocytes to functional preclinical safety assays. Toxicol Sci 134:412–426
33. Guo L, Coyle L, Abrams RMC et al (2013) Refining the human iPSC-cardiomyocyte arrhythmic risk assessment model. Toxicol Sci 136:581–594
34. Clements M, Thomas N (2014) High-throughput multi-parameter profiling of electrophysiological drug effects in human embryonic stem cell derived cardiomyocytes using multi-electrode arrays. Toxicol Sci 140:445–461
35. Xu C, Police S, Hassanipour M (2011) Efficient generation and cryopreservation of cardiomyocytes derived from human embryonic stem cells. Regen Med 6:53–66
36. Burridge PW, Matsa E, Shukla P et al (2014) Chemically defined generation of human cardiomyocytes. Nat Methods 11:855–860
37. Burridge PW, Thompson S, Millrod MA et al (2011) A universal system for highly efficient cardiac differentiation of human induced pluripotent stem cells that eliminates interline variability. PLoS One 6, e18293
38. Mummery CL, Zhang L, Ng ES et al (2012) Differentiation of human embryonic stem cells and induced pluripotent stem cells to cardiomyocytes: a methods overview. Circ Res 111:344–358
39. Brewer GJ, Cotman CW (1989) Survival and growth of hippocampal neurons in defined medium at low density: advantages of a sandwich culture technique or low oxygen. Brain Res 494:65–74
40. Brewer GJ, Torricelli JR, Evege EK et al (1993) Optimized survival of hippocampal neurons in B27-supplemented Neurobasal, a new serum-free medium combination. J Neurosci Res 35:567–576
41. RPMI Medium. https://www.thermofisher.com/uk/en/home/technical-resources/media-formulation.114.html
42. Leibovitz L-15 Medium. https://www.thermofisher.com/uk/en/home/technical-resources/media-formulation.81.html
43. Gee KR, Brown KA, Chen WNU et al (2000) Chemical and physiological characterization of fluo-4 Ca^{2+}-indicator dyes. Cell Calcium 27:97–106
44. Fiji. http://www.fiji.sc
45. George CH, Jundi H, Thomas NL et al (2006) Arrhythmogenic mutation-linked defects in ryanodine receptor autoregulation reveal a novel mechanism of Ca^{2+} release channel dysfunction. Circ Res 98:88–97
46. Liu J, Fu J-D, Siu C-W et al (2007) Functional sarcoplasmic reticulum for calcium handling of human embryonic stem cell-derived cardiomyocytes: insights for driven maturation. Stem Cells 25:3038–3044
47. Khan JM, Lyon AR, Harding SE (2013) The case for induced pluripotent stem cell-derived cardiomyocytes in pharmacological screening. Br J Pharmacol 169:304–317
48. Sheng X, Reppel M, Nguemo F et al (2012) Human pluripotent stem cell-derived cardiomyocytes: response to TTX and lidocain reveals strong cell to cell variability. PLoS One 7, e45963
49. Gorza L, Menabo R, Vitadello M et al (1996) Cardiomyocyte troponin T immunoreactivity is modified by cross-linking resulting from intracellular calcium overload. Circulation 93:1896–1904
50. Uesugi M, Ojima A, Taniguchi T et al (2014) Low-density plating is sufficient to induce cardiac hypertrophy and electrical remodelling in highly purified human iPS cell-derived cardiomyocytes. J Pharmacol Toxicol Methods 69:177–188
51. Kaestner L, Scholz A, Tian Q et al (2014) Genetically encoded Ca^{2+} indicators in cardiac myocytes. Circ Res 114:1623–1639
52. Fedorov VV, Lozinsky IT, Sosunov EA et al (2007) Application of blebbistatin as an excitation-contraction uncoupler for electrophysiologic study of rat and rabbit hearts. Heart Rhythm 4:619–626
53. Wang K, Brems JJ, Gamelli RL et al (2005) Reversibility of caspase activation and its role during glycochenodeoxycholate-induced hepatocyte apoptosis. J Biol Chem 280:23490–23495
54. Tang HL, Yuen KL, Tang HM et al (2009) Reversibility of apoptosis in cancer cells. Br J Cancer 100:118–122
55. Tang HL, Tang HM, Mak KH et al (2012) Cell survival, DNA damage, and oncogenic transformation after a transient and reversible apoptotic response. Mol Biol Cell 23:2240–2252
56. Izyumov DS, Avetisyan AV, Pletjushkina OY et al (2004) "Wages of Fear": transient threefold decrease in intracellular ATP level imposes apoptosis. Biochim Biophys Acta 1658:141–147
57. Lee P, Klos M, Bollensdorff C et al (2012) Simultaneous voltage and calcium mapping of genetically purified human induced pluripotent stem cell-derived cardiac myocyte monolayers. Circ Res 110:1556–1563

Chapter 10

Combined Impedance and Extracellular Field Potential Recordings from Human Stem Cell-Derived Cardiomyocytes

Alison Obergrussberger, Ulrich Thomas, Sonja Stölzle-Feix, Nadine Becker, Krisztina Juhasz, Leo Doerr, Matthias Beckler, Michael George, and Niels Fertig

Abstract

Measurement of contractility using impedance is a novel method for gaining information about a drug candidate's potential to disturb cardiac cell contraction. The impedance signal is recorded from a monolayer of cardiac cells, most commonly derived from human-induced pluripotent stem cells (hiPSCs), which are becoming an attractive model for safety testing, especially in the light of the Comprehensive In Vitro Proarrhythmia Assay (CiPA) initiative introduced in 2013. The goal of this initiative is, in part, to standardize assays, targets, and cell types but also to evaluate the potential of new technologies, in this context, such as impedance. The CardioExcyte 96 is a hybrid system that combines the impedance readout (a measure of cell contractility) with extracellular field potential (EFP) recordings. This chapter focuses on cell handling of hiPSC cardiomyocytes (CMs) and the short- and long-term investigation into pharmacological effects of a wide range of pharmacological agents, including flecainide, nifedipine, isoproterenol, and E4031 using the CardioExcyte 96.

Key words CardioExcyte 96, CiPA initiative, Early after-depolarizations, Extracellular field potential, hERG, hiPSC-derived cardiomyocytes, Impedance, Label-free, Safety pharmacology

1 Introduction

Multielectrode arrays (MEAs) have been developed over the last several decades as a noninvasive method for recording extracellular field potentials (EFP) of cardiac cells [1, 2] or neural activity in slices [3–5]. Much effort has been made to improve the quality of recordings, primarily reducing noise by increasing the number of electrodes per well (reviewed in [6]). More recently, MEAs have been used to characterize human stem cell-derived cardiomyocytes [7–9] for use as a preclinical model for drug safety testing. In addition, devices analyzing impedance as a measure of cell contractility,

Mike Clements and Liz Roquemore (eds.), *Stem Cell-Derived Models in Toxicology*, Methods in Pharmacology and Toxicology, DOI 10.1007/978-1-4939-6661-5_10,

the xCELLigence RTCA Cardio System (ACEA Biosciences and Roche Applied Biosciences) [10, 11] and the CardioExcyte 96 (Nanion Technologies, GmbH) (Fig. 1a) [8, 12], have been utilized to test compound effects on the impedance signal from human-induced pluripotent stem cell-derived cardiomyocytes (hiPSC-CMs) [10–12]. The CardioExcyte 96 combines both impedance (cell contractility) and MEA-like (EFP) recordings [8, 12] in a 96-well plate format. A monolayer of contractile cells is formed on the sensor plate (Fig. 1c) which enables cells to be studied within a physiological network, as opposed to isolated cells in the case of, for example, the patch clamp technique. The substantial changes in cell morphology and adhesion which accompany contraction are monitored in the impedance signal, whereas the EFP signal is passively recorded by differential voltage recordings (between the two electrodes in one well; *see* Fig. 1b). The xCELLigence RTCA Cardio is capable of a data acquisition rate of 12.9 ms [10], whereas the CardioExcyte 96 has a temporal resolution down to 1 ms [12]. The impedance and EFP signals can be monitored over long periods of time, up to several days, allowing the long-term investigation into the effects of compounds on

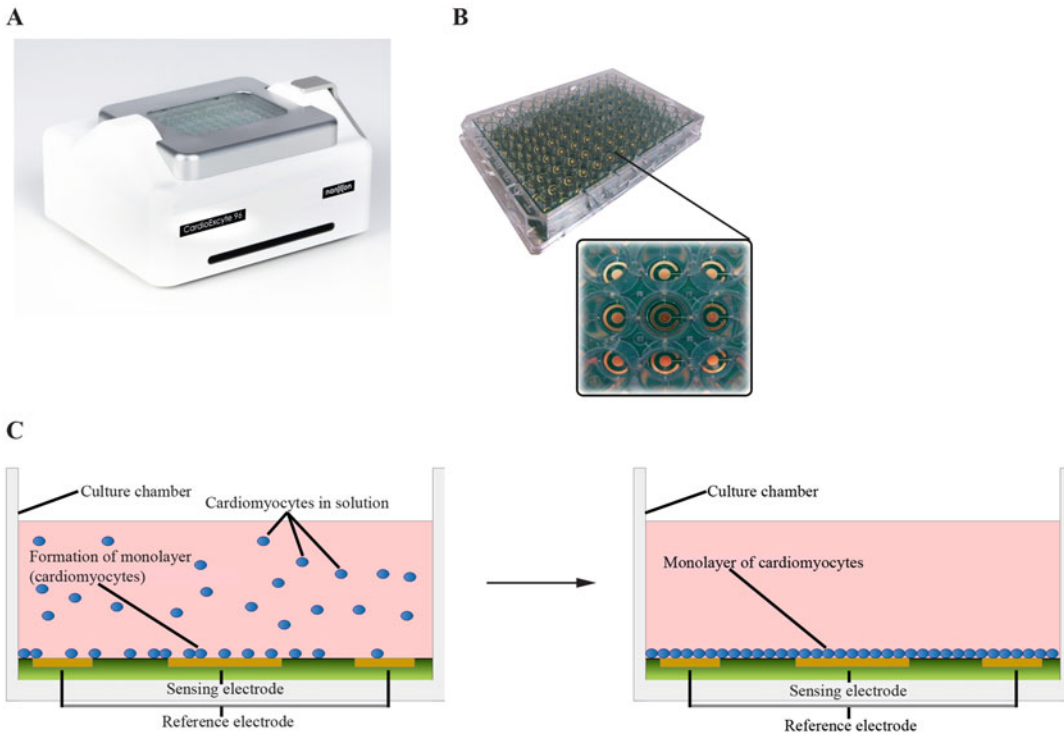

Fig. 1 (**a**) The CardioExcyte 96 with the recording chamber and NSP-96 sensor plate shown in position. The hand lever on the right is used to eject the plate. (**b**) The NSP-96 plate contains a single sensing electrode (see inset) in each of the 96 wells (adapted from Doerr et al. [12]). (**c**) The hiPSC-CMs thawed from frozen or harvested from culture are added as a suspension to the NSP-96 wells. The cells form a monolayer and begin to beat in synchrony

cardiomyocyte contractile function. The CardioExcyte 96 can be placed in an incubator or used in combination with an Incubation System to control temperature, humidity, and gas mixture, much like that of an incubator, making the device a stand-alone instrument. So far, a number of different in vitro cardiomyocyte preparations have been successfully validated on the CardioExcyte 96, including stem cell-derived cardiomyocytes from Axiogenesis (human, Cor.4U; murine, CorAt) [12], Cellular Dynamics International (iCell Cardiomyocytes) [12], GE Healthcare (Cytiva Plus) [8, 12], Cellectis (human, 3D clusters: hES-CMC™) [12], and ReproCELL (ReproCardio 2) [12]. Although the interpretation of impedance data from cardiac cells is complex, these have the potential to provide complementary information to patch clamp electrophysiology about compound effects. This chapter describes the methods involved in combined impedance and EFP measurements (from the same well) on the CardioExcyte 96, from seeding of cells on the NSP-96 plates through to short- and long-term investigation of compound effects on contractile function of stem cell-derived CMs. Indeed, this combined analysis of EFP and cell movement on an integrated instrument may offer some additional insights into drug liability for compounds such as blebbistatin which interfere with the cardiomyocyte contractile machinery but may not directly impact the cell's electrophysiology as measured by EFP alone (*see* Fig. 2; [11–15]). The hiPSC-CMs used to illustrate the methods in this chapter were Cor.4U (Axiogenesis AG), Pluricytes (Pluriomics), and iCell Cardiomyocytes^2 (CDI). A detailed description of the online analysis parameters used in this chapter is also provided.

2 Materials

2.1 Fibronectin Coating of the Sensor Plate

1. Stock solution of fibronectin (1 mg/ml; sterile)
2. Phosphate-buffered saline (PBS) including Ca^{2+} and Mg^{2+} (Dulbecco's PBS, Gibco, cat. no. 14040-166; Ca^{2+}/Mg^{2+} not stated)
3. NSP-96 sensor plate

2.2 Cell Thawing, Harvesting, and Seeding Procedures

1. Cultured or frozen cardiomyocytes to seed
2. Plating or thawing media provided by the manufacturer
3. PBS without Ca^{2+}/Mg^{2+} (Dulbecco's PBS, Gibco, cat. no. 14190-094), 2 mM EDTA
4. Trypsin-EDTA (1×)
5. Trypan blue for cell counting
6. Fibronectin-coated NSP-96

2.3 Medium Exchange

1. Manufacturer-supplied media

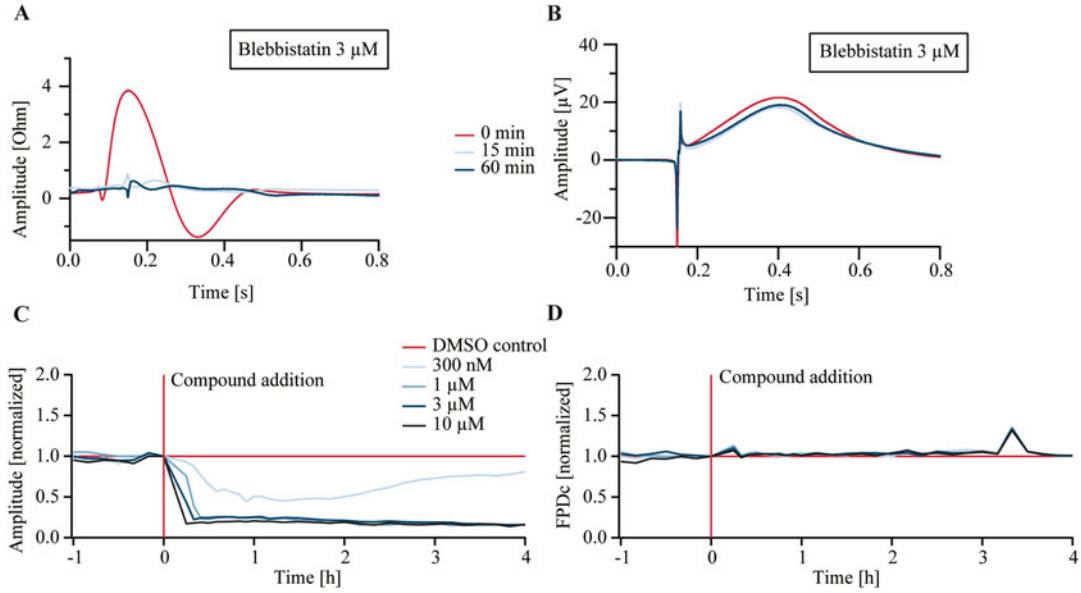

Fig. 2 The effect of the myosin II inhibitor, blebbistatin, on the impedance and EFP of Cor.4U cells (Axiogenesis AG). (**a**) The effect of 3 µM blebbistatin on the impedance mean beat and (**b**) the EFP mean beat at 15 and 60 min incubation in blebbistatin. Blebbistatin completely disrupts cell movement but has no significant effect on ion channel function as seen in (**a**) and (**b**), respectively. (**c**) Time course of the experiment in impedance mode. The effect of different concentrations of blebbistatin on the impedance mean beat amplitude plotted over time. (**d**) Time course of the experiment in EFP mode. The effect of different concentrations of blebbistatin on the EFP mean beat amplitude plotted over time

2.4 Compound Addition

1. Stock compound solutions, e.g., 1 mM E4031 in dimethyl sulfoxide (DMSO), 30 mM flecainide in DMSO, 10 mM nifedipine in DMSO (*see* **Note 1**), 10 mM isoproterenol in DMSO, 30 mM CMP1 (a blinded compound) in DMSO
2. Control (vehicle) solution, e.g., medium + 0.1 % DMSO
3. Manufacturer-supplied media

3 Methods

The CardioExcyte 96 (Fig. 1a) is a system for combined impedance and EFP recordings. This section describes the use of hiPSC-CMs from three different manufacturers, iCell Cardiomyocytes[2] (Cellular Dynamics International), Cor.4U (Axiogenesis AG), and Pluricytes (Pluriomics) on the CardioExcyte 96, from seeding the cells on the recording plates (NSP-96), through monitoring of impedance and EFP signals until a stable baseline is achieved up to compound application and data analysis. Since the technique is relatively new, some detail of the online analysis parameters used in this chapter is given.

3.1 Fibronectin Coating of the Sensor Plate

1. When working with the NSP-96 plates, perform the following steps aseptically inside a biosafety cabinet to avoid bacterial/fungal contamination (*see* **Note 2**). The NSP-96 plates are delivered sterile and vacuum-packed.
2. Fibronectin is used to coat the sensor plate (*see* **Note 3**). Dilute the fibronectin 1:100 with PBS (including Ca^{2+} and Mg^{2+}), e.g., 50 µl fibronectin in 5 ml PBS. Gently resuspend the fibronectin solution using a pipette (*see* **Note 4**).
3. Add 50 µl of the fibronectin solution into the wells to be used (*see* **Note 5**).
4. Incubate at 37 °C for at least 1.5 h or overnight at 4 °C.
5. Aspirate fibronectin solution just before adding the cell suspension. Ensure the wells do not dry out.

3.2 Cell Thawing, Harvesting, and Seeding Procedures

3.2.1 hiPSC-CM Thawing

1. Frozen cells (e.g., iCell Cardiomyocytes[2], Pluricytes, or Cor.4U) should be thawed as specified by the cell supplier. The common steps are briefly outlined here but should be adjusted according to the cell manufacturer's recommendations. After thawing, the cells are seeded directly onto the fibronectin-coated NSP-96.
2. Put the vial of cells in a 37 °C water bath for exactly 4 min.
3. Remove the vial of cells from the water bath, spray with 70% ethanol, and place into the sterile cell culture laminar flow hood.
4. Gently transfer the hiPSC-CMs to a new sterile 50 ml centrifuge tube using a 1 ml pipette. *See* **Note 6**.
5. Rinse the empty hiPSC-CM vial with 1 ml of plating/thawing medium (at room temperature) to recover any residual cells from the vial. Add the 1 ml plating/thawing medium rinse from the cryovial dropwise over 90 s (i.e., one drop every 4–5 s) to the 50 ml centrifuge tube containing the hiPSC-CM cell suspension. Gently swirl the tube while adding the media to ensure that the solution mixes completely; this also minimizes the osmotic shock to the thawed cells.
6. Slowly add 8 ml plating/thawing medium (at room temperature) to the 50 ml centrifuge tube containing the hiPSC-CM and the 1 ml of media. Add the first 1 ml dropwise over 30–60 s. Then add the remaining volume over the next ~30 s. Gently swirl the centrifuge tube while adding the medium.
7. Gently mix the contents of the 50 ml centrifuge tube by inverting 2–3 times. Gentle mixing is critical to ensure maximum viability. Avoid vigorous shaking or vortexing of the cell suspension.
8. Count cells using trypan blue staining to check viability (typically 90–95% viability).
9. Seed the cells on the NSP-96 as described in Sect. 3.2.3.

3.2.2 Harvesting Cells from Cultures

1. If cells are received as live cultures (e.g., Cor.4U) in T25 flasks, upon arrival remove media and replace with fresh media supplied by the manufacturer. Leave overnight in the incubator before harvesting for seeding on the NSP-96.
2. To harvest the cells, remove media and wash twice with PBS (without Ca^{2+} and Mg^{2+}, including 2 mM EDTA).
3. Add PBS (without Ca^{2+} and Mg^{2+}, including 2 mM EDTA) and incubate for 5 min at room temperature.
4. Following this time, remove PBS and add 3 ml of pre-warmed trypsin. Gently tip the culture flask to ensure an even distribution of trypsin over the bottom of the dish, and then remove most of the enzyme so that only a thin film of solution is left covering the cells.
5. Incubate 2–5 min at 37 °C, until the cells start to float.
6. Tap the flask gently to dislodge the remaining cells.
7. Add 2 ml of the manufacturer-provided culture media (room temperature).
8. Gently mix the cell suspension using a pipette.
9. Count cells using trypan blue staining to check viability (typically 90–95 %).
10. Centrifuge the cells at 100 g for 2 min. Gently pour off the media and resuspend the cell pellet to give a cell density of 20,000–40,000 viable cells per well.
11. Seed the cells on the NSP-96 as described in Sect. 3.2.3.

3.2.3 Seeding Procedure on the NSP-96

1. Cultured cells (harvested into suspension as described in Sect. 3.2.2) or frozen cells from liquid nitrogen (thawed as described in Sect. 3.2.1) can be seeded as a monolayer on the NSP-96. For 3D clusters, e.g., hES-CMC™ (Cellectis), *see* **Note** 7.
2. To seed the cells, it is not advisable to remove the fibronectin solution in all wells of the NSP-96 in one step as this may result in some of the wells drying out. For optimal results, remove the fibronectin solution in a column of eight wells, and then immediately replace these with 200 µl of cell suspension (20,000–40,000 viable cells per well). Repeat this process for each of the remaining rows in the NSP-96 plate. Cells should be seeded at a density of 20,000–40,000 viable cells per well in order to ensure the formation of a synchronously beating monolayer.
3. After seeding the cells, leave the NSP-96 under the cell culture hood for 30 min without moving it to allow the cells to settle evenly in the well.

3.3 Monitoring Formation of the Monolayer and Synchronous Beating

1. Place the CardioExcyte 96 inside the incubator (*see* **Note 8**) or turn on the Incubation System (*see* **Note 9**).
2. Place the NSP-96 on the recording chamber of the CardioExcyte 96, and use the hand lever to lower the NSP-96 into place.
3. Start the CardioExcyte Control software.
4. Monitor beat rate and amplitude in impedance and EFP modes every 30–60 min for 30 s for at least 4 days to allow formation of the monolayer and synchronous beating. It is possible to record more than one NSP-96 using the CardioExcyte 96. To do this simply manually swap the NSP-96 plates and select the correct recording file for each plate. *See* Figs. 3 and 4 for impedance and EFP signals at different time points using iCell Cardiomyocytes² (Cellular Dynamics International) and Fig. 5 for a time course of beat rate (impedance) and amplitude (EFP) over 6 days. Impedance and EFP mean beat parameters were stable 4 days after plating. Therefore, the cardiomyocytes can be used for experiments 4 days after plating.

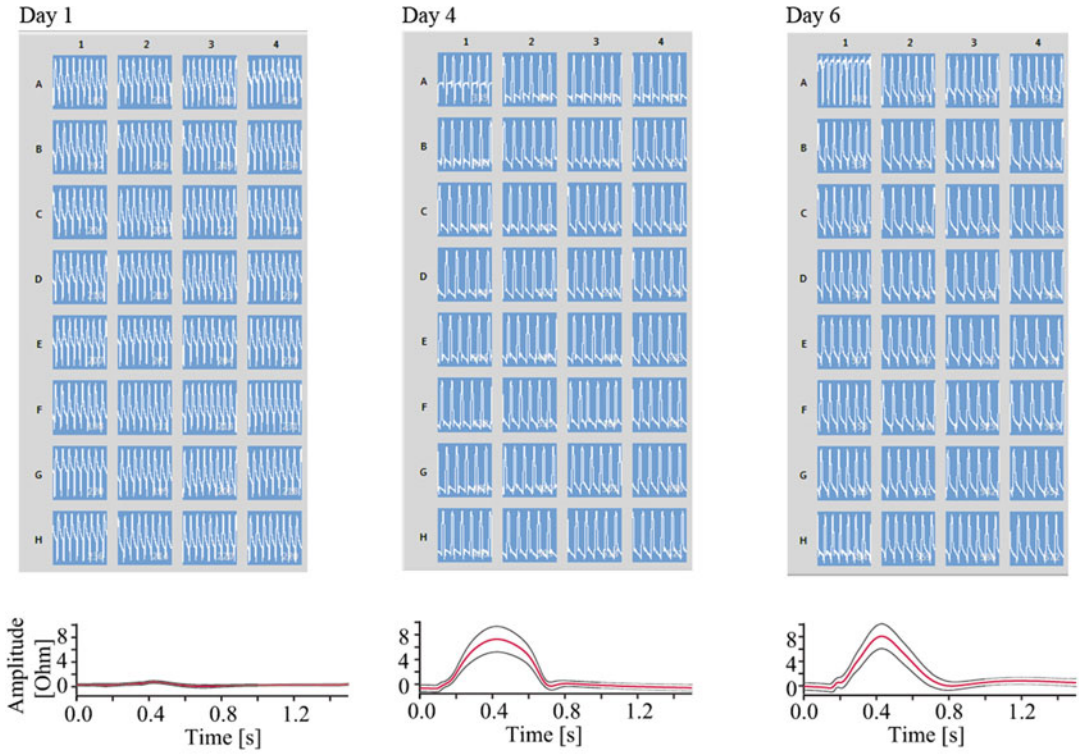

Fig. 3 Impedance measurements of iCell Cardiomyocytes² (Cellular Dynamics International) on the CardioExcyte 96 at different time points. The *top panels* show screenshots (four out of 12 columns) of the CardioExcyte 96 software during measurements in the impedance mode on days 1 (*left*), 4 (*middle*), or 6 (*right*) after plating. The *bottom panels* show impedance mean beat on days 1 (*left*), 4 (*middle*), and 6 (*right*) after plating. Impedance mean beat changes little between days 4 and 6, indicating that the cells can be used for experiments 4 days after plating as suggested by the manufacturer

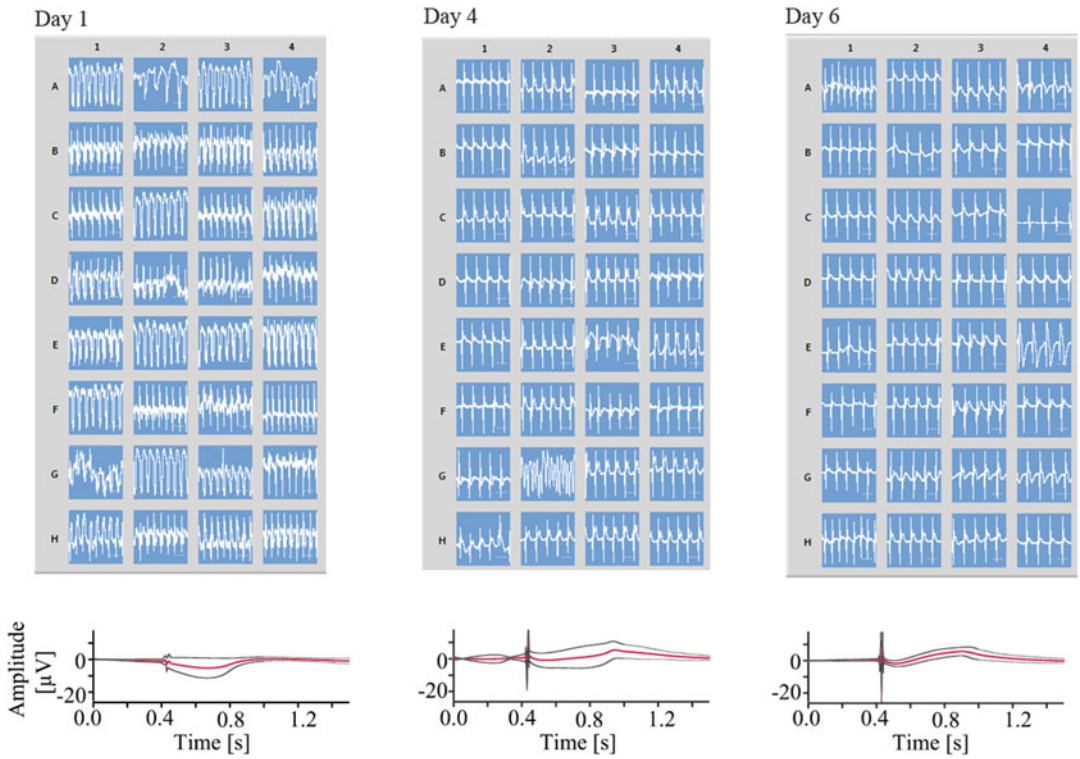

Fig. 4 EFP measurements of iCell Cardiomyocytes[2] (Cellular Dynamics International) on the CardioExcyte 96 at different time points. The *top panels* show screenshots (four out of 12 columns) of the CardioExcyte 96 software during measurements in the EFP mode on days 1 (*left*), 4 (*middle*), or 6 (*right*) after plating. The *bottom panels* show EFP mean beat on days 1 (*left*), 4 (*middle*), and 6 (*right*) after plating. EFP mean beat changes little between days 4 and 6, indicating that the cells can be used for experiments 4 days after plating as suggested by the manufacturer

5. Exchange medium (see Sect. 3.3.1) after 12 h and then once or twice per day (depending on cell type, see manufacturer's instructions) for 2–3 days. After this time, medium is exchanged once every 2 days.

3.3.1 Standard Medium Exchange

1. Disconnect the NSP-96 from the CardioExcyte 96 and place the NSP-96 in the laminar flow hood.
2. Aspirate 50 µl medium per well column by column, and add 50 µl of fresh medium (initial volume per well is 200 µl, medium supplied by the hiPSC manufacturer). *See* **Notes 10** and **11**.
3. Repeat step 2 four times to ensure a complete medium exchange. Do not to touch the bottom of the wells.

3.3.2 Medium Exchange Before Compound Addition

1. Before adding a compound, a complete medium exchange is required to ensure a volume of exactly 200 µl in each well (*see* **Note 12**). Remove the medium completely by placing the pipette at the bottom edge, ensuring minimal contact with the

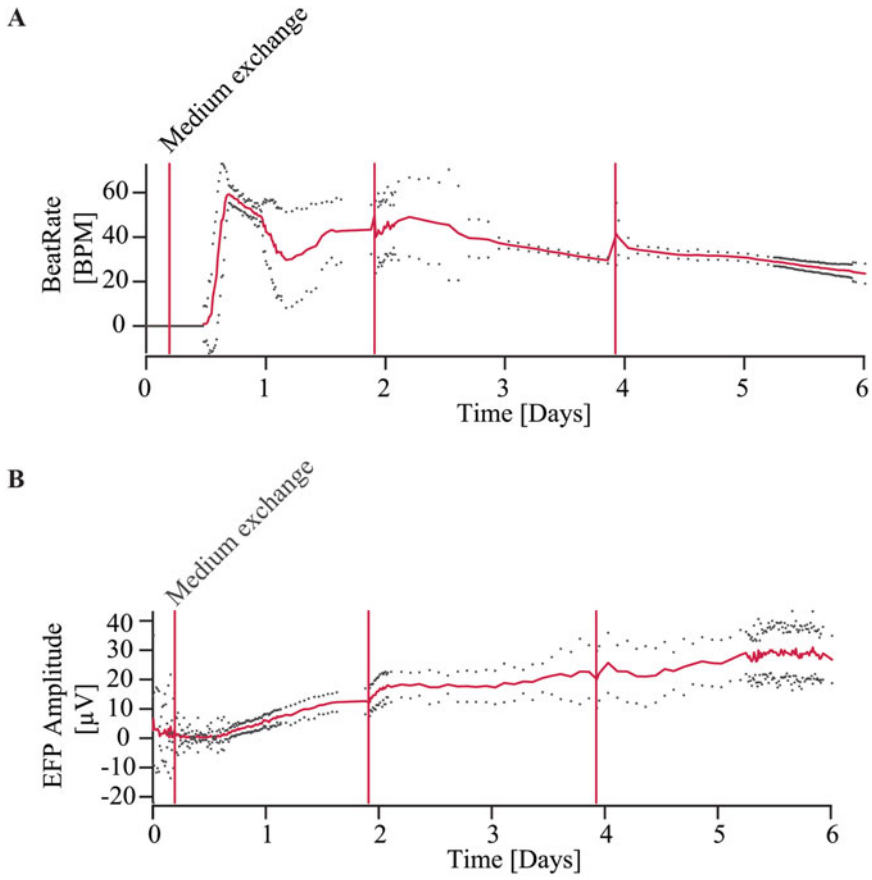

Fig. 5 Impedance beat rate (**a**) and EFP amplitude (**b**) of iCell Cardiomyocytes² (CDI) shown over time course of several days. The *red line* is the mean amplitude of multiple wells and the *dots* indicate the spread of the data. Medium exchanges were made as indicated by the *vertical red lines*. Impedance beat rate and EFP amplitude were stable after 4 days, at which point experiments could be started

bottom surface of the well. Immediately add fresh medium. Replace the medium well by well (single pipette) or column by column (eightfold multi-pipette). *See* **Notes 10** and **11**.

2. Let the cells equilibrate for 2–3 h before compound addition and monitor beat rate, base impedance, and beat amplitude to determine a stable baseline. The last four sweeps before compound addition (the last 30–45 min of control recording) should show stable amplitude and beat rate before compound is added. *See* **Note 13**.

3.4 Setting Up an Experiment

1. Open the CardioExcyte Control software.
2. Click on the "Recording" tab to display the experimental parameters to configure.
3. Select the "Edit" button under "Measurement Configuration." Under the "General" tab, choose Impedance, EFP mode, or Combined measurement mode.

4. Set the sweep duration (*see* **Note 14**).
5. For optional Pacemaker parameters, *see* **Note 15**. The user may wish to pace the activity of hiPSC-CMs as parameters such as field potential duration (FPD) are beat rate (BR) dependent. Therefore, in order to compare cells from different sources, it may be desirable to pace the cells. Additionally, it has been suggested that electrical stimulation may promote maturity of human embryonic stem cell-derived cardiomyocytes [16].
6. Click on the "Save file" button to save the settings.
7. Click on "OK" to close the "Configure settings" window.
8. Set up the compound plates and reference solutions by clicking on the "Edit Compounds" button.
9. Define compound names, concentrations, and reference solutions (e.g., culture medium). *See* **Note 16**.
10. Double-click on one of the defined plates (e.g., Rack A) to get an overview as displayed in Fig. 6a. *See* **Note 17**.
11. Configure the Incubation System if in use. Parameters are set in the left-hand panel in the "Configure Settings" window (*see* **Note 18**).
12. Start the experiment by clicking the button "Start Measurement." Enter a file name in the pop-up window.

3.5 Compound Addition

1. Prepare the compound at 2× the concentration to be measured.
2. Remove 100 µl of medium per well and add 100 µl of the compound solution using a multichannel pipette. *See* **Note 17**. We typically set up compound plates in 96-well plates at 2× concentration. When the 100 µl mixes with the 100 µl of solution present in the well, the resulting concentration is 1×. In this way, the compound addition is "mix and read."
3. Add a timestamp in the recording by clicking on the "Add Compound" button.
4. Make sure at least some of the wells (3–4 wells) per experiment are used for control (vehicle). *See* Fig. 6 for an example of an experiment using Cor.4U (Axiogenesis AG) on the CardioExcyte 96. Shown is a screenshot of the CardioExcyte Control software in control conditions (Fig. 6b) and in the presence of five different compounds across the plate (Fig. 6c). The compound plate shown in Fig. 6a gives an overview of the compounds and concentrations. Two columns of the plate were used for control solutions (vehicle). In our experiments, only vehicle controls were performed, but positive and negative controls could also be included in the compound plate depending on the experiment and lab practice. Online analysis parameters amplitude and beat rate should be stable for at least 30–45 min before addition of compound. *See* **Note 19** for an estimation of the time required for the experiment and, thus, throughput.

A

	1	2	3	4	5	6	7	8	9	10	11	12
A	control 0.000	E4031 1.000u	E4031 1.000u	Flecainide 30.0u	Flecainide 30.0u	Nifedipine 3.000u	Nifedipine 3.000u	Isoproterenol 5.000u	Isoproterenol 5.000u	CMP1 30.00u	CMP1 30.00u	control + DMSO 0.000
B	control 0.000	E4031 1.000u	E4031 1.000u	Flecainide 30.0u	Flecainide 30.0u	Nifedipine 3.000u	Nifedipine 3.000u	Isoproterenol 5.000u	Isoproterenol 5.000u	CMP1 30.00u	CMP1 30.00u	control + DMSO 0.000
C	control 0.000	E4031 500.0n	E4031 500.0n	Flecainide 15.00u	Flecainide 15.00u	Nifedipine 1.500u	Nifedipine 1.500u	Isoproterenol 2.500u	Isoproterenol 2.500u	CMP1 10.00u	CMP1 10.00u	control + DMSO 0.000
D	control 0.000	E4031 500.0n	E4031 500.0n	Flecainide 15.00u	Flecainide 15.00u	Nifedipine 1.500u	Nifedipine 1.500u	Isoproterenol 2.500u	Isoproterenol 2.500u	CMP1 10.00u	CMP1 10.00u	control + DMSO 0.000
E	control 0.000	E4031 250.0n	E4031 250.0n	Flecainide 7.500u	Flecainide 7.500u	Nifedipine 750.0n	Nifedipine 750.0n	Isoproterenol 1.250u	Isoproterenol 1.250u	CMP1 3.000u	CMP1 3.000u	control + DMSO 0.000
F	control 0.000	E4031 250.0n	E4031 250.0n	Flecainide 7.500u	Flecainide 7.500u	Nifedipine 750.0n	Nifedipine 750.0n	Isoproterenol 1.250u	Isoproterenol 1.250u	CMP1 3.000u	CMP1 3.000u	control + DMSO 0.000
G	control 0.000	E4031 125.0n	E4031 125.0n	Flecainide 3.750u	Flecainide 3.750u	Nifedipine 375.0n	Nifedipine 375.0n	Isoproterenol 625.0n	Isoproterenol 625.0n	CMP1 1.000u	CMP1 1.000u	control + DMSO 0.000
H	control 0.000	E4031 125.0n	E4031 125.0n	Flecainide 3.750u	Flecainide 3.750u	Nifedipine 375.0n	Nifedipine 375.0n	Isoproterenol 625.0n	Isoproterenol 625.0n	CMP1 1.000u	CMP1 1.000u	control + DMSO 0.000

B

C

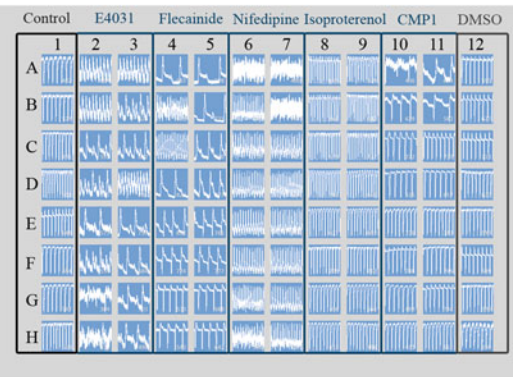

Fig. 6 Screenshot of the CardioExcyte Control software during an experiment using Cor.4U cells (Axiogenesis AG) in impedance mode. (**a**) The compound plate showing compounds and concentrations for panel **C**. (**b**) The impedance signal of the 96 wells in control conditions. (**c**) The impedance signal of the 96 wells after incubation in the five different compounds indicated. Eight wells were used for both media control and vehicle control (DMSO) solutions

3.6 Online Analysis

1. Open a file in CardioExcyte 96 Control and click on "Replay" to show the recorded data.
2. Set a "Reference Sweep" for easy comparison of data (e.g., before and after compound addition). To select a reference sweep, choose "Set Reference Sweep" under the Quality Control tab. The reference sweep is then displayed in red overlaid on the active sweep.
3. Choose the parameters to be analyzed (see Sect. 3.6.1 for a detailed description of online analysis parameters used in the data shown).

4. Online analysis parameters can be plotted against time using the Online Analysis (OA) Post-processing option under the "Extras" tab, i.e., online analysis parameters can be chosen from a list, allowing multiple parameters to be plotted in a single graph. If, during the experiment, a timestamp was added for compound addition, the different compound concentrations will be displayed as different shades of blue (*see* Fig. 7 for time courses of six different cells in response to nifedipine).
5. The data can be visually inspected and single wells selected or deselected to include or exclude them from the calculation. Furthermore, parameters can be normalized (e.g., to reference solution, to certain time points, secondary to primary beats, etc.). It is possible to export the data to a spreadsheet (including standard deviation) or as an image.
6. Mean beat at different concentrations of compound can be visualized (overlaid) and compared. Under the "Extras" tab, choose the "Mean Beat Post-processing" option. The mean beats of a selected sweep are grouped by the respective compound and averaged across all wells with the same compound and concentration. These average mean beats can then be plotted over time.
7. For concentration-response curves, open DataControl 96. Load the file to be analyzed. In the menu tab, click "CRC Results" and then "Start with Dialog." Alternatively, a previously analyzed file can be loaded and reanalyzed.
8. Modify fit parameters as appropriate. The raw data, time plots, and concentration-response curves (calculated using the OA parameter chosen) are shown for all enabled wells. Wells can be enabled or disabled based on visual inspection.
9. The wells are grouped by compound addition, so all wells which received the same compound are grouped together and used to construct the average concentration curve (*see* Fig. 7 for a screenshot of the DataControl 96 software showing the display of data including IC_{50} plots, time courses, and raw data traces for Cor.4U cells in the presence of nifedipine). *See* Fig. 7b for an example of the concentration-response curve for nifedipine on the impedance beat rate of Cor.4U cells. The IC_{50} calculated from the average concentration-response curve shown on the plot was 129 nM; the IC_{50} calculated from the individual IC_{50}s from the six wells was 139 ± 32 nM ($n = 6$) in good agreement with the literature value for nifedipine block of the cardiac voltage-gated calcium channel in guinea pig myocytes [17] using patch clamp electrophysiology. *See* Fig. 7c for an example of the concentration-response curve for E4031 on the impedance beat rate of Pluricytes. The IC_{50} calculated from the average response curve shown on the plot was 12.0 nM ($n = 6$) in good agreement with the literature value for block of hERG expressed in HEK cells [18] or atrial myocytes [19].

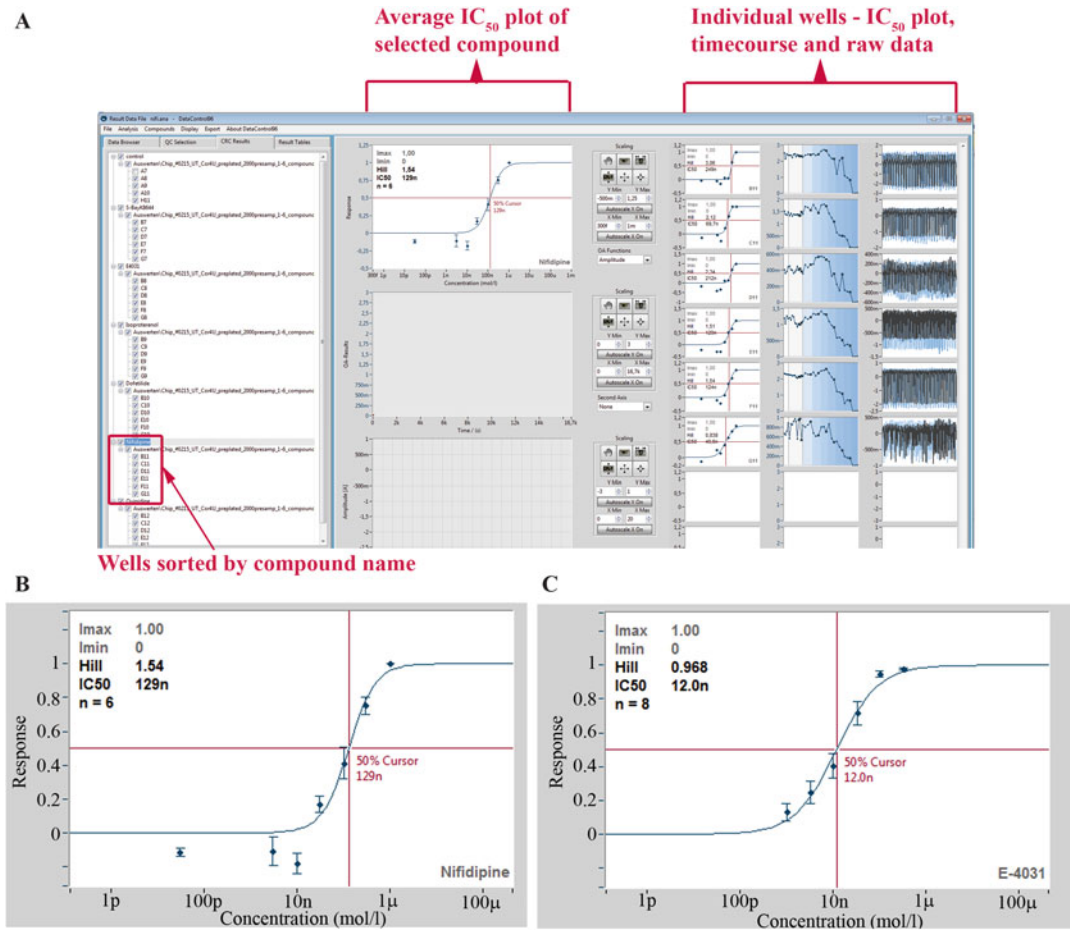

Fig. 7 Concentration-response curve construction and averaging using DataControl 96. (**a**) Screenshot of the DataControl 96 software for analysis of recorded data. Shown is an experiment on one NSP-96 plate using Cor.4U cells. The wells are grouped by compound name; the average concentration-response curve for each compound is displayed by clicking on the name, in this case nifedipine. The raw data traces, time course of the experiment and IC_{50} plot for each individual well are displayed on the right. Upon manual inspection, wells can be included or excluded from the analysis. (**b**) The concentration-response curve of nifedipine on impedance beat rate recorded from Cor.4U cells (Axiogenesis AG) for an average of six wells. The IC_{50} calculated from the average concentration-response curve is shown as 129 nM. The individual IC_{50}s can be exported. The IC_{50} calculated from the average ± S.E.M. of these values was 139 ± 32 nM ($n = 6$) in good agreement with the literature for nifedipine block of guinea pig myocytes [17]. (**c**) The concentration-response curve of E4031 on impedance beat rate recorded from Pluricytes (Pluriomics). The IC_{50} calculated from the average concentration-response curve was 12.0 nM in good agreement with the literature of E4031 block of hERG expressed in HEK cells [18] or atrial myocytes [19] using patch clamp electrophysiology

3.6.1 Online Analysis Parameters for Impedance and EFP

A detailed description of the online analysis parameters for impedance and EFP using the CardioExcyte 96 can be found in Doerr et al. [12]. An explanation of the online analysis parameters that were most commonly used for the data provided in this chapter is given below.

1. Mean beat (impedance and EFP)
   To generate a mean beat, the sweep is cut into sections of the same length, each section containing one beat. The sectioning occurs by detecting the peaks, then adding a pre-peak and a post-peak time window. These windows are automatically determined for each sweep. The sections are then aligned by peak time on the *x*-axis and by troughs on the *y*-axis. After alignment, a mean beat and its standard deviation are calculated and plotted (*see* Fig. 8a, c for an example of a mean beat in impedance and EFP modes, respectively).
2. Amplitude (impedance and EFP)
   Amplitude denotes the mean of the detected amplitudes as determined by peak-to-trough difference (*see* Fig. 8).
3. Beat rate (impedance and EFP)
   The inter-spike intervals (ISI, based on peak times) are averaged, and the reciprocal is calculated to determine beats per minute (*see* Fig. 8b, d).
4. Pulse width (impedance only)
   The parameter pulse width (10–90 %) is determined as the width of the mean beat in impedance mode at the amplitude level chosen by the percentile indicator. It indicates

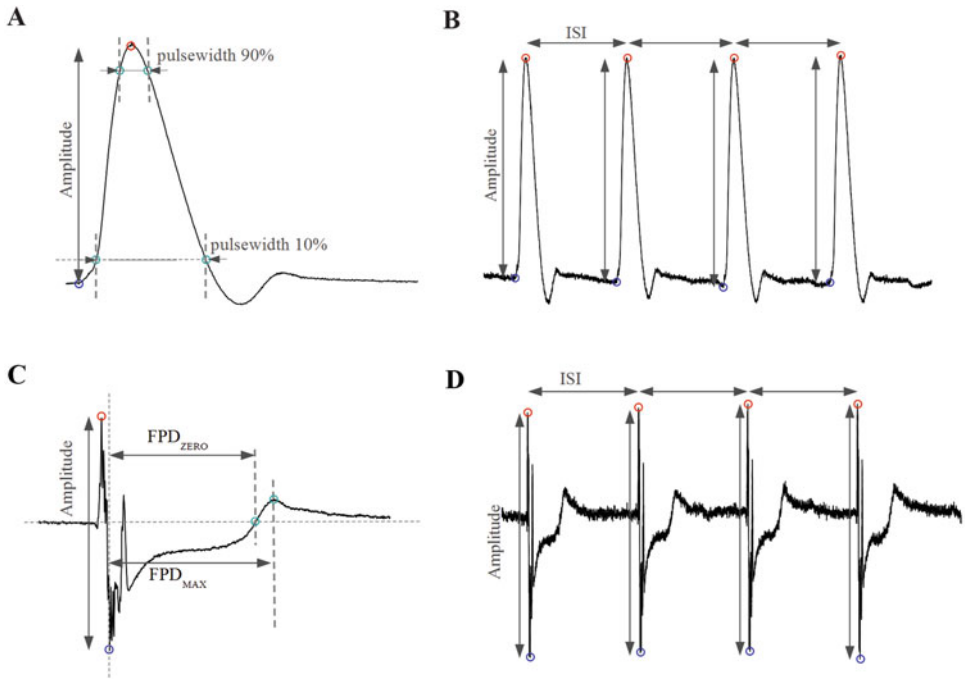

Fig. 8 Online analysis parameters available in CardioExcyte Control. An example of a mean beat in impedance mode (**a**) showing amplitude, pulse width 10 % and pulse width 90 %, and in EFP mode (**c**) showing amplitude, FPD_{ZERO} and FPD_{MAX}. An example of a recording in impedance mode (**b**) and EFP mode (**d**) showing amplitude and inter-spike interval (ISI) for calculation of beat rate

the duration of contraction. The accuracy of the pulse width is positively correlated with a low variance of the mean beat (*see* Fig. 8a).

5. Field potential duration (EFP only)
   The field potential duration (FPD) in EFP mode reflects the length of the action potential.
   The FPD is based on detecting the slow positive deflection after the initial fast deflection of the mean EFP (*see* Fig. 8c).

There are two different detection methods available:

(a) The FPD_{ZERO} is calculated as the time between the first negative deflection (blue circle) and the zero crossing of the repolarization curve (first green circle) (*see* Fig. 8c).

(b) The FPD_{MAX} is calculated as the time between the first negative deflection and the maximum of the repolarization curve (second green circle) (*see* Fig. 8c).

If the positive deflection of the repolarization is not very pronounced, FPD_{ZERO} can provide more reliable results.

If the FPD is taken as a measure for the QT interval, it can be corrected for beat rate-related changes using Fridericia's formula:

$$FPDc[ms] = \frac{FPD[ms]}{\sqrt[3]{ISI[s]}}$$

4 Notes

1. Nifedipine is light sensitive and should be stored in a vessel which protects it from light.
2. It is very important that work on the CardioExcyte 96 is carried out aseptically, all solutions should be kept sterile, and compound additions should be made within a biosafety cabinet. Experiments are performed over several days and bacterial or fungal contamination would be detrimental to the experiment.
3. In our experience fibronectin coating provides the best results, while gelatine, Geltrex©, or Matrigel© may impair the recorded signal quality.
4. Fibronectin should be pipetted very gently as it is sensitive to shear stress. Additionally, fibronectin in the wells should not be allowed to dry out at any point.
5. Partial use of the sensor plates (column by column) is possible and supported by the CardioExcyte 96 software. In this case, coat only the number of columns which will be used for the experiment. The unused columns can be used in

later experiments. To reduce the noise level, fill unused wells with PBS solution.

6. The use of a 50 ml centrifuge tube facilitates mixing of cells with plating/thawing media to minimize osmotic shock and increase cardiomyocyte viability. Precise timing is critical for maximizing viable cell recovery; the cells should not spend more than a few minutes thawed in the vial before adding plating media. Avoid repeated pipetting of the thawed hiPSC-CM cell suspension as this will adversely impact cell viability.
7. When seeding 3D clusters, e.g., hES-CMC™ (Cellectis), in our experience, placement of the cluster appears to be very important. For best results, the cluster should be placed directly on top of the sensing electrode using a single-channel pipette.
8. The CardioExcyte 96 takes about 2–3 h to warm up to 37 °C, so the instrument should be placed inside the incubator at least 2 h before fibronectin coating of the NSP-96.
9. The Incubation System consists of three parts, the Chamber which is heated, the Supply Unit, and the Ibidi Gas Mixer. The Chamber is connected to the Gas Mixer. This Gas Mixer provides the required atmosphere for the cells (5% CO_2 and desired humidity). The Chamber fits on top of the CardioExcyte 96 and contains the NSP-96 plate during recordings. If the Incubation System is used, the CardioExcyte 96 can be used on the benchtop and no longer needs to be in an incubator thus reducing the footprint. Recommended settings for the Incubation System are Lid = 40 °C and Chip = 36.5 °C.
10. To complete the solution exchanges as quickly as possible, use an 8-well multichannel pipette. This will minimize temperature-induced artifacts in the beat pattern.
11. To minimize temperature effects, use the Incubation System for the CardioExcyte 96 (*see* **Note 9**). Use the "Add Compound" dialog in the CardioExcyte 96 software to create a timestamp for every medium exchange.
12. The medium is completely removed and 200 µl added to ensure that exactly 200 µl solution is in each well at the start of the experiment, since solution can be lost over time due to evaporation.
13. In order to exchange the media and solutions, either the NSP-96 must be removed from the CardioExcyte 96 using the hand lever and placed in the laminar flow culture hood, or the whole CardioExcyte 96 must be removed from the incubator and placed in the laminar flow culture hood. The latter will reduce temperature artifacts. In order to minimize temperature artifacts, use the Incubation System for the CardioExcyte 96.

14. A sweep interval of 30 s is recommended for combined mode. If the sweep interval is too short and the beat rate low, the mean beat calculated may not be representative as not enough beats would be included in the analysis. For accurate results, as many beats as possible should be included. If the sweep interval is longer than 30 s, compound effects may occur during this time and valuable data not recorded. For the repetition interval, at least 3 min is recommended for combined mode as the system heats up if a shorter repetition interval is used. If a longer experiment time than 60 min is required, we recommend a repetition interval of 3 min for the first 60 min and then a repetition interval of 10 min after that.
15. In the "Pacemaker" tab, the stimulus parameters for pacing of the cells can be defined (if required). This feature is optional and was not used in the experiments shown in this chapter. If the box "Electrical stimulation active" is ticked, cells will be paced before (pre-stim time) and during each measurement. No stimulus is applied to the cells between sweeps. The Pacemaker option is only available in impedance mode.
16. It is mandatory to define a reference solution (Content Type "Reference") for calculating a concentration-response curve.
17. The compound is prepared at a 2× concentration. The solution is then diluted 1:2 in the well (100 µl remains in the well and 100 µl compound is added, thus giving a final concentration of 1×). In the compound table, the final concentration within the well is added by the user. Alternatively, a 10× concentrated stock solution could be prepared, and a medium exchange performed by removing all of the media and replacing it with 90 µl fresh media. 10 µl of the 10× compound stock is then added. The final concentration must be written in the table by the user.
18. Compounds can be added, deleted, or modified in the compound layout at any time before and during application, but not after they have been applied.
19. The timescale of a typical experiment includes 2–3 h for setup of the experiment (assuming prior formation of the synchronously beating monolayer), i.e., prewarming medium and performing a medium exchange 2 h prior to compound addition, taking control recordings, dilution of compounds, and setting up compounds in desired vessel, e.g., 96-well plate, setting up the compound plate in CardioExcyte Control; 3–4 h for testing compounds, one compound plate usually contains 5–10 compounds and analysis takes approximately 1–2 h depending on the number of parameters included. Therefore it is reasonable to assume that 5–10 compounds can be tested in an 8 h day.

5 Future Prospects

The CiPA initiative is a new paradigm which has arisen due to a need for more complete safety assessment of potential drug candidates [20, 21]. Stem cell-derived cardiomyocytes such as hiPSC-CMs are an attractive model for safety testing because of their recapitulation of native behavior, ease of use, and availability. However, if meaningful results are to be obtained, such models must be well characterized in terms of their ion channel expression profiles, using techniques such as patch clamp electrophysiology (*see* Chaps. 3 and 4 for methods for manual and automated patch clamp, respectively) and MEA (*see* Chap. 5. Additionally, novel technologies such as impedance are being evaluated as complementary tools to gain a more complete safety profile of a potential drug. As part of the CiPA initiative, manufacturers of impedance, MEA, and automated patch clamp instrumentation are working together with stem cell-derived cardiomyoycte providers to characterize the cells, standardize protocols, and validate technology. Impedance provides complementary information to MEA and patch clamp data about cardiac cell beat parameters and arrhythmia and will likely gain increasing attention as an alternative technology in safety screening.

Acknowledgments

We thank Cellular Dynamics International (CDI), Madison, Wisconsin, for the collaboration and for providing us with cardiomyocytes (iCell cardiomyocytes). We also thank Axiogenesis AG, Cologne, Germany, for the collaboration and for providing us with cardiomyocytes (Cor.4U). We also thank Pluriomics for the collaboration and for providing us with the Pluricytes.
The authors disclose receipt of the following financial support for the research, authorship, and/or publication of this article: The work presented here was funded in part by the Bayerische Forschungsstiftung (BayFor, Grant AZ-1036-12) and by the Bundesministerium für Bildung und Forschung (BMBF, Grant 01QE1502).

References

1. Connolly P, Clark P, Curtis ASG et al (1990) An extracellular microelectrode array for monitoring electrogenic cells in culture. Biosens Bioelectron 5:223–234. doi:10.1016/0956-5663(90)80011-2
2. Thomas C Jr, Springer P, Loeb G et al (1972) A miniature microelectrode array to monitor the bioelectric activity of cultured cells. Exp Cell Res 74:61–66. doi:10.1016/0014-4827(72)90481-8
3. Gross GW, Williams AN, Lucas JH (1982) Recording of spontaneous activity with photoetched microelectrode surfaces from mouse spinal neurons in culture. J Neurosci Methods 5:13–22. doi:10.1016/0165-0270(82)90046-2

4. Borkholder DA, Bao J, Maluf NI et al (1997) Microelectrode arrays for stimulation of neural slice preparations. J Neurosci Methods 77:61–66. doi:10.1016/S0165-0270(97)00112-X
5. Regehr WG, Pine J, Cohan CS et al (1989) Sealing cultured invertebrate neurons to embedded dish electrodes facilitates long-term stimulation and recording. J Neurosci Methods 30:91–106
6. Spira ME, Hai A (2013) Multi-electrode array technologies for neuroscience and cardiology. Nat Nanotechnol 8:83–94. doi:10.1038/nnano.2012.265
7. Harris K, Aylott M, Cui Y et al (2013) Comparison of electrophysiological data from human-induced pluripotent stem cell-derived cardiomyocytes to functional preclinical safety assays. Toxicol Sci 134:412–426. doi:10.1093/toxsci/kft113
8. Clements M, Thomas N (2014) High-throughput multi-parameter profiling of electrophysiological drug effects in human embryonic stem cell derived cardiomyocytes using multi-electrode arrays. Toxicol Sci 140:445–461. doi:10.1093/toxsci/kfu084
9. Clements M, Millar V, Williams A, Kalinka S (2015) Bridging functional and structural cardiotoxicity assays using human embryonic stem-cell derived cardiomyocytes for a more comprehensive risk assessment. Toxicol Sci 148:241–260. doi:10.1093/toxsci/kfv180
10. Xi B, Wang T, Li N et al (2011) Functional cardiotoxicity profiling and screening using the xCELLigence RTCA cardio system. J Lab Autom 16:415–421. doi:10.1016/j.jala.2011.09.002
11. Guo L, Abrams R, Babiarz JE et al (2011) Estimating the risk of drug-induced proarrhythmia using human induced pluripotent stem cell derived cardiomyocytes. Toxicol Sci 123:281–289. doi:10.1093/toxsci/kfr158
12. Doerr L, Thomas U, Guinot DR et al (2015) New easy-to-use hybrid system for extracellular potential and impedance recordings. J Lab Autom 20:175–188. doi:10.1177/2211068214562832
13. Abassi YA, Xi B, Li N et al (2012) Dynamic monitoring of beating periodicity of stem cell-derived cardiomyocytes as a predictive tool for preclinical safety assessment. Br J Pharmacol 165:1424–1441. doi:10.1111/j.1476-5381.2011.01623.x
14. Peters MF, Lamore SD, Guo L et al (2014) Human stem cell-derived cardiomyocytes in cellular impedance assays: bringing cardiotoxicity screening to the front line. Cardiovasc Toxicol 15:127–139. doi:10.1007/s12012-014-9268-9
15. Lamore SD, Scott CW, Peters MF (2015) Cardiomyocyte Impedance Assays. In: Assay Guidance Manual [Internet]. (Sittampalam GS, Coussens NP, Nelson H, Arkin M, Auld D, Austin C, Bejcek B, Glicksman M, Inglese J, Iversen PW, Li Z, McGee J, McManus O, Minor L, Napper A, Peltier JM, Riss T, Trask OJ Jr., Weidner J. Eds). Bethesda (MD): Eli Lilly & Company and the National Center for Advancing Translational Sciences; 2004–2015 Feb 25
16. Chan Y-C, Ting S, Lee Y-K et al (2013) Electrical stimulation promotes maturation of cardiomyocytes derived from human embryonic stem cells. J Cardiovasc Transl Res 6:989–999. doi:10.1007/s12265-013-9510-z
17. Shen JB, Jiang B, Pappano AJ (2000) Comparison of L-type calcium channel blockade by nifedipine and/or cadmium in guinea pig ventricular myocytes. J Pharmacol Exp Ther 294:562–570
18. Zhou Z, Gong Q, Ye B et al (1998) Properties of HERG channels stably expressed in HEK 293 cells studied at physiological temperature. Biophys J 74:230–241. doi:10.1016/S0006-3495(98)77782-3
19. Liu S, Rasmusson RL, Campbell DL et al (1996) Activation and inactivation kinetics of an E-4031-sensitive current from single ferret atrial myocytes. Biophys J 70:2704–2715. doi:10.1016/S0006-3495(96)79840-5
20. Sager PT, Gintant G, Turner JR et al (2014) Rechanneling the cardiac proarrhythmia safety paradigm: a meeting report from the Cardiac Safety Research Consortium. Am Heart J 167:292–300. doi:10.1016/j.ahj.2013.11.004
21. Fermini B, Hancox JC, Abi-Gerges N et al (2015) A new perspective in the field of cardiac safety testing through the comprehensive in vitro proarrhythmia assay paradigm. J Biomol Screen. doi:10.1177/1087057115594589

Chapter 11

Edge-Detection for Contractility Measurements with Cardiac Spheroids

Christian Zuppinger

Abstract

There is a growing appreciation of the requirement for a more physiological culture environment for in vitro research and toxicology testing. In the field of cardiovascular research, 3D cultures are often developed for regenerative medicine. However, recent innovations in 3D culture production and higher-throughput analysis methods, as well as the availability of human induced pluripotent stem cell-derived cardiomyocytes (hiPSC) with disease-specific genotypes, have opened new possibilities for toxicological studies in vitro. Spheroid contractility and other parameters of cardiac physiology can be measured using a variety of methods. We have adapted a label-free, video-based method originally used for primary rodent cardiomyocytes and used it with a model of 3D co-culture of hiPSC-derived cardiomyocytes and cardiac fibroblasts for the evaluation and development of new therapies and detection of cardiotoxicity.

Key words 3D culture, Spheroid, Cardiotoxicity, Contraction, Beating, Shortening, Image processing, Video analysis, hiPSC, Cardiomyocytes, Heart, Scaffold-free, Immunofluorescence

1 Introduction

1.1 Cardiomyocyte In Vitro Models

Ventricular cardiac muscle cells, the cardiomyocytes (not to be confused with smooth muscle myocytes of the arterial wall or myoblasts of skeletal muscle), are the working muscle cells of the heart that relentlessly maintain the body's circulation during a lifetime. Their high metabolic activity and low ischemic tolerance, sensitivity to changes in extracellular calcium, refractoriness to DNA transfection, and limited lifespan in culture, notably without proliferation, make these cells a demanding in vitro model system. Nevertheless, primary cardiomyocytes have been isolated from adult, fetal, and neonatal animals, and sometimes from patient tissue samples, for many different research applications. The cells are

Electronic supplementary material: The online version of this chapter (doi:10.1007/978-1-4939-6661-5_11) contains supplementary material, which is available to authorized users.

Mike Clements and Liz Roquemore (eds.), *Stem Cell-Derived Models in Toxicology*, Methods in Pharmacology and Toxicology,
DOI 10.1007/978-1-4939-6661-5_11,

either used fresh within a few hours after isolation, often for cell physiology and electrophysiology investigations [1, 2], or kept longer in culture for a variety of applications, for instance, the characterization of transgenic mouse models, research on the function of signaling pathways, developmental biology, or cardiotoxicity mechanisms [3–5]. However, limited availability of human primary cardiomyocytes has impeded widespread use of this approach. This issue is compounded by the lack of alternative immortalized cell lines with characteristics comparable to primary human cardiomyocytes. The technology of reprogramming somatic cells into induced pluripotent stem cells (hiPSC), which theoretically allows the production of human cardiomyocytes and other cardiovascular cell types in unlimited amounts, has become more popular as an alternative to primary rodent cells for disease modeling and toxicology [6]. Therefore, cardiomyocytes derived from human embryonic stem cells (hESC) and hiPSC are currently viewed as promising tools in pharmacological development, satisfying the need for both scalability and physiological relevance [7, 8]. Furthermore, in vitro studies are now possible with hiPSC-derived cardiomyocytes from patients with specific genotypes, and sometimes with access to their entire medical history. In our lab, we have used commercially available, hiPSC-derived cardiomyocytes to produce and analyze spheroid 3D cultures [9].

1.2 Currently Used 3D Cell Culture Systems with Cardiac Cells

Many innovative 3D cell culture models have been developed in recent years. What is common to all of them is that they attempt to replicate some aspects of native tissue organization and functionality more faithfully than analogous 2D culture models. Most cell types rapidly de-differentiate after isolation from the tissue, particularly when maintained in 2D culture formats. The sudden loss of a multitude of stimuli and cell–cell interactions has profound effects on the cells as they adapt to the new environment. This process becomes evident in cells by the formation of long actin stress fibers, motile activity, and rapid cell proliferation. These cells often show enhanced protein synthesis and degradation, and start to re-express genes from an earlier developmental phase. A typical example of such changes induced by culturing is the cardiac fibroblast. The process of fibroblast activation and transition to a myofibroblastic phenotype has been investigated in detail and was shown to be dependent on substrate stiffness and presence of inflammatory cytokines [10]. Similar differences have been observed in cells isolated from liver, pancreas, and kidney, where highly differentiated tissues and specialized cells exist that lose most of their functionality in standard 2D culture. 3D models have only recently been adopted for toxicology studies that aim to investigate more organ-specific cardiac parameters [11, 12].

Currently, the most commonly used 3D cell culture systems can be grouped into three categories: (1) models that use soft hydrogels where the cells reside within a gel matrix, filled in

multi-well plates or molded into a certain shape and made of matrigel, fibrin, collagen, or synthetic materials; (2) models that use pre-fabricated scaffolds where the cells grow on surfaces or within cavities of sponges, in foam-like filter inserts or de-cellularized tissues; and (3) models that use cellular self-organization without scaffold materials where the cells assemble to microtissues, clusters, aggregates, spheroids, or cell sheets. Additionally, cardiac microtissues have been integrated on larger technological platforms such as in miniaturized incubators ("organs-on-chip") as part of microfluidic systems, or served as building blocks for larger structures, for example, with bioprinting [13–15]. One of the most-studied 3D model systems in the field of cardiac tissue engineering is the so-called engineered heart tissue (EHT). Variants of this model are currently used by several groups for tissue replacement strategies (for review, see [16]), and smaller strip-formats have been used for drug testing [17]. The history of 3D culture as a technological concept and the use of cardiovascular cell types in such culture formats have been discussed elsewhere [18]. 3D cultures in the cardiovascular field have often been created for tissue replacement strategies. Therefore, many of those systems like collagen sponges, molded hydrogels, or cell sheets consist of relatively large tissues that can be manually handled and used for surgical implantation. However, large tissues need a considerable amount of cells and biomaterial resources.

In contrast to culture formats intended for tissue replacement applications, a drug-screening model using 3D in vitro technologies preferably contains smaller tissues allowing rapid diffusion of metabolites and test substances. There should be no interference with scaffold materials by forming a barrier, releasing undefined factors or adsorbing test substances. Such a system does not require a large number of costly cells, which is an important factor when primary cells or stem cell-derived cells are to be used. Furthermore, the microtissues should be of a uniform size that permits repetitions or replicates in the same experimental series. Ideally, multiple microtissues should be arranged or integrated in incubators such that they can be produced, treated, and analyzed by automatic devices. Spheroids—also called multicellular aggregates, organoids, organospheres, or microtissues—have been used for decades in cancer and stem cell research [19, 20]. Several production methods are available: in spinner flasks and rotation systems where aggregates form in non-uniform sizes, by the hanging drop method (gravity-assisted self-assembly), in microfluidic systems, in soft agar, and on non-adhesive surfaces such as coated multi-well plates or agarose micro-molds [21–24]. Cardiac spheroids show spontaneous contraction activity, and the resulting motion can be used to assess the viability of the spheroid, as well as cardiotoxic and pro-arrhythmic drug effects [9, 21, 24]. Equipment and methods have been developed in recent years to produce and analyze spheroids in

an automatic way [25], and complete systems for the automatic measurement of cardiac physiology in vitro have become commercially available.

1.3 Co-cultures

Co-cultures of several cell types may appear at first to be a less favorable option, since the effects of drugs and the results of biochemical assays are more difficult to relate to a single cell type. However, if the goal is to create more complex in vitro cultures with greater similarity to living tissue, especially with mature organotypic features, the inclusion of multiple cell types is unavoidable. Interesting data in this context has been published recently in the field of liver in vitro models. Multi-cell type 3D liver spheroids showed improved differentiation and extended stability in culture due to better cell polarization, which is required to maintain liver-specific functionality and cell–cell interactions [26]. In in vitro models comprising single or co-cultured liver and immune cells, troglitazone caused higher cytotoxicity when both cell types were present, than when single cultures of either cell type were used [27]. In a kidney 3D culture model, stromal cells supported epithelial morphogenesis, including improved preservation of the differentiation state and cell polarization of proximal tubule cells [28]. In the myocardium, cardiomyocytes and also endothelial cells, smooth muscle cells, fibroblasts, stem cells, and other cell types play an essential role in heart development, normal function of the organ, maintenance, and repair [29]. In contrast to standard 2D culture, the tissue-like conditions in 3D microtissues do not lead to overgrowth and suppression of co-cultured cell types [21, 23]. Therefore, 3D co-culture allows the interaction of cells showing a different proliferation potential to be studied in vitro, such as terminally differentiated cardiomyocytes and cardiac fibroblasts, that would rapidly overgrow other cell types in standard culture. In the last two decades, cardiac fibroblasts have been recognized as cells that actively contribute to the pathophysiology of adverse remodeling and electrical propagation in the myocardium [30–32]. New therapies targeted at these biological questions and pathologies could be tested in a tissue-like culture model. Another option in 3D culture is co-culture with endothelial cells that produce VEGF, which might improve vasculogenesis in the artificial tissue and facilitate the connection to the host vasculature after implantation, or serve as a model to test anti-angiogenic cancer therapies [33, 34]. By working with cell fractions of different purity after primary cell isolation, single- and co-cultures can be produced with cells from the same organ [35]. Ideally, pure cell populations are used as starting material for the co-culture so that a known ratio of different cell types is present. Recent progress in the maturation and selection of iPSC-derived cardiomyocytes make it possible to obtain pure cardiomyocyte populations to be used in single- or co-cultures [36], and many detailed protocols for working with hiPSC-derived cell types have been published in recent

years [37]. Culture conditions in co-cultures are not always straightforward, and optimization of culture media is needed to suit both or several cell types.

2 Video-Based Measurement of Cardiomyocyte Contractility In Vitro

Informative non-invasive and label-free methods are much sought after to complement the well-established electrophysiological and fluorescence imaging techniques [38]. Conceivable advantages of video-based measurement of contractility include the possibility to collect long-term observations of multiple cells and the relatively low consumables costs (no need for electrode-plates, lasers, and fluorescent dyes). The term "video-based" is generally used here for the analysis and optional recording of time-sequences of microscopy images using white light, whereby all contemporary digital systems offer much higher resolution and/or frame rates than the original television standards. A movie showing a variety of cardiac models that are currently in use to assess cardiac contractility is available in the electronic supplemental material (Movie 1).

2.1 Freshly Isolated Cardiomyocytes from Adult Mammals

Freshly isolated cardiomyocytes from adult mammals do not contract spontaneously, but can be paced by electrical field stimulation. These cells are commonly used immediately after isolation, but can also be kept in culture for several days, although with deteriorating response to field stimulation and cell function [39]. The morphology of these cells is marked by the slender rod-shaped form and the periodicity of sarcomeric striation, which is clearly visible in brightfield and phase contrast microscopy (*see* Figs. 1a and 2a, b). The measured kinetic parameters of shortening provide valuable information on basic cardiac mechanisms, pathologic changes in those hearts that served as the cell source, or effects of modulators of excitation–contraction coupling and other test substances. Unfortunately, the observed shortening cannot be directly related to crossbridge function, and therefore the absolute force developed during contraction is unknown in externally unloaded cells. Optical measurements on isolated cardiomyocytes and muscle strips were performed early in the history of video microscopy. Pioneering studies by Steadman et al. in 1988 used a diode array [40, 41]. Later, video digitization, faster computation, and CCD-cameras helped to obtain more precise and real-time measurements of shortening, by edge-detection on contrast-enhanced images, and sarcomere length by analysis of the sarcomeric striation pattern within a region of interest (Fig. 2a, b). Measurement of sarcomere shortening can be combined with simultaneous measurement of fluorescent signals from calcium-sensitive dyes such as fura-2, while the cells are kept in heated perfusion chambers [2]. Once the data have been recorded, analysis software enables the

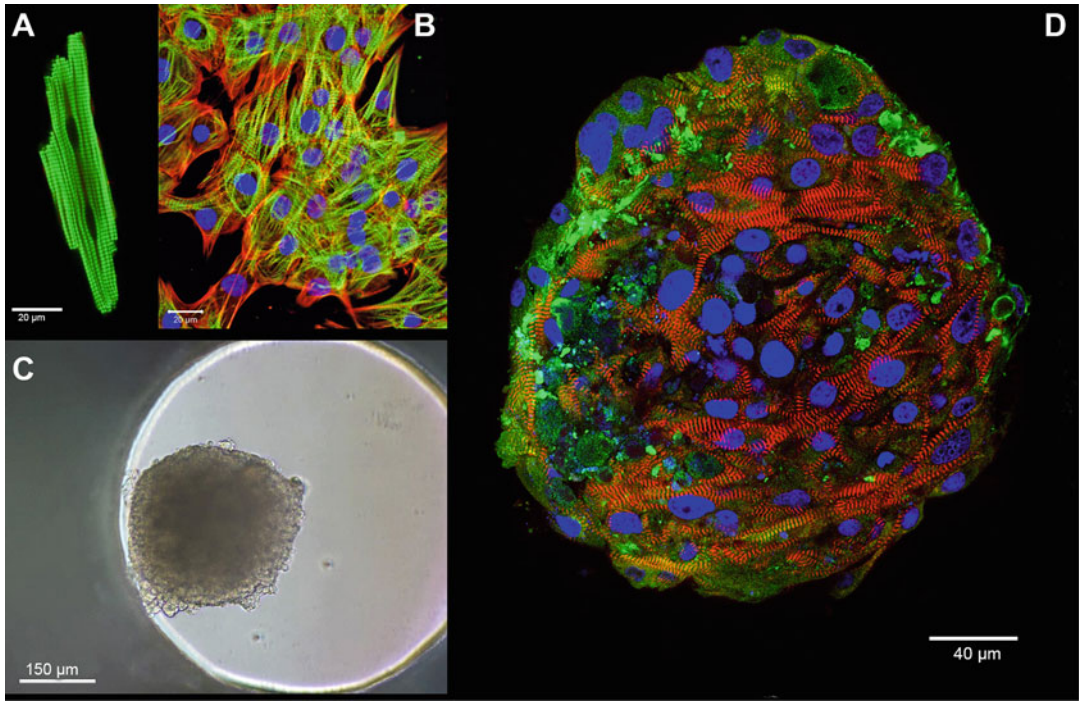

Fig. 1 Different types of cardiac muscle cells and culture formats. (**a**) A freshly isolated adult rat ventricular cardiomyocyte was fixed, immunostained for cardiac troponin-T (*green*), and imaged by confocal microscopy. (**b**) hiPSC-derived cardiomyocytes were purchased from Axol Biosciences (Cambridgeshire, UK) and cultured for 2 weeks before fixation and immunostaining for myosin heavy chain (*green*), all actin (*red*), and DNA (*blue*). (**c**) A spheroid microtissue made of hiPSC-derived cardiomyocytes after harvesting from hanging drops cultured in a multi-well plate "GravityTrap" (InSphero AG, Schlieren, Switzerland). (**d**) A microtissue made of human umbilical vein endothelial cells (Zen-Bio Inc., Durham, USA) and hiPSC-derived cardiomyocytes (Cellular Dynamics Intl., Madison, USA) was cultured for 3 weeks, then fixed and immunostained for von Willebrand factor (*green*), sarcomeric protein myomesin (*red*), and DNA (*blue*); a single image was then recorded by confocal microscopy

extraction of numerous kinetic and basic parameters of cellular contraction. These data can in turn be used to probe compound-induced changes to numerous cellular mechanisms (e.g., myofibril responsiveness, calcium handling proteins, and ion channels).

Fig. 2 (continued) of the frequency that has been derived from the signal (striation treated as a wave) making use of the mathematical method "fast Fourier transformation." (**b**) The video image of a cardiomyocyte is set to a hard contrast and the two cursors for edge-detection are placed at the opposite ends of the cell where they follow the motion of the edges during shortening. (**c**) The edge-detection method is used to capture beating of a cardiac microtissue. The *red curve below* shows the change of pixel values at the edges. (**d**) The *red marker* follows the sharp contrast at the edge of the beating spheroid at higher magnification using a 40× lens. (**e**) Typical shortening traces of an electrically paced, freshly isolated adult rat cardiomyocyte. (**f**) Typical shortening traces of a spontaneously contracting cardiac microtissue made of hiPSC-derived cardiomyocytes

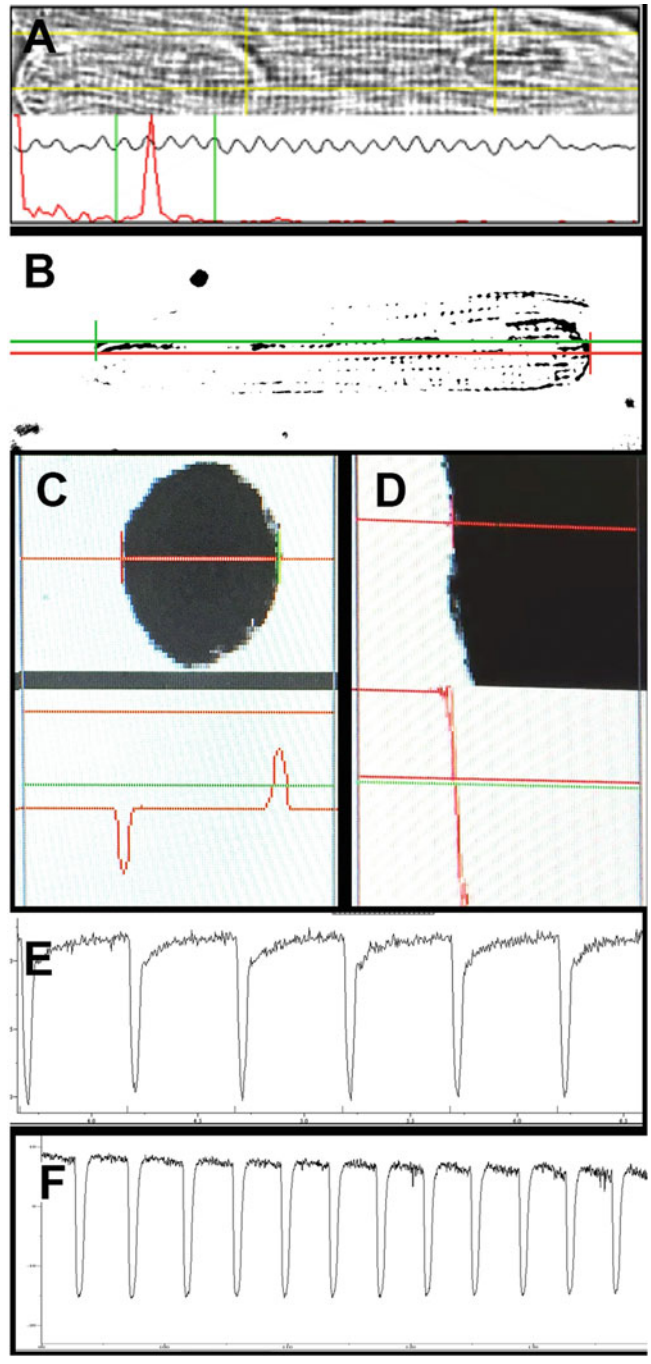

Fig. 2 Video-based methods for measuring the electrically paced shortening of freshly isolated adult rat cardiomyocytes (**a**, **b**, **e**), or spontaneously contracting spheroids made of human iPSC-derived cardiomyocytes (**c**, **d**, **f**). Screenshots were captured from the display of a contractility system for isolated myocytes purchased from IonOptix (Milton, MA, USA). Objects are not shown at the same scale (please refer to Fig. 1). (**a**) The video image of a single cardiomyocyte is centered in the capture window and a region of interest (ROI) is manually chosen. The graph below shows the periodicity of the sarcomeric striation inside the ROI and in *red* the peak

2.2 3D Cultures

Video edge-detection of unidirectional motion is not restricted to rod-shaped cardiomyocytes and can be used for contracting embryoid bodies, cardiac explant cultures, or 3D cultures [9, 42, 43]. The considerable thickness of 3D-cultured microtissues creates a strong contrast in light microscopy, so that methods such as real-time video edge-detection can be used also for spheroids made of immature primary or stem cell-derived cardiomyocytes (Fig. 2c, d). Figure 3 shows spontaneous contractions of cardiac microtissues exposed to different drugs and temperature conditions using the edge-detection module of the IonOptix software. Microtissues responded to the stimulation of beta-adrenergic receptors by isoproterenol (Fig. 3a). The spontaneous activity was rapidly inhibited by the myosin uncoupler blebbistatin (Fig. 3b), and the regular beating pattern was disrupted by the cardiotoxic cancer drug doxorubicin (Fig. 3c). Temperature alone had a significant impact on the rate of spontaneous contractions in these spheroids (Fig. 3d). A drawback of the measurement of clusters and entire tissues with edge-detection is that the visible displacement of the surface is often not concentric (showing regional heterogeneity) and may depend on several unknown factors related to tissue composition and cell–cell

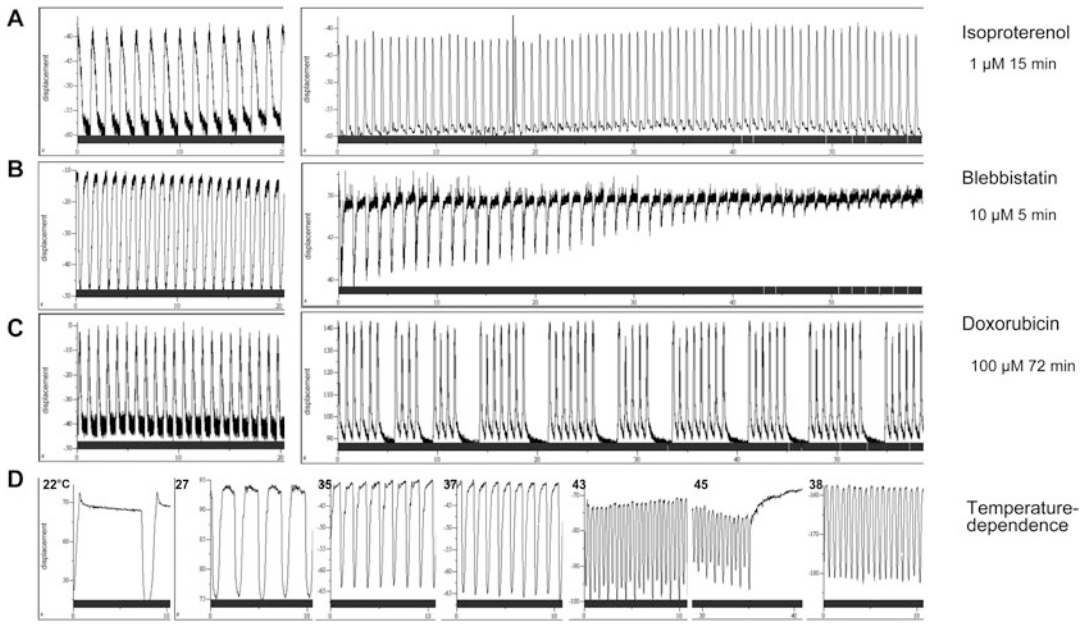

Fig. 3 Cardiac microtissues made of hiPSC-derived cardiomyocytes (Cellular Dynamics, Madison, USA) were used to validate edge-detection of spontaneous contractions. (**a**–**c**): Cultures were allowed to adapt to 37 °C and then an initial sequence of 60 s before and several sequences after the addition of a drug were recorded. Drug name, dose, and time-point after addition are indicated on the right. Representative traces are shown. (**d**) Microtissues were kept in the cold, then the bath temperature was steadily increased within 1 h while recordings were taken. Figure is adapted from our previous publication [9]

coupling. Also, rotational and out-of-focus movement of loosely or non-attached structures is not properly detected and may lead to errors. Nevertheless, even if only a part of the microtissue is captured by the measurement and the signal is not of the highest quality, progressive action of drugs on contractile function can be revealed over a timecourse, for example, as shown in response to the inhibitor of myosin II ATPase activity blebbistatin (Fig. 3b). In a recent paper, we have also shown a rapid response of fluo-4 calcium signals to external stimuli such as rapid switching to a caffeine-containing or calcium-free buffer in these cardiac microtissues [9].

2.3 Cardiomyocytes from Fetal or Newborn Animals and Stem Cell-Derived Cardiomyocytes

In contrast to freshly isolated rod-shaped primary cardiomyocytes, serum-containing cultures of adult cardiomyocytes, stem cell-derived, and primary fetal or neonatal cardiomyocytes form a monolayer of isotropically distributed, sometimes overlapping polygonal cells in standard cell culture (Fig. 1b). Only in optimal conditions, can sarcomeric periodicity be sporadically observed in monolayer cells by phase contrast microscopy. This option has been used in our lab to measure contractions simultaneously with Fura-2 calcium signals in long-term cultures of adult rat cardiomyocytes treated with cardiotoxic cancer therapies using the "SarcLen" software module by IonOptix LLC (Milton, MA, USA) (Fig. 2a) [3]. Edge-detection can be used in monolayer cultures making use of contrasting features such as nuclei or beads on the surface of the cells, but this motion is difficult to directly relate to the myofibrillar contraction–relaxation cycle. Instead of video, label-based methods (calcium and voltage sensitive, fluorescent dyes, and reporters) and culture on electrode arrays for the measurements of electric activity or impedance have been used. Impedance measurement of contractility has been used not only for 2D cell layers but also for cardiac 3D cultures and there are several commercial solutions available [12, 44]. With the advent of relatively inexpensive capture and storage options for digital high-speed video, optical assessment of contractile activity has become more attractive, even for very long observation times in devices offering a complete incubator environment and motorized stage. Some new or adapted techniques have been tested at the laboratory scale and some have already become commercially available such as SONY's SI8000 motion imaging system [38, 45, 46]. Methods based on motion vectors, as described here for monolayer cultures, can also be applied to 3D spheroid cultures (personal communication Dr. Tomohiro Hayakawa).

3 Production of a 3D Co-culture and Contractility Measurement Using Video Edge-Detection

3.1 Material

1. InSphero (Schlieren, CH) spheroid production platform consisting of the GravityPLUS™ Hanging Drop System and 96-well GravityTRAP™ ultra low-adhesion plates with conical wells, now exclusively available from PerkinElmer (10× pack catalog no ISP-06-001)
2. Myocyte contractility system from IonOptix LLC (Milton, MA, USA) includes hardware (Myocam™) and software components. This equipment is often used with an electrical pacing system. The method shown here does not use electrical field pacing or a flow-chamber, since the spheroids made of hiPSC-derived cardiomyocytes contract spontaneously in contrast to freshly isolated primary rod-shaped cardiomyocytes
3. Inverted research microscope (several vendors), with 10×–40× lenses and camera ports with optional heating chamber for cell culture plates, or an incubator-hood enclosing the entire microscope. Fluorescence equipment and green/red standard filters are needed for viability assays using fluorescent dyes such as the Live/Dead-assay (Biotium)
4. Dulbecco's Modified Eagle Medium (DMEM), with high glucose and GlutaMax, catalog no. 21885, Gibco/ThermoFisher Scientific (LuBio Science, Lucerne, CH). If the measurement is done outside of a cell culture incubator, a medium including the buffer substance 4-(2-hydroxyethyl)-1-piperazineethanesulfonic acid (HEPES) for the stabilization of pH may be considered such as Gibco/ThermoFisher Scientific DMEM catalog no. 21063
5. Bovine gelatin 2% solution in water, Sigma-Aldrich catalog no G1393. This solution is then diluted 100× in water, added to culture dishes so that the surface is just wet, and let dry before adding culture medium
6. hiPSC-derived cardiomyocytes. Tested with this protocol in our lab: iCell cardiomyocytes from Cellular Dynamics International (Madison, WI, USA), Cor.4U from Axiogenesis (Cologne, Germany) or cardiomyocytes ax2505 from Axol Biosciences (Cambridgeshire, UK)
7. Cryopreserved human cardiac fibroblasts (HCF), catalog no. 6300, ScienCell (Carlsbad, CA, USA) (*see* **Note 1**)
8. Fetal calf serum (FCS) from several vendors, heat-inactivated (30 min at 58 °C) in a waterbath
9. Antibiotics Gibco PenStrep, Cat no. 15140122, Gibco/ThermoFisher Scientific

10. Trypsin 10× 2.5%, Cat no. 15090, Gibco/ ThermoFisher Scientific
11. Sterile phosphate buffered saline (PBS), Gibco catalog no. 10010015, or Hank's balanced salt solution (HBSS)
12. Sterile glass Pasteur pipettes and serological pipettes, treated cell culture dishes 10 cm diameter or T75 cell culture flasks, laminar flow cabinet, incubator, and other standard cell culture equipment
13. Neubauer cell counting chamber or equivalent equipment
14. Integra ViaFlo automatic multi-pipette, catalog no. 4023, (Vitaris, Baar, CH), with pipette tips, Integra catalog no. 4434, 300 µl and liquid reservoirs for multi-pipettes
15. Phenylephrine-hydrochloride (PE), catalog no P6126, Sigma-Aldrich
16. L-ascorbic acid, catalog no A4544 (Sigma-Aldrich, Buchs, CH)
17. Live/Dead assay for viability testing using green/red fluorescence, Biotium, catalog no. 30002-T (Chemie Brunschwig, Basel, CH).

3.2 Method

1. Culture primary HCF from cryopreserved stocks in gelatin-coated culture flasks in DMEM with 10% FCS plus antibiotics and expand the cell population as needed. Passage cells at 80% confluency and split at a ratio of 1:3 (*see* **Note 2**). As general rule for seeding density, we use 1.5×10^4 cells/cm^2 for expansion of the cell population in standard culture.
2. HCF should not be used if older than passage number 10–15, or if the growth rate is declining before that. Keep some vials of cryopreserved cells from an early passage number as an archive sample for each lot. This can be instrumental, if the results of a specific lot deviate from the usual performance or a more detailed characterization of cell identity and purity is needed. For cryopreservation we use 1×10^6 cells per ml in a solution of 90% FCS and 10% dimethyl sulfoxide (DMSO).
3. Detach cultured fibroblasts using trypsin and PBS according to standard protocols. Wash the cells with medium several times and make sure that the fibroblasts are well separated from each other and don't form clusters. Gently stir or pass through a sterile nylon mesh if necessary. When the fibroblasts are ready, proceed with the cryopreserved hiPSC-derived cardiomyocytes.
4. Thaw the frozen vial of hiPSC-derived cardiomyocytes in a water bath at 37 °C for 4 min. Spray the vial with 70% ethanol and place in a sterile biosafety cabinet. Take care when opening, since pressure may have built up within the vial during cryopreservation. Dilute the cell solution by slowly adding

(drop by drop over 2 min) 8 ml DMEM with 10% FCS (*see* **Note 3**), with gentle shaking. Inspect the cells under the inverted microscope and assess the proportion of viable cells. Viability can be checked by staining a small sample with calcein-AM and propidium homodimer-1, which produces a bright green fluorescence in viable cells and a red signal from the nuclei of necrotic cells. The producers of the cells usually provide an evaluation of the expected proportion of viable cells. Only the portion of viable cells is considered in the following for the seeding number per spheroid. However, a viability of less than 50% may cause problems for the quality of the 3D culture, since cell debris can become mixed with the viable cells in the microtissue.

5. Count the density of cells in both cardiomyocyte and fibroblast solutions and adjust so that a mixture of viable cardiomyocyte/fibroblast at a ratio of 4:1 is made and the final co-culture concentration is 5000 cells per 40 µl (the volume of one hanging drop) of solution (*see* **Note 4**). This can be done in two steps where you first obtain the 4:1 mixture and then dilute or spin down to adjust the density for seeding. Optional: prepare cultures with only single cell types for comparison.
6. The size of the microtissues should be as small as possible in order to reduce cell usage and remain below the hypoxic limit of spheroids (approx. 400 µm in diameter). However, sizes below 5000 cells tend to show more variability in shape and beating activity (*see* Fig. 4, and *see* **Note 5**).

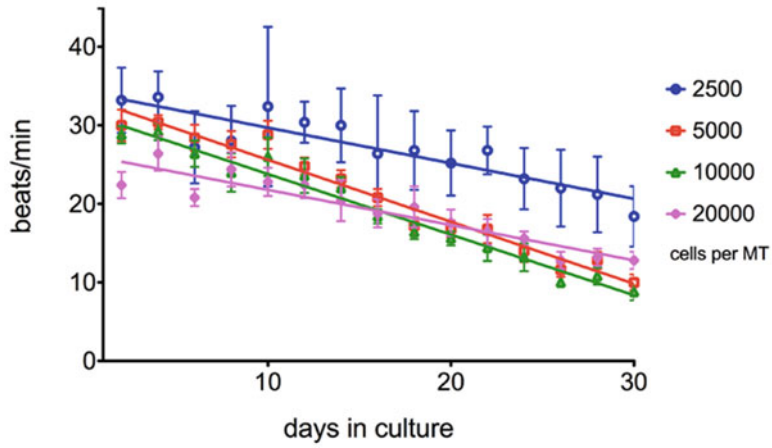

Fig. 4 Comparison of performance of cardiac microtissues over culture time with regular medium changes every 2 days. Groups of different starting cell numbers were assessed: 2500, 5000, 10000, and 20000 cell per spheroid. Although the group with the smallest number of cells performed best on average, it also showed the highest variability. Figure is adapted from our previous publication [9]

7. Add 40 µl of cell solution to each well of the GravityPlus hanging drop plate. Prepare the GravityPlus according to the manufacturer so that the droplets don't dry during culture and keep in an incubator at standard cell culture conditions for 4 days. This is the assembly phase (*see* **Note 6**).
8. Prepare GravityTrap plates for receiving the microtissues according to the manufacturer. These steps are shown in Fig. 5. Harvest the microtissues from hanging drops by slowly adding culture medium using the multichannel pipette from the top so that the droplets and microtissues fall into the wells of the GravityTrap plate. A centrifuge with inserts for cell culture multi-well plates can be used to gently spin-down (100 RPM, 2 min) the microtissues inside the conical wells.
9. Replace the culture medium using the motorized multi-pipette. Optionally add phenylephrine (PE) and L-ascorbic acid, at final concentrations of 10 µM and 0.3 µM, respectively, to the culture medium. This medium supplement increases spontaneous contraction frequency and keeps this parameter constant over culture time [9].
10. Culture microtissues, exchanging medium every 2 days and inspect for beating activity. The start of beating activity may depend on the type of hiPSC-derived cardiomyocytes and can start in the hanging drop phase, but should begin no later than 3 days after harvest from the drop. At 10 days of culture, microtissues should have arrived at stable and uniform beating activity of at least 40 beats per minute at 37 °C when PE is

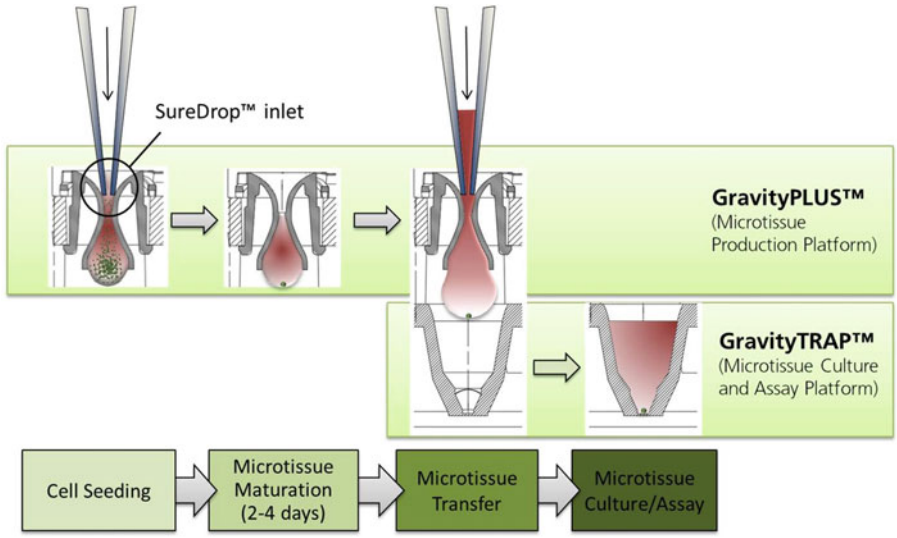

Fig. 5 Manual production of spheroids using an electronic multi-pipette and the two-part production platform consisting of GravityPlus for the hanging drop phase and the GravityTrap for further culture and analysis (image source: www.insphero.com)

present in the medium. Temperature can have a significant impact on spontaneous contractions (Fig. 3d), therefore, inspect microtissues only when the plate is still warm after taking it out of the incubator or in a heated chamber on the inverted microscope. For the measurement by edge-detection, keep microtissues and medium with test substances at constant temperature (either all at 37 °C or equilibrated to room temperature).

11. For measuring contractile activity, place the GravityTrap on the inverted microscope (also *see* **Note** 7) and adjust video contrast and brightness setting so that the spheroids appear as black circles. In the IonWizard software module for edge-detection, place one cursor at the edge of the spheroid and set the other end to "fixed" (i.e., record only one edge). Start the measurement and record shortening traces before and after drug application.
12. The timing of drug application and recording depends on the expected drug action, but can be divided into long and short treatments. Beta-stimulating drugs such as isoproterenol act fast (within 15 min) and can serve as positive control for the acceleration of beating frequency up to arrhythmic behavior and stopping, depending on the dose. For fast acting drugs, it is advised to record the same well before and after drug addition. In this way, the entire development is visible in the dataset, including the phase before drug addition, which should show stable contractions for at least 1 min, and up to one hour after the addition. The drugs can be added in the same way as a medium change is performed. Slowly acting drugs and factors changing gene expression may be added 24 h before measurement.
13. Several kinetic parameters can be extracted from the data using the "transient analysis" functions of IonWizard, such as amplitude of contraction, velocities, and duration of different phases of the contraction.

3.3 Notes

1. Typical marker proteins for fibroblasts are vimentin, collagen-I, and fibronectin. Several specific markers have been suggested for fibroblasts from cardiac origin, such as discoidin domain receptor-2 and cadherin-11 [30]. However, there might be different populations of fibroblasts with different origins in the heart, and their composition changes during inflammation and fibrosis-inducing events, so that several markers should be considered. A purely morphological description may not suffice, since smooth muscle and microvascular endothelial cells can show similar morphology.
2. Although cardiac fibroblasts are generally considered a well-growing cell type, being primary cells, they have a finite life span. Splitting is best done at a ratio of not more than 1:3 and

the cells should not become completely confluent. Otherwise, trypsinization is more difficult and cells might come off the culture surface in form of sheets leading to clumping.

3. Special media formulations are often used for hiPSC-derived cardiomyocyte cultures in standard culture. These medium formulations may not be compatible with co-cultured cells (for example, causing suppression of proliferating cells), therefore for the co-cultures we used DMEM as this is a well-described standard medium for use with FCS.
4. Cells may sediment quickly in medium, therefore keep mixing the cell solutions using a 10 ml serological pipette in the multi-pipette reservoirs to obtain regularly sized microtissues.
5. Microtissues can also be prepared with a smaller number of cells; as few as 2500 cells can be used for one spheroid with the cell types discussed here. However, the overall shape may not be perfectly spherical and tends to break up into sub-clusters. This is especially the case for hiPSC-cardiomyocytes as single culture, while the addition of HCF helps to improve cohesion of the spheroids.
6. Wells at the outer edge of 96-well plates may show more heterogeneity after 10 or more days of culturing because of evaporation of culture medium.
7. Cardiac microtissues can also be placed on glass coverslips coated with collagen or fibronectin. The microtissues usually adhere to such surfaces overnight in culture and can then be placed in special chambers for constant perfusion, electrical pacing, or staining with fluorescent dyes.

Acknowledgements

Funding was provided by the Swiss Heart Foundation. This study was performed with the support of the Microscopy Imaging Center (MIC), University of Bern. I am thanking Prof. Hugues Abriel and the entire channelopathies group (Department of Clinical Research, Univ. Bern) for valuable advice, stimulating discussions, and experimental support.

Glossary

3D Three-dimensional
DMSO Dimethyl sulfoxide
FCS Fetal Calf Serum
HBSS Hank's balanced salt solution
HCF Human cardiac fibroblasts
hESC Human embryonic stem cells

HEPES 4-(2-hydroxyethyl)-1-piperazineethanesulfonic acid
hiPSC Human induced pluripotent stem cells
PBS Phosphate buffered saline
PE Phenylephrine
ROI Region of interest

References

1. Roden DM, Lazzara R, Rosen M et al (1996) Multiple mechanisms in the long-QT syndrome. Current knowledge, gaps, and future directions. The SADS Foundation Task Force on LQTS. Circulation 94:1996–2012
2. Kondo RP, Apstein CS, Eberli FR et al (1998) Increased calcium loading and inotropy without greater cell death in hypoxic rat cardiomyocytes. Am J Physiol 275: H2272–H2282
3. Timolati F, Anliker T, Groppalli V et al (2009) The role of cell death and myofibrillar damage in contractile dysfunction of long-term cultured adult cardiomyocytes exposed to doxorubicin. Cytotechnology 61:25–36
4. Sawyer DB, Zuppinger C, Miller TA et al (2002) Modulation of anthracycline-induced myofibrillar disarray in rat ventricular myocytes by neuregulin-1 beta and anti-erbB2: potential mechanism for trastuzumab-induced cardiotoxicity. Circulation 105:1551–1554
5. Harder BA, Hefti MA, Eppenberger HM et al (1998) Differential protein localization in sarcomeric and nonsarcomeric contractile structures of cultured cardiomyocytes. J Struct Biol 122:162–175
6. Eschenhagen T, Mummery C, Knollmann BC (2015) Modelling sarcomeric cardiomyopathies in the dish: from human heart samples to iPSC cardiomyocytes. Cardiovasc Res 105:424–438
7. Rajamohan D, Matsa E, Kalra S et al (2013) Current status of drug screening and disease modelling in human pluripotent stem cells. Bioessays 35:281–298
8. Suter-Dick L, Alves PM, Blaauboer BJ et al (2015) Stem cell-derived systems in toxicology assessment. Stem Cells Dev 24:1284–1296
9. Beauchamp P, Moritz W, Kelm JM et al (2015) Development and characterization of a scaffold-free 3D spheroid model of iPSC-derived human cardiomyocytes. Tissue Eng Part C Methods 21:852–861
10. Hinz B, Celetta G, Tomasek JJ et al (2001) Alpha-smooth muscle actin expression upregulates fibroblast contractile activity. Mol Biol Cell 12:2730–2741
11. Eder A, Hansen A, Uebeler J. et al (2014) Basic Res Cardiol 109:436. doi:10.1007/s00395-014-0436-7
12. Jahnke H-G, Steel D, Fleischer S et al (2013) A novel 3D label-free monitoring system of hES-derived cardiomyocyte clusters: a step forward to in vitro cardiotoxicity testing. PLoS One 8, e68971
13. Rismani Yazdi S, Shadmani A, Bürgel SC et al (2015) Adding the "heart" to hanging drop networks for microphysiological multi-tissue experiments. Lab Chip 15:4138–4147
14. Mosadegh B, Xiong G, Dunham S et al (2015) Current progress in 3D printing for cardiovascular tissue engineering. Biomed Mater 10:034002
15. Kim J-Y, Fluri DA, Marchan R et al (2015) 3D spherical microtissues and microfluidic technology for multi-tissue experiments and analysis. J Biotechnol 205:24–35
16. Hirt MN, Hansen A, Eschenhagen T (2014) Cardiac tissue engineering: state of the art. Circ Res 114:354–367
17. Hansen A, Eder A, Bönstrup M et al (2010) Development of a drug screening platform based on engineered heart tissue. Circ Res 107:35–44
18. Zuppinger C (2016) 3D culture for cardiac cells. Biochim Biophys Acta 1863(7):1873–1881
19. Schaaf S, Eder A, Vollert I et al (2014) Generation of strip-format fibrin-based engineered heart tissue (EHT). Methods Mol Biol 1181:121–129
20. Hirschhaeuser F, Menne H, Dittfeld C et al (2010) Multicellular tumor spheroids: an underestimated tool is catching up again. J Biotechnol 148:3–15
21. Kelm JM, Ehler E, Nielsen LK et al (2004) Design of artificial myocardial microtissues. Tissue Eng 10:201–214
22. Rimann M, Graf-Hausner U (2012) Synthetic 3D multicellular systems for drug development. Curr Opin Biotechnol 23:803–809
23. Desroches BR, Zhang P, Choi B-R et al (2012) Functional scaffold-free 3-D cardiac microtissues: a novel model for the investigation of heart cells. Am J Physiol Heart Circ Physiol 302:H2031–H2042

24. Frey O, Misun PM, Fluri DA et al (2014) Reconfigurable microfluidic hanging drop network for multi-tissue interaction and analysis. Nat Commun 5:4250
25. Drewitz M, Helbling M, Fried N et al (2011) Towards automated production and drug sensitivity testing using scaffold-free spherical tumor microtissues. Biotechnol J 6:1488–1496
26. Messner S, Agarkova I, Moritz W et al (2013) Multi-cell type human liver microtissues for hepatotoxicity testing. Arch Toxicol 87:209–213
27. Edling Y, Sivertsson LK, Butura A et al (2009) Increased sensitivity for troglitazone-induced cytotoxicity using a human in vitro co-culture model. Toxicol In Vitro 23:1387–1395
28. Prange JA, Bieri M, Segerer S et al (2016) Human proximal tubule cells form functional microtissues. Pflugers Arch 468(4):739–50
29. Tirziu D, Giordano FJ, Simons M (2010) Cell communications in the heart. Circulation 122:928–937
30. Souders CA, Bowers SLK, Baudino TA (2009) Cardiac fibroblast: the renaissance cell. Circ Res 105:1164–1176
31. Desmoulière A, Gabbiani G (1995) Myofibroblast differentiation during fibrosis. Exp Nephrol 3(2):134–139
32. Rohr S, Kucera JP, Fast VG et al (1997) Paradoxical improvement of impulse conduction in cardiac tissue by partial cellular uncoupling. Science 275:841–844
33. Kelm JM, Diaz Sanchez-Bustamante C, Ehler E et al (2005) VEGF profiling and angiogenesis in human microtissues. J Biotechnol 118: 213–229
34. Bichsel CA, Hall SRR, Schmid RA et al (2015) Primary human lung pericytes support and stabilize in vitro perfusable microvessels. Tissue Eng Part A 21:2166–2176
35. Kelm JM, Djonov V, Hoerstrup SP et al (2006) Tissue-transplant fusion and vascularization of myocardial microtissues and macrotissues implanted into chicken embryos and rats. Tissue Eng 12:2541–2553
36. Veerman CC, Kosmidis G, Mummery CL et al (2015) Immaturity of human stem-cell-derived cardiomyocytes in culture: fatal flaw or soluble problem? Stem Cells Dev 24(9):1035–1052
37. van den Berg CW, Elliott DA, Braam SR et al (2016) Differentiation of human pluripotent stem cells to cardiomyocytes under defined conditions. Methods Mol Biol 1353:163–180
38. Hayakawa T, Kunihiro T, Ando T et al (2014) Image-based evaluation of contraction-relaxation kinetics of human-induced pluripotent stem cell-derived cardiomyocytes: Correlation and complementarity with extracellular electrophysiology. J Mol Cell Cardiol 77:178–191
39. Lipp P, Hüser J, Pott L et al (1996) Spatially non-uniform Ca2+ signals induced by the reduction of transverse tubules in citrate-loaded guinea-pig ventricular myocytes in culture. J Physiol 497(Pt 3):589–597
40. Steadman BW, Moore KB, Spitzer KW et al (1988) A video system for measuring motion in contracting heart cells. IEEE Trans Biomed Eng 35:264–272
41. Delbridge LM, Roos KP (1997) Optical methods to evaluate the contractile function of unloaded isolated cardiac myocytes. J Mol Cell Cardiol 29:11–25
42. Pieperhoff S, Wilson KS, Baily J et al (2014) Heart on a plate: histological and functional assessment of isolated adult zebrafish hearts maintained in culture. PLoS One 9, e96771
43. Brito-Martins M, Harding SE, Ali NN (2008) beta(1)- and beta(2)-adrenoceptor responses in cardiomyocytes derived from human embryonic stem cells: comparison with failing and non-failing adult human heart. Br J Pharmacol 153:751–759
44. Kloss D, Fischer M, Rothermel A et al (2008) Drug testing on 3D in vitro tissues trapped on a microcavity chip. Lab Chip 8:879–884
45. Seferidis VE, Ghanbari M (1993) General approach to block-matching motion estimation. Opt Eng 32:1464–1474
46. Ahola A, Kiviaho AL, Larsson K et al (2014) Video image-based analysis of single human induced pluripotent stem cell derived cardiomyocyte beating dynamics using digital image correlation. Biomed Eng Online 13:39

Chapter 12

Contractile Force Readout of hESC-Cardiomyocytes

Carlota Oleaga, Gregg Legters, L. Richard Bridges, Lee Kumanchik, Candace Martin, Yunqing Cai, Mark Schnepper, Christopher W. McAleer, Christopher J. Long, and James J. Hickman

Abstract

Promising pharmaceuticals frequently fail clinical trials due to cardiotoxicity or a decline in heart function not indicated from preclinical animal models and in vitro tests. The development of low-cost, high-throughput, and reliable in vitro human models remains a priority for pharmaceutical companies to avoid costly dead ends in clinical trials. Organ-on-a-chip systems allow the creation of functional, human tissue test beds that leverage the benefits of miniaturization using Biomicroelectromechanical System (BioMEMS) devices and the availability of differentiable human stem cells.

We have developed a 2D cardiac platform that allows the functional interrogation of human embryonic stem cell (hESC)-derived cardiomyocytes. The platform uses a laser to reflect off silicon cantilevers with adhered cardiomyocytes to monitor the contraction-induced deflection, enabling the calculation of contractile force.

Chips with up to 32 cantilevers can be scanned by an automated stage sending the cardiac signals to a high-speed detector that can record the spatial coordinates and transform them into force output. Separately, electrical conduction can also be monitored by patterning cardiomyocytes on top of microelectrode arrays. This platform enables physiologic characterization of inherited cardiomyopathies, as well as acute and chronic drug studies with arrhythmogenic and inotropic compounds, to predict their effect on in vivo cardiac output, as well as general toxicological evaluations.

Key words Human, Cardiomyocyte, Contractile force, Cantilever, Functional assay, Serum-free, Pharmacology, Toxicity, Organ-on-a-chip

1 Introduction

Cardiotoxicity is a recurrent drug side effect that has to be monitored during the development of new drugs [1]. Current preclinical cardiotoxicity models fail to reliably predict human toxicity; approximately 20% of drugs are withdrawn due to cardiotoxic events [3]. A more reliable means to predict drug-induced cardiotoxicity in humans [2] is required to reduce the failure rate of new commercialized molecules and reduce the cost of drug development [4–7].

Mike Clements and Liz Roquemore (eds.), *Stem Cell-Derived Models in Toxicology*, Methods in Pharmacology and Toxicology, DOI 10.1007/978-1-4939-6661-5_12, © Springer Science+Business Media New York 2017

The heart rhythmically distributes blood throughout the body to provide cells and tissues with oxygen and energy sources and to also eliminate carbon dioxide and metabolic waste. The heart is a pump that moves blood via contractile machinery, and its output is controlled by electrical impulses. Because the contractile machinery and the electrical activity are both critical for proper heart function, both systems should be interrogated for cardiotoxic effects [7]. Disruptions affecting cardiac innervation, conduction, and ion concentrations (sodium, calcium, and potassium) may interfere with the cardiac electrical activity. Additionally, disruption of the internal calcium concentration or sarcomere structure will also interfere with the contractile machinery. Inotropic drugs affect the strength of myocardium contraction, positively if force increases or negatively if force decreases. Examples of drug target points that regulate cardiac force include Ca^{2+} channels, Na^{+}/K^{+} ATPase, Na^{+}/Ca^{2+} exchanger (NCX), adrenergic receptors, cAMP-PKA pathway, ryanodine receptor (RyR), SERCA2a pathway, and sarcomere components [8].

We have validated a system that enables the simultaneous measurement of both of these cardiac functions from human stem cell (hSC)-derived cardiomyocytes. Only the method to record the force of cardiomyocyte contraction will be covered in this chapter. Further details of protocols to record electrical activity from hSC-cardiomyocytes are described here [7]. The contractile machinery module presented here improves previous published work in terms of having (1) complete contractile machinery, (2) reproducible fabrication, (3) accurate and comparable analysis, (4) human cardiomyocytes, and (5) a serum-free medium [7]. This module was adapted for cardiomyocytes from a previous design that studied skeletal muscle force in our laboratory [9–13]. In this system the cardiomyocytes are anchored along the top of a micro-cantilever, and a laser beam is used to target the cantilever tip to monitor the deflection after cellular contraction. The reflected light from the laser is registered by a photodetector and sent to a computer where algorithms convert the amount of deflection to force of contraction (Fig. 1).

2 Materials

2.1 Cantilever Fabrication and Cleaning

- Clean room facility
- AutoCAD software
- 4 in. silicon-on-insulator (SOI) wafer with 5 μm thick top layer of crystalline silicon bonded onto a 500 μm thick silicon handle wafer with 1–2 μm buried oxide layer (Ultrasil)
- Hexamethyldisilazane (HMDS) (Sigma-Aldrich)
- Resist spinner vacuum holder (Laurel or Headway Research)

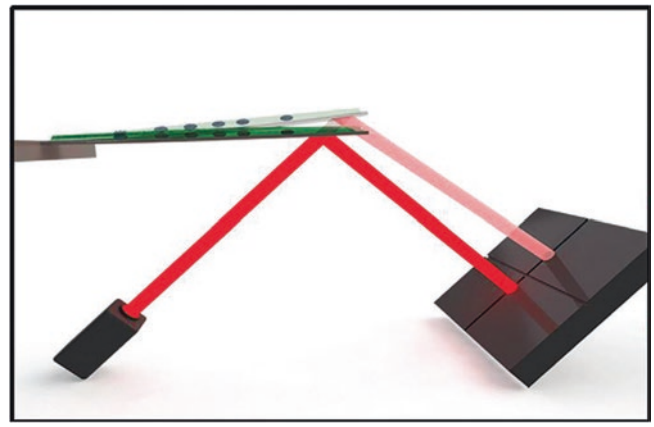

Fig. 1 Summary scheme of the cantilever technology. Cardiomyocyte contraction forces the cantilever to bend inducing a laser deflection that can be recorded and translated into force (figure provided by [11])

- Photoresist: S1818, SPR 220 (both from Shipley Co.)
- Oven (90–120 °C)
- Photomask aligner MA6 (SUSS MicroTec)
- Photoresist developer 726 MIF (MicroChemicals GmbH)
- 770 deep reactive-ion etching (DRIE) (Plasma-Therm)
- Metroline M4L plasma resist etcher (or a similar) (PVA TePla)
- Carrier wafer (University Wafer)
- Plasma-enhanced chemical vapor deposition (PECVD, GSI)
- Hot plate (80–170 °C)
- Thermal grease (MG Chemicals)
- Buffered hydrofluoric acid: 40% NH_4F in distilled water, 49% HF in distilled water (6:1 ratio) (Sigma)
- MeOH-HCl solution: 1 volume absolute methanol, 1 volume concentrated HCl
- PDC-326 oxygen plasma cleaner (or similar) (Harrick Plasma)
- Saturated (3 M) KOH: KOH, methanol (100%)
- 1% (w/v) Tergazyme: 1 g Tergazyme, q.s 100 mL distilled water
- Ultrapure water (mQ H_2O)
- Toluene (VWR) (optional step)
- 1 L Pyrex bottle (optional step)
- N_2 gas (optional step)
- Glove box (Mbraun) (optional step)

- (3-Trimethoxysilyl propyl) diethyltriamine (DETA) stock solution (100%) (United Chemical Technologies) (optional step)
- 0.1% (vol/vol) DETA, distilled toluene (optional step)
- Optical contact angle goniometer (Rame-Hart) (optional step)
- X-ray photoelectron spectroscopy (XPS) (Thermo Fisher) (optional step)
- Desiccator (VWR) (optional step)

2.2 Cell Culture

- Cryopreserved human embryonic stem cell-derived cardiomyocytes, Cytiva® stem cell line hESC-10-0061 (28976398) (GE Healthcare).
- Liquid nitrogen tank.
- Ultra-low temperature freezer (−80 °C) (Revco).
- Water bath (37 °C).
- Sterile 50 mL conical tubes.
- 5810R cell culture centrifuge (or a similar) (Eppendorf).
- 100 μg/mL L-thyroxine stock: 1 mg L-thyroxine (Sigma) and 10 mL 2 M ammonium hydroxide in methanol. Store aliquots at −20 °C.
- 10 μg/mL epidermal growth factor stock: 0.2 mg epidermal growth factor (Sigma), 20 mL 10 mM acetic acid. Store aliquots at −20 °C.
- 500 μg/mL hydrocortisone stock: 5 mg hydrocortisone (Sigma), 10 mL 10% ethanol (in water). Store aliquots at −20 °C.
- HSL2 serum-free culture medium (HSL2): 100 mL Ultraculture medium (BioWhittaker), 5× B27, 1× glutamax, 1× antibiotic/antimitotic, 1× MEM nonessential amino acids, 10 mM HEPES buffer (all from Gibco), 0.1 μg/mL of L-thyroxine, 10 ng/mL epidermal growth factor, 0.5 μg/mL hydrocortisone, 20 mM dextrose (Fisher Scientific).
- Cell culture 12-well plates.
- 50 μg/mL fibronectin: fibronectin 1 mg/mL (Millipore), 1× PBS.
- 1× PBS.
- Cell culture incubator (37 °C, 5% CO_2 and controlled humidity).
- Biosafety cabinet.
- 0.4% trypan blue solution (Sigma).
- Neubauer chamber or hemocytometer (Celeromics).

2.3 Drugs

Example drugs validated by [7]:

- Negative control: 2 mM sotalol (Sigma), HSL2 medium (prepare fresh each time)
- Positive control (positive inotropic): 20 μM norepinephrine (Sigma), HSL2 medium (prepare fresh each time)
- Positive control (negative inotropic): 100 μM verapamil (Sigma), HSL2 medium (prepare fresh each time)

2.4 AFM

- Upright Olympus BX51WI electrophysiology microscope (Olympus Inc.)
- KP-M2AN CCD Camera (or similar) (Hitachi)
- Microscope stage
- Class 2 red photodiode laser (Newport)
- Laser shutter (AutoMate Scientific) to prevent light-induced cellular toxicity
- 4-quadrant photodetector (Noah Industries)
- X-y-z-h translators (Newport)
- Temperature controller, Delta T4 culture dish controller (or similar) (Thermo Bioptechs)
- Homemade stimulation chamber: 15 mm × 15 mm (5 mm thick) polycarbonate square perimeter chamber with glass bottom—transparent base through which the laser beam could easily pass—and two silver wires (0.015 in. diameter) parallel to each other with a separation of 15 mm for broad-field stimulation
- Experimental medium: HSL2, 25 mM HEPES
- External pulse stimulator (A–M systems)
- Axoscope from pClamp 10.0 data acquisition software (Molecular Devices)
- Homemade LabVIEW software

3 Methods

3.1 Cantilever chip fabrication and cleaning

3.1.1 Cantilever chips are square (1 cm^2) with two etched rectangles in the middle, where the cantilevers (150 μm × 750 μm × 4 μm) are airlifted and attached only on the left side of the rectangle, thus, free to bend (Fig. 2a). Photomask design with AutoCAD software or alternative. To optimize fabrication, organize 24 cantilever chips in one SOI wafer. Two photomasks will be required—at the top and bottom—for

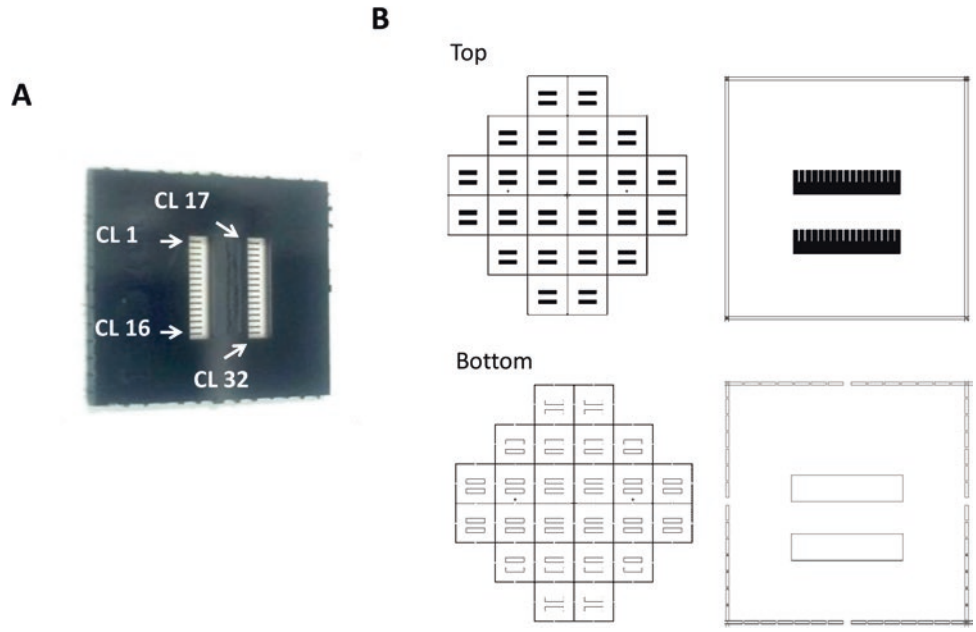

Fig. 2 Cantilever chip design. Picture of a silicon 1 × 1 cm cantilever chip. The cantilevers (CL) used for alignment are highlighted in the picture (**a**). Scheme of top and bottom photomask layers required to create the cantilever chip. *Alignment marks* are located in row 3 and columns 2 and 5 of both photomask grids. The bottom photomask includes perforated edges (**b**)

the difference in height of the chip and the cantilevers (Fig. 2b).

→ *Fabrication steps need to be performed in a clean room from this step onward.*

3.1.2 Prime the SOI wafer (with the 5 μm silicon side up) with an adhesion layer of HMDS through either vapor deposition or spin-on process (to a nearly monolayer thickness).

3.1.3 Move the wafer to a resist spinner vacuum holder; apply the photoresist S1818 in the center, and spin (1900 rpm) for 60 s to achieve a 2 μm thick layer.

3.1.4 Soft bake at 110 °C either in oven for 50 min or in hot plate for 1 min.

3.1.5 Align the wafer with the top photomask (Fig. 2b top) in the photomask aligner MA6 and expose (200 mJ/cm2).

3.1.6 Develop for 2 min in the photoresist developer 726 MIF.

3.1.7 Move the wafer to a 770 DRIE etcher; apply deep reactive-ion etching through the device layer to reach the buried oxide layer to define the cantilevers.

3.1.8 Remove the photoresist by plasma etching using Metroline M4L plasma resist etcher.

3.1.9 Protect the front side by depositing a 1 μm thick oxide layer using plasma-enhanced chemical vapor deposition (PECVD).

3.1.10 Flip the wafer (continue on this orientation unless mentioned), and deposit a 1.5 μm thick oxide layer using PECVD.

3.1.11 Prime with an adhesion layer of HMDS through either vapor deposition or spin-on process (to a nearly monolayer thickness).

3.1.12 Apply a 5 μm layer of SPR220 photoresist.

3.1.13 Soft bake at 110 °C either in oven for 50 min or in hot plate for 1 min.

3.1.14 Align the wafer with the bottom photomask in the MA6 and expose (200 mJ/cm2).

3.1.15 Develop for 2 min in the 726 MIF.

3.1.16 Hard bake at 120 °C in the oven for 30 min.

3.1.17 Etch the protective oxide mask by plasma etching to the silicon.

3.1.18 DRIE etch until there is 100 μm of the handle wafer remaining.

3.1.19 Mount the wafer on a carrier wafer using several spots of thermal grease, and complete the DRIE until arriving to the buried oxide layer.

3.1.20 Release the wafer from the carrier wafer using isopropanol alcohol.

3.1.21 Remove the photoresist by plasma etching using Metroline M4L plasma resist etcher until the resist is removed.

3.1.22 Run this last step inside a fume hood with corrosive acid protection. Soak the wafer in buffered hydrofluoric acid (HF, dilution 6:1) for 45 min.

3.1.23 Break wafer, to release individual chips, by bending either side of the defined line perforated holes etched during the DRIE steps).

3.1.24 Cleaning step:

- 3.1.24.1 Soak the cantilevers in 1 % Tergazyme solution for 2 h.
- 3.1.24.2 Rinse with distilled water.
- 3.1.24.3 O_2 plasma treatment for 15 min, prior to cell plating, to enhance surface hydrophilicity and fibronectin adsorption.
- 3.1.24.4 (*See* **Note 1**).

3.2 Cantilever chip surface chemistry modification (optional step to improve cell anchorage to chip) [14] (*see* **Note 2**).

3.2.1 Take the distilled toluene, and transfer into a water-free Pyrex bottle (dry in a 100 °C oven).

3.2.2 Replace the remaining air of the Pyrex bottle with dry nitrogen to minimize free oxygen.

3.2.3 Seal the bottle and transfer it to a glove box.

3.2.4 Inside the glove box, add DETA into the toluene to a final concentration of 0.1 % (vol/vol).

3.2.5 Remove the DETA-toluene solution from the glove box, and transfer it into a Pyrex beaker. Incubate the cantilever chips submerged in DETA-toluene solution at below boiling point (65 °C).

3.2.6 Remove the reaction vessel and chips from the hotplate, and allow them to cool for 30 min.

3.2.7 Wash three times with dry toluene.

3.2.8 Incubate in fresh toluene for 30 min, and heat to just below the boiling point of toluene over this period.

3.2.9 Analyze the positive deposition of DETA on the surface by XPS and contact angle goniometry.

3.3 Human cardiomyocyte culture

3.3.1 Sterilize cantilever chips by absolute ethanol soaking, and air-dry vertically in 12-well plates.

3.3.2 Once dry, incubate the cantilever chips (horizontally inside the well) with 50 μg/mL fibronectin. Place a 200 μL droplet of fibronectin solution on top of the micro-cantilever area. Incubate for 30 min in the cell culture incubator. Inside the hood, pipette out the fibronectin with a micropipette, and rinse the area twice with 1× PBS droplets. Maintain the second droplet until cell plating step (*see* **Note 3**).

3.3.3 Thaw the cryopreserved hSC-cardiomyocytes (following manufacturer's instructions):

3.3.3.1 Transfer one vial (or as many as required) from the liquid nitrogen tank to a −80 °C freezer, and incubate for 2 min.

3.3.3.2 Transfer the vial to a 37 °C water bath (without submerging the lid), and incubate for <2 min (goal: thaw the content almost entirely, maintaining a free ice piece in the middle of the tube).

3.3.4 Pipette the content in 9 mL of room temperature HSL2 medium in a 50 mL conical tube. Centrifuge at 300 × g for 5 min at room temperature.

3.3.5 Decant the supernatant and resuspend the pellet by rocking with 0.5–2 mL HSL2 (depending upon pellet size). Calculate cell density and viability by analyzing 10 μL of a 1:1 mix of cell suspension and 0.4% trypan blue solution in a Neubauer chamber.

3.3.6 Adjust cell density if necessary, and manually place the hSC-cardiomyocytes on top of cantilever chips at a cell density of 2500 cells/mm2 with a 100–200 μL droplet. Target the micro-cantilever area in the center of the chip to achieve full coverage of the cantilevers. Incubate the cell droplets for 3–4 h in a cell culture incubator, and afterward top up the droplets with 2 mL HSL2 to prevent them from drying out.

3.3.7 The following day replace entire volume of medium with fresh medium, and thereafter replace half of the medium every third day. The cardiomyocytes used to validate this instrument required 10–14 days in vitro, before expressing complete contractile machinery, to produce positive signals.

3.4 Cantilever recordings and drug experiments

3.4.1 Before transferring the cells, turn on the different parts of the AFM (atomic force microscopy) rig (microscope (1), camera (2), stimulator (5), laser-photodetector duo (6, 7), temperature controller to 37 ± 1 °C (8), computer, and software (9)), and add 2 mL experimental medium (HSL2, 25 mM HEPES) to the stimulation chamber (3) (component location is schemed in Fig. 3) (*see* **Note 4**).

3.4.1.1 Homemade LabVIEW software

3.4.1.1.1 A LabVIEW virtual instrument is needed to control the stepper motors that move the laser and detector and should be written with the following characteristics:

3.4.1.1.1.1 The software should allow the x and y stepper motors for the laser and the x and y stepper motors for the detector to be moved independently.

3.4.1.1.1.2 The software should allow for setting the laser and detector motors for alignment to the four corner

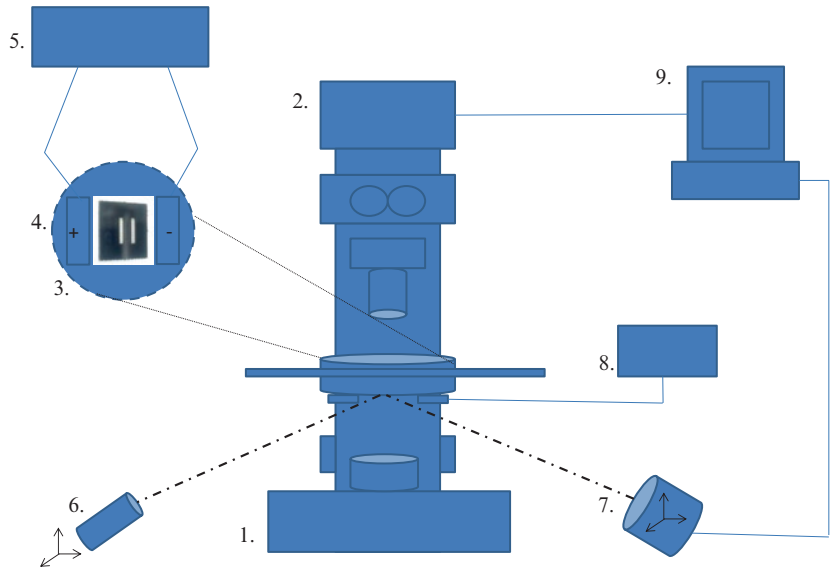

Fig. 3 AFM scheme. The AFM rig is composed of (1) an upright AFM, (2) a camera, (3) a stimulation chamber, (4) a bathing electrodes, (5) a stimulator, (6) a laser, (7) a detector, (8) a temperature controller, and (9) a computer

cantilever tips, and the software interpolates positions for the remaining cantilever tips.

3.4.1.1.1.3 After setting the positions of the cantilever tips (for both x and y motors for both the laser and detector), the software should cycle through the positions in order, stopping at each cantilever tip for a prescribed period of time before moving to the next cantilever tip. This time can be adjusted to suit the experiment. Typically, the time is set to 30 s.

3.4.2 Center the cantilever chip in between the two stimulation electrodes with the cantilever tips pointing to the right (*see* **Note 5**).

3.4.3 Align the laser-photodetector duo with the quadrant cantilevers. Start with cantilever 1, and then repeat with 16, 32, and 17 (Fig. 2a). Looking through the microscope eyepiece, position the laser beam on the tip of the cantilever, where the reflection achieves the brightest spot. Open Axoscope and LabVIEW software in the PC. Select cantilever 1 with LabVIEW (adjust manually laser beam location if misalignment), and lock the position. Align the detector to the baseline using the Axoscope software, and then lock the position in LabVIEW (*see* **Notes 6** and 7).

3.4.4 A cell stabilization period of 15 min to the lab atmosphere is required before recording (alignment time counts as part of the stabilization time).

3.4.5 Recording of the cantilever laser deflection due to cardiac contraction may be assessed on spontaneous contractile cells or under broad-field stimulation (*see* **Notes 8** and **9**). For both types of experiments, the software settings for recording will be:

3.4.5.1 Start recording in Axoscope.

3.4.5.2 Start an auto scan (10 s recording per cantilever) in LabVIEW on the selected cantilevers (32 or less).

3.4.5.3 Stop the recording in Axoscope after three complete rounds.

3.4.6 When recording field-controlled contractions, first start the stimulation by applying a square electrical pulse (40 ms) with 4–5 V in amplitude every 0.5–1 s (2–1 Hz), and then start the recording.

3.4.7 Before removing the chip out of the alignment position, pharmacological studies can be performed with a single dose or cumulative dosages to analyze a dose-response effect. Use the initial measurements (3.4.5. and 3.4.6. steps) as the baseline. Add a drug stock concentration to the volume of the stimulation chamber (2 mL) for a desired working concentration. Incubate for 5 min and record (spontaneous or stimulated). Repeat the process with increasing drug concentrations if planned [7] (*see* **Note 10**). We have validated this system with the following protocols:

3.4.7.1 Negative control: the arrhythmogenic agent sotalol is a potent hERG channel blocker.

3.4.7.1.1 After steps 3.4.5. and 3.4.6, add 100 μL of 2 mM sotalol to achieve a 100 μM final concentration in the 2 mL of the stimulation chamber. Incubate for 5 min.

3.4.7.1.2 Make spontaneous or stimulated recordings (5 min approx.).

3.4.7.2 Positive control (positive inotropic effect): the neurotransmitter and hormone norepinephrine, released by the parasympathetic nervous system, induces heart rate and contractile force.

3.4.7.2.1 After steps 3.4.5 and 3.4.6, add 100 μL of 20 μM norepinephrine to achieve a 1 μM final concentration in the 2 mL of the stimulation chamber. Incubate for 5 min.

3.4.7.2.2 Make spontaneous or stimulated recordings (5 min approx.).

3.4.7.3 Positive control (negative inotropic effect): the class-IV antiarrhythmic verapamil is an L-type calcium channel blocker.

3.4.7.3.1 After steps 3.4.5 and 3.4.6, add 20 μL of 100 μM verapamil to achieve a 1 μM final concentration in the 2 mL of the stimulation chamber. Incubate for 5 min.

3.4.7.3.2 Make spontaneous or stimulated recordings (5 min approx.).

3.4.7.3.3 Add 40 μL of 100 μM verapamil to achieve a 3 μM final concentration in the 2 mL of the stimulation chamber (cumulative dosage). Incubate for 5 min.

3.4.7.3.4 Make spontaneous or stimulated recordings (5 min approx.) (*see* **Notes 11** and **12**).

3.5 Stress calculation

3.5.1 Open the recorded files (.abf) from Axoscope with Campfit software to visualize the laser deflection on space, recorded by the photodetector, due to the cantilever bending (Fig. 4).

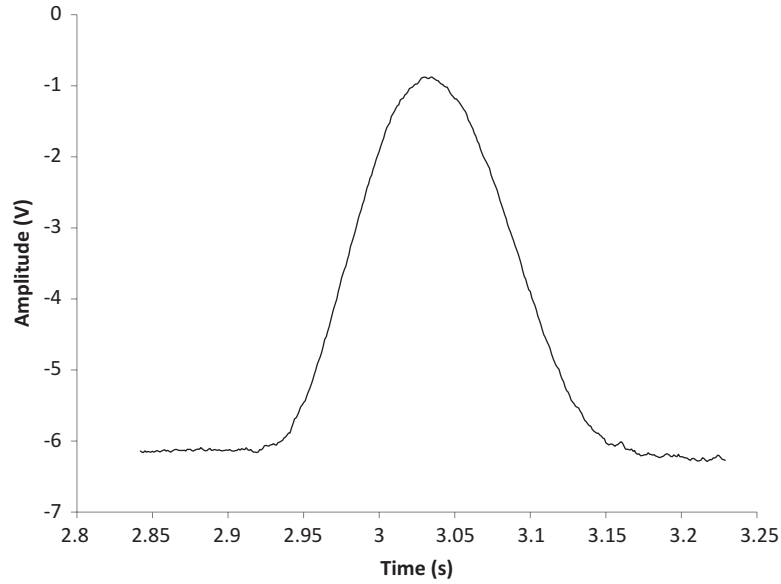

Fig. 4 Cardiomyocyte contraction. Deflection of the laser beam read by the photodetector due to the cantilever bending is plotted as amplitude versus time

3.5.1.1 Measure the amplitude of the originated picks (voltage) of individual cantilevers.

3.5.2 To calculate the contractile force of cardiomyocytes, use the amplitude as a coefficient of the Stoney equation (adapted for the cardiomyocyte cantilever chip [7, 11, 13]).

3.5.2.1 The adapted Stoney equation includes all the system parameters (Fig. 5) as coefficients:

3.5.2.1.1 θ: the angle of the laser and detector relative to the plane of the cantilever

3.5.2.1.2 P: the path length of the laser from the cantilever tip to the detector

3.5.2.1.3 C detector: the system-specific coefficient relating voltage to laser position on the photodetector

3.5.2.1.4 Voltage: peak amplitude recorded (Fig. 4). E_{Si}: the elastic modulus of silicon

3.5.2.1.5 ν_{Si}: Poisson's ratio of silicon

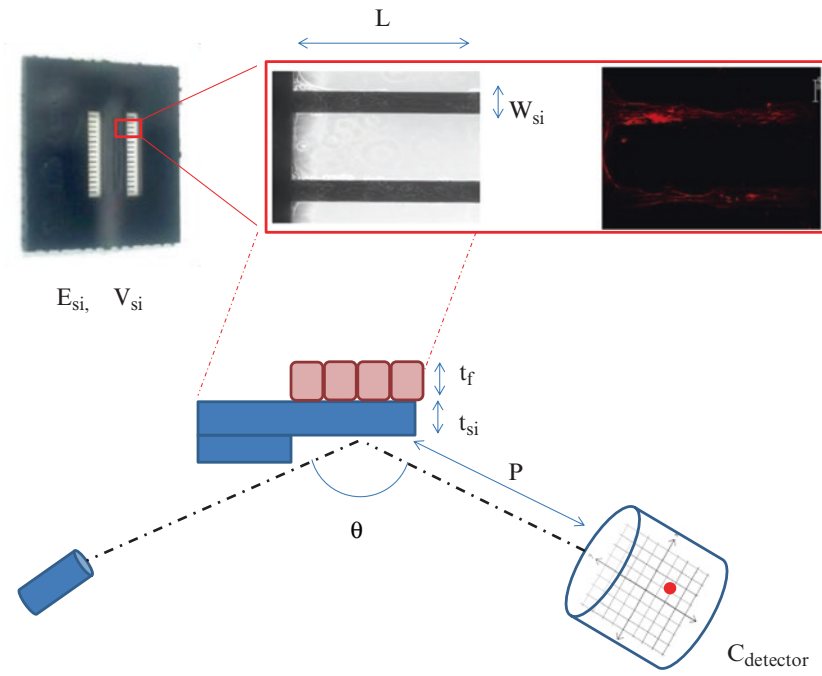

Fig. 5 Force system parameters. The physical parameters that characterize the system and are considered to calculate the force output are the cantilever chip (E_{Si}, v_{Si}, L, W_{Si}, t_{Si}), the cardiomyocytes (tf), and the light alignment (θ, P, t_{Si}, $C_{detector}$)

3.5.2.1.6 L: the cantilever length

3.5.2.1.7 t_{Si}: the thicknesses of thecantilever

3.5.2.1.8 w_{Si}: the cantilever width

3.5.2.1.9 t_f: the thickness of the cardiomyocyte layer

3.5.2.2 The cantilever tip deflection:

$$\delta = \frac{2L}{3}\tan\left[\frac{\theta}{2} - \frac{1}{2}\arctan\left(\tan\theta - \frac{\text{Voltage}}{C_{\text{detector}} \times P \times \cos\theta}\right)\right].$$

3.5.2.3 It will be needed to calculate the stress of contraction:

$$\sigma_c = \frac{E_{Si} t_{Si}^3}{6t_f\left(1-\nu_{Si}\right)\left(t_f + t_{Si}\right)} \frac{3\delta}{2L^2} \times \frac{1}{1+\frac{t_f}{t_{Si}}}.$$

3.5.2.4 The force (nN) in the cardiomyocyte layer is equal to the stress times the cross sectional area (width × thickness):

$$F_{\text{cardiomyocytes}} = \sigma_c \times t_f \times w_{Si}.$$

3.5.2.5 Following this protocol the contraction should show forces in the tens to hundreds of nN range.

3.5.2.6 Pharmacological tests can express percentage of change upon drug incubation compared initial baseline recording.

4 Drug Validation Data

The incubation of a negative control (sotalol) and two positive controls, positive (norepinephrine) and negative (verapamil) inotropic compounds, as described in the method section were used to validate this system. The measured forces of control cardiomyocytes and drug-treated ones are shown in Fig. 6.

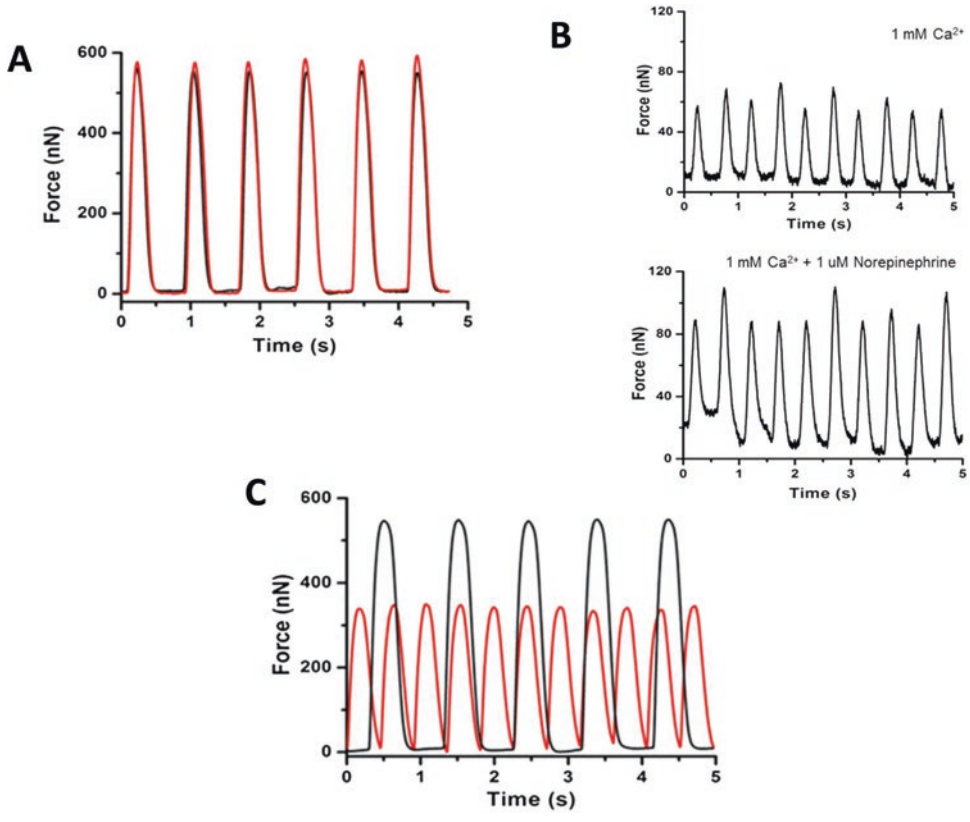

Fig. 6 Drug validation data. Cantilever force measurements indicating the effect of 100 mM sotalol (*red*) compared to control (*black*) (**a**), 1 μM norepinephrine (*bottom*) compared to control (*top*) (**b**), and 3 mM verapamil (*red*) compared to control (*black*) (**c**) on the cardiomyocytes (figure provided by [7])

5 Conclusion

This chapter describes, in detail, the methodology of a novel high-content phenotypic in vitro system that measures the force of the cardiac contractile machinery, in a high-throughput way, for the study of cellular physiology or the response to drugs that may affect cardiomyocyte contraction. The system has been previously validated with drug-specific response of human embryonic stem cell-derived cardiomyocytes to three known compounds, under serum-free conditions [7]. This in vitro model improves upon other published systems developed for the study of cardiac contractile force, because it (1) studies the complete contractile machinery, (2) has a reproducible fabrication, (3) generates accurate and comparable data, and (4) uses mature human cardiomyocytes under (5) serum-free medium conditions [7]. With this detailed protocol, the reproducibility of this system should be possible in other laboratories with other cardiac cells and even in the pharmaceutical and chemical industries to better predict human cardiotoxicity.

6 Notes

1. After the fabrication process and before releasing the chip for cell culture, cantilever inspection is recommended, utilizing a scanning electron microscope (SEM) (JEOL 6400 SEM or similar) to confirm successful fabrication of the chip.
2. To improve cellular anchorage to the surface of the chip, it is recommended a DETA coating is added to the surface of the cantilever [13].
3. To prevent cell migration from the cantilever tips to the bottom of the cell culture well, it is recommended to place a hydrophobic surface underneath the chip, such as tridecafluoro-1,1,2,2-tetrahydrooctyl-1-trichlorosilane (13 F) [15].
4. AFM should be installed on a high-performance anti-vibration platforms and workstations for microscopy to prevent vibrations during force recordings.
5. Ensure that the bottom surface of the glass dish is thoroughly cleaned to reduce laser deflection of opaque dirt on the glass surface.
6. On occasions when muscle tissue amasses at the tip of the cantilever making it difficult to align the laser beam, choose the next closest cantilever board to align, and make subsequent changes in the LabVIEW software. The algorithm in the software will account for this change and allow the full range of laser and detector for each individual cantilever.

7. After aligning the laser beam to the cantilever tip, ensure that a split laser beam does not appear on the detector. This is an indication that the cantilever fails to make proper contact with the surface, which will affect the intensity of the signal.
8. Laboratory lights should be turned off to prevent ambient perturbations in baseline.
9. To the same effect, the AFM should be placed within a faraday cage.
10. Drugs can be washed out by rinsing the cells five times with experimental medium [7].
11. Cantilever chips may be reused several times (6–10 times); after the cell culture and the experiment are done, the chip can be soaked in 1% Tergazyme overnight. Then follow the steps in list 1.24, and inspect the surface of the chip with a metallurgical or stereo microscope.
12. To extend half-life of cantilever chips, avoid:
    - Flipping the chip upside down—surface tension to remove it afterward will rip off the micro-cantilevers.
    - Pipetting liquid directly to the micro-cantilevers, with the exception of cell plating.

References

1. Braam SR, Tertoolen L, van de Stolpe A, Meyer T, Passier R, Mummery CL (2010) Prediction of drug-induced cardiotoxicity using human embryonic stem cell-derived cardiomyocytes. Stem Cell Res 4(2):107–116
2. Esch MB, Smith AS, Prot JM, Oleaga C, Hickman JJ, Shuler ML (2014) How multi-organ microdevices can help foster drug development. Adv Drug Deliv Rev 69–70:158–169
3. Cook D, Brown D, Alexander R, March R, Morgan P, Satterthwaite G et al (2014) Lessons learned from the fate of AstraZeneca's drug pipeline: a five-dimensional framework. Nat Rev Drug Discov 13(6):419–431
4. Gwathmey JK, Tsaioun K, Hajjar RJ (2009) Cardionomics: a new integrative approach for screening cardiotoxicity of drug candidates. Expert Opin Drug Metab Toxicol 5(6):647–660
5. Raschi E, Ceccarini L, De Ponti F, Recanatini M (2009) hERG-related drug toxicity and models for predicting hERG liability and QT prolongation. Expert Opin Drug Metab Toxicol 5(9):1005–1021
6. Redfern W, Carlsson L, Davis A, Lynch W, Mackenzie I, Palethorpe S et al (2003) Relationships between preclinical cardiac electrophysiology, clinical QT interval prolongation and torsade de pointes for a broad range of drugs: evidence for a provisional safety margin in drug development. Cardiovasc Res 58(1):32–45
7. Stancescu M, Molnar P, McAleer CW, McLamb W, Long CJ, Oleaga C et al (2015) A phenotypic in vitro model for the main determinants of human whole heart function. Biomaterials 60:20–30
8. Tamargo J, Duarte J, Caballero R, Delpon E (2011) New therapeutic targets for the development of positive inotropic agents. Discov Med 12(66):381–392
9. Das M, Gregory CA, Molnar P, Riedel LM, Wilson K, Hickman JJ (2006) A defined system to allow skeletal muscle differentiation and subsequent integration with silicon microstructures. Biomaterials 27(24):4374–4380
10. Das M, Wilson K, Molnar P, Hickman JJ (2007) Differentiation of skeletal muscle and integration of myotubes with silicon microstructures using serum-free medium and a synthetic silane substrate. Nat Protoc 2(7):1795–1801
11. Pirozzi KL, Long CJ, McAleer CW, Smith AS, Hickman JJ (2013) Correlation of embryonic skeletal muscle myotube physical characteristics with contractile force generation on an atomic force microscope-based bio-

microelectromechanical systems device. Appl Phys Lett 103(8):83108

12. Smith AS, Long CJ, Pirozzi K, Najjar S, McAleer C, Vandenburgh HH et al (2014) A multiplexed chip-based assay system for investigating the functional development of human skeletal myotubes in vitro. J Biotechnol 185:15–18
13. Wilson K, Das M, Wahl KJ, Colton RJ, Hickman J (2010) Measurement of contractile stress generated by cultured rat muscle on silicon cantilevers for toxin detection and muscle performance enhancement. PLoS One 5(6), e11042
14. Wilson K, Stancescu M, Das M, Rumsey J, Hickman J (2011) Direct patterning of coplanar polyethylene glycol alkylsilane monolayers by deep-ultraviolet photolithography as a general method for high fidelity, long-term cell patterning and culture. J Vac Sci Technol B Nanotechnol Microelectron 29(2):21020
15. Smith AS, Long CJ, McAleer C, Bobbitt N, Srinivasan B, Hickman JJ (2014) Utilization of microscale silicon cantilevers to assess cellular contractile function in vitro. J Vis Exp 92, e51866

Chapter 13

In Vitro Cardiotoxicity Investigation Using High Content Analysis and Human Stem Cell-Derived Models

Liz Roquemore, M. Ariel Kauss, Catherine Hather, Nick Thomas, and Hirdesh Uppal

Abstract

In the quest for more effective approaches to reduce the time, cost, and risks associated with development of new pharmaceuticals, High Content Analysis (HCA) is emerging as a valuable tool for in vitro predictive toxicity testing. Enabling rapid collection and analysis of information-rich cell images from thousands of samples a day, HCA offers high enough throughput for routine screening (High Content Screening, HCS) and mechanistic investigations to be performed at the early stages of discovery and preclinical development. By interrogating multiple endpoints simultaneously in the context of the same cells, candidate drugs can be grouped and prioritized according to the types and severity of cell effects they induce relative to reference compounds. At the same time, the signature drug response profiles captured by HCA provide valuable insights into mechanisms of toxicity. This chapter provides step-by-step protocols used for HCA cardiotoxicity testing of kinase inhibitors and other compounds of interest in oncology. Critical to the success of this approach is the selection and careful handling of a cell model that is amenable to high throughput HCA techniques while faithfully recapitulating human cardiomyocyte physiology in the dish with minimal batch-to-batch variability. Commercial human stem cell-derived cardiomyocytes (hSC-CM) provide a tractable and highly relevant model for this purpose. With robust quality-controlled hSC-CM cultures serving as a common test system, cardiotoxicity data obtained by HCA has the potential to be integrated with data from complementary in vitro tests—particularly those assessing electrophysiological effects—to provide more comprehensive evaluation and improved prediction of clinical responses.

Key words HCA, HCS, High content analysis, Cardiotoxicity, Human stem cell models, Cardiomyocytes, Mitochondrial toxicity, Cell profiling, Preclinical drug development, In vitro toxicity testing

1 Introduction

1.1 Improving Predictivity with High Content Analysis

High Content Analysis (HCA) is a drug discovery tool that harnesses the power of cell imaging to examine multiple endpoints and mechanistic pathways simultaneously at relatively high throughput. The technology has gained substantial momentum over the past decade due to advances on several fronts, including sensitivity and robustness of automated microscopy, accuracy and user friendliness of analysis software, improved solutions for data

Mike Clements and Liz Roquemore (eds.), *Stem Cell-Derived Models in Toxicology*, Methods in Pharmacology and Toxicology, DOI 10.1007/978-1-4939-6661-5_13,

visualization and mining, and the introduction of more relevant human cell models. HCA methodologies are being adopted for safety assessments at the discovery, preclinical and clinical stages of drug development to identify potential liabilities as early as possible and gain a deeper understanding of toxic mechanisms to inform drug design and lead optimization.

The use of HCA to facilitate earlier and more predictive cytotoxicity assessment promises to reduce costly late-stage attrition, lower the risk of market withdrawals for safety reasons, and decrease reliance on animal models at preclinical stages. Given that the average cost of progressing a drug from the point of discovery to registration has been estimated at nearly two billion dollars, and that over the period from 2006 to 2010 safety issues accounted for almost a quarter of failures in clinical development stages [1], the potential impact of HCA could be quite significant.

Although HCA technology cannot be expected to replace conventional in vitro test formats and animal-based methodologies in the near term, it offers unique advantages [2] that are likely to ensure its continued development and longevity as a complementary platform for early stage in vitro toxicity testing.

A major benefit of HCA is its capacity to collect multichannel spatial and morphological measurements at the subcellular level without compromising the integrity of the cell population. This allows multivariate investigation of diverse drug-induced changes including biomarker translocations, loss of mitochondrial integrity, alteration of mitochondrial morphology, disruption of calcium homeostasis, induction of reactive oxygen species, loss of nuclear integrity, changes in DNA content, formation of micronuclei, and many more. Subject to availability of appropriate fluorescent probes, many of these toxicity indicators can be monitored in live cells, facilitating detailed study of effects on the same cell population at multiple time points without disrupting cell behavior or risking fixation artifacts. This is especially advantageous when working with adherent 2D monolayers and 3D models such as organoids, where spatial relationships between cells and intercellular communication may play an important part in the phenotype of the population. For example, the spontaneous rhythmic beating of hSC-CM monolayers, which can be quantified by high frame rate HCA using a reporter of intracellular calcium such as Fluo-4 [3], is dependent on intercellular gap junctions, ion channel coordination, and intact contractile machinery. Preserving structural integrity can be critical for obtaining relevant results. As a case in point, Pointon et al. found that inhibiting spontaneous beating of hSC-CM renders them less sensitive to a number of structural cardiotoxins [4]. It is worth noting that even dyes compatible with live imaging may be toxic, degrade, or change their properties over extended time periods in live cells, and for this reason it is often best to configure longer time course studies in endpoint format (as in the example in this chapter, where the time course is carried out over 3 days).

Another key feature of image-based approaches is the collection of individual cell measurements, rather than population averages. The ability to quantify effects on single cells and sub-populations can increase assay sensitivity by detecting changes that would be masked if averaged across all cells in the sample well. For example, a plate reader assay quantifying total fluorescence intensity from a well population would register no net signal change if a chronic drug treatment were to induce both an adaptive increase in mitochondrial membrane potential in 50% of the cells and an equal magnitude of signal loss in the other half of the population due to loss of mitochondrial membrane integrity. Single cell analysis also makes it possible to quantify relatively rare events, such as micronuclei formation, an indicator of genotoxicity. While flow cytometry is widely employed to capture single cell and sub-population effects such as these, it necessitates disruption of 2D and 3D architecture during sample preparation, disturbing intercellular communication and causing damage that can potentially compromise the results.

Yet another advantage of HCA is the speed of both imaging and analysis. Automated HCA systems are optimized to capture and analyze high quality images very rapidly, enabling multivariate analysis of thousands of sample wells per day. For example, a single screening run of the magnitude described in this chapter—e.g., comprising 130 compounds, three time points, triplicate 10-point dose curves, four colors (i.e., dyes) per field of view, four fields of view per well—would require capture of over 200,000 images. With full automation, the image acquisition and analysis could be completed in under a week.

The utility of HCA for predictive toxicology rests on the premise that sub-acute drug-induced changes and damage at the cellular level may be informative biomarkers of the gross physiological responses manifesting as clinical toxicity. While the validity of this assumption is highly dependent upon a number of variables, especially choice of endpoints and relevance of the cell model, there is a growing body of evidence supporting the relative effectiveness of HCA compared to more conventional cytotoxicity assays [2]. The majority of these studies have focused on application of HCA for predicting hepatotoxicity, which alongside cardiotoxicity is a leading cause of safety related attrition [5–7]. However, with the advent of more relevant and tractable human heart cell models, HCA approaches are also being implemented for assessment of cardiotoxicity [4, 8].

1.2 Using hSC-CM Models for HCA Cardiotoxicity Testing

The development of human cardiomyocyte models from embryonic stem cells (hESC-CM) and induced pluripotent stem cells (hiPSC-CM) is a significant breakthrough for cardiotoxicity testing [9]. Renewable, reproducible, and well-characterized commercial hSC-CM have the potential to supersede the diverse assortment of non-human, immortalized, and genetically engineered cell

models more conventionally used in cardiotoxicity testing, offering a unifying model system that can be interrogated across a range of detection platforms and assay types for more relevant, integrated, and comprehensive toxicity assessment.

At present, the majority of in vitro cardiotoxicity assessments aim to identify adverse effects on cardiac electrophysiology and ion channel function. This is in part due to the high incidence of TdP (Torsades de Pointes) related drug withdrawals and consequent revision of safety guidelines for new chemical entities encouraging implementation of in vitro I_{Kr} assays (hERG potassium channel block) as part of integrated non-clinical risk assessment for proarrhythmic potential [10]. However, it is recognized that a significant proportion of clinical cardiovascular toxicities may arise as a result of structural and metabolic damage that conventional patch clamp electrophysiological assessments cannot detect [5].

An accepted mechanism for integrating structural integrity assays into preclinical in vitro testing is thus an unmet need. HCA has the potential to address this need when paired with appropriate human model systems. A study employing HCA to profile toxicity of known functional and structural cardiotoxins demonstrated the utility of HCA for this purpose [4]. In conjunction with assessment of ATP, the HCA method was able to predict in vivo outcomes with an overall sensitivity and specificity of 74%. Comparative analysis of model cell types used in the study revealed that hSC-CM provided better prediction of structural cardiotoxicity than the conventional H9c2 myoblast line.

1.3 Cardiotoxicity of Anti-cancer Drugs

The methods and results in this chapter derive from an ongoing study investigating the cardiotoxicity of anti-cancer agents [8]. The cardiovascular risks of anti-cancer agents have become more evident in recent years, particularly as the lifespan of patients with metastatic disease increases, but also as new classes and combinations of drugs may have on- or off-target effects on mechanistic pathways that are common to both cancer cell survival and cardiomyocyte health [11, 12]. Small molecules and biologics targeting key cellular kinases have generated significant interest and success as therapeutic agents. Nevertheless, a number of anti-cancer drugs in clinical use have been associated with adverse cardiotoxic effects (Table 1; [12–15]).

1.4 Detecting Mitochondrially Mediated Cardiotoxicity

Cardiac tissue is energetically demanding and rich in mitochondria [16], and direct or indirect action of anti-cancer drugs, including kinase inhibitors, on mitochondria has been identified as a key contributing factor in cardiotoxicity associated with oncology therapeutics [11]. It is important to be aware that most cell types cultured in glucose-containing media, including cardiomyocytes, have a tendency to shift bioenergetic metabolism to generate the bulk of their ATP from glycolysis rather than oxidative phosphorylation (OXPHOS), despite having abundant and fully

Table 1
Cardiotoxicity induced by tyrosine kinase (TK) inhibitors in cancer therapeutics

Drug	TK target	Indications	Cardiotoxicity
Imatinib	Bcr-Abl, c-kit, PDGFR	CML, PhALL, GIST, CMML, CEL, DFSP	CHF, LVEF depression
Dasatinib	Bcr-Abl, c-kit, PDGFR, Src	CML	QT prolongation, Peripheral edema
Nilotinib	Bcr-Abl, c-kit, PDGFR	CML	QT prolongation
Sunitinib	VEGFR, RET, PDGFR, c-kit	RCC, GIST	Hypertension, LVEF depression, CHF, MI
Sorafenib	VEGFR, c-kit, PDGFR, FLT3, RAF1	RCC, HCC	Acute coronary syndrome, MI, hypertension
Lapatinib	EGFR, ERBB2	Breast cancer	Asymptomatic LVEF depression
Gefitinib	EGFR	NSCLC	Not reported
Erlotinib	EGFR	NSCLC, pancreatic cancer	Not reported

Data from Orphanos et al. [13]
CML chronic myelogenous leukemia, *PhALL* Philadelphia chromosome-positive acute lymphoblastic leukemia, *GIST* gastrointestinal stromal tumors, *CMML* chronic myelomonocytic leukemia, *CEL* chronic eosinophilic leukemia, *DFSP* dermatofibrosarcoma protuberans, *CHF* congestive heart failure, *LVEF* left ventricular ejection fraction, *RCC* renal cell carcinoma, *MI* myocardial infarction, *HCC* hepatocellular carcinoma, *NSCLC* non-small cell lung cancer

metabolically competent mitochondria [17]. This phenomenon can lead to partial or complete resistance of hSC-CM to mitochondrial toxicants [18]. Replacing glucose with galactose as the primary energy source (protocol 3.2, **step 7**) renders glycolysis energetically unfavorable, forcing the cells to rely on mitochondria for ATP production, and more closely mimicking the in vivo metabolic state of healthy heart tissue. One study of four tyrosine kinase (TK) inhibitors in isolated mitochondria and rat H9c2 cells demonstrated a fourfold increase in Sorafenib toxicity in galactose medium [19]. A more recent study testing a variety of culture conditions demonstrated that hiPSC-CM are bioenergetically closest to adult heart tissue cells when cultured in galactose media [20].

1.5 Screening of 130 Anti-Cancer Agents (and Reference Compounds) for Cardiotoxicty

As part of an ongoing study investigating cardiotoxicity of kinase inhibitors and other compounds of interest in oncology, blinded HCA screens comprising a set of 130 anti-cancer drugs and controls were conducted using spontaneously beating hSC-CM in a live 4-color (dye) assay (Fig. 1). With control and reference compounds included for normalization and comparison, responses generated in the course of the study proved to be remarkably similar across replicate wells, plates, instruments, and operators. The following materials and methods were used to conduct the screening, which was configured in 384-well format. Dose–response data were collected

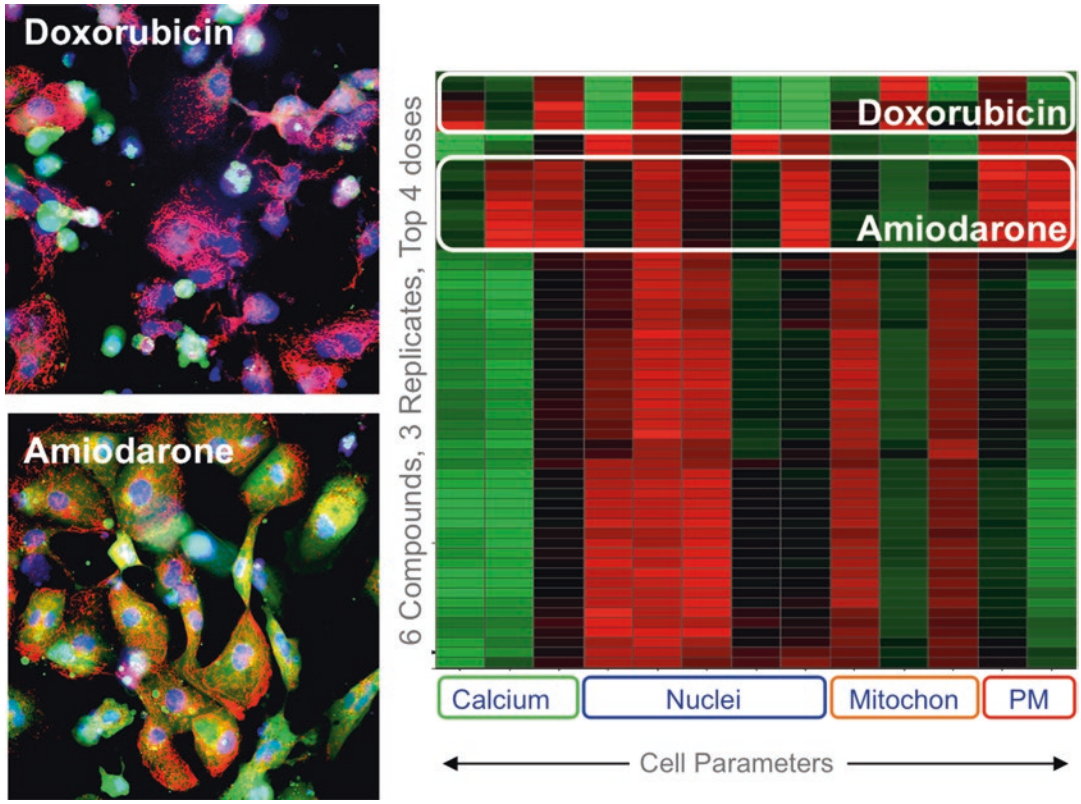

Fig. 1 High content analysis cell health assay. Cytiva cardiomyocytes treated with doxorubicin, amiodarone, and vehicle only (control), as indicated, and stained for intracellular calcium (Fluo-4; *green*), nuclear status (Hoechst; *blue*), mitochondrial health (TMRM; *red*), and plasma membrane (PM) integrity (TOTO-3; not visible in these three-color RGB images). Imaged with IN cell analyzer HCA platform using 40×/0.6 NA objective. Many cell health metrics can be extracted by high content image analysis from each fluorophore to construct multiparametric "signatures" for each compound and concentration (each row of the (heat map)

for every compound in triplicate at 24, 48, and 72 h time points. To explore the utility of bioenergetic modulation in sensitizing hSC-CM to mitochondrial toxicants, assay plates were prepared in duplicate with hSC-CM cultured in standard medium (RPMI 1640/B27 containing 11 mM glucose) for one set, and glucose-free medium (replacing glucose with galactose) for the other. Included in the screen were compounds that previously had been shown to cause signal change for all of the assay endpoints ("positive" reference compound, Amiodarone) or none of them ("negative" reference compound, Nifedipine). Although Nifedipine (an L-type Ca2+ channel blocker) will perturb the spontaneous beating of hSC-CMs, it was useful as a negative reference compound for this particular assay, since we had previously validated that it would not induce changes in the endpoints of interest. Full 10-point dose–response series were run for both of these compounds at all time points and in both glucose and galactose media. In addition, top, middle, and bottom dose concentrations of each were included as in-plate controls in the empty edge wells.

2 Materials

2.1 General Equipment and Consumables

1. Adjustable pipettes and tips
2. Serological pipettes, sterile, 5–25 ml
3. Liquid nitrogen vapor store
4. Biosafety cabinet—Class II laminar flow providing sterile environment for cell culture
5. 37 °C water bath
6. Centrifuge
7. Tissue culture incubator—humidified and equilibrated to 37 °C, 5% CO_2
8. Inverted light microscope (routine culture assessment)
9. Hemocytometer or automated cell counter
10. HCA System—IN Cell Analyzer 2200 or 6000 (GE Healthcare), or similar caliber automated epifluorescence microscope with digital imaging capability, multi-well plate compatible stage, 40× objective, and excitation and emission filters suitable for chosen dyes
11. Image analysis software—IN Cell Investigator (GE Healthcare) or similar, validated for HCA applications and capable of image pre- and post-processing, cell-by-cell analysis, feature segmentation, target identification (nuclei, mitochondria, and cytoplasmic sampling region), sub-population filtering, and sub-population analysis.

2.2 Plate Preparation and Cell Culture Media

1. Cardiomyocytes—well-characterized hSC-CM cell line (**Note 4.1**) such as Cytiva Plus Cardiomyocytes (GE Healthcare, 29-0918-80). Refer to product data sheet and manufacturer's instructions for thawing from frozen stocks; cell count and viability determinations; and culture maintenance
2. Glucose medium (same formulation as "RPMI + B27 medium" referred to in published literature and Instructions for Use documents): glucose-free RPMI 1640 supplemented with 1× B27 and 11 mM glucose; sterile filtered (**Note 4.4**)
3. Galactose medium: RPMI 1640, no glucose supplemented with 1× B27 and 11 mM galactose; sterile filtered (**Note 4.4**)
4. Fibronectin (1 mg, human)
5. Sterile distilled H_2O
6. 50 ml centrifuge tube
7. Phosphate buffered saline, sterile distilled (D-PBS)
8. 384-well culture plates, sterile (e.g., Greiner μClear 781091)
9. 20 μl pipette and sterile 1–40 μl tips
10. 1000 μl pipette and sterile 1–1000 μl tips.

2.3 Cell Health Dye Assay and Imaging

Ionomycin (optional control, e.g., Sigma-Aldrich i0634-5 mg)

FCCP (optional control, e.g., Sigma-Aldrich c2929-10 mg)

Triton X-100 (optional control, e.g., Sigma-Aldrich 9443-100 ml)

Hoechst 33342 (e.g., BD Biosciences 561908)

Tetramethylrhodamine, Methyl Ester, Perchlorate (TMRM)

4 μM Fluo-4-AM

4 μM TOTO-3 iodide

Breathe Easier sealing membranes for multi-well plates (Sigma-Aldrich Z763624)

3 Methods

Table 2 summarizes the overall workflow encompassing the methods that follow. The protocols have been optimized for use with spontaneously beating Cytiva™ or Cytiva Plus™ human stem cell-derived cardiomyocytes, which were used to generate all results presented in the chapter. If using alternative cell lines, *see* **Note 4.1** and refer to manufacturer's recommendations for preparation and maintenance. Details of the fibronectin coating and cell seeding procedures are included because quality and consistency at these stages can significantly affect the hSC-CM phenotype and resulting images.

3.1 Fibronectin Coating of Assay Plates

For best results, prepare extracellular matrix (ECM)-coated plates on the day of use.

1. Reconstitute 1 mg fibronectin to 1 ml with sterile distilled water (1 mg/ml final concentration).
2. In a sterile 50-ml tube, prepare a 12.5 μg/ml solution by diluting 125 μl of the 1 mg/ml fibronectin into 9875 μl D-PBS.
3. To each well of a sterile 384-well plate, add 30 μl of 12.5 μg/ml fibronectin. Cover the plate with its sterile lid, and place in the tissue culture incubator for at least 2 h (**Note 4.2**).

3.2 Seeding and Culture of Cells in the Assay Plate

For 384-well HCA experiments, cells are typically seeded at $9–15 \times 10^3$ viable cells per well to obtain a confluent monolayer. It may be advantageous to seed cells to all wells of the plate, even if it is planned to exclude edge wells from the assay (**Note 4.3**). Even if the outer wells are not seeded with cells, keep them filled with an aqueous solution (e.g., culture medium or D-PBS) at all times in order to minimize evaporation and variability in the test wells. The following protocol specifies 10,000 viable Cytiva Plus cells per well; seeding density optimization is recommended for different cell lines and intended applications. For mitochondrial sensitization, precondition cells in galactose medium 24 h prior to compound addition (at **step 7**; **Note 4.4**).

Table 2

HCS cardiotoxicity assay workflow

Protocol (section)	Step	Procedure	Value	Description
3.1	1	Fibronectin-coat	30 µl	12.5 µg/ml fibronectin
3.2	2	Plate cells	50 µl, 1×10^4 cells	hSC-CM (Cytiva Plus)
	3	Incubate	5 days	37 °C/5% CO_2
	4	Media change	40 µl	Glucose or galactose medium
	5	Incubate	24 h	37 °C/5% CO_2
3.3	6	Add compounds	20 µl	Dilution series in Glu or Gal medium; 0.03–300 µM final concentration range
	7	Incubate	24, 48, 72 h	37 °C/5% CO_2
3.4	8	Add fluorescent probe cocktail	20 µl	Final concentrations: 1 µM Hoechst, 20 nM TMRM, 1 µM Fluo-4, 1 µM TOTO-3 in Glu or Gal medium
	9	Incubate	1 h	37 °C/5% CO_2
3.5	10	Image	40×/0.6 NA objective, four fields per well	Automated HCA/HCS with environmental control (37 °C, humidified CO_2)
3.6	11	Image analysis	Multivariate	Mitochondrial morphology, calcium homeostasis, plasma membrane integrity, nuclear status (IN Cell Investigator)
3.7	12	2° Data analysis	IC_{50}, profile plots, SOM clustering	Statistical data package (Spotfire DecisionSite via IN Cell Investigator)

1. Preheat water bath to 37 °C
2. In 37 °C water bath, warm 25 ml glucose medium (RPMI/B27)
3. Dilute the thawed cardiomyocyte cell suspension to 2×10^5 viable cells/ml using warm glucose medium

$$\text{Required volume}(\text{ml}) = \frac{(\text{number of viable cells})}{(2 \times 10^5 \text{ viable cells} / \text{ml})}$$

4. Remove fibronectin-coated culture plate from the incubator
5. Aspirate the fibronectin solution from each well and *immediately* replace with 50 µl cardiomyocyte suspension
6. After seeding required wells, replace the sterile lid on the culture plate, and place in the cell culture incubator (**Note 4.5**)

7. At 5 days post-seeding, or 24 h prior to compound addition (**Note 4.6**), flick the media out of the plate onto clean tissues and replace with 40 µl pre-warmed (37 °C) glucose medium or galactose medium, taking care not to disturb the seeded cells or introduce bubbles. Return to the incubator for a further 24 h, at which point the cells will be ready for compound addition.

3.3 Compound Plate Preparation and Addition of Compound to Assay Plate

Compound Plates (at 3× concentration) are configured in a layout that mirrors that of the Assay Plates, so that the assay can be initiated with minimal chance of error by transferring from the Compound Plate to corresponding wells on the Assay Plate. For each test compound, a dose series is arrayed on the Compound Plate in triplicate, as illustrated in Fig. 2, which shows a 10-point series prepared using a dilution factor of 3.16. Each 384-well plate can accommodate eight compounds, arrayed in blocks of 30 wells (i.e., 10 doses × 3 replicates per compound, as shown), excluding edge wells. For mitochondrial sensitization, prepare compounds in galactose medium, (**steps 2** and **4** below). Compound Plates may be prepared up to 18 h before the experiment, stored at 4 °C, and then equilibrated to 37 °C prior to use. The following protocol specifies a final compound concentration range of 0.03–300 µM in the Assay Plate.

1. Prepare 30 mM stock solutions of all test compounds and controls in sterile vehicle solvent of choice (e.g., DMSO);
2. Dilute each compound stock solution 33.3 fold by adding 9 µl stock to 291 µl of culture medium (glucose or galactose medium). This yields a 900 µM solution (3× the concentration of the highest dose on the Assay Plate) containing 3% vehicle solvent;
3. To a sterile 384-well plate, transfer 80 µl of each 900 µM compound solution to the wells designated for the highest dose in the range. (i.e., columns 12 and 22, Fig. 2a);
4. Dispense 54 µl of media containing 3% (v/v) of the appropriate vehicle solvent into each of the remaining wells in the compound blocks (columns 3–11 and 13–21);
5. Create the dilution series by successively transferring 25 µl compound solution from the starting wells (highest compound concentration) into the 54 µl of medium in the next-concentration wells of the series, thoroughly mixing after each addition. Continue in this fashion to complete each series (to columns 4 and 14, Fig. 2). *See* **Note 4.7**.
6. Prior to adding compounds to the cells, equilibrate the Compound Plate to 37 °C in a tissue culture incubator.

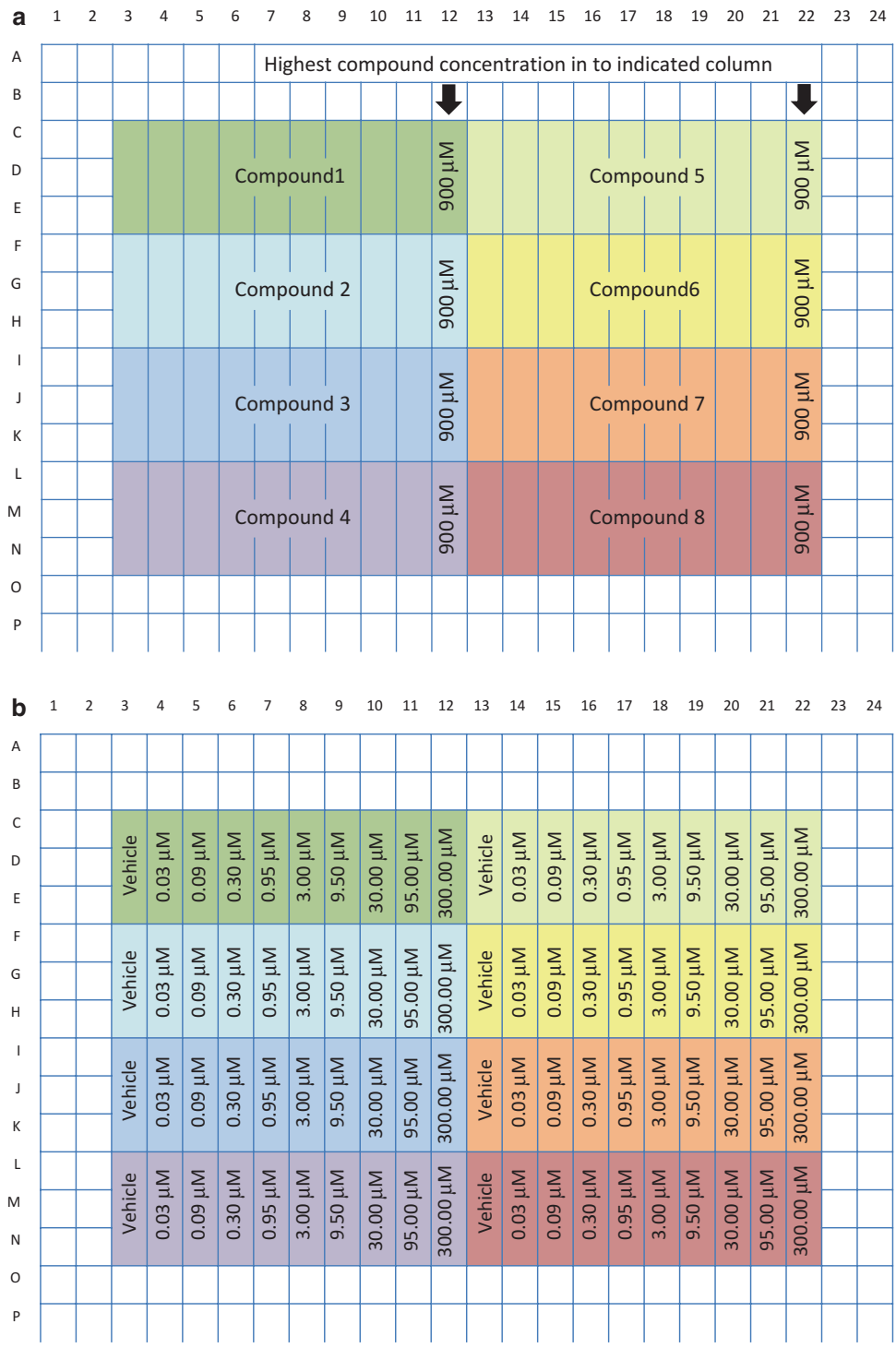

Fig. 2 Compound and assay plate maps. (**a**) Compounds are arrayed in dose–response series at 3× concentration on the compound plate. (**b**) Assay plate layout mirrors that of the compound plate, with final dilutions indicated

7. To start the HCA assay, transfer 20 μl compound solution from the Compound Plate into the corresponding well of the Assay Plate, taking care not to disturb the cell monolayer or create bubbles.
8. Cover the Assay Plate with its sterile lid, and return it to the tissue culture incubator for the desired drug exposure period (24–72 h).

3.4 Cytotoxicity Assay

The fluorophores employed in this assay monitor nuclear status, calcium homeostasis, mitochondrial health, and cell viability. In keeping with the features of an effective cytotoxicity assay, summarized by O'Brien [2], the chosen combination of endpoints is designed to capture a wide variety of potential processes involved in cell injury, providing surveillance of both morphological and functional changes. The assay workflow is summarized in Table 2.

1. Twenty minutes prior to loading the cells with dyes to probe cell health, add 20 μl of 4× concentrated controls to designated control wells (**Note 4.8**).
2. Remove fluorescent probes of choice ("dyes") from storage and equilibrate to room temperature, briefly vortexing and centrifuging if needed to ensure mixing and full recovery of contents.
3. Warm cell culture media (glucose and/or galactose) by placing in a 37 °C water bath.
4. In a sterile tube, prepare 4× cocktail of dyes (**Note 4.9**) in prewarmed culture medium. For the studies in this chapter, the 4× cocktail contained:
   - 4 μM Hoechst 33342
   - 80 nM TMRM
   - 4 μM Fluo-4-AM
   - 4 μM TOTO-3 iodide
5. Decant the 4× dye mix into a sterile reagent reservoir and use a multichannel pipette to dispense 20 μl into each treated well of the 384-well cell Assay Plate, changing tips as necessary to avoid cross contamination of drug treatments. Take care not to disturb the cells or introduce bubbles during reagent additions.
6. Cover the Assay Plate with its sterile lid, and return it to the incubator for 1 h.

3.5 High Content Imaging

Prior to imaging, ensure that there is sufficient storage space (memory) available for the image files (**Note 4.10**). It is also helpful to create and test the image acquisition protocol ahead of time, checking that plate scan times will not be likely to exceed 90 min per plate.

1. Pre-equilibrate the HCA system with environmental control unit to 37 °C, 5 % CO_2.
2. Remove lid from plate(s) and replace with Breathe Easier plate seal (**Note 4.11**).
3. Load plate into the instrument.
4. Open or create an acquisition protocol, specifying plate type, objective, and excitation/emission pathways. On IN Cell Analyzer systems, the 40×/0.6 NA objective is recommended to ensure adequate resolution of mitochondria, and the Quad 2 polychroic is selected in conjunction with the following excitation (x) and emission (m) filter combinations: 350/50×, 455/50 m (Hoechst); 490/20×, 525/20 m (Fluo-4); 579/34×, 624/40 m (TMRM); and 645/30×, 705/72 m (TOTO-3).
5. For each channel, optimize exposure time and focus parameters using negative (vehicle only) and positive control wells.
6. Choose number of fields sufficient to collect a minimum of 250 cells per untreated/vehicle-only control well (**Note 4.12**).
7. Start acquisition (**Note 4.13**)

3.6 Image Analysis

1. *Identify (segment) nuclei on the basis of staining in the Hoechst channel*. The nuclear region thus defined will be used to (1) determine cell count (from the Hoechst channel image); (2) extract nuclear size and morphology measurements (Hoechst channel image); (3) identify dead cells on the basis of nuclear staining in the TOTO-3 channel image; and (4) measure Fluo-4 fluorescence (calcium) in the nuclear region. Depending on the image quality, one or more pre-processing steps (shading removal, de-noising, etc.) may be helpful to improve segmentation results. Choose a segmentation method that best distinguishes nuclei from each other and from any background signal, so that the segmentation result (visualized by a mask or outline) corresponds as closely as possible with the objects observed in the image. If needed, use post-processing steps (erosion, dilation, fill holes, sieve, clump breaking, etc.) to further improve delineation of nuclei.
2. *Define the cytoplasmic region*. This region will be used to (1) sample Fluo-4 fluorescence (calcium) in the cytoplasmic region of the Fluo-4 image, and (2) assign mitochondria (falling within each cytoplasm + nucleus region in the TMRM image) to their corresponding nucleus (Hoechst channel), and thus to an individual cell. For the purposes of cell health assessment, it is not necessary to identify the entire region of the cytoplasm, but rather is sufficient to sample a representative area surrounding the nucleus. Typically this is achieved by dilating

outwards from the nucleus (in the Hoechst channel image) to create a ring or "collar" of sufficient width to capture representative data from the cytoplasm.

3. *Segment mitochondria in the TMRM channel image.* Mitochondria characteristically present as granular structures and/or thread-like networks distributed throughout the body of the cell. Since mitochondrial morphology and staining intensity may vary with different drug treatments, refer to positive and negative control samples when setting up the segmentation parameters. Choose a segmentation method that will best distinguish mitochondrial structures from each other and the surrounding background signal. As with nuclear segmentation, experiment with available pre- and post-processing steps as needed to achieve acceptable segmentation.
4. *Define live-cell and dead-cell populations.* TOTO-3 will stain the nuclei of dead cells only. Apply the nuclear mask defined in **step 1** to the TOTO-3 channel image to measure average intensity of nuclei in the TOTO-3 channel. Referring to positive and negative controls, set up an intensity threshold to distinguish live and dead sub-populations. Configure the analysis routine to report the number and percentage of live and dead cells.
5. *Extract cell health measurements.* A variety of measurements may be taken from the features identified in each fluorescence channel. Set up the analysis routine to report individual cell measurements and the respective population averages for each well. The following metrics (per cell, unless otherwise specified) may be helpful for cell health profiling.
    - Hoechst channel (Nuclei): Mean nuclear area, mean nuclear form factor (degree of "roundness"), mean nuclear intensity, total nuclear intensity (average pixel intensity × area, as an indicator of DNA content), and total nuclear count (sum of nuclei detected in all fields of view captured within a well).
    - Fluo-4 channel (Calcium): mean nuclear signal intensity, mean cell (nuclear + cytoplasm) signal intensity, and total cell signal intensity (mean pixel intensity × area).
    - TMRM channel (Mitochondria): total (sum) mitochondrial area (indicator of mitochondrial mass), mean mitochondrial area, total (sum) mitochondrial count, mean mitochondrial count, mean mitochondrial form factor ("roundness"), mean mitochondrial intensity, and mean mitochondrial length.
    - TOTO-3 (dead cells) and Hoechst (all cells):

$$\%\text{Viability}(\text{per well}) = 100 \times \frac{[\text{total cell count} - \text{dead cell count}]}{\text{total cell count}}$$

6. Configure analysis protocol to export data in a format (e.g., xls or csv) compatible with the statistical data analysis software of choice. All data for the examples in this chapter were analyzed with Spotfire or Spotfire DecisionSite (Tibco), using the Functional Genomics package for Self-Organizing Map clustering.

3.7 Data Visualization, Phenotypic Profiling, and Cluster Analysis

Once image analysis is complete, import well-averaged and individual cell data into statistical analysis software for secondary analysis. For example:

1. *Plot dose–response curves and extract IC50 values for measures of interest* such as % viability (based on TOTO-3), Mitochondrial Form Factor (TMRM) (Fig. 3). At lead optimization and prioritization stages it may be informative to rank compounds of the same series based on IC_{50} values for one or more parameters such as % viability. If maximal in vivo plasma concentration values (C_{max}) are available, therapeutic index may be calculated by normalizing the % viability IC_{50} to C_{max} (i.e., IC_{50}/C_{max}). A threshold of 100 would be typical as a rough and ready means of distinguishing toxic from non-toxic species. If C_{max} is unavailable, in vitro efficacious concentration could be substituted.
2. *Profile drug responses based on multiple parameters.* In contrast to prioritization based on IC_{50} values, multivariate response profiling takes greater advantage of the high information con-

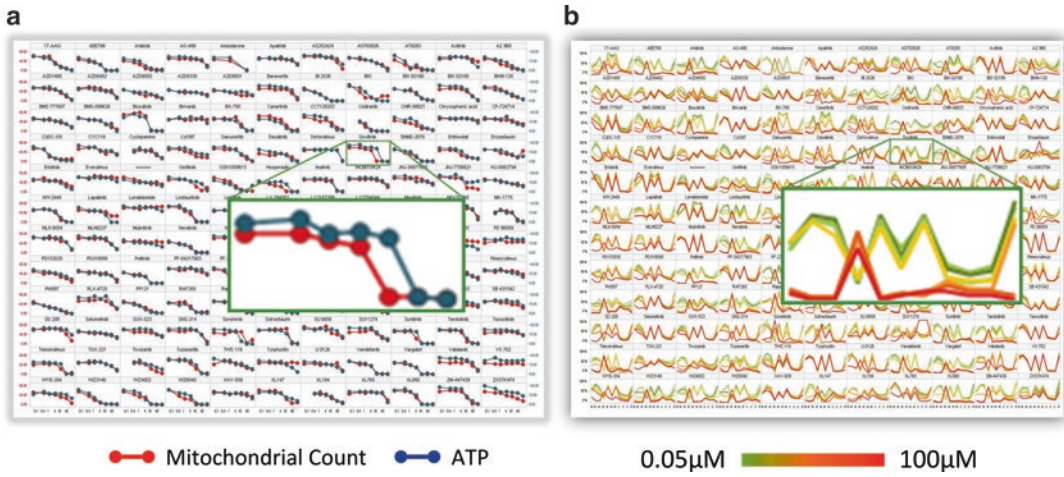

Fig. 3 Dose–response and profile plots. (**a**) Dose–response plots for all compounds in the screen for a single mitochondrial parameter. Data from other assays can be plotted for comparison. For example, ATP content plotted here was determined using a non-HCA in vitro ATP assay (not discussed in this chapter); (b) 11-parameter profile plots were created for every compound in the set at every dose (shown here over the range from 0.05 to 100 µM, as indicated in the color legend). Parameters (*x*-axis) are group together by fluorophore, as indicated in Fig. 4. Reproduced from [8]

tent of HCA screens, for more informed decision-making and more mechanistic information. For this purpose, parallel coordinate plots are useful (Figs. 3 and 4). Plot each parameter on a separate vertical axis, expressing as % maximum response to normalize. As illustrated in Fig. 4, grouping parameters based on endpoint (fluorescent probe) provides insight into mechanisms of toxicity. Since mitochondrial parameters were of particular interest in this study, we found it informative to create profile plots comprising seven measures relating to mitochondrial health, three relating to intracellular calcium levels in subcellular regions, and percentage viability as determined from TOTO-3 signal. By grouping like parameters together on the profile plot, it has readily become apparent that, relative to a negative control reference compound (Nifedipine in this case), the MEK1 inhibitor PD325901 elevated intracellular calcium, the principal regulator of cardiac contractility (Fig. 4a), while Entinostat, a histone deacetylase inhibitor, caused a similar change in calcium levels, and also affected some but not all of the mitochondrial measures, consistent with reported Entinostat-induced mitochondrial damage mediated by generation of reactive oxygen species (Fig. 4b) [21]. By contrast, Imatinib (Gleevek) affected all of parameters, including mitochondrial rounding ("form factor"), increases in which are highly correlated with cell death (Fig. 4c). The extensive mitochondrial damage observed in response to Imatinib is consistent with literature reports of Imatinib cardiotoxicity in humans, including mitochondrial abnormalities observed in biopsies from patients presenting with severe congestive heart failure while taking Imatinib [22].

3. *Cluster profiles according to similarity.* A Self-Organizing Map (SOM) tool, such as that available in Spotfire software, will assign profiles to a user-selected number of bins based on similarity. The larger the number of profiles being compared, the more bins are required. Too few bins will fail to adequately distinguish phenotypic signatures, while too many will lead to meaningless distinctions. For the set of 130 compounds in this example (Fig. 5), binning was set to 12, resulting in negative and positive reference compounds falling into bins 1 and 12, respectively. As shown in Fig. 5, the majority (85%) of compounds in the set for which we could find reports of clinical cardiotoxicity or adverse reactions [13, 23] clustered in group 12, including the positive reference compound Amiodarone. It is worth noting here that although Amiodarone is a prescribed antiarrhythmic drug, it is known to produce side effects related to its therapeutic mechanism of action, and there has been at least one associated adverse cardiovascular drug reaction [23]. None of the compounds in our study known to have reported

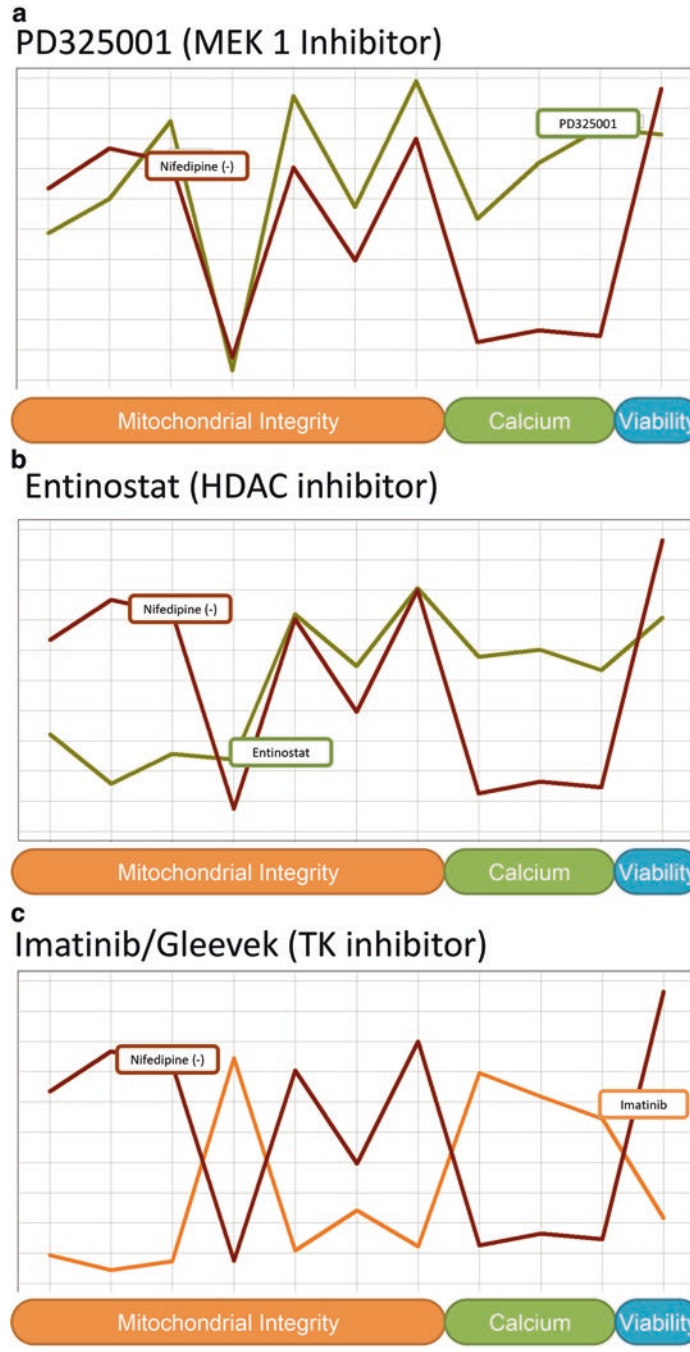

Fig. 4 Profile plot interpretation. Grouping related endpoints reveals mechanistic information. Nifedipine (*brown line*) was used as a negative reference compound for comparison. All plots are for compound concentration of 33 μM. (**a**) Effect of MEK1 inhibitor on calcium parameters only; (**b**) effect of Entinostat (a histone deacetylase inhibitor) on calcium and some mitochondrial parameters; (**c**) effect of Imatinib (a tyrosine kinase inhibitor) on all parameters in the profile. Reproduced from [8]

a

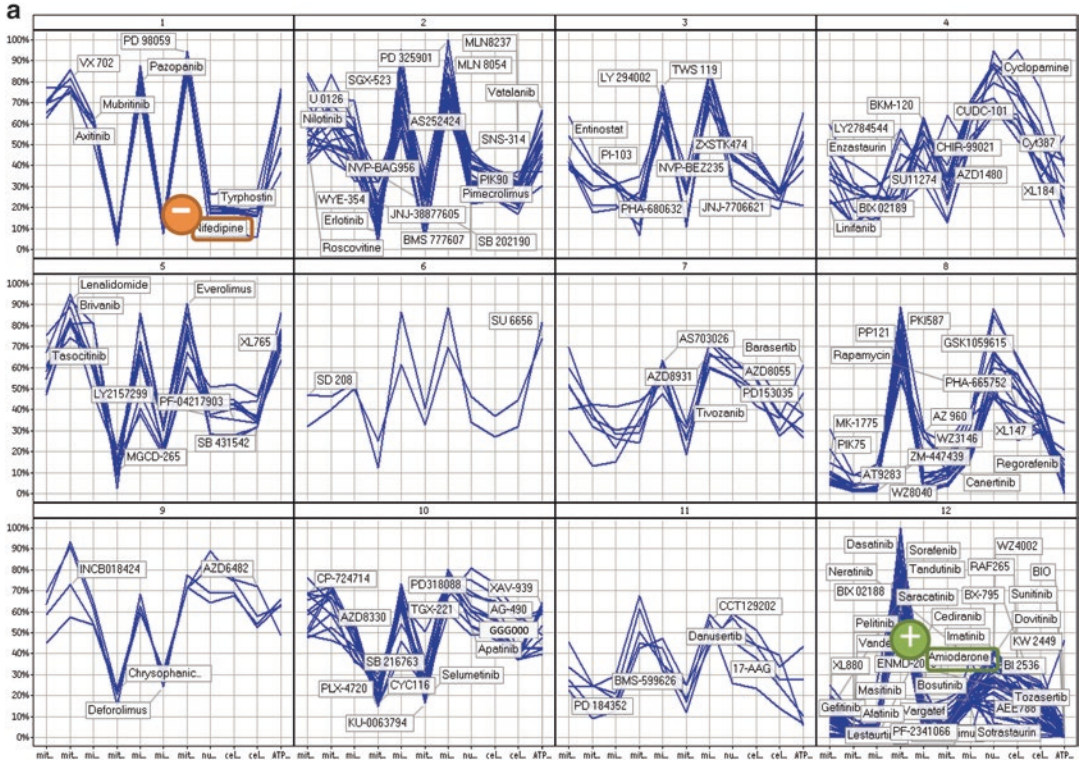

b

Cluster 12			
Amiodarone (+)	Dasatinib	Masitinib	Tandutinib
AEE788	Dovitinib	Neratinib	Temsirolimus
Afatinib	ENMO-2076	Pelitinib	Tozastertib
BI2536	Gefitinib	PF-2341066	Vandetanib
BIO	Hesperadin	RAF265	Vargatef
BIX 02188	Imatinib	Saracatinib	WZ4002
Bosutinib	KW 2449	Sorafenib	XL880
BX-795	Lapatinib	Sotrastaurin	
Cediranib	Lestaurtinib	Sunitinib	

Fig. 5 Profile clustering. (**a**) SOM clustering results from the screen of 130 compounds in glucose medium, effectively segregating negative and positive reference compounds, Nifedipine and Amiodarone, into bins 1 and 12, respectively. Parameters (*x*-axis) are grouped together by fluorophore, as indicated in Fig. 4. (**b**) Compounds assigned to cluster 12, with those having reported clinical toxicities highlighted in *orange* [13, 23]. Reproduced from [8]

clinical cardiotoxicities clustered in group with the negative reference compound Nifedipine. These results suggest that with further validation this profile clustering approach could be a useful tool in compound prioritization, helping identify compounds most likely to lead to clinical cardiotoxicity (i.e.,

those clustering with positive reference compounds), and to generate testable hypotheses as to the underlying basis of profile similarities within clusters.

4. *Use 2-D plots to explore variable dependencies as well as dose- and time-dependent effects.* Screening in hSC-CM cultured in glucose medium indicated that Mubritinib, which clustered in group 1 with the negative reference compound, was not toxic over the dose range at either the 24-h or 72-h time point (Fig. 6). However, culture in galactose medium revealed that after 72 h of treatment, doses at the low end of the concentration range elicited a steep drop in cell viability concomitant with mitochondrial morphology changes. At the 24-h time point there is less time for drug to elicit its full effects, and in this case the change in mitochondrial morphology is revealed to occur at a lower concentration than the drop in cell viability, suggesting that the effect of Mubritinib on mitochondrial health may be a direct one which potentiates cell death. Mubritinib is a protein kinase inhibitor that was under development for cancer treatment by Takeda. It was discontinued for unknown reasons after completing phase 1 clinical trials [24]. The results with Mubritinib are contrasted with the data from Amiodarone treatment, where toxicity is detected in both glucose and galactose media at both time points, and there is a fairly linear correlation between mitochondrial form factor and viability.

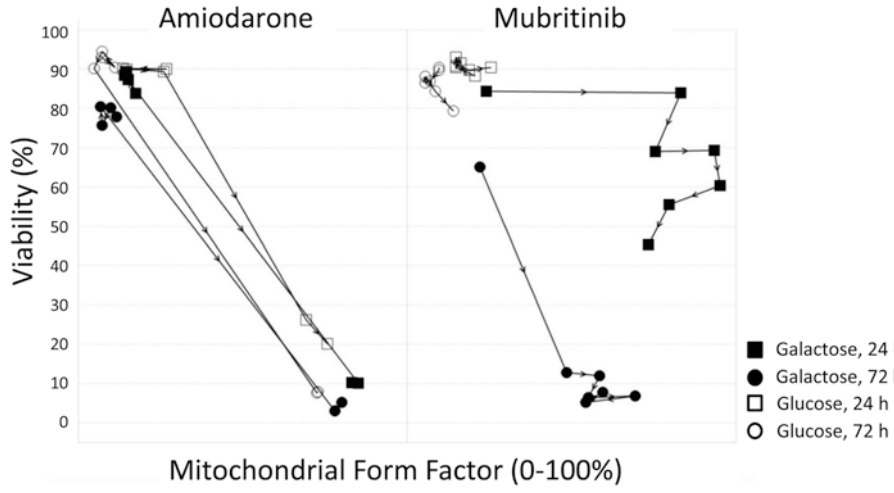

Fig. 6 Galactose medium unmasks mitochondrial toxicity of Mubritinib. Correlation plots for % cell viability and mitochondrial form factor for Amiodarone (**a**) and Mubritinib (**b**) treatments in the presence of glucose or galactose media at 24 and 72 h (as indicated in the key). *Arrows* indicate increasing doses

4 Notes

4.1 For meaningful results, it is essential to use a well-characterized hSC-CM line, preferably one that has previously been validated for HCA and demonstrated to possess tissue specific markers and characteristics expected of authentic human cardiomyocytes. There are a number of commercial hSC-CM products to choose from, typically generated from either human embryonic stem cells (hESC) or human induced pluripotent stem cells (hiPSC).

4.2 The 2 h fibronectin incubation period may be used to prepare fresh cardiomyocyte culture medium, thaw frozen cells, and perform cell count and viability determinations. Refer to product data sheet and manufacturer's recommendations for instructions on thawing and cell count determinations.

4.3 It is recommended that outer wells of the Assay Plate be seeded with cells but not used for testing compound due to the increased evaporation rates at the edge of the plate. Cells in the edge wells can be used for dye loading and function controls on the day of the assay.

4.4 Avoid repeated warming of glucose and galactose media. Warm only the required volume of medium to complete the task. If preparing the media in bulk, aliquot in convenient volumes (e.g., 25 ml) for storage at 2–8 °C. Use within 1 week of preparation.

4.5 Monitor cells on a manual microscope daily, assessing general morphology and watching for signs of spontaneous monolayer beating, which typically becomes apparent from day 4 post-seeding. An additional feeding step (replacing medium with fresh) around day 4 is optional if medium appears spent or there are signs of stress in the culture.

4.6 The optimal time to begin the HCA assay (by compound addition) is at 5–7 days post-seeding to allow time for the cells to fully recover from cryostorage and develop the physiological characteristics expected of authentic human cardiomyocytes. It may be necessary to perform optimization experiments to determine appropriate culture period for the intended application.

4.7 Precise aspiration, dispensing, and mixing are essential for robust and reproducible results. Ensure dispensing equipment is calibrated before use. If preparing the Compound Plate manually, a multichannel pipette is suitable; mix between transfers by gently pipetting up and down. To avoid cross contamination, always dilute from higher to lower concentrations,

changing to fresh tips for each compound. If using an automated dispenser, follow the manufacturer's recommendations to select appropriate parameters for aspirate, dispense, and mix steps.

4.8 Example controls (final concentration) include: 20 μM ionomycin (calcium ionophore that disrupts calcium homeostasis); 10 μM FCCP (carbonyl cyanide 4-(trifluoromethoxy) phenylhydrazone), a protonophore that leads to loss of mitochondrial membrane potential; 0.25% Triton X-100, a detergent that compromises plasma membrane integrity.

4.9 Prepare enough 4× dye mix for 20 μl per sample well plus excess appropriate for the dispensing device/reservoir; e.g., 12 ml would be typical for a 384-well plate when pipetting by hand from a reagent reservoir with a multichannel pipette. Dyes may be varied to suit the detection platform and endpoints of interest. Optimal incubation time (for Step 3.6) may vary, depending on dye choices and cell model. Freeze-thaw of stock reagents is not recommended. Do not re-use reagents once prepared. For convenience and quality assurance, commercial kits are available for monitoring cell health. Protocols are compatible with use of Cytiva Cell Health Assay for HCA (GE Healthcare, 29024468), which was specifically formulated and validated for use with Cytiva/Cytiva Plus cardiomyocytes and IN Cell Analyzer imaging platforms. The reagents of this kit are proprietary, but report on the same endpoints. However, the excitation/emission filters and image analysis approach differ slightly from those provided in this chapter; refer to Instructions for Use for guidance.

4.10 Required storage will depend on image file size, number of channels collected per field, number fields per well, number of wells imaged per plate, and number of plates in the run.

4.11 The gas permeable plate seal applied after the cells have equilibrated to 37 °C/5% CO_2 helps maintain environmental conditions when the plate is not under active environmental control (within the tissue culture incubator or imaging platform).

4.12 For the studies in this chapter, which used a 40×/0.6 NA objective, four fields of view were sufficient to image on average a total of 320 cells.

4.13 Plates may be loaded manually or using automation. If using automation, ensure plates are housed at 37 °C/5% CO_2 when not in the environmental control of the HCA unit, and ideally use a gas permeable plate seal to stabilize the culture microenvironment during transfers.

5 Conclusion

Effective preclincial toxicity assessment of kinase inhibitors and other anti-cancer agents requires comprehensive surveillance of cardiac drug impact in an appropriately sophisticated human model coupled with an equally sophisticated analytical toolbox. The use of HCA in combination with hSC-CM has enabled toxicity screening of a 130-compound data set, integrating measurements from a range of mechanistically informative endpoints monitored at sub-cytotoxic drug concentrations. Phenotypic profiling and cluster analysis identified 85% of compounds with reported clinical cardiotoxicities. With robust quality-controlled hSC-CM cultures serving as a common test system, cardiotoxicity data obtained by HCA has the potential to be combined with data from complementary in vitro tests. For example, multielectrode array (MEA) and impedance assays can now be performed in screening (multiwell) formats to provide valuable information about electrophysiological and mechanical properties essential for cardiomyocyte action potentials and spontaneous beating. Data from such assays can be incorporated into multiparametric profile plots alongside HCA measurements to provide even more comprehensive evaluation and improved prediction of clinical responses.

Disclaimer

GE Healthcare Cytiva: In Cell Analyzer products are for research use only and not for diagnostic or therapeutic use.

References

1. Segall MD, Barber C (2014) Addressing toxicity risk when designing and selecting compounds in early drug discovery. Drug Discov Today. doi:10.1016/j.drudis.2014.01.006
2. O'Brien PJ (2014) High-content analysis in toxicology: screening substances for human toxicity potential, elucidating subcellular mechanisms and in vivo use as translation safety biomarkers. Basic Clin Pharmacol Toxicol 115:4–17. doi:10.1111/bcpt.12227
3. GE Healthcare Application Note 2916473AA (2016) Assessing cardiac activity with high-content analysis: quantitating dynamic calcium flux and contractility with Cytiva Plus Cardiomyocytes and IN Cell Analyzer. https://www.gelifesciences.com/gehcls_images/GELS/Related%20Content/Files/1444842538846/litdoc29164723_20151014190842.pdf. Accessed 20 July 2016
4. Pointon A, Abi-Gerges N, Cross MJ, Sidaway JE (2013) Phenotypic profiling of structural cardiotoxins in vitro reveals dependency on multiple mechanisms of toxicity. Toxicol Sci 132(2):317–326. doi:10.1093/toxsci/kft005
5. Laverty HG et al (2011) How can we improve our understanding of cardiovascular safety liabilities to develop safer medicines? Br J Pharmacol 163(4):675–693

6. Redfern WS et al (2010) Impact and frequency of different toxicities throughout the pharmaceutical life cycle. The Toxicologist 114:232 (abstract 1081)
7. Vishal BS et al (2016) WITHDRAWN—a resource for withdrawn and discontinued drugs. Nucleic Acids Res 44:D1080–D1086
8. Roquemore L (2016) Improving predictivity. Innov Pharm Technol 52:25–29
9. Chi KR (2013) Revolution dawning in cardiotoxicity testing. Nat Rev Drug Discov 12:565–567
10. ICH Expert Working Group (2005) ICH harmonized tripartite guideline: the non-clinical evaluation of the potential for delayed ventricular repolarization (QT interval prolongation) by human pharmaceuticals S7B. Available via ICH: http://www.ich.org/fileadmin/Public_Web_Site/ICH_Products/Guidelines/Safety/S7B/Step4/S7B_Guideline.pdf. Accessed 20 July 2016
11. Force T, Krause DS, Van Etten RA (2007) Molecular mechanisms of cardiotoxicity of tyrosine kinase inhibition. Nat Rev Cancer 7(5):332–344. doi:10.1038/nrc2106
12. Mellor HR, Bell AR, Valentin J-P et al (2011) Cardiotoxicity associated with targeting kinase pathways. Toxicol Sci 120(1):14–32. doi:10.1093/toxsci/kfq378
13. Orphanos GS, Ioannidis GN, Ardavanis AG (2009) Cardiotoxicity induced by tyrosine kinase inhibitors. Acta Oncol 48(7):964–70
14. Cheng H, Force T (2010) Why do kinase inhibitors cause cardiotoxicity and what can be done about it? Prog Cardiovasc Dis 53(2):114–120
15. Gupta R, Maitland ML (2011) Sunitinib, hypertension and heart failure: a model for kinase inhibitor-mediated cardiotoxicity. Curr Hypertens Rep 13(6):430–435
16. Lemieux H, Hoppel CL (2009) Mitochondria in the human heart. J Bioenerg Biomembr 41:99–106
17. Young JD (2013) Metabolic flux rewiring in mammalian cell culture. Curr Opin Biotechnol 24(6). doi:10.1016/j.copbio.2013.04.016
18. Marroquin LD, Hynes J, Dykens JA et al (2007) Circumventing the Crabtree effect: replacing media glucose with galactose increases susceptibility of HepG2 cells to mitochondrial toxicants. Toxicol Sci 97(2):153–161
19. Will Y, Dykens JA, Nadanaciva S et al (2008) Effect of the multitargeted tyrosine kinase inhibitors imatinib, dasatinib, sunitinib and sorafenib on mitochondrial function in isolated rat heart mitochondria and H9c2 cells. Toxicol Sci 106(1):153–161
20. Rana P, Anson B, Engle S et al (2012) Characterization of human-induced pluripotent stem cell-derived cardiomyocytes: bioenergetics and utilization in safety screening. Toxicol Sci 130(1):117–131
21. Rosato RR, Almenara JA, Grant S (2003) The histone deacetylase inhibitor MS-275 promotes differentiation or apoptosis in human leukemia cells through a process regulated by generation of reactive oxygen species and induction of p21CIP1/WAF1. Cancer Res 63(13):3637–3645
22. Kerkela R et al (2006) Cardiotoxicity of the cancer therapeutic agent imatinib mesylate. Nat Med 12:908–916
23. Omar HR (2012) Amiodarone-induced T-U fusion. Am J Emerg Med 30(9):2081.e1-e2
24. ClinicalTrials.gov (2012) Safety and tolerability study of TAK-165 in subjects with tumors expressing HER-2. https://clinicaltrials.gov/ct2/show/NCT00034281?term=TAK165&rank=1. Accessed 22 July 2016

Chapter 14

Structural Toxicity: Hypertrophy Models of Human Pluripotent Stem Cell-Derived Cardiomyocytes

Janos Kriston-Vizi, Sian E. Harding, and Gábor Földes

Abstract

Human pluripotent stem cells (hPSC) are investigated as a source of authentic human cardiac cells for drug discovery and toxicological tests. Cell-based assays performed using an automated fluorescence imaging platform and high-content analysis are valuable in characterizing hypertrophic states that may be induced in hPSC-derived cardiomyocytes upon exposure to cardiotoxic compounds. In high-purity populations of hPSC-derived cardiomyocytes loaded with cell tracer probes and other cell markers, detailed hypertrophic profiles can be assessed based on information captured at cellular and subcellular levels.

Key words Human pluripotent stem cells, Cardiomyocyte, Hypertrophy, Automated high-content imaging

1 Introduction

Cardiac hypertrophy is the abnormal enlargement of the heart muscle, resulting from a thickening of cardiomyocytes and changes in other heart muscle components, such as extracellular matrix, and can lead to heart failure. Physiological hypertrophy occurring in pregnancy and athletes is not detrimental and results in normal or enhanced heart function. Causes can also be pathological, as a result of pressure overload in response to hypertension or valvular disease.

1.1 Human Pluripotent Stem Cell-Derived Cardiomyocytes

Human PSC are being investigated as a new source of cells for cardiac disease modelling. Predominant manifestations of cardiac pathologies investigated in engineered hPSC-CM are short-term, including depressed cell contraction, electrophysiological changes, and arrhythmia, or longer-term, such as abnormal morphology, hypertrophy, and increased susceptibility to cell death. While the acute characteristics show close similarities to those observed in adult cardiomyocytes, a marked difference in viability is seen in the long-term survival (months) of hPSC-CM cultures compared to ex vivo adult cell cultures (~2 days). This of course is one of the

Mike Clements and Liz Roquemore (eds.), *Stem Cell-Derived Models in Toxicology*, Methods in Pharmacology and Toxicology, DOI 10.1007/978-1-4939-6661-5_14,

main attractions of hPSC-CM as a model system. Pharmaceutical companies are showing growing interest in using these cells for drug development and toxicology, hoping that these human cell-based platforms will increase predictive capabilities and decrease drug development costs.

A number of human induced pluripotent stem cell-derived cardiomyocyte (hiPSC-CM) models for genetic diseases have a hypertrophic phenotype, including the LEOPARD syndrome and hypertrophic cardiomyopathy (HCM) (Table 1). Human iPSC-CM of LEOPARD syndrome display increased cell size along with increased expression of nuclear factor of activated T-cells (NFAT) [11]. Patient-derived HCM hiPSC-CM exhibit increased basal cell size compared to controls [27, 38]. On the other hand, it still remains to be determined whether HCM patient-derived cardiomyocytes or control cells treated with hypertrophic stimuli are the best model to use for the study of hypertrophy. The majority of these disease models originate from patient-derived hiPSC, but the trisomy 21 model described by Bosman and co-workers utilizes

Table 1
Human PSC-derived cardiomyocyte models for inherited disorders with hypertrophic phenotype

Condition	Cell source	Mutation	Cardiac phenotype	References
LEOPARD syndrome	hiPSC	Protein tyrosine phosphatase, non-receptor type 11 gene (PTPN11)	Cardiac hypertrophy, electrocardiographic abnormalities, pulmonary valve stenosis	[11]
Hypertrophic cardiomyopathy (HCM)	hiPSC	Missense mutation on exon 18 of the β-myosin heavy chain gene; myosin binding protein C	Non-ischemic cardiomyopathy, enlargement of the cardiac cells	[14, 27]
Dilated cardiomyopathy (DCM)	hiPSC	Point mutation R173W in exon 12 of troponin T2 gene	Non-ischemic cardiomyopathy, increased heterogeneous sarcomeric organization	[23], [37], [41]
Barth syndrome	hiPSC	Mutation of gene encoding tafazzin	Cardiomyopathy, cardiolipin abnormalities	[40]
Duchenne muscular dystrophy (DMD)	hiPSC	Mutation in DMD gene encoding dystrophin	Muscle degeneration, disorganized sarcomere	[28]
Down's syndrome	hESC	Trisomy 21	Increased expression of hypertrophic cardiomyopathy genes	[5]

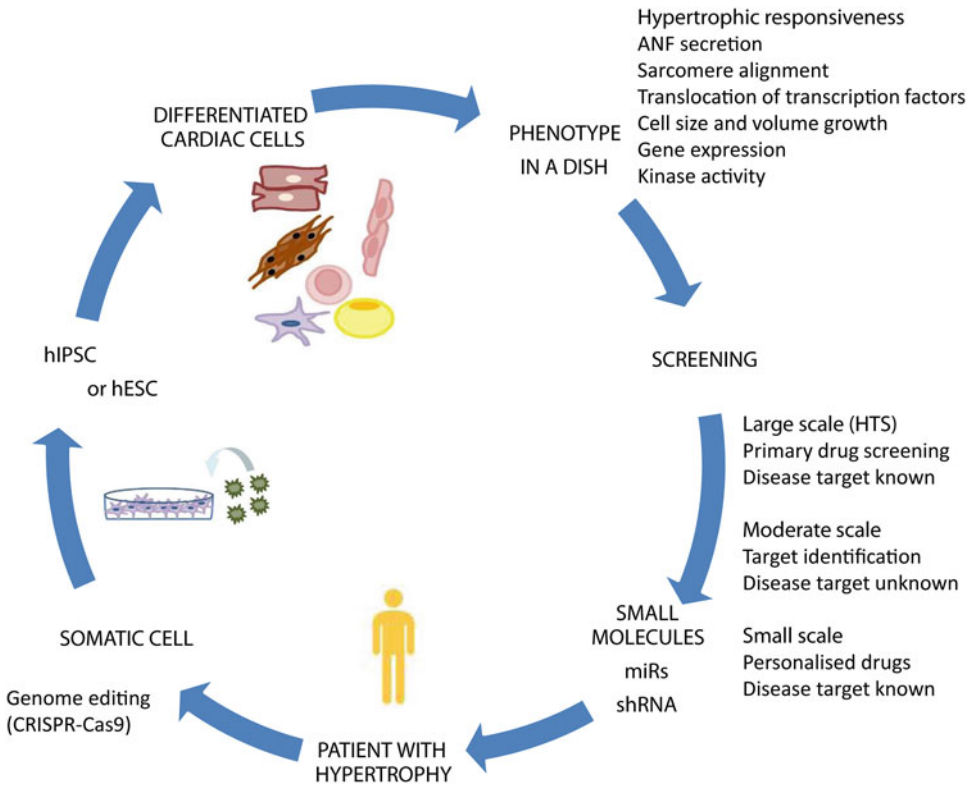

Fig. 1 Schematic drawing of various approaches in hypertrophy modelling and drug screening (CRISPR-Cas9 models, pharmacological approaches, and patient-derived hiPSC trials in vitro)

patient human embryonic stem cell-derived cardiomyocytes (hESC-CMs) [5]. In this study trisomic cells showed an increased expression of HCM genes in comparison to those in euploid control [5]. A greater understanding of hypertrophic signalling in hPSC-CM is required to ensure conclusions drawn from these models are physiologically relevant. In this chapter we describe scalable high-content microscopy-based methods for the detection of cell growth and hypertrophy in hPSC-CM (using the assay measures such as cell area, volume, sarcomere organization, and atrial natriuretic factor (ANF) subcellular distribution) that can serve for personalized in vitro cardiomyocyte screens (Fig. 1 and Table 2).

1.2 Intracellular Signalling in hPSC-CM Hypertrophy

We have reported an increase in cell size in hESC-CM in response to phenylephrine (PE) [19], attributed to activation of p38 MAPK signalling pathways. It was found that a combination of small molecule inhibitors such as those targeting the STAT3 pathway can partially restore the PE response in hiPSC-CM. However, using pharmacological approaches, the hypertrophic response in hPSC-CM remains controversial. In contrast to hESC-CM, our results showed that hiPSC-CM are unresponsive to alpha-adrenergic stimuli, with cell

Table 2

Phenotypic assays to assess cardiomyocyte hypertrophy

Hypertrophy assay	Technology	Reference
Mechanical analysis of hypertrophied cells and myocardial tissue constructs	Cardiac microtissue platform; single cell microarray post detectors (mPads); engineered heart tissue; heart-on-chip model; muscular thin film; applied stretch for single cells with Flexercell	[21, 22, 34, 40]
Imaging intracellular changes	Flow cytometry for troponin/BNP-positive cells; spontaneous Ca2+ transient imaging and measurements; translocation of transcription factors; extracellular flux analysis (Seahorse) to detect altered metabolism; traction force microscopy for single cell contractility; cellular impedance monitoring for cell growth	[17, 25, 38, 40, 41]
Gene profiling/gene regulatory networks and related pathway analysis	Real-time PCR; TaqMan microfluidic cards; single cell PCR; small RNA assays; microarray; RNAseq; miRNASeq; GSEA pre-ranked analysis	[2, 17, 22]
Production and release of hypertrophic factors	ANF, BNP, ET-1, FABP3, troponin I	[10, 17, 38]
Comparison with engineered or native cells	Isolated human ventricular myocytes; neonatal mouse/rat cells, rat embryonic cardiomyocytes (H9C2); CRISPR/Cas9-isogenic control	[18, 22, 32, 40]

size and ANF expression remaining unchanged [18]. In other studies, mild increases in hiPSC-CM size (10% or less) have been seen with alpha-adrenergic PE, and up to 25% with endothelin-1 [38]. Data are also conflicting for the presence of cardiomyocyte hypertrophy in response to β-adrenergic stimulation. We found no increase in hiPSC-CM size [18], whereas Zhi et al. found the opposite in HCM cells [42]. In that model, β-adrenergic stimulation exacerbated cellular hypertrophy as well as abnormal calcium handling and arrhythmia [27]. Enhanced myofibrillar disarray and NFAT nuclear translocation were also reported [42]. It has been shown that serum-containing media causes hypertrophy in hESC-CM and hiPSC-CM, which may explain the lack of further cellular growth in response to hypertrophic stimuli in some studies [14].

We postulate that the difference between hESC-CM and hiPSC-CM is caused by an imbalance in anti-hypertrophic signalling pathways. The predominant α-adrenergic receptors (AR) in the myocardium are α_1-ARs [7], and stimulation with catecholamines induces pathological cardiac hypertrophy [33, 43]. We found that the expression of α-ARs in hPSC-CMs shows an early and transient up-regulation during differentiation followed by a rapid down-regulation of α_{1A}-AR mRNA levels both in hiPSC-CM and hESC-CM. Conversely α_{1B}-AR was found to be increased in an

apparently compensatory manner [18]. The analysis of signalling pathways identified an EGFR/Src/GSK3β/STAT3 network modulated by α_{1B}-AR that could drive the hypertrophic process.

Endothelin-A receptor (ET_A) is expressed in the cardiovascular system and has a number of roles including vasoconstriction, tachycardia, positive inotropy, and hypertrophy [8, 12, 16]. We found that ET_A as well as angiotensin II (Ang II) and cyclic stretch can increase cell size in hESC-CM with corresponding increases in ANF expression [18, 19]. In hPSC-CM, ET_A also induces expression of hypertrophic genes such as BNP and ANF [18]. ET_A and Ang II did not result in significant increases in cell size and correspondingly increased ANF and BNP expression was only seen in response to ET_A activation. Hypertrophic modelling in commercially available hiPSC-CM assays relies therefore on detection of BNP expression in response to ET_A [36].

1.3 3D high-content Screening and 3D high-Content Analysis

Image-based 3D high-content screening is still in its infancy, even though a large body of literature has presented a rich set of 3D cell culture techniques in the past decades [3, 15, 30, 36]. Cell-based 3D high-content screening can be approached at tumor spheroid [26, 39] or single cell level [18]. Assessment of complex structural changes in cardiomyocyte hypertrophy, such as rearrangements of sarcomere structure and dynamic translocation of natriuretic peptides or transcription factors, requires 3D imaging. 3D high-content image acquisition requires a plate reader equipped with a high resolution microscope capable of optical sectioning [24]. We used an Opera LX spinning disk confocal plate reader (PerkinElmer) for 3D high-content image acquisition. The specifications of computer hardware for 3D high-content analysis (HCA) are similar to the 2D HCA. General HCA hardware considerations [13] are applicable; however, the extra spatial dimension requires the additional memory for image analysis and hard drive space for data storage that server-grade workstations can provide. For 3D HCA, third party, standalone software is currently preferred over the dedicated software solutions typically shipped with HCA imaging platforms [24]. Although the dedicated analysis solutions tend to be designed for the biologist with user-friendly interfaces, they are typically intended to analyze common 2D assays, and are insufficient for analysis of 3D assays [20]. We use ImageJ [1] for image analysis, and R [31] for statistical data processing.

2 Materials

2.1 Human Pluripotent Stem Cell-Derived Cardiomyocytes

1. Extracellular matrix Matrigel-coated plates as substrates for feeder-independent human ESC or hiPSC cultures.
2. Pre-defined stem cell qualified medium such as mTESR1 for culturing undifferentiated stem cells.

3. Serum-free basal medium for hypertrophy experiments: a. DMEM:M199 medium, in 3:1 ratio. Add 1 ml penicillin/streptomycin, 0.2 g bovine serum albumin (0.2% wt/vol), 0.00176 g ascorbic acid, 0.066 g creatine, 0.0626 g taurine, and 0.03224 g carnitine to 100 ml DMEM/M199 medium. Dilute insulin 1:10 (final concentration 10 mg/ml) and then add 8.2 μl of this to 50 ml DMEM/M199 on the day of experiments. Alternatively, RPMI basal medium supplemented with B27 can be used for screening experiments.
4. For dissociation of cultures into single cardiomyocytes, remove media from cells and add TrypLE (0.5 or 1 ml, Gibco) at room temperature (RT), and incubate for 8 min at 37 °C. Triturate cells four times and transfer to a 15 ml tube. Spin 4 min at 240 g. Remove media after spin. Add RPMI-B27 (with insulin) and triturate gently. Plate cells at the density desired (5×10^5 for 24-well plate and 750 K for 12-well plate) and RPMI-B27 (with insulin). It can take 2–3 days to see beating cells.

2.2 Hypertrophic Stimuli

1. Hypertrophic alpha-adrenoceptor agonist PE (10 μM) for 48 h. Use serum-free basal medium for dilution. Prepare fresh PE solution from powder before each experiment. Alternatively, treat cells with angiotensin II (100 nM) or endothelin-1 (1, 10, and 100 nM) for 48 or 24 h, respectively.
2. Cultures of hPSC-CM can be exposed to cyclic equiaxial mechanical stretch. Use 0.5 Hz as the frequency of cyclic stretch with pulsation of 10–25% elongation of cells for 24 h. Cells are stretched by applying a cyclic vacuum suction under Bioflex plates with computer-controlled equipment (FX-2000; Flexcell International). Use control cultures on the same plate without stretch.

2.3 Screening Molecules for Effects on Cardiac Hypertrophy

In order to determine the effect of protein kinase inhibition on growth in cell size of hPSC-CM, use selective small molecule inhibitors, e.g., p38 inhibitor SB202190 (1 μM, Sigma), PKG inhibitor KT5823 (1 μM), HDAC II inhibitor trichostatin A (0.25 μM), ERK inhibitor PD98059 (10 μM), JNK inhibitor SP600125 (1 μM), GSK3β inhibitor 1-azakenpaullone (10 μM), CaMK II inhibitor KN93 (10 μM), calcineurin inhibitor cyclosporine A (0.2 μM), mTOR inhibitor rapamycin (10 ng/ml), and calcineurin/FKBP inhibitor FK506 (0.1 μM) in the presence or absence of PE for 48 h. Drug discovery methodologies in cardiac hypertrophy may typically start with a phenotype-based high-throughput screen for small molecule inhibitors [29]. Approaches to validate cardiomyocyte hypertrophy responses include gene transduction into isolated cardiomyocytes, use of transgenic and knockout animals, and pharmacological studies, including human stem cell models.

2.4 Antibodies and Vital Dyes

1. Primary antibodies for immunocytochemistry: anti-Ki67 (proliferation marker, 1:100), anti-ANF (hypertrophy signalling, 1:300, Santa Cruz), anti-troponin T (sarcomere protein, 1:200, Abcam), anti-alpha-actinin (sarcomere protein, 1:500, Sigma-Aldrich), and anti-NFAT (transcription factor, 1:100, ab93628, Abcam) primary antibodies (Fig. 2).
2. Detection of primary antibodies: Alexa 488-, Alexa 647-, and Alexa 546-conjugated secondary antibodies (all 1:400, ThermoFisher Scientific). Dilute probes in RPMI medium supplemented with B27.

2.5 Gene Expression and Proteome Profiling

To assess gene transcriptional changes, TaqMan chemistry-based real-time PCR assays and microfluidic PCR cards are used.

2.6 Instrumentation for 3D High-Content Image Acquisition and Analysis

1. 3D high-content screening requires a plate reader equipped with a high resolution microscope (typically confocal) for optical sectioning. At image acquisition, we use a spinning disk confocal Opera LX plate reader (PerkinElmer) with triple bandpass filters for 488/561/640 nm and UV (365 nm) wavelengths. Various objectives can be used in the Opera setup: 4× air NA = 0.16, 40× air NA = 0.6, 60× water NA = 1.2. We recommend using either of these two types of multiwell plates: for BD Optilux (BD Biosciences) 96-well plate use the 40× air lens, and for skirtless CellCarrier (PerkinElmer) clear bottom TC treated 384-well plate use the 60× water lens (*see* **Note 4.1**).
2. Hardware specifications of the high-content analysis computer. Volume quantification in a high-content environment is resource intensive and computationally demanding. The speed of the analysis can be maximized by loading and processing as much image data into the memory as the system allows. HCA system server motherboards are designed to accommodate a large amount of memory and suitable servers are commercially available. Use a Tyan FT48-B8812 barebone computer for high-content analysis of the images and quantify cell volume, sarcomere reorganization, and ANF redistribution. Our Tyan FT48-B8812 is equipped with four pieces of 12-core AMD Opteron 6174 CPUs and 256 GB memory. In total 48 threads could run in parallel and the overall computational speed can be further improved with the use of a 1 terabyte NAND flash memory as solid state drive integrated on a PCI express card (Supertalent Raiddrive II). As a very fast hard drive it supported 2.4GB/sec read speed through a PCIe (Gen.2) ×8 interface.

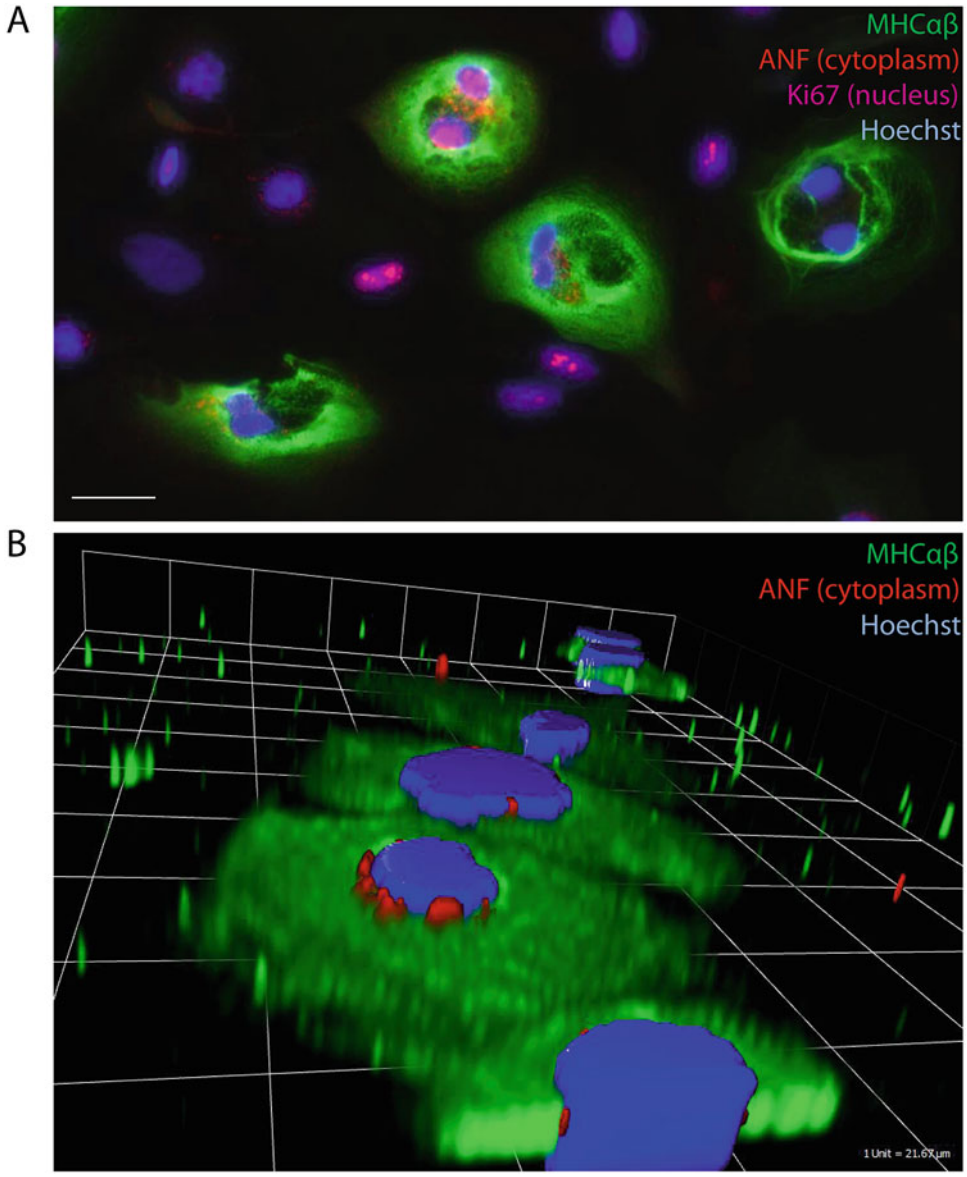

Fig. 2 Cultured human pluripotent stem cell-derived cardiomyocytes. (**a**) Depending on the nature of the stimulus and its intensity (example shows PE treatment in the presence of proliferation/cytokinesis inhibitor agent blebbistatin, 48 h), hPSC-CM can undergo hypertrophy, activation of cell death pathways, or progression into cell division. Cells were stained with Hoechst; sarcomere protein troponin I or MHC α/β; atrial natriuretic factor ANF; and proliferation marker Ki67. Scale bar 10 μm. (**b**) Example 3D reconstructions (Volocity) of these cells are also shown

3 Methods

3.1 Cardiomyocyte Differentiation

Differentiation protocols for production of cardiomyocytes from hPSC, including embryonic and induced pluripotent stem cells, are now efficient, relying on sequential exposure to small molecule modulators that mimic early cardiac development [9]. One of the most efficient protocols is:

Day 0

Take a Matrigel-coated 6-well plate and culture hESCs in mTESR1 (2 ml/well). Change media to RPMI-B27 without insulin (2 ml) when hPSC culture (maintained in mTESR1) is between 75 and 90% confluency (d3-4 after thaw or split). Add selective GSK3β inhibitor CHIR99021 at 6 or 8 μM to each well (using 10 mM stock). Optimal level and duration of CHIR99021 can be tested with 6 or 8 μM for both 1 day and 2 days incubation. CHIR99021 is stable at 4 °C for a minimum of 2–4 weeks.

Day 1

Exchange media to RPMI-B27 without insulin, if CHIR99021 is used for 1 day.

Day 2

Exchange media to RPMI-B27 without insulin if CHIR99021 is used for 2 days.

Day 3

Add 2 ml RPMI-B27 without insulin and with Wnt pathway inhibitor such as C59 (2.5 μM). Change media every 2 days when feeding cells with RPMI-B27 without insulin.

Days 11–13

For metabolic selection, replace media with glucose-free RPMI basal medium (Life Technologies: 11879–020) supplemented with B27. Exposing the cells for 2–4 days with this media selects against proliferating non-cardiomyocytes (*see* **Notes 4.2** and **4.3**).

3.2 Gene Expression Assays

Experiments by the authors and others suggest mRNA levels of natriuretic peptides do not usually predict their protein levels. Therefore, a combination of mRNA levels of ANF versus an imaging-based assessment of ANF is expected to work better than either approach alone to clarify disease mechanisms.

1. Lyse undifferentiated and differentiated hESC and hiPSC cultures in TriReagent buffer (Sigma Aldrich) for total RNA

extraction. As controls, obtain total RNA from fetal heart (Clontech) and fetal fibroblast (MRC5 lung fetal fibroblast line, ATCC). Purify RNA using RNeasy columns (Qiagen), quantify, and check for quality.

2. Use the High Capacity cDNA Reverse Transcription Kit (ThermoFisher Scientific) to generate double-stranded cDNA.

For quantifying mRNA levels of ANF in undifferentiated hESC and hiPSC cultures, fetal lung fibroblast (MRC5), adult isolated ventricular myocytes, hESC-CM, and hiPSC-CM, real-time PCR analyses are performed with TaqMan Gene Expression Assays (ThermoFisher Scientific). Use GAPDH Endogenous Control (FAM/MGB TaqMan gene expression probe, ThermoFisher Scientific) as a housekeeping control. By calculating the gene expression stability measure M, which is the mean pair-wise variation for a gene from all other tested genes, GAPDH is considered as stable reference gene. GAPDH and ACTB show similar stability, as measured with coefficient of variation and standard deviation.

3.3 Phospho-Kinase Assay

Downstream signalling pathways can be assessed by using proteome screening for kinase phosphorylation. In many cases, despite the significant functional responses in hypertrophy-related parameters, evidence of active signalling was seen in hPSC-CM. Seed hPSC-CM in 6-well plates and treat with pro-hypertrophic agents such as PE (10 μM) for 48 h. Collect cells by centrifugation and wash once with phosphate buffered saline (PBS). Resuspend cell pellets in lysis buffer and incubate for 20 min at 4 °C. Determine protein concentration using the Pierce protein assay reagent. Perform screening for different phospho-kinases in cell lysates with a Human Phospho-Kinase Antibody Array (R&D Systems).

3.4 High-Content Imaging of hPSC-CM

3.4.1 Live Staining and Immunocytochemistry

1. To perform live staining, use high-purity cardiomyocyte populations. Add drugs 3–5 days after cell plating or recovery from frozen stocks. After drug treatment, incubate cells with Cell Tracker Red (ThermoFisher Scientific) for 45 min at 37 °C with 5% CO_2. Place cells in 100 μl fresh media (RPMI-B27) in 96-well or 384-well plate. Keep labelled cultures at 37 °C/5% CO_2 and scan using automated microscope.
2. To characterize detailed hypertrophic properties of hPSC-CM, use combinations of immunocytochemistry markers. Fix cells with 4% paraformaldehyde, permeabilize with 0.2% Triton X-100, block with 4% fetal bovine serum in PBS for 1 h, and label with anti-ANF (Santa Cruz, sc20518, 1:300) and anti-troponin I (Abcam, ab47003, 1:200) primary antibodies. Use Alexa 488- and Alexa 546-conjugated secondary antibodies (all 1:400, ThermoFisher Scientific, in 3% bovine serum albumin in PBS as a carrier solution). Use Hoechst (0.5 μg/ml; Sigma-Aldrich) to visualize DNA.

3.4.2 Cell Proliferation in Fixed Cardiomyocytes Cultures

Although proliferation rates in hPSC-CM are initially far higher than in adult cardiomyocytes, these drop around 1 month after differentiation. Cell morphology is initially less organized, but can become more ordered with time or external physical cues. As our earlier data show that PE can increase cell size independently from cell cycle, use of a cell proliferation assay may serve as an internal control.

1. Fix cells after drug treatment and stain with anti-troponin I or anti-alpha-actinin with Alexa 488; anti-Ki67 with Alexa 568; and Hoechst.
2. Quantitate DNA content and visualize DNA intensity as a histogram. Quantitate percentage of 2N and 4N DNA content subpopulations. Quantitate the ratio of Ki67-positive (or phospho-histone H3-positive) nuclei in the culture to assess proliferating fraction of the population.

3.4.3 2D Image Acquisition

1. For 2D acquisition, scan plates on high-content analysis instrument platforms using modified bioapplication protocols for morphology assessment or compartmental analysis. Using an automated highly sensitive fluorescence imaging microscope with 10× objective and suitable filter sets, the stained cells can be identified with Hoechst, antibody against cardiac specific sarcomere protein (such as troponin I or alpha-actinin), and ANF.
2. When the cardiomyocyte undergoes hypertrophy, we expect an orchestrated induction in cell size, sarcomere alignment, and cytoplasmic ANF redistribution (Fig. 3 shows example images of positive and negative controls). As assay readouts, use cell size; sarcomere content; alignment/abnormalities and length; ANF intensity and distribution; and nuclear translocation of transcription factors such as NFAT [22].

Higher magnification Opera images can be acquired either using a 40× air or a 60× water immersion objective. However, with the Opera system one encounters plate restrictions when working with a water immersion objective. The water holder collar on the objective will not fit under the skirt of a 96- or 384-well plate. Therefore, the Opera can only image skirtless plates with a water immersion objective, and currently those are only available in 384-well format. The Opera Phenix system (PerkinElmer) allows the use of water immersion objectives with 96-well plates with skirt on a restricted plate area, omitting the edge wells. The skirtless CellCarrier-96 Ultra plate (PerkinElmer) will allow the imaging all 96-wells with a water immersion objective. It is at pre-release test phase at the time of writing the manuscript.

3.4.4 3D Image Acquisition

Here we present an image acquisition protocol for both a 40× air objective and a 60× water immersion objective, combining the latter with the PreScanReScan approach.

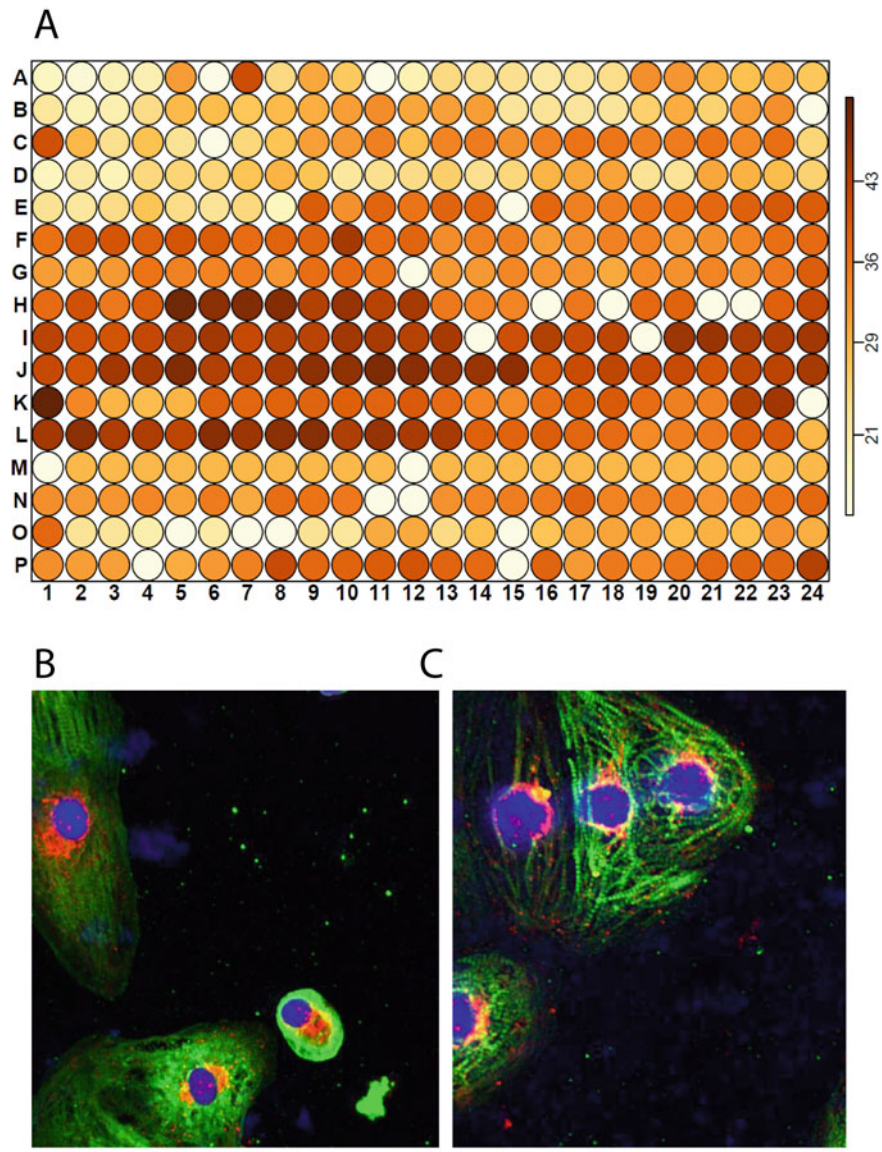

Fig. 3 (**a**) Whole plate level visualization of ANF distribution. Mean ANF-nucleus distances in μm were calculated with an R script and the results are shown as a plate heatmap, generated using the Prada (version 1.42) package from Bioconductor, R (version 3.2.3). Representative images of the wells that show, (**b**) no change in ANF distribution, and (**c**) significant changes in ANF distribution

40× Air Objective (96-Well Plate, BD Optilux, and BD Biosciences)

1. Use Opera LX plate reader for image acquisition. Apply 40× air NA = 0.6 objective to image the cells seeded into BD Optilux (BD Biosciences) 96-well plates. Apply 30 ms exposure time at the Hoechst channel 1 (365 nm) for nuclear imaging; 400 ms with 3330 μW laser power at the MHC α/β-Alexa 488 in channel 2 (488 nm); and 400 ms with 1600 μW laser power at the ANF-Alexa546 in channel 3 (561 nm). Camera pixels can be binned by 2, resulting in a nominal pixel size of

0.32×0.32 μm with 1.0 μm axial resolution of the imaged six optical slices. Image 25 fields of view (FoV) in the central position of each well.

60× Water Immersion Objective with PreScanReScan (384-Well Plate, CellCarrier, and PerkinElmer)

Use the PreScanReScan system (version 0.91 (10/02/2012) by Achim Kirsch, PerkinElmer Cellular Technologies Germany GmbH), a set of Acapella scripts to (1) prescan with a low magnification objective to identify the location of cardiomyocytes in each well and (2) rescan those locations with high magnification objective and acquire an image stack. The PreScanReScan can only be run from the Acapella Player environment, and version 0.91 requires Opera software version 2.0 or later.

1. Start the prescan component of the system with imaging the cells, seeded on a CellCarrier (PerkinElmer) clear bottom TC treated 384-well plate. Use a 4× air NA = 0.16 objective for the prescanning, applying 500 ms exposure time at the Hoechst channel 1 (365 nm) for nuclear imaging; 800 ms with 3330 μW laser power at the MHC α/β-Alexa 488 in channel 2 (488 nm); and 800 ms with 1600 μW laser power at the ANF-Alexa546 in channel 3 (561 nm). The camera pixels are not binned resulting in a nominal pixel size of 1.6×1.6 μm for the imaged optical slice. This 1 FoV (2219×1677 μm) covers the central region of the well.
2. Execute the first Acapella script component of the PreScanReScan system, "PreScanReScan_Create_Sublayouts_Objects_framelimit.script," on the prescanned images, in order to analyze, identify, and record the in-well position of the cells. Each detected cell is supposed to fit in the 60× rescan FoV. The maximum number of cells can be specified in the "framelimit" option. In this example, record the Sublayout of the first ten cells.
3. Several input parameters are requested by the script file. Besides trivial ones such as "Path to the OperaDB," "Path to the Images:Illustrations," and "Magnification of next lens"(=60), other parameters need some additional effort in optimization. The "Offset in X direction [μm]," and "Offset in Y direction [μm]," parameters are two experimentally specified constants that represent the offset between the centers of the low and high resolution images. Signs indicate directionality, with negative values virtually shifting the 60× FoV left and up in X and Y directions, respectively. Use X offset = −230 μm and Y offset = −150 μm values, which are surprisingly large when we compare the 146×110 μm size of a whole 60× FoV.

   The Image Analysis section specifies the image processing parameters that result in the identification of rescan FoVs. The PreScanReScan algorithm is designed to identify rescan FoVs based on the location of nuclei. However, in this study, cells express strong signal at 488 nm; therefore channel 2, the MHC α/β-Alexa 488 channel, is used ("Channel for Cell Detection"),

providing an intensity filter at the same time. Use the value 100 for size filter ("Minimum Nuclei Size for Rescan"). Instead of nuclei, tune the "Nuclei Detection" section for whole cell detection, using the following parameters:

- Nuclei Detection Algorithm = "A", which is a proprietary segmentation algorithm.
- Threshold Adjustment = 1.5, which ranges from 0 to 3, and fine tunes the segmentation by shrinking (low values) or expanding (high values) the mask.
- Minimum Nuclei Distance = 7, which splits artificially merged nuclei by specifying a minimal distance between centers of nuclei.
- Nuclear Splitting Adjustment = 7, which is another parameter to split artificially merged nuclei.
- Individual Threshold Adjustment = 0.4, which ranges from 0 to 1.0, and fine tunes the segmentation of nuclei.
- Minimum Nuclear Area = 100, which is a size filter in terms of pixels. Discard objects smaller than the specified value.
- Discard minimum Nuclear Contrast = 0.35, which ranges from 0 to 1.0, and is an intensity filter for objects with contrast less than the specified value.
- Parameter SCAN = "None," which is intended for optimization of the parameters above.

4. Acquire images of the 384-well plate with a 60× water NA = 1.2 objective. A 100 ms exposure time can be applied at the Hoechst channel 1 (365 nm) for nuclear imaging; 800 ms with 3330 μW laser power at the MHC α/β-Alexa 488 in channel 2 (488 nm); and 800 ms with 1600 μW laser power at the ANF-Alexa546 in channel 3 (561 nm). Camera pixels are not binned, resulting in a nominal pixel size of 0.11 × 0.11 μm with 0.5 μm axial resolution of the imaged 12 optical slices.
5. Determine the number and position of image stacks by the PreScanReScan Opera scripts (maximum 10 stacks per well). Use the script collection PreScanReScan version 0.91-2012-02-10 with Opera software 2.0 to identify the location of the cells within each well of the 384-well plate prescanned with 4× objective. Segment cells detected in channel 2 and filter by minimum contrast >0.35, and area >100 for rescan at 60× magnification (Fig. 4).

3.4.5 3D Fluorescence Image Processing

A diagram of the 3D high-content analysis workflow is shown in Fig. 5.

Hardware

Use a server-grade Tyan FT48-B8812 barebone computer; the specifications are described at Sect. 2.5.

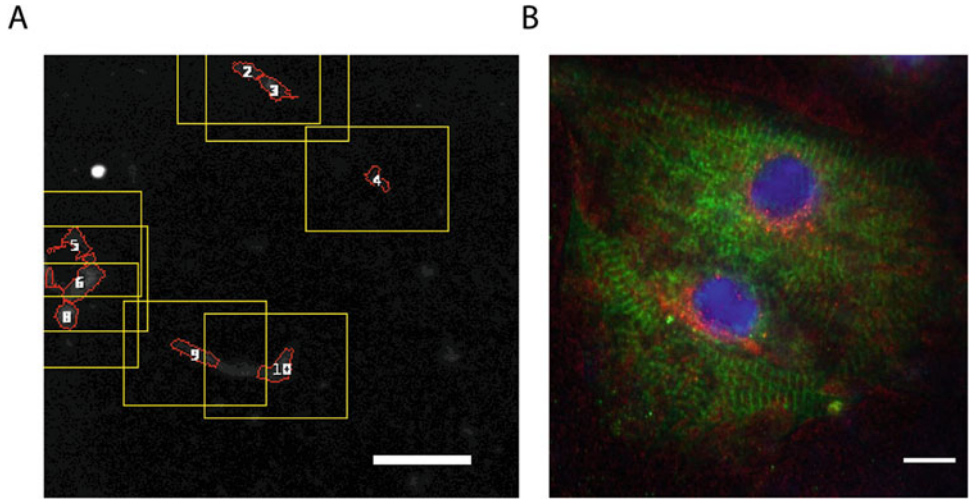

Fig. 4 (**a**) Illustration of cardiomyocytes imaged with 4× lens at PreScan step after image analysis. The identified cells were re-imaged with 60× lens in the ReScan step. *Yellow* rectangles show the contours of the 60× field of views. Scale bar 100 μm. (**b**) Maximum intensity projection of cardiomyocytes imaged with PerkinElmer Opera, 60× (NA = 1.2) water immersion lens. Cells were stained with Hoechst, MHC α/β-Alexa, and ANF-Alexa546 on *blue*, *green*, and *red* channels and imaged in 365, 488, and 561 nm excitation wavelengths, respectively. Scale bar 10 μm

Software

Perform the image analysis under a 64-bit version of Kubuntu Linux 10.10, ImageJ version 1.45 s, and Fiji [35] with Java 1.6.0_20.

Acquire the 3-channel, fluorescence, 12-bit depth images as Opera LX *.flex files, and analyze after conversion into *.tif format by the Acapella FlexToVolocity.script.

Feature Extraction

Extract three features of interest from the images using Fiji: (1) cell volume; (2) texture features related to sarcomere reorganization; and (3) ANF distance from the nucleus related to ANF redistribution.

Cell Volume Measurement

Perform cell volume measurement on MHC α/β-Alexa 488 in channel two images. The image resolution does not allow us to separate each individual cell; therefore calculate the average cell volume in each well by the total volume of the stained voxels divided by the number of nuclei. Perform the 3D cell volume measurement by a custom Fiji macro. The workflow starts with manual selection of a suitable threshold (=273) that provides optimal segmentation results both at the lowest and highest optical slices. The 3D Object Counter plugin [4] implemented under Fiji can be used for a 26 neighbor connection, size filter, and volume measurement of the foreground voxels. The gelatine cover on the well bottom results in an image noise corrected by a size filter that removes objects smaller than 166 μm^3 (1000 voxel at 40×, 27,400 voxel at 60× magnification). Record the 3D object map of each image stack for quality control purposes. Record the volume of each 26

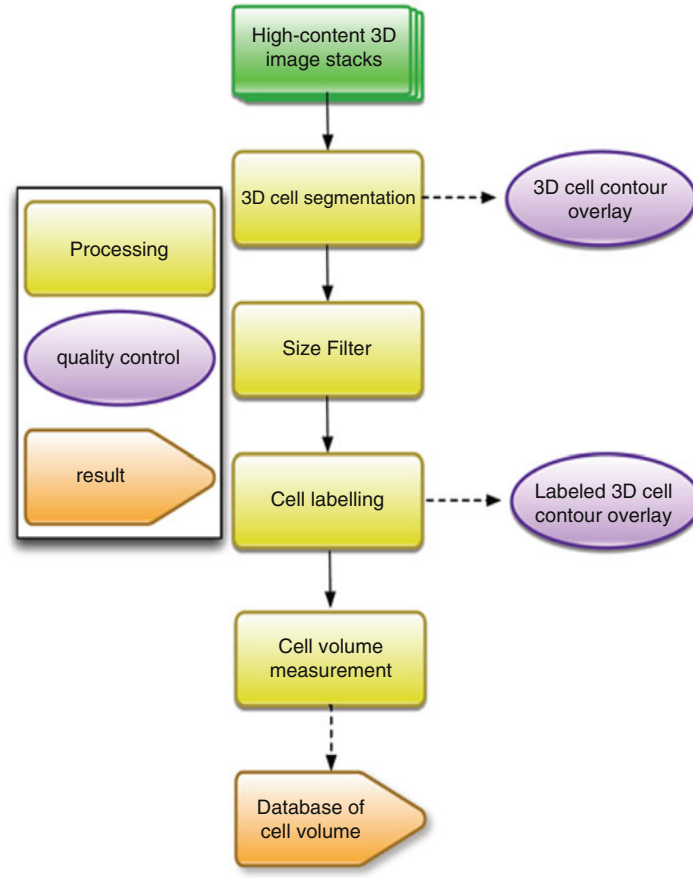

Fig. 5 Illustrative diagram of the high-content analysis workflow applied. 3D image stack of confocal slices serves as input and a database of cell volumes is the output. Overlay images play an important role; the workflow quality is checked at every step

neighbor-connected 3D object, together with its well and field of view identifiers. Measure the nuclear number and position by custom ImageJ macros, which create a maximum intensity projection of the optical slices, and apply a local maxima finder algorithm with noise tolerance = 500. Perform the texture measurement by a custom ImageJ macro using the plugin GLCM Texture Too. Determine cellular foreground area by applying a 10 pixel radius median filter on the maximum intensity projection of a channel 2 image converted to 8-bit, and segment with threshold = 6. Measure texture features on the maximum intensity projection pixel intensities of channel 2 under the binary mask.

3D Localization

Measure the ANF position in the cell with a custom ImageJ macro that applies a maximum intensity projection of the channel 3 optical slices, and the macro records of the coordinates of local pixel maxima with noise tolerance = 200.

3.4.6 Statistical Data Analysis for Widefield and Confocal High-Content Screens

The volumetric, texture, and distributional results of the image analysis are stored in ASCII tables and can be evaluated statistically with R, the well-established, open source statistical software [31] (http://r-project.org). Use R scripts to calculate single values per well for (1) average cell volume, (2) texture descriptors, and (3) average ANF distance to the center of the nucleus. Calculate the average cell volume as a ratio of the total volume of MHC α/β--Alexa and total number of nuclei in each well. Calculate the mean value of the texture features in each field of view in a separate R script. Quantify the ANF redistribution by the mean Euclidean ANF distance from the closest nucleus (Fig. 3).

Use the cellHTS2 package [6] in custom R scripts for statistical analysis. Normalize the results by a robust *Z* score method using the median and the median absolute deviation (MAD) of the sample wells. Following normalization, calculate the *Z* score of each well, based on the sample workflow described in "End-to-end analysis of cell-based screens: from raw intensity readings to the annotated hit list" (last retrieved on 15/02/2016 from the website https://www.bioconductor.org/packages/3.3/bioc/vignettes/cellHTS2/inst/doc/cellhts2Complete.pdf).

Regarding replicates, consider biological replicates to be a batch of differentiated cardiomyocytes taken through a complete experiment (a run of high-content microscopy or real-time PCR data) (*see* **Note 4.4**). Technical replicates refer to numbers of repeats within a run for real-time PCR and number of wells for high-content microscopy. Data from each well for the 2D high-content microscopy will be taken from up to 2000 cells, but this is only represented as one value for each well.

3.5 Conclusion

Providing multiple endpoints is a great advantage of high-content imaging-based assays. The assays can therefore readily predict molecular targets as well as off-target effects of test compounds, such as cytotoxicity or changes in cardiovascular cell morphology. Toxicology and early stages of drug discovery benefit enormously from the advanced 3D high-content screening systems that were, until recently, primarily employed in low-throughput research.

4 Notes

4.1 Only a skirtless plate can operate with a water immersion lens, because a plate skirt hinders the free access of edge wells of an objective with water collar.

4.2 Regarding differentiation of cardiomyocytes, at day 1 check cell morphology at 20× magnification to predict if differentiated cells are going to beat. Cells at the border of the wells should be square and tightly joined and look gray where cells in the middle

of cultures are triangular and edged and have gap in between and look "shiny." On days 9–11 one can see cardiomyocyte contraction (start depends on hPSC-CM line). Once cells start beating, feed them with RPMI-B27 containing insulin.

4.3 Regarding metabolic selection, cardiomyocytes rely on oxidative phosphorylation, while the non-cardiomyocytes tend to rely on glycolysis. Using metabolic selection, cells relying on glycolysis die and only cardiomyocytes survive.

4.4 This is the typical understanding of biological replicates from a cell lines such as HEK or CHO. (For in-house experiments this would usually include the differentiation of a new batch of hESC or hiPSC-derived cardiomyocytes, but this may not be possible from commercial lines where one is reliant on available batch numbers.) In many of the experiments here we also have a number of different lines, which can also be considered biological replicates.

Acknowledgements

This work was supported by the UK Medical Research Council core funding to the MRC-UCL University Unit (Ref. MC_EX_G0800785) (JKV), the European Union Seventh Framework Programme(FP7/2007-2013,grantno.PIRG08-GA-2010-276811) (JKV), and the Hungarian Scientific Research Fund (OTKA K-105555) (GF).

Glossary

ANF	Atrial natriuretic peptide
BNP	B-type natriuretic peptide
ESC	Embryonic stem cell
GSK	Glycogen synthase kinase
HCM	Hypertrophic cardiomyopathy
hESC	Human embryonic stem cell
hESC-CM	Human embryonic stem cell-derived cardiomyocyte
hiPSC	Human induced pluripotent stem cell
hiPSC-CM	Human induced pluripotent stem cell-derived cardiomyocyte
hPSC	Human pluripotent stem cell
hPSC-CM	Human pluripotent stem cell-derived cardiomyocyte
MAPK	Mitogen activated protein kinase
NFAT	Nuclear factor of activated T-cells

References

1. Abramoff MD, Magalhaes PJ, Ram SJ (2016) Image Processing with ImageJ. Biophoton Int 7(4):36–43
2. Aggarwal P, Turner A, Matter A, Kattman SJ, Stoddard A, Lorier R, Swanson BJ, Arnett DK, Broeckel U (2014) RNA expression profiling of human iPSC-derived cardiomyocytes in a cardiac hypertrophy model. PLoS One 9(9), e108051
3. Ansari N, Muller S, Stelzer EH, Pampaloni F (2013) Quantitative 3D cell-based assay performed with cellular spheroids and fluorescence microscopy. Methods Cell Biol 113:295–309
4. Bolte S, Cordelieres FP (2006) A guided tour into subcellular colocalization analysis in light microscopy. J Microsc 224(3):213–232
5. Bosman A, Letourneau A, Sartiani L, Del LM, Ronzoni F, Kuziakiv R, Tohonen V, Zucchelli M, Santoni F, Guipponi M, Dumevska B, Hovatta O, Antonarakis SE, Jaconi ME (2015) Perturbations of heart development and function in cardiomyocytes from human embryonic stem cells with trisomy 21. Stem Cells 33(5):1434–1446
6. Boutros M, Bras LP, Huber W (2006) Analysis of cell-based RNAi screens. Genome Biol 7(7):R66
7. Bruckner R, Mugge A, Scholz H (1985) Existence and functional role of alpha 1-adrenoceptors in the mammalian heart. J Mol Cell Cardiol 17(7):639–645
8. Bupha-Intr T, Haizlip KM, Janssen PM (2012) Role of endothelin in the induction of cardiac hypertrophy in vitro. PLoS One 7(8), e43179
9. Burridge PW, Holmstrom A, Wu JC (2015) Chemically defined culture and cardiomyocyte differentiation of human pluripotent stem cells. Curr Protoc Hum Genet 87:21
10. Carlson C, Koonce C, Aoyama N, Einhorn S, Fiene S, Thompson A, Swanson B, Anson B, Kattman S (2013) Phenotypic screening with human iPS cell-derived cardiomyocytes: HTS-compatible assays for interrogating cardiac hypertrophy. J Biomol Screen 18(10):1203–1211
11. Carvajal-Vergara X, Sevilla A, D'Souza SL, Ang YS, Schaniel C, Lee DF, Yang L, Kaplan AD, Adler ED, Rozov R, Ge Y, Cohen N, Edelmann LJ, Chang B, Waghray A, Su J, Pardo S, Lichtenbelt KD, Tartaglia M, Gelb BD, Lemischka IR (2010) Patient-specific induced pluripotent stem-cell-derived models of LEOPARD syndrome. Nature 465(7299):808–812
12. Concas V, Laurent S, Brisac AM, Perret C, Safar M (1989) Endothelin has potent direct inotropic and chronotropic effects in cultured heart cells. J Hypertens Suppl 7(6):S96–S97
13. Copeland J, Shamu CE (2016) Informatics considerations. In: An introduction to high content screening, Wiley, pp 81–102. Steven A. Haney, Douglas Bowman, Arijit Chakravarty (Edt); Anthony Davies, Caroline Shamu (Associate Editors) John Wiley and Sons Inc. Hoboken, New Jersey
14. Dambrot C, Braam SR, Tertoolen LG, Birket M, Atsma DE, Mummery CL (2014) Serum supplemented culture medium masks hypertrophic phenotypes in human pluripotent stem cell derived cardiomyocytes. J Cell Mol Med 18(8):1509–1518
15. Debnath J, Brugge JS (2005) Modelling glandular epithelial cancers in three-dimensional cultures. Nat Rev Cancer 5(9):675–688
16. Drawnel FM, Archer CR, Roderick HL (2013) The role of the paracrine/autocrine mediator endothelin-1 in regulation of cardiac contractility and growth. Br J Pharmacol 168(2):296–317
17. Drawnel FM, Boccardo S, Prummer M, Delobel F, Graff A, Weber M, Gerard R, Badi L, Kam-Thong T, Bu L, Jiang X, Hoflack JC, Kiialainen A, Jeworutzki E, Aoyama N, Carlson C, Burcin M, Gromo G, Boehringer M, Stahlberg H, Hall BJ, Magnone MC, Kolaja K, Chien KR, Bailly J, Iacone R (2014) Disease modeling and phenotypic drug screening for diabetic cardiomyopathy using human induced pluripotent stem cells. Cell Rep 9(3):810–821
18. Foldes G, Matsa E, Kriston-Vizi J, Leja T, Amisten S, Kolker L, Kodagoda T, Dolatshad NF, Mioulane M, Vauchez K, Aranyi T, Ketteler R, Schneider MD, Denning C, Harding SE (2014) Aberrant alpha-adrenergic hypertrophic response in cardiomyocytes from human induced pluripotent cells. Stem Cell Rep 3(5):905–914
19. Foldes G, Mioulane M, Wright JS, Liu AQ, Novak P, Merkely B, Gorelik J, Schneider MD, Ali NN, Harding SE (2011) Modulation of human embryonic stem cell-derived cardiomyocyte growth: a testbed for studying human cardiac hypertrophy? J Mol Cell Cardiol 50(2):367–376
20. Ghosh RN, Lapets O, Haskins JR (2007) Characteristics and value of directed algorithms in high content screening. Methods Mol Biol 356:63–81
21. Hansen A, Eder A, Bonstrup M, Flato M, Mewe M, Schaaf S, Aksehirlioglu B, Schwoerer AP, Uebeler J, Eschenhagen T (2010) Development of a drug screening platform based on engineered heart tissue. Circ Res 107(1):35–44
22. Hinson JT, Chopra A, Nafissi N, Polacheck WJ, Benson CC, Swist S, Gorham J, Yang L,

Schafer S, Sheng CC, Haghighi A, Homsy J, Hubner N, Church G, Cook SA, Linke WA, Chen CS, Seidman JG, Seidman CE (2015) HEART DISEASE. Titin mutations in iPS cells define sarcomere insufficiency as a cause of dilated cardiomyopathy. Science 349(6251):982–986

23. Karakikes I, Ameen M, Termglinchan V, Wu JC (2015) Human induced pluripotent stem cell-derived cardiomyocytes: insights into molecular, cellular, and functional phenotypes. Circ Res 117(1):80–8
24. Ketteler R, Kriston-Vizi J (2016) High-content screening in cell biology. In: Bradshaw R, Stahl P (eds) Encyclopedia of cell biology, 4th edn. Academic, Waltham, MA, pp 234–244
25. Kijlstra JD, Hu D, Mittal N, Kausel E, van der Meer P, Garakani A, Domian IJ (2015) Integrated analysis of contractile kinetics, force generation, and electrical activity in single human stem cell-derived cardiomyocytes. Stem Cell Rep 5(6):1226–1238
26. Kunz-Schughart LA, Freyer JP, Hofstaedter F, Ebner R (2004) The use of 3-D cultures for high-throughput screening: the multicellular spheroid model. J Biomol Screen 9(4):273–285
27. Lan F, Lee AS, Liang P, Sanchez-Freire V, Nguyen PK, Wang L, Han L, Yen M, Wang Y, Sun N, Abilez OJ, Hu S, Ebert AD, Navarrete EG, Simmons CS, Wheeler M, Pruitt B, Lewis R, Yamaguchi Y, Ashley EA, Bers DM, Robbins RC, Longaker MT, Wu JC (2013) Abnormal calcium handling properties underlie familial hypertrophic cardiomyopathy pathology in patient-specific induced pluripotent stem cells. Cell Stem Cell 12(1):101–113
28. Lin B, Li Y, Han L, Kaplan AD, Ao Y, Kalra S, Bett GC, Rasmusson RL, Denning C, Yang L (2015) Modeling and studying mechanism of dilated cardiomyopathy using induced pluripotent stem cells derived from Duchenne Muscular Dystrophy (DMD) patients. Dis Model Mech 8(5):457–466
29. McKinsey TA, Kass DA (2007) Small-molecule therapies for cardiac hypertrophy: moving beneath the cell surface. Nat Rev Drug Discov 6(8):617–635
30. Pampaloni F, Reynaud EG, Stelzer EH (2007) The third dimension bridges the gap between cell culture and live tissue. Nat Rev Mol Cell Biol 8(10):839–845
31. R Core Development Team (2016) A language and environment for statistical computing. R Foundation for Statistical Computing, Vienna, Austria
32. Ren R, Oakley RH, Cruz-Topete D, Cidlowski JA (2012) Dual role for glucocorticoids in cardiomyocyte hypertrophy and apoptosis. Endocrinology 153(11):5346–5360
33. Rokosh DG, Stewart AF, Chang KC, Bailey BA, Karliner JS, Camacho SA, Long CS, Simpson PC (1996) α1-adrenergic receptor subtype mRNAs are differentially regulated by α1-adrenergic and other hypertrophic stimuli in cardiac myocytes in culture and in vivo. Repression of α1B and α1D but induction of α1C. J Biol Chem 271(10):5839–5843
34. Schaaf S, Shibamiya A, Mewe M, Eder A, Stohr A, Hirt MN, Rau T, Zimmermann WH, Conradi L, Eschenhagen T, Hansen A (2011) Human engineered heart tissue as a versatile tool in basic research and preclinical toxicology. PLoS One 6(10), e26397
35. Schindelin J, Arganda-Carreras I, Frise E, Kaynig V, Longair M, Pietzsch T, Preibisch S, Rueden C, Saalfeld S, Schmid B, Tinevez JY, White DJ, Hartenstein V, Eliceiri K, Tomancak P, Cardona A (2012) Fiji: an open-source platform for biological-image analysis. Nat Methods 9(7):676–682
36. Shamir ER, Ewald AJ (2014) Three-dimensional organotypic culture: experimental models of mammalian biology and disease. Nat Rev Mol Cell Biol 15(10):647–664
37. Sun N, Yazawa M, Liu J, Han L, Sanchez-Freire V, Abilez OJ, Navarrete EG, Hu S, Wang L, Lee A, Pavlovic A, Lin S, Chen R, Hajjar RJ, Snyder MP, Dolmetsch RE, Butte MJ, Ashley EA, Longaker MT, Robbins RC, Wu JC (2012) Patient-specific induced pluripotent stem cells as a model for familial dilated cardiomyopathy. Sci Transl Med 4(130):130ra47.
38. Tanaka A, Yuasa S, Mearini G, Egashira T, Seki T, Kodaira M, Kusumoto D, Kuroda Y, Okata S, Suzuki T, Inohara T, Arimura T, Makino S, Kimura K, Kimura A, Furukawa T, Carrier L, Node K, Fukuda K (2014) Endothelin-1 induces myofibrillar disarray and contractile vector variability in hypertrophic cardiomyopathy-induced pluripotent stem cell-derived cardiomyocytes. J Am Heart Assoc 3(6), e001263
39. Vinci M, Gowan S, Boxall F, Patterson L, Zimmermann M, Court W, Lomas C, Mendiola M, Hardisson D, Eccles SA (2012) Advances in establishment and analysis of three-dimensional tumor spheroid-based functional assays for target validation and drug evaluation. BMC Biol 10:29
40. Wang G, McCain ML, Yang L, He A, Pasqualini FS, Agarwal A, Yuan H, Jiang D, Zhang D, Zangi L, Geva J, Roberts AE, Ma Q, Ding J, Chen J, Wang DZ, Li K, Wang J, Wanders RJ, Kulik W, Vaz FM, Laflamme MA, Murry CE, Chien KR, Kelley RI, Church GM, Parker KK, Pu WT (2014) Modeling the mitochon-

drial cardiomyopathy of Barth syndrome with induced pluripotent stem cell and heart-on-chip technologies. Nat Med 20(6):616–623

41. Wu H, Lee J, Vincent LG, Wang Q, Gu M, Lan F, Churko JM, Sallam KI, Matsa E, Sharma A, Gold JD, Engler AJ, Xiang YK, Bers DM, Wu JC (2015) Epigenetic regulation of phosphodiesterases 2A and 3A underlies compromised beta-adrenergic signaling in an iPSC model of dilated cardiomyopathy. Cell Stem Cell 17(1):89–100
42. Zhi D, Irvin MR, Gu CC, Stoddard AJ, Lorier R, Matter A, Rao DC, Srinivasasainagendra V, Tiwari HK, Turner A, Broeckel U, Arnett DK (2012) Whole-exome sequencing and an iPSC-derived cardiomyocyte model provides a powerful platform for gene discovery in left ventricular hypertrophy. Front Genet 3:92
43. Zhong H, Minneman KP (1999) Alpha1-adrenoceptor subtypes. Eur J Pharmacol 375(1–3):261–276

Chapter 15

Addressing Functional Neurotoxicity Using the Microelectrode Array (MEA)

Udo Kraushaar, Elke Guenther, and Dietmar Hess

Abstract

Early drug development requires tests for compound-induced neurotoxic effects, i.e., to investigate possible alterations of neuronal activity as a result of the test compound. In vivo and in vitro animal models transpire not to be overly predictive of neurotoxic effects in humans and furthermore are in contradiction to the efforts of the European Community to reduce the number of animal experiments. Consequently, alternatives to these animal model-based assays are currently being investigated. Human induced pluripotent stem cell (hiPSC)-derived neurons offer several advantages, including being of human origin and offering the possibility of developing disease models from patient-derived cells. The development of electrophysiological assays based on microelectrode array systems (MEA) allows one to study alterations of neuronal activity in samples of varying complexity ranging from single cells to neuronal networks. As a non-invasive method it supports not only acute but also long-term experiments for extended time periods. Here we describe how to record neuronal activity from neurons and provide exemplarily insights into a validation study for a commercially available hiPSC-derived neuronal cell type.

Key words Microelectrode array, MEA, Multi-well, Assay development, Spike analysis, Neuronal activity, Threshold detection

1 Introduction

Detailed pharmacological in vitro profiling of new chemical entities is imperative in the early phase of drug development in order to predict adverse effects of test compounds. Most of the neurotoxic effects until now are investigated using either in vivo or in vitro animal models, with the latter usually not being highly predictive. The translation from data obtained using animal models to humans is problematic, in addition to the ethical issues associated with animal experiments [1]. One reason for the insufficient translation to the clinic is the lack of disease-specific phenotypes, which often cannot be modelled easily in animals. The development of neurons differentiated from human embryonic stem cells (hESC) and human induced pluripotent stem cells (hiPSC) was a

Mike Clements and Liz Roquemore (eds.), *Stem Cell-Derived Models in Toxicology*, Methods in Pharmacology and Toxicology,
DOI 10.1007/978-1-4939-6661-5_15,

milestone in science, opening the possibility of overcoming the limitations of animal models, thereby allowing one to use human material in compound screening and drug validation. hiPSC can be differentiated into different neuronal subtypes and glia cells by a precisely timed exposure to a combination of growth factors and cell culture reagents. The usage of hiPSC-derived neurons is the only practicable strategy to study the development and function of live human neurons.

Cell sources are not limited to healthy individuals. This technique also allows the study of human neurons carrying genetically encoded disorders from patients with neurological diseases or specific mutations as well as other terminally differentiated cell types, by exposure to a combination of growth factors and cell culture conditions. Human iPSCs thus make it possible to study human neurons, a previously inaccessible cell type, carrying the genetic information from patients with a specific mutation or a neuropsychiatric disease [2, 3]. These diseases are difficult to replicate in genetically modified animals due to the fact that multiple mutation sites seem to be involved in many disorders, including schizophrenia, depression, and autism [4].

The typical approach to measure the function of primary and hiPSC-derived neurons is by means of manual patch clamp technique. Here a glass capillary carefully contacts a single neuron, allowing the changes in voltage or transmembrane currents to be recorded. Even though this method offers high spatial and temporal resolution it has numerous limitations. First of all, the number of cells recorded at a given time is typically limited to one (with more recordings in parallel being possible but relatively challenging), making it difficult to investigate neuronal network activity (i.e., cell–cell communication). Secondly, these patch clamp recordings are invasive and not suitable for long-term measurements. In contrast, microelectrode array (MEA) systems enable multiple parallel electrical recordings of neuronal signals to be collected non-invasively making this technique particularly suitable for long-term experiments [5–7]. Consequently, MEA provides a means to investigate the activity within the neuronal network. The heart of an MEA chip consists of substrate-integrated microelectrodes (diameters between 10 and 100 μm, depending on chip and manufacturer) that are arranged in an array. This array is embedded in a recording chamber, which also serves as a culture dish. The number of electrodes typically ranges between 60 and 256 arranged as an 8×8 or 16×16 array, respectively, depending on the system used. Neurons are plated directly on top of the electrodes and electrical activity is recorded extracellularly as field action potentials from all electrodes simultaneously. The defined geometry of the 2D array provides information of not only the activity at the individual electrodes but also the 2D flow of excitation of the neuronal network under investigation. Optional lids on top of the chamber

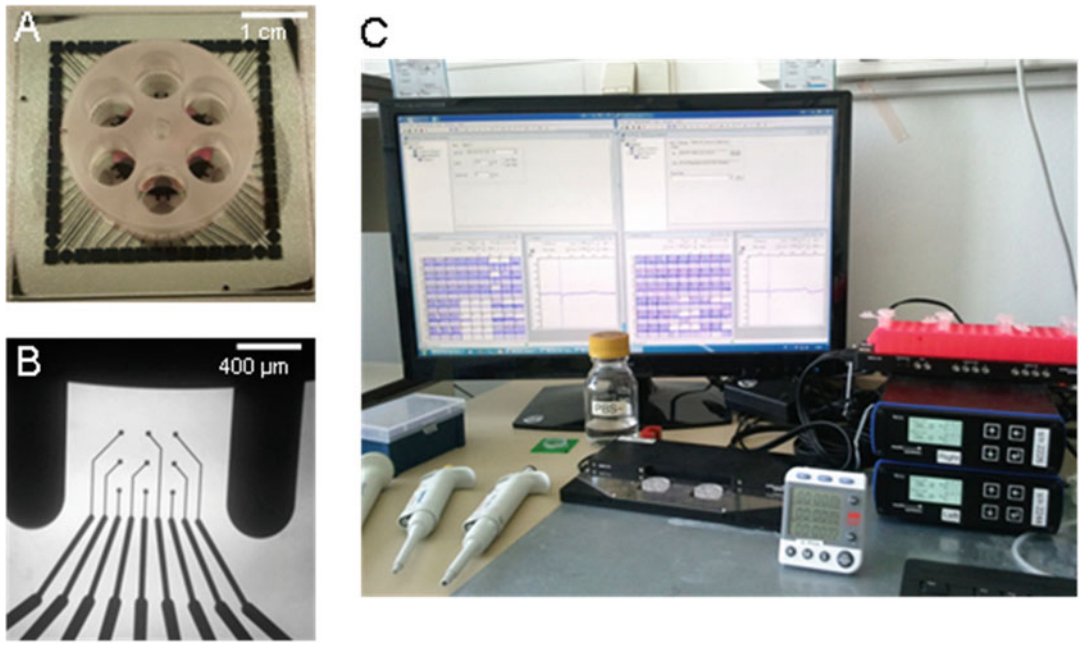

Fig. 1 MEA setup. (**a**) MEA chip consisting of six independent wells allowing the recording of up to six experiments in parallel. (**b**) Magnification of the electrode array within one of the wells. Nine electrodes (round structures at the end of each lead, 30 µm diameter) are placed in a 3×3 array (200 µm pitch). (**c**) MEA setup consisting of the amplifier (located between the pipettes and the timer, consisting of two headstages for the parallel recording of two MEA chips), a heating unit (*right*), and a computer

ensure sterile conditions, a requirement for long-term recordings. Academic research experiments typically use single-well MEA chips that, due to the high number of electrodes, permit extensive investigation of network activity even over a long period of time. In areas where higher throughputs are of interest, chips with 6–9 wells are available. For even higher throughput, multi-well plates are available in which up to 96 parallel recordings can be achieved. A limitation of this increase in number of experimental wells is the concomitant decrease in number of electrodes per well. Whilst this decreased electrode density is still sufficient to investigate the overall activity, it limits the significance of information regarding the signal propagation.

In this chapter we will address functional neurotoxicity on hiPSC-derived neurons using 6-well MEA chips containing nine electrodes per well (Fig. 1).

2 Materials

hiPSC-derived neurons can either be generated in house or obtained from one of several commercial manufacturers. As the field is highly dynamic at the time of preparation of this chapter, a list of

manufacturers will not necessarily reflect the current market status. Therefore no recommendation can be given about the best cell source. The data and figures depicted here are from the product line Peri.4U™ (Axiogenesis, Germany) a fully differentiated neuronal line with a peripheral neuron profile according to the manufacturer (e.g., 90% peripherin positive cells [8]). When using cells obtained from commercial sources, best results are achieved when the recommended protocols and culturing conditions are followed. Special attention should be given to the cell thawing procedure, since there are several critical steps that can make the difference between a high yield of healthy cells and a major loss of cells.

MEA systems are available from several companies including Multi Channel Systems (MCS) (Germany), Axion BioSystems (USA), and AlphaMed (Japan), to mention just a few. They all are based on the same recording principle, i.e., extracellular recordings from substrate-integrated electrodes, and are all suitable for experiments with hiPSC-derived neurons. Differences are subtle and include the software integrated for analysis, maximal sampling frequency, the capability to be used in cell culture incubators (not all of them are resistant to the humidity inside the incubator), and material and durability of the MEA electrodes. The system used for the experiments in this chapter consisted of an MEA2100 system (MCS) attached to a PC running the software MC_Rack which comes with the system. The MEA chips used were 6-well chips (60-6wellMEA200/30iR-Ti). This type of MEA chip comes in two varieties: one with small round chambers (60-6wellMEA200/30iR-Ti-rcr) comparable to the wells of a 96-well plate, and one with triangular chambers (60-6wellMEA200/30iR-Ti-tcr) that support a larger media volume. In both MEA chips, nine electrodes per well (arranged as a 3×3 array) are integrated with an electrode diameter of 30 μm and a pitch of 200 μm. The material of the electrodes is sputtered titanium nitrate (TiN) which provides low electrode impedance resulting in very low noise.

Sterilization of the chips prior to cultivation can be achieved either by autoclaving procedures (unless recommended differently by the chip manufacturer) or submersion of the chips for approximately 30–45 min in 70% (non-denatured) ethanol followed by air drying in a laminar flow hood/biosafety cabinet.

Several different cell attachment substrates are available including laminin and polyethylenimide (PEI solution, *see* **Note 1**). Unless an alternative is specifically recommended by the cell manufacturer, these are suitable provided the pH is maintained within the range of 4–9. A pH outside of this range tends to destroy the insulation of the electrode leads, which in turn leaves the chip damaged.

Cleaning of the chips is best done by rinsing the chips with a powerful (deionized) water jet from a squirt bottle, with a subsequent submersion in a solution containing 1% Tergazyme

(Alconox, USA) in distilled water over night at room temperature. Following a careful rinsing with distilled water, any remaining residue can be washed off by placing the chips overnight in large beaker with distilled water (approx. 1 L for 4–6 chips). Air drying completes the cleaning cycles, and the chips can then be sterilized for further use.

Test compounds often cannot be dissolved directly in aqueous solutions but require a solvent. Typically either ethanol or dimethylsulfoxide (DMSO) is used to prepare stock solutions. In most cell systems, final concentrations of up to 0.1% are well tolerated by the cells. However, running vehicle control tests in parallel to the experiments is highly recommended.

Cell cultivation for MEA does not require special equipment compared to that recommended in other typical cell culture procedures. A horizontal laminar flow hood is beneficial when a stereomicroscope is used during plating of the cells (e.g., when plating small droplets). When seeding the cells in small droplets, low adhesion surface 10 µm pipette tips are ideal for forming a defined droplet.

3 Methods

3.1 Cell Seeding on MEA Chips

The surface of an MEA chip is to some extent hydrophobic, depending on both storage condition and duration. The longer the storage period in a dry environment, the greater the hydrophobic effect. A hydrophobic surface is suboptimal for two reasons: (a) cells tend not to adhere to hydrophobic surfaces resulting in a limited cell attachment; and (b) the nanostructured TiN is not fully wetted which results in a lower signal-to-noise ratio during experimental recordings. There are basically two different strategies to make the surface of the chips hydrophilic: (1) store the MEA chip submerged in distilled water until use; or (2) plasma clean the chip prior to use (*see* **Note 2**). Coating of the MEA chip requires a fairly steady hand. To optimize the signal-to-noise ratio of recording, plating of the cells onto the reference electrode should be avoided. For MEAs obtained from MCS the reference electrode can easily be identified because it is a very large solitary electrode placed some distance from the array of recording electrodes (Fig. 2b). To avoid the reference electrode, only small droplets directly spotted on top of the electrode array are optimal. Depending on the number and spacing of the electrodes within the area, droplet volumes of 1–3 µl can easily be achieved without moistening the reference electrode (Fig. 2b). When placing the droplet it is critical NOT to touch the electrodes of the array with the pipette tip, since the TiN is very fragile and will easily be damaged by the mechanical stress. A stereomicroscope is a very helpful tool for both coating and plating of the cells (*see* **Note 3**). When using the stereomicroscope it is

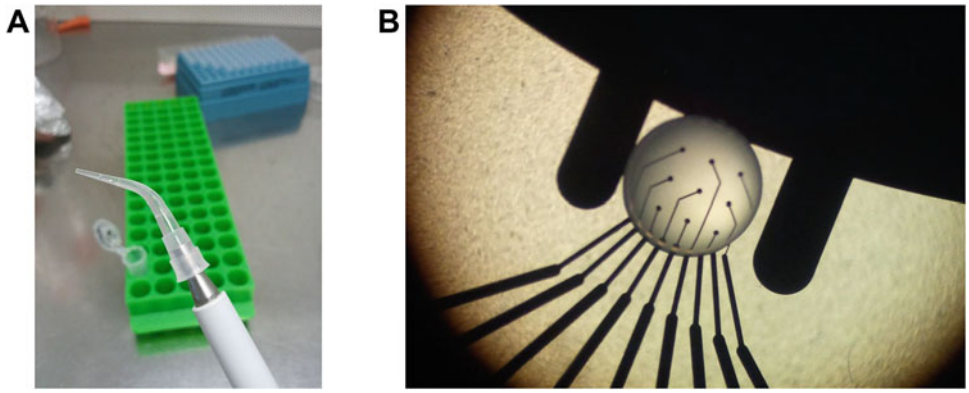

Fig. 2 (**a**) Kinked pipet tip for optimized pipetting into MEA under visual control. The pipet tip was rapidly moved through a Crème brulee torch and bent using a sterile forceps to an angle of approx. 50°. (**b**) Cell suspension droplet of approx. 0.75 μl applied to the electrode array of a single MEA well

difficult to insert the pipet tip with the cells (or coating substrate) for steric reasons. A solution is to kink the pipet tip to an angle of approx. 45–60° (Fig. 2a, *see* **Note 4**). When plating these small amounts of liquid, evaporation is a major issue. To minimize this it is advised to (1) place the MEA chips into a sufficiently large petri dish containing a moist filter paper at the bottom, and (2) perform the chip coating and cell plating steps rapidly and return the MEA chip back to the cell culture incubator as quickly as possible. The optimal cell density depends on the type of cells under investigation and can range from 0.3×10^6 to 6×10^6 cells/cm^2. Usually cells should be allowed to rest in the incubator for 1–3 h in order to attach to the surface of the MEA chip within the droplet before each well is slowly filled with medium (200 μl for 6-well and 9-well MEAs, 1 ml for single-well MEAs) with the pipet touching the inner wall of the well to avoid disturbing the plated cells. Unless stated differently by the manufacturer's manual, a 50% media exchange for the 6-well and 9-well MEAs should be performed 1 day post-plating and twice a week thereafter.

3.2 Recording of Spontaneous Electrical Activity

For most of the commercially available neuronal lines, spontaneous electrical activity can already be detected 3–5 days post-plating. To record this activity the cells should be transferred to the MEA setup for a minimum of 10 min prior to the recordings. This allows the cells to recover from mechanical stress introduced by vibrations and movement from the incubator to the MEA setup and ensures that the activity stabilizes. Additionally the heat system located below the MEA chip in the platform is typically set to 37 °C. When experiments are performed in bicarbonate buffered solutions or media, stabilization of recordings for long-time periods can be achieved by covering the top of the MEA with a small chamber in which humidified carbogen (typically 5% CO_2 and 95% O_2, depending on

the bicarbonate concentration in the medium) is flowing constantly. The carbogen stabilizes the pH of the solution and the humidified environment minimizes evaporation of the recording solution which would otherwise result in an increased osmolarity. This could be suboptimal for cell survival and increase the effective test compound concentration. To ensure that the field action potential (fAP) amplitude is recorded in full, the sampling frequency of the MEA setup should be sufficiently high to avoid under-sampling effects [9]. A sampling frequency set to 20–40 kHz is sufficient for most preparations. Please note that the data file size depends on the sampling frequency and easily can reach sizes of several tens of GBytes. Unless required differently in the experimental design, a hardware bandpass filter of 10 Hz–3 kHz is a good choice.

Figure 3 depicts a typical experiment at an early cultivation stage. Each of the boxes shown in A is the oscillographic voltage representation of a single electrode. Each of the wells of the 6-well MEA used in this experiment contains 9 electrodes. The black box in Fig. 3a indicates the nine electrodes comprising one well. It can be seen that spontaneous fAPs could be recorded on some of the electrodes. On the right-hand side a recording from one electrode is shown. The fAP activity displays a burst pattern which can be identified more clearly in the time-magnified picture below where the individual underlying fAPs within a single burst can be resolved. The magnitude and deflection (up- or downwards) of a single fAP can vary depending on the localization of the respective neurons relative to the recording electrodes [10, 11].

3.3 Spike and Burst Detection

There are many different strategies published regarding the analysis of the fAPs in neurons (e.g., see [12–16]), but most start with a simple threshold detection for identification of fAPs. In principle two possible strategies can be followed to set a threshold: (1) to set a fixed threshold for all electrodes. The downside of this is that in recordings where the noise level between the respective electrodes is different one tends to set a threshold which is still suitable for the most noisy electrode, thereby reaching threshold values where signals on the other electrodes might be missed; (2) to determine the standard deviation of the noise at a defined time window (e.g., 500 ms) of each of the electrodes individually and to set the threshold to a multiplied factor of the SD for each electrode (Fig. 4a). This procedure helps to convert the raw data into time markers which in turn can be used to calculate spike frequency and to define bursts. A burst consists of a series of fAPs within a defined time window, with defined time windows without activity before and after the fAP series (Fig. 4b). The parameter definition required for burst analysis includes:

- maximal interspike interval within a burst
- minimal burst duration

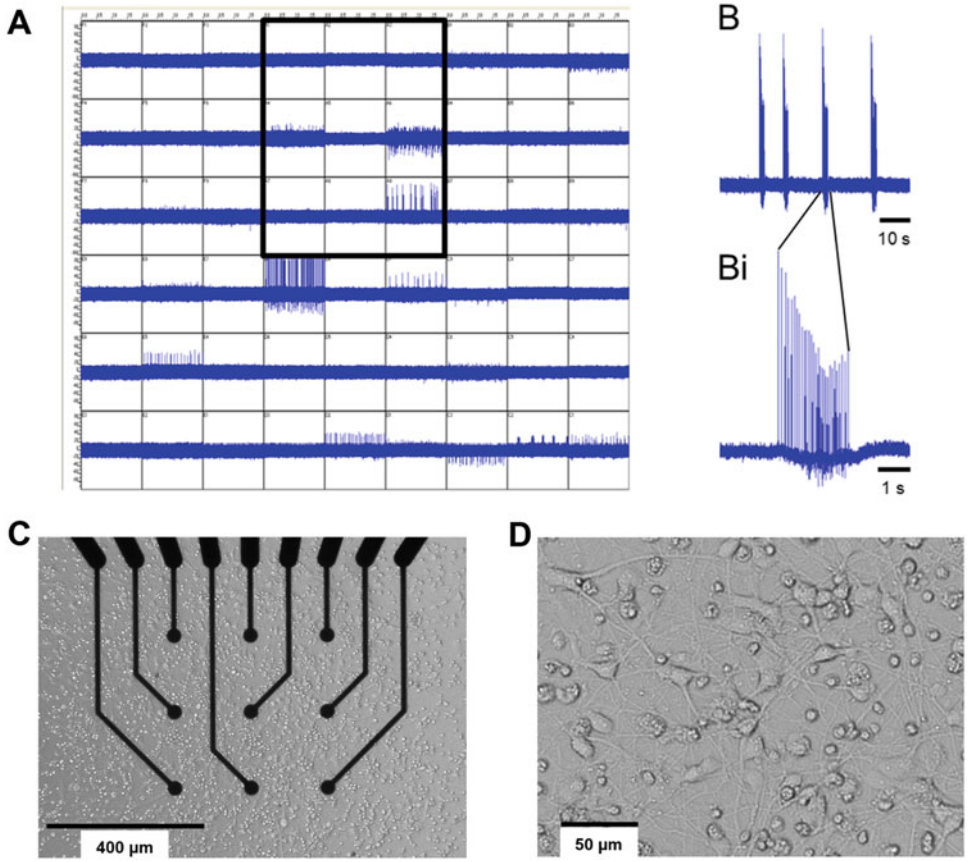

Fig. 3 Voltage traces of fAP recordings at 6 days in vitro. (**a**) Overview over all 54 electrodes of the 6-well MEA. Each box consists of the voltage representation of one electrode. The large box indicates the nine electrode representations of a single well. In some of the traces electrical activity can be recorded, shown as rapid voltage deflections. (**Bi**) Magnification of fAPs grouped in four bursts. (**Bii**) Magnification of one burst shown in **Bi**. The single fAPs underlying the burst can clearly be distinguished. (**c**) Neuronal culture on top of an MEA array. (**d**) Magnification. Cell density was $0.25 \times 10^6/\text{cm}^2$

- maximal burst duration
- minimal numbers of spikes within a burst
- minimal interval between bursts (which determines if the activity under investigation consists of one burst with variable activity or several bursts separated by inactivity phases).

The application of the optimal settings in order to adequately characterize burst behavior is one of the most challenging parts of this data analysis. Once these parameters are determined, a typical routine characterization of the electrical activity of hiPSC-derived neurons can consist of the following parameters:

- Mean spike frequency (Hz)
- Mean burst frequency (1/min)

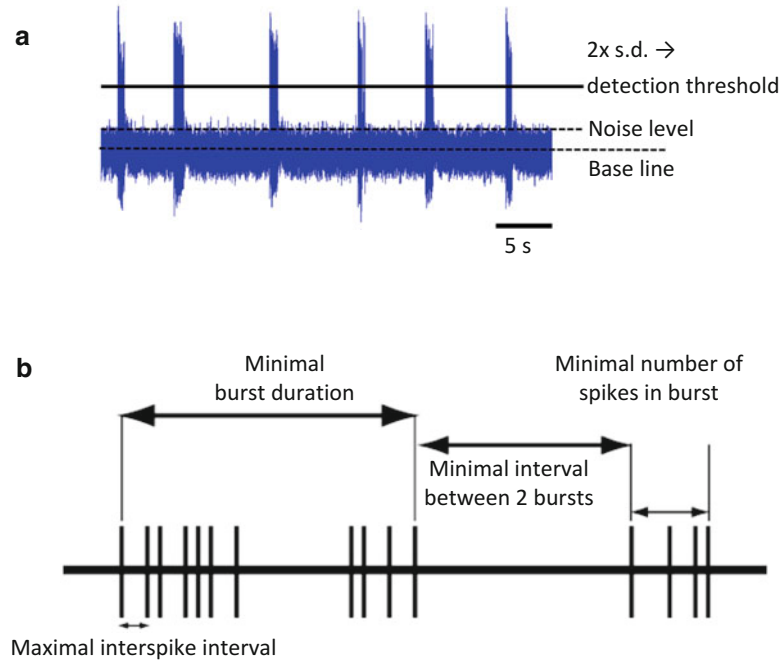

Fig. 4 Spike detection parameter. (**A**) Definition of threshold settings. An exemplary trace is shown displaying six bursts. Marked in dashed lines are both base line and noise level, a straight line indicates the value where standard deviation (s.d.) of the noise level was multiplied by 2. (**b**) Sketch to illustrate some of the analysis parameters mentioned in the text

- Mean burst duration (ms)
- Mean spike frequency within the burst (Hz)
- Mean spike proportion within a burst (%).

Sample analysis for Peri.4U™ neurons is shown in Fig. 5. Here recordings of spontaneously active neuronal activity were obtained under control conditions. Each data point represents the measurement from a single MEA recording.

3.4 Compound Application

There are two possible methods to apply compounds to the cells, either applied as a single test concentration per well or as the consecutive application of increasing test concentrations, which is more frequently used in compound screens. For both cases a time segment without compound is recorded which serves as control to which the compound condition is normalized. Usually compounds will be added followed by a wash-in time prior to recording (Fig. 6). For further details, *see* **Note 5**.

3.4.1 Vehicle Control Experiments

As noted in the method section many compounds require the use of either DMSO or ethanol (the solvent or vehicle) to prepare a stock solution. To ensure that neuronal activity changes are not an

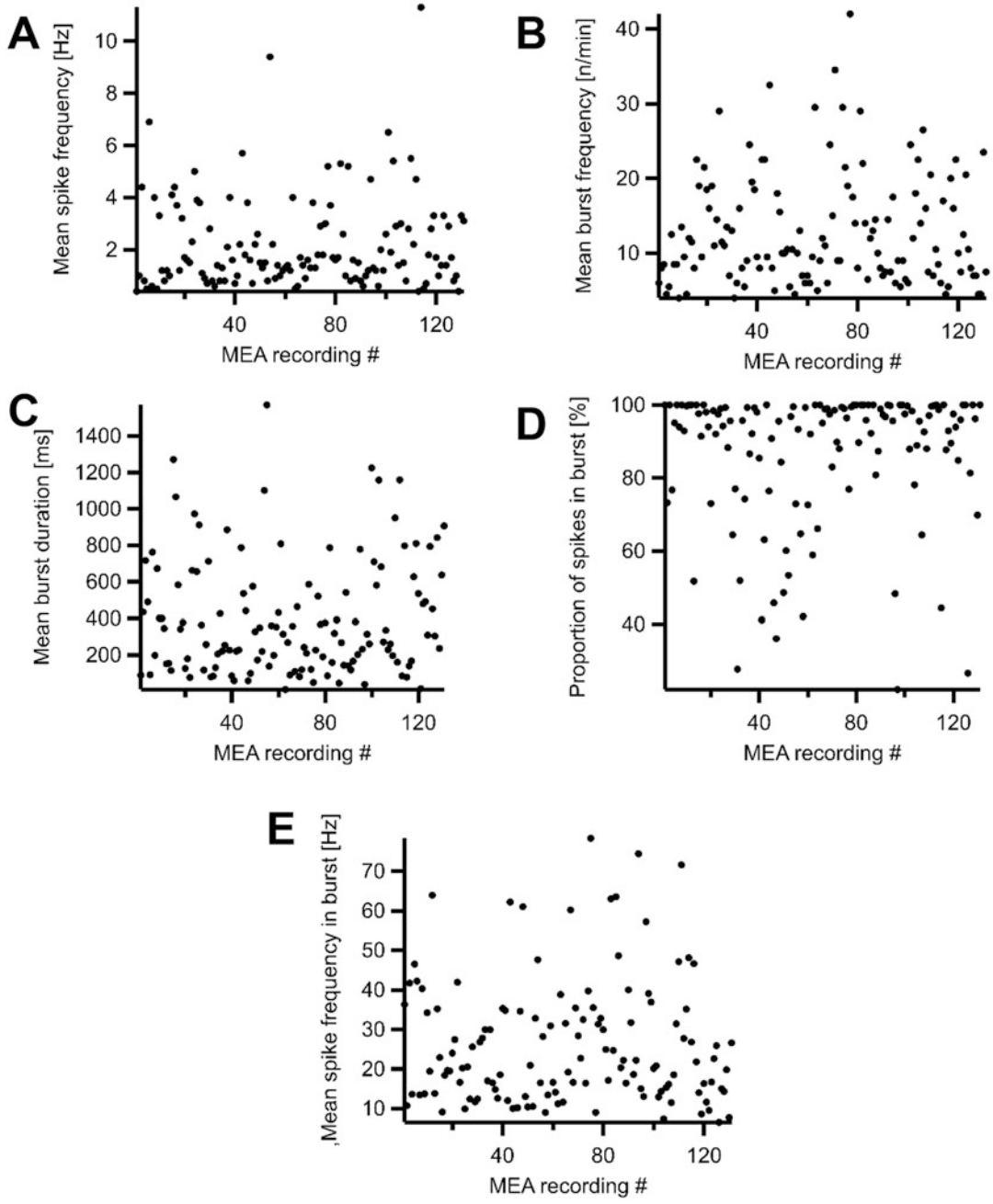

Fig. 5 Analysis of five parameters describing the spontaneous electrical activity of Peri.4U™ neurons. Each data point represents the recording of a single MEA recording. (**a**) Mean spike frequency in Hz; (**b**) mean burst frequency in n/min; (**c**) mean burst duration in ms; (**d**) proportion of spikes in burst in %; (**e**) mean spike frequency in burst in Hz

effect of the solvent used, it is highly recommended that vehicle control experiments are run in parallel to the test compounds. The concentration of solvent used for the vehicle control should be equivalent to the solvent concentration introduced with the test

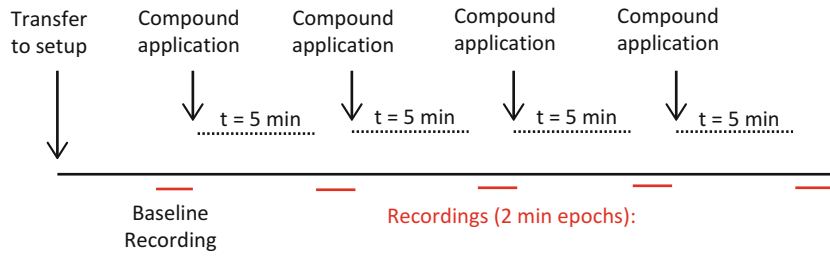

Fig. 6 Routine application scheme for consecutive compound application. After transfer of the cells to the MEA setup and a defined recovery period a control recording is obtained. Compound is applied directly thereafter and allowed to equilibrate in the MEA well for 5 min after which a recording is performed. This sequence is continued until the end of the experiment

compound. Figure 7 displays the analysis of different parameters after eight consecutive vehicle applications (here DMSO) up to a final concentration of 0.1 %. Ideally the vehicle does not influence the neuronal activity. In rare cases application of vehicle leads to a disturbance of the activity, which needs to be considered when assessing the compound-induced effects.

3.4.2 Compound Experiments

In the following, an exemplary validation study is displayed for Peri.4U™ neurons on MEA chips. Nine neurotoxic compounds were applied (*see* Table 1) and the effect on burst activity was investigated. The effect for all but one compound was also investigated using manual patch clamp on these cells to further understand the underlying mode of action if possible (data not shown). For one of the compounds tested, Fipronil, a $GABA_A$ receptor blocker in insects (i.e., a broad-use insecticide), results are presented in more detail. Application of Fipronil induced a concentration-dependent reduction of all parameters investigated including the mean spike frequency with an IC_{50} of 4.4 ± 1.2 µM (Fig. 8). This reduction of the spontaneous activity was accompanied by a reduction of the mean burst frequency. Furthermore fewer spikes were located within a burst, i.e., more solitary events were recorded. Patch clamp recordings revealed a significant inhibitory effect of Fipronil on voltage activated Na^+ currents in voltage clamp and a reduction of the numbers of APs following a current injection in current clamp mode. This reduction was in line with the effects seen in the MEA recordings indicating the same mode of action.

A summary of the effects induced by the test compounds on the measured parameters for both MEA and patch clamp can be seen in Table 2. Table 3 compares the data obtained from hiPSC-derived neurons (Peri.4U™) with primary neurons (rat cortex [17]) using an MEA system in both cases. The compound-induced effects on both neuronal activity and sensitivity are highly comparable in hiPSC-derived neurons and the primary rat cell system.

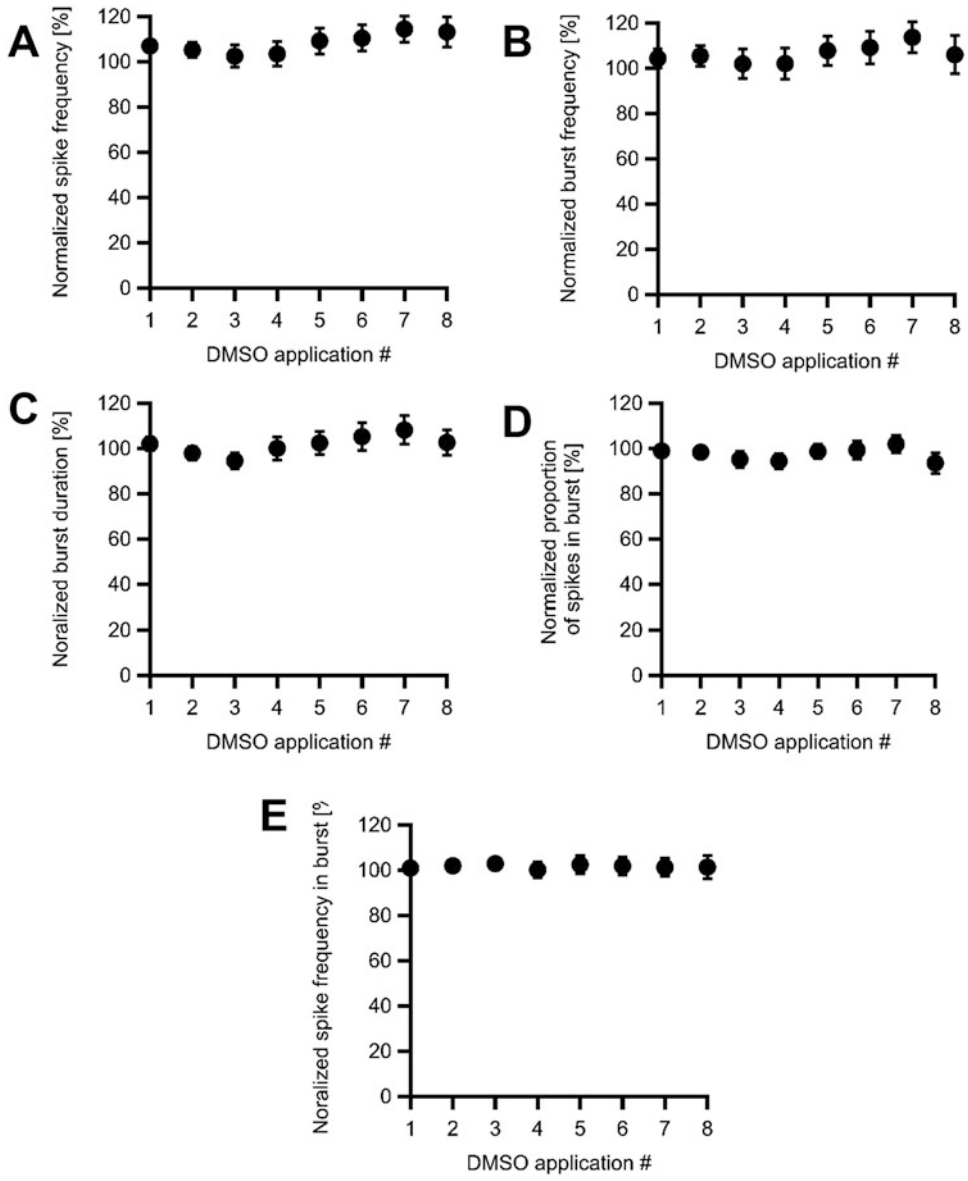

Fig. 7 Vehicle control experiments: analysis of five parameters on the spontaneous electrical activity of Peri.4U™ neurons. (**a**) Normalized spike frequency; (**b**) normalized burst frequency; (**c**) normalized burst duration; (**d**) normalized proportion of spikes in burst; (**e**) normalized spike frequency in burst. Data from $n = 26$ experiments. Error bars indicate SEM

These results suggest that the recording of electrical activity from hiPSC-derived neurons on an MEA system is a promising tool for the development of assays investigating the neurotoxicity of test compounds in human neurons.

Table 1
Reference compounds used for the investigation of neurotoxicity of hiPSC neurons on MEA

Compound name	Neurotoxic effect	Literature
Fipronil	Insecticide, $GABA_A$ receptor antagonist in insects	[17]
Loxapine	Neuroleptic, D2 and 5-HT_2 receptor antagonist	[18, 19]
Nomifensine	Antidepressant, DAT, and NET inhibitor	[20]
Trimethyltin	Organotin induces major cell damages, chromatin condensation, and internucleosomal DNA fragmentation	[17, 21]
Eugenol	Phenylpropene in plants, Na^+ channel inhibitor	[22, 23]
Nicotine	nACh receptor agonist	[24, 25]
Diphenhydramine	H1 receptor antagonist	[17, 26]
Ranitidine	H2 receptor antagonist	[27, 28]
Mepiquat	Plant growth regulator, mode of action unknown	[29]

4 Notes

1. To prepare a PEI solution, a solution containing 50 mM boric acid and 12.5 mM borax is dissolved in distilled water. After stirring overnight add 0.1 ml of a 5% polyethylenimide solution. Sterile filter and store at 4 °C. For coating add a droplet (ideally 1–2 μl) of PEI solution to the well and leave at room temperature for 1 h. Discard the solution and wash 3× with distilled water. Allow well to dry until use.
2. When using a plasma cleaner to make the surface of the MEA chip hydrophilic it is beneficial not to plasma clean the chip for an extensive time period. Typically 1 min is sufficient to achieve optimal hydrophilicity. With longer exposure times any droplet added to the surface will spread out making it difficult to achieve the cell density one is aiming for.
3. When placing droplets onto the MEA chip a simple stereomicroscope comes in handy. Ideally the bottom of the stage plate is illuminated by a regular light bulb (e.g., halogen bulb) rather than an LED field as with the latter the *Z*-axis resolution of the view is suboptimal.
4. To kink a pipet tip for the seeding of the cells simply move the pipet tip rapidly through a small flame (e.g., a Crème brulee torch) until the hot area becomes a bit more transparent compared to the cold plastic material. Bend the tip by application

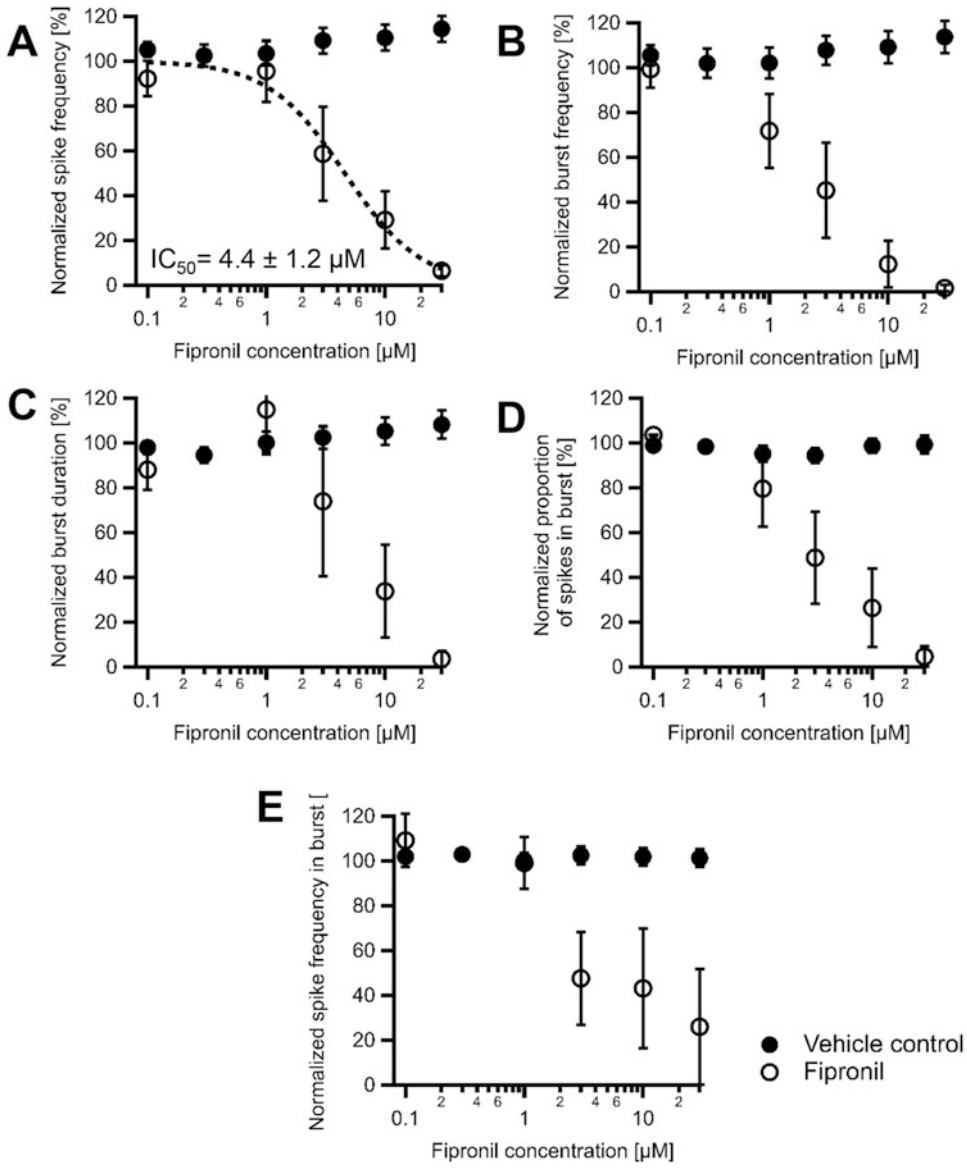

Fig. 8 Effect of Fipronil on the spontaneous electrical activity of Peri.4U™ neurons. (**a**) normalized spike frequency; (**b**) normalized burst frequency; (**c**) normalized burst duration; (**d**): normalized proportion of spikes in burst; (**e**) normalized spike frequency in burst. *Solid circles*: vehicle control ($n=24$), *open circles*: compound data ($n=5$). Error bars indicate SEM

of force using a sterile forceps until the material has cooled down. Make sure that the tip is still hollow after this procedure (Fig. 2a).

5. To minimize the mechanical stress of the neurons during application of a compound, an optimal media exchange is in the order of 10% of the well volume. This implies that the com-

Table 2
Summary of compound-induced effects on both MEA and patch clamp recordings

	MEA recordings					Patch clamp		
Compound name	**MSF**	**SPIB**	**BPM**	**MBD**	**MBF**	**INa**	**RMP**	**NS**
Fipronil	▼	▼	▼	▼	▼	▼	0	▼
Loxapine	▼	▼	▼	▼	▼	0	0	▼
Nomifensine	▼	▼	▼	▼	▼	▼	0	▼
Trimethyltin	▼	▼	▼	▼	▼	▼	0	▼
Eugenol	▼	▼	▼	▼	▼	0	0	▼
Nicotine	▲	0	▲	▲	0	0	0	0
Diphenhydramine	▼	▼	▼	▼	▼	▲		▼
Ranitidine	0	0	0	0	0	▲	0	0
Mepiquat	0	0	0	0	0	nt	nt	nt

MSF mean spike frequency, *SPIB* spike proportion in burst, *BPM* bursts per minute, *MDB* mean burst duration, *MBF* mean spike frequency in burst, *INa* peak amplitude of Na^+ current, *RPM* resting membrane potential, *NS* number of spikes, ▼ reduction, ▲ increase, *0* no change, *nt* not tested

Table 3
Comparison between MEA recordings on hiPSC neurons (Peri.4U™) and primary neurons (rat cortex)

	Overall activity	
Compound name	**Rat cortical neurons [17]**	**Peri.4U™ hiPSC neurons**
Fipronil	Reduction ≥ 10 μM	Reduction $IC_{50} = 4.4 \pm 1.6$ μM
Loxapine	Not tested	Reduction $IC_{50} = 1.4 \pm 0.3$ μM
Nomifensine	Reduction ≥ 10 μM	Reduction $IC_{50} = 6.2 \pm 0.8$ μM
Trimethyltin	Reduction ≥ 10 μM	Reduction $IC_{50} = 50.2 \pm 8.5$ μM
Eugenol	Reduction ≥ 1 μM	Reduction ≥ 10 μM
Nicotine	Increase ≥ 10 μM	Increase ≥ 100 nM
Diphenhydramine	Reduction ≥ 1 μM	Reduction $IC_{50} = 4.1 \pm 0.7$ μM
Ranitidine	Not tested	No effect up to 100 μM
Mepiquat	No effect up to 100 μM	No effect up to 100 μM

pound to be added consists of a stock solution with the respective high concentration. To simplify the calculations it is advised to keep the volume within the well constant by withdrawing the pipetting volume prior to adding the compound.

Acknowledgements

Parts of the research leading to these results has received support from the Innovative Medicines Initiative Joint Undertaking under grant agreement n° 115439, resources of which are composed of financial contribution from the European Union's Seventh Framework Programme (FP7/2007-2013) and EFPIA companies' in kind contribution. This publication reflects only the author's views and neither the IMI JU nor EFPIA nor the European Commission are liable for any use that may be made of the information contained therein.

References

1. Dragunow M (2008) The adult human brain in preclinical drug development. Nat Rev Drug Discov 7:659–666. doi:10.1038/nrd2617
2. Peitz M, Jungverdorben J, Brustle O (2013) Disease-specific iPS cell models in neuroscience. Curr Mol Med 13:832–841. doi:10.2174/1566524011313050014
3. Imaizumi Y, Okano H (2014) Modeling human neurological disorders with induced pluripotent stem cells. J Neurochem 129:388–399. doi:10.1111/jnc.12625
4. Vassos E, Collier DA, Holden S et al (2010) Penetrance for copy number variants associated with schizophrenia. Hum Mol Genet 19:3477–3481. doi:10.1093/hmg/ddq259
5. Thomas CA, Springer PA, Loeb GE et al (1972) A miniature microelectrode array to monitor the bioelectric activity of cultured cells. Exp Cell Res 74:61–66. doi:10.1016/0014-4827(72)90481-8
6. Potter SM (2001) Distributed processing in cultured neuronal networks. Prog Brain Res 130:49–62
7. Stett A, Egert U, Guenther E et al (2003) Biological application of microelectrode arrays in drug discovery and basic research. Anal Bioanal Chem 377:486–495. doi:10.1007/s00216-003-2149-x
8. Peri.4U – hiPSC Peripheral Neurons - AXIOGENESIS - iPSC Human Cardiomyocytes Neurons Hypertrophy Disease Model Cells. http://axiogenesis.com/products/neuronal-cells/peri-4u-hipsc-peripheral-neurons.html. Accessed 25 Feb 2016
9. Nyquest H (1928) Certain topics in telegraph transmission theory. Trans Am Inst Electr Eng 47:617–644
10. Holt GR, Koch C (1999) Electrical interactions via the extracellular potential near cell bodies. J Comput Neurosci 6:169–184. doi:10.1023/A:1008832702585
11. Buzsáki G, Anastassiou CA, Koch C (2012) The origin of extracellular fields and currents—EEG, ECoG, LFP and spikes. Nat Rev Neurosci 13:407–420. doi:10.1038/nrn3241
12. Canepari M, Bove M, Maeda E et al (1997) Experimental analysis of neuronal dynamics in cultured cortical networks and transitions between different patterns of activity. Biol Cybern 77:153–162. doi:10.1007/s004220050376
13. Morefield SI, Keefer EW, Chapman KD, Gross GW (2000) Drug evaluations using neuronal networks cultured on microelectrode arrays. Biosens Bioelectron 15:383–396. doi:10.1016/S0956-5663(00)00095-6
14. Quiroga RQ, Nadasdy Z, Ben-Shaul Y (2004) Unsupervised spike detection and sorting with wavelets and superparamagnetic clustering. Neural Comput 16:1661–1687. doi:10.1162/089976604774201631
15. Muthmann J-O, Amin H, Sernagor E et al (2015) Spike detection for large neural populations using high density multielectrode arrays. Front Neuroinform 9:28. doi:10.3389/fninf.2015.00028
16. Ness TV, Chintaluri C, Potworowski J et al (2015) Modelling and analysis of electrical potentials recorded in microelectrode arrays

(MEAs). Neuroinformatics 13:403–426. doi:10.1007/s12021-015-9265-6

17. Defranchi E, Novellino A, Whelan M et al (2011) Feasibility assessment of microelectrode chip assay as a method of detecting neurotoxicity in vitro. Front Neuroeng 4:6. doi:10.3389/fneng.2011.00006
18. Singh AN, Barlas C, Singh S et al (1996) A neurochemical basis for the antipsychotic activity of loxapine: interactions with dopamine D1, D2, D4 and serotonin 5-HT2 receptor subtypes. J Psychiatry Neurosci 21:29–35
19. Kapur S, Zipursky R, Remington G et al (1997) PET evidence that loxapine is an equipotent blocker of 5-HT2 and D2 receptors: implications for the therapeutics of schizophrenia. Am J Psychiatry 154:1525–1529. doi:10.1176/ajp.154.11.1525
20. Kinney JL (1985) Nomifensine maleate: a new second-generation antidepressant. Clin Pharm 4:625–636
21. Fiedorowicz A, Figiel I, Kamińska B et al (2001) Dentate granule neuron apoptosis and glia activation in murine hippocampus induced by trimethyltin exposure. Brain Res 912:116–127. doi:10.1016/S0006-8993(01)02675-0
22. Cho JS, Kim TH, Lim J-M, Song J-H (2008) Effects of eugenol on Na+ currents in rat dorsal root ganglion neurons. Brain Res 1243:53–62. doi:10.1016/j.brainres.2008.09.030
23. Moreira-Lobo DCA, Linhares-Siqueira ED, Cruz GMP et al (2010) Eugenol modifies the excitability of rat sciatic nerve and superior cervical ganglion neurons. Neurosci Lett 472:220–224. doi:10.1016/j.neulet.2010.02.009
24. Lindstrom J (1997) Nicotinic acetylcholine receptors in health and disease. Mol Neurobiol 15:193–222. doi:10.1007/BF02740634
25. Yoshida T, Sakane N, Umekawa T, Kondo M (1994) Effect of nicotine on sympathetic nervous system activity of mice subjected to immobilization stress. Physiol Behav 55:53–57. doi:10.1016/0031-9384(94)90009-4
26. Sewell RG, Nanry KP, Kennedy J et al (1985) Supra-additive toxic interaction of nicotine with antihistamines, and enhancement by the proconvulsant pentylenetetrazole. Pharmacol Biochem Behav 22:469–477
27. Chen K, Wang J-J, Yung WH et al (2005) Excitatory effect of histamine on neuronal activity of rat globus pallidus by activation of H2 receptors in vitro. Neurosci Res 53:288–297. doi:10.1016/j.neures.2005.07.008
28. Zhang J, Han X-H, Li H-Z et al (2008) Histamine excites rat lateral vestibular nuclear neurons through activation of post-synaptic H2 receptors. Neurosci Lett 448:15–19. doi:10.1016/j.neulet.2008.10.027
29. EFSA (2008) Conclusion regarding the peer review of the pesticide risk assessment of the active substance mepiquat. EFSA Journal 6(7). http://dx.doi.org/10.2903%2Fj.efsa.2008.146r

Chapter 16

Micropatterned Co-Cultures of Induced Pluripotent Stem Cell-Derived Hepatocytes and Stromal Cells for Drug Toxicity Studies

Brenton R. Ware and Salman R. Khetani

Abstract

As opposed to a limited supply of primary human hepatocytes (PHHs), induced pluripotent stem cell-derived human hepatocytes (iPSC-HHs) could provide a nearly unlimited supply of cells needed for screening large compound libraries in the early stages of drug discovery when SAR (structure–activity relationship) approaches are still feasible. With multiple donors of iPSC-HHs, the role of genetics on drug toxicity can also be evaluated as opposed to the limited genetic diversity of available PHH donors. However, like PHHs, iPSC-HHs in pure monolayers suffer from a rapid decline in hepatic functions and morphology, making them inadequate for chronic drug toxicity assessments. We adapted the micropatterned co-culture (MPCC) technology to commercially available iPSC-HHs, whereby these cells were organized onto collagen-coated domains of empirically optimized dimensions and then surrounded by 3T3-J2 murine embryonic fibroblasts in industry-standard multiwell plates. These so-called iMPCCs maintain high levels of hepatic functions, including basal cytochrome P450 activities and drug-mediated enzyme induction, for at least 4 weeks in vitro and reduced expression of fetal markers (i.e., alpha-fetoprotein) as compared to a declining phenotype in confluent iPSC-HH monolayers. Furthermore, iMPCCs correctly classified 24 of 37 hepatotoxic drugs (65% sensitivity), while all 10 non-toxic drugs tested were classified as such in iMPCCs (100% specificity). These results for drug toxicity detection in iMPCCs were remarkably similar to published data in PHH-based MPCCs that were treated with the same drugs. In this chapter, we describe the methods for micropatterning collagen in multiwell plates, establishing an iMPCC in those plates with commercially available iPSC-HHs, and conducting an initial drug toxicity screen with the cultures.

Key words Induced pluripotent stem cell-derived hepatocytes, Co-culture, Polydimethylsiloxane, Micropatterning, Photolithography, High-throughput screening, Drug-induced liver injury

1 Introduction

Drug-induced liver injury (DILI) remains a leading cause of acute liver failures and the pre-launch attrition, use restrictions, and post-market withdrawal of pharmaceuticals [1]. In particular, DILI is responsible for ~40% of the drug failures in the clinical trial stage of development and has been associated with ~1000 drugs brought

Mike Clements and Liz Roquemore (eds.), *Stem Cell-Derived Models in Toxicology*, Methods in Pharmacology and Toxicology, DOI 10.1007/978-1-4939-6661-5_16,

to market [2]. The US Food and Drug Administration mandates drug testing on both a rodent and non-rodent species before proceeding to human clinical trials [3]. While useful to understand some toxicity pathways, animal models do not provide a comprehensive understanding of *human-relevant* drug toxicity and metabolism [4, 5]. Most human-relevant systems including microsomes, hepatocarcinoma cell lines, and liver slices either do not enable complete drug metabolism, do not display normal hepatic morphology and functions, or do not maintain liver functions beyond a few days, respectively. Thus, primary human hepatocytes (PHHs) are frequently used to construct models of the human liver because they retain phenotypic functions for several weeks in vitro when subjected to the appropriate culture conditions [6, 7]. Even so, the scarcity of available healthy liver tissue and significant lot-to-lot variability in phenotypic functions impede PHH use for screening the toxic potential of large (millions) compound libraries in early drug discovery.

One of the most problematic forms of DILI is idiosyncratic, whereby only a small portion of the population experiences severe toxicity. Widespread instances of DILI tend to have a strong dose-dependence, whereas idiosyncratic DILI generally shows rare occurrences with little to no correlation with dose [8]. For example, troglitazone (Rezulin®) caused one liver failure for every 8000–20,000 patients before being withdrawn from US markets [9]. While there could be many underlying causes (i.e., age, nutritional status, and immune system responses) for such toxicity, it is believed that genetics are a significant, albeit unproven, contributing factor [10]. Thus, the limited number of available PHH donors reduces the genetic diversity of in vitro drug studies and may not give a fully accurate representation of the patient population's genetic background.

Induced pluripotent stem cell-derived human hepatocyte-like cells (iPSC-HHs) could not only address the limited genetic diversity of PHHs, but also provide a sustainable source of cells for building high-throughput models for preclinical drug screening [11]. However, iPSC-HHs generated using temporal delivery of growth factors and extracellular matrix proteins alone have very low and declining liver functions relative to adult PHHs [12, 13]. Furthermore, recent drug toxicity screens with iPSC-HH cultures have been restricted to acute doses of highly toxic compounds; even then, multiple overtly hepatotoxic compounds known in the clinic were not correctly flagged in such cultures [14, 15], potentially due to the very low activities of drug metabolism enzymes.

The in vitro phenotype of cultured primary hepatocytes has long been known to be improved via co-culture with liver- and non-liver-derived stromal cells from multiple species [16, 17]. Longevity and functions of such co-cultures are then further

improved significantly in micropatterned co-cultures (MPCCs) in which primary hepatocytes are arranged onto collagen-coated domains of empirically optimized dimensions and subsequently surrounded by 3T3-J2 murine embryonic fibroblasts, which allows better control over both homotypic and heterotypic cell–cell interactions [7, 18]. MPCCs created from primary hepatocytes of multiple species display high levels of long-term liver functions and have been shown to have superior prediction of clinical drug outcomes when compared to conventional culture models [18–22].

We have optimized the aforementioned MPCC technique for use with commercially available iPSC-HHs (iCell® Hepatocytes from Cellular Dynamics International) and demonstrated substantial improvements in mature iPSC-HH functions for at least 4 weeks in vitro as opposed to a declining liver phenotype in confluent iPSC-HH monolayers [23]. In particular, iPSC-HHs in these so-called iMPCCs maintain an in vivo-like hepatocyte morphology and polarity, secrete albumin and urea, display activities of major cytochrome P450s (CYP450s) and Phase II enzymes, show drug-mediated CYP450 induction, and down-regulate fetal markers such as alpha-fetoprotein. Furthermore, iPSC-HHs in iMPCCs displayed prototypical polygonal hepatic shape, distinct nuclei/nucleoli, and formed bile canaliculi with adjacent cells. More quantitatively, albumin secretion from iMPCCs was within the range of donor diversity observed in PHH-MPCCs, whereas urea synthesis was ~30–50% of PHH-MPCCs. CYP450 activity levels in iMPCCs ranged from ~5% (CYP2C19) to ~70% (CYP1A2) of PHH-MPCCs. Some of these differences are likely due to the maturation status of iPSC-HHs in iMPCCs, while other differences could be due to donor-dependent factors between the cell types.

Given the high levels of drug metabolism enzyme activities, we sought to explore iMPCC utility for an initial drug toxicity screening in the early stages of drug development [24]. Using 47 drugs of different classes and mechanisms of action, we found a 65% sensitivity (ability to detect compounds toxic to the liver) and 100% specificity (ability to detect non-toxins), which are remarkably similar to results observed using PHH-MPCCs treated with an identical drug set [20]. Furthermore, we demonstrated the potential of iMPCCs for detecting the differential toxicity of structural drug analogs (as would occur in a prospective drug screening campaign) and to probe mechanisms of toxic action (for utility in investigative toxicology). In this chapter, we describe the process of iMPCC creation and drug dosing. Specifically, we cover the soft lithographic techniques for micropatterning collagen in multiwell plates, the seeding techniques for establishing co-cultures, the procedure for applying the compounds of interest to the co-cultures, and the formulae for evaluating drug toxicity results using a limited number of drug doses.

2 Materials

2.1 Preparing Polydimethylsiloxane Lithography Mask

1. Silicon wafer with specific pattern of photoresist such as SU-8 (multiple vendors such as Trianja Technologies, SimTech, and FlowJem) (*see* Fig. 1a)
2. Glass petri dish
3. Arch punch (5 mm diameter for a 96-well plate; McMaster Carr)
4. Vacuum desiccator
5. Weighing dishes
6. Hexamethyldisilazane
7. Sylgard 184 PDMS kit (Dow Corning)
8. Teflon block (multiple vendors such as Star Prototype and 3D Systems).

2.2 Preparing Micropatterned Collagen Plates

1. Industry-standard tissue culture-treated 96-well plate
2. Rat tail collagen-I
3. Double-distilled water (ddH_2O)
4. Oxygen plasma chamber that utilizes radio frequency waves (multiple vendors such as PlasmaEtch and SPI Supplies)
5. PDMS lithography mask (materials and methods described in Sects. 2.1 and 3.1)
6. Plate compression clamp (multiple vendors such as Star Prototype and 3D Systems)

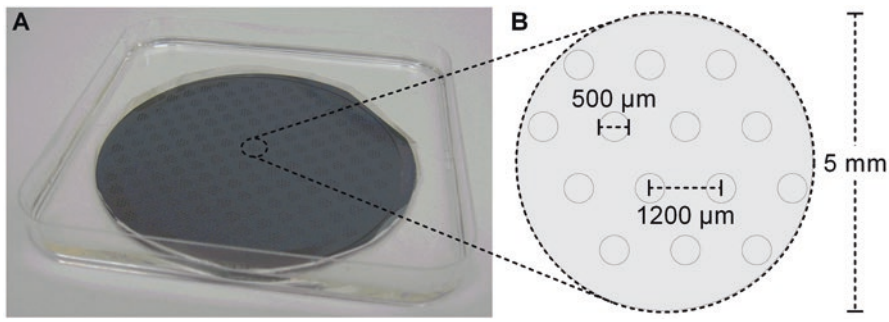

Fig. 1 Arrangement of islands in MPCC pattern. (**a**) Silicon and SU-8 master should be designed and manufactured to contain islands of 500 μm diameter and 1200 μm center-to-center spacing. This geometry results in ~9.2 % of the available surface area being covered with hepatocyte-like cells and the remaining area being covered with stromal cells. In our previous work, we have demonstrated this as the optimal geometry to support iPSC-HH functions when using 3T3-J2 murine embryonic fibroblasts as the supporting stromal cell type [23]. Islands should have a depth of 150–250 μm to ensure proper patterning. (**b**) PDMS is molded using the silicon master and circular "buttons" are then cored out from the PDMS sheet using a commercially available arch punch. A total of 14–16 islands should be present in a 5 mm diameter button that will fit in a single well of a 96-well plate in subsequent steps

7. 70% (v/v) ethanol
8. Bovine serum albumin fraction V

2.3 Culturing 3T3-J2 Fibroblasts

1. 3T3-J2 fibroblasts (courtesy of Howard Green, Harvard Medical School) [25]
2. Dulbecco's modified Eagle's medium (DMEM) with high glucose and L-glutamine
3. Bovine serum
4. Penicillin-streptomycin solution (100×)
5. 150 cm^2 tissue culture T-flasks
6. 1× phosphate buffered saline (PBS)
7. 0.25% (m/v) trypsin with 0.21 mM EDTA
8. Trypan blue viability stain
9. Hemocytometer

2.4 Seeding iPSC-HHs

1. Commercially available iPSC-HHs (Cellular Dynamics International)
2. Reagents to process iPSC-HHs (according to manufacturer protocols)
3. Hemocytometer
4. Trypan blue viability stain
5. 96-well plate with micropatterned collagen (materials and methods described in Sects. 2.2 and 3.2)

2.5 Seeding 3T3-J2 Fibroblasts

1. Dulbecco's modified Eagle's medium (DMEM) with high glucose and L-glutamine
2. Bovine serum
3. HEPES buffer
4. B27 supplement (Thermo-Fisher)
5. ITS+ premix (Corning)
6. Penicillin-streptomycin solution (100×)
7. Oncostatin-M, reconstituted to 10 μg/mL in 1× PBS with 0.1% (m/v) bovine serum albumin
8. Dexamethasone, reconstituted to 10 mM in dimethyl sulfoxide
9. Glucagon, reconstituted to 0.7 mg/mL in 0.05 M acetic acid
10. Propagating 3T3-J2 fibroblasts (materials and methods described in Sects. 2.3 and 3.3)
11. Fibroblast media (methods described in Sects. 2.3 and 3.3)
12. 1× phosphate buffered saline (PBS)
13. 0.25% (m/v) trypsin with 0.21 mM EDTA
14. Hemocytometer.

2.6 Maintaining Cultures

1. Hepatocyte culture media (materials and methods described in Sects. 2.5 and 3.5).

2.7 Drug Dosing

1. Drugs of interest
2. Dimethyl sulfoxide (vehicle control)
3. Dulbecco's modified Eagle's medium (DMEM) with high glucose and L-glutamine
4. HEPES buffer
5. B27 supplement (Thermo-Fisher)
6. ITS+ premix (Corning)
7. Penicillin-streptomycin solution (100×)
8. Oncostatin-M, reconstituted to 10 μg/mL in 1× PBS with 0.1% (m/v) bovine serum albumin
9. Dexamethasone, reconstituted to 10 mM in dimethyl sulfoxide
10. Glucagon, reconstituted to 0.7 mg/mL in 0.05 M acetic acid
11. Deep-well plates (2 mL/well capacity)
12. 96-well U-bottom low-binding collection plates
13. Aluminum plate sealers

2.8 Biochemical Assays and Data Analysis

1. Human albumin ELISA kit (Bethyl Laboratories)
2. Urea nitrogen (BUN) test (Stanbio Laboratory)
3. Spectrophotometer capable of reading 96-well assay plates
4. Data analysis software (e.g., Microsoft Excel, GraphPad Prism).

3 Methods

3.1 Preparing PDMS Lithography Mask

The procedural steps below need to be completed only once, since the PDMS lithography mask is reusable for several years.

1. Glue the silicon master onto the glass petri dish with a few drops of PDMS (10:1 base to curing agent by weight), ensure that the wafer is pressed flat against the petri dish, and allow curing at 65 °C overnight. The resulting assembly should look like Fig. 1a.
2. Silanize the silicon master by adding a few drops of silane to a plastic weighing dish, and then placing the silicon master and plastic weighing dish together in a vacuum desiccator chamber. Keep under vacuum until the silane has evaporated.
3. Mix PDMS components together (10:1 base to curing agent by weight) thoroughly. It is important that the mixing be done well over several minutes since otherwise the PDMS polymerization will be inconsistent across the length of the device.

4. Pour PDMS over the silanized silicon master, ensuring all features on the master (areas with micropatterning) are uniformly covered with PDMS. Degas the PDMS under vacuum and cure at 65 °C overnight on a level surface. *See* **Note 4.1**.
5. Carefully remove the PDMS from the silicon master by using a razor blade to cut along the edges of the PDMS and peeling the PDMS upwards. Peeling the PDMS too fast will tear the micropatterned features and cause poor patterning.
6. Core out the PDMS buttons with the arch punch, resulting in a geometry similar to Fig. 1b.
7. Machine two interconnecting Teflon pieces that, when connected, form a base and pillars for a 96-well tissue culture plate.
8. Properly connect the two machined Teflon pieces (similar to Fig. 2a) to prevent PDMS from leaking through in **step (10)** below.
9. Silanize Teflon pieces following **step (2)** above.
10. Pour PDMS (10:1 base to curing agent by weight) into the Teflon mold, ensuring that each pillar is filled and that a flat, rectangular base of PDMS (~1 cm thick) is maintained above all pillars.
11. Degas the PDMS under vacuum until all bubbles have been removed. Bubbles remaining in the PDMS can cause inconsistent patterning and pillars to break off easily. *See* **Note 4.2**.
12. Cure the PDMS in a 65 °C oven overnight, ensuring that the PDMS is level. Carefully remove the cured PDMS from the Teflon mold so as to not tear the posts. Figure 2b, c shows a sample of what the resulting PDMS base should look like.
13. Attach the PDMS buttons, created in **step (6)**, to the PDMS base that was constructed with the Teflon block in **step (12)**. On the bottom of each pillar, place a small drop of PDMS (10:1 base to curing agent by weight) and a PDMS button

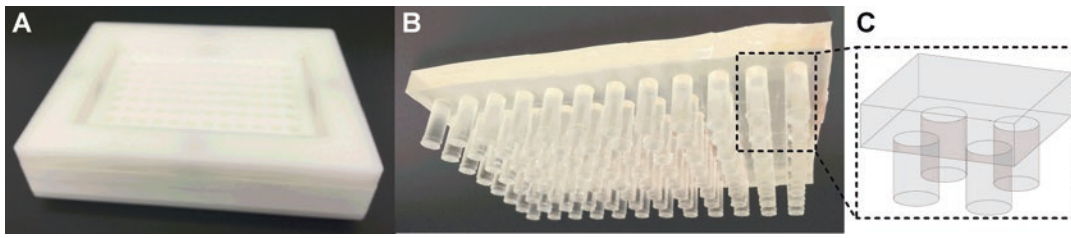

Fig. 2 Manufacturing the PDMS base. (**a**) Two interconnecting Teflon pieces should be manufactured to match the geometry of an industry-standard 96-well plate. Pillars should be 5 mm in diameter, ~12.5 mm in height, and spaced to match the wells of a 96-well plate. (**b**) After silanization, PDMS is poured into the Teflon mold, degassed in a vacuum desiccator, and allowed to cure. The final PDMS base should have both rectangular base and pillars for each well of a 96-well plate. The rectangular base should be ~1 cm thick to ensure that pillars can only be minimally distorted. (**c**) An expanded illustration of four wells of the PDMS mold

(with micropatterned features pointing away from the base, *see* Fig. 3). Ensure that the buttons are at a uniform height with light, even pressure. Allow to cure at 65 °C overnight on a level surface.

3.2 Preparing Micropatterned Collagen Plates

These procedures can be completed well before the cell culture experiments, because the plates are stable when stored as indicated.

1. Dilute rat tail collagen-I to 25 μg/mL in ddH_2O.
2. In a biosafety cabinet, add 50 μL diluted collagen solution to each well of the 96-well plate.
3. Place the 96-well plate at 37 °C in a humidified incubator for 2 h.
4. Rinse the plate twice with ddH_2O.
5. Let the 96-well plate dry thoroughly (with lid off in the biosafety cabinet) for at least 2 h, and overnight if needed due to the ambient humidity. Incomplete drying will cause water to become trapped in subsequent steps and lead to improper patterning.

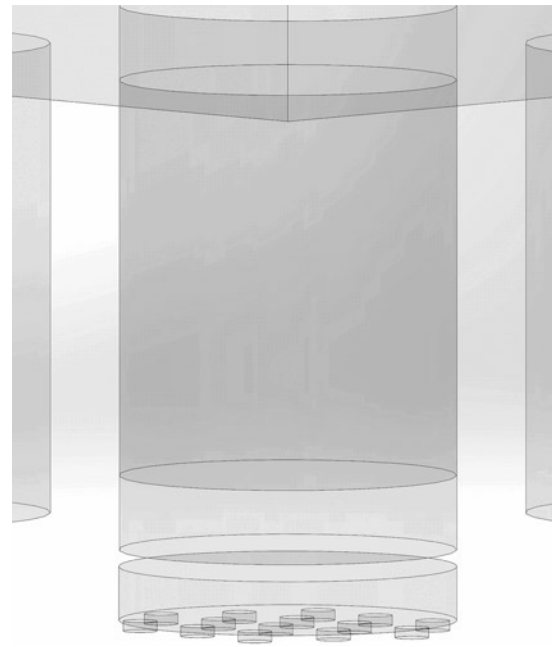

Fig. 3 Attachment of PDMS buttons to the PDMS base. Upon completion of both the PDMS base (from Teflon mold shown in Fig. 2) and buttons (from silicon master shown in Fig. 1), the two should be attached using a small drop of uncured PDMS. The micropatterned posts/islands on the buttons should be pointing away from the base so they can contact the cell culture plate during the oxygen plasma ablation process. After applying light pressure to the buttons and ensuring they are at a uniform height, cure the fixture at 65 °C overnight

6. Clamp the PDMS lithography mask (from Sect. 3.1) into the plate ensuring that all PDMS posts/islands are pressing up against the collagen-coated plastic. Each post/island should appear circular and not "doughnut-like," which indicates over-compression and buckling of the PDMS. *See* Fig. 4 and **Note 4.3**.
7. Insert the assembly into the plasma machine and close the chamber door.
8. Run the oxygen plasma at 50–100 W for 30–120 s. Consult the plasma machine documentation on operation of the specific model used. The combination of plasma power and time will likely need to be optimized for a given machine. It is recommended to use a radio frequency-based machine as opposed to microwave-based since the latter can cause heat gradients, which will non-specifically degrade the collagen.
9. Remove the assembly from the plasma machine and separate the base from the plate. The remaining collagen islands in the 96-well plate should resemble those shown in Fig. 5.
10. In a biosafety cabinet, sterilize the plate by adding 70% (v/v) ethanol to completely cover the bottom of each well and allow to sit for at least 45 min. Ultraviolet (UV) sterilization can also be used; however, the time and intensity of UV will need to be optimized to ensure sterility.
11. Rinse the plate three times with ddH_2O and allow to dry in the biosafety cabinet with the lid removed.
12. Dilute bovine serum albumin to 0.05% (m/v) in ddH_2O.
13. Add 50 μL/well bovine serum albumin solution and place at 37 °C in a humidified incubator for 45–60 min.

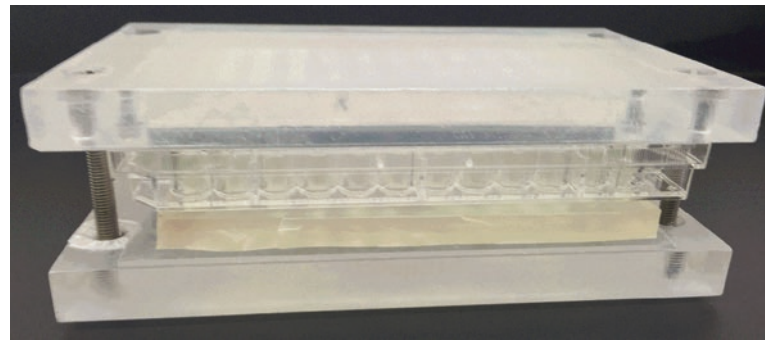

Fig. 4 Assembly for micropatterning collagen in plates. After a 96-well tissue culture polystyrene plate is coated with rat tail collagen, the PDMS mold (from Fig. 3) is placed into the plate and secured with the plate compression clamp. Oxygen plasma will ablate all exposed regions of collagen, while the collagen protected by the PDMS posts will remain intact/adsorbed for cell attachment

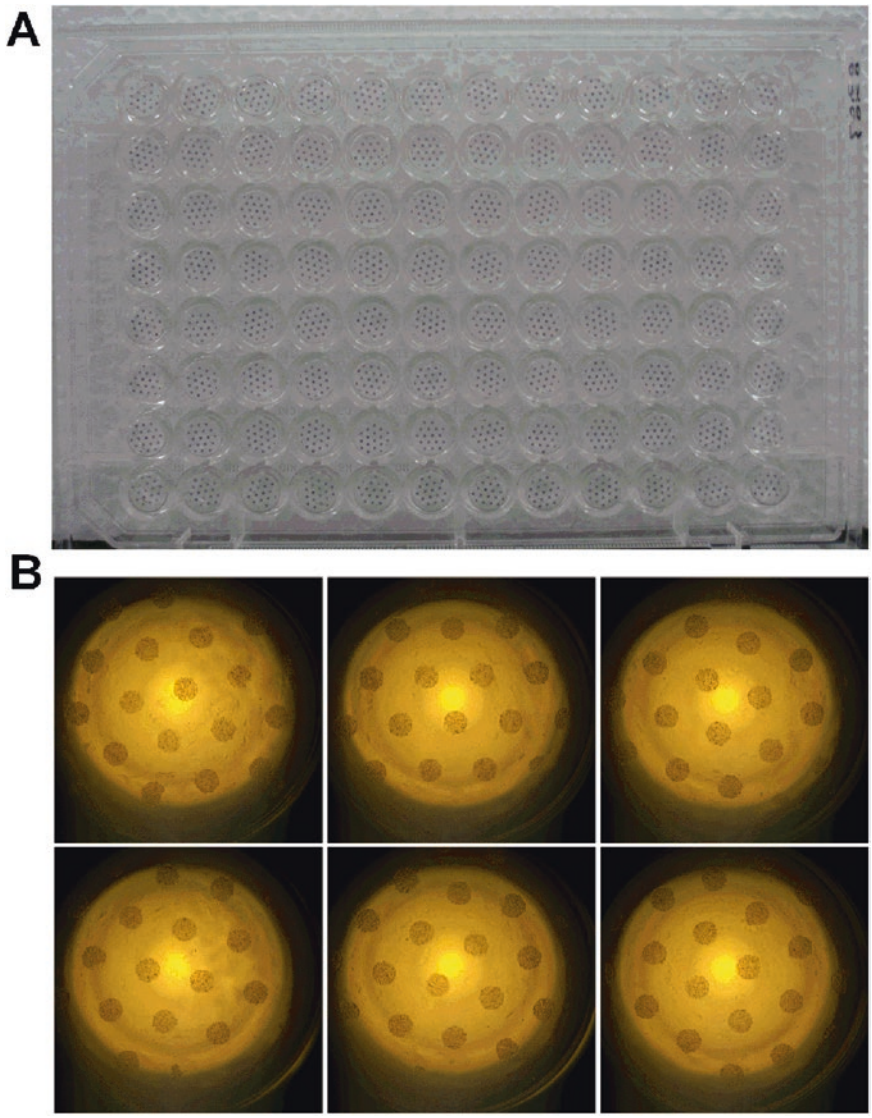

Fig. 5 Micropatterned 96-well plate for iPSC-HH seeding. (**a**) Image of a 96-well tissue culture polystyrene plate with hepatocyte islands stained with the MTT [3-(4,5-dimethylthiazol-2-yl)-2,5-diphenyltetrazolium bromide] dye. (**b**) Magnified image of six wells with hepatocyte islands. Adapted with permission from Oxford University Press [24]

14. Rinse plate twice with ddH_2O and allow to dry for 2 h in the biosafety cabinet with plate lid removed.
15. Once the 96-well plates are dry, they can be sealed with the lid on and put at 4 °C in a sealed plastic bag with a desiccant pack to keep the plates dry. The plates can be stored as such for at least 2 months without noticeable degradation in cell patterning in Sect. 3.4.

3.3 Culturing 3T3-J2 Fibroblasts

These procedures should be started at least a week before starting procedures outlined in Sect. 3.4.

1. Prepare fibroblast culture medium by supplementing DMEM with 10% (v/v) bovine serum and 1% (v/v) penicillin-streptomycin stock solution (at 100×).
2. Thaw a vial of 3T3-J2 fibroblasts by removing from liquid nitrogen dewar and swirling in a 37 °C water bath until only a small crystal of ice remains (~2 min). *See* **Note 4.4**.
3. Sterilize vial by spraying thoroughly with 70% (v/v) ethanol and transferring to a biosafety cabinet.
4. Pipette vial contents into a 50 mL conical.
5. Rinse vial with 1 mL fresh fibroblast medium and pipette into the 50 mL conical of **step (4)**.
6. Add ~28 mL fibroblast medium to the 50 mL conical in a dropwise manner (over ~2 min) to bring the total contents to 30 mL. The dropwise addition of media allows the cryoprotectant in the cell interior to be released without lysing the cells.
7. Transfer the contents of the 50 mL conical to a 150 cm^2 tissue culture-treated T-flask and maintain in a 37 °C humidified incubator.
8. Change fibroblast medium every third day by aspirating the old media (while being careful not to disturb the adherent cell monolayer) and adding 30 mL of fresh medium.
9. Observe the fibroblasts under a microscope periodically. When the cells reach 80–90% confluency, they will need to be passaged according to **steps (10)–(21)**. *See* **Note 4.5**.
10. Aspirate media from the flask and replace with 10 mL 1× PBS.
11. Aspirate the PBS and replace with 10 mL 0.25% (m/v) trypsin with EDTA, ensuring that the trypsin covers the flask surface.
12. Place the flask for 7 min at 37 °C in a humidified incubator.
13. Tap the flask on the side of a table (without breaking the plastic) to detach cells still adhered to the flask surface. View under a microscope to ensure that at least 90% of the cells are detached.
14. Quickly add 10 mL of fresh serum-supplemented fibroblast medium to the flask in order to neutralize the trypsin.
15. Using a serologic pipette, rinse the suspension over the flask surface to collect any remaining cells and then transfer the suspension to a 50 mL conical.
16. Centrifuge the cell suspension at 420×*g* for 8 min.
17. Carefully remove the supernatant with a serologic pipette, ensuring not to disturb the cell pellet.

18. Resuspend the pellet in fresh fibroblast medium (~4 mL) and ensure complete mixing to the point where there are no visible clumps.
19. Use a hemocytometer and trypan blue (for viability assessment) to count the cells. An 80–90% confluent 150 cm^2 T-flask will typically yield 4–4.5 million viable cells. Note that if fibroblasts are maintained and trypsinized as described above, the viability should be greater than 99%.
20. Calculate the appropriate amount of cell suspension necessary. A 150 cm^2 T-flask seeded with 0.4–0.5 million cells will typically need to be passaged again in 4–5 days with a media change on the third day after seeding.
21. Mix an appropriate amount of cell suspension and fresh fibroblast medium to reach 30 mL total volume, seed into a new 150 cm^2 T-flask, and place at 37 °C in a humidified incubator.

3.4 Seeding iPSC-HHs

Start these procedures only when 3T3-J2 fibroblasts are propagating successfully and 96-well plates have been micropatterned with collagen.

1. Process the iPSC-HHs according to manufacturer-supplied protocols. We have successfully incorporated both fresh and cryopreserved iPSC-HHs from Cellular Dynamics International (iCell® Hepatocytes) into the iMPCC platform.
2. Use a hemocytometer and trypan blue (for viability assessment) to count the cells. Using manufacturer-recommended seeding medium, bring the cell density to 0.667 million viable cells/mL.
3. Ensuring a homogeneous cell suspension, add 50 μL/well of the cell suspension to each well, and then place at 37 °C in a humidified incubator.
4. Shake the plate every 20 min in both the horizontal and then the vertical perpendicular planar axes to homogenize the cells since otherwise they will typically settle to the sides of the well. Circular shaking will cause cells to aggregate in the center of the well and is not recommended. The cells start adhering onto the collagen-coated islands in 15–20 min, and cell-laden islands should be visible from the bottom of the plate macroscopically under appropriate lighting, similar to the appearance in Fig. 5b. It typically takes ~4–6 h for the islands to be >90% filled with iPSC-HHs. *See* **Note 4.6**.
5. Once the collagen-coated islands are filled at least 90% with iPSC-HHs, rinse each well three times with fresh DMEM (no supplements required) to remove unattached cells. It is not recommended to use vacuum aspiration on micropatterned cultures at any point in the culture lifetime. Use of micropipettes

(manual or electronic) is recommended for all cell culture and drug dosing steps.

6. Replace the culture medium on the cells to that recommended by the manufacturer.
7. Place the cultures at 37 °C in a humidified incubator until 3T3-J2 fibroblasts are ready to be seeded on top of the micropatterned iPSC-HH cultures.

3.5 Seeding 3T3-J2 Fibroblasts

These procedures should be completed 12–24 h after completing procedures in Sect. 3.4.

1. Prepare the hepatocyte culture medium. For a 50 mL conical, combine 42.25 mL DMEM, 5 mL bovine serum, 1.5 mL HEPES buffer stock (at 1 M), 1 mL B27 stock (at 50×), 500 μL ITS+ premix stock (at 100×), 500 μL penicillin-streptomycin stock (at 100×), 12.5 μL oncostatin-M stock (at 10 μg/mL), 0.5 μL dexamethasone stock (at 10 mM), and 0.5 μL glucagon stock (at 0.7 mg/mL). Scale volumes as necessary. Pre-warm this medium in a 37 °C water bath for 15–30 min before use. Excess medium can be stored at 4 °C and used for up to 1 week.
2. Follow the procedure outlined in **steps (10)–(17)** of Sect. 3.3 to pellet suspended fibroblasts.
3. Resuspend the fibroblast pellet in fresh hepatocyte culture medium to reach a density of 0.5–1 million cells/mL. Ensure complete mixing to the point where there are no visible clumps.
4. Use a hemocytometer and trypan blue to count the viable cells. See **step (19)** in Sect. 3.3 for expected cell counts.
5. Add fresh hepatocyte culture medium to bring the suspension to a density of 0.3 million cells/mL.
6. Remove the existing cell culture medium from the iPSC-HH plates and either discard or store at −20 °C to −80 °C for future assays if desired.
7. Ensuring a homogeneous cell suspension from **step (5)**, add 50 μL/well of the fibroblast suspension to each well of the 96-well plate and place at 37 °C in a humidified incubator. It is recommended to execute **steps (6)** and **(7)** such that wells with iPSC-HHs do not get desiccated. One strategy is to execute the steps for one row or column of the 96-well plate at a time.
8. Shake the plate every 30 min (for a total of 1.5 h) in both the horizontal and then the vertical perpendicular planar axes to homogenize the fibroblasts since otherwise they will settle to the center of the well typically. Circular shaking will cause cells to aggregate in the center of the well and is not recommended. *See* **Note 4.6**. The process of preparing and seeding plates is summarized in Fig. 6.

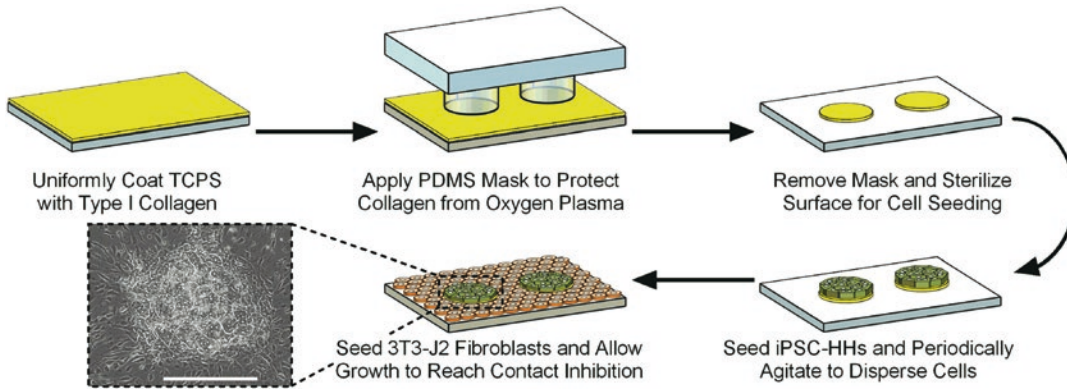

Fig. 6 Process overview of preparing and seeding plates. Industry-standard 96-well plates are homogeneously coated in rat tail collagen-I and subjected to PDMS mask-based micropatterning via oxygen plasma (see Sect. 3.2). iPSC-HHs will selectively bind to the remaining collagen islands (see Sect. 3.4). Subsequent seeding of 3T3-J2 fibroblasts completes the iMPCC (see Sect. 3.5). After 1 week in culture, iMPCC islands should appear similar to the micrograph shown (scale bar = 400 μm). Adapted with permission from Wiley [23]

3.6 Maintaining Cultures

Following the completion of steps outlined in Sect. 3.5, the following steps need to be performed every other day for ~1 week prior to use of the co-cultures for drug dosing studies.

1. Pre-warm the hepatocyte culture medium (recipe given in **step (1)** of Sect. 3.5) in a 37 °C water bath for 15–30 min.
2. Remove the existing medium from the cell culture plate. Store the collected media at −20 °C to −80 °C for future assays if desired.
3. Add 50 μL/well fresh culture medium to each well of the 96-well plate and continue to incubate at 37 °C in a humidified incubator. It is recommended to execute **steps (2)** and **(3)** such that wells with cells do not get desiccated. One strategy is to execute the steps for one row or column of the 96-well plate at a time.

3.7 Drug Dosing

After the cultures have been stabilized for ~1 week and appear similar to the phase contrast micrograph shown in Fig. 6, the steps outlined below should be completed every other day over the course of 6 days. We have found that 6 days of dosing with fresh drug added to culture medium every 2 days provides for high specificity (i.e., no false positives from non-toxic drugs tested) and high sensitivity (~65%) [24]. However, the duration of dosing with drugs can be adjusted (i.e., 2 or 4 days of dosing or beyond 6 days) depending on the hypotheses being posed.

1. Reconstitute drugs to 1000× the highest desired dose in DMSO. For our studies and the remaining protocols here, we base our doses on the C_{max} value, or the maximum/peak plasma concentration of the drug [20, 26]. Since our highest dose is typically 100 × C_{max}, we reconstitute the drugs at 100,000 × C_{max}.

Excess of this drug stock can be stored at −20 °C to −80 °C and used for future time points. *See* **Note 4.7**.

2. Prepare *serum-free* hepatocyte culture medium. For a 50 mL conical, combine 47.25 mL DMEM, 1.5 mL HEPES buffer stock (at 1 M), 1 mL B27 stock (at 50×), 500 μL ITS+ premix stock (at 100×), 500 μL penicillin-streptomycin stock (at 100×), 12.5 μL oncostatin-M stock (at 10 μg/mL), 0.5 μL dexamethasone stock (at 10 mM), and 0.5 μL glucagon stock (at 0.7 mg/mL). Scale volumes as necessary. Pre-warm this medium to 37 °C in a water bath for 15–30 min before use. Excess media can be stored at 4 °C and used for up to 1 week.
3. Supplement a portion of this media with 0.1 % (v/v) DMSO so that it can be used for drug dilutions in subsequent steps.
4. Using a deep-well plate, arrange the dosing media according to your desired plate layout. In our studies, we typically use 100 × C_{max} and 25 × C_{max} doses, so we will focus our example on that. In one column of the deep-well plate, thoroughly mix 1 μL of the 100,000 × C_{max} drug stock with 999 μL fresh medium (can be scaled as necessary) to bring the drug concentration to 100 × C_{max} and the DMSO concentration to 0.1 % (v/v) (*see* Fig. 7a).
5. In an adjacent column of the deep-well plate, add 600 μL of the DMSO-supplemented media created in **step (3)** (or scale with the total volume used in **step (4)**, *see* Fig. 7a).
6. Transfer 200 μL (or scale as appropriate) from the column created in **step (4)** to the column created in **step (5)** and mix thoroughly (*see* Fig. 7b). This will reduce the drug concentration to 25 × C_{max} while maintaining DMSO at 0.1 % (v/v) (*see* Fig. 7c).
7. Include DMSO-only controls in the deep-well plate that have 800 μL of the DMSO-supplemented media created in **step (3)** (or scale with the total volume used in **step (4)**).
8. Remove the existing cell culture medium from the plate and collect for future assays by freezing at −20 °C to −80 °C.
9. Add 50 μL/well of the appropriate medium (drug-containing or DMSO-only control) to each well of the 96-well plate and place in a 37 °C humidified incubator. It is recommended to execute **steps (8)** and **(9)** such that wells with cells do not get desiccated. One strategy is to execute the steps for one row or column of the 96-well plate at a time.

3.8 Biochemical Assays

In our experience with the MPCC platform, albumin and urea have been the most sensitive markers for drug toxicity detection in comparison to intracellular ATP and glutathione levels [20, 24]. Thus, measurements of albumin and urea in the supernatants allow assessment of time-dependent toxicity in the same wells.

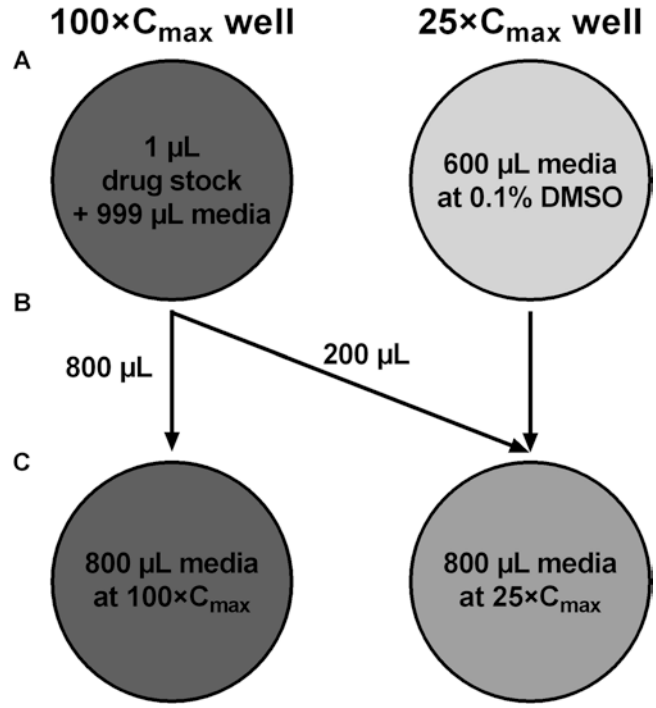

Fig. 7 Preparation of the deep-well plate for drug dosing. (**a**) To make the 100 × C_{max} dosing media, combine 999 µL serum-free, DMSO-free media with 1 µL 100,000 × C_{max} drug stock. In the adjacent well for the 25 × C_{max} dosing media, add 600 µL serum-free media supplemented with 0.1 % (v/v) DMSO. (**b**) To make the 25 × C_{max} dosing media, transfer 200 µL of the 100 × C_{max} dosing media to the well containing 600 µL serum-free media supplemented with 0.1 % (v/v) DMSO. (**c**) The wells will have a total volume of 800 µL at 0.1 % (v/v) DMSO and a drug concentration of either 100 × C_{max} or 25 × C_{max}. All volumes can be scaled as necessary

Further, albumin and urea are secreted only by the iPSC-HHs and not the 3T3-J2 fibroblasts. If we are testing a drug for the first time on iMPCCs, we will measure biomarkers such as albumin and urea in supernatants collected after 2, 4, and 6 days of dosing with the drug. The data allows us to determine how the toxicity profile changed over time for that specific drug and whether the day of dosing needs to be adjusted for future studies with that drug. Evaluation of cell responses at multiple time points can also be useful in an investigative toxicology setting. However, for a rapid screening protocol whereby both high sensitivity and high specificity are needed, we only measure the biomarkers in the supernatants after 6 days of dosing as we have shown in our previous study [24]. Other markers such as ATP, glutathione, or alanine aminotransferase might be necessary for further mechanistic studies. In such cases, fibroblast-only controls need to be prepared and dosed in an identical manner as the iMPCCs. The difference

in functions between the iMPCCs and fibroblast-only controls will yield the approximate hepatic contribution to each signal.

1. Thaw samples only when ready to run assays. Avoid multiple freeze-thaw cycles to prevent sample degradation.
2. Follow manufacturer-supplied protocols for completing the assays chosen for analysis. Ensure that the specific spectrophotometer of choice will be compatible with the assay outputs before using the samples.
3. For assays that require making a standard curve for analysis (i.e., albumin, urea), we recommend making those standards in the DMSO-supplemented media created in **step (3)** of Sect. 3.7 and using a serial dilution method. Note that the urea nitrogen (BUN) test from Stanbio Laboratory can be miniaturized to a 96-well plate format by using 10 μL of sample per well that is incubated with 150 μL of a mixture of color and acid reagent provided in the kit at a 1:2 ratio of color:acid reagent. The plate can then be incubated in the oven at 60 °C for 90 min while ensuring that evaporation is minimal by completely sealing the plate with a plate sealer.

3.9 Data Processing and Binary Toxicity Calls

The analysis described below assumes that three doses were used per drug ($0 \times C_{max}$, $25 \times C_{max}$, and $100 \times C_{max}$). With only three doses, it is difficult to fit the data to a sigmoidal (or multiparametric) dose–response curve since the curve will likely be highly inaccurate. Thus, our analysis below is meant for an initial binary decision on the compound, similar to strategies used by others [26, 27], especially in early stages of drug discovery. However, with additional drug doses—potentially 7 to 10—one can fit the data to a more complex curve and calculate various parameters as described below.

1. Normalize the liver functions/end-points in drug-dosed wells to the functions/end-points in the DMSO-only control wells. Express the normalized values as percentages.
2. For cultures whose functions at $25 \times C_{max}$ of drug were below 50% of control wells, linearly interpolate between the functions at $0 \times C_{max}$ and $25 \times C_{max}$ to calculate the compound's TC_{50} value (*see* Fig. 8a). The following equation is the reduced form of the linear interpolation:

$$TC_{50} = \frac{1250}{100 - F_{25}}$$

where TC_{50} = interpolated concentration that reduces functions to 50% of DMSO-only controls (multiples of C_{max})

F_{25} = functional levels at a drug dose of $25 \times C_{max}$ (% of DMSO-only control).

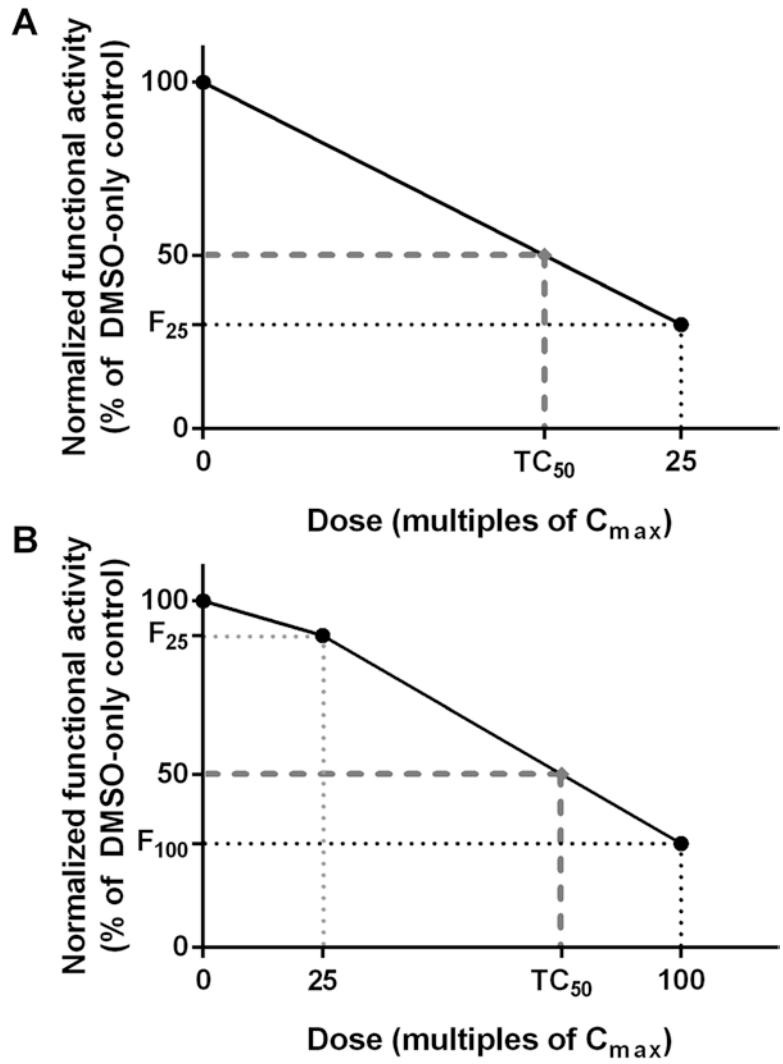

Fig. 8 Calculating the TC_{50} value. (**a**) If a compound causes the cultures to lose at least 50% of their liver function at 25 × C_{max}, linear interpolation is performed between the 0 × C_{max} (DMSO control) and 25 × C_{max} doses to calculate the compound's TC_{50} value. (**b**) For cultures that do not show at least a 50% reduction in function at the 25 × C_{max} dose but do at the 100 × C_{max} dose, linear interpolation is performed between the 25 × C_{max} and 100 × C_{max} doses to calculate the compound's TC_{50} value

3. For cultures not flagged at 25 × C_{max} but whose functions at 100 × C_{max} were below 50% of controls, linearly interpolate between the functions at 25 × C_{max} and 100 × C_{max} to calculate the compound's TC_{50} value (*see* Fig. 8b). The following equation is the reduced form of the linear interpolation:

$$TC_{50} = -75 \cdot \left(\frac{50 - F_{100}}{F_{25} - F_{100}} \right) + 100$$

where TC_{50} = interpolated concentration that reduces functions to 50% of DMSO-only controls (multiples of C_{max})

F_{25} = functional levels at a drug dose of 25 × C_{max} (% of DMSO-only control)

F_{100} = functional levels at a drug dose of 100 × C_{max} (% of DMSO-only control).

4. If a function was not below 50% of DMSO-only controls at the 100 × C_{max} dose, declare the drug "non-toxic" with respect to the liver. *See* **Note 4.8** for a discussion on the TC_{50} criteria and **Note 4.9** for examples of using this TC_{50} algorithm.
5. Calculate the assay sensitivity by dividing the number of drugs picked up as toxic (had an applicable TC_{50} value and are indeed true positives as opposed to false positives) by the total number of liver toxic drugs tested.
6. Calculate the assay specificity by dividing the number of drugs declared non-toxic (did not have an applicable TC_{50} value and are indeed true negatives as opposed to false negatives) by the total number of non-hepatotoxic drugs tested.

4 Notes

4.1 Fabricating PDMS Buttons

Uniform PDMS button (from silicon master) thickness is essential for proper patterning. To minimize the batch-to-batch variability in button thickness, place the petri dish containing the silicon master on a scale to measure the amount of PDMS actually used.

4.2 Degassing PDMS in a Vacuum Desiccator

If removing air bubbles from PDMS is taking a long time, try releasing and reapplying the vacuum pressure every 5–10 min. This pressure change will pop the bubbles already at the surface and draw embedded bubbles out towards the PDMS surface.

4.3 Clamping the PDMS Mask into a 96-Well Plate

Appropriate tightness is necessary for optimal patterning. With too little pressure, not all posts/islands will be properly protected from oxygen plasma. Too much pressure will cause the PDMS posts to form "doughnut" shapes (over-compression due to buckling of the PDMS) and might lead to inconsistent patterning. If the clamp is ever over-tightened, release the pressure entirely and retighten.

4.4 Selection of Fibroblasts

3T3-J2 fibroblasts have been found to induce the highest hepatic functions from multiple stromal cell types tested [28]. If these cells cannot be obtained, other 3T3 clones such as NIH-3T3 or Swiss-3T3 (from American Type Culture Collection or ATCC) can be used, albeit with lower induction of hepatic functions.

4.5 Erratic Growth of Fibroblasts

The doubling rate of 3T3-J2 fibroblasts is 1.5 days, on average. In some cases, the 3T3-J2 fibroblasts can grow more slowly or quickly

due to the specific lot of bovine serum used in the medium. Screen several lots of serum before banking one.

4.6 Shaking of the Plates to Homogenize the Cells

The plate should be out of the incubator for no more than 30 s each time. In addition, ensure that shaking is not done so vigorously so as to splash the cell suspension out of the well and into the space between the wells.

4.7 Limited DMSO Solubility of Drugs

For some drugs, the solubility in DMSO will not permit the drug to be dissolved at 100,000 × C_{max}. If vortexing and brief sonication do not lead to the drug becoming soluble in the DMSO, the DMSO volume should be doubled to reduce the stock concentration of the drug to 50,000 × C_{max}. During the drug dosing, this drug stock should be added at a ratio of 2 μL for every 998 μL of media. Thus, the overall DMSO concentration will be 0.2% (v/v). It is important to keep DMSO to as low of a level as possible since increasing concentrations of DMSO can lead to the down-regulation of CYP3A4 activity in iPSC-HHs [24].

4.8 Choice of TC_{50} Binary Decision Criteria

In our initial studies, we measured high assay sensitivity without sacrificing specificity when dosing the iMPCCs with drug three times over 6 days, weighing each assay equally in our decision-making, and utilizing the TC_{50} criteria [24]. Such parameters can be adjusted using statistical techniques as desired based on the number of data points available.

4.9 Sample Data Processing

Sample albumin data for mebendazole, acetaminophen, and aspirin are presented in Table 1. Each compound has data from both the 25 × C_{max} and 100 × C_{max} dose expressed as a percent of the DMSO-only control (F_{25} and F_{100}, respectively) along with the reported C_{max} value of the compound. For mebendazole, since the F_{25} value (15.96%) is below the 50% threshold, the equation in Sect. 3.9(2) applies:

$$TC_{50} = \frac{1250}{100 - F_{25}} = \frac{1250}{100 - 15.96} = 14.87$$

Table 1
Sample toxicity data in iMPCCs after 6 days of drug dosing

Compound	Albumin data at 25 × C_{max} dose (% of control, F_{25})	Albumin data at 100 × C_{max} dose (% of control, F_{100})	C_{max} (μM)
Mebendazole	15.96	6.09	0.126
Acetaminophen	72.35	7.37	151.170
Aspirin	90.92	63.47	5.526

Since this value has units of multiples of C_{max}, multiplying by the C_{max} value (0.126 μM) yields a TC_{50} of 1.87 μM. For acetaminophen, since the F_{25} value (72.35%) is above the 50% cutoff while the F_{100} value (7.37%) is below, the equation given in Sect. 3.9(3) applies:

$$TC_{50} = -75 \cdot \left(\frac{50 - F_{100}}{F_{25} - F_{100}}\right) + 100 = -75 \cdot \left(\frac{50 - 7.37}{72.35 - 7.37}\right) + 100 = 50.80$$

Multiplying this by the C_{max} value (151.170 μM) converts the TC_{50} to units of molarity, or 7679.44 μM. For aspirin, neither the F_{25} nor F_{100} values are below 50%, so it is designated as a "non-toxic" compound with respect to the liver based on our criteria.

5 Conclusions and Future Prospects

Despite being widely used for constructing in vitro models of the human liver, PHHs are ultimately a scarce resource with variable quality and limited genetic diversity. iPSC-HHs can be a sustainable tool for the preclinical screening of drug candidates, especially during early drug discovery when SAR (structure–activity relationship) approaches are still feasible [11]. However, the hepatic phenotype of the iPSC-HHs rapidly declines in conventional confluent monolayers [23]. Engineering tools, such as those adapted from the semiconductor industry, can be used to control the microenvironment (i.e., cell–cell interactions, soluble factors, etc.) around hepatocytes and stromal cells, which has shown great promise in stabilizing the liver phenotype for several weeks in vitro [3].

We and others are applying the aforementioned engineering tools to stem cell-derived hepatocyte-like cells to further differentiate these cells towards the adult PHH phenotype and maintain such functions for several weeks in vitro [11]. In particular, we adapted and optimized the micropatterned co-culture (MPCC) technique for iPSC-HHs, specifically iCell® Hepatocytes by Cellular Dynamics International [23]. Liver functions (i.e., albumin secretion, urea synthesis, and CYP450 activities) in these so-called iMPCCs were found to be significantly higher and stable for at least 4 weeks in vitro as compared to conventional confluent iPSC-HH monolayers [23]. We then showed a remarkable similarity between the iMPCCs and PHH-based MPCCs for DILI assessment using a set of 47 drugs (65–70% sensitivity, 100% specificity) [24]. Furthermore, iMPCCs detected the differential toxicity of structural drug analogs and recapitulated known bioactivation mechanisms underlying acetaminophen toxicity. In this chapter, we described in detail our protocols to create iMPCCs and then apply them to an initial/early drug toxicity

screen where quantities of novel drugs can be limiting and thus fewer doses are desired. Some of the steps in our protocol require specialized engineered devices that can be outsourced to prototyping foundries, while most other steps can be executed in any standard biological laboratory.

Some of the hepatotoxic drugs picked up by in vitro models of the human liver, including iMPCCs, cause idiosyncratic liver failure (i.e., troglitazone, isoniazid) in the clinic [20, 24, 26, 27]. However, in a cellular screen, stress markers (i.e., 50% or greater down-regulation of albumin secretion, urea synthesis, or ATP levels) were still able to classify these drugs as "toxic" over their "non-toxic" counterparts (i.e., high specificity). Such an outcome suggests that cellular stresses are potentially the first step in a series of mechanisms that eventually cause major liver injury (i.e., acute liver failure) in some patients. The livers of other patients who lack certain risk factors (i.e., genetics, diseases, and other medications) may instead adapt and recover from the initial hepatic stress. It should be noted, however, that until a very large panel of iPSC-HH donors are available (thousands of lines), it is not possible to predict which *specific* patient may fall into the "liver failure" or "recovery/adaptation" categories. Nonetheless, the goal of early drug development is to identify potential hazards associated with drugs and come up with design strategies to mitigate risks of clinical failure to the greatest extent possible. For such purposes, engineered models of the human liver provide for a robust preclinical drug screening strategy.

In vitro models of the human liver still fail to pick up several drugs as toxic (i.e., false negatives), which could indicate more complex toxicity mechanisms that are not currently replicated in hepatocyte-centric systems. For instance, inclusion of immune and liver stromal cell types (i.e., sinusoidal endothelial cells, Kupffer macrophages, and stellate cells) is likely to improve DILI predictions, as some drugs may not be directly toxic to the hepatocytes or may trigger an immune response that causes toxicity. More recently, several investigators have embarked on creation of multicellular models of the human liver, though validation studies with key drug sets are still ongoing [3]. We have designed iMPCCs to be modular in that interactions between iPSC-HHs and different types of stromal cells can be studied without significant changes to iPSC-HH homotypic interactions on the micropatterned extracellular matrix domains.

In the future, we anticipate that advances to the iMPCC platform will improve the in vitro screening of novel pharmaceuticals before launching clinical trials. As more iPSC-HH lines are established through rapid advances in iPSC technology, we anticipate that multiple iPSC-HH donors will reflect at least part of the genetic diversity seen in the human population that impacts idiosyncratic

drug toxicity. Ultimately, the advancements in iPSC technology coupled with a long-term culture model like the iMPCC will enable personalized drug screening applications.

Acknowledgments

We thank Cellular Dynamics International (Madison, WI) for providing the iPSC-HHs as well as Mitchell Durham and Wendy Sunada for assisting in compiling the protocols. Funding was provided by the National Science Foundation (CAREER CBET-1351909 to S.R.K.) and the National Institute of Allergy and Infectious Diseases (1R03AI115171-01 to S.R.K.).

Competing Interests Statement

S.R.K. consults for and holds stock in Ascendance Biotechnology, which has exclusively licensed the iMPCC technology from Colorado State University for drug development applications. B.R.W. has no potential conflicts of interest to disclose.

Glossary

BSA	Bovine serum albumin
C_{max}	Maximum or peak drug concentration measured in human plasma
CYP450	Cytochrome P450 enzyme
DMEM	Dulbecco's Modified Eagle's Medium
DMSO	Dimethyl sulfoxide
FDA	US Food and Drug Administration
HEPES	2-[4-(2-hydroxyethyl)piperazin-1-yl]ethanesulfonic acid
iPSC-HHs	Induced pluripotent stem cell-derived human hepatocytes
iMPCC	Micropatterned co-cultures containing iPSC-HHs and stromal cells
ITS+	Insulin/transferrin/selenious acid with BSA and linoleic acid
MPCC	Micropatterned co-culture containing PHHs and stromal cells
PBS	Phosphate buffered saline
PDMS	Polydimethylsiloxane
PHHs	Primary human hepatocytes
TCPS	Tissue culture polystyrene
TC_{50}	Interpolated concentration that reduces functions to 50% of DMSO-only controls (can be reported as multiples of C_{max})
UV	Ultraviolet

References

1. Kaplowitz N (2005) Idiosyncratic drug hepatotoxicity. Nat Rev Drug Discov 4:489–499
2. Zhang M, Chen M, Tong W (2012) Is toxicogenomics a more reliable and sensitive biomarker than conventional indicators from rats to predict drug-induced liver injury in humans? Chem Res Toxicol 25:122–129
3. Khetani SR, Berger DR, Ballinger KR et al (2015) Microengineered liver tissues for drug testing. J Lab Autom 20:216–250
4. Olson H, Betton G, Robinson D et al (2000) Concordance of the toxicity of pharmaceuticals in humans and in animals. Regul Toxicol Pharmacol 32:56–67
5. Shih H, Pickwell GV, Guenette DK et al (1999) Species differences in hepatocyte induction of CYP1A1 and CYP1A2 by omeprazole. Hum Exp Toxicol 18:95–105
6. Godoy P, Hewitt NJ, Albrecht U et al (2013) Recent advances in 2D and 3D in vitro systems using primary hepatocytes, alternative hepatocyte sources and non-parenchymal liver cells and their use in investigating mechanisms of hepatotoxicity, cell signaling and ADME. Arch Toxicol 87:1315–1530
7. Khetani SR, Bhatia SN (2008) Microscale culture of human liver cells for drug development. Nat Biotechnol 26:120–126
8. Ulrich RG (2007) Idiosyncratic toxicity: a convergence of risk factors. Annu Rev Med 58:17–34
9. Isley WL (2003) Hepatotoxicity of thiazolidinediones. Expert Opin Drug Saf 2:581–586
10. Yuan L, Kaplowitz N (2013) Mechanisms of drug-induced liver injury. Clin Liver Dis 17:507–518
11. Davidson MD, Ware BR, Khetani SR (2015) Stem cell-derived liver cells for drug testing and disease modeling. Discov Med 19:349–358
12. Gerbal-Chaloin S, Funakoshi N, Caillaud A et al (2014) Human induced pluripotent stem cells in hepatology: beyond the proof of concept. Am J Pathol 184:332–347
13. Schwartz RE, Fleming HE, Khetani SR et al (2014) Pluripotent stem cell-derived hepatocyte-like cells. Biotechnol Adv 32: 504–513
14. Takayama K, Kawabata K, Nagamoto Y et al (2013) 3D spheroid culture of hESC/hiPSC-derived hepatocyte-like cells for drug toxicity testing. Biomaterials 34:1781–1789
15. Medine CN, Lucendo-Villarin B, Storck C et al (2013) Developing high-fidelity hepatotoxicity models from pluripotent stem cells. Stem Cells Transl Med 2:505–509
16. Bhatia SN, Balis UJ, Yarmush ML et al (1999) Effect of cell–cell interactions in preservation of cellular phenotype: cocultivation of hepatocytes and nonparenchymal cells. FASEB J 13: 1883–1900
17. Guillouzo A (1998) Liver cell models in in vitro toxicology. Environ Health Perspect 106(Suppl 2):511–532
18. Lin C, Shi J, Moore A et al (2015) Prediction of drug clearance and drug-drug interactions in microscale cultures of human hepatocytes. Drug Metab Dispos 44:127–136
19. Wang WW, Khetani SR, Krzyzewski S et al (2010) Assessment of a micropatterned hepatocyte coculture system to generate major human excretory and circulating drug metabolites. Drug Metab Dispos 38:1900–1905
20. Khetani SR, Kanchagar C, Ukairo O et al (2013) Use of micropatterned cocultures to detect compounds that cause drug-induced liver injury in humans. Toxicol Sci 132: 107–117
21. Ramsden D, Tweedie DJ, Chan TS et al (2014) Bridging in vitro and in vivo metabolism and transport of faldaprevir in human using a novel cocultured human hepatocyte system, HepatoPac. Drug Metab Dispos 42:394–406
22. Dixit V, Moore A, Tsao H et al (2016) Application of micropatterned cocultured hepatocytes to evaluate the inductive potential and degradation rate of major xenobiotic metabolizing enzymes. Drug Metab Dispos 44:250–261
23. Berger DR, Ware BR, Davidson MD et al (2014) Enhancing the functional maturity of iPSC-derived human hepatocytes via controlled presentation of cell-cell interactions in vitro. Hepatology 61:1370–1381
24. Ware BR, Berger DR, Khetani SR (2015) Prediction of drug-induced liver injury in micropatterned co-cultures containing iPSC-derived human hepatocytes. Toxicol Sci 145: 252–262
25. Rheinwald JG, Green H (1975) Serial cultivation of strains of human epidermal keratinocytes: the formation of keratinizing colonies from single cells. Cell 6:331–343
26. Xu JJ, Henstock PV, Dunn MC et al (2008) Cellular imaging predictions of clinical drug-induced liver injury. Toxicol Sci 105:97–105
27. O'Brien PJ, Irwin W, Diaz D et al (2006) High concordance of drug-induced human hepatotoxicity with in vitro cytotoxicity measured in a novel cell-based model using high content screening. Arch Toxicol 80:580–604
28. Khetani SR, Szulgit G, Del Rio JA et al (2004) Exploring interactions between rat hepatocytes and nonparenchymal cells using gene expression profiling. Hepatology 40:545–554

INDEX

A

Activin 33
Adrenergic receptors (AR) 274
Albumin data 330
Amplitude heterogeneity index (AHI) 180
Antihistamines 38
Antipsychotics 38
ApoTox-Glo 187
Atrial natriuretic factor (ANF) 282
Automated patch clamp (APC)
  HTS 57
  materials 59–61
  nifedipine 77
  Patchliner 58, 59
  pluricytes and cellectis 58
  SyncroPatch 384PE 58, 59
Axiogenesis 168
Axoscope software 239

B

Beating 218, 222–224
Biochemical assays 325–327
Blebbistatin 193

C

Caffeine 33
Calcium
  channel 154, 156, 163
  transient 137, 138
Calcium-induced calcium release (CICR) 135
Campfit software 240
Cardiac hypertrophy
  antibodies and dyes 277
  AR 274
  cardiac hypertrophy 276
  cardiomyocyte differentiation 279
  cell proliferation 281
  cell volume measurement 285
  2D and 3D image acquisition 281
  gene expression assays 277, 279–280
  hESC-CM and hiPSC-CM 274
  high-content analysis 286
  human PSC 271
  hypertrophic stimuli 276
  intracellular signalling 273–275
  MAD 287
  microscopy-based methods 273
  natriuretic peptides 275
  phenotypic assays 274
  physiological hypertrophy 271
  proteome profiling 277
  serum-free basal medium 276
  software 285
  tumor spheroid 275
Cardiac Safety Research Consortium 39
Cardiac Two-Channel Time Series algorithm 157
CardioExcyte 96 ..... 192, 193, 200, 206
CardioExcyte Control software 204
Cardiotoxicity 250
CaViar 115
Cell density 33
Cell profiling 260
Cellular Dynamics International 155, 168, 193
CheRiff 111, 115
CiPA initiative 208
Co-cultures 214–215
Coefficient of variance (CV) 32
Compound experiments 303–305
Comprehensive in vitro proarrhythmia assay (CIPA) 10, 84, 137, 174
Consortium for Safety Assessment Using Human iPS Cells (CSAHi) 137
Contractile force
  AFM 233, 238
  cantilever chip design 233, 234
  cantilever fabrication and cleaning 230–233, 235
  cantilever recordings and drug experiments 237, 239, 240
  cantilever technology 230, 231
  cardiomyocyte contraction 241
  cardiotoxicity 229
  cell culture 232
  drug validation data 243
  drugs 233
  force system parameters 242
  heart 230
  hSC-derived cardiomyocytes 230
  human cardiomyocyte culture 236, 237

Mike Clements and Liz Roquemore (eds.), *Stem Cell-Derived Models in Toxicology*, Methods in Pharmacology and Toxicology,
DOI 10.1007/978-1-4939-6661-5, © Springer Science+Business Media New York 2017

Contractile force (*cont.*)
inotropic drugs....230
machinery module....230
stress calculation....240–242
surface chemistry modification, cantilever chip....236
Cor.4U hiPSC-Cardiomyocytes....155
Cor.4U®....137
CRISPR-Cas9....12
Culturing 3T3-J2 fibroblasts....321–322
CYP450 activity....313
CyteSeer™....157
Cytiva Cell Health Assay....267
Cytiva Plus™....254
Cytiva™....175, 254

D

Danio rerio....3
DataControl software....60, 75, 77
3D cell culture systems....212–214
3D cultures....218–219
3D fluorescence image processing....284–286
Dimethyl sulfoxide (DMSO)....44
2D monolayers....11
DMSO solubility....330
Downstream signalling pathways....280
Drosophila melanogaster....3
Drug-drug interactions....102–103
Drug-induced liver injury (DILI)....311
Drug metabolism enzyme activities....313
Drug screening....8
Drug toxicity....175, 188
Dulbecco's modified Eagle's medium (DMEM....220, 315, 316

E

Early after depolarization (EADs)....37, 86, 124, 169
Electrical field stimulation (EFS)....138
Electrocardiogram....37
Electrophysiologic phenotypes....6–8
Electrophysiology....105
Endothelin-A receptor (ET_A)....275
Extracellular field potentials (EFP)....191

F

Fabricating PDMS buttons....329
fAP recordings....300
Fibroblasts....329
Fibronectin....78, 205
Field of view (FOV)....180
Field potential duration (FPD)....86
Fipronil....303
Fluo-4....161
Fluorescent calcium-sensitive dye....151
Fluorescent voltage-sensitive dye....136
Fluoroquinolone antibiotics....38
FluoVolt....120, 151, 161
FluoVolt®....138
Fluoxetine....154
Fruit fly....3

G

$GABA_A$ receptor blocker....303
GE healthcare....193
Genetically encoded fluorescent indicators (GEFIs)....109
Genotoxicity....249
GlutaMax....220
Glycolysis....251
GravityPlus....223
GravityTrap....223, 224

H

Hank's balanced salt solution (HBSS)....221
Health and Environmental Sciences Institute (HESI)....39, 84, 87
Heart....211, 213–215
Hepatotoxic drugs....332
High content analysis (HCA)....260
anti-cancer drugs....250–253
cardiotoxicity assay workflow....249, 254, 255
cell health dye assay and imaging....254
cell imaging....247
cell population....248
CHCA methodologies....248
clinical toxicity....249
compound plates....256, 266
cytoplasmic region....259
cytotoxicity assay....258
cytotoxicity assessment....248
data visualization....261–266
equipment and consumables....253
extract cell health measurements....260
fibronectin....254, 266
flow cytometry....249
genotoxicity....249
glucose and galactose media....266
Hoechst channel....259
hSC-CM models....249–250
hSC-CM monolayers....248
image-based approaches....249
imaging....258–259
live-cell and dead-cell populations....260
mitochondria....250
monitor cells....266
organoids....248
phenotypic profiling, and cluster analysis....261–266
plate preparation and cell culture media....253

seeding and culture, cells....254–256
TMRM channel image....260
High-throughput screening (HTS)....57
Cal-520-AM dye....151
calcium ions....135
calcium transient assay stability....151
calcium transient recording....142
cardiac pacemaker cells....135
cardiomyocytes....135
cell preparation and dye loading....141
cell preparation, VSD assay....142–143
centrifugation....150
compound-induced changes....144–146
Cor.4U cardiomyocytes....136, 140
edge effects....150
FDSS system....140–141
fluorescent voltage- and calcium-sensitive dyes....136
FluoVolt dye....151
frozen Cor.4U Cardiomyocytes....148
Hamamatsu FDSS μCell andFDSS7000EX....136, 137
Hamamatsu Wave Checker Software....143–144
harsh suction and pipetting disrupts cardiomyocyte monolayers....150–151
L-type calcium channels....135
materials....137–138
microelectrode array recordings....137
microplates....139–140, 146–147
multiwell plates....138–139
VSD assays....137
hiPSC-derived cardiomyocytes
defrosting frozen aliquots....61–62
Patchliner....63
SyncroPatch 384PE....63
hPST assay....32–34
Human cardiac fibroblasts (HCF)....220
Human embryonic stem cells (hESC)....293
Human ether-à-go-go related gene (hERG)....87
Human pluripotent stem cell (hPSC)....23, 25–32
standard protocol
change media....25
differentiation and first compound treatment....26–28
differentiation and stain cells....29–30
differentiation medium I....23
H9 human ES cell line....23
hPST experiment....32
IC_{50} values....30–31
media change and second compound treatment....29
SOX17-IC_{50}....30
96-well plates (*see* Plate pluripotent stem cells)
Human pluripotent stem cell test (hPST)
cell culture....21
immunofluorescence staining....20
immunostaining....20
karyotype analysis....21
matrigel....22
mesendoderm differentiation....19–21
mesendoderm lineage....18
mycoplasma....21
pipetting....21
plate pluripotent stem cells....23–25
preparation of compounds....26, 28
preparation, cell bank....22
routine stem cell culture....21
stock solution....22
teratogens....17
Human stem cell-derived cardiomyocytes (hESC-CMs)
arrhythmogenic mechanisms....39
assay protocol....45–49
blebbistatin....193
cardiac action potential and ionic currents....37, 38
CardioExcyte 96....206
cell capacitance....51
cell culture components....39–40
compounds....45, 200
cytiva cardiomyocytes....43
data analysis....49–50
1\:2 diluted matrigel aliquots....41
1\:30 diluted matrigel solution....41–42
eurofins....52, 54
experiment....199–200
extracellular and intracellular solution compositions....44–45
fibronectin....195, 205
gramicidin....45, 51
harvesting cells....196
hiPSC-CMs....193, 195
I_{Kr}....55
materials....193–194
matrigel....42, 51
matrigel-coated coverslips....42, 51
medium exchange....198–199
monolayer and synchronous beating....197–199
nifedipine....52, 53, 55, 205
NSP-96....196
online analysis (OA)....201–205
patch-clamp instrumentation....40
plating cells....44
QT interval....37
quinidine....52
RPMI 1640/B27 Medium....41
sensor plate, fibronectin coating....193
sotalol....52, 53
test compound preparation....44
Human-induced pluripotent stem cell-derived cardiomyocytes (hiPSC-CMs)
maturation....5–6
screening drug effects....8–10

I

IC200—Kinetic Image Cytometer....156
Imatinib....34
Impedance. *See* Human stem cell-derived cardiomyocytes
Induced pluripotent stem cell-derived cells (iPSCs)
arrhythmic phenotypes....2
autocrine and paracrine....3
biomedical and pharmaceutical researchers....3
cardiomyocytes....1
cell autonomous diseases....2
congenital diseases....2
"disease-in-a-dish" models....2
endocrine/exocrine factors....3
genome engineering....2
hiPSC-CMs....4
neuronal and hepatocyte models....2
neurons and hepatocytes....1
proclinical space....11–12
vitro cellular models....3
Induced pluripotent stem cell-derived CMs (iPSC-CMs)....154, 173
InSphero....220
Inter-transient noise (ITN)....180
In vitro toxicity testing....248
Ion channels....57, 58, 63, 67, 72, 80
IonOptix LLC....220
IonWizard software....224

J

Japan iPS Cardiac Safety Assessment (JiCSA)....88, 137

K

Kinetic image cytometry™ (KIC™)
antibiotic Puromycin....162
APs, calcium transients and contraction....154, 155
axiogenesis....168
calcium influx....154, 155
calcium transient....163–167
cardiac myocytes....154
Cor.4U hiPSC-Cardiomyocytes....155
cytoplasmic calcium....154
cytoplasmic mask....158
drug arrhythmogenic liability....169
drug effects....154
drug-induced arrhythmias....153
FLIPR\FDSS....158
Fluo-4 No-Wash (NW)....161–162
hERG K^+ channel block....153
heterologous expression system....155
iCell Cardiomyocytes....155
ion channels....154, 155
kinetic image cytometry....158, 159
materials....156
"pace-maker" cells....158
phosphodiesterase inhibitors....168
plate map....156, 157
preparation....158–160
procedure....160–161
QT interval duration....164
recombinant heterologous cells....154
TdP....153
Kinked pipet tip....298
Krebs-Ringer-HEPES (KRH)....177

L

LabVIEW software....244
L-ascorbic acid....221
LEOPARD syndrome....272
Live staining and immunocytochemistry....280

M

MEA chip....295, 297–298
Mean spike frequency....300
Median absolute deviation (MAD)....287
Membrane potential....136, 138
Microelectrode array (MEA) technology
automation....101–102
cardiac electrophysiology signals....84, 85
cardiac safety evaluation....86–88
cell plating and culture....89–91
cell type-specific beating characteristics....105
chronic assays....84, 100
compound addition and data acquisition....92–93
conduction velocity metrics....104
data analysis....93–96
double delta calculation....105
drug-drug interactions....102–103
electrical pacing....96–99
electrodes embedded....83
electrophysiological signal....84
extracellular probe electrodes....85
field potential....85, 86
golden channel *vs.* well mean....104
isolated cardiomyocyte....84
Maestro multiwell MEA platform....89
materials....88
neurons and cardiomyocytes....83
optimizing assay quality....104
optogenetics....100–101
pacing rate....105
pH sensitivity....103
single *vs.* sequential dosing....103
structure-function relationships....103
transmembrane voltage....84
Micropatterned co-culture (MPCC)

pattern 314
technique 313
Micropatterned collagen plates 314–315, 318–320
Mitochondria 250
Mitochondrial toxicity 265
Mouse 3
Mouse embryonic stem cell test (mEST) 17
Mubritinib 265
Multielectrode arrays (MEAs) 191, 295, 297–298
Mus musculus 3
Myocam™ 220

N

Neurotoxicity
biochemical assays and data analysis 316
cell sources 294
data processing and binary toxicity calls 327–329
drug dosing 316, 324–325
electrode density 295
fipronil 306
hiPSC 305
hiPSC-derived neurons 295
maximal burst duration 300
MEA 296
minimal burst duration 299
MPCC technique 313
PDMS Lithography Mask 316–318
pharmacological in vitro profiling 293
sterilization 296
in vitro phenotype 312
Nifedipine 52, 55, 77, 205, 252
Nuclear factor of activated T-cells (NFAT) 272

O

Optogenetics 100–101
AP shape 131
blue laser intensity 130
calcium handling 131
calcium transients (CTs) 111
Cardiac Optopatch platform 111, 130
cardiomyocytes 114–115
cell plating efficiency 128
cell source and preparation 113–118
cellular physiology 109
CheRiff- and CaViar 111, 129
depolarized resting potential 132
drug addition and imaging 122–124
drug stocks 120–122
FluoVolt 120
GCaMP6f 112
incomplete ion channel expression 132
lentivirus 129
light-controlled stimulation 111
materials 113
measurements 131
mixed populations 131
morphology 131
optical actuators 110
optopatch vectors 115
signaling networks 110
spontaneous beating and paced action potentials 118–119
transfection method 129
treatment 118
voltage and calcium imaging 110, 115–119
voltage sensor QuasAr2 111
Optopatch
action potentials and calcium transients 124
baseline characteristics and drug effects 125–128
statistical analyses 125
Oxygen plasma 319

P

PatchControl 384 software 60, 71–73
Patchliner 58, 59
cell capture and sealing procedure 63–66
CiPA 58
current clamp recordings 68–71
data analysis 68
hiPSC-CMs 63
planar patch clamp electrophysiology 60
voltage and current clamp modes 67
voltage-gated recordings 66–68
Peri.4U™ 296, 301
Phenylephrine-hydrochloride (PE) 221
Phosphate buffered saline (PBS) 221
Phospho-kinase assay 280
Plate pluripotent stem cells
count cells 24
dilute cells 25
dilution of matrigel 23
dissociate cells 24
matrigel solidification 23
plate cells 25
storage 24
thawing 23
transfer to 96-well plate 23
washing 23
Plate reader 136, 138
Polydimethylsiloxane (PDMS) 113, 116, 316, 317
Polydimethylsiloxane lithography mask 314
Potassium channel 153, 162
PreScanReScan
algorithm 283
system 283
Primary human hepatocytes (PHHs) 312
Proclinical space 11–12

Q

Quinidine 52

R

Rat 3
Rattus norvegicus 3
ReproCELL (ReproCardio 2) 193
Retinoic acid (RA) 33
Rezulin® 312
Rofecoxib 174
Routine application scheme 303

S

Sarco-/endoplasmic reticulum ATPase (SERCA) 136
Sarcoplasmic reticulum (SR) 135
SB-431542 33
Scanning electron microscope (SEM) 244
Scientific CMOS (sCMOS) 119
Seeding 3T3-J2 Fibroblasts 315, 323–324
Seeding iPSC-HHs 315, 322–323
Self-Organizing Map (SOM) 262
Serum-free 230, 232, 244
Shortening 215, 224
Signal-to-noise ratio (SNR) 118
Sodium channel 154
Sotalol 52, 53
Spheroid
  cardiac microtissues 225
  cardiomyocytes 211, 212
  co-cultures 214–215
  3D cell culture systems 212–214
  3D cultures 218–219
  fetal/newborn animals 219
  fibroblasts 224
  freshly isolated cardiomyocytes 215
  microtissues 225
  stem cell-derived cardiomyocytes 219
  video-based measurement 215–219
Spike and burst detection 299–301
Spontaneous electrical activity 298
Stem cell 84
Stem cell-derived cardiomyocytes. *See* Induced pluripotent stem cell-derived cells (iPSCs)
Stem cell-derived cardiomyocytes (CMs) 177–183
  axial alignment, cells 183
  calcium (Ca^{2+}) signals 174
  cardiac troponin-T (cTnT) 175
  cardiovascular (CV) drug 173
  caspase 3/7 activation assays 187
  confocal microscopy 188
  Cytiva™ 175
  electrophysiological (EP) 174
  equipment, Ca^{2+} Imaging 177
  KnockOut DMEM (KO-DMEM) 175
  Krebs-Ringer-HEPES (KRH) 177
  Leibovitz L-15 Medium 177
  methods
    Ca^{2+} imaging 179
    cell viability and apoptosis 179–180
    data extraction and processing 180–183
    data processing and visualisation 180, 182
    freezing and plating 177–179
  RPMI Medium 176
  silicon gaskets 175
Superoxide dismutase 1 (*SOD1*) 11
SyncroPatch 384PE 58–61
  cell capture and sealing procedure 71–72
  data analysis 75–77
  experimental setup 71
  hiPSC-CMs 63
  planar patch clamp electrophysiology 60–61
  voltage protocols 73
  voltage-gated recordings 72–75

T

Temporal heterogeneity index (THI) 180
Terminal deoxynucleotidyl transferase dUTP nick end labelling (TUNEL) method 179
Tetramethylrhodamine, methyl ester, perchlorate (TMRM) 254
Thalidomide 33, 34
Threshold detection 299
3T3-J2 Fibroblasts 315
Tokyo Women's Medical University (TWMU) 58
Torsades de pointes (TdP) 37, 87, 153
Toxicity 229
Translational 1, 3, 9

U

US Food and Drug Administration (FDA) 39

V

Vala Sciences Inc. 157
Valdecoxib 175
Vehicle control experiments 301–304
Verapamil 154
Video analysis
  beta-stimulating drugs 224
  bovine 220
  cardiomyocyte and fibroblast 222
  cryopreservation 221
  culture microtissues 223
  detach cultured fibroblasts 221
  dimethyl sulfoxide (DMSO) 221

fetal calf serum (FCS).....220
GravityPlus.....223
HCF.....221
hiPSC-derived cardiomyocytes.....220
InSphero.....220
microtissues.....222
transient analysis.....224
Vioxx™.....174
Voltage-gated Ca2+.....60, 61, 63, 66, 68, 72, 79, 80
Voltage-gated K+.....60, 68, 71, 72
Voltage-sensitive dye (VSD) assays.....137

Z

Zebrafish.....3